Productie van groene basischemicaliën
door conventionele en opkomende pyrolyseprocessen

Production of Green Base Chemicals
through Conventional and Emerging Pyrolysis Processes

Ruben De Bruycker

Promotor: prof. dr. ir. K. Van Geem
Proefschrift ingediend tot het behalen van de graad van
Doctor in de Ingenieurswetenschappen: Chemische Technologie

Vakgroep Chemische Proceskunde en Technische Chemie
Voorzitter: prof. dr. ir. G. B. Marin
Faculteit Ingenieurswetenschappen en Architectuur
Academiejaar 2015 - 2016

UNIVERSITEIT
GENT

ISBN 978-90-8578-910-9
NUR 952
Wettelijk depot: D/2016/10.500/42

Promotor

Prof. dr. ir. Kevin M. Van Geem
Laboratorium voor Chemische Technologie
Vakgroep Chemische Proceskunde en Technische Chemie
Universiteit Gent

De auteur genoot tijdens de onderzoekactiviteiten de steun van het Bijzonder Onderzoekfonds (BOF), Universiteit Gent.

Examencommissie

Leescommissie

prof. dr. Frédérique Battin-Leclerc
Laboratoire Réactions et Génie des Procédés
ENSIC, Université de Lorraine, Nancy

dr. Véronique Dias
Thermodynamics and Fluid Mechanics
Université Catholique de Louvain

prof. dr. Marie-Françoise Reyniers
Laboratorium voor Chemische Technologie
Vakgroep Chemische Proceskunde en Technische Chemie
Universiteit Gent

prof. dr. ir. Frederik Ronsse
Thermal Conversion of Biomass
Vakgroep Biosysteemtechniek
Universiteit Gent

dr. ir. Maarten K. Sabbe [secretaris]
Laboratorium voor Chemische Technologie
Vakgroep Chemische Proceskunde en Technische Chemie
Universiteit Gent

Andere leden

prof. dr. ir. Guy B. Marin
Laboratorium voor Chemische Technologie
Vakgroep Chemische Proceskunde en Technische Chemie
Universiteit Gent

prof. dr. ir. Rik Van De Walle [voorzitter]
Data Science Lab
Vakgroep Elektronica en Informatiesystemen
Universiteit Gent

prof. dr. ir. Kevin M. Van Geem [promotor]
Laboratorium voor Chemische Technologie
Vakgroep Chemische Proceskunde en Technische Chemie
Universiteit Gent

Acknowledgements

In de eerste plaats wil ik mijn promotor prof. Kevin Van Geem bedanken voor de kans een doctoraat te beginnen onder zijn hoede. Bedankt om me tijdens de afgelopen vier jaar sterk verschillende processen te laten onderzoeken en dat je deur altijd openstond voor discussies. Verder wil ik ook prof. Guy Marin danken om dit doctoraat te laten doorgaan binnen zijn labo, zijn waardevolle input betreffende verschillende publicaties en zijn aandacht voor detail.

I would like to thank Dr. Hans-Heinrich Carstensen, a very valuable partner for several of the publications presented in this thesis. Understanding the pyrolysis and combustion of the selected model components would have been impossible without your expertise and your quantum chemical calculations.

Furthermore, I would like to thank Prof. Frédérique Battin-Leclerc for the opportunity to spend three months in her research group at Université de Lorraine, Nancy. This thesis wouldn't have been the same without the fruitful collaboration with you, dr. Luc-Sy Tran and Prof. Olivier Herbinet.

Een speciaal woord van dank gaat ook naar de thesisstudenten die me hebben bijgestaan met het experimenteel werk en het modelleren, Frederik Vercruysse, Ibe Pattyn, Charlotte Cluydts en Michiel Sulmon. Hopelijk heeft de bench scale jullie niet volledig tot waanzin gedreven.

Het experimentele luik van deze thesis vergde veel tijd van het technisch personeel van het LCT, Bert, Marcel, Michaël, Erwin, Brecht, Tim, Tom, Hans, Wim en Lambert. Bedankt om altijd klaar te staan en me te helpen. Here, a special mentioning to Marko is also in place. Thanks for teaching me the art of performing experiments!

De goede sfeer die op het labo heerst is één van de belangrijkste redenen waarom ik graag naar het werk kwam. De collega's zijn hier voornamelijk voor verantwoordelijk. Specifiek wil ik de mensen bedanken die elke dag op mijn gezicht moesten kijken: Nick, Thomas, Carl, Pieter, Ismaël en David. Numerous other colleagues provided sufficient entertainment during coffee and lunch breaks: Andres, Ezgi, Florence, Jonas, Laurien, Lukas, Maarten, Marko, Natalia, Nenad, Pieter, Ruben, Shekhar, Sri Bala, Stamatis, Stephanie, Yu to name a few.

Acknowledgements

Veel dank gaat uit naar vrienden en familie die me tijdens mijn doctoraat hebben gesteund. Behalve steun hebben jullie me ook van de nodige ontspanning kunnen voorzien. Vele leuke avonden/feesten/reizen de afgelopen vier jaar zijn herinneringen voor het leven. Jullie pogingen om dit doctoraat te begrijpen worden ook enorm gewaardeerd! In het bijzonder wil ik Niels, Lies, papa en mama bedanken voor hun aanhoudende zorg/steun/hulp/interesse/… kortom, voor alles! Ten slotte, mijn toeverlaat Silke, bedankt voor alle liefde die je me de afgelopen jaren gegeven hebt!

Ruben De Bruycker

Gent 2016

Contents

Notation

Roman symbols

A	pre-exponential factor	$m^3\ mol^{-1}\ s^{-1}$ or s^{-1}
$\widetilde{A}$	single-event pre-exponential factor	$m^3\ mol^{-1}\ s^{-1}$ or s^{-1}
$\widetilde{A}_{ref}$	single-event pre-exponential factor of the reference reaction	$m^3\ mol^{-1}\ s^{-1}$ or s^{-1}
c_j	concentration of species j	$mol\ m^{-3}$
Δc_j^s	instantaneous error on c_j when applying the PSSA	$mol\ m^{-3}$
d_t	internal tube diameter	m
E_a	activation energy	$kJ\ mol^{-1}$
$E_{a,ref}$	activation energy of the reference reaction	$kJ\ mol^{-1}$
F_j^0	inlet molar flow rate of species j	$mol\ s^{-1}$
F_V	volumetric flow rate	$m^3\ s^{-1}$
G	Gibbs free energy	$kJ\ mol^{-1}$
h	Planck constant	$6.62\ 10^{-34}\ J\ s^{-1}$
H	enthalpy	$kJ\ mol^{-1}$
k	rate coefficient	$m^3\ mol^{-1}\ s^{-1}$ or s^{-1}
k_B	Boltzmann constant	$1.38\ 10^{-23}\ J\ K^{-1}$
n_e	number of single events	
P	pressure	MPa
R	Universal gas constant	$8.314\ J\ mol^{-1}\ K^{-1}$
r_j	rate of reaction j	$mol\ m^{-3}\ s^{-1}$
T	temperature	K
$v_{i,j}$	stoichiometric coefficient of species i in reaction j	
x_i	mole fraction of component i	
z	axial position	m

Greek

$\alpha_j(T)$	stoichiometric coefficient of species j in a single-step equivalent reaction, obtained after elimination of the concentration of μ-radicals using the pseudo-steady-state approximation, at temperature T	
$\Delta_f H$	enthalpy of formation	kJ mol^{-1}
$\Delta_r H$	enthalpy of reaction	kJ mol^{-1}
Δn	molecularity of the reaction (2 for bimolecular, 1 for monomolecular)	
$\Delta_r S$	entropy of reaction	J K^{-1} mol^{-1}
φ	equivalence ratio	
τ	residence time	s
$\chi(T)$	quantum mechanical tunneling correction factor	

Acronyms

4PA	4-pentenoic acid	
ASTM	American society for testing and materials	
BAC	bond additivity correction	
BDE	bond dissociation energy	
CBS	complete basis set	
CIP	coil inlet pressure	MPa
CIT	coil inlet temperature	K
COP	coil outlet pressure	MPa
COT	coil outlet temperature	K
CPD	1,3-cyclopentadiene	
CTO	crude tall oil	
Ci:j	methyl ester with an acid chain length of i carbon atoms with y C=C double bonds	
DTO	distilled tall oil	
FID	flame ionization detector	
GAV	group additivity value	
GC	gas chromatograph	

GC×GC	two dimensional gas chromatograph
GBL	γ-butyrolactone
GVL	γ-valerolactone
HDO	hydrodeoxygenation
JSR	jet-stirred reactor
LOA	light oxygenates analyzer
MON	motor octane number
MTHF	2-methyl-tetrahydrofuran
NGC	natural gas condensate
PAH	polycyclic aromatic hydrocarbon
PFR	plug flow reactor
PSSA	pseudo-steady-state approximation
RGA	refinery gas analyzer
RME	rapeseed methyl esters
RON	research octane number
ROP	rate of production
TCD	thermal conductivity detector
TOFA	tall oil fatty acids
THF	tetrahydrofuran
THP	tetrahydropyran
TOF-MS	time-of-flight mass spectrometer
TST	transition state

Summary

Scope

Environmental awareness has triggered an increased demand for renewable consumer goods. A lot of commodities are made by the petrochemical industry from a limited number of platform chemicals, e.g. ethene, propene, 1,3-butadiene and benzene. In turn, the bulk of these chemicals are produced by steam cracking of crude oil fractions which is inherently non-renewable.

The route that requires the lowest capital investment for the production of green chemicals is the use of existing petrochemical facilities while (partially) shifting towards bio-derived feedstocks. Triglyceride-based biomass is an excellent candidate. The global vegetable oil production was over 150 million tons in 2015. It has a low oxygen content and deoxygenation forms hydrocarbon mixtures that have high selectivities towards ethene and propene following steam cracking. Lignocellulose is more abundant and sustainable compared to triglycerides. Therefore, a wide range of conversion routes from lignocellulose to fuels and chemicals are currently being investigated, including biochemical, catalytic, thermochemical processes or a combination thereof.

This thesis focusses on two thermochemical processes, i.e. steam cracking of catalytically upgraded triglyceride-based biomass and fast pyrolysis of lignocellulose. Experimental investigation and the use of advanced fundamental models can raise the performance of these processes, required to be economically viable.

Automated generation of compact fundamental kinetic models

Single-event microkinetic models for thermochemical processes are characterized by a large number of species and reactions which increases exponentially with molecular weight of the feedstock. Kinetic models that describe the thermochemical conversion of high molecular weight feedstocks, such as biomass, are impractical for large-scale computations.

A network generation tool called PRIM-O has been developed that allows automatic generation of thermal decomposition schemes. PRIM-O also reduces the number of species by a posteriori lumping of the feedstock, in situ lumping of molecular products and application of the pseudo steady state approximation to μ-radicals, i.e. radicals for which bimolecular

consumption reactions can be neglected. Compared to the earlier version called PRIM, PRIM-O allows the generation of kinetic models for pyrolysis of oxygenated molecules and the list of defined reaction families has been extended.

The generation of a kinetic model for the pyrolysis of methyl esters is presented as case study. A good agreement was obtained between experimental and model calculated mole fraction profiles, indicative that the model reduction strategies introduce a negligible error.

Steam cracking of renewable feedstocks

Green chemicals can be produced by the two-step process (i) catalytic upgrading of biomass to hydrocarbons and (ii) steam cracking of hydrocarbons to alkenes and aromatics. As the catalytic upgrading step requires the consumption of hydrogen for the removal of oxygen, biomass feedstocks with a low oxygen content are preferred. Possible feedstocks include vegetable oils, waste fats and tall oil.

Hydrodeoxygenation of vegetable oils and waste fats followed by hydrocracking/isomerization results in a mixture of normal and branched alkanes. Steam cracking of two such mixtures has been investigated experimentally in a dedicated bench scale setup. Selectivities towards ethene and propene were higher than in steam cracking of crude oil fractions. A detailed kinetic model was developed to identify the dominant reaction paths towards alkenes and aromatics. This model aids in optimizing operating conditions of the steam cracking step. Furthermore, it can create a feedback loop to the preceding catalytic step to modify the hydrocarbon mixture composition. For example, a higher degree of branching in the hydrocarbon mixture results in higher propene/aromatic yields following steam cracking.

Steam cracking of hydrodeoxygenated crude tall oil has also been investigated. Crude tall oil is a by-product of the Kraft wood-pulping process and consists of fatty acids, resin acids and sterols. The resulting deoxygenated hydrocarbon mixture is characterized by the high fraction of naphthenes. Also here, high ethene and propene yields were obtained following steam cracking. Hydrodeoxygenation of crude tall oil at high temperatures increases the fraction of naphthenoaromatics in the hydrocarbon mixture. As these molecules have a high selectivity towards low-value chemicals following steam cracking, hydrodeoxygenation should proceed at sufficiently low temperatures but still ensuring high deoxygenation conversion.

Fast pyrolysis of model compounds for lignocellulose and derivatives

Fast pyrolysis of lignocellulose is a complex chemical process and, therefore, first the pyrolysis chemistry of its core constituents and reactive intermediates, formed during the thermochemical process, has to be unraveled. In this thesis, model components relevant to the pyrolysis of carbohydrates have been selected, i.e. γ-valerolactone, 2-methyl-tetrahydrofuran and tetrahydropyran. These molecules can also be produced by catalytic and enzymatic routes from lignocellulose and have been proposed as next-generation bio-fuels. Pyrolysis experiments were performed for all three molecules. Combustion experiments have been performed for 2-methyl-tetrahydrofuran. New detailed kinetic models, primarily based on quantum chemical calculations, are in good agreement with the experimental data. For γ-valerolactone and 2-methyl-tetrahydrofuran pyrolysis, unimolecular ring opening reactions to respectively 4-pentenoic acid and 4-pentenol have been identified. Scission of the ring bonds was found to be unimportant for γ-valerolactone and 2-methyl-tetrahydrofuran pyrolysis. Interestingly, scission of the ring bonds is important for decomposition of tetrahydrofuran and tetrahydropyran. Clearly, the presence of an alkyl group has a big impact on the reactivity of cyclic ethers.

The decomposition chemistry of three unsaturated molecules has been investigated, i.e. 3-methyl-2-butenol, 3-methyl-3-butenol and 1,5-hexadiene. Unsaturated alcohols, such as 3-methyl-2-butenol and 3-methyl-3-butenol, are formed in the fast pyrolysis of carbohydrates and the low-temperature oxidation of alcohols. The self-recombination product of allyl radicals, i.e. 1,5-hexadiene, has been identified as an important intermediate in the formation of benzene in the oxidation and pyrolysis of both hydrocarbon and oxygenated molecules, e.g. in the pyrolysis of γ-valerolactone. Given the importance of these three unsaturated molecules as intermediates in the aforementioned processes, their pyrolysis and oxidation chemistry has been investigated. The two unsaturated alcohols react entirely different despite their obvious molecular similarities. In the investigated conditions, over 99% of 3-methyl-3-butenol is consumed by a unimolecular retro-ene reaction to isobutene and formaldehyde. In contrast, oxidation and pyrolysis of 3-methyl-2-butenol is dominated by radical chemistry. Thus, the position of the C=C double bond with respect to the hydroxyl group has a big impact on the reactivity of unsaturated alcohols. Thermal decomposition of 1,5-hexadiene has a high selectivity towards benzene and 1,3-cyclopentadiene. Below 1100K, benzene formation is dominated by three competing reaction pathways: (i) hydrogen abstraction from 1,5-hexadiene, intramolecular radical addition and dehydrogenation; (ii) addition of vinyl on 1,3-

butadiene, intramolecular radical addition and dehydrogenation; (iii) recombination of cyclopentadienyl plus methyl, hydrogen abstraction and ring enlargement. Analogous pathways were found to be important for the formation of other aromatics.

Samenvatting

Toepassingsgebied

Ons groeiend milieubewustzijn zorgt voor een stijging van de vraag naar hernieuwbare consumentengoederen. Heel wat alledaagse artikelen worden geproduceerd door de petrochemische industrie startend van een beperkt aantal platformchemicaliën, zoals etheen, propeen, 1,3-butadieen en benzeen. Het merendeel van deze chemicaliën wordt echter gemaakt door stoomkraken van ruwe aardoliefracties, wat een niet-hernieuwbare grondstof is. Daarom wordt er gezocht naar alternatieve processen voor de productie van groene chemicaliën.

Het proces dat de laagste kapitaalinvestering vraagt is het gebruik van hernieuwbare grondstoffen in bestaande, conventionele, stoomkrakers. Plantaardige oliën en afvalvetten zijn een uitstekende kandidaat om aardoliefracties, gedeeltelijk, te vervangen gezien hun moleculaire gelijkenissen, bijvoorbeeld lage zuurstofinhoud. De globale productie van plantaardige oliën was meer dan 150 miljoen ton in 2015. De katalytische verwijdering van zuurstof uit triglyceriden resulteert in koolwaterstofmengsels die een hoge selectiviteit hebben naar etheen en propeen tijdens stoomkraken. Hoewel dit proces al relatief veel commercieel succes kent, lijdt dit proces onder de relatief beperkte beschikbaarheid van plantaardige oliën en afvalvetten. Grootschalige productie vereist toewijzing van oliën die normaal bedoeld zijn voor de voedingsindustrie. Daarom worden ook conversieroutes onderzocht die starten van lignocellulose, waarvan grotere (afval-) hoeveelheden beschikbaar zijn, bijvoorbeeld biochemische, katalytische en thermochemische processen.

Deze thesis focust op twee thermochemische processen, namelijk stoomkraken van katalytisch opgewaardeerde triglyceriden/vetzuren en de snelle pyrolyse van lignocellulose. De prestaties van deze processen kunnen verbeterd worden door experimenteel onderzoek en geavanceerd fundamentele modellen, noodzakelijk om ze economisch rendabel(er) te maken

Automatische generatie van compacte kinetische modellen

Single-event microkinetische modellen voor thermochemische processen zijn gekenmerkt door vele species en reacties, waarvan het aantal exponentieel stijgt met het moleculair gewicht van de voeding. Kinetische modellen die de thermochemische conversie van

voedingen met groot moleculair gewicht, zoals biomassa, beschrijven, zijn onpraktisch voor berekeningen op grote schaal.

Een netwerkgeneratiesoftwarepakket, genaamd PRIM-O, werd ontwikkeld dat toelaat thermische decompositieschema's automatische te genereren. PRIM-O reduceert het aantal species door a posteriori lumping van de voeding, in situ lumping van moleculaire producten en toepassing van de pseudo-stabiele toestandsbenadering voor μ-radicalen, dit zijn radicalen waarvoor bimoleculaire consumptiereacties verwaarloosd kunnen worden. In vergelijking met de voorgaande versie PRIM is PRIM-O in staat kinetische modellen te genereren voor zuurstofhoudende moleculen en is de lijst van gedefinieerde reactiefamilies uitgebreid.

De generatie van een kinetisch model voor de pyrolyse van methylesters is voorgesteld als gevalsstudie. Er is een goede overeenkomst tussen experimentele data en modelvoorspellingen. Dit duidt aan dat de voorgenoemde strategieën voor modelreductie een verwaarloosbare fout introduceren.

Stoomkraken van hernieuwbare voedingen

Groene chemicaliën kunnen geproduceerd worden door het tweestapproces (i) katalytische conversie van biomassa naar koolwaterstofmengsel en (ii) stoomkraken van dat koolwaterstofmengsel naar alkenen en aromaten. In de katalytische stap wordt kostbaar waterstof verbruikt om zuurstof te verwijderen uit de biomassa. Daarom is dit proces vooral geschikt voor biomassavoedingen met een lage zuurstofinhoud, zoals plantaardige oliën, afvalvetten en tallolie.

Hydrodeoxygenering van plantaardige oliën en afvalvetten gevolgd door hydrokraken/isomerisatie resulteert in een mengsel van normaal en vertakte alkanen. Stoomkraken van twee zulke mengsels is experimenteel onderzocht geweest gebruikmakend van een proefbank-schaalreactoropstelling. De opgemeten selectiviteit naar etheen en propeen was groter dan die in stoomkraken van typische aardoliefracties. Een gedetailleerd kinetisch model werd ontwikkeld om reactiepaden naar alkenen en aromaten te identificeren. Dit model helpt om procescondities voor stoomkrakers te optimaliseren. Verder kan het terugkoppelen naar de voorgaande katalytische stap om de samenstelling van het koolwaterstofmengsel te manipuleren. Bijvoorbeeld, een hogere graad van vertakkingen in het koolwaterstofmengsel resulteert in grotere propeen en aromaat opbrengsten tijdens stoomkraken.

Verder werd ook stoomkraken van hydrodeoxygeneerd ruwe tallolie onderzocht. Ruwe tallolie is een bijproduct van het Kraft-houtpulpingproces en bestaat uit vetzuren, harszuren en sterolen. Het resulterend gedeoxygeneerd koolwaterstofmengsel wordt gekarakteriseerd door de grote fractie naftenen. Ook hier werden hoge etheen- en propeenopbrengsten opgemeten tijdens stoomkraken. Hydrodeoxygenering van ruwe tallolie op hoge temperaturen vergroot de fractie naftenoaromaten in het koolwaterstofmengsel. Deze moleculen hebben een hoge selectiviteit naar chemicaliën met een lage economische waarde bij stoomkraken. Hydrodeoxygenering moet daarom doorgaan op voldoende lage temperaturen, terwijl wel nog steeds hoge deoxygeneringconversie moet bereikt worden.

Snelle pyrolyse van modelcomponenten voor lignocellulose en afgeleiden

Snelle pyrolyse van lignocellulose is een complex chemisch proces en daarom moet eerst de pyrolyse van de kernbestanddelen en reactieve intermediairen, gevormd tijdens het thermochemisch proces, begrepen worden. In deze thesis zijn modelcomponenten die relevant zijn voor de pyrolyse van sachariden geselecteerd, met name γ-valerolacton, 2-methyl-tetrahydrofuraan en tetrahydropyraan. Deze moleculen kunnen ook geproduceerd worden door katalytische en enzymatische routes vertrekkende van lignocellulose. Ze worden voorgesteld als biobrandstoffen van de volgende generatie. Pyrolyse-experimenten werden uitgevoerd voor deze drie moleculen. Verbrandingsexperimenten werden uitgevoerd voor 2-methyl-tetrahydrofuraan. Nieuwe gedetailleerde kinetische modellen, voornamelijk gebaseerd op kwantumchemische berekeningen, zijn in overeenstemming met experimentele data. Unimoleculaire ringopeningreacties werden geïdentificeerd voor γ-valerolacton en 2-methyl-tetrahydrofuraan, naar respectievelijk 4-penteenzuur en 4-penteenol. Breken van ringbindingen is onbelangrijk in de pyrolyse van γ-valerolacton en 2-methyl-tetrahydrofuraan terwijl dit type reactie wel belangrijk is in de pyrolyse van tetrahydrofuraan en tetrahydropyraan. Hieruit blijkt dat alkylgroepen een grote impact hebben op de reactiviteit van cyclische ethers.

De decompositiechemie van drie ongesatureerde moleculen werd onderzocht, met name 3-methyl-2-buteenol, 3-methyl-3-buteenol en 1,5-hexadieen. Ongesatureerde alcoholen, zoals 3-methyl-2-buteenol en 3-methyl-3-butenol, worden gevormd in de snelle pyrolyse van sachariden en de oxidatie van alcoholen op lage temperatuur. 1,5-hexadieen, gevormd door zelfrecombinatie van allyl radicalen, is een belangrijk intermediair in de vorming van benzeen bij oxidatie en pyrolyse van zowel koolwaterstoffen als zuurstofhoudende moleculen,

bijvoorbeeld in de pyrolyse van γ-valerolacton. Vanwege het belang van deze drie ongesatureerde moleculen als intermediair in de voorgenoemde processen werd hun pyrolyse- en oxidatiechemie onderzocht. De twee ongesatureerde alcoholen reageren geheel verschillend ondanks hun duidelijke moleculaire gelijkenissen. In de onderzochte procescondities werd meer dan 99% van 3-methyl-3-buteenol geconsumeerd door een unimoleculaire retro-ene reactie naar isobuteen en formaldehyde. In tegenstelling, oxidatie en pyrolyse van 3-methyl-2-buteenol wordt gedomineerd door radicalaire chemie. Klaarblijkelijk heeft de positie van de C=C dubbele binding relatief ten opzicht van de hydroxyl groep een groot effect op de reactiviteit van ongesatureerde alcoholen. Thermische decompositie van 1,5-hexadieen heeft een grote selectiviteit naar benzeen en 1,3-cyclopentadieen. Beneden 1100K wordt benzeenvorming gedomineerd door drie competitieve reactiepaden: (i) waterstofabstractie van 1,5-hexadieen, intramoleculaire radicaaladditie en dehydrogenering, (ii) additie van vinyl op 1,3-butadieen, intramoleculaire radicaaladditie en dehydrogenering en (iii) recombinatie van cyclopentadieenyl en methyl, waterstofabstractie en ringvergroting. Analoge reactiepaden zijn belangrijk in de vorming van andere aromaten.

Glossary

Arrhenius expression	The mathematical expression of rate coefficient $k = A \exp\left(\frac{-E_a}{RT}\right)$ where A is the temperature independent pre-exponential factor and E_a is the activation energy.
Bond dissociation energy	The bond dissociation energy is the enthalpy change for a hemolytic bond scission.
Comprehensive two-dimensional gas chromatography	Advanced analytical technique that provides two-dimensional separation by combining two different analytical columns connected with an interface, called the modulator, that ensures that the entire sample is comprehensively subjected to both separations.
Elementary reaction	A chemical reaction in which one or more species react to products in a single step and with a single transition state.
Goldfinger-Letort-Niclause formalism	A formalism for describing free-radical chemistry by distinguishing between β radicals, that are assumed to be involved in second-order propagation reactions, and μ radicals, that are assumed to be involved in first-order propagation reactions.
Green chemicals	Platform chemicals like ethene, propene and 1,3-butadiene produced from renewable resources in a sustainable production process.

Group additivity method	A group additivity method is a technique that allows to predict properties from molecular structures. For example, within Benson's group additivity method a property can be written as a sum of contributions arising from its constituent groups.
Hydrodeoxygenation	A catalytic process which, in the presence of hydrogen, removes oxygen from organic components in the form of water. Common side-reactions are decarboxylation and decarbonylation producing carbon dioxide and carbon monoxide respectively.
Lumping	Grouping of species, which are generally isomers or homologous species with similar reactivity, in order to reduce the total number of species in a kinetic model.
Modified Arrhenius expression	The mathematical expression of rate coefficient $k = A\,T^{n}\exp\left(\frac{-E_a}{RT}\right)$ where A is the temperature independent pre-exponential factor, E_a is the activation energy and n is a constant.
Molecularity	An elementary step is uni-, bi-, or ter-molecular if it involves respectively one, two or three reactants.
Natural gas condensate	A low-density mixture of hydrocarbons that are present as gaseous components in raw natural gas and are extracted therefrom by condensation.
Pyrolysis	The unanalyzed decomposition of organic components resulting from exposure to high temperature, in the absence of molecular oxygen.
Reaction family	A class of reactions that are characterized by the same pattern of electronic/atomic rearrangement steps.

Single-event microkinetic model	A kinetic model that describes processes using only elementary reactions.
Steam cracking	A petrochemical process in which saturated hydrocarbons are converted into small unsaturated hydrocarbons by exposure to high temperature in the presence of steam.
Tall oil	A viscous yellow-black odorous liquid obtained as a by-product of the Kraft process of wood pulp manufacture when pulping mainly coniferous trees.
Wall effect	The rate of many homogeneous reactions can be affected by the presence and state of reactor walls.

Chapter 1

Introduction and outline

1.1 Scope and objective

The current petrochemical industry is based upon a limited number of building blocks, such as ethene, propene, 1,3-butadiene, benzene and toluene. These molecules are generally produced from non-renewable fossil feedstocks by thermal cracking, catalytic cracking and dehydrogenation units. The building blocks are used as raw material in other chemical processes. For example, ethene is used in the manufacture of polyethylene, ethylene oxide, ethylene dichloride, ethylbenzene and numerous other organic chemicals, see Figure 1-1.

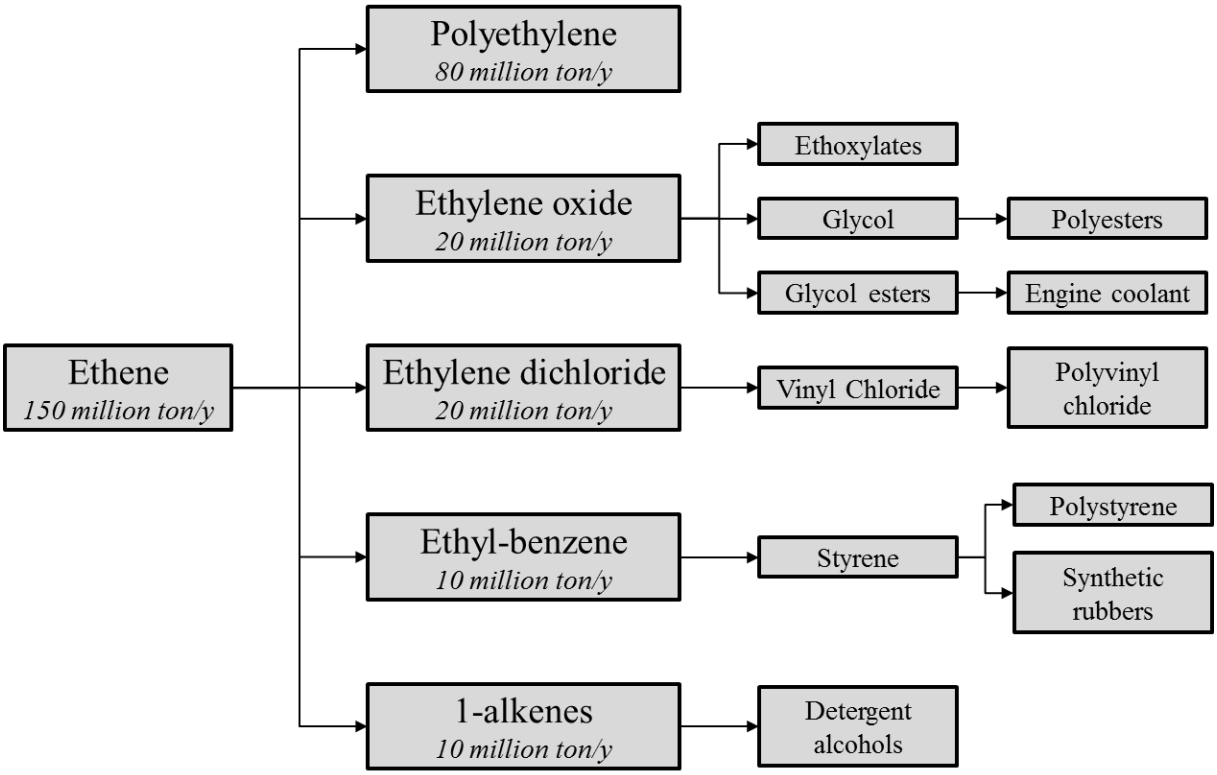

Figure 1-1 Common ethene derivatives [1]

The petrochemical industry relies heavily on crude oil availability and price. As the availability of conventional oil reserves deplete, oil majors and oil-producing countries are investigating the exploration of unconventional oil sources, such as oil sands, oil shale and tight oil. For example, the production from Canadian oil sands is projected to grow from 3.7 million barrels per day in 2014 to 5.3 million barrels per day in 2030 [2]. The crude recovery

from unconventional sources is accompanied with an increase in greenhouse gas emissions. The well-to-wheel emissions of gasoline and diesel from Canadian oil sands is approximately 20% higher than from conventional crudes [3].

At the time of writing this thesis, the oil price was at 40$ per barrel, coming from 100$ per barrel mid-2014, also see Figure 1-2. The sudden drop is mainly caused by the increase in supply by the United States, Canada, Iraq and Iran and the decreased demand due to the economic slowdown in China. Crude oil price forecasts are unclear. Continued low oil-prices will work inhibitive for new investments and increase dependency on oil-producing countries while a return to normal of oil-prices will continue the exploration of unconventional oil sources and the associated increase in greenhouse gas emissions[4].

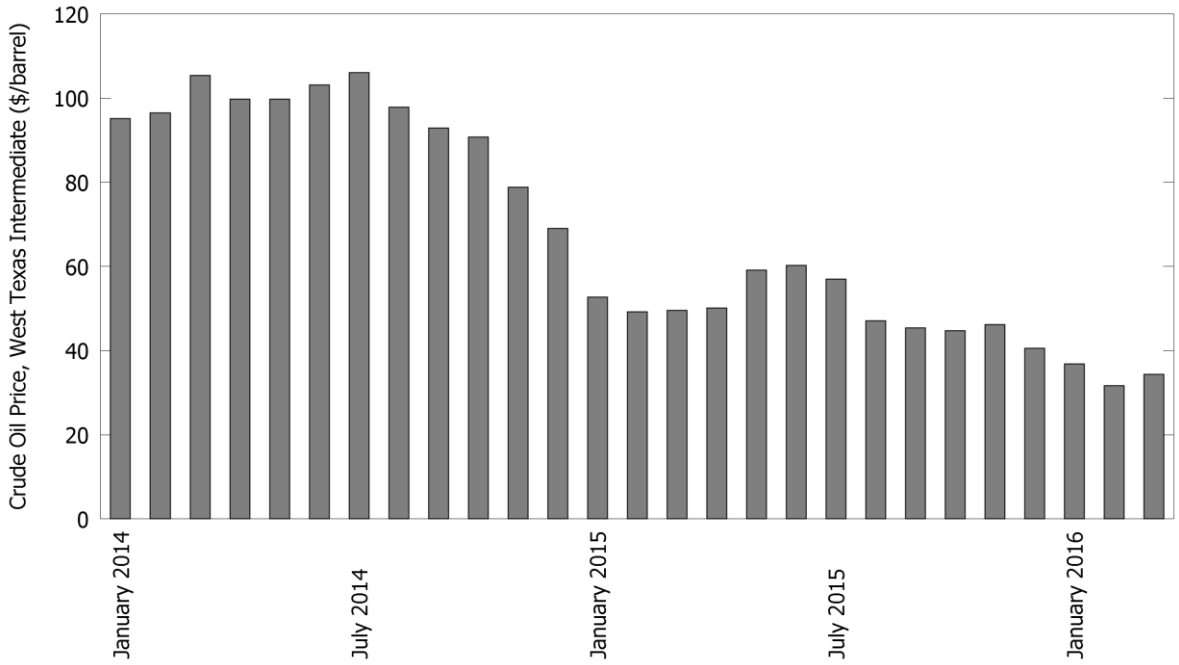

Figure 1-2 Evolution of West Texas Intermediate crude oil price

The production of chemicals from biomass improves sustainability and allows diversification of feedstocks. In this thesis, the production of green chemicals through two different pyrolysis processes has been investigated. The first process is steam cracking of catalytically upgraded triglyceride-based biomass and is discussed in section 1.2. The second process is fast pyrolysis of lignocellulosic biomass and is discussed in section 1.3. In section 1.4, the outline of this thesis is presented.

1.2 Steam cracking of renewable feedstocks

1.2.1 Steam cracking

The bulk of ethene and propene is produced by steam cracking of hydrocarbons[1, 5]. In this process, a hydrocarbon feedstock is evaporated, heated and mixed with steam. This stream enters a tubular reactor suspended in a furnace. Heat is supplied by burners in the furnace floor and side walls. In the reactor, the temperature of the gas increases from 500-650°C at the inlet to approximately 750°C-875°C at the outlet. The residence time is below 0.5s. The hydrocarbon feedstocks fragments into alkenes such as ethene, propene and 1,3-butadiene and aromatics such as benzene and toluene through a free-radical mechanism [6]. The outlet gas is rapidly quenched to avoid reaction of valuable products. The complex product mixture has to be separated and purified. This is accomplished by compressing the mixture followed by a number of distillation columns. A schematic overview of a depropanizer first front-end naphtha cracker is presented in Figure 1-3.

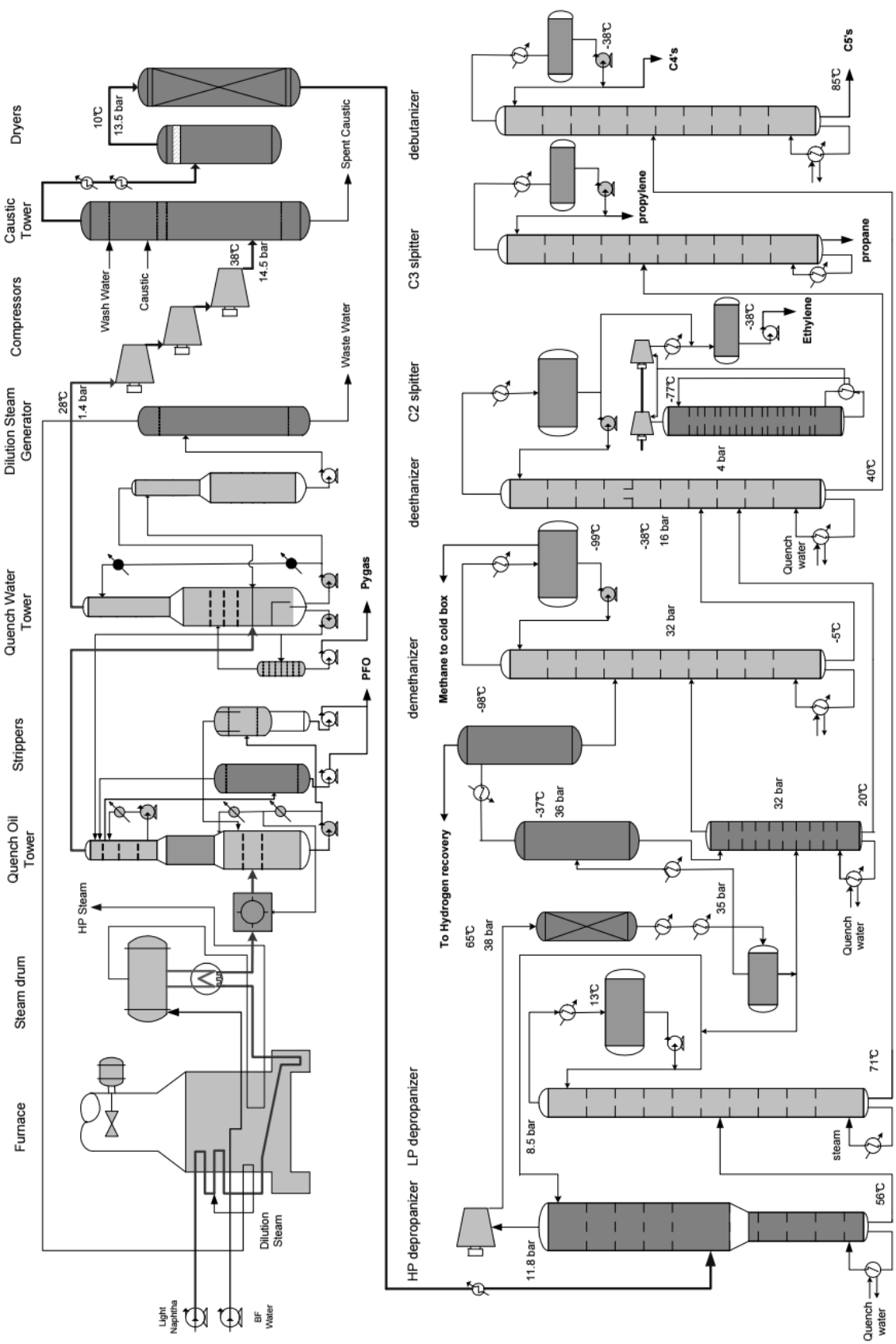

Figure 1-3 Depropanizer first front-end naphtha cracker[7]

A wide range of hydrocarbons can be used as feedstock for steam crackers. Steam crackers, especially in Europe, often rely on refined oil products, such as naphtha[8]. The current economic situation has pushed investments to steam crackers that utilize very light and very heavy feedstocks. This is caused by shale gas and the unconventional heavy oil. The production of shale gas through hydraulic fracking has boomed the past years. Besides methane, shale gas may contain over 20% of C_{2+} components, also known as "wet" shale gas [9]. For example, wet shale gas from the Marcellus play consists of 74.7% of methane, 15.6% of ethane, 5.5% of propane, 1.4% of normal butane, 0.7% of iso-butane and 2.1% of C_{5+} alkanes [9]. The availability of cheap hydrocarbon feedstock is projected to cause a 30% increase in ethene capacity in the US [10]. As worldwide reserves of crude oil deplete, oil derived from unconventional sources, such as tar sands, have an increased market share. Therefore, feedstock flexibility for steam crackers becomes an important asset. An interesting opportunity is the direct use of crude oil in petrochemical facilities as this reduces emissions and energy consumption by eliminating refining steps. In 2013, ExxonMobil launched the first steam cracker that can process crude oil in Singapore[11].

1.2.2 Triglyceride and fatty acid based biomass as feedstock for steam crackers

Climate change, public opinion and policy makers are pushing for a reduction in the consumption of natural gas and crude oil. For petrochemical companies, one interesting option is the use of bio-derived feedstocks in existing production facilities, such as steam crackers, reducing investment cost. The main difference with traditional hydrocarbon feedstocks is the presence of oxygen atoms. Pyrolysis of bio-derived feedstocks results in the formation of carbon monoxide, carbon dioxide, water and other oxygenated molecules [12]. Conventional separation systems, as in Figure 1-3, are incapable of handling the increase in carbon monoxide and carbon dioxide. Furthermore, the produced small oxygenates may contaminate the alkene streams. For example, methanol in the reactor effluent will end up in C_3 and C_4 streams[13]. Hence, the direct use of bio-derived feedstocks in steam crackers is troublesome. Catalytic processes that remove the oxygen content prior to its pyrolysis are often required.

Triglyceride and fatty acid based biomass shows similarities with hydrocarbon feedstocks given its high carbon and low oxygen content, see Figure 1-4. This type of biomass can be derived from vegetable oils, waste oils/fats and tall oil, a by-product of the Kraft pulping process [14]. Catalytic upgrading via conventional hydrodeoxygenation over NiMo/CoMo catalysts results in a mixture of long chain normal alkanes, typically having between 14 and

18 carbons depending on the acid chain length [15]. This process consumes hydrogen which is required to remove oxygen as water, carbon monoxide and carbon dioxide. Pyrolysis of long chain normal alkanes has a high selectivity to ethene and propene [16]. Several processes have been developed where the hydrodeoxygenation step is followed by hydrocracking [17, 18]. The long-chain normal alkanes formed in the first step are converted into smaller normal and branched alkanes in the second step. The hydrocarbon fraction having 10 or more carbon atoms can be used as diesel or jet-fuel while the hydrocarbon fraction having 9 or less carbon atoms can be used as a renewable naphtha for steam crackers.

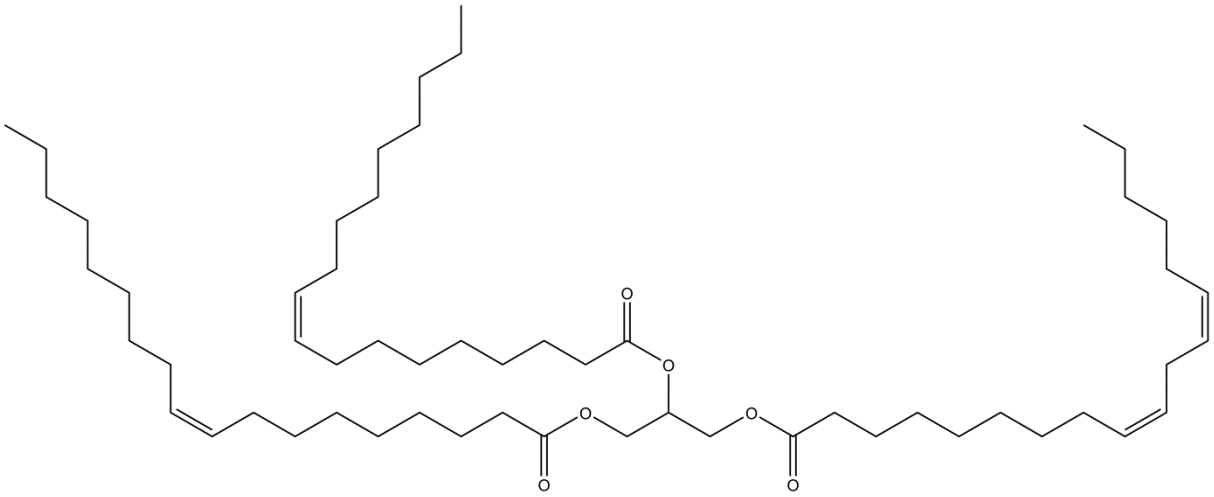

Figure 1-4 Example structure of triglyceride

1.3 Fast pyrolysis of lignocellulosic biomass

The aforementioned section highlighted the possibility to use triglyceride biomass as feedstock in steam crackers following catalytic upgrading. For triglycerides, relatively simple catalytic processes and minor amounts of hydrogen are required to produce hydrocarbons, as this solely involves removal of the ester functionality. Large-scale production of green chemicals using triglycerides would require the allocation of vegetable oils which inevitably competes with food production for land and water.

Lignocellulosic biomass is low-cost, more abundant and is considered to be more sustainable[19]. Agricultural residues and wood are important sources of lignocellulose. Also for this type of biomass, life-cycle-analysis is required to evaluate its sustainability. Agricultural residues are often scattered while the use of woody biomass requires short-rotation crops[19].

Several bio-refineries that utilize lignocellulosic biomass have been conceptualized. Their environmental and economic viability requires complete utilization of the feedstock. The heart of a bio-refinery can be a bio-chemical, catalytic and/or thermochemical process which converts the lignocellulose in a variety of chemicals. Subsequent processes upgrade the product stream into high-value chemicals and/or bio-fuels. An example of a pyrolysis-based bio-refinery is presented in Figure 1-5.

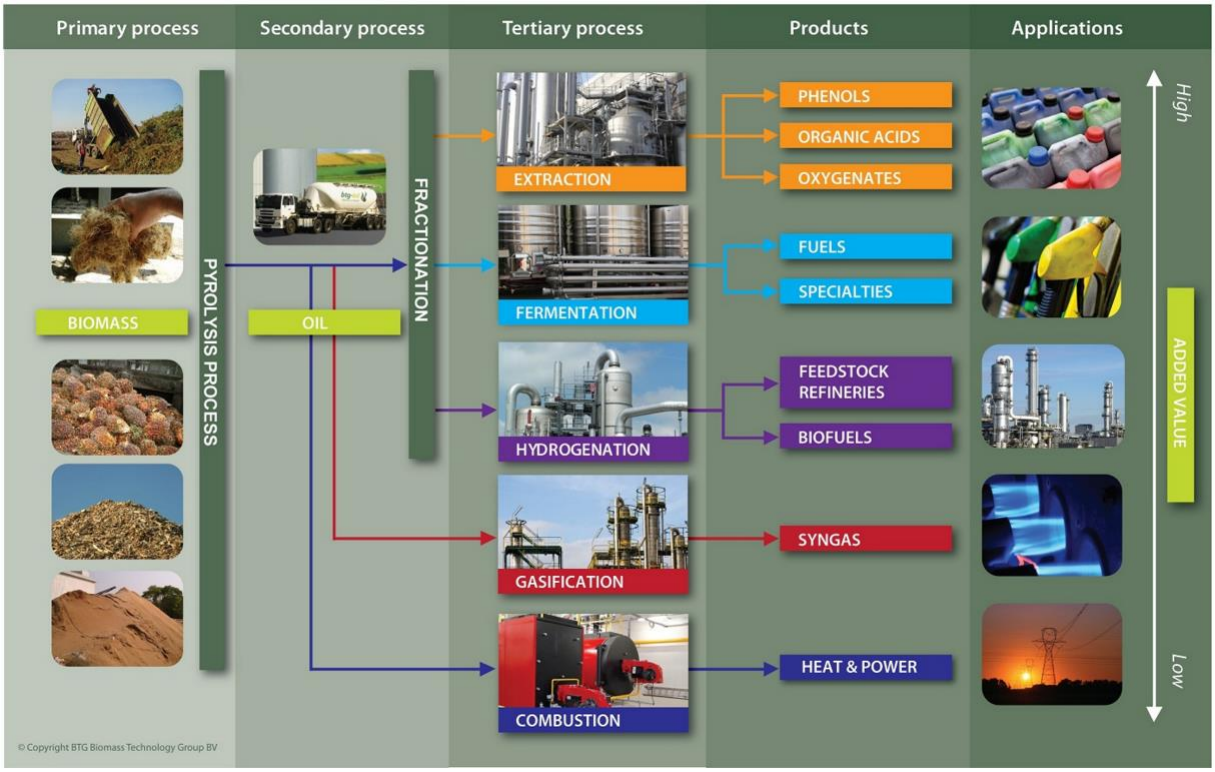

Figure 1-5 Bio-liquids refinery proposed by BTG[20]

In the remainder of this section, the molecular structure of lignocellulose is discussed, see 1.3.1, and several conversion methods of lignocellulose to chemicals are presented, see 1.3.2. The conversion method of interest in this thesis is fast pyrolysis. Optimization of a pyrolysis-based bio-refinery requires control of bio-oil yield and composition which necessitates a detailed understanding of the underlying chemistry. In 1.3.3 an overview of past and current efforts regarding kinetic modeling of biomass fast pyrolysis is presented.

1.3.1 Lignocellulosic biomass structure

Lignocellulosic biomass mainly composes of cellulose, hemicellulose and lignin with minor amounts of extractives and inorganic salts.

Cellulose is a linear polysaccharide chain consisting of glucose units connected by β-(1,4)-linkages. The degree of polymerization depends on the origin of the material, e.g. between 300 and 1700 for wood pulp and between 800 and 10 000 for cotton and plant fibers [21]. The presence of hydroxyl groups allows formation of intra and intermolecular hydrogen bonds, see Figure 1-6, which results in partially crystalline fiber structures and morphologies.

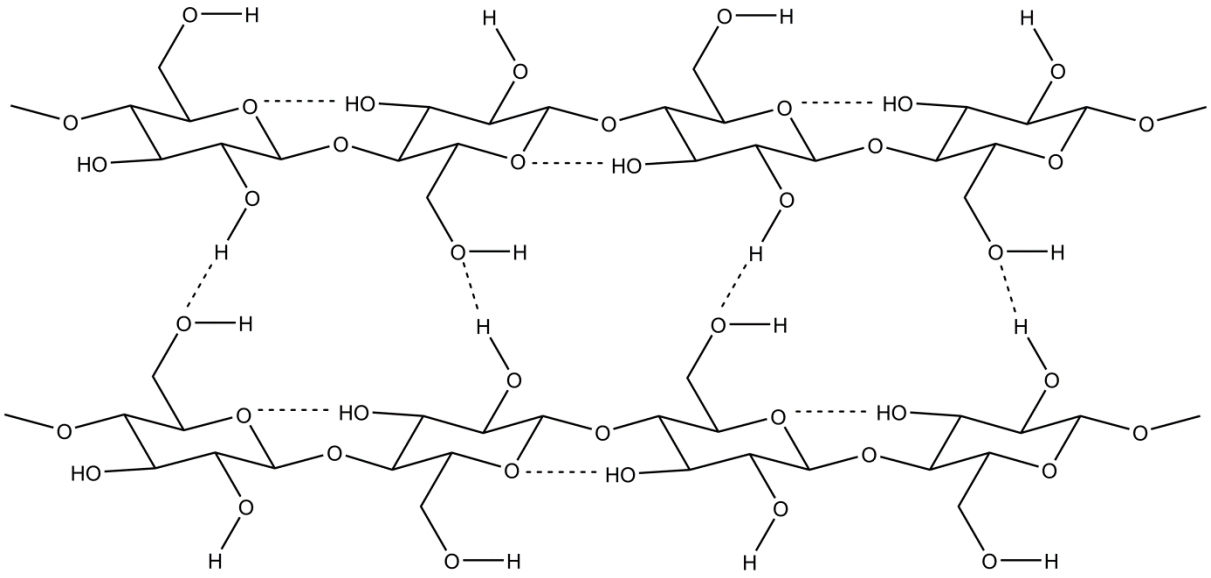

Figure 1-6 Structure of cellulose. Dashed lines indicate hydrogen bonding

The chemical structure of hemicellulose is less well-defined. It is a polysaccharide consisting of pentose and hexose sugars. Compared to cellulose, hemicellulose is amorphous and has a low degree of polymerization [22]. Xylan is often used to represent hemicellulose in hardwoods while glucomannan is used to represent hemicellulose in softwoods [23].

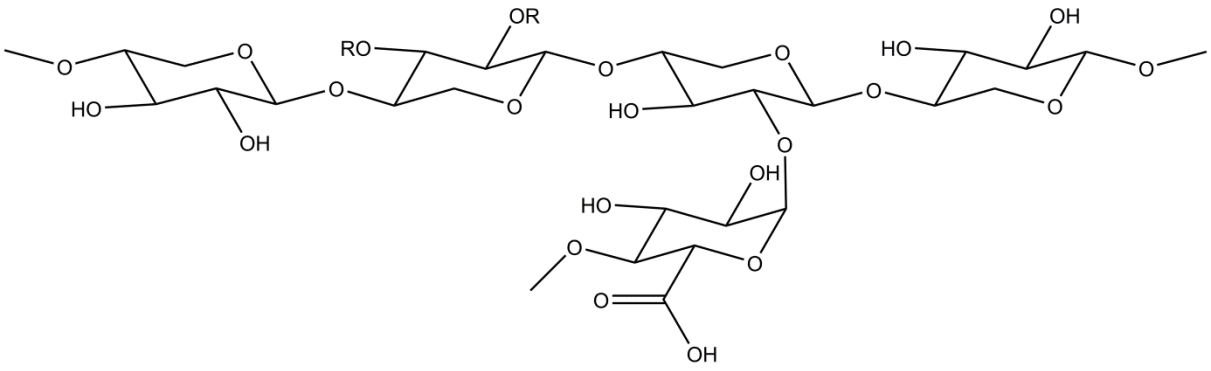

Figure 1-7 Structure of xylan, representative for hemicellulose in hardwoods

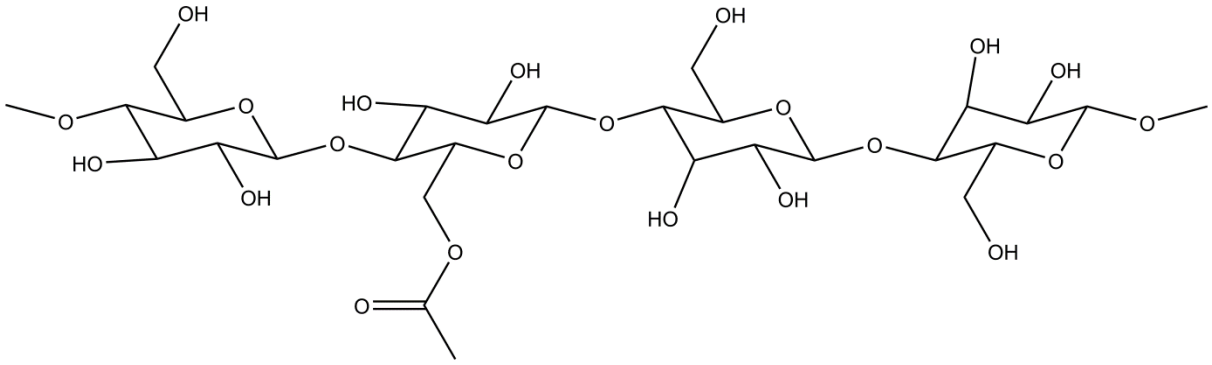

Figure 1-8 Structure of glucomannan, representative for hemicellulose in softwoods

Lignin is a three-dimensional cross-linked resin and can be considered to be built of p-coumaryl alcohol, coniferyl alcohol and sinapyl alcohol units, so-called lignin monomers, see Figure 1-9 [22, 24]. Softwoods are mostly composed of units of coniferyl alcohol, while hardwoods have higher amounts of sinapyl alcohol units [25]. Softwoods have a higher lignin content compared to hardwoods [25].

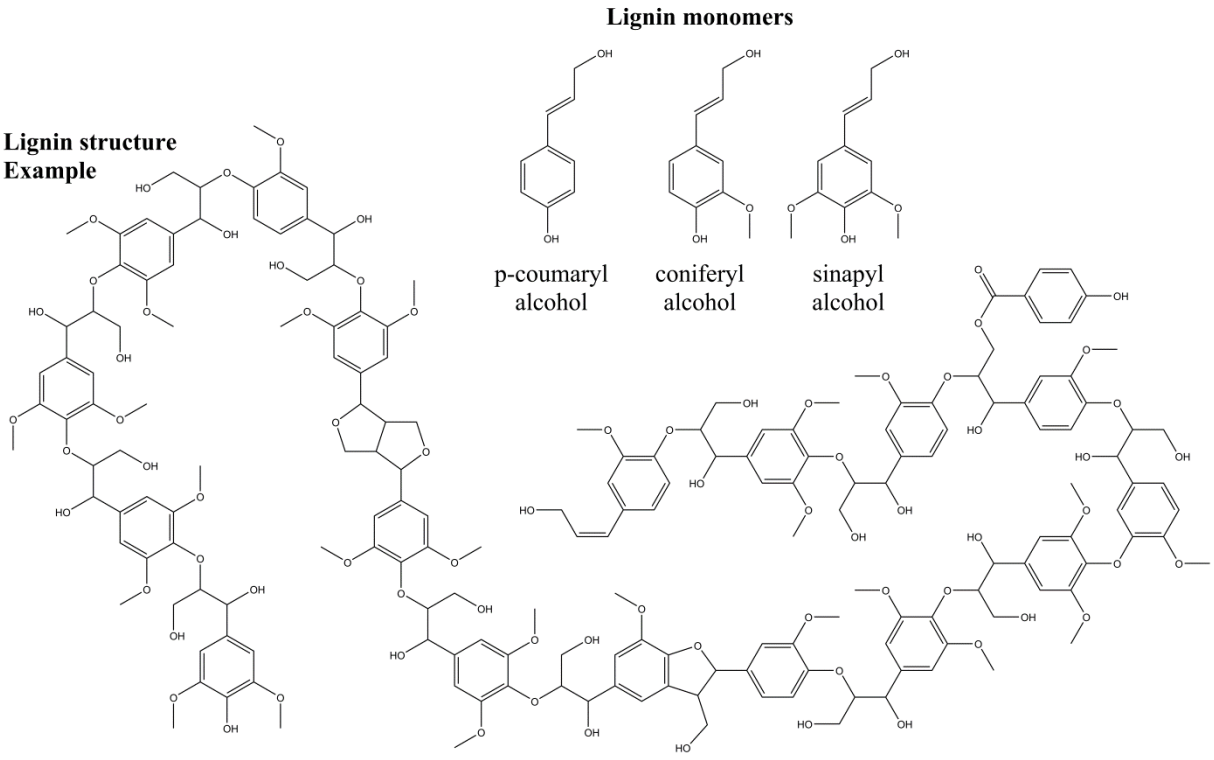

Figure 1-9 Structure of lignin and lignin monomers

Cellulose, hemicellulose and lignin usually account for more than 90% of the total biomass [26]. Extractives, the residual fraction in biomass, can be divided into two groups, i.e. hydrophilic and hydrophobic components [27]. Hydrophilic components include lignans and

sugars, while hydrophobic components include fatty acids, fatty alcohols, resin acids, sterols and terpenoids[27].

1.3.2 Conversion of lignocellulosic biomass to green chemicals

1.3.2.1 Biochemical processes

Biochemical processes often operate under relatively mild operating conditions and are selective towards specific products. Fermentation of sugars and starch to ethanol is a well-known example. The production of ethanol from lignocellulose requires separation of the major components of biomass, i.e. cellulose, hemicellulose and lignin. Subsequently, the carbohydrates can be hydrolyzed to sugars, catalyzed by acids or enzymes, and eventually fermented to ethanol [28, 29]. Recently, a wide variety of novel biochemical processes have been developed that enable production of other green chemicals and biofuels, such as bio-butanol [30].

1.3.2.2 Catalytic processes

Lignocellulose has a high degree of functionality. A wide variety of products can be formed following catalysis, e.g. hydrolysis, dehydration, (de-)hydrogenation, isomerization, aldol condensation [31]. Possible chemicals that are produced from cellulose include 5-hydroxymethyl-furfural [32, 33], lactic acid [34, 35] and levulinic acid [36]. Possible chemicals that are produced from hemicellulose include xylitol and furfural [37]. The aforementioned chemicals can be processed further into bio-fuels and/or platform molecules.

One such high-potential molecule is γ-valerolactone [38-40]. It can be produced from furfural, 5-hydroxymethyl-furfural, levulinic acid by relatively simple, high-selective catalytic processes [39], see Figure 1-10. γ-valerolactone has interesting fuel-properties [41], is an excellent green solvent [42] and can be used to produce other high-value fuels, such as 2-methyl-tetrahydrofuran and valeric esters, and chemicals, such as 1,4-pentandiol and α-methylene-γ-valerolactone, in a bio-refinery [39, 43, 44].

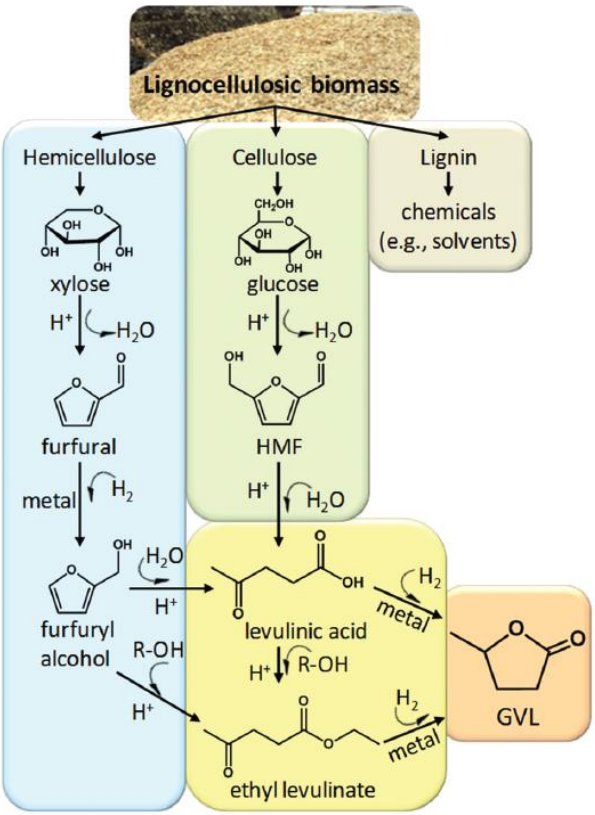

Figure 1-10 Production of γ-valerolactone from lignocellulose [39]

Several catalytic processes have been developed that enable the direct production of liquid hydrocarbons from lignocellulose by depolymerization and complete defunctionalization. Op de Beeck et al. presented a route for the direct catalytic conversion of cellulose to hexane, pentane and methyl-cyclopentane [45]. The reaction proceeds at elevated temperatures under hydrogen pressure in the presence of tungstosilicic acid, dissolved in the aqueous phase, and modified Ru/C, suspended in the organic phase. Liu et al. carried out a one-pot conversion of cellulose to hexane over a Ir-ReO_x/SiO_2 catalyst with H-ZSM-5 as co-catalyst in a biphasic reaction system under hydrogen pressure[46]. These conversion routes are still in their infancy but provide an interesting opportunity to obtain bio-derived naphtha from lignocellulose.

1.3.2.3 Thermochemical processes

Thermochemical conversion methods that have been considered include gasification, liquefaction and pyrolysis[28].

Gasification of biomass differs from the other thermochemical conversion methods given its high operating temperature, i.e. higher than 1000K [28, 47]. Minor amounts of air are added in order to partially oxidize the biomass. Excess air would result in complete combustion

which allows to obtain heat. Gasification has a high selectivity to gaseous products, e.g. CO, CO_2, H_2O, H_2 and CH_4 [28, 47]. Fischer-Tropsch synthesis allows to obtain long chain hydrocarbons from the formed CO and H_2.

Liquefaction of biomass is typically performed under relatively low temperature, i.e. 600K, high pressure, i.e. 10 MPa, and in the presence of a catalyst, for example sodium hydroxide [28, 48]. During liquefaction, biomass is decomposed into small reactive molecules which repolymerize to oily compounds, so-called bio-crudes. Bio-crudes have a higher H/C ratio and lower O/C ratio compared to the original biomass[48].

Pyrolysis is thermal degradation in the absence of an oxidizing agent. Biomass pyrolysis products are often classified into three categories, i.e. char, gases and liquids (at room temperature), so-called bio-oil [22, 49]. Produced gases include CO, CO_2, H_2, CH_4 and NH_3. Bio-oil is a complex mixture of acids, aldehydes, ketones, furans, phenols and sugars[50]. The yield of each product class depends on feedstock composition, heating rate, temperature and residence time. Two types of pyrolysis process can be distinguished. Slow pyrolysis maximizes char yield through slow heating rates, low end temperature and high residence times [51]. Fast pyrolysis maximizes bio-oil yield through high heating rates, moderate end temperature, i.e. 800K, and short vapor residence times, i.e. below 2s [52]. The effect of reaction temperature on product yields is displayed in Figure 1-11 [53]. At 773K, a maximum in organics, i.e. bio-oil yield, is observed. At higher temperatures the yield of gaseous products increases due to secondary reactions consuming the organics.

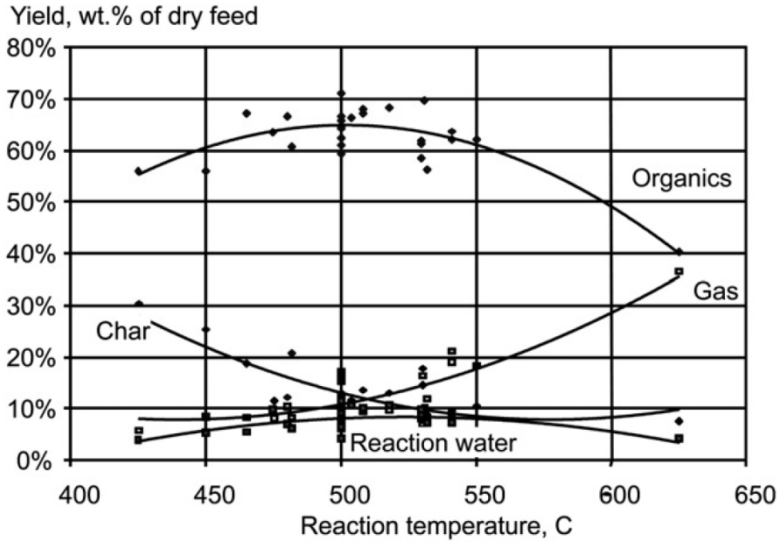

Figure 1-11 Product yields in the fast pyrolysis of Aspen Poplar as a function of reaction temperature. Figure adopted from [53]

Reactor technologies for fast pyrolysis should enable a very rapid heating of the biomass to an operating temperature around 800K and a rapid quenching of the produced vapors[54]. Proposed processes include fluidized beds, rotating cone pyrolysis and ablative pyrolysis [54, 55]. Commercialized and semi-commercialized processes include the "Rapid Thermal Processing" technology by Ensyn [56] and the "Empyro" project by BTG-BTL [57].

1.3.3 Unraveling fast pyrolysis chemistry by experiments and detailed kinetic modeling

It has been recognized that commercialization of the fast pyrolysis technology requires control of the bio-oil composition, and not solely maximization of the total bio-oil yield. Bio-oil composition depends on various process variables, such as feedstock composition, presence of inorganic salts, temperature… [49, 58]

Control of the bio-oil composition requires a thorough understanding of the underlying chemistry. Thermogravimetric analysis has been widely used to understand biomass pyrolysis but this only provides information regarding the global decomposition rate. Furthermore, the product spectrum following biomass pyrolysis is often reported as the overall yield of bio-oil, char and non-condensable gas. Kinetic models that attempt to reproduce such experiments (i) split up the biomass into its main macromolecular constituents, i.e. cellulose, hemicellulose and lignin, (ii) propose global decomposition reactions and (iii) assign reaction rate coefficients through regression with the available experimental data [22]. For example, the cellulose pyrolysis model by Shafizadeh and Bradbury proposed that cellulose first depolymerizes to so-called active cellulose which can decompose by a slow reaction to char and gas and by a fast reaction to bio-oil [59], see Figure 1-12.

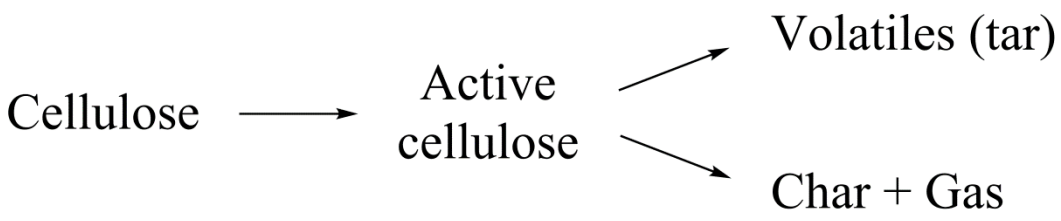

Figure 1-12 Shafizadeh scheme for cellulose pyrolysis

State-of-the-art experiments regarding biomass fast pyrolysis are performed using setups that allow analysis of the complex product spectrum. Brown, Shanks and coworkers conducted a series of fast pyrolysis experiments using a micro-pyrolyzer, for cellulose [60], hemicellulose

[61] and lignin [62]. The experimentally-obtained primary pyrolysis product distribution is listed in Table 1-1.

Table 1-1 Primary pyrolysis product distribution following cellulose[60], hemicellulose[61] and lignin[62] fast pyrolysis at 773K.

Cellulose		**Hemicellulose (extracted from switch gras)**		**Lignin (isolated from cornstover)**	
Fast pyrolysis product	wt%	Fast pyrolysis product	wt%	Fast pyrolysis product	wt%
Formic Acid	6.6	CO	2.8	CO	1.8
Furan/Acetone	0.7	CO2	18.8	CO2	15.2
Glycolaldehyde	6.7	Acetaldehyde	0.7	Acetaldehyde	0.9
Acetic acid	0.1	Formic Acid	11	Formic acid/Acetone	0.7
2-Methyl furan	0.4	2-methyl furan	1.5	2-methyl furan	0.1
Acetol	0.3	Acetic acid	1.1	Acetic acid	11.5
2-Furaldehyde	1.3	Acetol	3	2-furaldehyde	0.2
2-Furan methanol	0.5	2-furaldehyde	2.2	Phenol	1.9
3-Furan methanol	0.3	Dianhydroxyloses	9.2	2-methoxy phenol	0.9
5-Methyl furfural	0.2	Anhydro xylopyranose	3.4	2-methyl phenol	0.1
2-Hydroxy-3-methyl-cyclopenten-1-one	0.2	Xylose	4.9	4-methyl phenol	0.6
Levoglucosenone	0.4			2-methoxy-4-methyl phenol	0.7
5-Hydroxymethyl furfural	2.8			3,5-dimethyl phenol	0.1
Anhydro xylopyranose	3			3-ethyl phenol	0.6
Levoglucosan - pyranose	58.8			4-ethyl-2-methoxy phenol	0.4
Levoglucosan - furanose	4.1			4-vinyl phenol	3.5
Other Anhydro Sugars	1.4			2-methoxy-4-vinyl phenol	1.8
				2,6-dimethoxy phenol	1
				Euginol	0.2
				4-methyl-2,6-dimethoxyphenol	0.8
				3,5-dimethoxy-4-hydroxy benzaldehyde	0.4
				3,4-dimethoxy acetophenone	0.8
				4-allyl-2,6-dimethoxyphenol	0.2
				4-allyl-2,5-dimethoxyphenol	0.3
				3,5-dimethoxy-4-hydroxy acetophenone	0.3
				Sinapyl alcohol	0.7
Char	5.4	Char	10.7	Char	37
Total	93.2	Total	58.6	Total	82.7

Kinetic models have been developed that incorporate experimental speciation data while maintaining the original concept of global decomposition reactions. The most successful kinetic model has been developed by Ranzi and coworkers [26, 63, 64]. In this model, the original global decomposition reactions are retained but the lumped components such as “gas” and “volatiles” are replaced by the product spectrum obtained in the speciation experiments. For example, Ranzi and co-workers use a similar scheme for cellulose pyrolysis as Shafizadeh and Bradbury, see Figure 1-13[64]. However, the products are now identified as levoglucosan, acetic acid, glycolaldehyde etc. with stoichiometric coefficients and reaction rate coefficients that fit available experimental data. Note that the semi-detailed scheme by

Ranzi and coworkers describes the primary decomposition reactions of biomass. The scheme can be extended with detailed networks containing secondary reactions of primary products.

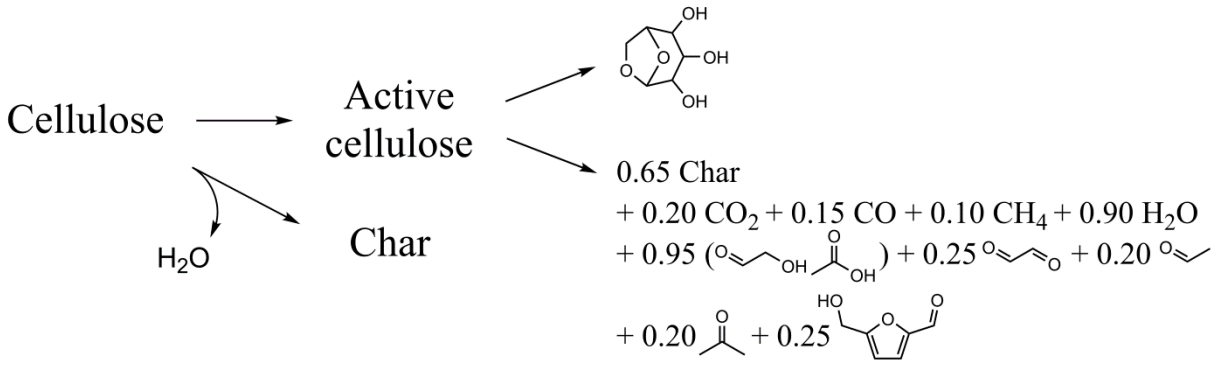

Figure 1-13 Ranzi scheme for cellulose pyrolysis

The success of these decomposition schemes lies in their simplicity. Unfortunately, the rate coefficients do not have any physical meaning. They are mostly fitted to experimental thermogravimetric weight loss profiles and are only valid for a narrow temperature range, narrow heating rate range and certain feedstock compositions. Furthermore, these schemes do not take into account the effect of inorganics on biomass pyrolysis which can drastically alter the product composition [58]. Finally, the molecular structure, and presence, of "active" biomass remains a topic of debate [65].

In order to encompass these issues, mechanistic models for biomass pyrolysis are being developed. Mechanistic models require a detailed characterization of the feedstock and identification of all possible reaction families. Broadbelt and coworkers have developed a first mechanistic model for the pyrolysis of cellulose [66-68]. Utilized reaction families include initiation, depropagation, dehydration, isomerization, decarbonylation, retro-Diels-Alder, retro-aldol, keto-enol tautomerization, ring-opening/closing and fragmentation. Associated reaction rate coefficients were taken from (i) experimental studies, (ii) quantum chemical calculations or (iii) fitted to the available experimental data. The pyrolysis of cellulose results in a wide range of intermediates, such a furans, unsaturated alcohols, cyclic ethers and lactones [66]. The model is in good agreement with the experimental data obtained using a micro-pyrolyzer [67]. Mechanistic models for the other biomass macromolecules are less well-established, partially due to their complex structure compared to cellulose. Klein, Virk and co-workers proposed a molecular-level model for lignin pyrolysis [69, 70]. First, the lignin molecular structure was presented using three possible lignin monomer alcohols, i.e. coniferyl, coumaryl and sinapyl, and eight possible linkages. The probability for each type of

lignin monomer and each type of linkage was taken from the lignin model proposed by Freudenberg [71]. Subsequently, reaction paths are generated that consume the linkages and side chains while leaving the aromatic cores intact. Lignin pyrolysis products include CH_4, CO, CO_2, H_2, H_2O, CH_3OH and phenolics. Finally, reaction rate coefficients are assigned using linear free-energy relationships [69].

It is noteworthy that despite the efforts in mechanistic modeling of biomass pyrolysis, the pyrolysis of small oxygenated molecules that are part of the biomass molecular structure is still not fully understood. An improved understanding regarding the thermal decomposition of such species, also known as model components, aids in understanding the thermal decomposition of biomass.

1.4 Outline

Green chemicals can be produced by using bio-derived feedstocks in thermochemical processes. Such processes compete with existing well-established technologies that use fossil feedstocks. Therefore, every novel process has to be optimized in order to be economically and environmentally viable. This can only be accomplished by understanding the underlying chemistry. The combination of a detailed kinetic model with a reactor model allows to predict yields and selecitivities of products as a function of feedstock composition and operating conditions.

In **Chapter 2**, a network generation tool called PRIM-O is presented that facilitates the development of kinetic models. PRIM-O automatically generates thermal decomposition schemes for hydrocarbons and oxygenates and applies the pseudo steady state approximation to radicals that only undergo monomolecular reactions. The procedure in PRIM-O allows to drastically reduce the number of species in the final kinetic model which is particularly useful for high molecular weight feedstocks, such as biomass.

Chapter 3 contains three papers that discuss the use of bio-derived feedstocks in steam crackers, i.e. the conventional pyrolysis process. The first paper investigates the steam cracking of linear and branched alkanes, produced by hydrodeogyenation and isomerization of vegetable oils and waste fats. The second paper assesses the potential of hydrodeoxygenated crude tall oil for the production of green chemicals. The composition of the hydrocarbon mixtures are affected by the operating conditions of the catalytic upgrading step. Hence, the kinetic models for pyrolysis in these papers allow (i) selection of operating conditions of steam crackers for maximization of alkene yield and (ii) steering of the catalytic

deoxygenation process to the most optimal hydrocarbon feedstock composition. The final paper discusses the pyrolysis of rapeseed methyl esters. A kinetic model was developed using PRIM-O. The presence of an ester functionality unavoidably results in the formation of oxygenated species, such as formaldehyde. The use of non-deoxygenated bio-derived feedstocks in steam crackers should therefore be avoided.

Chapter 4 contains four papers that discuss the pyrolysis of three cyclic oxygenated species, i.e. 2-methyl-tetrahydrofuran, tetrahydropyran and γ-valerolactone. Understanding their decomposition chemistry helps understand lignocellulose fast pyrolysis as they are integral parts of the bio-polymer molecular structure. Furthermore, they are considered to be next-generation biofuels, produced from cellulose by biochemical and catalytic processes. For 2-methyl-tetrahydrofuran, both pyrolysis and combustion chemistry has been investigated by experiments and detailed kinetic modeling. The pyrolysis of γ-valerolactone highlighted the importance of a unimolecular ring opening reaction. A similar reaction was identified in the pyrolysis of 2-methyl-tetrahydrofuran. The proposed kinetic models are building blocks for detailed mechanistic biomass fast pyrolysis models.

Steam cracking and biomass fast pyrolysis results in a wide range of intermediates that can be formed. A thorough understanding of reaction paths consuming these species is important for accurate prediction of the reaction effluent composition. In **Chapter 5**, the reactivity of 1,5-hexadiene and two unsaturated alcohols is investigated. In the pyrolysis of both hydrocarbons and oxygenated species, recombination of allyl radicals, forming 1,5-hexadiene, followed by hydrogen abstraction, intramolecular radical addition and dehydrogenation has been highlighted as an important benzene formation pathway. Unsaturated alcohols are formed by thermal decomposition of long chain alcohols and dehydration of cellulose. The presence of both a C=C double bond and a hydroxyl group has a big impact on their reactivity. Both the oxidation and pyrolysis of the aforementioned intermediates has been investigated which allows for validation of the developed kinetic models over a wide range of conditions and can aid in the mechanistic understanding of biomass pyrolysis and gasification.

Finally, in **Chapter 6**, the general conclusions and an outlook for future research are presented.

1.5 References

[1] H. Zimmermann, R. Walzl, Ethylene, in Ullmann's Encyclopedia of Industrial Chemistry, John Wiley & Sons, Inc.: New York, 2009.
[2] CAPP 2015 CAPP Crude Oil Forecast, Markets & Transportation. http://www.capp.ca/publications-and-statistics/publications/264673 (09/03/2016),
[3] H. Cai, A. R. Brandt, S. Yeh, J. G. Englander, J. Han, A. Elgowainy, M. Q. Wang, Well-to-Wheels Greenhouse Gas Emissions of Canadian Oil Sands Products: Implications for U.S. Petroleum Fuels, Environmental Science & Technology 49 (2015) 8219-8227
[4] International Energy Agency, World Energy Outlook (2015)
[5] P. Eisele, R. Killpack, Propene, in Ullmann's Encyclopedia of Industrial Chemistry, John Wiley & Sons, Inc.: New York, 2005.
[6] M. Dente, G. Bozzano, T. Faravelli, A. Marongiu, S. Pierucci, E. Ranzi, Kinetic Modelling of Pyrolysis Processes in Gas and Condensed Phase, Adv. Chem. Eng. 32 (2007) 51-166
[7] K. M. Van Geem, G. B. Marin, N. Hedebouin, J. Grootjans, Energy efficiency of the cold train of an ethylene cracker, Oil Gas-European Magazine 34 (2008) 95-99
[8] T. Ren, M. Patel, K. Blok, Olefins from conventional and heavy feedstocks: Energy use in steam cracking and alternative processes, Energy 31 (2006) 425-451
[9] Marcellus Shale Coalition, Natural Gas Production in the Marcellus and Utica Shales (2012)
[10] pwc, Shale gas. Reshaping the US chemicals industry (2012)
[11] F. Tan, S. L. Peng, Exxon starts world's 1st crude-cracking petrochemical unit, Reuters (2014)
[12] S. P. Pyl, K. M. Van Geem, P. Puimège, M. K. Sabbe, M.-F. Reyniers, G. B. Marin, A comprehensive study of methyl decanoate pyrolysis, Energy 43 (2012) 146-160
[13] J. A. Reid, G. Nowowiejski, Overview of Oxygenates in Olefin Units in Relation to Corrosion, Fouling, Product Specifications, and Safety, Ethylene Producers Conference, New Orleans, USA (2003)
[14] R. Patt, O. Kordsachia, R. Süttinger, Y. Ohtani, J. F. Hoesch, P. Ehrler, R. Eichinger, H. Holik, U. Hamm, M. E. Rohmann, P. Mummenhoff, E. Petermann, R. F. Miller, D. Frank, R. Wilken, H. L. Baumgarten, G.-H. Rentrop, Paper and Pulp, in Ullmann's Encyclopedia of Industrial Chemistry, Wiley-VCH Verlag GmbH & Co. KGaA: 2000.
[15] R. W. Gosselink, S. A. W. Hollak, S.-W. Chang, J. van Haveren, K. P. de Jong, J. H. Bitter, D. S. van Es, Reaction Pathways for the Deoxygenation of Vegetable Oils and Related Model Compounds, ChemSusChem 6 (2013) 1576-1594
[16] T. Dijkmans, S. P. Pyl, M.-F. Reyniers, R. Abhari, K. M. Van Geem, G. B. Marin, Production of bio-ethene and propene: alternatives for bulk chemicals and polymers, Green Chem. 15 (2013) 3064-3076
[17] S. P. Pyl, C. M. Schietekat, M.-F. Reyniers, R. Abhari, G. B. Marin, K. M. Van Geem, Biomass to olefins: Cracking of renewable naphtha, Chem. Eng. J. 176-177 (2011) 178-187
[18] Axens, Axens' technologies, products and services (2015)
[19] H. R. Ghatak, Biorefineries from the perspective of sustainability: Feedstocks, products, and processes, Renew. Sust. Energ. Rev. 15 (2011) 4042-4052
[20] R. H. Venderbosch BTG Bio-liquids Refinery. https://www.btg-btl.com/en/applications/biochemicals
[21] D. Klemm, B. Heublein, H.-P. Fink, A. Bohn, Cellulose: Fascinating Biopolymer and Sustainable Raw Material, Angew. Chem. Int. Ed. 44 (2005) 3358-3393
[22] A. Anca-Couce, Reaction mechanisms and multi-scale modelling of lignocellulosic biomass pyrolysis, Prog. Energy Combust. Sci. 53 (2016) 41-79
[23] F. Shafizadeh, Introduction to pyrolysis of biomass, J. Anal. Appl. Pyrolysis 3 (1982) 283-305
[24] D. Mohan, C. U. Pittman, P. H. Steele, Pyrolysis of wood/biomass for bio-oil: A critical review, Energ. Fuel. 20 (2006) 848-889
[25] J. L. McCarthy, A. Islam, Lignin Chemistry, Technology, and Utilization: A Brief History, in Lignin: Historical, Biological, and Materials Perspectives, American Chemical Society: 1999; Vol. 742, pp 2-99.
[26] P. E. A. Debiagi, C. Pecchi, G. Gentile, A. Frassoldati, A. Cuoci, T. Faravelli, E. Ranzi, Extractives Extend the Applicability of Multistep Kinetic Scheme of Biomass Pyrolysis, Energ. Fuel. 29 (2015) 6544-6555
[27] A. Oasmaa, E. Kuoppala, S. Gust, Y. Solantausta, Fast pyrolysis of forestry residue. 1. Effect of extractives on phase separation of pyrolysis liquids, Energ. Fuel. 17 (2003) 1-12
[28] M. Fatih Demirbas, Biorefineries for biofuel upgrading: A critical review, Applied Energy 86, Supplement 1 (2009) S151-S161
[29] V. Menon, M. Rao, Trends in bioconversion of lignocellulose: Biofuels, platform chemicals & biorefinery concept, Prog. Energy Combust. Sci. 38 (2012) 522-550
[30] M. Kumar, K. Gayen, Developments in biobutanol production: New insights, Applied Energy 88 (2011) 1999-2012

[31] J. N. Chheda, G. W. Huber, J. A. Dumesic, Liquid-Phase Catalytic Processing of Biomass-Derived Oxygenated Hydrocarbons to Fuels and Chemicals, Angew. Chem. Int. Ed. 46 (2007) 7164-7183
[32] T. Wang, M. W. Nolte, B. H. Shanks, Catalytic dehydration of C6 carbohydrates for the production of hydroxymethylfurfural (HMF) as a versatile platform chemical, Green Chem. 16 (2014) 548-572
[33] J.-P. Lange, E. van der Heide, J. van Buijtenen, R. Price, Furfural—A Promising Platform for Lignocellulosic Biofuels, ChemSusChem 5 (2012) 150-166
[34] M. Dusselier, P. Van Wouwe, A. Dewaele, E. Makshina, B. F. Sels, Lactic acid as a platform chemical in the biobased economy: the role of chemocatalysis, Energ. Environ. Sci. 6 (2013) 1415-1442
[35] E. de Jong, A. Higson, P. Walsh, M. Wellisch, Product developments in the bio-based chemicals arena, Biofuels, Bioproducts and Biorefining 6 (2012) 606-624
[36] R. Weingarten, W. C. Conner, G. W. Huber, Production of levulinic acid from cellulose by hydrothermal decomposition combined with aqueous phase dehydration with a solid acid catalyst, Energ. Environ. Sci. 5 (2012) 7559-7574
[37] J. J. Bozell, G. R. Petersen, Technology development for the production of biobased products from biorefinery carbohydrates-the US Department of Energy's "Top 10" revisited, Green Chem. 12 (2010) 539-554
[38] X. Tang, X. Zeng, Z. Li, L. Hu, Y. Sun, S. Liu, T. Lei, L. Lin, Production of γ-valerolactone from lignocellulosic biomass for sustainable fuels and chemicals supply, Renew. Sust. Energ. Rev. 40 (2014) 608-620
[39] D. M. Alonso, S. G. Wettstein, J. A. Dumesic, Gamma-valerolactone, a sustainable platform molecule derived from lignocellulosic biomass, Green Chem. 15 (2013) 584-595
[40] I. T. Horvath, H. Mehdi, V. Fabos, L. Boda, L. T. Mika, γ-Valerolactone - a sustainable liquid for energy and carbon-based chemicals, Green Chem. 10 (2008) 238-242
[41] Á. Bereczky, K. Lukács, M. Farkas, S. Dóbé, Effect of γ-Valerolactone Blending on Engine Performance, Combustion Characteristics and Exhaust Emissions in a Diesel Engine, Natural Resources 5 (2014) 177-179
[42] G. Strappaveccia, E. Ismalaj, C. Petrucci, D. Lanari, A. Marrocchi, M. Drees, A. Facchetti, L. Vaccaro, A biomass-derived safe medium to replace toxic dipolar solvents and access cleaner Heck coupling reactions, Green Chem. 17 (2015) 365-372
[43] J. Q. Bond, D. M. Alonso, D. Wang, R. M. West, J. A. Dumesic, Integrated Catalytic Conversion of γ-Valerolactone to Liquid Alkenes for Transportation Fuels, Science 327 (2010) 1110-1114
[44] J. Q. Bond, D. Martin Alonso, R. M. West, J. A. Dumesic, γ-Valerolactone Ring-Opening and Decarboxylation over SiO2/Al2O3 in the Presence of Water, Langmuir 26 (2010) 16291-16298
[45] B. Op de Beeck, M. Dusselier, J. Geboers, J. Holsbeek, E. Morre, S. Oswald, L. Giebeler, B. F. Sels, Direct catalytic conversion of cellulose to liquid straight-chain alkanes, Energ. Environ. Sci. 8 (2015) 230-240
[46] S. Liu, M. Tamura, Y. Nakagawa, K. Tomishige, One-Pot Conversion of Cellulose into n-Hexane over the Ir-ReOx/SiO2 Catalyst Combined with HZSM-5, ACS Sustainable Chemistry & Engineering 2 (2014) 1819-1827
[47] M. Balat, E. Kirtay, H. Balat, Main routes for the thermo-conversion of biomass into fuels and chemicals. Part 2: Gasification systems, Energy Convers. Manage. 50 (2009) 3158-3168
[48] M. Balat, Mechanisms of Thermochemical Biomass Conversion Processes. Part 3: Reactions of Liquefaction, Energy Sources, Part A: Recovery, Utilization, and Environmental Effects 30 (2008) 649-659
[49] C. Di Blasi, Modeling chemical and physical processes of wood and biomass pyrolysis, Prog. Energy Combust. Sci. 34 (2008) 47-90
[50] M. R. Djokic, T. Dijkmans, G. Yildiz, W. Prins, K. M. Van Geem, Quantitative analysis of crude and stabilized bio-oils by comprehensive two-dimensional gas-chromatography, J. Chromatogr. A 1257 (2012) 131-140
[51] M. J. Antal, M. Grønli, The Art, Science, and Technology of Charcoal Production, Ind. Eng. Chem. Res. 42 (2003) 1619-1640
[52] A. V. Bridgwater, Renewable fuels and chemicals by thermal processing of biomass, Chem. Eng. J. 91 (2003) 87-102
[53] A. V. Bridgwater, Review of fast pyrolysis of biomass and product upgrading, Biomass Bioenerg. 38 (2012) 68-94
[54] R. H. Venderbosch, W. Prins, Fast pyrolysis technology development, Biofuels Bioproducts & Biorefining-Biofpr 4 (2010) 178-208
[55] A. V. Bridgwater, Upgrading biomass fast pyrolysis liquids, Environmental Progress & Sustainable Energy 31 (2012) 261-268
[56] Ensyn http://www.ensyn.com/
[57] BTG-BTL https://www.btg-btl.com/en/company/projects/empyro
[58] P. R. Patwardhan, J. A. Satrio, R. C. Brown, B. H. Shanks, Influence of inorganic salts on the primary pyrolysis products of cellulose, Bioresour. Technol. 101 (2010) 4646-4655

[59] F. Shafizadeh, A. G. W. Bradbury, Thermal degradation of cellulose in air and nitrogen at low temperatures, J. Appl. Polym. Sci. 23 (1979) 1431-1442
[60] P. R. Patwardhan, J. A. Satrio, R. C. Brown, B. H. Shanks, Product distribution from fast pyrolysis of glucose-based carbohydrates, J. Anal. Appl. Pyrolysis 86 (2009) 323-330
[61] P. R. Patwardhan, R. C. Brown, B. H. Shanks, Product Distribution from the Fast Pyrolysis of Hemicellulose, ChemSusChem 4 (2011) 636-643
[62] P. R. Patwardhan, R. C. Brown, B. H. Shanks, Understanding the Fast Pyrolysis of Lignin, ChemSusChem 4 (2011) 1629-1636
[63] M. Calonaci, R. Grana, E. Barker Hemings, G. Bozzano, M. Dente, E. Ranzi, Comprehensive Kinetic Modeling Study of Bio-oil Formation from Fast Pyrolysis of Biomass, Energ. Fuel. 24 (2010) 5727–5734
[64] E. Ranzi, A. Cuoci, T. Faravelli, A. Frassoldati, G. Migliavacca, S. Pierucci, S. Sommariva, Chemical Kinetics of Biomass Pyrolysis, Energ. Fuel. 22 (2008) 4292-4300
[65] V. Agarwal, P. J. Dauenhauer, G. W. Huber, S. M. Auerbach, Ab Initio Dynamics of Cellulose Pyrolysis: Nascent Decomposition Pathways at 327 and 600 °C, J. Am. Chem. Soc. 134 (2012) 14958-14972
[66] X. Zhou, M. W. Nolte, H. B. Mayes, B. H. Shanks, L. J. Broadbelt, Experimental and Mechanistic Modeling of Fast Pyrolysis of Neat Glucose-Based Carbohydrates. 1. Experiments and Development of a Detailed Mechanistic Model, Ind. Eng. Chem. Res. 53 (2014) 13274-13289
[67] X. Zhou, M. W. Nolte, B. H. Shanks, L. J. Broadbelt, Experimental and Mechanistic Modeling of Fast Pyrolysis of Neat Glucose-Based Carbohydrates. 2. Validation and Evaluation of the Mechanistic Model, Ind. Eng. Chem. Res. 53 (2014) 13290-13301
[68] R. Vinu, L. J. Broadbelt, A mechanistic model of fast pyrolysis of glucose-based carbohydrates to predict bio-oil composition, Energ. Environ. Sci. 5 (2012) 9808-9826
[69] Z. Hou, C. A. Bennett, M. T. Klein, P. S. Virk, Approaches and Software Tools for Modeling Lignin Pyrolysis, Energ. Fuel. 24 (2010) 58-67
[70] M. T. Klein, P. S. Virk, Modeling of lignin thermolysis, Energ. Fuel. 22 (2008) 2175-2182
[71] K. Freudenberg, A. C. Neish, Constitution and Biosynthesis of Lignin, Springer-Verlag, New York, 1968

Chapter 2

PRIM-O: Primary decomposition schemes for hydrocarbons and oxygenates

2.1 Abstract

Kinetic models for pyrolysis and combustion are developed with increasing detail and complexity. Especially for high molecular weight feedstocks such as crude oil and biomass-related molecules, reactor simulations can become computationally expensive. This issue can be addressed using the network generation tool "PRIM-O". Its general features are discussed in this chapter. PRIM-O requires the user to provide reactants and a reaction family for which rate coefficients and the product spectrum have to be generated. The algorithm starts by executing the reaction family. Radicals for which bimolecular reactions can be neglected, i.e. μ-radicals, are identified and decomposition reactions, e.g. β-scission, are generated. Reaction rate coefficients of each elementary step are estimated using a comprehensive kinetic library, mainly through group-additivity methods. The pseudo-steady-state approximation is applied to μ-radicals which allows to generate a so-called one-step equivalent reaction. The μ-radicals are no longer present in the equivalent reaction. Instead, they are replaced by their products following decomposition. This algorithm, coupled with in situ lumping of primary molecular products and a posteriori lumping of the feedstock, allows to significantly reduce the number of species compared to conventional kinetic models while retaining a high level of accuracy.

Keywords: PRIM-O, network generation, μ-hypothesis, pseudo-steady-state approximation, lumping

2.2 Introduction

The chemistry involved in the pyrolysis of hydrocarbons has been investigated for decades. The pioneering work of Rice and co-workers in the 1930's established the importance of free radicals[1, 2]. Since then, the understanding of the associated chemistry has continuously increased. Now, industrial pyrolysis reactors are operated using tools that are able to predict product yields as a function of feedstock composition and operating conditions[3-5].

State-of-the-art kinetic models for pyrolysis and combustion are developed manually, which requires a thorough understanding of the chemistry by the scientist, or automatically, which necessitates a code that is able to provide reliable estimates for thermodynamic and kinetic parameters, or a combination of both[6]. Lu and Law showed that the number of reactions increases linearly with the number of species in the kinetic model, which, in turn, increases exponentially with the number of heavy, i.e. non-hydrogen, atoms in the reactant[7], see Figure 2-1. Most kinetic models, especially those describing species with a large number of heavy atoms, are impractical for large scale computations, e.g. reactive computational fluid dynamics[7, 8]. Moreover, 1D-reactor simulations are insufficiently fast for the optimal operation of pyrolysis reactors.

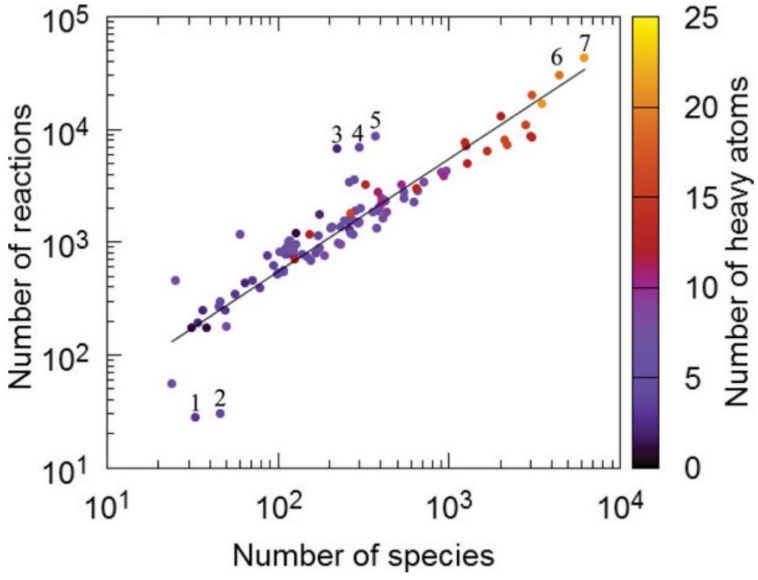

Figure 2-1 Number of reactions as a function of species for gas phase kinetic models of pyrolysis, oxidation and combustion processes. The secondary axis is the number of heavy (non-hydrogen) atoms in the reactant molecule. Outliers: (1) – dimethyl ether combustion [9], (2) – 1,3-butadiene combustion [10], (3) – ethene/methane combustion [11], (4) – propanol combustion [12], (5) – iso-butanol combustion and pyrolysis [13], (6) – methyl palmitate combustion [14], (7) – methyl stearate combustion [14]. Figure adopted from De Vijver et al. [6]

Kinetic models can be reduced by incorporating the chemical knowledge regarding reactivity of free radicals in the models themselves and in engineering tools in general. Two

characteristics of free radicals will be highlighted in this section. The first, widely applied, characteristic is the pseudo-steady-state approximation for radicals, which is the mathematical expression that the time rate of change of the concentration is equal to zero. The second characteristic is the μ-hypothesis, which states that bimolecular reactions for certain radicals can be neglected. These approximations can be used during development of a kinetic model or as post-treatment.

Both characteristics are often used in manually-developed kinetic models, without being explicitly mentioned. These assumptions are applied to a selected, and often non-systematic, number of radicals. For example, in the propene oxidation model by Burke et al.[15], frequently applied as base mechanism in this thesis, hydrogen abstraction from but-3-en-2-one is written as a one-step reaction to vinyl plus ketene without explicitly taking into account the but-3-en-2-one-1-yl intermediate, see Figure 2-2. Thus, Burke et al. assumed that but-3-en-2-one-1-yl solely reacts by the unimolecular C-C β-scission reaction and applied the pseudo-steady-state approximation.

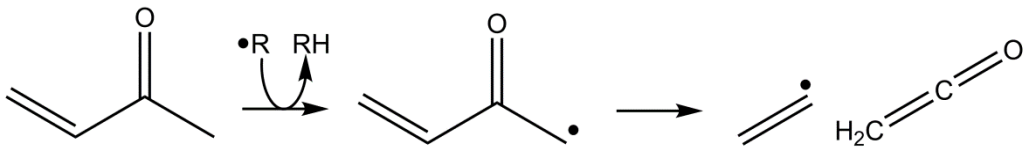

Figure 2-2 Hydrogen abstraction from but-3-en-2-one and subsequent C-C β-scission

Several automatic network generation tools have been developed that systematically take into account the pseudo-steady-state approximation and the μ-hypothesis for radicals. EXGAS[16] only considers hydrogen abstraction, a bimolecular reaction, by small and relatively stable radicals that cannot easily decompose by C-C and C-O β-scission, such as formyl, hydroxyl-methyl, methoxy, ethyl, iso-propyl and tert-butyl. Furthermore, radicals formed by consumption of primary products are not explicitly considered in EXGAS. Instead, only the major species formed following decomposition are retained. For example, in unsaturated methyl esters, primary products in the pyrolysis and oxidation of saturated methyl esters, hydrogen can be abstracted from the allylic carbon atom. The resulting resonantly stabilized radical is not present in the kinetic model as it has been replaced by 1,3-butadiene plus an ester radical [17], the products following C-C β-scission, see Figure 2-3. These assumptions allow to significantly reduce the kinetic model with a minimal loss in accuracy.

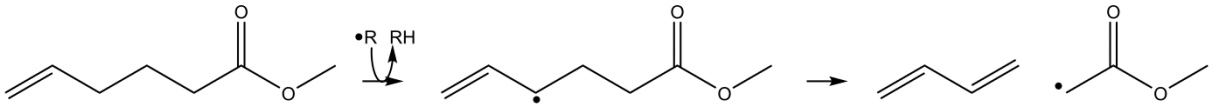

Figure 2-3 Hydrogen abstraction from methyl hex-5-enoate and subsequent C-C β-scission

MAMA[18, 19], a network generation tool developed by Dente, Ranzi and co-workers, applies the pseudo-steady-state approximation to all radicals for which the μ-hypothesis is valid, also known as μ-radicals, when generating the thermal decomposition paths of molecules. The mass balance for each μ-radical j is of the form:

$$C_j \sum_{i \in I_j} k_{j,i}^{isom} + C_j \sum_{i \in D_j} k_{j,i}^{decomp} = \sum_{i \in I_j} C_i \, k_{i,j}^{isom} + \sum_{i \in D_j} C_i \, k_{i,j}^{decomp} + P_{j,0} \qquad (1)$$

In equation (1), C_j is the concentration of component j, I_j is the set of isomerization reactions that involve component j, D_j is the set of decomposition reactions that involve component j, $k_{j,i}^{isom}$ is the reaction rate coefficient for isomerization of component j to component i, $k_{j,i}^{decomp}$ is the reaction rate coefficient for decomposition of component j forming component i and $P_{j,0}$ is the production of component j by reaction of the feed molecule. The left-hand side of equation (1) equals the consumption of radical j while the right-hand side equals the production of component j. The set of algebraic equations is linear with respect to radical concentrations – as only mono-molecular reactions are considered for μ-radicals. MAMA evaluates the reaction rate coefficients at a certain temperature, solves the linear system and uses the solution to obtain the distribution of end-products.

PRIM[20, 21], a network generation tool developed at the Laboratory for Chemical Technology, shows similarities with the MAMA program. The main difference is that the temperature dependence of the product distribution is retained in the output. PRIM has originally been developed for the pyrolysis of hydrocarbons. The interest regarding the use of bio-derived feedstocks in conventional steam crackers and the fast pyrolysis of lignocellulosic biomass has motivated the extension of PRIM to PRIM-O, which is able to generate decomposition schemes for oxygenated molecules. The general features of PRIM-O are discussed in this chapter. The pyrolysis of methyl esters is presented as case-study in section 3.3 of this thesis.

2.3 PRIM-O overview

PRIM-O requires the user to provide a kinetic library, which consists of a list of reaction families and parameters to calculate associated reaction rate coefficients, reactants and the desired reaction family for which a decomposition scheme has to be generated. This is the subject of section 2.4.

The network generation algorithm starts by constructing connectivity matrices for the reactants. Atoms that are part of an aromatic ring, that are part of a double bond and that are oxygen atoms are tracked by separate vectors. Subsequently, PRIM-O executes the desired reaction family by changing the connectivity matrix and vectors by means of matrix operations. PRIM-O identifies μ-radicals and generates all possible isomerization and decomposition reactions, again using matrix operations. Each elementary reaction is assigned a rate coefficient. The network generation stops when decomposition paths have been generated for all μ-radicals. PRIM-O applies the pseudo-steady-state approximation to μ-radicals, solves the set of linear algebraic equations and uses the solution to obtain formation rates of end-products and end-radicals. This is the subject of section 2.5.

PRIM-O writes out a list of so-called "relative pseudo rate coefficients", which can be used to calculate reaction rates when performing reactor simulations. The complete decomposition scheme can be written as a one-step equivalent reaction. Thermodynamic data of reactants and product species are estimated using external programs, such as Genesys's ThermoGenerator and RMG's ThemoDataEstimator. This is the subject of section 2.6.

2.4 Input

2.4.1 Kinetic library

A set of reaction families is defined in PRIM-O. This set can be divided in three groups: (i) reaction families that consume stable species and produce μ-radicals, (ii) reaction families that consume μ-radicals, (iii) reaction families that consume stable species and produce non-radical products. The defined reaction families are listed in Table 2-1.

Table 2-1 Reaction families in PRIM-O

Reaction family	Reaction template	Methodology	Ref.
Formation of µ-radicals			
Bond scission			
C-C	C_1-C_2 → •C_1 + •C_2	Rate rules	[22]
C-H	C_1-H → •C_1 + •H	Rate rules	[22]
C-O	C_1-OX → •C_1 + •OX	Rate rules	[17]
Intermolecular hydrogen abstraction			
by •C	C_1-H + •C_2 → •C_1 + C_2-H	Group additivity	[23, 24]
by •H	C_1-H + •H → •C_1 + H_2	Group additivity	[25]
by •O	C_1-H + •OX → •C_1 + H-OX	Group additivity	[26]
Intermolecular radical addition			
by •C	C_1=C_2 + •C_3 → •C_1-C_2-C_3	Group additivity	[27]
by •H	C_1=C_2 + •H → •C_1-C_2-H	Group additivity	[28]
by •O	C_1=C_2 + •OX → •C_1-C_2-OX	Rate rules	[29]
Ipso-addition by h atoms			
alkyl-aromatics	Aro-C_1 + •H → Aro-H + •C_1	Rate rules	[30]
naphtheno-aromatics	Naphteno-aromatic + •H → Aro-C_1-C_2-C_3-C_4•	Rate rules	[30]
Decomposition of µ-radicals			
β-scission			
•C-C-C	•C_1-C_2-C_3 → C_1=C_2 + •C_3	Group additivity	[27]
•C-C-H	•C_1-C_2-H → C_1=C_2 + •H	Group additivity	[28]
•C-O-C	•C_1-O-C_2 → C_1=O + •C_2	Rate rules[b]	a
•O-C-C	•O-C_1-C_2 → C_1=O + •C_2	Rate rules[c]	a
•C-C-O	•C_1-C_2-OX → C_1=C_2 + •OX	Rate rules[d]	a
•C-O-H	•C_1-O-H → C_1=O + •H	Rate rules[e]	a
•O-C-H	•O-C_1-H → C_1=O + •H	Rate rules[f]	a
α-scission			
•C(=O)-C	•C(=O)-C_1 → CO + • C_1	Rate rules[g]	a
Intramolecular hydrogen abstr.	•C_1-(C)n-C_2-H → H-C_1-$(C)_n$-C_2•	Rate rules	[31, 32]
Intramolecular radical addition			
endo	•C_1-$(C)_n$-C_2=C_3→ cy(C_1-$(C)_n$-C_2•-C_3)	Rate rules	[31]
exo	•C_1-$(C)_n$-C_2=C_3→ cy(C_1-$(C)_n$-C_2)-C_3•	Rate rules	[31]
Unimolecular decomposition reactions forming stable species			
Retro-ene	C_1=C_2-C_3-C_4-C_5→ C_1-C_2=C_3 + C_4=C_5	Rate rules	[33]
Retro Diels-Alder	cy(C_1=C_2-C_3-C_4-C_5-C_6) → C_6=C_1-C_2=C_3 + C_4=C_5	Rate rules	[34]

a CBS-QB3 calculated value using methodology described in 4.2 (unpublished)
b analogy with •CH_2-O-CH_3 → CH_2=O + •CH_3
c analogy with •O-CH_2-CH_3 → CH_2=O + •CH_3
d analogy with •CH_2-CH_2-OH → CH_2=CH_2 + •OH
e analogy with CH_3-•CH- OH → CH_3-CHO + •H
f analogy with CH_3-CH_2-O• → CH_3-CHO + •H
g analogy with CH_3-C(=O)• → CO + •CH_3

This set of reaction families has been used to construct kinetic models for the pyrolysis of normal alkanes, branched alkanes, naphthenes, aromatics and methyl esters. Each reaction family is accompanied by a methodology to calculate reaction rate coefficients. Preferably, the methodology should be able to take into account the effect of functional groups influencing the reactive moiety. If desired, the user can modify the methodology and/or

change associated parameters. The remainder of this section discusses the standard kinetic library in PRIM-O.

Group additivity is one possible way to estimate rate coefficients. Marin and coworkers applied Benson's group additivity method to transition state theory[27]. Group additive values for hydrogen abstraction and β-scission reactions were derived from quantum chemical calculations using the CBS-QB3 composite method[23-28]. More information about the method to calculate rate coefficients can be found in the referenced works. In short, each rate coefficient is function of 3 parameters, i.e. the number of single-events n_e, the pre-exponential factor for each single-event $\widetilde{A}$ and the activation energy E_a. The number of single-events is the number of energetically equivalent paths from reactant(s) to transition state. The activation energy and pre-exponential factor are estimated by taking kinetic parameters of the reference reactions of the considered reaction family, $E_{a,ref}$ and $\widetilde{A}_{ref}$, and adding group additive contributions that take into account the difference in transition state between the considered reaction and the reference reaction.

$$k(T) = n_e \, \widetilde{A} \exp\left(-\frac{E_a}{R\,T}\right) \quad (2)$$

$$E_a = E_{a,ref} + \sum_{i=1}^{n} \Delta GAV^0_{E_a,i} \quad (3)$$

$$\log\left(\widetilde{A}\right) = \log\left(\widetilde{A}_{ref}\right) + \sum_{i=1}^{n} \Delta GAV^0_{\widetilde{A},i} \quad (4)$$

In PRIM-O, the group additive framework by Marin and coworkers was applied to estimate reaction rate coefficients for hydrogen abstraction by carbon-centered radicals, hydrogen abstraction by hydrogen atoms, hydrogen abstraction by oxygen-centered radicals, carbon-centered radical addition on C=C double bonds, carbon-centered β-scission, hydrogen atom addition on C=C double bonds and hydrogen-centered β-scission.

A group additive framework is unavailable for other reaction families in Table 2-1.

Rate rules for C-C and C-H scission are implemented in PRIM-O as suggested by Mehl et al.[22]. Reaction rate coefficients for C-O scission are estimated using an analogy with methyl decanoate[17]. Kinetic parameters for addition of hydroxyl radicals on C=C double bonds are taken from hydroxyl addition on propene[29]. Ipso-addition by hydrogen atom involves the addition of a hydrogen atom on an aromatic carbon atom connected to a carbon chain and subsequent release of that carbon chain. In the case of alkyl aromatics this leads to release of

the alkyl side chain. In the case of naphtheno-aromatics this leads to opening of the naphthenic ring. Rate coefficients for both reaction families were estimated using an analogy with toluene plus hydrogen atom to benzene plus methyl[30].

A comprehensive kinetic study regarding β-scission reactions which causes the formation of a C=O double bond and/or an oxygen-centered radical is currently unavailable, i.e. $\bullet C_1\text{-}O\text{-}C_2 \rightarrow C_1{=}O + \bullet C_2$, $\bullet O\text{-}C_1\text{-}C_2 \rightarrow C_1{=}O + \bullet C_2$, $\bullet C_1\text{-}C_2\text{-}OX \rightarrow C_1{=}C_2 + \bullet OX$, $\bullet C_1\text{-}O\text{-}H \rightarrow C_1{=}O + \bullet H$ and $\bullet O\text{-}C_1\text{-}H \rightarrow C_1{=}O + \bullet H$. Nonetheless, these reaction families are implemented in PRIM-O as they can be important in the pyrolysis of esters, aldehydes, alcohols and acids. Currently, rate coefficients for these reactions are estimated by taken the rate coefficient from an analogous reaction. For example, reactions that belong to the $\bullet O\text{-}C_1\text{-}C_2 \rightarrow C_1{=}O + \bullet C_2$ reaction family are assigned reaction rate coefficients from $\bullet O\text{-}CH_2\text{-}CH_3 \rightarrow CH_2{=}O + \bullet CH_3$. Rate coefficients for CO α-scission are estimated from $CH_3\text{-}C(=O) \rightarrow CO + \bullet CH_3$.

Intramolecular hydrogen abstraction and intramolecular radical addition reactions proceed through a cyclic transition state. Wang et al. proposed that the pre-exponential factor is function of the number of hindered rotors in the transition state while the activation energy is the sum of the activation energy of the analogous bimolecular reaction and the ring strain in the transition state[31, 32]. The proposed rate rules are implemented in PRIM-O.

Two unimolecular decomposition reactions are included in PRIM-O that do not involve radicals. The first reaction family is the retro-ene reaction. Reaction rate coefficients were taken from 1-pentene to propene plus ethene[33]. The second reaction family is the retro-diels-alder reaction. Reaction rate coefficients from cyclohexene to 1,3-butadiene plus ethene are assigned[34].

2.4.2 Feed molecule and requested decomposition scheme

The user has to specify the connectivity of the molecule of interest together with its functional groups, e.g. oxygen atoms, double bonds, aromaticity, to PRIM-O, using an in-house developed chemical representation nomenclature. Furthermore, the reaction family for which a decomposition scheme has to be generated needs to be supplied.

2.5 Network generation

2.5.1 Molecular representation

The molecule provided by the user is converted to a connectivity matrix in PRIM-O. Furthermore, information regarding functional groups, such as oxygen atoms, double bonds, aromaticity, are tracked in separate vectors.

Guaiacol is presented in Figure 2-4 as example. PRIM-O gives a label to each heavy atom, i.e. non-hydrogen atom. Subsequently, a 9 x 9 connectivity matrix is constructed. The element on row i and column j is 1 or 0 whether a bond is present between atom i and j or not. The aromaticity is stored in a vector with 9 elements. Element i is 1 or 0 whether the atom is part of an aromatic ring or not. The oxygen atoms are stored in a vector with 9 elements. Element i is 1 or 0 whether the atom is an oxygen atom or not.

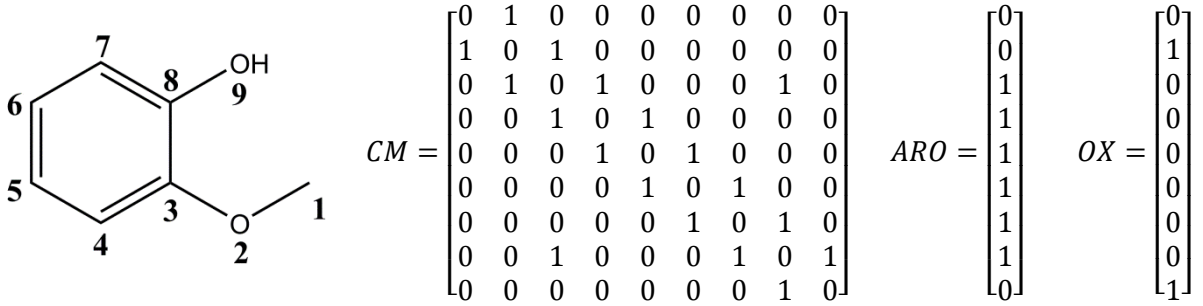

Figure 2-4 Guaiacol and the associated connectivity matrix CM, aromaticity vector ARO and oxygen atom vector OX

2.5.2 Executing reaction families and matrix operations

PRIM-O identifies all reactive centra in the feed molecule for the desired reaction family. PRIM-O does not consider reactions that result in the formation of vinylic and/or phenylic radicals, as these are not favored kinetically. Reaction rate coefficients are assigned to each elementary reaction. Subsequently, the connectivity matrices and vectors representing the products are constructed. For example, in the case of hydrogen abstraction and C-H scission, the connectivity matrix and vectors of the resulting radical is the same as the feed structure. Only a variable which specifies radical position is initialized.

Subsequently, β-radicals are identified amongst the formed radicals. All possible β-radicals are defined explicitly in PRIM-O. In general, β-radicals are radicals that have less than 6 carbon atoms. The benzyl radical is an exception to this rule. Radicals that are not β-radicals are considered μ-radicals. The formed μ-radicals are matched with all μ-radical decomposition reaction families listed in Table 2-1. PRIM-O does not allow formation of vinylic, phenylic radicals and/or allenic species. Connectivity matrices and vectors

representing the products are generated. This procedure continues until all μ-radicals are assigned decomposition paths.

The C-C β-scission of the primary methyl butanoate radical to ethene and methyl acetate radical is presented as example, see Figure 2-5 and Figure 2-6. First, PRIM-O identifies atoms that are in the β-position with respect to the radical. Atoms j that are in β-position with respect to atom i can be tracked by taking the square of the connectivity matrix minus the unit matrix. Elements i,j and j,i in the resulting matrix are 1. In the presented example, carbon atom 3 is in β-position with respect to carbon atom 1 containing the radical center, see Figure 2-5. Breaking of the C_2-C_3 bond does not cause formation of vinylic, phenylic radicals or allenic species. Therefore, PRIM-O executes the reaction family.

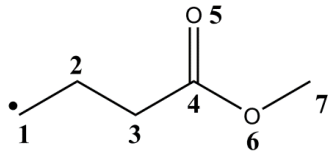

$$CM = \begin{bmatrix} 0 & 1 & 0 & 0 & 0 & 0 & 0 \\ 1 & 0 & 1 & 0 & 0 & 0 & 0 \\ 0 & 1 & 0 & 1 & 0 & 0 & 0 \\ 0 & 0 & 1 & 0 & 1 & 1 & 0 \\ 0 & 0 & 0 & 1 & 0 & 0 & 0 \\ 0 & 0 & 0 & 1 & 0 & 0 & 1 \\ 0 & 0 & 0 & 0 & 0 & 1 & 0 \end{bmatrix} \quad OX = \begin{bmatrix} 0 \\ 0 \\ 0 \\ 0 \\ 1 \\ 1 \\ 0 \end{bmatrix} \quad CM^2 - I = \begin{bmatrix} 0 & 0 & 1 & 0 & 0 & 0 & 0 \\ 0 & 0 & 0 & 1 & 0 & 0 & 0 \\ 1 & 0 & 0 & 0 & 1 & 1 & 0 \\ 0 & 1 & 0 & 0 & 0 & 0 & 1 \\ 0 & 0 & 1 & 0 & 0 & 1 & 0 \\ 0 & 0 & 1 & 0 & 1 & 0 & 0 \\ 0 & 0 & 0 & 1 & 0 & 0 & 0 \end{bmatrix}$$

Figure 2-5 Primary methyl butanoate radical and the associated connectivity matrix CM, oxygen atom vector OX and CM^2-I

As the bond between atom 2 and atom 3 breaks, PRIM-O modifies the connectivity matrix by putting elements 2,3 and 3,2 to zero, see Figure 2-6. Two submatrices can be derived representing the connectivity of the products, ethene and methyl acetate radical. Vectors and variables are modified to represent the change in radical position and double bonds.

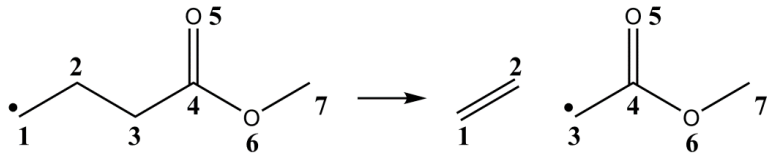

$$CM' = \left[\begin{array}{cc|ccccc} 0 & 1 & 0 & 0 & 0 & 0 & 0 \\ 1 & 0 & \mathbf{0} & 0 & 0 & 0 & 0 \\ \hline 0 & \mathbf{0} & 0 & 1 & 0 & 0 & 0 \\ 0 & 0 & 1 & 0 & 1 & 1 & 0 \\ 0 & 0 & 0 & 1 & 0 & 0 & 0 \\ 0 & 0 & 0 & 1 & 0 & 0 & 1 \\ 0 & 0 & 0 & 0 & 0 & 1 & 0 \end{array}\right] \quad CM_{C2H4} = \begin{bmatrix} 0 & 1 \\ 1 & 0 \end{bmatrix} \quad CM_{MA} = \begin{bmatrix} 0 & 1 & 0 & 0 & 0 \\ 1 & 0 & 1 & 1 & 0 \\ 0 & 1 & 0 & 0 & 0 \\ 0 & 1 & 0 & 0 & 1 \\ 0 & 0 & 0 & 1 & 0 \end{bmatrix}$$

Figure 2-6 C-C β-scission of primary methyl butanoate radical to ethene plus methyl acetate radical and associated connectivity matrices

2.5.3 In-situ lumping of products

Network generation may result in a wide variety of products. A pre-defined list of molecules that are allowed to be formed is present in PRIM-O. Species in this list differ regarding number of carbon atoms and functional groups, e.g. branching, oxygen atoms, double bonds, presence of naphthenic and aromatic rings. These species, generally, do not specify the exact position of the functional group(s). Therefore, each species in the list should be considered as a lump of molecules that possess the same features. The list can be found in Appendix A.

PRIM-O matches each generated product with a species in the list. Multiple products can be matched with the same species. PRIM-O treats these isomers as one molecule, also known as in-situ lumping. In-situ lumping drastically reduces the number of products at the cost of lower accuracy. For example, radicals formed following hydrogen abstraction from normal alkanes can form 1-alkenes by C-C β-scission and 2-alkenes/3-alkenes/4-alkenes/… by C-H β-scission. PRIM-O distinguishes between alkenes whether the C=C double bond is located on the end of the carbon chain or not. Therefore, 2-alkenes/3-alkenes/4-alkenes… with the same number of carbon atom are lumped.

It is the task of the user to manage the PRIM-O species list and modify when needed. If a molecule is formed that cannot be matched with the PRIM-O species list, the network generation terminates. The user can add the specific species to the list and re-run the algorithm to generate output.

For some products it is valid to assume that they dominantly react by molecular re-arrangements forming a molecule that is present in the pre-defined list. In such a case, only the latter molecule is retained. For example, the pyrolysis of dienes may result in the formation of trienes. Trienes are not present in the PRIM-O species list. These molecules react quickly to cyclohexadienes by molecular rearrangement, see Figure 2-7. The CBS-QB3 calculated reaction rate coefficient for 1,3,5-hexatriene to 1,3-cyclohexadiene is $k=7.70\ 10^{+14}\ T^{-0.82}\ \exp(-14400/T)$, $k(1000K)=1.49\ 10^{+6}\ s^{-1}$. Therefore, PRIM-O matches trienes with the corresponding cyclohexadienes when searching through the species list.

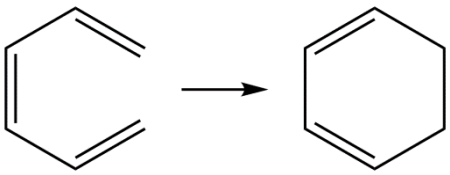

Figure 2-7 Cyclization of 1,3,5-hexatriene to 1,3-cyclohexadiene

2.5.4 Pseudo steady-state approximation

After μ-radicals are assigned decomposition paths, PRIM-O applies the pseudo-steady-state approximation to μ-radicals. The set of algebraic equations is solved with respect to μ-radical concentrations. These are substituted in the equations of the end-products and end-radicals to obtain production rates as function of reactant concentration and rate coefficients of the involved elementary reactions.

This illustrated in Figure 2-8 for hydrogen abstraction from hexane. The hexyl radicals are μ-radicals. They can react by C-C β-scission and intramolecular hydrogen abstraction. The resulting set of differential equations for the species presented in Figure 2-8 are listed in equations (5) to (12). Applying the pseudo-steady-state approximation to the hexyl radicals results in equation (13). The solution, equation (14), can be substituted in equations (9) to (12).

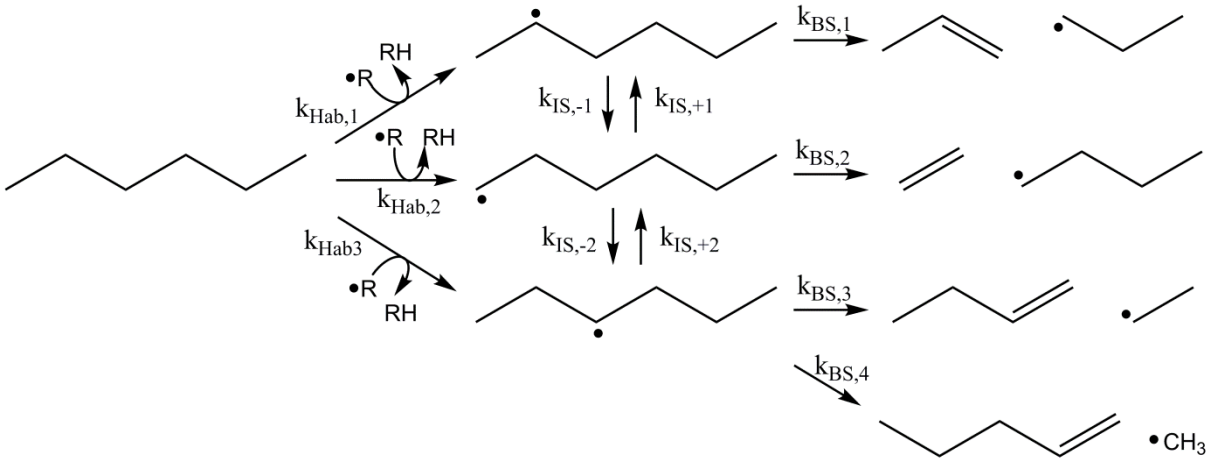

$$\frac{dC_{nC6H14}}{dt} = \frac{dC_R}{dt} = -\frac{dC_{RH}}{dt} = -\left(k_{Hab,1} + k_{Hab,2} + k_{Hab,3}\right) C_{nC6H14} C_R \quad (5)$$

$$\frac{dC_{nC6H13-2\bullet}}{dt} = k_{Hab,1} C_{nC6H14} C_R + k_{IS,+1} C_{nC6H13-1\bullet} - \left(k_{BS,1} + k_{IS,-1}\right) C_{nC6H13-2\bullet} \quad (6)$$

$$\frac{dC_{nC6H13-1\bullet}}{dt} = k_{Hab,2} C_{nC6H14} C_R + k_{IS,-1} C_{nC6H13-2\bullet} + k_{IS,+2} C_{nC6H13-3\bullet} - \left(k_{BS,2} + k_{IS,+1} + k_{IS,-2}\right) C_{nC6H13-1\bullet} \quad (7)$$

$$\frac{dC_{nC6H13-3\bullet}}{dt} = k_{Hab,3} C_{nC6H14} C_R + k_{IS,-2} C_{nC6H13-1\bullet} - \left(k_{BS,3} + k_{BS,4} + k_{IS,+2}\right) C_{nC6H13-3\bullet} \quad (8)$$

$$\frac{dC_{C3H6}}{dt} = \frac{dC_{C3H7-1\bullet}}{dt} = k_{BS,1} C_{nC6H13-2\bullet} \quad (9)$$

$$\frac{dC_{C2H4}}{dt} = \frac{dC_{nC4H9-1\bullet}}{dt} = k_{BS,2} C_{nC6H13-1\bullet} \quad (10)$$

$$\frac{dC_{1-C4H8}}{dt} = \frac{dC_{C2H5\bullet}}{dt} = k_{BS,3} C_{nC6H13-3\bullet} \quad (11)$$

$$\frac{dC_{1-C5H10}}{dt} = \frac{dC_{CH3\bullet}}{dt} = k_{BS,4} C_{nC6H13-3\bullet} \quad (12)$$

Applying the pseudo-steady-state approximation to hexyl radicals

$$\begin{bmatrix} k_{BS,2} + k_{IS,+1} + k_{IS,-2} & -k_{IS,-1} & -k_{IS,+2} \\ -k_{IS,+1} & k_{BS,1} + k_{IS,-1} & 0 \\ -k_{IS,-2} & 0 & k_{BS,3} + k_{BS,4} + k_{IS,+2} \end{bmatrix} \begin{bmatrix} C_{nC6H13-1\bullet} \\ C_{nC6H13-2\bullet} \\ C_{nC6H13-3\bullet} \end{bmatrix} = \begin{bmatrix} k_{Hab,2} C_{nC6H14} C_R \\ k_{Hab,1} C_{nC6H14} C_R \\ k_{Hab,3} C_{nC6H14} C_R \end{bmatrix} \quad (13)$$

$$\begin{bmatrix} C_{nC6H13-1\bullet} \\ C_{nC6H13-2\bullet} \\ C_{nC6H13-3\bullet} \end{bmatrix} = \begin{bmatrix} k_{BS,2} + k_{IS,+1} + k_{IS,-2} & -k_{IS,-1} & -k_{IS,+2} \\ -k_{IS,+1} & k_{BS,1} + k_{IS,-1} & 0 \\ -k_{IS,-2} & 0 & k_{BS,3} + k_{BS,4} + k_{IS,+2} \end{bmatrix}^{-1} \begin{bmatrix} k_{Hab,2} C_{nC6H14} C_R \\ k_{Hab,1} C_{nC6H14} C_R \\ k_{Hab,3} C_{nC6H14} C_R \end{bmatrix} \quad (14)$$

Figure 2-8 Hydrogen abstraction from n-hexane and subsequent decomposition paths

2.6 Output

2.6.1 Pseudo rate coefficients and relative pseudo rate coefficients

After substituting the µ-radical concentrations, the formation of products becomes a complex function of elementary reaction rate coefficients and, thus, temperature. The output of PRIM-O tackles this complexity by introducing so-called "pseudo rate coefficients" (PSC) and "relative pseudo rate coefficients" (PRC). The formation rate of each product i can be written as:

$$R_i = PSC(i)\, C_{reactant} \quad (15)$$

$$R_i = PRC(i)\, k_{ref}\, C_{reactant} \quad (16)$$

k_{ref} is the rate coefficient of the reference reaction of the considered reaction family, e.g. CH_4+•H→•CH_3+H_2 for hydrogen abstraction from carbon-centered radicals by hydrogen atoms. The PRC's vary little with temperature as the major temperature dependency is located in the reference rate coefficients[35]. PRIM-O writes out a list of PRC's for a user-defined temperature domain, typically from 773 to 1173K in 20K increments. When calculating the formation rate of a species i in a reactor simulation, k_{ref} has to be evaluated at the reactor temperature while $PRC(i)$ can be taken from the PRIM-O output.

In the example presented in Figure 2-8, equation (14) can be rewritten as follows:

$$\begin{bmatrix} C_{nC6H13-1\bullet} \\ C_{nC6H13-2\bullet} \\ C_{nC6H13-3\bullet} \end{bmatrix} = \begin{bmatrix} k_{BS,2} + k_{IS,+1} + k_{IS,-2} & -k_{IS,-1} & -k_{IS,+2} \\ -k_{IS,+1} & k_{BS,1} + k_{IS,-1} & 0 \\ -k_{IS,-2} & 0 & k_{BS,3} + k_{BS,4} + k_{IS,+2} \end{bmatrix}^{-1} \begin{bmatrix} \frac{k_{Hab,2}}{k_{Hab,ref}} \\ \frac{k_{Hab,1}}{k_{Hab,ref}} \\ \frac{k_{Hab,3}}{k_{Hab,ref}} \end{bmatrix} k_{Hab,ref} C_{nC6H14} C_R \quad (17)$$

Substituting equation (17) in equations (9) to (12) allows obtaining reaction rates as presented in equation (16).

2.6.2 Equivalent reaction

The set of reaction rates for reactants and products can be converted into a so-called one-step equivalent reaction by dividing formation rates of products by the total reaction rate. This allows to obtain selectivities of species, which are temperature dependent, for a given reaction.

This will again be illustrated using the example presented in Figure 2-8. Assuming the intramolecular hydrogen abstraction reaction rate coefficients are 0 s^{-1}, which facilitates calculating the inverse of the matrix in equation (14), hexyl radical concentrations are:

$$C_{nC6H13-2\bullet} = \frac{k_{Hab,1}}{k_{BS,1}} C_{nC6H14} C_R \quad \textbf{(18)}$$

$$C_{nC6H13-1\bullet} = \frac{k_{Hab,2}}{k_{BS,2}} C_{nC6H14} C_R \quad \textbf{(19)}$$

$$C_{nC6H13-3\bullet} = \frac{k_{Hab,3}}{k_{BS,3} + k_{BS,4}} C_{nC6H14} C_R \quad \textbf{(20)}$$

The continuity equations for products become:

$$\frac{dC_{C3H6}}{dt} = \frac{dC_{C3H7-1\bullet}}{dt} = k_{Hab,1} C_{nC6H14} C_R \quad \textbf{(21)}$$

$$\frac{dC_{C2H4}}{dt} = \frac{dC_{nC4H9-1\bullet}}{dt} = k_{Hab,2} C_{nC6H14} C_R \quad \textbf{(22)}$$

$$\frac{dC_{1-C4H8}}{dt} = \frac{dC_{C2H5\bullet}}{dt} = \frac{k_{BS,3}}{k_{BS,3} + k_{BS,4}} k_{Hab,3} C_{nC6H14} C_R \quad \textbf{(23)}$$

$$\frac{dC_{1-C5H10}}{dt} = \frac{dC_{CH3\bullet}}{dt} = \frac{k_{BS,4}}{k_{BS,3} + k_{BS,4}} k_{Hab,3} C_{nC6H14} C_R \quad \textbf{(24)}$$

Dividing the formation rates by the total reaction rate, equation (5), allows to obtain species selectivities:

$$S_{C3H6} = S_{C3H7-1\bullet} = \frac{k_{Hab,1}}{k_{Hab,1} + k_{Hab,2} + k_{Hab,3}} \quad \textbf{(25)}$$

$$S_{C2H4} = S_{nC4H9-1\bullet} = \frac{k_{Hab,2}}{k_{Hab,1} + k_{Hab,2} + k_{Hab,3}} \quad \textbf{(26)}$$

$$S_{1-C4H8} = S_{C2H5\bullet} = \frac{k_{BS,3}}{k_{BS,3} + k_{BS,4}} \frac{k_{Hab,3}}{k_{Hab,1} + k_{Hab,2} + k_{Hab,3}} \quad \textbf{(27)}$$

$$S_{1-C5H10} = S_{CH3\bullet} = \frac{k_{BS,4}}{k_{BS,3} + k_{BS,4}} \frac{k_{Hab,3}}{k_{Hab,1} + k_{Hab,2} + k_{Hab,3}} \quad \textbf{(28)}$$

Equations (5) and (21) to (24) can be represented by the one-step equivalent reaction:

$$\begin{aligned} nC_6H_{14} + R \xrightarrow{k_{Hab,1}+k_{Hab,2}+k_{Hab,3}} & \frac{k_{Hab,1}}{k_{Hab,1}+k_{Hab,2}+k_{Hab,3}}(C_3H_6 + C_3H_7 - 1\bullet) \\ & + \frac{k_{Hab,2}}{k_{Hab,1}+k_{Hab,2}+k_{Hab,3}}(C_2H_4 + nC_4H_9 - 1\bullet) \\ & + \frac{k_{BS,3}}{k_{BS,3}+k_{BS,4}}\frac{k_{Hab,3}}{k_{Hab,1}+k_{Hab,2}+k_{Hab,3}}(1 - C_4H_8 + C_2H_5\bullet) \\ & + \frac{k_{BS,4}}{k_{BS,3}+k_{BS,4}}\frac{k_{Hab,3}}{k_{Hab,1}+k_{Hab,2}+k_{Hab,3}}(1 - C_5H_{10} + CH_3\bullet) + RH \end{aligned} \quad (29)$$

The resulting equivalent reaction can help the model developer to identify dominant reaction paths. When substituting the reaction rate coefficients in equation (29), the stoichiometric coefficients can be derived, at 1073K:

$$\begin{aligned} nC_6H_{14} + R \rightarrow & 0.44\,(C_3H_6 + C_3H_7 - 1\bullet) + 0.12\,(C_2H_4 + nC_4H_9 - 1\bullet) + 0.29\,(1 - C_4H_8 + C_2H_5\bullet) \\ & + 0.15\,(1 - C_5H_{10} + CH_3\bullet) + RH \end{aligned} \quad (30)$$

Hydrogen abstraction from secondary carbon atoms is favored over hydrogen abstraction from primary carbon atoms in hexane. Therefore, ethene and 1-butyl, decomposition products of 1-hexyl, have lower stoichiometric coefficients than the other products in equation (30). 3-hexyl radicals can decompose by C-C β-scission forming 1-butene plus ethyl and by C-C β-scission forming 1-pentene plus methyl. The former reaction is favored as an ethyl radical is more stable than a methyl radical. Hence, 1-butene and ethyl have larger stoichiometric coefficients than 1-pentene and methyl. The 2-hexyl radical has the same formation rate as the 3-hexyl radical. As 2-hexyl only has one C-C β-scission reaction, the stoichiometric coefficients of the corresponding products, i.e. propene and 1-propyl, is the sum of the stoichiometric coefficients of the products formed by the two competing β-scission reactions of 3-hexyl.

2.6.3 Thermodynamic data

Calculation of thermodynamic data for reactants and products is not part of the PRIM-O algorithm itself. After model generation, PRIM-O converts the connectivity matrices and vectors of all species to adjacency lists and/or IUPAC International Chemical Identifiers, also known as InChI's. Ethyl-benzene is given as example in Figure 2-9. Adjacency lists and InChI's are used as input for external programs, such as RMG's ThermoDataEstimator[36] and Genesys's ThermoGenerator[37]. These programs estimate thermodynamic properties using Benson group contribution method[38].

Molecule: Ethyl-benzene

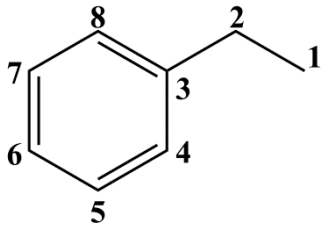

Representation in PRIM-O:

$$\mathrm{CM} = \begin{bmatrix} 0 & 1 & 0 & 0 & 0 & 0 & 0 & 0 \\ 1 & 0 & 1 & 0 & 0 & 0 & 0 & 0 \\ 0 & 1 & 0 & 1 & 0 & 0 & 0 & 1 \\ 0 & 0 & 1 & 0 & 1 & 0 & 0 & 0 \\ 0 & 0 & 0 & 1 & 0 & 1 & 0 & 0 \\ 0 & 0 & 0 & 0 & 1 & 0 & 1 & 0 \\ 0 & 0 & 0 & 0 & 0 & 1 & 0 & 1 \\ 0 & 0 & 1 & 0 & 0 & 0 & 1 & 0 \end{bmatrix} \quad \mathrm{ARO} = \begin{bmatrix} 0 \\ 0 \\ 1 \\ 1 \\ 1 \\ 1 \\ 1 \\ 1 \end{bmatrix}$$

Adjacencey list:

1 C 0 (2,S)
2 C 0 (1,S) (3,S)
3 C 0 (2,S) (4,S) (8,D)
4 C 0 (3,S) (5,D)
5 C 0 (4,D) (6,S)
6 C 0 (5,S) (7,D)
7 C 0 (6,D) (8,S)
8 C 0 (3,D) (7,S)

InChI: 1S/C8H10/c1-2-8-6-4-3-5-7-8/h3-7H,2H2,1H3

Figure 2-9 Representation of ethyl benzene in PRIM-O and corresponding adjacency list and InChI

2.6.4 A posteriori lumping of the feedstock

When developing a kinetic model using output from PRIM-O, the number of species can be further reduced by a posteriori lumping. So-called "pseudo-components" are introduced, which are defined as a weighted mixture of isomers. The associated weights can be derived by analyzing the investigated feedstock. If this is impossible with the available analytical techniques, weights can be adopted from literature sources[18, 39]. The rate of formation of products originating from the pseudo component is the sum of the rates of formation of products from the individual isomers multiplied by their respective weight.

A typical example is the lumping of branched alkanes. The pseudo component "branched heptane" is the weighted sum of the eight possible isomers: 2-methyl-hexane, 3-methyl-hexane, 2,2-dimethyl-pentane, 2,3-dimethyl-pentane, 2,4-dimethyl-pentane, 3,3-dimethyl-pentane, 3-ethyl-pentane and 2,2,3-trimethyl-butane. The selectivity of the pseudo-component

"branched heptane" towards products is the weighted average of the selectivities of the individual isomers, see Table 2-2.

Table 2-2 Product selectivities of individual branched heptane isomers and the branched heptane lump

Molecule	2-methyl-hexane	3-methyl-hexane	2,2-dimethyl-pentane	2,3-dimethyl-pentane	2,4-dimethyl-pentane	3,3-dimethyl-pentane	3-ethyl-pentane	2,2,3-trimethyl-butane	Branched heptane
Weight	0.52	0.26	0.04	0.04	0.04	0.04	0.04	0.01	
Product spectrum following hydrogen abstraction									
hydrogen atom	0.023	0.022	0.005	0.021	0.012	0.002	0.025	0.013	0.021
methyl	0.161	0.233	0.401	0.385	0.251	0.289	0.254	0.485	0.215
ethyl	0.079	0.293	0.000	0.187	0.000	0.405	0.487	0.000	0.162
1-propyl	0.252	0.157	0.141	0.000	0.000	0.000	0.000	0.000	0.179
2-propyl	0.150	0.000	0.000	0.201	0.561	0.000	0.000	0.257	0.112
1-butyl	0.086	0.000	0.000	0.000	0.000	0.000	0.000	0.000	0.045
2-butyl	0.000	0.189	0.000	0.134	0.000	0.000	0.000	0.000	0.055
iso-butyl	0.163	0.000	0.000	0.000	0.177	0.000	0.000	0.000	0.092
tert-butyl	0.000	0.000	0.321	0.000	0.000	0.000	0.000	0.245	0.016
2-pentyl	0.000	0.067	0.000	0.000	0.000	0.000	0.000	0.000	0.017
3-pentyl	0.000	0.000	0.000	0.000	0.000	0.000	0.233	0.000	0.010
2-methyl-1-butyl	0.000	0.040	0.000	0.000	0.000	0.000	0.000	0.000	0.010
2-methyl-2-butyl	0.000	0.000	0.000	0.000	0.000	0.304	0.000	0.000	0.012
2-methyl-3-butyl	0.000	0.000	0.000	0.072	0.000	0.000	0.000	0.000	0.003
2-methyl-4-butyl	0.086	0.000	0.000	0.000	0.000	0.000	0.000	0.000	0.045
2,2-dimethyl-1-propyl	0.000	0.000	0.131	0.000	0.000	0.000	0.000	0.000	0.005
ethene	0.086	0.106	0.131	0.072	0.000	0.304	0.233	0.000	0.103
propene	0.249	0.189	0.321	0.134	0.177	0.000	0.000	0.245	0.208
1-butene	0.150	0.039	0.000	0.060	0.000	0.000	0.000	0.000	0.091
2-butene	0.000	0.119	0.000	0.141	0.000	0.000	0.000	0.000	0.037
isobutene	0.252	0.000	0.141	0.000	0.561	0.000	0.000	0.257	0.163
1-pentene	0.000	0.039	0.000	0.000	0.000	0.000	0.000	0.000	0.010
2-pentene	0.000	0.081	0.000	0.000	0.000	0.000	0.487	0.000	0.042
2-methyl-1-butene	0.000	0.173	0.000	0.000	0.000	0.173	0.000	0.000	0.052
3-methyl-1-butene	0.079	0.000	0.000	0.016	0.000	0.000	0.000	0.000	0.042
2-methyl-2-butene	0.000	0.000	0.000	0.171	0.000	0.232	0.000	0.000	0.016
1-hexene	0.045	0.000	0.000	0.000	0.000	0.000	0.000	0.000	0.024
2-hexene	0.095	0.062	0.000	0.000	0.000	0.000	0.000	0.000	0.066
3-hexene	0.000	0.043	0.000	0.000	0.000	0.000	0.000	0.000	0.011
branched hexene	0.022	0.128	0.401	0.385	0.251	0.289	0.254	0.485	0.114
branched heptene	0.023	0.022	0.005	0.021	0.012	0.002	0.025	0.013	0.021

2.7 Coupling of μ-network with β-network

The set of equivalent single-step reactions generated by PRIM-O is often referred to as the μ-network, as this set describes the chemistry of reactions which generate μ-radicals. Dedicated kinetic models have to contain chemistry for both μ and β-radicals. Therefore, the μ-network has to be coupled with a β-network. A β-network consists of a set of elementary reactions involving β-radicals and associated thermochemistry.

In this work, literature reported kinetic models regarding pyrolysis of small species, such as ethane and methyl butanoate[33, 40], were taken as β-network. Note that these literature-reported kinetic models also contain reactions of μ-radicals. Such reactions have to be removed from the model before coupling with the μ-network generated with PRIM-O.

Practically, the coupling of μ-network and β-network is performed using an algorithm called SORT. The user of SORT specifies the β-network and the equivalent single-step reactions that have to be incorporated in the kinetic model. The most essential feature of the algorithm is the correct matching of species that appear in both the μ-network and β-network. The output of SORT can be (i) a CHEMKIN-readable kinetic model which contains equivalent single-step reactions where stoichiometric coefficients are evaluated at a certain temperature or (ii) a kinetic model where the temperature-dependence of the stoichiometric coefficients of the equivalent single-step reactions is retained and which can be coupled with CHEMKIN using a user-defined subroutine.

2.8 Outlook

PRIM has been extended to PRIM-O to generate decomposition schemes for the pyrolysis of oxygenated molecules. The pyrolysis of methyl esters is presented as case study in Chapter 3.3. This necessitates the inclusion of chemistry relevant for the decomposition of esters in PRIM-O. Furthermore, the list of defined species in PRIM-O, see Appendix A, is extended to contain esters and derived products.

The current framework can be expanded to other oxygenates, such as triglycerides, sterols and biomass model components. This does require a thorough understanding of the underlying chemistry. The currently-implemented reaction families should contain parameters, e.g. group additive values, that enable accurate prediction of associated rate coefficients. Possibly, several reaction families need to be added to describe the pyrolysis of oxygenated molecules.

For example, the generation of kinetic models for the pyrolysis of ethers using PRIM-O requires extension of the list of defined species and list of reaction families. Acyclic ethers are known to react by a combination of radical and unimolecular chemistry in pyrolysis conditions [41]. The current kinetic library allows the estimation of kinetic parameters for radical chemistry of ethers. Hydrogen abstraction from ethers and subsequent β-scission results in unsaturated ethers. The latter species have to be added to the list of defined species in PRIM-O prior to network generation. The unimolecular elimination of alcohols is an important reaction route in the thermal decomposition of ethers [41]. This reaction family is currently unavailable in PRIM-O and has to be added in order to generate an adequate kinetic model.

Currently, it is not possible to generate decomposition schemes for the pyrolysis of sulfur and nitrogen containing components. The representation of such molecules in PRIM-O necessitates the addition of vectors specifying the position of sulfur and nitrogen atoms, analogous to oxygen containing molecules – see section 2.4. The reaction families need to be modified accordingly.

2.9 Conclusion

The general features of PRIM-O, a network generation tool for the pyrolysis of hydrocarbons and oxygenates, are presented. The algorithm starts by reacting a molecule according to a reaction family, specified by the user. In the code, the reactant is presented by a connectivity matrix and a set of vectors containing information regarding its functional groups. The execution of a reaction family is equivalent with matrix operations. Subsequently, μ-radicals are identified. All possible unimolecular decomposition reactions are generated for each μ-radical, causing new radicals and products to be formed. Each elementary step is assigned a reaction rate coefficient calculated using group additivity or rate rules. Products are lumped according to carbon number and functional groups. The network generation stops when all μ-radicals are assigned decomposition reactions. Then, PRIM-O applies the pseudo-steady-state approximation to μ-radicals and solves the linear set of algebraic equations. The μ-radical concentrations can be substituted in the rates of formation of other end-products. The resulting “pseudo” rate coefficients are the output of PRIM-O and can be used for reactor simulations.

This procedure allows to significantly reduce the number of species in the kinetic model while maintaining a high level of detail, hence, facilitating their use in large-scale computations.

2.10 References

[1] F. O. Rice, W. R. Johnston, B. L. Evering, The Thermal Decomposition of Organic Compounds from the Standpoint of Free Radicals. II. Experimental Evidence of the Decomposition of Organic Compounds into Free Radicals, J. Am. Chem. Soc. 54 (1932) 3529-3543

[2] F. O. Rice, The Thermal Decomposition of Organic Compounds from the Standpoint of Free Radicals. I. Saturated Hydrocarbons, J. Am. Chem. Soc. 53 (1931) 1959-1972

[3] M. W. M. van Goethem, F. I. Kleinendorst, C. van Leeuwen, N. van Velzen, Equation-based SPYRO model and solver for the simulation of the steam cracking process, Comput. Chem. Eng. 25 (2001) 905-911

[4] M. Dente, E. Ranzi, A. G. Goossens, Detailed prediction of olefin yields from hydrocarbon pyrolysis through a fundamental simulation program SPYRO, Comput. Chem. Eng. 3 (1979) 61-75

[5] K. M. Van Geem, M.-F. Reyniers, G. B. Marin, Challenges of modeling steam cracking of heavy feedstocks, Oil. Gas. Sci. Technol. 63 (2008) 79-94

[6] R. Van de Vijver, N. M. Vandewiele, P. L. Bhoorasingh, B. L. Slakman, F. Seyedzadeh Khanshan, H.-H. Carstensen, M.-F. Reyniers, G. B. Marin, R. H. West, K. M. Van Geem, Automatic Mechanism and Kinetic Model Generation for Gas- and Solution-Phase Processes: A Perspective on Best Practices, Recent Advances, and Future Challenges, Int. J. Chem. Kinet. 47 (2015) 199-231

[7] T. F. Lu, C. K. Law, Toward accommodating realistic fuel chemistry in large-scale computations, Prog. Energy Combust. Sci. 35 (2009) 192-215

[8] P. A. Reyniers, C. M. Schietekat, D. J. Van Cauwenberge, L. A. Vandewalle, K. M. Van Geem, G. B. Marin, Necessity and Feasibility of 3D Simulations of Steam Cracking Reactors, Ind. Eng. Chem. Res. 54 (2015) 12270-12282

[9] X. L. Zheng, T. F. Lu, C. K. Law, C. K. Westbrook, H. J. Curran, Experimental and computational study of nonpremixed ignition of dimethyl ether in counterflow, P. Combust. Inst. 30 (2005) 1101-1109

[10] X. L. Zheng, T. F. Lu, C. K. Law, Experimental counterflow ignition temperatures and reaction mechanisms of 1,3-butadiene, P. Combust. Inst. 31 (2007) 367-375

[11] A. Cuoci, A. Frassoldati, T. Faravelli, E. Ranzi, A computational tool for the detailed kinetic modeling of laminar flames: Application to C2H4/CH4 coflow flames, Combust. Flame 160 (2013) 870-886

[12] A. Frassoldati, A. Cuoci, T. Faravelli, U. Niemann, E. Ranzi, R. Seiser, K. Seshadri, An experimental and kinetic modeling study of n-propanol and iso-propanol combustion, Combust. Flame 157 (2010) 2-16

[13] S. S. Merchant, E. F. Zanoelo, R. L. Speth, M. R. Harper, K. M. Van Geem, W. H. Green, Combustion and pyrolysis of iso-butanol: Experimental and chemical kinetic modeling study, Combust. Flame 160 (2013) 1907-1929

[14] O. Herbinet, J. Biet, M. H. Hakka, V. Warth, P.-A. Glaude, A. Nicolle, F. Battin-Leclerc, Modeling study of the low-temperature oxidation of large methyl esters from C11 to C19, P. Combust. Inst. 33 (2011) 391-398

[15] S. M. Burke, W. Metcalfe, O. Herbinet, F. Battin-Leclerc, F. M. Haas, J. Santner, F. L. Dryer, H. J. Curran, An experimental and modeling study of propene oxidation. Part 1: Speciation measurements in jet-stirred and flow reactors, Combust. Flame 161 (2014) 2765-2784

[16] V. Warth, N. Stef, P. A. Glaude, F. Battin-Leclerc, G. Scacchi, G. M. Côme, Computer-Aided Derivation of Gas-Phase Oxidation Mechanisms: Application to the Modeling of the Oxidation of n-Butane, Combust. Flame 114 (1998) 81-102

[17] O. Herbinet, P.-A. Glaude, V. Warth, F. Battin-Leclerc, Experimental and modeling study of the thermal decomposition of methyl decanoate, Combust. Flame 158 (2011) 1288-1300

[18] E. Ranzi, M. Dente, A. Goldaniga, G. Bozzano, T. Faravelli, Lumping procedures in detailed kinetic modeling of gasification, pyrolysis, partial oxidation and combustion of hydrocarbon mixtures, Prog. Energy Combust. Sci. 27 (2001) 99-139

[19] E. Ranzi, M. Dente, S. Plerucci, G. Biardi, Initial product distributions from pyrolysis of normal and branched paraffins, Ind. Eng. Chem. Fund. 22 (1983) 132-139

[20] P. J. Clymans, G. F. Froment, Computer generation of the reaction paths and rate equations in the thermal cracking of normal and branched paraffins, Comput. Chem. Eng. 8 (1984) 137-142

[21] L. P. Hillewaert, J. L. Dierickx, G. F. Froment, Computer-Generation of Reaction Schemes and Rate-Equations for Thermal-Cracking, AlChE J. 34 (1988) 17-24

[22] M. Mehl, G. Vanhove, W. J. Pitz, E. Ranzi, Oxidation and combustion of the n-hexene isomers: A wide range kinetic modeling study, Combust. Flame 155 (2008) 756-772

[23] M. K. Sabbe, A. Vandeputte, M.-F. Reyniers, M. Waroquier, G. B. Marin, Modeling the influence of resonance stabilization on the kinetics of hydrogen abstractions, Phys. Chem. Chem. Phys. 12 (2010) 1278-1298

[24] P. D. Paraskevas, M. K. Sabbe, M.-F. Reyniers, N. G. Papayannakos, G. B. Marin, Kinetic Modeling of α-Hydrogen Abstractions from Unsaturated and Saturated Oxygenate Compounds by Carbon-Centered Radicals, ChemPhysChem 15 (2014) 1849-1866

[25] P. D. Paraskevas, M. K. Sabbe, M.-F. Reyniers, N. G. Papayannakos, G. B. Marin, Kinetic Modeling of α-Hydrogen Abstractions from Unsaturated and Saturated Oxygenate Compounds by Hydrogen Atoms, J. Phys. Chem. A 118 (2014) 9296-9309
[26] P. D. Paraskevas, M. K. Sabbe, M.-F. Reyniers, N. G. Papayannakos, G. B. Marin, Group Additive Kinetics for Hydrogen Transfer Between Oxygenates, J. Phys. Chem. A (2015)
[27] M. K. Sabbe, M.-F. Reyniers, V. Van Speybroeck, M. Waroquier, G. B. Marin, Carbon-centered radical addition and beta-scission reactions: Modeling of activation energies and pre-exponential factors, ChemPhysChem 9 (2008) 124-140
[28] M. K. Sabbe, M.-F. Reyniers, M. Waroquier, G. B. Marin, Hydrogen Radical Additions to Unsaturated Hydrocarbons and the Reverse beta-Scission Reactions: Modeling of Activation Energies and Pre-Exponential Factors, ChemPhysChem 11 (2010) 195-210
[29] J. Zador, A. W. Jasper, J. A. Miller, The reaction between propene and hydroxyl, Phys. Chem. Chem. Phys. 11 (2009) 11040-11053
[30] D. L. Baulch, C. J. Cobos, R. A. Cox, P. Frank, G. Hayman, T. Just, J. A. Kerr, T. Murrells, M. J. Pilling, J. Troe, R. W. Walker, J. Warnatz, Evaluated Kinetic Data for Combustion Modeling - Supplement I, J. Phys. Chem. Ref. Data 23 (1994) 847-1033
[31] K. Wang, S. M. Villano, A. M. Dean, Reactivity–Structure-Based Rate Estimation Rules for Alkyl Radical H Atom Shift and Alkenyl Radical Cycloaddition Reactions, J. Phys. Chem. A 119 (2015) 7205-7221
[32] K. Wang, S. M. Villano, A. M. Dean, The Impact of Resonance Stabilization on the Intramolecular Hydrogen-Atom Shift Reactions of Hydrocarbon Radicals, Chemphyschem 16 (2015) 2635-2645
[33] M. K. Sabbe, K. M. Van Geem, M.-F. Reyniers, G. B. Marin, First principle-based simulation of ethane steam cracking, AlChE J. 57 (2011) 482-496
[34] Z. Wang, L. Ye, W. Yuan, L. Zhang, Y. Wang, Z. Cheng, F. Zhang, F. Qi, Experimental and kinetic modeling study on methylcyclohexane pyrolysis and combustion, Combust. Flame 161 (2014) 84-100
[35] C. Vercauteren. Rigoureuze kinetische schema's voor de thermische kraking van koolwaterstoffen. Ghent University, Ghent, 1991.
[36] C. W. Gao, J. W. Allen, W. H. Green, R. H. West, Reaction Mechanism Generator: Automatic construction of chemical kinetic mechanisms, Comput. Phys. Commun. 203 (2016) 212-225
[37] N. M. Vandewiele, K. M. Van Geem, M.-F. Reyniers, G. B. Marin, Genesys: Kinetic model construction using chemo-informatics, Chem. Eng. J. 207 (2012) 526-538
[38] S. W. Benson, Thermochemical Kinetics: Methods for the Estimation of Thermochemical Data and Rate Parameters, John Wiley & Sons, New York, 1976
[39] M. Dente, G. Bozzano, T. Faravelli, A. Marongiu, S. Pierucci, E. Ranzi, Kinetic Modelling of Pyrolysis Processes in Gas and Condensed Phase, Adv. Chem. Eng. 32 (2007) 51-166
[40] L. K. Huynh, A. Violi, Thermal decomposition of methyl butanoate: Ab initio study of a biodiesel fuel surrogate, J. Org. Chem. 73 (2008) 94-101
[41] K. Yasunaga, J. M. Simmie, H. J. Curran, T. Koike, O. Takahashi, Y. Kuraguchi, Y. Hidaka, Detailed chemical kinetic mechanisms of ethyl methyl, methyl tert-butyl and ethyl tert-butyl ethers: The importance of uni-molecular elimination reactions, Combust. Flame 158 (2011) 1032-1036

Chapter 3

Steam cracking of renewable feedstocks

This chapter discusses the use of bio-derived feedstocks in steam crackers. The first paper investigates the steam cracking of deoxygenated vegetable oils and waste fats. The second paper investigates the steam cracking of deoxygenated crude tall oil. The third paper investigates the pyrolysis of methyl esters. These three processes were investigated by both experimental work and kinetic modeling. Experiments were performed in a dedicated bench scale pyrolysis setup. Kinetic models were developed using PRIM-O, discussed in Chapter 2.

3.1 Steam cracking of bio-derived normal and branched alkanes: Influence of branching on product distribution and formation of aromatics

3.1.1 Abstract

The presence of large amounts of oxygen in the molecular structure of triglyceride and fatty acid based feedstocks makes direct use in conventional steam crackers impossible without substantial modifications to the cold section. Full or partial catalytic deoxygenation has potential to resolve this, giving a mixture which consists primarily of normal and branched alkanes. Two of these deoxygenated mixtures have been investigated theoretically and experimentally in a dedicated bench setup (P=0.17 MPa, T=1050-1150K, F_{HC}=4.17 10^{-2} g s^{-1}, steam dilution of 0.3 and 0.5 g_{H2O}/g_{HC}). Furthermore, the degree of branching of the hydrocarbon mixtures impacts the product distribution, in particular the alkene selectivity. The newly generated, validated detailed kinetic model shows that small alkenes are formed by hydrogen abstraction and successive C-C β-scission reactions. In the studied temperature range, mono-aromatics are formed by three competing pathways: a series of recombination reactions of allylic radicals followed by hydrogen abstraction and intramolecular radical additions, additions of allylic and vinyl radicals on dienes followed by intramolecular radical addition, and finally recombination reactions of carbon-centered radicals with 1,3-cyclopentadienyl followed by hydrogen abstraction and ring enlargement.

Keywords: Triglycerides, steam cracking, normal and branched alkanes, detailed kinetic model, aromatics

3.1.2 Introduction

The increasing demand for biomass derived chemicals and polymers has triggered academic and industrial research towards the use of bio-derived feedstocks for olefin production, ideally without any additional investments[1, 2].

A reasonable successful commercialized process starts from hydrolysis of starch or cellulose followed by fermentation of the sugars to ethanol, the current biofuel market leader. Dehydration of bio-derived ethanol forms bio-derived ethene, also known as bio-ethene. Commercial bio-ethene, which is almost identical to ethene derived from non-renewable/fossil sources, can be used in existing petrochemical facilities[1, 3], if the oxygenate impurities are sufficiently low.

A different type of feedstock that has been investigated for the production of sustainable fuels and chemicals is triglyceride and fatty acid based biomass. The direct use of triglycerides as a fuel is not feasible given their high kinematic viscosity and low volatility. Fuels are therefore produced from this type of biomass by (i) transesterification with methanol forming methyl-esters, also known as biodiesel[4], or (ii) catalytic upgrading via deoxygenation processes[5], also known as green diesel[6]. Catalytic upgrading typically involves a hydrotreating step, forming a mixture of long chain normal alkanes, followed by a hydrocracking or isomerization step, forming a mixture of normal and branched alkanes. Green diesel has several advantages over biodiesel such as greater thermal and oxidation stability[6, 7]. The production of green diesel has been commercialized, examples are NExBTL[8], produced by Neste, the UOP/Eni ecofining[9] process and the Axens Vegan technology[10]. Recently, Total announced plans to transform an unprofitable oil refinery in La Mède, France, to manufacture green diesel, implementing the Axens Vegan technology[11].

Hydrocarbon mixtures produced by the aforementioned processes can also be used for the production of bio-derived chemicals[12] by utilization of existing steam cracking facilities[13]. The composition of these mixtures, e.g. degree and type of branching, affects yields of alkenes and aromatics formed following steam cracking[14]. Facilitating the use of a new feedstock, such as catalytically upgraded vegetable oils, in steam crackers requires detailed models that select reactor operating conditions which maximize the overall profit[15]. Furthermore, such models can provide feedback to the preceding catalytic processes to optimize the steam cracker feedstock composition, e.g. increase or decrease the degree of branching of the hydrocarbons. This is illustrated in Figure 3.1-1.

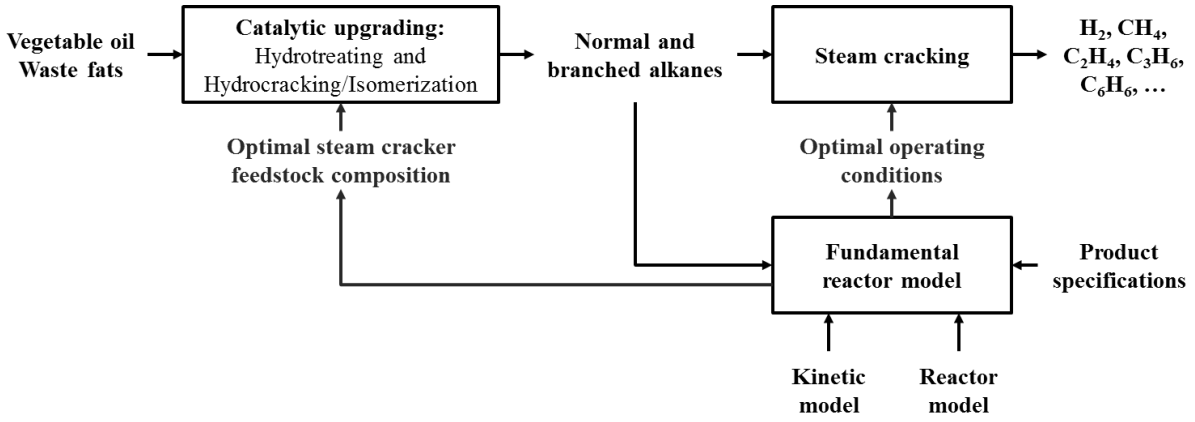

Figure 3.1-1 Fundamental reactor model which selects operating conditions of both the catalytic upgrading step and the steam cracking step in order to obtain the desired product specification

While the pyrolysis of n-alkanes is a mature scientific research field, new experimental data are still reported and kinetic models are continuously being improved, e.g. for heptane [16], decane [17, 18] or dodecane [18, 19]. In comparison, the availability of experimental data and kinetic models regarding the pyrolysis of branched alkanes is remarkably lower although depending on the size and the number of side branches substantial different product yields are expected. Recent models that describe the decomposition of branched alkanes, have solely been validated for oxidation and combustion conditions[20-22]. Furthermore, experimental kinetic data regarding the pyrolysis of branched alkanes having more than 10 carbon is unavailable to the best of the author's knowledge.

In this work, a detailed kinetic model has been developed which is able to describe the pyrolysis of normal and branched alkanes, having 30 carbon atoms or less. Steam cracking experiments for two hydrocarbon mixtures, consisting of normal and branched alkanes provided by Neste, were performed in a dedicated bench-scale setup. These mixtures differ strongly in the degree of branching. The obtained experimental mass fraction profiles are compared with model calculated mass fraction profiles. Finally, a reaction paths analysis is performed to understand how the formation paths of small alkenes and aromatics are affected by a change in feedstock composition to help steer the hydrodeoxygenation reactions.

3.1.3 Experimental methods

3.1.3.1 Feedstock

In this work, two hydrocarbon mixtures, consisting of normal and branched alkanes, were produced through a Neste-patented two-step process[8].

In a first step, triglyceride based biomass is deoxygenated over a NiMo catalyst supported on Al_2O_3 under hydrogen pressure[8]. Sulphur components are added to the inlet stream to keep the catalyst in the sulphided state. This first step essentially produces n-alkanes with minor amounts of by-products, e.g. branched alkanes. Note that the oxygen content can be removed under the form of water (hydrodeoxygenation), carbon monoxide (decarbonylation) and carbon dioxide (decarboxylation)[5]. Oxygen removal by decarbonylation and decarboxylation consumes less hydrogen compared to hydrodeoxygenation but causes the resulting alkane to have one carbon atom less compared to the original fatty acid chain.

In a second step, the mixture of n-alkanes are isomerized over a molecular sieve impregnated with platinum, e.g. Pt/ZSM-22[8]. At medium conversion, the isomerization step is selective towards mono-methyl branching[23, 24]. Methyl branching on the second carbon is preferred, but becomes less pronounced as the carbon chain length of the feed n-alkane increases[24]. At higher conversion/temperature, the selectivity towards multi-branched and cracked products increases[25].

The two obtained hydrocarbon feedstocks were analyzed with a two-dimensional gas chromatograph, equipped with a flame ionization detector and a time-of-flight mass spectrometer. Their compositions are listed in Table 3.1-1. The high fraction of alkanes with an uneven carbon number indicates that a large fraction of the oxygen in the original triglycerides and fatty acids is removed by decarbonylation and decarboxylation reactions. The two mixtures differ in the degree of branching, i.e. hydrocarbon mixture 1 consists of 49wt% branched alkanes while hydrocarbon mixture 2 consists of 89wt% branched alkanes. Unique identification of single, branched, isomers was impossible, even with the utilized advanced analysis equipment[26]. Therefore, branched alkanes with the same number of carbon atoms were quantified as a group.

Table 3.1-1 Composition of the investigated hydrocarbon mixtures

	Hydrocarbon mixture 1		**Hydrocarbon mixture 2**	
#C atoms	branched alkanes (wt%)	normal alkanes (wt%)	branched alkanes (wt%)	normal alkanes (wt%)
5	0.00	0.00	0.01	0.01
6	0.00	0.01	0.07	0.01
7	0.19	0.08	0.08	0.05
8	0.24	0.12	0.24	0.13
9	0.29	0.14	0.65	0.22
10	0.36	0.14	1.02	0.22
11	0.41	0.15	1.15	0.19
12	0.48	0.21	1.23	0.18
13	0.53	0.29	1.42	0.19
14	1.06	0.60	2.06	0.36
15	6.53	6.92	9.46	1.56
16	13.62	16.41	19.35	2.34
17	9.87	7.89	20.95	2.47
18	14.35	17.88	29.93	2.78
19	0.28	0.11	0.62	0.05
20	0.20	0.18	0.58	0.00
21	0.05	0.02	0.10	0.02
22	0.05	0.03	0.11	0.01
23	0.04	0.02	0.04	0.01
24	0.03	0.03	0.04	0.00
25	0.01	0.00	0.00	0.00
26	0.04	0.00	0.00	0.00

3.1.3.2 Bench scale set-up for steam cracking

Steam cracking experiments were performed in a dedicated bench-scale setup. This setup has been described extensively in the past and only a brief discussion is given here[27-29]. The apparatus consists of a feed, reactor and analysis section, see Figure 3.1-2. In the feed section, the hydrocarbon mixture is fed towards an evaporator at 623K using a Coriolis flow meter controlled pump. Water is fed towards an evaporator at 623K using a peristaltic pump. Both gaseous streams are mixed before entering the reactor.

The tubular reactor has an inner diameter of 6 mm, is 1.475m long and is made out of Incoloy 800HT. Heat is provided by an external rectangular furnace. The temperature is measured and controlled by eight thermocouples contained in thermowells positioned in small bends along the length of the reactor, see Figure 3.1-2. The pressure in the reactor was controlled by a

needle valve downstream of the reactor. The pressure drop over the reactor was found to be negligible, below 5kPa.

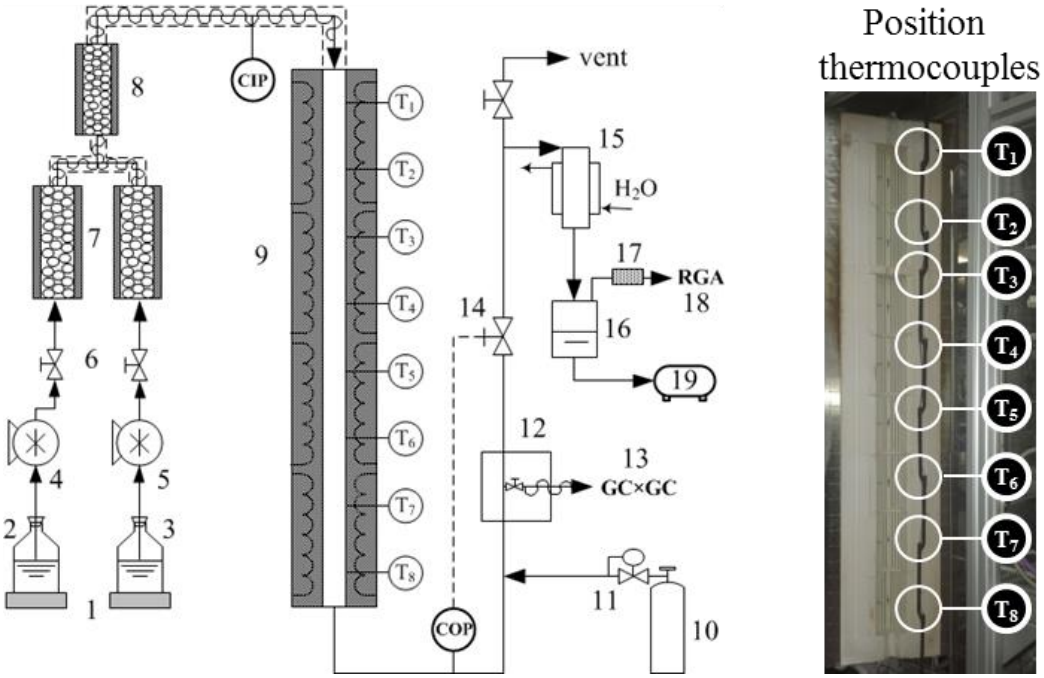

Figure 3.1-2 Schematic overview of the experimental steam cracking set-up and details regarding position of thermocouples. (1: electronic balance, 2: hydrocarbon reservoir, 3: water reservoir, 4: peristaltic pump, 5: water pump, 6: valve, 7: evaporators, 8: mixer, 9: reactor, 10: internal standard, 11 coriolis mass flow controller, 12 heated sampling oven, 13: GC×GC-FID/TOF-MS, 14: outlet pressure restriction valve, 15: water cooled heat exchanger, 16: gas/liquid separator, 17: dehydrator, 18: refinery gas analyzer, 19: condensate drum)

The reactor effluent enters a heated sampling system kept at 623K to avoid condensation. There, a flow of N_2 was added to the reactor effluent, which was used as internal standard. The sampling system is connected with two gas chromatographs. The first gas chromatograph is equipped with two thermal conductivity detectors and one flame ionization detector. It allows quantification of H_2 and C_{4-} hydrocarbons using the known flow rate of the internal standard N_2. The sampling system is also connected with a two-dimensional gas chromatograph, equipped with a flame ionization detector and a time-of-flight mass spectrometer, through a heated transfer line. This analytical device allows identification and quantification of all hydrocarbons in the reactor effluent. Methane, detected and quantified on the first gas chromatograph, was used as secondary internal standard. Response factors of N_2, H_2 and C_{4-} hydrocarbons were determined using a calibration mixture provided by Air Liquide. Response factors of other hydrocarbons were calculated using the effective carbon number approach. The followed procedure showed good repeatability. C and H molar balance closed within 5%.

3.1.4 Modeling methodology

A kinetic model has been developed for the pyrolysis of normal and branched alkanes having 30 carbon atoms or less. The pyrolysis of large alkanes results in the formation of a large number of radicals and products. Common assumptions to constrain the size of the reaction network, without losing accuracy, include the pseudo-steady-state approximation and the μ-hypothesis[15, 28, 30, 31]. The pseudo-steady-state approximation is the mathematical expression that the time rate of change of the concentration of radicals is equal to zero. The μ-hypothesis assumes that for certain radicals bimolecular reactions can be neglected. The μ-hypothesis is typically assumed to be valid for radicals that have six carbon atoms or more, also known as μ-radicals[30, 32].

In this work, the pseudo-steady-state approximation was applied to μ-radicals. Therefore, the developed kinetic model can be split up into two parts. The first part contains reactions that generate radicals for which bimolecular reactions cannot be neglected. This subnetwork is often called the β-network. The second part contains reactions that generate μ-radicals. This subnetwork is often called the μ-network and has been generated automatically using PRIM-O, a network generation tool that applies the pseudo-steady-state approximation and the μ-hypothesis to μ-radicals[32, 33]. These assumptions allow to eliminate the μ-radicals from the model.

Both β- and μ-network are discussed more elaborately in the following section. Also, how the hydrocarbon feedstock is described by the components included in the kinetic model is discussed in the following sections.

3.1.4.1 β-network

The β-network contains kinetic and thermodynamic data for reactions that generate radicals for which bimolecular reactions cannot be neglected, typically radicals having less than six carbon atoms. Therefore, the β-network mostly contains pyrolysis chemistry for relatively small hydrocarbons. In this work, the β-network contains the ethane steam cracking mechanism developed by Sabbe et al. [34] as seed mechanism. Note that reactions that include μ-radicals were removed from the latter mechanism as they are part of the μ-network in this work. A limited number of reactions and species were manually added to the β-network. These include recombination of allylic radicals and recombination of cyclopentadienyl with carbon-centered radicals. Reaction rate coefficients were estimated by analogy with allyl plus allyl[35] and cyclopentadienyl plus methyl[36] respectively.

Furthermore, decomposition chemistry of benzyl was implemented as proposed by da Silva et al.[37]. Note that bimolecular reactions cannot be neglected for the benzyl radical, e.g. recombination with methyl forming ethylbenzene[38], and, hence, it is an exception to the six carbon atom rule.

3.1.4.2 μ-network

The μ-network consists of reactions that form μ-radicals. These reactions have been generated using PRIM-O[32, 33]. The μ-networks contains decomposition reactions, e.g. scission and hydrogen abstraction, for alkanes that have six carbons or more.

3.1.4.2.1 PRIM-O

The PRIM-O algorithm is displayed in Figure 3.1-3. The user of PRIM-O has to provide the structure of the molecule and the reaction family for which kinetic and thermodynamic data has to be generated. Possible reaction families include hydrogen abstraction, radical addition and scission, see Table 3.1-3. The algorithm starts by reacting the molecule with the desired reaction family. PRIM-O generates the product species and radicals, and corresponding kinetic data. Subsequently, PRIM-O reacts each product μ-radical with all defined monomolecular decomposition reaction families, e.g. β-scission. After all μ-radicals are assigned a decomposition path, the pseudo-steady-state approximation is applied to the μ-radicals. This allows to eliminate the μ-radicals from the model, i.e. the μ-radicals are replaced by their product spectrum in the reaction equations.

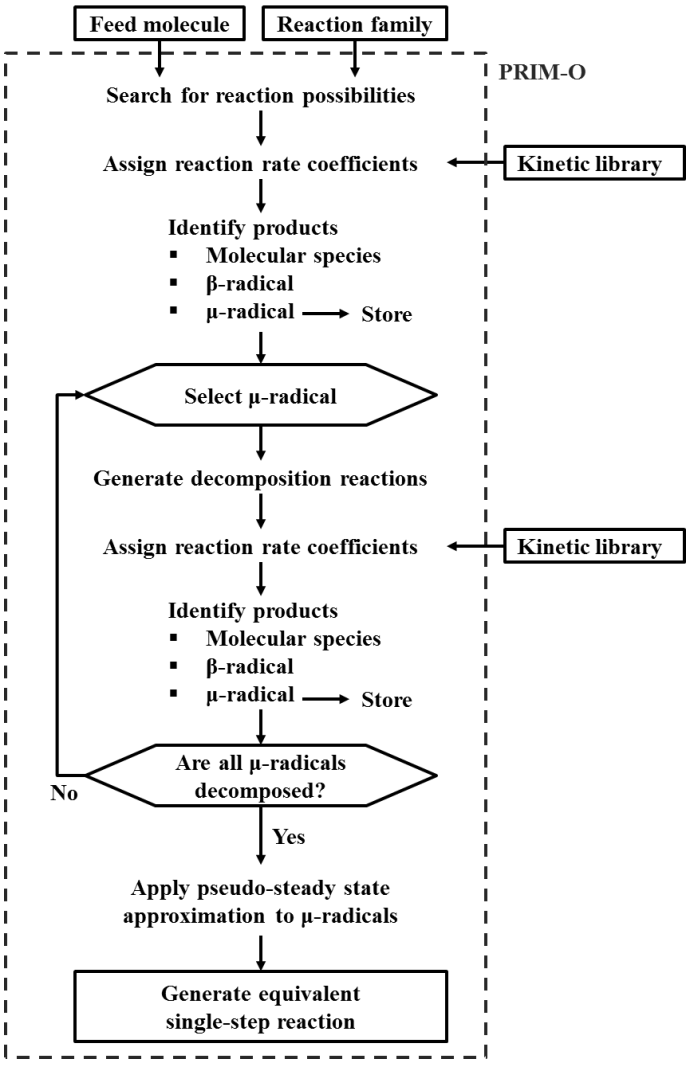

Figure 3.1-3 PRIM-O algorithm

3.1.4.2.2 Example: hydrogen abstraction from 2,4-dimethyl-pentane

Hydrogen abstraction from 2,4-dimethylpentane and its subsequent decomposition in PRIM-O is presented as example in Figure 3.1-4. Seven possible reactive centra for hydrogen abstraction are recognized by PRIM-O forming three different radicals. These radicals have seven carbon atoms and consumption by bimolecular reactions, e.g. recombination with other radicals and addition on C=C double bonds, can be neglected. PRIM-O generates possible unimolecular decomposition reactions for the μ-radicals. In Figure 3.1-4, only C-C β-scission is considered for simplicity. The continuity equations for the species associated with Figure 3.1-4 are listed in Table 3.1-2- equations (1) to (9). When all generated μ-radicals have decomposition paths, PRIM-O applies the pseudo-steady-state approximation to the μ-radicals, in this case the 2,4-dimethylpentane radicals, see Table 3.1-2 - equations (2) to (4). The 2,4-dimethylpentane radical concentrations can be eliminated from equations (5) to (9)

in Table 3.1-2. This procedure allows to describe hydrogen abstraction from 2,4-dimethylpentane and subsequent decomposition by a single equivalent reaction, equation (10) in Table 3.1-2. Note that the stoichiometric coefficients of the products in equation (10) are function of the reaction rate coefficients of the various elementary steps.

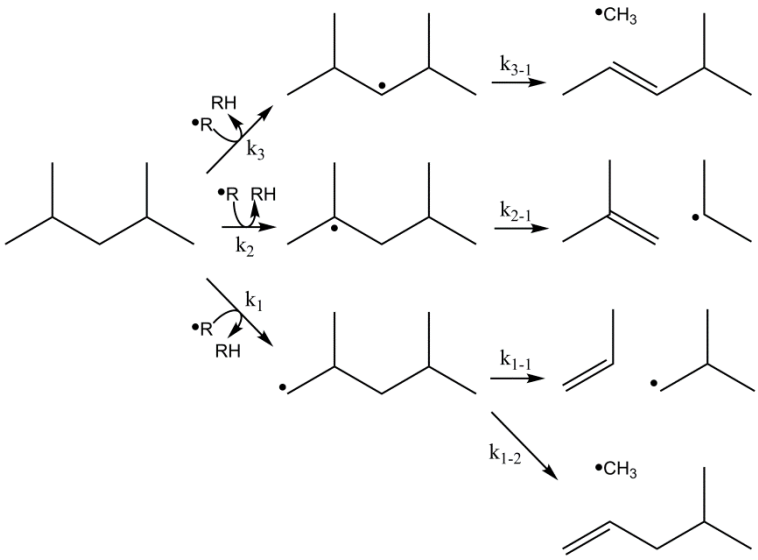

Figure 3.1-4 Hydrogen abstraction from 2,4-dimethyl-pentane and subsequent C-C β-scission reaction

Table 3.1-2 Set of differential equations associated with hydrogen abstraction from 2,4-dimethyl-pentane and subsequent C-C β-scission reaction. The equivalent single step reaction is obtained by applying the pseudo-steady-state approximation to μ-radicals.

Set of differential equations:

$$\frac{dC_{24DMC5}}{dt} = \frac{dC_R}{dt} = -\frac{dC_{RH}}{dt} = -(k_1 + k_2 + k_3)\, C_{24DMC5} C_R \quad (1)$$

$$\frac{dC_{24DMC5-1\bullet}}{dt} = k_1 C_{24DMC5} C_R - (k_{1-1} + k_{1-2}) C_{24DMC5-1\bullet} = 0 \rightarrow C_{24DMC5-1\bullet} = \frac{k_1 C_{24DMC5} C_R}{k_{1-1} + k_{1-2}} \quad (2)$$

$$\frac{dC_{24DMC5-2\bullet}}{dt} = k_2 C_{24DMC5} C_R - k_{2-1} C_{24DMC5-2\bullet} = 0 \rightarrow C_{24DMC5-2\bullet} = \frac{k_2 C_{24DMC5} C_R}{k_{2-1}} \quad (3)$$

$$\frac{dC_{24DMC5-3\bullet}}{dt} = k_3 C_{24DMC5} C_R - k_{3-1} C_{24DMC5-3\bullet} = 0 \rightarrow C_{24DMC5-3\bullet} = \frac{k_3 C_{24DMC5} C_R}{k_{3-1}} \quad (4)$$

$$\frac{dC_{C3H6}}{dt} = \frac{dC_{iC4H9}}{dt} = k_{1-1} C_{24DMC5-1\bullet} = k_1 C_{24DMC5} C_R \frac{k_{1-1}}{k_{1-1} + k_{1-2}} \quad (5)$$

$$\frac{dC_{4M1C5}}{dt} = k_{1-2} C_{24DMC5-1\bullet} = k_1 C_{24DMC5} C_R \frac{k_{1-2}}{k_{1-1} + k_{1-2}} \quad (6)$$

$$\frac{dC_{iC4H8}}{dt} = \frac{dC_{iC3H7}}{dt} = k_{2-1} C_{24DMC5-2\bullet} = k_2 C_{24DMC5} C_R \quad (7)$$

$$\frac{dC_{4M2C5}}{dt} = k_{3-1} C_{24DMC5-3\bullet} = k_3 C_{24DMC5} C_R \quad (8)$$

$$\frac{dC_{CH3}}{dt} = k_{1-2} C_{24DMC5-1\bullet} + k_{3-1} C_{24DMC5-3\bullet} = k_1 C_{24DMC5} C_R \frac{k_{1-2}}{k_{1-1} + k_{1-2}} + k_3 C_{24DMC5} C_R \quad (9)$$

(10)

Equivalent single step reaction:

$$24DMC5 + R \xrightarrow{k_1+k_2+k_3} \frac{k_1}{k_1+k_2+k_3}\frac{k_{1-1}}{k_{1-1}+k_{1-2}}(C_3H_6 + iC_4H_9) + \frac{k_1}{k_1+k_2+k_3}\frac{k_{1-2}}{k_{1-1}+k_{1-2}}4M1C5$$
$$+ \frac{k_2}{k_1+k_2+k_3}(iC_4H_8 + iC_3H_7) + \frac{k_3}{k_1+k_2+k_3}4M2C5$$
$$+ \left(\frac{k_1}{k_1+k_2+k_3}\frac{k_{1-1}}{k_{1-1}+k_{1-2}} + \frac{k_3}{k_1+k_2+k_3}\right)CH_3 + RH$$

3.1.4.2.3 Kinetic data

Reactions that are generated by PRIM-O can be divided in two groups, i.e. reactions that produce μ-radicals and reactions that consume μ-radicals. Reaction families that belong to the first group include C-C-scission, hydrogen abstraction by carbon-centered radicals, hydrogen abstraction by hydrogen atoms, carbon-centered radical addition on C=C double bonds and hydrogen atom addition on C=C double bonds. Reaction families that belong to the second group include C-C β-scission, C-H β-scission, intramolecular hydrogen abstraction and intramolecular radical addition.

Table 3.1-3 Reaction families in PRIM-O

Reaction family	Reaction template	Methodology	Ref.
Formation of μ-radicals			
Bond scission			
C-C	C_1-C_2 → •C_1 + •C_2	Rate rules	[39]
C-H	C_1-H → •C_1 + •H	Rate rules	[39]
Intermolecular hydrogen abstraction			
by •C	C_1-H + •C_2 → •C_1 + C_2-H	Group additivity	[40]
by •H	C_1-H + •H → •C_1 + H_2	Group additivity	[41]
Intermolecular radical addition			
by •C	C_1=C_2 + •C_3 → •C_1-C_2-C_3	Group additivity	[42]
by •H	C_1=C_2 + •H → •C_1-C_2-H	Group additivity	[43]
Decomposition of μ-radicals			
β-scission			
C-C	•C_1-C_2-C_3 → C_1=C_2 + •C_3	Group additivity	[42]
C-H	•C_1-C_2-H → C_1=C_2 + •H	Group additivity	[43]
Intramolecular hydrogen abstraction	•C_1-(C)n-C_2-H → H-C_1-$(C)_n$-C_2•	Rate rules	[44, 45]
Intramolecular radical addition			
endo	•C_1-$(C)_n$-C_2=C_3→ cy(C_1-$(C)_n$-C_2•-C_3)	Rate rules	[44]
exo	•C_1-$(C)_n$-C_2=C_3→ cy(C_1-$(C)_n$-C_2)-C_3•	Rate rules	[44]

Kinetic data for intermolecular hydrogen abstraction by carbon-centered radicals, intermolecular hydrogen abstraction by hydrogen atoms, carbon-centered β-scission / intermolecular radical addition by carbon-centered radicals on C=C double bonds and hydrogen-centered β-scission / intermolecular hydrogen atom addition on C=C double bonds were estimated using the comprehensive group additive framework developed by Marin and

coworkers[46]. Reaction rate coefficients for scission of hydrocarbons were estimated using the rate rules proposed by Mehl et al.[30, 39]. Reaction rate coefficients for intramolecular hydrogen abstraction and intramolecular radicals addition were estimated using the reactivity-structure-based rate estimate rules developed by Wang et al.[44, 45].

3.1.4.2.4 Thermodynamic data

Thermodynamic data were estimated using Benson's group additivity method[47]. NASA polynomials were generated using Genesys's ThermoGenerator[48].

3.1.4.3 Modeling hydrocarbon feedstock composition

The use of the developed microkinetic model requires a detailed molecular feedstock composition. As explained in section 3.1.3.1, it was not possible to identify and quantify each branched alkane individually. Martens et al. investigated the isomerization of C_8 to C_{24} alkanes over a Pt/H-ZSM-22 catalyst, the same catalyst used in this work, and obtained the distribution of the resulting branched alkanes for each carbon number[24]. The same distribution of branched alkanes is assumed in this work in order to "reconstruct" the detailed molecular composition of the hydrocarbon mixtures. For example, the distribution of C_{18} branched alkanes is 25.6% 2-methyl-heptadecane, 17.4% 3-methyl-heptadecane, 8.5% 4-methyl-heptadecane, 10.6% 5-methyl-heptadecane, 9% 6-methyl-heptadecane, 11.8% 7-methyl-heptadecane, 11.6% 8-methyl-heptadecane and 5.5% 9-methyl-heptadecane.

3.1.5 Results and discussion

3.1.5.1 Experimental results

Steam cracking of the paraffinic mixtures was performed at a constant pressure of 0.17 MPa and a constant hydrocarbon mass flow rate of 4.17 10^{-2} g s^{-1}. The temperature in the reactor was varied between 1053 and 1133K. Water was used as diluent. Two dilutions were investigated, i.e. $\delta=F_{m,H2O}/F_{m,HC}$=0.5 and 0.35.

Eighty species were detected and quantified in the reactor effluent. The conversion of normal and branched alkanes is over 90% in the investigated conditions. A number of product profiles are presented in Figure 3.1-5 (steam cracking of hydrocarbon mixture 1) and Figure 3.1-6 (steam cracking of hydrocarbon mixture 2). The presented species have high yields during steam cracking and/or are important aromatics in the reactor effluent.

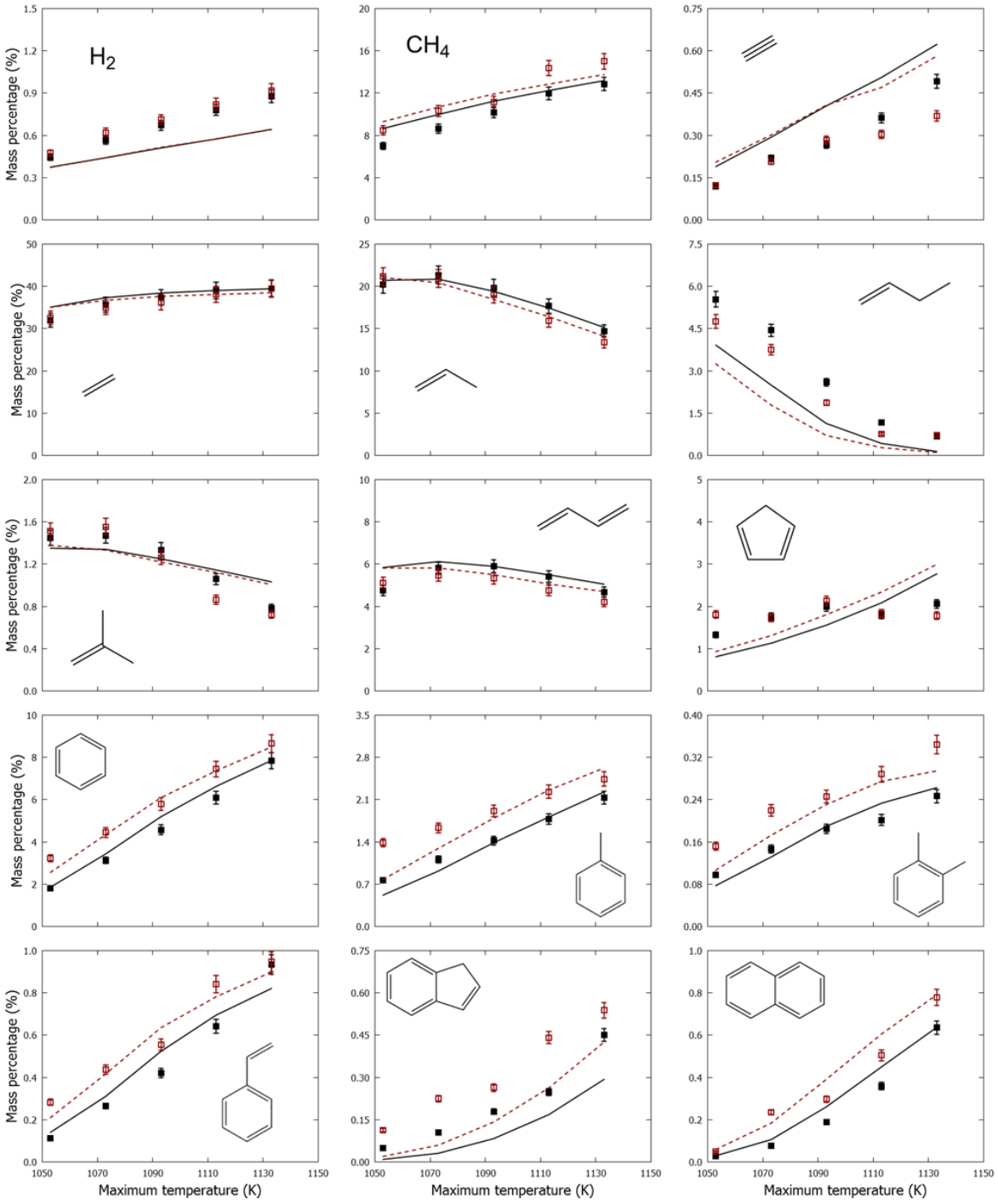

Figure 3.1-5 Mass fraction profiles of as a function of maximum temperature in the tubular reactor for steam cracking of hydrocarbon mixture 1 (see Table 3.1-1); P=0.17MPa, F_{HC}=4.17 10^{-2} g s^{-1}; symbols, experimental mole fraction profile of molecule represented in graph (filled black, F_{H2O}=2.08 10^{-2} g s^{-1} – open red, F_{H2O}=1.44 10^{-2} g s^{-1}); lines, mole fraction profiles calculated with CHEMKIN using the plug flow reactor model and the developed kinetic model (full black, F_{H2O}=2.08 10^{-2} g s^{-1} – dashed red, FH2O=1.44 10^{-2} g s^{-1})

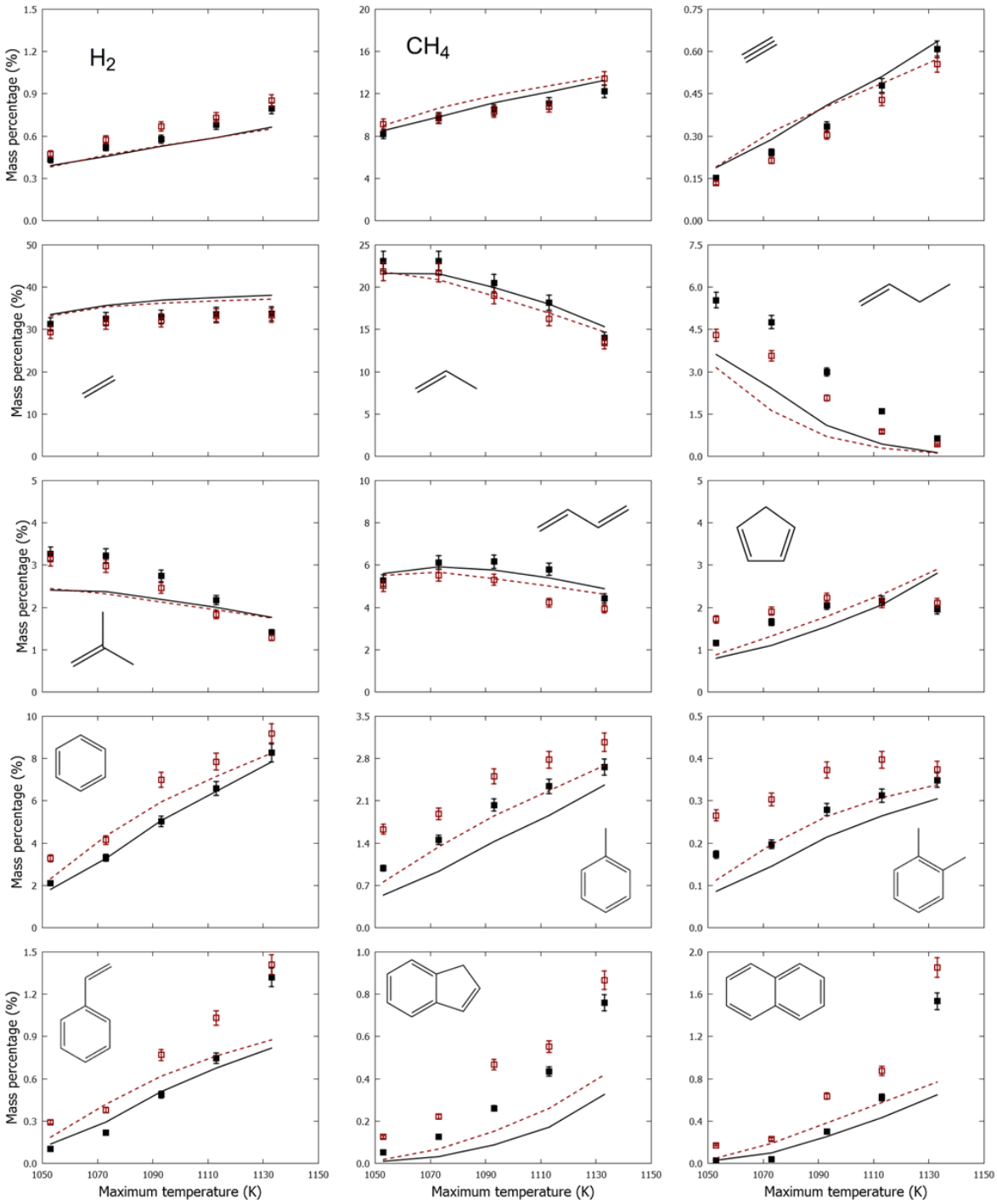

Figure 3.1-6 Mass fraction profiles of as a function of maximum temperature in the tubular reactor for steam cracking of hydrocarbon mixture 2 (see Table 3.1-1); P=0.17MPa, F_{HC}=4.17 10^{-2} g s^{-1}; symbols, experimental mole fraction profile of molecule represented in graph (filled black, F_{H2O}=2.08 10^{-2} g s^{-1} – open red, F_{H2O}=1.44 10^{-2} g s^{-1}); lines, mole fraction profiles calculated with CHEMKIN using the plug flow reactor model and the developed kinetic model (full black, F_{H2O}=2.08 10^{-2} g s^{-1} – dashed red, FH2O=1.44 10^{-2} g s^{-1})

Steam cracking of the investigated hydrocarbon mixtures has a high selectivity towards small alkenes. Hydrocarbon mixture 1 has a maximum ethene yield of 40wt% and a maximum propene yield of 21wt%. Hydrocarbon mixture 2 has a maximum ethene yield of 34wt% and a maximum propene yield of 23wt%. The isobutene yield of hydrocarbon mixture 2 is approximately twice as high compared to the isobutene yield of hydrocarbon mixture 1. Differences in the selectivities to the alkenes of the hydrocarbon mixtures can be attributed to change in degree of branching[14]. Under comparable operating conditions, fossil naphtha has a maximum ethene yield of 32 wt% and a maximum propene yield of 18wt%[13, 28].

The selectivities to aromatics increases at higher temperatures and higher hydrocarbon partial pressures. The yield of aromatics is higher during steam cracking of hydrocarbon mixture 2 compared to steam cracking of hydrocarbon mixture 1.

3.1.5.2 Model performance and reaction path analysis

Model calculated mass fraction profiles have been added to Figure 3.1-5 and Figure 3.1-6. The model is in good agreement with the experimental data. Note that no kinetic parameter was fit to improve model performance. The main discrepancies can be observed for 1-butene, which is underpredicted, and molecular hydrogen, however the differences are still within 25%. The model calculated slope of the molecular hydrogen profile is smaller than the experimental slope.

The normal and branched alkanes are mainly consumed by hydrogen abstraction reactions. Hydrogen abstraction from tertiary carbon atoms is favored over hydrogen abstraction from secondary carbon atoms which, in turn, is favored over hydrogen abstraction from primary carbon atoms[40]. The resulting alkyl radicals mainly react by C-C β-scission. In the case of normal alkanes, this reaction path causes high ethene selectivity. In the case of branched alkanes, the alkyl branch is incorporated in the alkene formed following C-C β-scission, e.g. methyl branching will result in propene formation. As mentioned earlier, the majority of branched alkanes are 2-methyl-alkanes. Hydrogen abstraction from the tertiary carbon atom and subsequent C-C β-scission forms isobutene and an alkyl radical.

The pyrolysis of alkanes forms large 1-alkenes. 1-alkenes with five or more carbon atoms can react by retro-ene reactions forming propene and a smaller 1-alkene[49]. Scission of the weak allylic bond in 1-alkenes forms an alkyl radical and an allyl radical. Retro-ene and hydrogen abstraction by allyl radicals are important reaction paths to propene in the investigated operating conditions, in line with earlier work[13, 28].

The aforementioned discussion provides guidelines regarding the ideal feedstock composition as function of desired product composition. Maximum propene and isobutene yields are obtained with a high degree of branching while maximum ethene yields are obtained with a low degree of branching.

3.1.5.3 Formation of substituted aromatics

In the pyrolysis of alkanes, aromatics are formed by secondary reactions[49]. Aromatic formation pathways are presented in Figure 3.1-7. Note that some elementary steps were grouped to constrain the size of the figure. The formation of aromatics starts with the consumption of small alkenes such as propene, 1-butene and isobutene. These species form resonantly stabilized radicals upon hydrogen abstraction.

Consumption of allyl by recombination with other radicals is favored over C-H β-scission to allene. The self-recombination of allyl forms 1,5-hexadiene. Hexa-2,5-dien-1-yl is formed following hydrogen abstraction from 1,5-hexadiene and addition of vinyl on 1,3-butadiene. The hexa-2,5-dien-1-yl radical plays an important role in the formation of aromatics[50, 51]. It can form benzene by endo intramolecular radical addition to a six-membered ring and subsequent dehydrogenation steps. Alternatively, hexa-2,5-dien-1-yl can form cyclopentadiene by intramolecular hydrogen abstraction to hexa-2,4-dien-1-yl, endo intramolecular radical addition to a five-membered ring and C-C β-scission of the methyl side group. Note that in the investigated operating conditions cyclopentadiene is mainly formed by intramolecular radical addition of penta-1,4-dien-1-yl, formed by addition of allyl on acetylene, and penta-2,4-dien-1-yl, formed by hydrogen abstraction from 1,3-pentadiene and 1,4-pentadiene, followed by C-H β-scission.

The kinetic model predicts that substituted aromatics are formed through similar reaction pathways as benzene. Several reaction paths to toluene have been added to Figure 3.1-7 based on a rate of production analysis. Butenyl radicals can recombine with allyl forming heptadienes. Subsequent hydrogen abstraction leads to resonantly stabilized heptadienyl radicals that can react by endo intramolecular radical addition to methyl-cyclohexenyl radicals. The latter radicals can form toluene, by dehydrogenation reactions, and benzene, by dehydrogenation reactions and β-scission of the methyl side group. The resonantly stabilized heptadienyl radicals can also be formed by addition of the vinylic prop-1-en-1-yl and prop-1-en-2-yl radicals on 1,3-butadiene, addition of vinyl on 1,3-pentadiene and addition of allyl on

1,3-butadiene. The addition of vinylic and allylic radicals on 1,3-dienes is important as the formed adduct is resonantly stabilized.

Aromatics are also formed from cyclopentadienyl. Cyclopentadienyl may recombine with other carbon centered radicals. The resulting adduct can undergo hydrogen abstraction and ring enlargement to a six-membered ring, through a bicyclic intermediate[52-54]. The reaction route leads to benzene, toluene and styrene in the case of recombination of cyclopentadienyl with methyl, ethyl and allyl respectively.

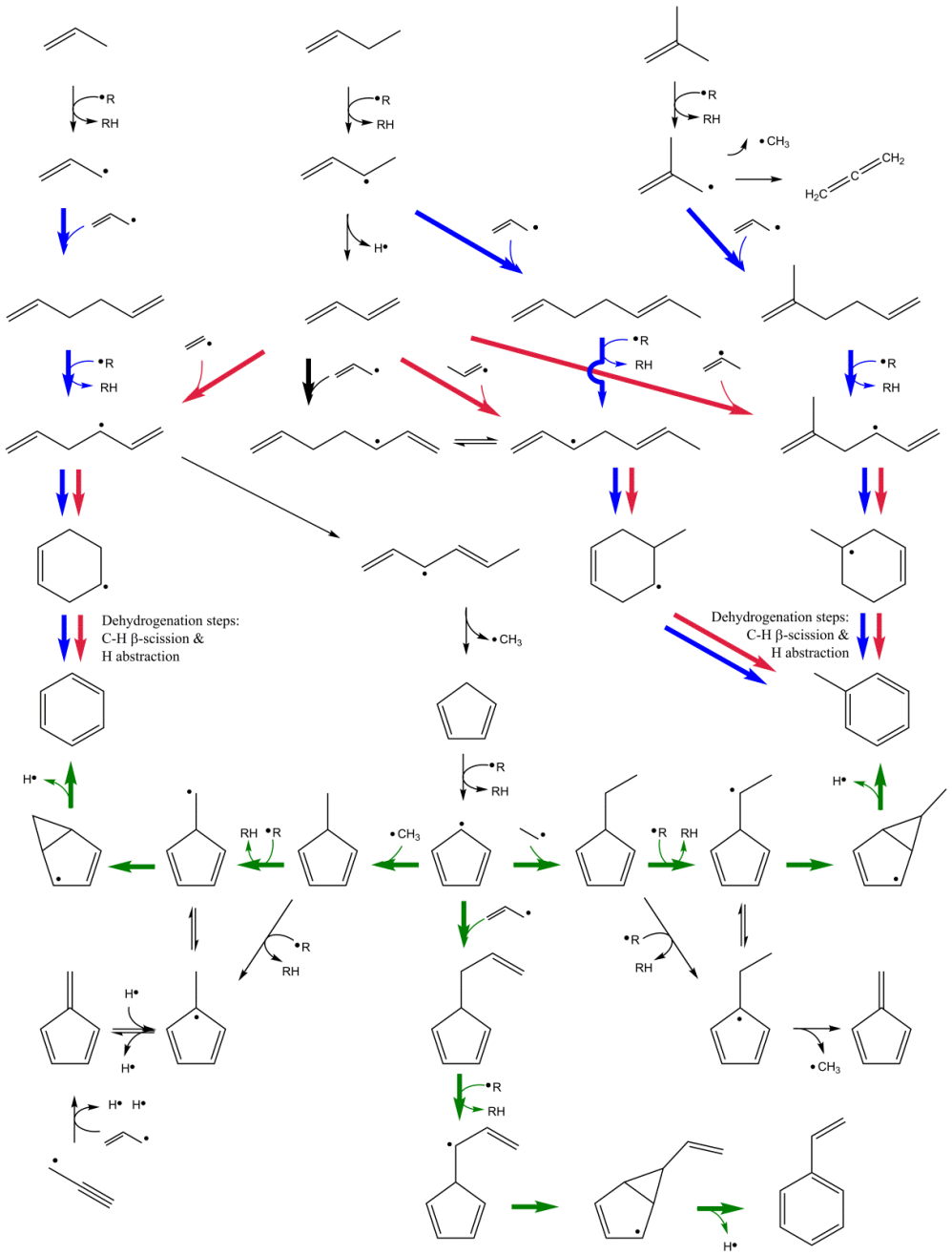

Figure 3.1-7 Reaction path analysis for steam cracking of hydrocarbon mixture 1 (see Table 3.1-1) starting from propene, 1-butane and 1,3-butadiene to benzene, toluene and styrene at P=0.17MPa, T=1093K, F_{HC}=4.17 10^{-2} g s^{-1}

In short, there are three important formation paths that lead to aromatics, i.e. recombination of allylic radicals followed by hydrogen abstraction, addition of vinylic and allylic radicals on dienes and recombination of cyclopentadienyl with carbon-centered radicals. The importance of each pathway depends on the operating conditions and the specific aromatic compound. Note that the reaction paths displayed in Figure 3.1-7 start from the consumption of propene and butenes. As hydrocarbon mixture 2 has a higher selectivity to these alkenes, a higher aromatic yield is expected and obtained in comparison to hydrocarbon mixture 1. Hence, changing operating conditions of the catalytic upgrading step of triglyceride-based biomass, preceding steam cracking, that result in an increase/decrease in branching will result in an increase/decrease of aromatic yield following steam cracking.

A rate of production analysis with respect to benzene and toluene was performed for steam cracking of hydrocarbon mixture 1 at 1093K. The rates of production of the most important reactions are presented in Figure 3.1-8 and Figure 3.1-9 as function of axial coordinate. At the investigated operating conditions, over 90% of the hydrocarbon mixture is converted in the first 20cm of the reactor. Radical concentration is highest in this zone, as it is very sensitive to scission of C-C bonds of the feedstock. As all reactions displayed in Figure 3.1-8 and Figure 3.1-9 involve the consumption of radicals, a maximum in rate of production is observed in the first 20cm of the reactor.

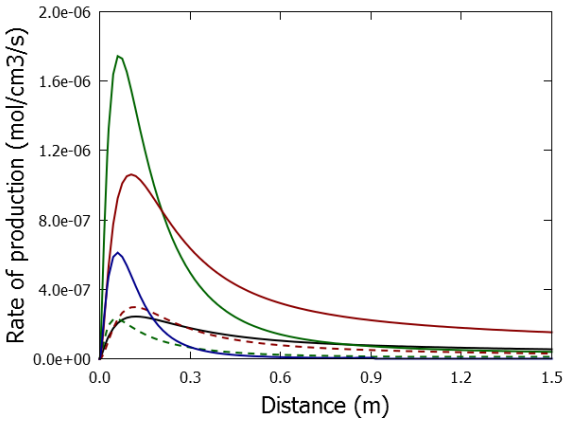

Figure 3.1-8 Rate of production plot with respect to benzene for steam cracking of hydrocarbon mixture 1 (see Table 3.1-1) as a function of axial coordinate at P=0.17MPa, T=1093K, F_{HC}=4.17 10^{-2} g s^{-1}; ——- C≡CC•+C=CC•, ——- C=CC=C+C=C•, - - - - - C=CC=C+C=CC•, ——- hydrogen abstraction from methyl-1,3-cyclopentadiene, - - - - hydrogen abstraction from ethyl-1,3-cyclopentadiene, ——- hydrogen abstraction from 1,5-hexadiene (formed by self-recombination of allyl radicals)

Benzene is mainly formed by the reaction path starting with recombination of methyl and cyclopentadienyl (beginning of the reactor) and addition of vinyl on 1,3-butadiene (middle

and end of the reactor), see Figure 3.1-8. Self-recombination of allyl followed by hydrogen abstraction is an important formation channel in the first 20 cm of the reaction. Minor benzene formation pathways that are displayed in Figure 3.1-8 start with recombination of allyl plus propargyl, recombination of ethyl with cyclopentadienyl and addition of allyl on butadiene. Note that the latter two pathways involve the loss of methyl in the subsequent cyclization and decomposition reactions.

Addition of allyl on butadiene is the main toluene producing channel, see Figure 3.1-9. Other addition reactions displayed in Figure 3.1-9 are vinyl plus 2-methyl-1,3-butadiene, addition of but-1en-3-yl on 1,3-butadiene and addition of prop-1-en-2-yl plus butadiene. The recombination of ethyl with cyclopentadienyl is relatively less important for toluene production compared to recombination of methyl with cyclopentadienyl for benzene production. As presented in Figure 3.1-7, hydrogen abstraction from ethyl-cyclopentadiene and decomposition to toluene plus H is in competition with hydrogen abstraction from ethyl-cyclopentadiene and β-scission to fulvene plus methyl radical. Furthermore, the consumption of ethyl by recombination with cyclopentadienyl is in competition with its unimolecular decomposition to ethene plus hydrogen atom.

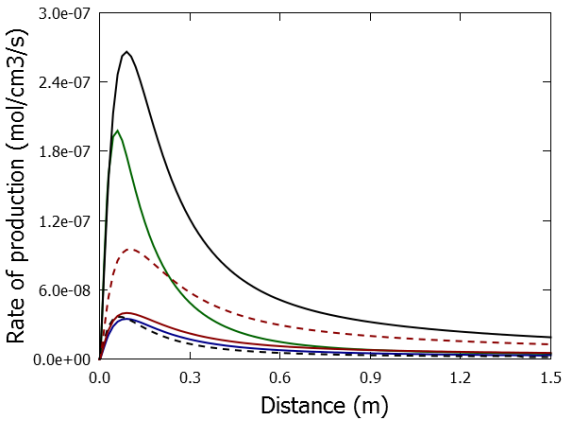

Figure 3.1-9 Rate of production plots with respect to toluene for steam cracking of hydrocarbon mixture 1 (see Table 3.1-1) as a function of axial coordinate at P=0.17MPa, T=1093K, F_{HC}=4.17 10^{-2} g s^{-1}; ——- C=CC=C+C=CC•, - - - - - C=CC=C+C=CC•C, ——- C=C(C)C=C+C=C•, - - - - - C=CC=C+C=C•C, ——- hydrogen abstraction from ethyl-1,3-cyclopentadiene, ——- hydrogen abstraction from 1,5-heptadiene (formed by recombination of allyl with 1-buten-3-yl)

3.1.6 Conclusions

The two-step process (i) deoxygenation of triglyceride based biomass and (ii) steam cracking of the resulting hydrocarbons is a promising production route for bio-derived base chemicals. The main focus is on the second step in this work.

Steam cracking of two hydrocarbon mixtures, produced through deoxygenation of triglycerides, was found to have a high selectivity to small alkenes, higher than conventional petroleum derived naphthas. The hydrocarbon mixture with the highest degree of branching had lower ethene yields but higher propene and isobutene yields compared to the hydrocarbon mixture with the lowest degree of branching.

Experimental mass fraction profiles are in good agreement with calculated mass fraction profiles using a newly developed kinetic model for these specific feeds. Small alkenes are formed by typical hydrogen abstraction, β-scission chemistry. Reaction paths to aromatics are more complex and involve secondary reactions that consume these small alkenes. The hydrocarbon mixture with the highest degree of branching has the highest yield of aromatics. This is caused by the higher yield of propene and butenes which are consumed forming resonantly-stabilized radicals. The latter radicals have a higher lifetime than non-resonantly-stabilized radicals and can therefore react with other species leading to molecular growth.

Guidelines for operating conditions in the catalytic deoxygenation of triglyceride based biomass can be summarized as follows: propene, isobutene and aromatic yields following steam cracking can be maximized by increasing branching while ethene yields following steam cracking can be maximized by decreasing branching.

3.1.7 References

[1] E. de Jong, A. Higson, P. Walsh, M. Wellisch, Product developments in the bio-based chemicals arena, Biofuels, Bioproducts and Biorefining 6 (2012) 606-624
[2] P. S. Nigam, A. Singh, Production of liquid biofuels from renewable resources, Prog. Energy Combust. Sci. 37 (2011) 52-68
[3] L. Shen, E. Worrell, M. Patel, Present and future development in plastics from biomass, Biofuels, Bioproducts and Biorefining 4 (2010) 25-40
[4] F. Ma, M. A. Hanna, Biodiesel production: a review, Bioresour. Technol. 70 (1999) 1-15
[5] R. W. Gosselink, S. A. W. Hollak, S.-W. Chang, J. van Haveren, K. P. de Jong, J. H. Bitter, D. S. van Es, Reaction Pathways for the Deoxygenation of Vegetable Oils and Related Model Compounds, ChemSusChem 6 (2013) 1576-1594
[6] S.-Y. No, Application of hydrotreated vegetable oil from triglyceride based biomass to CI engines – A review, Fuel 115 (2014) 88-96
[7] A. Vonortas, N. Papayannakos, Comparative analysis of biodiesel versus green diesel, Wiley Interdisciplinary Reviews: Energy and Environment 3 (2014) 3-23
[8] J. Myllyoja, P. Aalto, P. Savolainen, V. M. Purola, V. Alopaeus, J. Gronqvist Process for the manufacture of diesel range hydrocarbons. 2015.
[9] T. Kalnes, T. Marker, D. R. Shonnard, K. P. Koers, Green diesel production by hydrorefining renewable feedstocks, Biofuels (2008)
[10] Axens, Axens' technologies, products and services (2015)
[11] R. Kotrba, A Transformative Project: Total's La Mède Conversion, Biomass Magazine (2015)
[12] I. Kubičková, D. Kubička, Utilization of Triglycerides and Related Feedstocks for Production of Clean Hydrocarbon Fuels and Petrochemicals: A Review, Waste and Biomass Valorization 1 (2010) 293-308
[13] T. Dijkmans, S. P. Pyl, M.-F. Reyniers, R. Abhari, K. M. Van Geem, G. B. Marin, Production of bio-ethene and propene: alternatives for bulk chemicals and polymers, Green Chem. 15 (2013) 3064-3076

[14] P. Zámostný, Z. Bělohlav, L. Starkbaumová, J. Patera, Experimental study of hydrocarbon structure effects on the composition of its pyrolysis products, J. Anal. Appl. Pyrolysis 87 (2010) 207-216
[15] K. M. Van Geem, M.-F. Reyniers, G. B. Marin, Challenges of modeling steam cracking of heavy feedstocks, Oil. Gas. Sci. Technol. 63 (2008) 79-94
[16] P. Zámostný, A. Karaba, N. Olahová, J. Petrů, J. Patera, E. Hájeková, M. Bajus, Z. Bělohlav, Generalized model of n-heptane pyrolysis and steam cracking kinetics based on automated reaction network generation, J. Anal. Appl. Pyrolysis 109 (2014) 159-167
[17] M. Zeng, W. Yuan, Y. Wang, W. Zhou, L. Zhang, F. Qi, Y. Li, Experimental and kinetic modeling study of pyrolysis and oxidation of n-decane, Combust. Flame 161 (2014) 1701-1715
[18] T. Malewicki, K. Brezinsky, Experimental and modeling study on the pyrolysis and oxidation of n-decane and n-dodecane, P. Combust. Inst. 34 (2013) 361-368
[19] S. Banerjee, R. Tangko, D. A. Sheen, H. Wang, C. T. Bowman, An experimental and kinetic modeling study of n-dodecane pyrolysis and oxidation, Combust. Flame 163 (2016) 12-30
[20] S. Li, S. M. Sarathy, D. F. Davidson, R. K. Hanson, C. K. Westbrook, Shock tube and modeling study of 2,7-dimethyloctane pyrolysis and oxidation, Combust. Flame 162 (2015) 2296-2306
[21] S. M. Sarathy, T. Javed, F. Karsenty, A. Heufer, W. Wang, S. Park, A. Elwardany, A. Farooq, C. K. Westbrook, W. J. Pitz, M. A. Oehlschlaeger, G. Dayma, H. J. Curran, P. Dagaut, A comprehensive combustion chemistry study of 2,5-dimethylhexane, Combust. Flame 161 (2014) 1444-1459
[22] S. M. Sarathy, C. K. Westbrook, M. Mehl, W. J. Pitz, C. Togbe, P. Dagaut, H. Wang, M. A. Oehlschlaeger, U. Niemann, K. Seshadri, P. S. Veloo, C. Ji, F. N. Egolfopoulos, T. Lu, Comprehensive chemical kinetic modeling of the oxidation of 2-methylalkanes from C-7 to C-20, Combust. Flame 158 (2011) 2338-2357
[23] C. S. Laxmi Narasimhan, J. W. Thybaut, G. B. Marin, P. A. Jacobs, J. A. Martens, J. F. Denayer, G. V. Baron, Kinetic modeling of pore mouth catalysis in the hydroconversion of n-octane on Pt-H-ZSM-22, J. Catal. 220 (2003) 399-413
[24] J. A. Martens, G. Vanbutsele, P. A. Jacobs, J. Denayer, R. Ocakoglu, G. Baron, J. A. Muñoz Arroyo, J. Thybaut, G. B. Marin, Evidences for pore mouth and key–lock catalysis in hydroisomerization of long n-alkanes over 10-ring tubular pore bifunctional zeolites, Catal. Today 65 (2001) 111-116
[25] J. A. Martens, D. Verboekend, K. Thomas, G. Vanbutsele, J. Pérez-Ramírez, J.-P. Gilson, Hydroisomerization and hydrocracking of linear and multibranched long model alkanes on hierarchical Pt/ZSM-22 zeolite, Catal. Today 218–219 (2013) 135-142
[26] K. M. Van Geem, S. P. Pyl, M.-F. Reyniers, J. Vercammen, J. Beens, G. B. Marin, On-line analysis of complex hydrocarbon mixtures using comprehensive two-dimensional gas chromatography, J. Chromatogr. A 1217 (2010) 6623-6633
[27] M. R. Harper, K. M. Van Geem, S. P. Pyl, G. B. Marin, W. H. Green, Comprehensive reaction mechanism for n-butanol pyrolysis and combustion, Combust. Flame 158 (2011) 16-41
[28] R. De Bruycker, J. M. Anthonykutty, J. Linnekoski, A. Harlin, J. Lehtonen, K. M. Van Geem, J. Räsänen, G. B. Marin, Assessing the Potential of Crude Tall Oil for the Production of Green-Base Chemicals: An Experimental and Kinetic Modeling Study, Ind. Eng. Chem. Res. 53 (2014) 18430-18442
[29] S. P. Pyl, C. M. Schietekat, K. M. Van Geem, M.-F. Reyniers, J. Vercammen, J. Beens, G. B. Marin, Rapeseed oil methyl ester pyrolysis: On-line product analysis using comprehensive two-dimensional gas chromatography, J. Chromatogr. A 1218 (2011) 3217-3223
[30] M. Dente, G. Bozzano, T. Faravelli, A. Marongiu, S. Pierucci, E. Ranzi, Kinetic Modelling of Pyrolysis Processes in Gas and Condensed Phase, Adv. Chem. Eng. 32 (2007) 51-166
[31] E. Ranzi, M. Dente, S. Plerucci, G. Biardi, Initial product distributions from pyrolysis of normal and branched paraffins, Ind. Eng. Chem. Fund. 22 (1983) 132-139
[32] R. De Bruycker, S. P. Pyl, M.-F. Reyniers, K. M. Van Geem, G. B. Marin, Microkinetic model for the pyrolysis of methyl esters: From model compound to industrial biodiesel, AlChE J. 61 (2015) 4309-4322
[33] P. J. Clymans, G. F. Froment, Computer generation of the reaction paths and rate equations in the thermal cracking of normal and branched paraffins, Comput. Chem. Eng. 8 (1984) 137-142
[34] M. K. Sabbe, K. M. Van Geem, M.-F. Reyniers, G. B. Marin, First principle-based simulation of ethane steam cracking, AlChE J. 57 (2011) 482-496
[35] A. Fridlyand, P. T. Lynch, R. S. Tranter, K. Brezinsky, Single Pulse Shock Tube Study of Allyl Radical Recombination, J. Phys. Chem. A 117 (2013) 4762-4776
[36] S. Sharma, W. H. Green, Computed Rate Coefficients and Product Yields for c-C(5)H(5) + CH(3) -> Products, J. Phys. Chem. A 113 (2009) 8871-8882
[37] G. da Silva, J. A. Cole, J. W. Bozzelli, Kinetics of the Cyclopentadienyl + Acetylene, Fulvenallene + H, and 1-Ethynylcyclopentadiene + H Reactions, The Journal of Physical Chemistry A 114 (2010) 2275-2283
[38] W. Yuan, Y. Li, P. Dagaut, J. Yang, F. Qi, Investigation on the pyrolysis and oxidation of toluene over a wide range conditions. I. Flow reactor pyrolysis and jet stirred reactor oxidation, Combust. Flame 162 (2015) 3-21

[39] M. Mehl, G. Vanhove, W. J. Pitz, E. Ranzi, Oxidation and combustion of the n-hexene isomers: A wide range kinetic modeling study, Combust. Flame 155 (2008) 756-772
[40] M. K. Sabbe, A. Vandeputte, M.-F. Reyniers, M. Waroquier, G. B. Marin, Modeling the influence of resonance stabilization on the kinetics of hydrogen abstractions, Phys. Chem. Chem. Phys. 12 (2010) 1278-1298
[41] P. D. Paraskevas, M. K. Sabbe, M.-F. Reyniers, N. G. Papayannakos, G. B. Marin, Group Additive Kinetics for Hydrogen Transfer Between Oxygenates, J. Phys. Chem. A (2015)
[42] M. K. Sabbe, M.-F. Reyniers, V. Van Speybroeck, M. Waroquier, G. B. Marin, Carbon-centered radical addition and beta-scission reactions: Modeling of activation energies and pre-exponential factors, ChemPhysChem 9 (2008) 124-140
[43] M. K. Sabbe, M.-F. Reyniers, M. Waroquier, G. B. Marin, Hydrogen Radical Additions to Unsaturated Hydrocarbons and the Reverse beta-Scission Reactions: Modeling of Activation Energies and Pre-Exponential Factors, ChemPhysChem 11 (2010) 195-210
[44] K. Wang, S. M. Villano, A. M. Dean, Reactivity–Structure-Based Rate Estimation Rules for Alkyl Radical H Atom Shift and Alkenyl Radical Cycloaddition Reactions, J. Phys. Chem. A 119 (2015) 7205-7221
[45] K. Wang, S. M. Villano, A. M. Dean, The Impact of Resonance Stabilization on the Intramolecular Hydrogen-Atom Shift Reactions of Hydrocarbon Radicals, Chemphyschem 16 (2015) 2635-2645
[46] R. Van de Vijver, N. M. Vandewiele, P. L. Bhoorasingh, B. L. Slakman, F. Seyedzadeh Khanshan, H.-H. Carstensen, M.-F. Reyniers, G. B. Marin, R. H. West, K. M. Van Geem, Automatic Mechanism and Kinetic Model Generation for Gas- and Solution-Phase Processes: A Perspective on Best Practices, Recent Advances, and Future Challenges, Int. J. Chem. Kinet. 47 (2015) 199-231
[47] S. W. Benson, Thermochemical Kinetics: Methods for the Estimation of Thermochemical Data and Rate Parameters, John Wiley & Sons, New York, 1976
[48] N. M. Vandewiele, K. M. Van Geem, M.-F. Reyniers, G. B. Marin, Genesys: Kinetic model construction using chemo-informatics, Chem. Eng. J. 207 (2012) 526-538
[49] O. Herbinet, P. M. Marquaire, F. Battin-Leclerc, R. Fournet, Thermal decomposition of n-dodecane: Experiments and kinetic modeling, J. Anal. Appl. Pyrolysis 78 (2007) 419-429
[50] K. Wang, S. M. Villano, A. M. Dean, Reactions of allylic radicals that impact molecular weight growth kinetics, Phys. Chem. Chem. Phys. 17 (2015) 6255-6273
[51] Z. J. Buras, E. E. Dames, S. S. Merchant, G. Liu, R. M. I. Elsamra, W. H. Green, Kinetics and Products of Vinyl + 1,3-Butadiene, a Potential Route to Benzene, J. Phys. Chem. A 119 (2015) 7325-7338
[52] H. Richter, J. B. Howard, Formation of polycyclic aromatic hydrocarbons and their growth to soot - a review of chemical reaction pathways, Prog. Energy Combust. Sci. 26 (2000) 565-608
[53] S. Sharma, M. R. Harper, W. H. Green, Modeling of 1,3-hexadiene, 2,4-hexadiene and 1,4-hexadiene-doped methane flames: Flame modeling, benzene and styrene formation, Combust. Flame 157 (2010) 1331-1345
[54] K. Wang, S. M. Villano, A. M. Dean, Fundamentally-based kinetic model for propene pyrolysis, Combust. Flame 162 (2015) 4456-4470

3.2 Assessing the potential of crude tall oil for the production of green base chemicals

This section is based on the following paper:

Ruben De Bruycker, Jinto M. Anthonykutty, Juha Linnekoski, Ali Harlin, Juha Lehtonen, Kevin M. Van Geem, Jari Räsänen, Guy B. Marin, "Assessing the potential of crude tall oil for the production of green-base chemicals: an experimental and kinetic modeling study" *Industrial & Engineering Chemistry Research* 2014, 53 (48), 18430 – 18442

3.2.1 Abstract

Crude tall oil (CTO) is a cost-competitive bio-material available from the Kraft pulping process that contains approximately 50% fatty acids, 30% resin acids and 20% neutral polycyclic oxygenated species such as sterols. Although CTO differs drastically from conventional fossil-derived feedstocks, it proves to be an interesting drop-in alternative to produce renewable base chemicals. The proposed two-step process in which, first, CTO is converted into a highly paraffinic/naphthenic feedstock through hydrodeoxygenation (HDO) over a NiMo catalyst, followed by steam cracking produces up to 34wt% of ethene, 15wt% of propene and 5wt% of 1,3-butadiene. A dedicated kinetic model was developed for HDO-CTO steam cracking containing over 500 species to further optimize its industrial potential. Reaction path analysis shows that the HDO severity must be optimized to remove all oxygen but dehydrogenation should be avoided so that valuable light olefins and aromatic production are maximized instead of low value fuel-oil.

Keywords: Crude tall oil, hydrodeoxygenation, steam cracking, kinetic modeling, polycyclic hydrocarbons

3.2.2 Introduction

Ethene and propene, the platform chemicals used for the production of plastics and base chemicals, are regarded as one of the few petrochemical building blocks that could be produced from biomass using existing petrochemical technology. At present, most of the world-wide production of ethene is still based on various fossil-fuel based feedstocks. For instance, in Europe and Asia, ethene is mainly produced from cracking of naphtha, gas oil and condensate; whereas in US, Canada and Middle East, in addition to naphtha cracking, ethene is also produced by cracking of ethane and propane [1-3]. Especially in the US, the shale gas boom causes chemical companies to expand/build facilities focused on ethane cracking [2].

In 2013 over 143 million tons of ethene was produced entirely from feedstocks of fossil origin[4]. As the demand for ethene increases, along with concerns over the excessive use of fossil feedstocks[2], alternative pathways for the production of ethene from bio-based feedstocks, such as bioethanol[5], are being investigated and commercialized. Bio-based ethene can act as a monomer for the production of bio-analogues of petroleum-derived plastics, the so-called bio-plastics. Today, the bio-plastics market is growing, especially in the United States and Europe, and an increase in bio-plastics demand from 890 thousand tons in 2012 to 2.9 million tons by 2017 is prospected [6].

Steam cracking of bio-derived feedstocks is one possible method to produce bio-ethene and other valuable chemicals[7], next to catalytic dehydration of bioethanol. The main advantage of using steam cracking technology for production of olefins is that existing facilities can be used without billion dollar investment costs. However, the oxygen content in typical raw bio-oils can give rise to substantial operation problems in the separation section of conventional steam cracking plants[8]. Catalytic upgrading via hydrodeoxygenation (HDO) has been proposed for many bio-feedstocks to reduce their oxygen content. HDO requires hydrogen pressures up to 20MPa and, as such, the oxygen content in the raw bio-derived feedstock will have a significant impact on the overall costs because of the use of expensive hydrogen. For example, bio-oils produced from fast pyrolysis of lignocellulosic biomass typically have a high oxygen content of over 40% [9]. Hence, HDO of these bio-oils is not economically feasible or sustainable for steam crackers considering the low margins per tonne ethene produced. Furthermore, bio-oil’s chemical composition differs greatly from conventional naphtha and additional finishing steps would be required.

The use of fatty acids and/or glycerides, derived from vegetable oils, waste fats/greases or algae, is an attractive alternative. Their low oxygen content, solely situated in the glycerol/acid functionality, makes HDO more viable, for example through the Bio-SynfiningTM process [7]. Saudi Basic Industries Corp., or SABIC, plans to use cooking oil and fat waste for the production of renewable olefins which will be situated next to a naphtha-fed unit in Geerlen, Netherlands[10].

Tall oil, a byproduct of the Kraft pulping process[11] and, thus, derived from non-food sources, is a promising bio-derived feedstock with a low oxygen content[12, 13]. Bio-ethene may be produced through hydrodeoxygenation and steam cracking, similar to vegetable oils and waste fats. Tall oil is derived from woody biomass which is typically grown in non-arable land. Therefore, the use of land is minimal in the case of tall oil production from any woody starting material. The greenhouse gas emissions related to land use changes, which are significant during the cultivation and harvesting of feed crops for vegetable oil production[14], are negligible for tall oil production. Allocation of tall oil for the production of bio-olefins requires substitute chemicals which replace their current use. The associated cost is expected to be lower for tall oil compared to vegetable oil given the lower economic value of tall oil compared to vegetable oil[12, 14]. This creates a prospect in terms of economic and environmental perspective for utilizing tall oil as a low carbon footprint bio-refinery feedstock in countries where ample production capacity of tall oil is available from Kraft pulping such as Finland, Sweden and USA[12]. A thorough life cycle assessment should asses and compare the greenhouse emissions for production of bio-ethene and bio-plastics from various bio-derived feedstocks, including HDO and steam cracking of vegetable oils, HDO and steam cracking of tall oil and dehydration of ethanol[5]. Such studies are currently unavailable to the best of our knowledge.

HDO of fractionated tall oil such as HDO-TOFA, i.e. tall oil fatty acids, and HDO-DTO, i.e. distilled tall oil, followed by their use as a steam cracker feedstock has been studied previously by Pyl et al.[15]. It has been reported that pure HDO-TOFA gives rise to a high yield of ethene (>30 wt. %) in a conventional steam cracker[15]. Direct use of crude tall oil (CTO), which is produced by skimming off and acidification of tall oil soap from the black liquor obtained from pulping, is more cost competitive compared to TOFA and DTO, which are produced through distillation of CTO. It is thus of interest to utilize this material, readily available from pulp and paper mills, for steam cracking via catalytic upgrading. Hydrotreating of CTO over a sulfided NiMo catalyst produces a hydrocarbon mixture comprising of mainly

paraffins and naphthenes, as reported by Anthonykutty et al. [16]. The aforementioned study also mentions that steam cracking of HDO-CTO is not obvious due to the significant amounts of polycyclic structures that are not available in classical fossil based feedstocks. These molecules have a higher selectivity towards (poly-)aromatic species compared to simple alkanes[17], reducing the olefin yield and potentially increased coking/fouling[18].

Nowadays, operating conditions of steam crackers are selected based on advanced simulation tools, maximizing the overall profit based on the detailed composition coming out of the gas-fired furnaces [19, 20]. As such, development of accurate kinetic models describing the pyrolysis of polycyclic molecules is indispensable for the optimal use of HDO-CTO in steam crackers considering their large quantities present in these renewable feedstock. Several studies regarding the kinetics of decalin pyrolysis, i.e., the simplest polycyclic hydrocarbon, have been published recently[21, 22]. However, according to the authors' knowledge, there are no reported studies regarding the thermal decomposition of norabietane, one of the main compounds in HDO-CTO, see Figure 3.2-1. Hence, this issue needs to be resolved to assess the economic viability of HDO-CTO steam cracking or co-cracking it as drop-in with other (fossil) feedstocks.

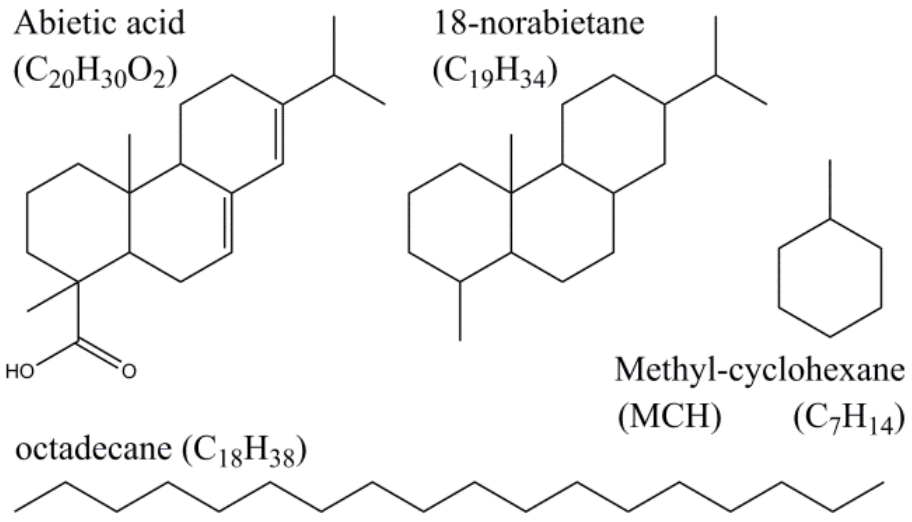

Figure 3.2-1 Structure and molecular formula of abietic acid, 18-norabietane, methyl-cyclohexane (MCH) and octadecane

This research reports a two-step process for the production of olefins from CTO. In the first step, CTO was hydrodeoxygenated over a commercial NiMo catalyst under 5MPa hydrogen pressure and at 623K in a continuous down flow, fixed bed reactor. In the second step, steam cracking of HDO-CTO was investigated in a dedicated bench-scale setup. The effect of temperature on product yield distribution was evaluated and compared to conventional steam

cracking feedstocks. Furthermore, a detailed kinetic modeling of the pyrolysis of polycyclic hydrocarbons is presented in this work with specific attention to the compounds present in HDO-CTO. The proposed modeling methodology has been validated earlier for n-alkanes[23] and rate rules are derived from pyrolysis of mononaphthenes.

3.2.3 Experimental methods

3.2.3.1 Feedstock preparation

The feedstock for steam cracking was prepared by hydrodeoxygenation of CTO obtained from the Stora Enso Oyj pulp mill in Finland. CTO is a very viscous mixture[12]. Volatilization is difficult without causing decomposing of fatty acids and resin acids[24]. In this work, CTO analysis through standard GC and advanced GC×GC methods[25-27] proved to be insufficient. Therefore, CTO was analyzed by Nablabs laboratories (Espoo, Finland) using the dedicated ASTM 5974-00 method[16, 24]. In the ASTM D 5974-00 method, acids are converted to more volatile and more stable methyl esters prior to gas chromatography[24]. The group composition and major components present in CTO are listed in Table 3.2-1.

Table 3.2-1 Group type composition of CTO and HDO-CTO.

	CTO		**HDO-CTO**
Group type composition (wt%)		*Group type composition (wt%)*	
Fatty acids	**48.1**	**N-alkanes**	**55.1**
Palmitic acid ($C_{16}H_{32}O_2$)	2.1	C16	2.6
Margaric acid ($C_{17}H_{34}O_2$)	0.4	C17	16.0
Stearic acid ($C_{18}H_{36}O_2$)	0.8	C18	27.0
Oleic acid ($C_{18}H_{34}O_2$)	9.1	**Iso-alkanes**	**2.7**
Linoleic acid ($C_{18}H_{32}O_2$)	27.6	**Mono-naphthenes**	**6.8**
Pinolenic acid ($C_{18}H_{30}O_2$)	1.6	**di-naphthenes**	**8.5**
Resin acids (tricyclic acids)	**28.5**	C18	4.1
Abietic acid ($C_{20}H_{30}O_2$)	9.2	C19	2.2
Palustric acid ($C_{20}H_{30}O_2$)	3.9	**tri-naphthenes**	**18.9**
Neoabietic acid ($C_{20}H_{30}O_2$)	3.3	C18	6.2
Pimaric acid ($C_{20}H_{30}O_2$)	2.6	C19	9.5
Dehydroabietic acid ($C_{20}H_{28}O_2$)	2.4	**tetra-naphthenes**	2.3
Other (including sterols)	**23.0**	**Aromatics**	**5.6**
Sitosterol ($C_{29}H_{50}O$)	3.6	C18 dinapthenoaromatics	1.6
24-methenecycloartenol ($C_{31}H_{50}O$)	2.5	C19 dinapthenoaromatics	1.7

CTO was pre-heated to approximately 340K and subsequently fed to the reactor using a Lewa, Sarl FC-1 model pump. HDO was carried out in a continuous down flow, fixed bed reactor at VTT Technical Research Centre of Finland (Espoo, Finland). The reactor tube (500

mm long, 20 mm internal diameter stainless steel tube) was placed co-axially in an oven (Oy Meyer Vastus) and the catalyst bed temperature was monitored by a temperature controller (TTM-339 series). A commercial NiMo catalyst was used for HDO, which was sulfided with a H_2S/H_2 gas mixture for 12 hours at 673K before the start of the experiment. The reactor was operated at a temperature of 623K and 5MPa hydrogen pressure. In total 4kg of liquid product was produced from CTO. This was carefully separated into an aqueous and an organic phase using a separating funnel as aqueous phase was clearly settled at the bottom level. The organic phase (HDO-CTO) was collected in airtight glass bottles (Schott) and sent to Ghent University (Ghent, Belgium) by road transport for steam cracking experiments. The oxygen content of HDO-CTO, determined by elemental analysis, was 0.1wt%, before and after transport. This corresponds to an oxygen conversion of 99% during HDO.

3.2.3.2 Feedstock analysis

HDO-CTO was analyzed using a 2D-gas chromatograph equipped with both a flame ionization detector and time-of-flight mass spectrometer (GC×GC-FID/TOF-MS). Figure 3.2-2 shows a GC×GC-FID chromatogram with indication of the most important species detected. Over 300 components have been identified which can be divided in approximately 4 groups, i.e. n-alkanes (55.1 wt %), iso-alkanes (2.7 wt%), naphthenes (36.5 wt%) and aromatics (5.6 wt%), see Table 3.2-1. Traces of oxygenated molecules were identified in HDO-CTO using TOF-MS. Quantification of this residual fraction was not possible because of the very small quantities given the high conversion during HDO and overlap with the complex product spectrum after HDO, e.g. linoleic acid with tricyclic hydrocarbons having between 19 and 20 carbon atoms. HDO operating conditions have a direct effect on the composition, which has been discussed earlier [13, 16]. The vast majority of n-alkanes comprises of octadecane and heptadecane which are produced from oleic (C18:1) and linoleic (C18:2) acid present in the virgin crude tall oil[13]. The high fraction of heptadecane reflects the high degree of decarboxylation under the applied HDO conditions[13]. In comparison, iso-alkanes only comprise a small fraction of HDO-CTO. The majority of this fraction consists of branched $C_{18}H_{38}$ and $C_{17}H_{36}$ alkanes formed by isomerization of their normal analogues during HDO[13]. Smaller iso-alkanes can also be formed through cracking of the naphthenic hydrocarbons[16]. The high fraction of naphthenic hydrocarbons in HDO-CTO is no surprise, given the large amount of resin acids and sterols in the virgin crude tall oil. HDO of abietic acid ($C_{20}H_{30}O_2$), the most abundant resin acid in CTO, results in formation of 18-norabietane ($C_{19}H_{34}$)[16]. Under the applied HDO conditions 18-norabietane can crack with

formation of mono-naphthenic and di-naphthenic hydrocarbons as observed in the experiments[16]. HDO of sterols leads to tetra-naphthenic hydrocarbons, such a stigmastane ($C_{29}H_{52}$) in the case of β-sitosterol ($C_{29}H_{50}O$). Obviously these structures can break-down further as well. The fraction of tetra-naphthenic hydrocarbons in HDO-CTO was found to be 2.3wt%. Note that the high fraction of cyclo-alkanes and the presence of tetra-naphthenic hydrocarbons makes the feedstock substantially more challenging compared to previously investigated hydrodeoxygenated tall oil fractions [15], i.e. distilled tall oil and tall oil fatty acids, both from an experimental (increased fouling[18, 28]) and kinetic modeling[22] standpoint. Aromatics, the last group of hydrocarbons observed, comprise about 5.6 wt% of the feedstock. The majority of this group consists of octahydro-phenanthrene with a variety of alkyl side groups. 19-norabieta-8, 11, 13-triene is the main constituent and is mainly formed during HDO through decarboxylation and dehydrogenation of abietic acid [13, 16].

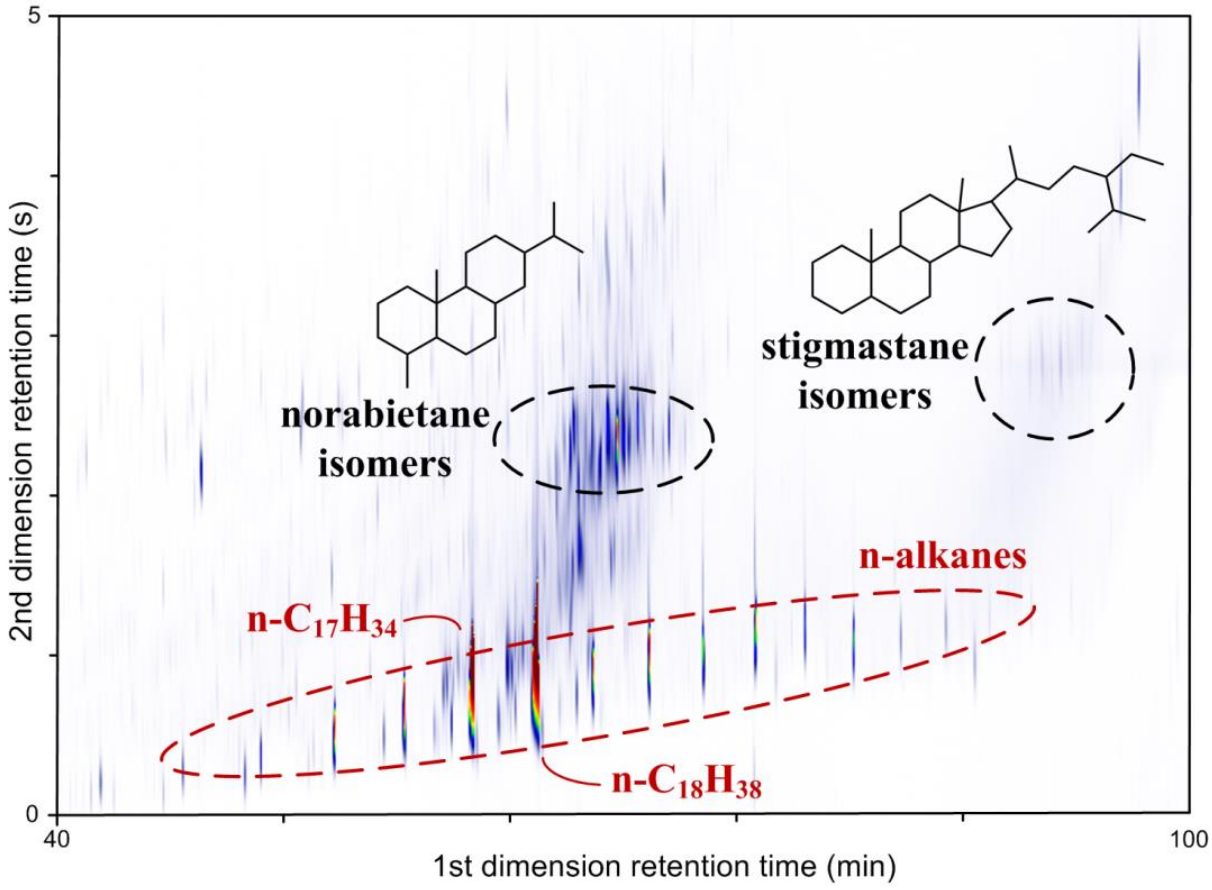

Figure 3.2-2: GC×GC-FID chromatogram of HDO-CTO with indication of the most important components

While it is possible to differentiate molecules based on carbon number and functional groups, e.g. alkanes, mono-naphthenes, di-naphthenes, tri-naphthenes, identification of single isomers

is difficult, even with advanced analysis equipment[29]. Hence, in this work, molecules with the same carbon number and the same chemical functionalities are grouped.

3.2.3.3 Bench scale set-up for steam cracking

In order to evaluate the potential of HDO-CTO as a renewable source of olefins and aromatics, steam cracking of HDO-CTO, as well as a naphtha and a natural gas condensate, was performed in a bench scale steam cracking set-up which has been described extensively in the past [30, 31]. A schematic overview is presented in Figure 3.2-3 (A) and only a brief discussion is given here.

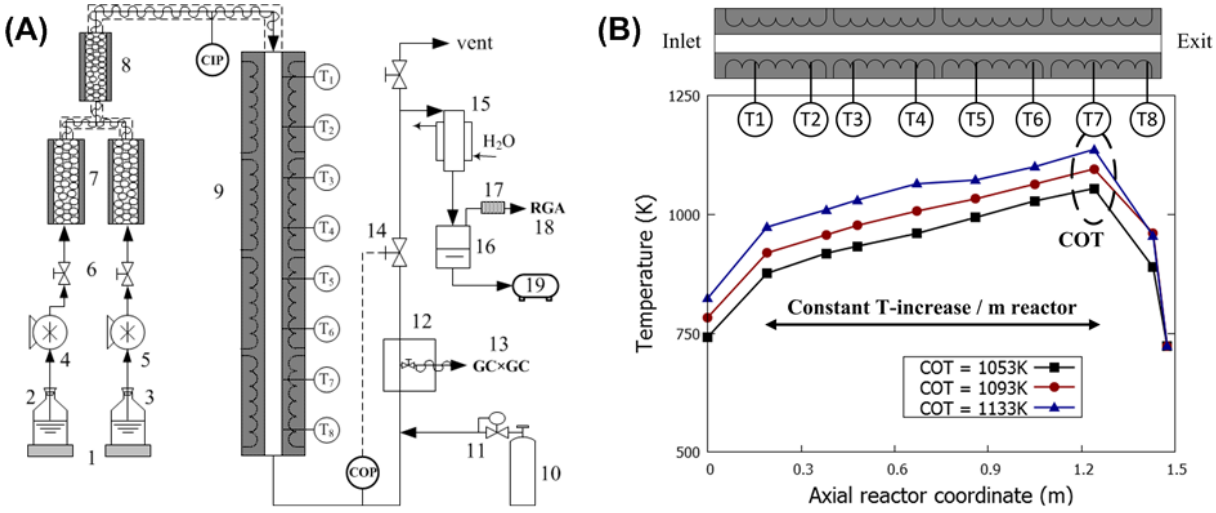

Figure 3.2-3: (A) Schematic overview of the experimental steam cracking set-up indicating temperature and pressure measurements. (1: electronic balance, 2: hydrocarbon reservoir, 3: water reservoir, 4: peristaltic pump, 5: water pump, 6: valve, 7: evaporators, 8: mixer, 9: reactor, 10: internal standard, 11 coriolis mass flow controller, 12 heated sampling oven, 13: GC×GC-FID/TOF-MS, 14: outlet pressure restriction valve, 15: water cooled heat exchanger, 16: gas/liquid separator, 17: dehydrator, 18: refinery gas analyzer, 19: condensate drum) (B) Process gas temperature profile along the axial reactor coordinate measured by the eight thermocouples for steam cracking of HDO-CTO, corresponding to a set coil outlet temperature of respectively 1053, 1093 and 1133K. (figure after Djokic et al. [31] and Vandewiele et al. [32])

The hydrocarbon feedstock is fed to an evaporator kept at 673 K using a peristaltic pump. In a similar way, water gets evaporated. Both hydrocarbon and steam are mixed prior to entering the reactor. The reactor is 1.475m long and has an internal diameter of 6mm. It is made of Incoloy 800HT with following elemental composition: Ni 30-35wt%, Cr 19-23wt% and Fe > 39.5wt%. The process gas temperature is measured through eight thermocouples which are positioned along the axial reactor coordinate. The reactor is positioned vertically in an electrically heated furnace which consists of four separate sections, controlled by four thermocouples. The temperature in the last section of the furnace was set at the desired coil outlet temperature (COT). The other sections have set temperatures that allow for a constant temperature increase over the length of the reactor in line with industrial practice. The

resulting measured temperature profile hence consisted of a steep temperature increase at the inlet of the reactor up to the first set temperature, followed by the set linear temperature increase to the coil outlet temperature, and finally a steep temperature decrease at the outlet of the reactor, see Figure 3.2-3 (B).

A fixed flow of N_2, controlled using a Coriolis mass flow controller, was added to the reactor effluent for further quenching and as internal standard. The resulting mixture was sent to a heated sampling system kept at 573 K to avoid condensation [29]. A part of the mixture is injected on a refinery gas analyzer (RGA) after removal of the condensable fraction. This chromatograph is able to calculate the flow rate of all permanent gases using two thermal conductivity detectors (TCD), of which one is dedicated to H_2 quantification, and C_4- hydrocarbons using a FID based on the fixed flow rate of N_2. The response factors were determined using a calibration mixture provided by Air Liquide, Belgium. Furthermore, the effluent is injected on a GC×GC-FID through transfer lines, kept at 573 K which is above the dew point of the reactor effluent[33]. The flow rates of the detected molecules were calculated using CH_4, identified and quantified on the RGA, as secondary internal standard. Response factors were calculated using the effective carbon number approach [34]. A more detailed description of data quantification has been described previously [35]. The followed experimental procedure allows online analysis of the complete product spectrum and avoids separate gas-phase and condensate analysis.

The obtained results had good repeatability and the error for the major species is estimated to be 5%, mainly caused by uncertainties in flow rate, calibration factors and temperature. Elemental balances typically closed within 5%.

3.2.4 Results and discussion

3.2.4.1 Experimental results

Steam cracking of HDO-CTO was investigated at a constant pressure of 0.17 MPa and a constant inlet flow rate of 2.8×10^{-2} g s^{-1} hydrocarbon feedstock and 1.4×10^{-2} g s^{-1} steam. The coil outlet temperature (COT) was varied between 1053 and 1133 K. Furthermore, steam cracking of 3 other hydrocarbon feedstocks, i.e., a naphtha, a natural gas condensate (NGC) and a naphtha (50 wt%) – HDO-CTO (50 wt%) blend, has been investigated at comparable operating conditions as fossil references. Online analysis allowed identification and quantification of over 100 products present in the reactor effluent. A summary of the obtained results is given in Table 3.2-2. The product distribution can be divided in permanent gases,

light alkanes, light alkenes, aromatics and a residual fraction. At a COT of 1053K, 2wt% of HDO-CTO is unconverted, which is in line with other comparable studies[15, 23].

Compared to the investigated fossil liquid feedstocks, i.e. naphtha and NGC, the cracking effluent of HDO-CTO has a lower fraction of permanent gases although all feedstocks have comparable ethene and propene yield. H_2 and CH_4 are mainly formed by hydrogen abstraction of H and CH_3 from the feed and other molecules under steam cracking conditions[36]. HDO-CTO comprises for the vast majority of molecules with 16 or more carbon atoms. According to the so-called μ-hypothesis [37], decomposition of the accompanying large radicals, formed by hydrogen abstraction, will result in the formation of a high number of light olefins and one small radical. Hence, the low permanent gases to small olefins ratio for HDO-CTO is mainly a consequence of the higher average molecular weight of the feedstock. Small amounts of carbon oxides are formed through steam reforming of carbonaceous deposits, catalyzed by Ni present in the reactor wall material[38]. Furthermore, the thermal decomposition of residual oxygenated molecules in the feedstock can contribute as well[15].

The HDO-CTO feedstock consists of 58 wt% alkanes and 42 wt% polycyclic hydrocarbons. Steam cracking of the former components is known to lead to a high fraction of ethene in the reactor effluent by subsequent beta scission of alkyl radicals, as stated previously[7, 39, 40]. While polynaphthenic hydrocarbons have a relatively high yield towards small olefins, the selectivity is lower compared to n-alkanes[17, 21, 41]. Decomposition of large naphthenic radicals leads to the formation of unsaturated cyclic intermediates, see section 3.2.4.2, which can further dehydrogenate to aromatics, resulting in a relatively high yield for benzene, toluene, styrene and xylenes[21]. This was observed experimentally, see Table 3.2-2.

Table 3.2-2: Summary of the measured product distribution (wt%) for steam cracking of naphtha, natural gas condensate, naphtha/HDO-CTO blend and HDO-CTO at different coil outlet temperatures (COT). [$F_{hydrocarbons}$ = 2.8E-2 g s^{-1}, F_{H2O} = 1.4E-2 g s^{-1}]

Feedstock	Naphtha			NGC			Naphta (50wt%) - HDO-CTO (50wt%)			HDO-CTO				
COT (K)	1093	1113	1133	1093	1113	1133	1093	1113	1133	1053	1073	1093	1113	1133
C_3H_6/C_2H_4	0.71	0.57	0.45	0.58	0.47	0.35	0.59	0.46	0.33	0.59	0.53	0.43	0.34	0.24
Permanent Gases														
H_2	0.98	1.13	1.23	0.86	0.95	1.10	0.87	0.95	1.12	0.59	0.70	0.78	0.92	0.93
CH_4	14.36	17.76	19.30	14.57	16.88	19.53	14.30	15.82	18.36	10.84	12.81	14.11	15.83	16.39
CO	0.07	0.07	0.12	0.05	0.06	0.09	0.09	0.08	0.14	0.03	0.07	0.08	0.09	0.09
CO_2	0.06	0.03	0.02	0.02	0.02	0.01	0.05	0.03	0.03	0.01	0.05	0.03	0.03	0.02
Light Alkanes														
C_2H_6	4.08	4.25	3.85	4.34	4.22	3.96	4.49	4.06	3.77	4.69	4.90	4.55	4.33	3.81
C_3H_8	0.49	0.44	0.35	0.52	0.43	0.31	0.52	0.41	0.30	0.64	0.62	0.50	0.40	0.28
Light Alkenes														
C_2H_4	24.80	28.19	30.07	28.75	30.54	31.99	26.98	29.31	32.68	25.82	27.60	29.29	32.07	33.95
C_3H_6	17.67	15.96	13.60	16.58	14.36	11.07	15.82	13.51	10.67	15.24	14.57	12.71	10.98	8.18
1-C_4H_8	1.95	1.20	0.72	1.83	0.93	0.36	1.47	0.76	0.42	2.40	1.78	0.89	0.43	0.23
iso-C_4H_8	3.49	2.76	1.94	2.82	2.02	1.15	2.23	1.68	1.01	1.01	0.97	0.77	0.59	0.40
1,3-C_4H_6	4.35	3.93	3.34	4.01	3.64	2.91	4.54	4.02	2.94	5.32	5.53	5.12	4.32	2.86
Aromatics														
Benzene	6.42	9.08	10.40	7.99	9.24	10.99	7.53	8.54	10.37	5.41	6.04	8.34	9.34	11.90
Toluene	3.01	3.49	3.58	3.40	3.41	3.66	3.79	3.64	3.67	4.03	4.43	4.62	5.24	5.95
Styrene	0.57	0.99	1.25	1.02	1.15	1.46	1.07	1.22	1.44	1.13	1.35	1.56	2.01	2.36
Xylenes	0.20	0.29	0.31	0.91	0.82	0.78	0.65	0.56	0.50	1.27	1.25	1.14	1.16	1.11
Other														
C_2H_2	0.30	0.50	0.70	0.37	0.53	0.70	0.31	0.44	0.62	0.17	0.23	0.29	0.43	0.48
CPD	1.40	1.68	1.79	1.20	1.37	1.43	1.44	1.72	1.48	0.94	1.60	1.86	1.91	1.46

The above discussion illustrates the high dependence of product distribution on the considered feedstock. While the experimental ethene yield during steam cracking of HDO-CTO is only 4wt% higher compared to steam cracking of naphtha, this can have a big effect on the overall economics of an industrial plant, given the low profit margins on ethene[42]. Nowadays, steam crackers of liquid feeds have a reasonable flexibility regarding feedstock composition. The extent to which cracking has occurred is tracked through so-called severity indices, of which the propene to ethene ratio (P/E-ratio) [kg kg^{-1}] is often favored [43, 44]. Mostly, this ratio is kept between 0.5 and 0.4 in industry. Higher ratios indicate (above 0.5) a low degree of cracking and a large amount of liquid byproducts while lower ratios (below 0.5) indicate a high degree of secondary cracking which correlates with increased coke formation and, thus, decreased run lengths[45]. Figure 3.2-4 illustrates that given P/E-ratio, and thus a similar extent of cracking, is reached at lower temperatures for HDO-CTO compared to conventional

feedstocks such as naphtha. The desired ratio of 0.5 is reached at a COT of 1070 K, 1130 K and 1100 K for HDO-CTO, naphtha and a 50wt%/50wt% blend thereof respectively, demonstrating that a comparably lower heat input is required for the considered renewable feedstock. This result is similar to earlier observations for hydrodeoxygenated tall oil fatty acids [15] and hydrodeoxygenated waste oils [7], both primarily consisting of large n-alkanes in contrast to the naphthenic/paraffinic mixture investigated here.

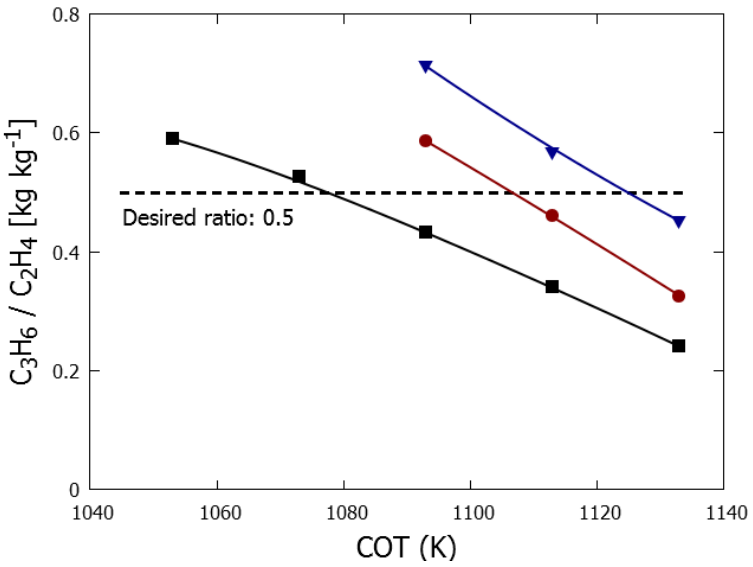

Figure 3.2-4: Propene/Ethene-ratio (kg kg^{-1}) as a function of coil outlet temperature (COT): ■ - HDO-CTO, ▲ - naphtha, ● - 50wt% HDO-CTO / 50wt% naphtha blend

3.2.4.2 Kinetic modeling of steam cracking of HDO-CTO

Better understanding the effect of operating conditions and feedstock composition on product distribution requires fundamental understanding of the underlying chemistry. Only then operating conditions can be selected which maximize olefin yield, vital for optimal use of any new feedstock such as HDO-CTO.

The followed kinetic modeling approach has been discussed extensively in the past[20, 23, 46, 47] and only a brief discussion will be given here. Steam cracking proceeds through a free radical mechanism. Given the high average molecular weight of HDO-CTO, taking into account every possible elementary step, every radical and every isomer would render the kinetic model to be impractically large[48, 49] and the solution of the resulting set of differential equations extremely slow, even using advanced solution techniques such as using a GPU[50]. In line with the earlier observations, the μ-hypothesis is applied to reduce the size of the kinetic model. The mechanism can be further reduced by combining the μ-hypothesis with the pseudo-steady-state approximation (PSSA) for radicals having 6 or more carbon

atoms [51]. The μ-hypothesis assumes that bimolecular reactions for large radicals, μ-radicals, can be neglected and as such only isomerize or decompose to smaller molecules and radicals[37, 52]. Combined with the PSSA, these radicals can be eliminated from the model equations.

As example, the hydrogen abstraction from methyl-cyclohexane (MCH) followed by carbon-centered β-scission is given in Figure 3.2-5. Radical reactions such as hydrogen shifts and hydrogen-centered β-scission are not included to keep the figure representable. Five possible methyl-cyclohexane radicals can be formed. Subsequent ring opening forms heptenyl radicals. These radicals are μ-radicals and, as such, they will, dominantly, react through monomolecular reactions. Only carbon centered β-scissions are considered for illustrative reasons, hence, decomposition leads to formation of ethene, propene, butenyl and pentenyl radicals only. Butenyl and pentenyl radicals are C_{5-} radicals for which bimolecular reactions, such as hydrogen abstraction from the feed molecule, cannot be neglected. Hence, they are not eliminated from the model equations and appear as final products in the presented scheme. Their further decomposition reactions are considered in the β-network of the complete kinetic model. Besides ring opening, the 1-methyl-cyclohex-2-yl radical can react further and form methyl and cyclohexene (cC_6H_{10}). The μ-radicals, in this example methyl-cyclohexane radicals and heptenyl radicals, can now be eliminated from the model equations using the pseudo-steady-state approximation. This allows to represent the hydrogen abstraction of methyl-cyclohexane and subsequent monomolecular decomposition of μ-radicals by a single reaction where the rate constant is the sum of the individual hydrogen abstraction rate constants and where the stoichiometric coefficients depend on the rate constants of the various elementary steps[46].

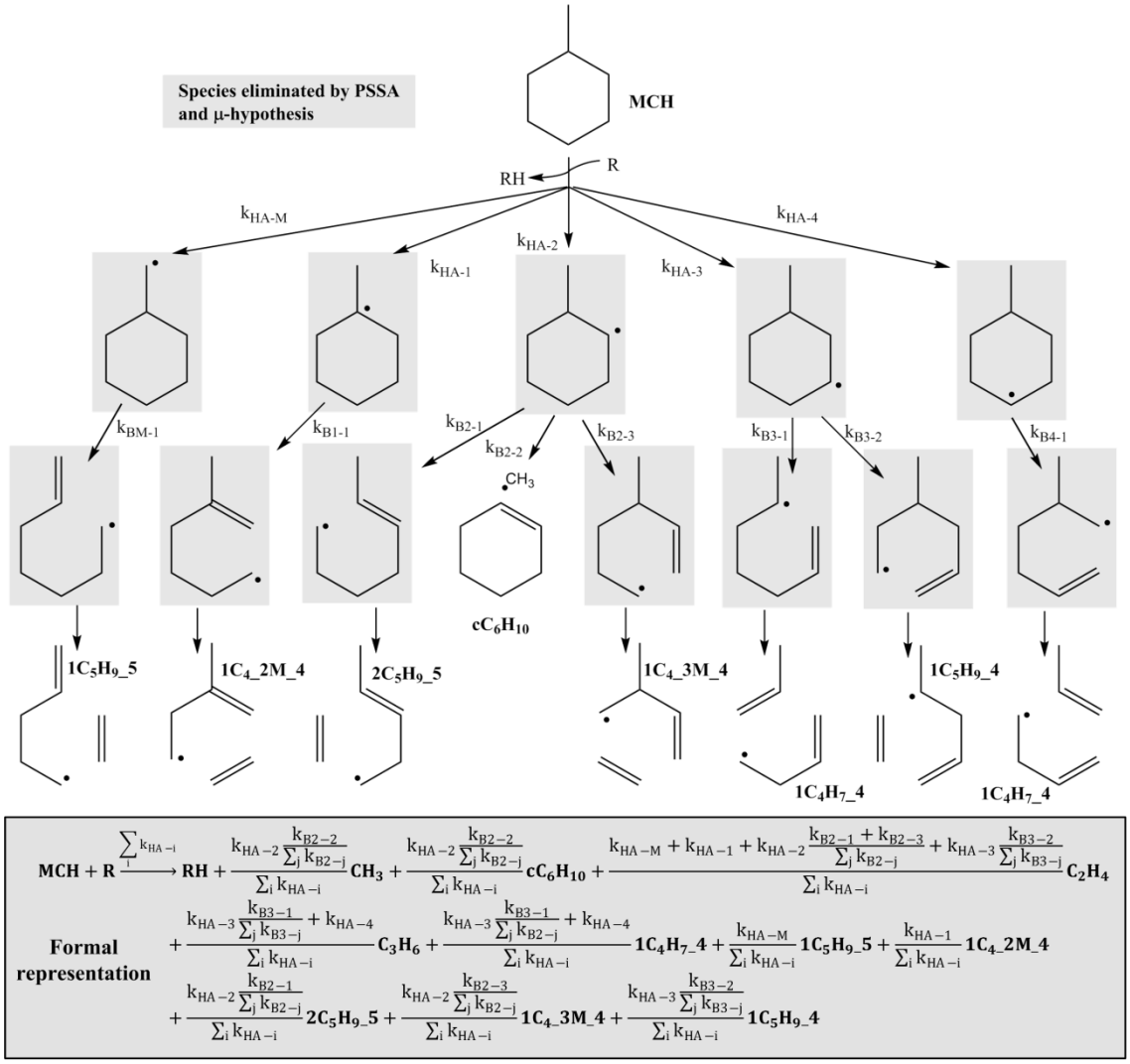

$$\mathbf{MCH} + \mathbf{R} \xrightarrow{\sum_i k_{HA-i}} \mathbf{RH} + \frac{k_{HA-2}\frac{k_{B2-2}}{\sum_j k_{B2-j}}}{\sum_i k_{HA-i}}\mathbf{CH_3} + \frac{k_{HA-2}\frac{k_{B2-2}}{\sum_j k_{B2-j}}}{\sum_i k_{HA-i}}\mathbf{cC_6H_{10}} + \frac{k_{HA-M} + k_{HA-1} + k_{HA-2}\frac{k_{B2-1}+k_{B2-3}}{\sum_j k_{B2-j}} + k_{HA-3}\frac{k_{B3-2}}{\sum_j k_{B3-j}}}{\sum_i k_{HA-i}}\mathbf{C_2H_4}$$

Formal representation

$$+ \frac{k_{HA-3}\frac{k_{B3-1}}{\sum_j k_{B3-j}} + k_{HA-4}}{\sum_i k_{HA-i}}\mathbf{C_3H_6} + \frac{k_{HA-3}\frac{k_{B3-1}}{\sum_j k_{B2-j}} + k_{HA-4}}{\sum_i k_{HA-i}}\mathbf{1C_4H_7\_4} + \frac{k_{HA-M}}{\sum_i k_{HA-i}}\mathbf{1C_5H_9\_5} + \frac{k_{HA-1}}{\sum_i k_{HA-i}}\mathbf{1C_4\_2M\_4}$$

$$+ \frac{k_{HA-2}\frac{k_{B2-1}}{\sum_j k_{B2-j}}}{\sum_i k_{HA-i}}\mathbf{2C_5H_9\_5} + \frac{k_{HA-2}\frac{k_{B2-3}}{\sum_j k_{B2-j}}}{\sum_i k_{HA-i}}\mathbf{1C_4\_3M\_4} + \frac{k_{HA-3}\frac{k_{B3-2}}{\sum_j k_{B3-j}}}{\sum_i k_{HA-i}}\mathbf{1C_5H_9\_4}$$

Figure 3.2-5 Hydrogen abstraction from methyl-cyclohexane (MCH) and subsequent decomposition reactions. The equivalent single-step of this reaction set is obtained after elimination of the concentration of μ-radicals using the pseudo-steady-state approximation, considering all the elementary reactions.

The kinetic model consists of two parts: (i) a μ-reaction network containing reactions of large molecules where μ-radicals (C_{6+}) have been eliminated using the pseudo-steady-state approximation and (ii) a β-reaction network containing elementary reactions of generally small molecules which do not form μ-radicals. For example, the equivalent single-step reaction of hydrogen abstraction of methyl-cyclohexane, where μ-radicals have been eliminated using the pseudo-steady-state approximation, is part of the μ-network while the unimolecular decomposition reactions of butenyl and pentenyl radicals are part of the β-network. Thermodynamic data was taken from extensive databases whenever possible [53]. Otherwise, they were evaluated using Benson's group additivity method [54, 55]. Kinetic data for the elementary steps required for generation of reactions in the μ-network were calculated using group additivity values derived by Sabbe et al.[56-58] who applied Benson's group additivity concept to transition state theory. The β-network consists of an ethane steam

cracking reaction network[36] appended with several polycyclic aromatic hydrocarbon pathways[59, 60].

This methodology has been validated for the thermal decomposition of n-alkanes [23] but not for substituted naphthenic hydrocarbons present in HDO-CTO. Hence, in the next section, the methodology and rate rules will first be validated for methyl-cyclohexane (MCH), i.e., the most simple and the most investigated substituted cyclo-alkane for which several extensive datasets are available in literature [61, 62], before extension to polycyclic hydrocarbons such as 18-norabietane. Describing the pyrolysis of naphthenes required implementation of several new reaction families compared to n-alkane pyrolysis, i.e., cyclo-alkyl decomposition[63], retro Diels-Alder reactions of unsaturated napthenes[64] and ipso-addition on substituted aromatics[65].

The use of equivalent single-step reactions, by eliminating μ-radicals using the pseudo-steady-state approximation, should not be considered a simplification. One such reaction can contain information of over 100 elementary reactions, e.g. hydrogen abstractions, isomerizations, cyclizations, β-scissions, also see Figure 3.2-5. Both assumptions made, i.e. pseudo-steady-state approximation and μ-hypothesis, allow writing the model more comprehensively without losing accuracy[66, 67]. Moreover, the elimination of μ-radicals has a computational advantage as the reduced number of species facilitates the use of the kinetic model in large-scale computations [66, 68]. This model in particular can be used in 3D simulations of steam cracking reactors which helps in understanding coke formation and aids in reactor design.[69]

Reactor simulations were performed using the ideal plug flow reactor model of CHEMKIN-PRO[70]. The plug flow assumption has been validated earlier for the setup discussed in section 3.2.3.3[30]. The measured temperature profiles and pressure profiles were given as input to the simulations. For HDO-CTO, each group of feed molecules with the same carbon number and the same chemical functionalities, see section 3.2.3.2, was assigned a representative molecule. Such a molecule is typically the molecule with the highest weight fraction belonging to that group, e.g. 18-norabietane represents tri-naphthenes with 19 carbon atoms. These representative molecules with weight fractions corresponding to their respective groups were given as inlet composition to the simulations. Given the structure of the developed reaction mechanism, the USRPROD routine was used to couple the kinetic model

with the CHEMKIN framework. This option enables the user to define a subroutine that calculates the rate of production of all species for certain reactor conditions.

3.2.4.2.1 Thermal decomposition of the simplest alkylated cyclo-alkane, methyl-cyclohexane

Most studies regarding the thermal decomposition of methyl-cyclohexane aim at improving the current understanding of its oxidation characteristics[61, 62, 71]. Some datasets available in literature thus consider an experimental operating range which is different than what has been applied here such as high pressure (> 0.3 MPa), high temperature (>1200 K) or short residence times (< 100 ms). Wang et al. studied the pyrolysis of methyl-cyclohexane in an alumina flow reactor at 0.1 MPa and residence times around 0.2 s [62]. A complete description of the pyrolysis experiments of methyl-cyclohexane falls outside the scope of this study and, thus, only the model performance will be presented in this work. A selected number of experimentally recorded mole percentages below 1200 K together with simulations using the generated model and the Wang et al. model[62] are displayed in Figure 3.2-6 as a function of the maximum temperature (Tmax), the maximum temperature of the temperature profile corresponding to the experiment, as stated previously. The developed kinetic model is able to accurately predict conversion and trends in species profiles. The main discrepancies can be observed for ethene, which is overpredicted, and 1,3-butadiene, which is underpredicted. The model by Wang et al. has been added for comparison.

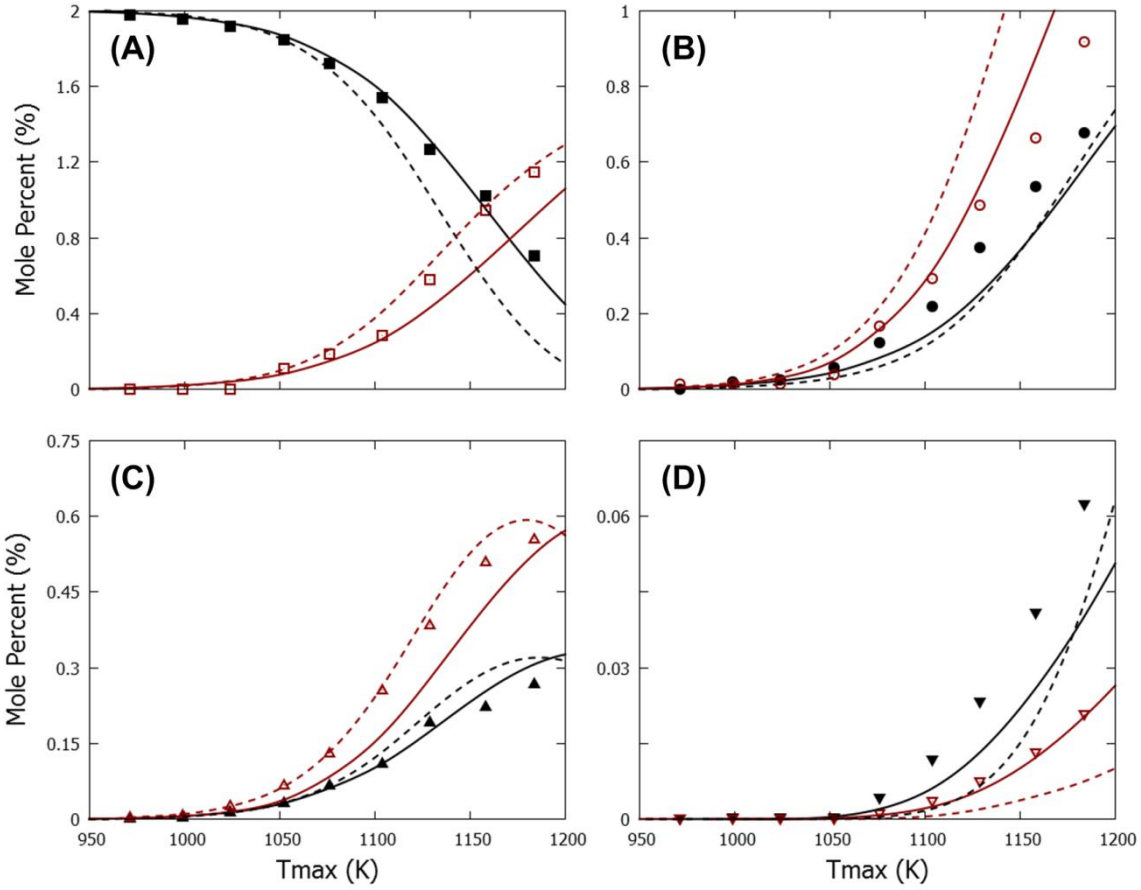

Figure 3.2-6: Mole percentage profiles as a function of Tmax, i.e. the maximum temperature in the flow reactor, for the pyrolysis of methyl-cyclohexane (MCH)[62]: ■ - MCH (A), □ - H_2 (A), ● - CH_4 (B), ○ - C_2H_4 (B), ▲ - C_3H_6 (C), ▲ - 1,3-butadiene (C), ▼ - benzene (D), ▼- toluene x 2 (D) ; lines, mole percentage profiles calculated with CHEMKIN using the plug flow reactor model: ——- the developed kinetic model, - - - - the kinetic model by Wang et al.[62]

The major difference between both models is methyl-cyclohexane conversion which is overpredicted by Wang et al. This has an effect on all other product yields, which are typically higher for the Wang et al. model. The unimolecular decomposition of methyl-cyclohexane forming methyl and cyclohexyl has the biggest effect on the conversion profile[62]. The rate coefficient used by Wang et al., from a theoretical study by Zhang et al.[72], is approximately a factor 5 higher than the one used in this work, from Klippenstein et al.[73].

The applied kinetic data was first validated for acyclic hydrocarbons[23]. The extension to cyclic hydrocarbons, by extrapolating existing reaction families and introducing new reaction families discussed above, can be considered successful given the good agreement between experiment and simulation for methyl-cyclohexane pyrolysis without any adjustments of the reaction coefficients, i.e. tuning. This good agreement is a prerequisite before extending to polycyclic hydrocarbons what will be discussed in the next section.

3.2.4.2.2 Modeling the steam cracking of polynaphthenic substituted hydrocarbons

The proposed modeling methodology has been extended to polynaphthenic hydrocarbons and the final mechanism is able to describe the pyrolysis of the complete HDO-CTO feedstock. The β-network of the kinetic model comprises 113 species and 1585 reactions while the μ-network comprises the reactions of an additional 413 species. Figure 3.2-7 presents a selection of experimental results with model predictions for the steam cracking of HDO-CTO as a function of COT.

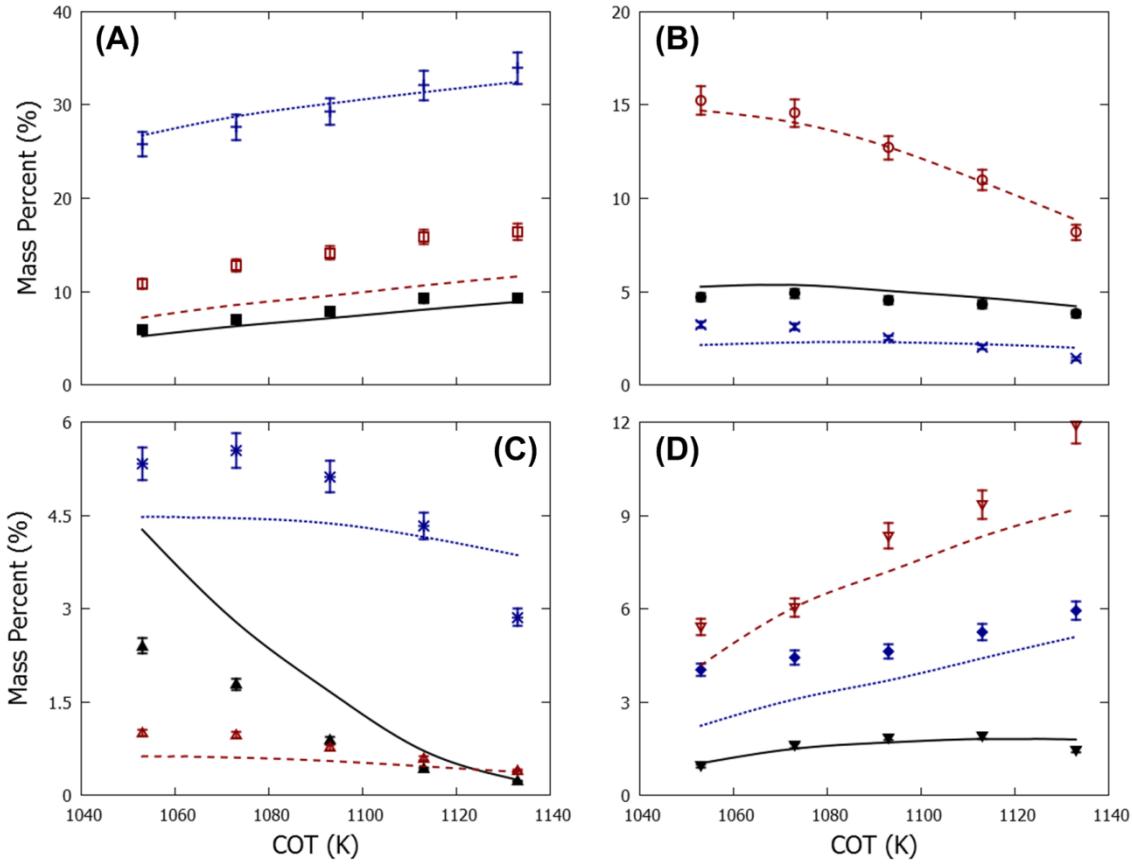

Figure 3.2-7: Mass percentage profile as a function of coil outlet temperature (COT) for steam cracking of HDO-CTO: ■ - H_2 x 10 (A), □ - CH_4 (A), + - C_2H_4 (A), ● - C_2H_6 (B), ○ - C_3H_6 (B), × - C3H8 x 5 (B), ▲ - 1-butene (C), ▲ - isobutene (C), ✱ - 1,3-butadiene (C), ▼ - 1,3-cyclopentadiene (D), ▼- benzene (D), ◆ - toluene (D); lines, mass percentage profiles calculated with CHEMKIN using the plug flow reactor model and the developed kinetic model.

The simulated species profiles match the experimental yields, both quantitatively and qualitatively, also given the complexity of the feedstock. The main discrepancies can be observed for methane which is underpredicted. Note that some group additive values applied in this work were originally derived for acyclic hydrocarbons, e.g. isomerization. The effect of a cyclic structure on the kinetic parameters, as is the case for isomerization in Figure 3.2-8, is, thus, not accounted for. Possibly, this can explain some of the model discrepancies observed in Figure 3.2-7. Further experimental and kinetic modeling work regarding thermal

decomposition of polycyclic model components can help in this respect. Model discrepancies can also be related with feedstock characterization, see 3.2.3.2 and 3.2.4.2, as molecules with the same carbon number and chemical functionalities were grouped and a representative molecule was selected for each group. As steam cracking of n-alkanes has been discussed earlier [7], the remainder of this section will focus on understanding the pyrolysis of polycyclic hydrocarbons.

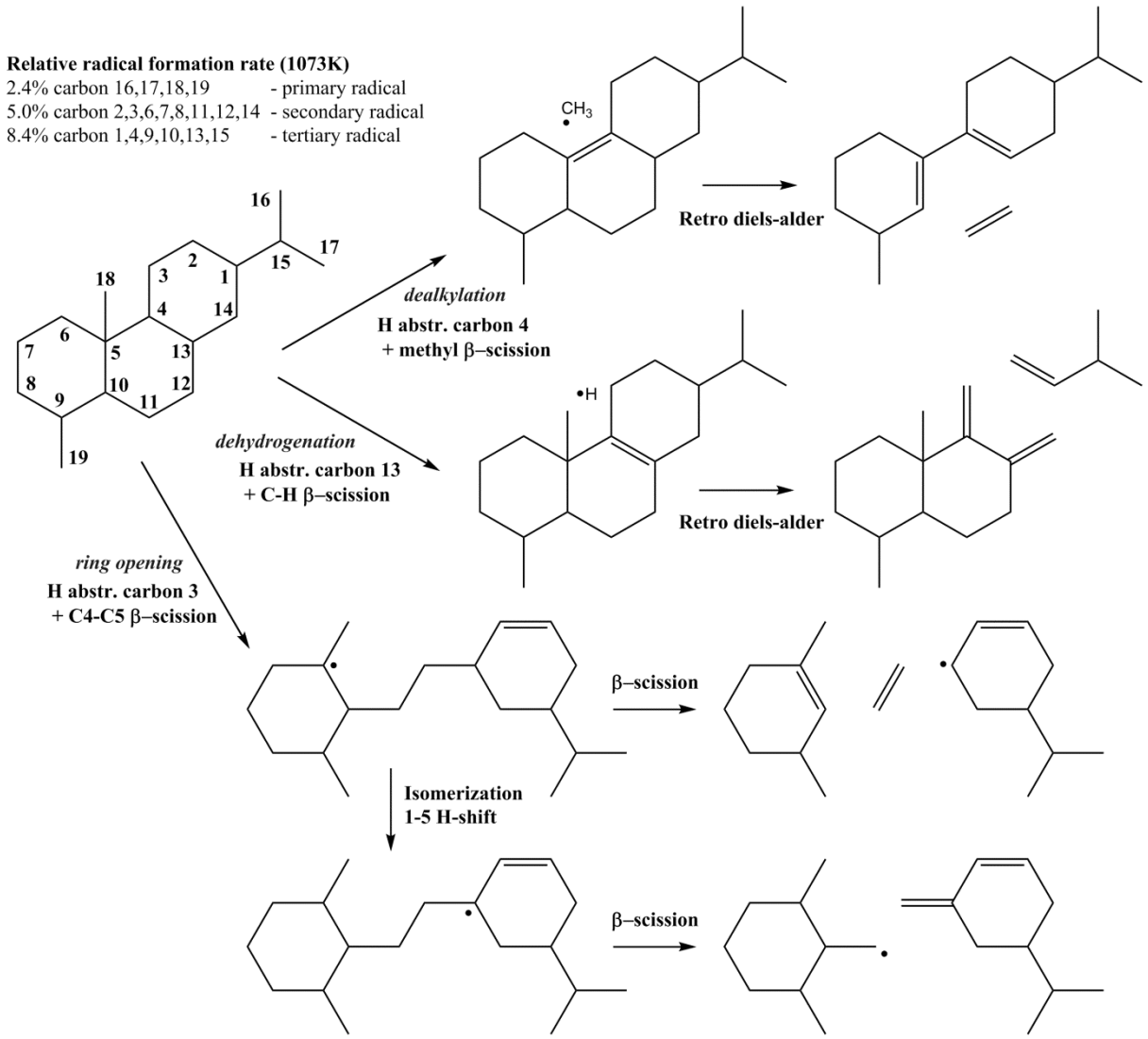

Figure 3.2-8 Selected decomposition paths for norabietane following hydrogen abstraction.

Resin acids present in crude tall oil form hydrogenated phenanthrene structures with various alkyl groups following hydrodexoygenation [13]. As mentioned in section 3.2.3.2, 18-norabietane is the most abundant polycyclic hydrocarbon in HDO-CTO. Unimolecular decomposition occurs primarily through scission of an alkyl group from the naphthenic structure, similar to methyl-cyclohexane[62]. The majority of 18-norabietane is however consumed by hydrogen abstraction in the investigated temperature range. Hydrogen

abstraction from 18-noarbietane leads to approximately 10% primary radicals, 40% secondary radicals and 50% tertiary radicals at 1073K, calculated using reaction path analysis. This distribution is a weak function of temperature[67].

Some examples of possible decomposition paths following hydrogen abstraction are presented in Figure 3.2-8. There are three possible pathways, i.e., dealkylation, dehydrogenation and ring opening. The generated model predicts that C-C β-scission of an alkyl side chain, so-called dealkylation, is favored compared to other reaction pathways. A similar result has been reported earlier in the theoretical work of Sirjean et al. on 1-methyl-cylopent-2-yl decomposition[63]. Note that not all cyclic radicals can undergo dealkylation as this requires a carbon atom with an alkyl chain in position α to the radical site. Sirjean et al. reported that the formation of cyclopentene and methyl is approximately a factor 10 faster than ring opening in the considered temperature range[63]. The rates of the C-H β-scission and ring opening are competitive, with the latter being favored[63]. Each 18-norabietane radical ($C_{19}H_{33}$) can decompose through C-H β-scission forming an unsaturated tricyclic hydrocarbon with 19 carbon atoms ($C_{19}H_{32}$) and a hydrogen radical. In contrast, the product distribution following ring opening and subsequent decomposition is different for each 18-norabietane radical. The global hydrogen abstraction reaction of 18-norabietane has a relatively high selectivity towards $C_{19}H_{32}$ isomers as such an isomer can be formed through all 19 hydrogen abstraction channels.

Ring opening of 18-norabietane radicals and subsequent decomposition results in the formation of a wide spectrum of species. While ethene and propene can be formed directly, there is a high selectivity to polyunsaturated hydrocarbons, unsaturated naphthenes and resonantly stabilized radicals. These species can form aromatics through stepwise dehydrogenation and/or dealkylation steps. Aromatics can thus be believed to be primary products of 18-norabietane, directly originating from the feed structure and, as such, they are not solely formed through secondary chemistry such as propargyl recombination [74] or vinyl addition on butadiene followed by cyclization [36, 75]. This explains the high experimental yield for the latter species. Billaud et al. obtained a similar result for pyrolysis of decalin and described its initial decomposition as a sum of aromatics, light alkenes and permanent gases [41]. Reaction path analysis shows that secondary reactions of primary products formed following hydrogen abstraction from 18-norabietane are important sources of ethene during steam cracking of HDO-CTO, e.g. retro diels-alder of unsaturated cyclic molecules. This is different compared to steam cracking of the conventional feedstocks and n-alkanes in HDO-

CTO where ethene is mainly formed through primary reactions of the hydrocarbons present in the feedstock, i.e. hydrogen abstraction followed by (repeated) β-scission.

Naphthenoaromatics comprise about 5wt% of the HDO-CTO feedstock and are products of polycyclic alkanes through dehydrogenation of one of the rings. 19-norabieta-8,11,13-triene has a rather different reactivity compared to its hydrogenated counterpart, 18-norabietane. Its unimolecular decomposition through scission of a methyl group is significantly faster due to formation of a resonantly stabilized radical. The majority of naphthenoaromatics is however consumed through reactions with radicals. Besides hydrogen abstraction, ipso-addition on the aromatic ring causing either dealkylation and ring opening are possible[76]. The latter pathway is responsible for about 10% of naphthenoaromatic consumption in the investigated temperature range. Hydrogen abstraction on positions rendering a benzylic radical will dominate over hydrogen abstractions from other carbon atoms. Subsequent decomposition routes, dehydrogenation and ring opening, are presented in Figure 3.2-9. The former reaction pathway leads to formation of substituted hexahydrophenanthrene which will react to substituted tetrahydrophenanthrene following hydrogen abstraction and dehydrogenation or dealkylation. Thermal decomposition of unsaturated naphthenoaromatics have a high selectivity towards poly-aromatics at typical pyrolysis conditions (T=1000K, P=0.1MPa) as observed during pyrolysis of tetralin[77, 78]. The thermal decomposition of 19-norabieta-8,11,13-triene will, thus, have a high selectivity for pyrolysis fuel oil (C_{10+}) and permanent gases but a low selectivity for light olefins.

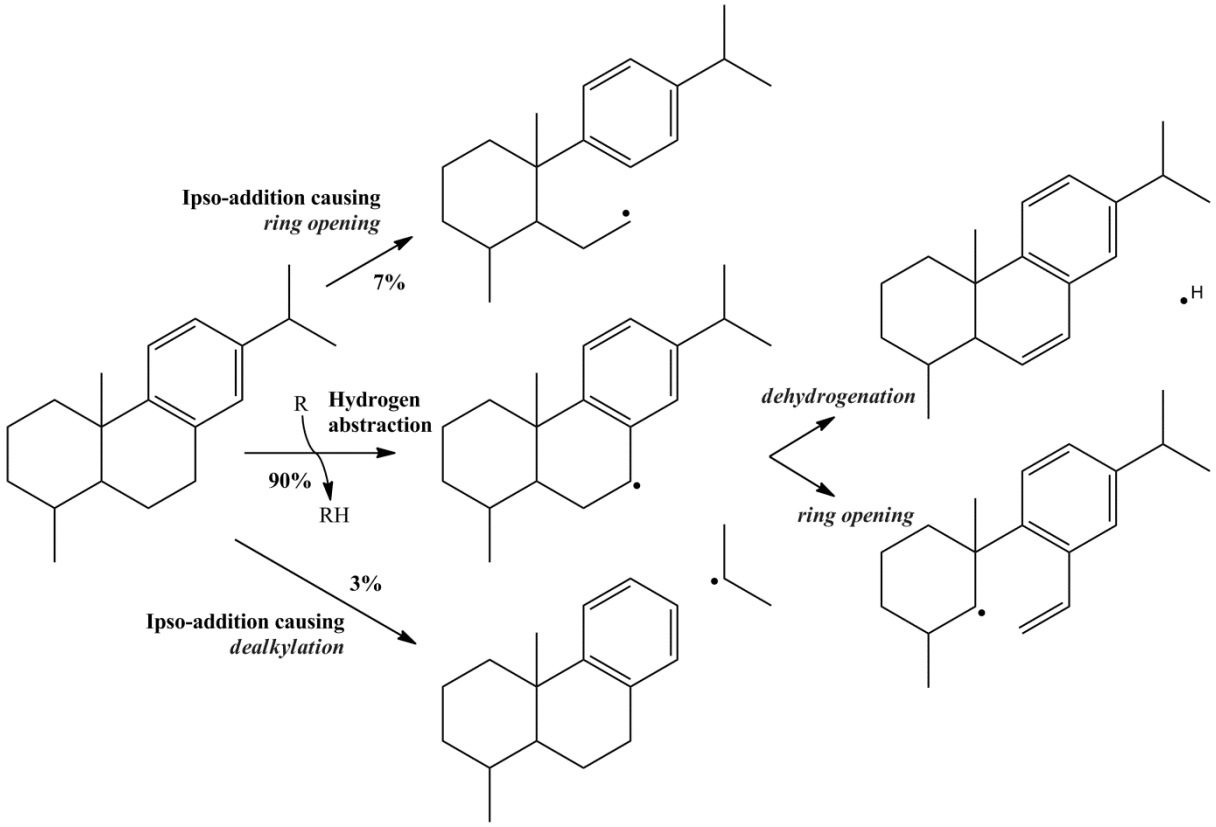

Figure 3.2-9 Selected reaction paths of 19-norabieta-8,11,13-triene with radicals. Numbers indicate relative consumption rate.

The selected operating conditions for HDO have an important effect on the product distribution obtained during steam cracking of HDO-CTO. These HDO conditions should be severe enough that no residual oxygen remains to avoid formation of small oxygenated molecules such as formaldehyde or methanol which can lead to downstream fouling and off-spec ethene/propene streams[8]. On the other hand, HDO of CTO at high temperatures will yield a large amount of (poly-)aromatics[13, 16]. Dehydrogenation of cyclo-alkanes, such as norabietane, is an endothermic reaction, hence, favoring formation of aromatics at these conditions[79]. As discussed earlier, polycyclic hydrocarbons with unsaturated rings have a high selectivity for low-value chemicals.

3.2.5 Conclusions

Crude tall oil is a high-potential renewable feedstock for the production of bio-ethene, bio-propene and bio-aromatics. Production of light olefins from CTO can be achieved in a two-step process, i.e., hydrodeoxygenation followed by steam cracking.

Steam cracking of HDO-CTO has been investigated experimentally and ethene yields up to 34wt% and propene yields up to 15 wt% have been measured, in line with conventional

feedstock's such as naphtha and natural gas condensate. Furthermore, a similar propene over ethene ratio can be achieved at lower temperatures for CTO upon comparison with the aforementioned fossil feedstocks, which makes that CTO derived olefins require a lower heat input.

Optimal use of the proposed feedstock in conventional steam crackers is only possible when the reactions governing its thermal decomposition are well understood. Therefor a dedicated micro-kinetic model has been developed which is able to describe the pyrolysis of alkanes and polycyclic hydrocarbons present in HDO-CTO. The kinetics describing the decomposition of cyclic hydrocarbons were first validated for the simplest alkylated naphthene, i.e. methyl-cyclohexane. The final generated model is also able to accurately reproduce the experiments that have been performed with CTO next to methyl-cyclohexane. Rate of production analysis shows that the naphthenes give rise to a high yield of valuable olefins and mono-aromatics. On the other hand naphthenoaromatics form mainly permanent gases and poly-aromatics. Both species are formed through hydrodeoxygenation of resin acids present in the crude tall oil. The formation of naphthenoaromatics can be suppressed by performing hydrodeoxygenation of crude tall oil at relatively low temperatures[16]. In this case, space time and hydrogen pressure should be high enough to ensure complete oxygen conversion.

3.2.6 References

[1] International Energy Agency - Energy Technology Systems Analysis Programme and International Renewable Energy Agency, Production of Bio-ethylene, Technology Brief I13 (2013)
[2] Q. Wang, X. Chen, A. N. Jha, H. Rogers, Natural gas from shale formation – The evolution, evidences and challenges of shale gas revolution in United States, Renew. Sust. Energ. Rev. 30 (2014) 1-28
[3] A. E. Muñoz Gandarillas, K. M. Van Geem, M.-F. Reyniers, G. B. Marin, Influence of the Reactor Material Composition on Coke Formation during Ethane Steam Cracking, Ind. Eng. Chem. Res. 53 (2014) 6358-6371
[4] W. R. True, Global ethylene capacity poised for major expansion, Oil & Gas J. (2013)
[5] M. Zhang, Y. Yu, Dehydration of Ethanol to Ethylene, Ind. Eng. Chem. Res. 52 (2013) 9505-9514
[6] Smithers Rapra, The future of bioplastics, Market forecasts to 2017 (2012)
[7] S. P. Pyl, C. M. Schietekat, M.-F. Reyniers, R. Abhari, G. B. Marin, K. M. Van Geem, Biomass to olefins: Cracking of renewable naphtha, Chem. Eng. J. 176-177 (2011) 178-187
[8] J. A. Reid, G. Nowowiejski, Overview of Oxygenates in Olefin Units in Relation to Corrosion, Fouling, Product Specifications, and Safety, Ethylene Producers Conference, New Orleans, USA (2003)
[9] A. V. Bridgwater, Review of fast pyrolysis of biomass and product upgrading, Biomass Bioenerg. 38 (2012) 68-94
[10] N. Andrew, SABIC eyes biological feedstocks for polymers, Hydrocarb. Process. (2014)
[11] R. Patt, O. Kordsachia, R. Süttinger, Y. Ohtani, J. F. Hoesch, P. Ehrler, R. Eichinger, H. Holik, U. Hamm, M. E. Rohmann, P. Mummenhoff, E. Petermann, R. F. Miller, D. Frank, R. Wilken, H. L. Baumgarten, G.-H. Rentrop, Paper and Pulp, in Ullmann's Encyclopedia of Industrial Chemistry, Wiley-VCH Verlag GmbH & Co. KGaA: 2000.
[12] L.-H. Norlin, Tall Oils, in Ullmann's Encyclopedia of Industrial Chemistry, John Wiley & Sons, Inc.: New York, 2005.
[13] J. M. Anthonykutty, K. M. Van Geem, R. De Bruycker, J. Linnekoski, A. Laitinen, J. Räsänen, A. Harlin, J. Lehtonen, Value Added Hydrocarbons from Distilled Tall Oil via Hydrotreating over a Commercial NiMo Catalyst, Ind. Eng. Chem. Res. 52 (2013) 10114-10125

[14] A. Thomas, Fats and Fatty Oils, in Ullmann's Encyclopedia of Industrial Chemistry, Wiley-VCH Verlag GmbH & Co. KGaA: 2000.
[15] S. P. Pyl, T. Dijkmans, J. M. Antonykutty, M.-F. Reyniers, A. Harlin, K. M. Van Geem, G. B. Marin, Wood-derived olefins by steam cracking of hydrodeoxygenated tall oils, Bioresour. Technol. 126 (2012) 48-55
[16] J. Anthonykutty, J. Linnekoski, A. Harlin, A. Laitinen, J. Lehtonen, Catalytic upgrading of crude tall oil into a paraffin-rich liquid, Biomass Conv. Bioref. 1 (2014) 1-11
[17] W. Hillebrand, W. Hodek, G. Kölling, Steam cracking of coal-derived oils and model compounds: 1. Cracking of tetralin and t-decalin, Fuel 63 (1984) 756-761
[18] F. D. Kopinke, G. Zimmermann, G. C. Reyniers, G. F. Froment, Relative Rates of Coke Formation from Hydrocarbons in Steam Cracking of Naphtha. 2. Paraffins, Naphthenes, Mono-olefins, di-olefins, cyclo-olefins, and acetylenes, Ind. Eng. Chem. Res. 32 (1993) 56-61
[19] S. Barendregt, P. J. M. Valkenburg, E. S. Wagner, M. Dente, E. Ranzi, History and Recent Developments in SPYRO, a Review, AIChE Spring National Meeting, New Orleans, LA, USA (2002)
[20] K. M. Van Geem, M.-F. Reyniers, G. B. Marin, Challenges of modeling steam cracking of heavy feedstocks, Oil. Gas. Sci. Technol. 63 (2008) 79-94
[21] P. Dagaut, A. Ristori, A. Frassoldati, T. Faravelli, G. Dayma, E. Ranzi, Experimental and semi-detailed kinetic modeling study of decalin oxidation and pyrolysis over a wide range of conditions, P. Combust. Inst. 34 (2013) 289-296
[22] Y. Zhu, D. F. Davidson, R. K. Hanson, Pyrolysis and oxidation of decalin at elevated pressures: A shock-tube study, Combust. Flame 161 (2014) 371-383
[23] T. Dijkmans, S. P. Pyl, M.-F. Reyniers, R. Abhari, K. M. Van Geem, G. B. Marin, Production of bio-ethene and propene: alternatives for bulk chemicals and polymers, Green Chem. 15 (2013) 3064-3076
[24] ASTM International, Standard Test Methods for Fatty and Rosin Acids in Tall Oil Fractionation Products by Capillary Gas Chromatography (2010)
[25] H. E. Toraman, T. Dijkmans, M. R. Djokic, K. M. Van Geem, G. B. Marin, Detailed compositional characterization of plastic waste pyrolysis oil by comprehensive two-dimensional gas-chromatography coupled to multiple detectors, J. Chromatogr. A 1359 (2014) 237-246
[26] T. Dijkmans, K. M. Van Geem, M. R. Djokic, G. B. Marin, Combined Comprehensive Two-Dimensional Gas Chromatography Analysis of Polyaromatic Hydrocarbons/Polyaromatic Sulfur-Containing Hydrocarbons (PAH/PASH) in Complex Matrices, Ind. Eng. Chem. Res. 53 (2014) 15436-15446
[27] T. Dijkmans, M. R. Djokic, K. M. Van Geem, G. B. Marin, Comprehensive compositional analysis of sulfur and nitrogen containing compounds in shale oil using GCxGC – FID/SCD/NCD/TOF-MS, Fuel 140 (2015) 398-406
[28] M. R. Djokic, K. M. Van Geem, C. Cavallotti, A. Frassoldati, E. Ranzi, G. B. Marin, An experimental and kinetic modeling study of cyclopentadiene pyrolysis: First growth of polycyclic aromatic hydrocarbons, Combust. Flame 161 (2014) 2739-2751
[29] K. M. Van Geem, S. P. Pyl, M.-F. Reyniers, J. Vercammen, J. Beens, G. B. Marin, On-line analysis of complex hydrocarbon mixtures using comprehensive two-dimensional gas chromatography, J. Chromatogr. A 1217 (2010) 6623-6633
[30] M. R. Harper, K. M. Van Geem, S. P. Pyl, G. B. Marin, W. H. Green, Comprehensive reaction mechanism for n-butanol pyrolysis and combustion, Combust. Flame 158 (2011) 16-41
[31] M. Djokic, H.-H. Carstensen, K. M. Van Geem, G. B. Marin, The thermal decomposition of 2,5-dimethylfuran, P. Combust. Inst. 34 (2013) 251-258
[32] N. M. Vandewiele, G. R. Magoon, K. M. Van Geem, M.-F. Reyniers, W. H. Green, G. B. Marin, Experimental and Modeling Study on the Thermal Decomposition of Jet Propellant-10, Energ. Fuel. (2014)
[33] K. M. Van Geem, I. Dhuyvetter, S. Prokopiev, M. F. Reyniers, D. Viennet, G. B. Marin, Coke Formation in the Transfer Line Exchanger during Steam Cracking of Hydrocarbons, Ind. Eng. Chem. Res. 48 (2009) 10343-10358
[34] J. Beens, H. Boelens, R. Tijssen, J. Blomberg, Quantitative aspects of comprehensive two-dimensional gas chromatography (GC x GC), J. High. Resolut. Chromatogr. 21 (1998) 47-54
[35] S. P. Pyl, C. M. Schietekat, K. M. Van Geem, M.-F. Reyniers, J. Vercammen, J. Beens, G. B. Marin, Rapeseed oil methyl ester pyrolysis: On-line product analysis using comprehensive two-dimensional gas chromatography, J. Chromatogr. A 1218 (2011) 3217-3223
[36] M. K. Sabbe, K. M. Van Geem, M.-F. Reyniers, G. B. Marin, First principle-based simulation of ethane steam cracking, AlChE J. 57 (2011) 482-496
[37] K. J. Laidler, Chemical Kinetics, Harper & Row, New York, 1987
[38] M. F. Reyniers, G. F. Froment, Influence of metal-surface and sulfur addition on coke deposition in the thermal cracking of hydrocarbons, Ind. Eng. Chem. Res. 34 (1995) 773-785
[39] O. Herbinet, P. M. Marquaire, F. Battin-Leclerc, R. Fournet, Thermal decomposition of n-dodecane: Experiments and kinetic modeling, J. Anal. Appl. Pyrolysis 78 (2007) 419-429

[40] C. Ji, S. M. Sarathy, P. S. Veloo, C. K. Westbrook, F. N. Egolfopoulos, Effects of fuel branching on the propagation of octane isomers flames, Combust. Flame 159 (2012) 1426-1436
[41] F. Billaud, P. Chaverot, E. Freund, Cracking of decalin and tetralin in the presence of mixtures of n-decane and steam at about 810°C, J. Anal. Appl. Pyrolysis 11 (1987) 39-53
[42] H. Zimmermann, R. Walzl, Ethylene, in Ullmann's Encyclopedia of Industrial Chemistry, John Wiley & Sons, Inc.: New York, 2009.
[43] M. Golombok, J. van der Bijl, M. Kornegoor, Severity Parameters for Steam Cracking, Ind. Eng. Chem. Res. 40 (2000) 470-472
[44] K. M. Van Geem, M. F. Reyniers, G. B. Marin, Two severity indices for scale-up of steam cracking coils, Ind. Eng. Chem. Res. 44 (2005) 3402-3411
[45] A. E. Muñoz Gandarillas, K. M. Van Geem, M.-F. Reyniers, G. B. Marin, Coking Resistance of Specialized Coil Materials during Steam Cracking of Sulfur-Free Naphtha, Ind. Eng. Chem. Res. 53 (2014) 13644-13655
[46] P. J. Clymans, G. F. Froment, Computer generation of the reaction paths and rate equations in the thermal cracking of normal and branched paraffins, Comput. Chem. Eng. 8 (1984) 137-142
[47] E. Ranzi, M. Dente, S. Plerucci, G. Biardi, Initial product distributions from pyrolysis of normal and branched paraffins, Ind. Eng. Chem. Fund. 22 (1983) 132-139
[48] D. M. Fake, A. Nigam, M. T. Klein, Mechanism based lumping of pyrolysis reactions: Lumping by reactive intermediates, Appl. Catal. A-Gen. 160 (1997) 191-221
[49] M. Mehl, W. J. Pitz, S. M. Sarathy, C. K. Westbrook, Modeling the combustion of high molecular weight fuels by a functional group approach, Int. J. Chem. Kinet. 44 (2012) 257-276
[50] T. Dijkmans, C. M. Schietekat, K. M. Van Geem, G. B. Marin, GPU based simulation of reactive mixtures with detailed chemistry in combination with tabulation and an analytical Jacobian, Comput. Chem. Eng. 71 (2014) 521-531
[51] M. Dente, G. Bozzano, T. Faravelli, A. Marongiu, S. Pierucci, E. Ranzi, Kinetic Modelling of Pyrolysis Processes in Gas and Condensed Phase, Adv. Chem. Eng. 32 (2007) 51-166
[52] A. Nigam, D. M. Fake, M. T. Klein, Simple Approximate Rate Law for Both Short-chain and Long-chain Rice-Herzfeld Kinetics, AlChE J. 40 (1994) 908-910
[53] B. Ruscic, R. E. Pinzon, G. von Laszewski, D. Kodeboyina, A. Burcat, D. Leahy, D. Montoya, A. F. Wagner, Active Thermochemical Tables: thermochemistry for the 21st century, in SciDAC 2005: Scientific Discovery Through Advanced Computing, A. Mezzacappa, (Ed.) Iop Publishing Ltd: Bristol, 2005; Vol. 16, pp 561-570.
[54] S. W. Benson, Thermochemical Kinetics: Methods for the Estimation of Thermochemical Data and Rate Parameters, John Wiley & Sons, New York, 1976
[55] M. K. Sabbe, F. De Vleeschouwer, M.-F. Reyniers, M. Waroquier, G. B. Marin, First Principles Based Group Additive Values for the Gas Phase Standard Entropy and Heat Capacity of Hydrocarbons and Hydrocarbon Radicals, J. Phys. Chem. A 112 (2008) 12235-12251
[56] M. K. Sabbe, A. Vandeputte, M.-F. Reyniers, M. Waroquier, G. B. Marin, Modeling the influence of resonance stabilization on the kinetics of hydrogen abstractions, Phys. Chem. Chem. Phys. 12 (2010) 1278-1298
[57] M. K. Sabbe, M.-F. Reyniers, M. Waroquier, G. B. Marin, Hydrogen Radical Additions to Unsaturated Hydrocarbons and the Reverse beta-Scission Reactions: Modeling of Activation Energies and Pre-Exponential Factors, ChemPhysChem 11 (2010) 195-210
[58] M. K. Sabbe, M.-F. Reyniers, V. Van Speybroeck, M. Waroquier, G. B. Marin, Carbon-centered radical addition and beta-scission reactions: Modeling of activation energies and pre-exponential factors, ChemPhysChem 9 (2008) 124-140
[59] C. Cavallotti, D. Polino, A. Frassoldati, E. Ranzi, Analysis of Some Reaction Pathways Active during Cyclopentadiene Pyrolysis, J. Phys. Chem. A 116 (2012) 3313-3324
[60] C. Cavallotti, D. Polino, On the kinetics of the C5H5 + C5H5 reaction, P. Combust. Inst. 34 (2013) 557-564
[61] S. Zeppieri, K. Brezinsky, I. Glassman, Pyrolysis studies of methylcyclohexane and oxidation studies of methylcyclohexane and methylcyclohexane/toluene blends, Combust. Flame 108 (1997) 266-286
[62] Z. Wang, L. Ye, W. Yuan, L. Zhang, Y. Wang, Z. Cheng, F. Zhang, F. Qi, Experimental and kinetic modeling study on methylcyclohexane pyrolysis and combustion, Combust. Flame 161 (2014) 84-100
[63] B. Sirjean, P. A. Glaude, M. F. Ruiz-Lopez, R. Fournet, Theoretical Kinetic Study of Thermal Unimolecular Decomposition of Cyclic Alkyl Radicals, J. Phys. Chem. A 112 (2008) 11598-11610
[64] J. H. Kiefer, J. N. Shah, Unimolecular dissociation of cyclohexene at extremely high temperatures: behavior of the energy-transfer collision efficiency, J. Phys. Chem.-US 91 (1987) 3024-3030
[65] C. Ellis, M. S. Scott, R. W. Walker, Addition of toluene and ethylbenzene to mixtures of H2 and O2 at 772 K: Part 2: formation of products and determination of kinetic data for H+ additive and for other elementary reactions involved, Combust. Flame 132 (2003) 291-304

[66] A. Stagni, A. Cuoci, A. Frassoldati, T. Faravelli, E. Ranzi, Lumping and Reduction of Detailed Kinetic Schemes: an Effective Coupling, Ind. Eng. Chem. Res. 53 (2013) 9004-9016
[67] E. Ranzi, M. Dente, A. Goldaniga, G. Bozzano, T. Faravelli, Lumping procedures in detailed kinetic modeling of gasification, pyrolysis, partial oxidation and combustion of hydrocarbon mixtures, Prog. Energy Combust. Sci. 27 (2001) 99-139
[68] T. F. Lu, C. K. Law, Toward accommodating realistic fuel chemistry in large-scale computations, Prog. Energy Combust. Sci. 35 (2009) 192-215
[69] C. M. Schietekat, M. W. M. van Goethem, K. M. Van Geem, G. B. Marin, Swirl flow tube reactor technology: An experimental and computational fluid dynamics study, Chem. Eng. J. 238 (2014) 56-65
[70] R. J. Kee, F. M. Rupley, J. A. Miller, M. E. Coltrin, J. F. Grcar, E. Meeks, H. K. Moffat, A. E. Lutz, G. Dixon-Lewis, M. D. Smooke, J. Warnatz, G. H. Evans, L. R. S., R. E. Mitchell, L. R. Petzold, W. C. Reynolds, M. Caracotsios, W. E. Stewart, P. Glarborg, C. Wang, O. Adigun, in: 15101 ed.; Reaction Design, Inc.: San Diego (CA), 2010.
[71] J. P. Orme, H. J. Curran, J. M. Simmie, Experimental and modeling study of methyl cyclohexane pyrolysis and oxidation, J. Phys. Chem. A 110 (2006) 114-131
[72] F. Zhang, Z. Wang, Z. Wang, L. Zhang, Y. Li, F. Qi, Kinetics of Decomposition and Isomerization of Methylcyclohexane: Starting Point for Studying Monoalkylated Cyclohexanes Combustion, Energ. Fuel. 27 (2013) 1679-1687
[73] S. J. Klippenstein, Y. Georgievskii, L. B. Harding, Predictive theory for the combination kinetics of two alkyl radicals, Phys. Chem. Chem. Phys. 8 (2006) 1133-1147
[74] L. B. Harding, S. J. Klippenstein, Y. Georgievskii, On the combination reactions of hydrogen atoms with resonance-stabilized hydrocarbon radicals, J. Phys. Chem. A 111 (2007) 3789-3801
[75] C. Cavallotti, R. Rota, S. Carrà, Quantum Chemistry Computation of Rate Constants for Reactions Involved in the First Aromatic Ring Formation, J. Phys. Chem. A 106 (2002) 7769-7778
[76] P. Dagaut, A. Ristori, A. Frassoldati, T. Faravelli, G. Dayma, E. Ranzi, Experimental Study of Tetralin Oxidation and Kinetic Modeling of Its Pyrolysis and Oxidation, Energ. Fuel. 27 (2013) 1576-1585
[77] M. L. Poutsma, Progress toward the mechanistic description and simulation of the pyrolysis of tetralin, Energ. Fuel. 16 (2002) 964-996
[78] Y. Li, L. Zhang, Z. Wang, L. Ye, J. Cai, Z. Cheng, F. Qi, Experimental and kinetic modeling study of tetralin pyrolysis at low pressure, P. Combust. Inst. 34 (2013) 1739-1748
[79] R. Biniwale, N. Kariya, M. Ichikawa, Dehydrogenation of Cyclohexane Over Ni Based Catalysts Supported on Activated Carbon using Spray-pulsed Reactor and Enhancement in Activity by Addition of a Small Amount of Pt, Catal. Lett. 105 (2005) 83-87

3.3 Microkinetic model for the pyrolysis of methyl esters

This section is based on the following paper:

Ruben De Bruycker, Steven Pyl, Marie-Françoise Reyniers, Kevin M. Van Geem, Guy B. Marin, "Microkinetic model for the pyrolysis of methyl esters: From model compound to industrial biodiesel" *AIChE Journal* 2015, 61 (12), 4309 – 4322

3.3.1 Abstract

A tool for the generation of decomposition schemes of large molecules has been developed. These decomposition schemes contain radicals which can be eliminated from the model equations if both the μ-hypothesis and the pseudo-steady-state approximation are valid. The reaction rate coefficients and thermodynamic parameters have been calculated by incorporating a comprehensive group additive framework. A microkinetic model for the pyrolysis of methyl esters with a carbon number of up to 19 has been generated using this tool. It is validated by comparing calculated and experimental product yields of the pyrolysis of methyl decanoate and novel rapeseed methyl ester pyrolysis data in the temperature range from 800 to 1100K and methyl ester partial pressure range from 1 10^{-3} to 1 10^{-2} MPa. This modeling frame work allows to not only assess the use of methyl ester mixtures as potential feedstock for olefin production but also their effect as blend-in or trace impurity.

Keywords: pyrolysis, methyl esters, kinetic modeling, group additivity, C=C double bond

3.3.2 Introduction

Pyrolysis of alkanes, cycloalkanes, alkenes, aromatics, alcohols and methyl esters, mainly proceeds through a free-radical mechanism[1, 2]. This process is characterized by a vast number of species and reactions which increases dramatically with the molecular mass of the feed[1, 3]. Developing microkinetic models which describe the thermal decomposition of large molecules thus requires the use of automatic reaction network generation software. Most of these tools require the input of the feed as well as a set of reaction families. The reaction generator subsequently matches molecules and reaction families to add new reactions and molecules to the reaction network. Examples of such tools are Genesys[4], RING[5], RMG[6], EXGAS[7], NETGEN[8, 9], REACTION[10]… The output of these network generators is generally a CHEMKIN readable file containing thermodynamic data, derived from the group additivity method originally developed by Benson[11], and elementary reactions, with kinetic parameters often derived from rate rules such as the Evans-Polanyi relationship[12]. Despite being general, the aforementioned tools require constrains to limit the number of species and reactions. Thus, automated reaction network generation has mainly been used for relatively small molecules.

The need for reaction networks of heavy feeds will however increase. Notable examples are the steam cracking of vacuum gas oils and the fast pyrolysis of biomass. MAMA[1] is a reaction network generator that has been used to create kinetic models for molecules with a high molecular mass. This program decomposes large radicals, for example formed by hydrogen abstraction of large molecules, until a distribution of primary products remains. The obtained product spectrum is retained in such reactions, rather than the large radical itself. MAMA makes use of a library of kinetic parameters and the temperature dependence of the stoichiometric coefficients of the various products in the final equivalent reactions is neglected.

In this work a new automated network generation code is presented called PRIM-O, based on the earlier version called PRIM[13], that can be used for large hydrocarbons, large oxygen containing compounds, and mixtures thereof. The main differences compared to previous version is (i) the use of group additivity for both kinetics and thermodynamics, based on the work by Benson[11], and (ii) the extension towards oxygenated components.

The pyrolysis of methyl esters has been chosen to assess its capabilities and limitations. Methyl esters have received a lot of interest in the past few decades given their potential to be

a sustainable alternative to fossil fuels. Engine studies showed that these oxygenated fuels have the tendency to reduce soot formation [14-16] but result in increased NO_x formation compared to traditional diesel fuels [15, 17-19]. Methyl esters are generally produced through the transesterfication of vegetable oils with methanol [20, 21] which can be used as an alternative feedstock for olefin production[22-25].

A kinetic model for the thermal decomposition of methyl esters has been generated. In order to validate this model, experimental pyrolysis data with detailed product distribution is required. To the best of our knowledge, such data is currently unavailable for real rapeseed methyl ester mixtures. Therefore, pyrolysis experiments have been performed using a continuous flow tubular reactor setup with dedicated online analysis section for product identification and quantification. Furthermore, commonly used assumptions such as the μ-hypothesis[26] and the pseudo-steady-state approximation[27-29] (PSSA), also known as the quasi-steady-state-approximation (QSSA), are verified.

3.3.3 Experimental methods

The experimental reactor setup has been described in detail elsewhere[30-32] and therefore only a brief description based on Djokic et al.[31] and Pyl et al.[32] will be given here.

The rapeseed methyl ester feed (RME) was provided by CARGILL[33] and was used without further treatment. The mixture comprises methyl esters with alkyl chains up to 24 carbon atoms and up to 3 double bonds. The major constituents are methyl palmitate (21mol%), methyl stearate (2.5mol%), methyl oleate (53mol%), methyl linoeate (15mol%) and methyl linolenate (5mol%). The (liquid) methyl ester feedstock was fed using a mass flow controlled pump (LIQUI-FLOW Bronkhorst) into a vaporizer. The mass flow of the diluent, i.e. nitrogen (Air Liquide, purity +99.999mol%), was controlled using a Coriolis mass flow controller (CORI-FLOW Bronkhorst). A heated quartz pellet-filled mixer upstream of the reactor ensures a homogeneous nitrogen – methyl ester gas mixture.

This mixture enters a 1.475m long reactor with an internal diameter of 6 mm made out of Incoloy 800HT. The reactor is placed vertically in an electrically heated rectangular furnace and the pressure is kept constant by a valve downstream of the reactor. In all experiments, the reactor is operated nearly isothermally with a steep temperature increase at the inlet and a steep temperature drop at the reactor outlet. Eight thermocouples along the reactor monitor the process gas temperature at different positions. Two manometers, positioned at the inlet

and outlet of the reactor, record the coil inlet pressure (CIP) and the coil outlet pressure (COP), respectively. The pressure drop over the reactor was found to be negligible.

The analysis section of the pyrolysis setup has been discussed previously[32]. In short, it consists of several dedicated gas chromatographs, i.e., a refinery gas analyzer (RGA), a light oxygenates analyzer (LOA) and a 2D-gas chromatograph (GC×GC) equipped with a flame ionization detector (FID) and time of flight mass spectrometer (TOF-MS). The RGA quantifies hydrogen and other permanent gases using two thermal conductivity detectors (TCD) and the C_{4-} hydrocarbon fraction using a FID. Nitrogen, the diluent used in this work, was used as primary internal standard. The LOA detects small oxygenates such as formaldehyde, methanol and water using a TCD. Propene was used as secondary internal standard for this chromatogram. The GC×GC is able to identify (TOF-MS) and quantify (FID) the complete effluent stream ranging from methane to pyrene. Methane was used as secondary internal standard. For each studied condition, at least 3 repeat analyses were performed. For all runs the mass balances were within the range of 95-105%. Deviations are attributed to uncertainties in the mass flow rates of the feed and the internal standard (N_2). After normalization of the total mass balance, elemental balances (C, H, O) were verified. The estimated experimental error of the measured product yields is 5% rel. in line with previous work[31]. The experimental error is lower for components with higher mole fractions.

3.3.4 Modeling methodology

Radicals, formed during the pyrolysis of methyl esters, can react further through various channels such as β-scission, intermolecular/intramolecular hydrogen abstraction and intermolecular/intramolecular radical addition. As long as the feed molecules are sufficiently small, it is possible to account for each individual reaction which leads to an accurate kinetic model. A higher number of heavy atoms, i.e., non-hydrogen atom, in the feed molecules leads to a dramatic increase in species and reactions[8, 34, 35]. The strategies followed to overcome the aforementioned issue will be discussed in the subsequent sections.

In line with earlier work[13, 34, 36-38], the kinetic network has been split up into two sub-networks, i.e. a β-network containing all thermodynamic and kinetic data of small molecules (typically C_{5-}), and a μ-network containing decomposition schemes for larger molecules (typically C_{6+}). The proposed separation originates from the μ-radical hypothesis[26] which proposes that radicals with a high number of heavy atoms primarily react via monomolecular reactions, μ-reactions, while bimolecular reactions, β-reactions, can be neglected.

Every reaction which forms a μ-radical is present in the μ-network. These μ-radicals react by intramolecular hydrogen abstraction and β-scission, i.e. monomolecular reactions, until only non-radical species and C_{5-} radicals remain. Rather than incorporating the μ-radicals explicitly in the μ-network, they can be substituted by their decomposition product spectrum. This is possible by combining the μ-radical hypothesis with the pseudo-steady-state approximation (PSSA)[13]. Reactions in the μ-network are collections of elementary reactions appearing as an equivalent single-step reaction[1, 13, 39].

In the following sections, the various parts of the kinetic model are discussed in detail. First, the origin of the β-network is discussed. This is followed by details regarding the generation of the μ-network using PRIM-O. Special attention is dedicated to validation of the μ-hypothesis and PSSA for ester radicals. Finally, the coupling of the complete kinetic model with CHEMKIN, a software tool for solving complex chemical kinetics problems, is discussed.

3.3.4.1 β-network

The β-network mainly contains thermodynamic data of small molecules (C_{5-}) and an appropriate set of elementary reactions. Three classes of molecules are present in the β-network, i.e., non-radical species, radicals that are solely involved in bimolecular reactions (such as H• and CH_3•) and radicals that are involved in mono and bimolecular reactions. In this work the β-network describes thermal decomposition of methyl butanoate, pyrolysis of C_{5-} hydrocarbons, reactions of small oxygenates and polycyclic aromatic hydrocarbon (PAH) formation through cyclopentadienyl chemistry.

The primary decomposition reactions of methyl butanoate were taken from an ab initio study by Huynh and Violi[40]. Their results were successfully applied to predict ignition delays as well as the formation of CO, CO_2, CH_3 and C_2H_4 during methyl butanoate pyrolysis in a shock tube[41-43]

A hydrocarbon pyrolysis mechanism developed by Sabbe et al.[44] and validated for steam cracking of small alkanes was also added to the β-network. The kinetics of the referred mechanism are obtained from the same CBS-QB3-based group additive models as applied in the μ-network, see subsequent section. Thermodynamic data were determined using accurate quantum chemical CBS-QB3 calculations.

Reactions and thermochemistry of small oxygenated species were taken from the mechanism by Li et al. [45], which includes decomposition of formaldehyde and methanol. While this reaction network was developed for combustion, it has been validated for pyrolysis conditions as well[45].

Finally, reaction paths for formation of PAH through cyclopentadienyl radicals were based on the work of Cavallotti et al.[46, 47].

3.3.4.2 Generation of the μ-network using PRIM-O

Each reaction in the μ-network was generated using PRIM-O. As input, PRIM-O requires the structure of the molecule and the desired reaction. The algorithm searches for possible reactive moieties corresponding to that specific reaction and calculates the kinetic parameters associated with each elementary step. Subsequently, μ-radicals are identified. For these species, all possible monomolecular reaction routes are generated, e.g. β-scission, intramolecular hydrogen abstraction, intramolecular radical addition… PRIM-O reiterates this procedure until all generated μ-radicals have decomposition paths. Finally, the μ-radicals can be eliminated from the model equations using the pseudo-steady-state approximation[48]. The μ-radicals are replaced by their complex product spectrum, comprising of non-radical species and small (C_{5-}) radicals, which leads to the so-called equivalent single-step reactions. All feed molecules and accompanying C_{6+} products were given as input to PRIM-O together with the possible reaction types, e.g. hydrogen abstraction scission, radical addition.

As example, the hydrogen addition on methyl hept-6-enoate and its subsequent decomposition in PRIM-O is presented in Figure 3.3-1. Intramolecular hydrogen abstraction and hydrogen-centered β-scission are not included to reduce the complexity of the figure. Two possible reactive centra are recognized forming methyl heptanoate-6-yl and methyl heptanoate-7-yl. For both radicals, bimolecular reactions can be neglected and they are further decomposed in PRIM-O. Methyl heptanoate-6-yl reacts with formation of propene and methyl butanoate-4-yl. The latter radical is assumed to be the largest radical for which bimolecular reactions cannot be neglected, hence, it is not further decomposed. Methyl heptanoate-7-yl forms ethene and methyl pentanoate-5-yl. The latter radical is a μ-radical and reacts further through carbon centered β-scission forming methyl propanoate-3-yl and, again, ethene. The complete hydrogen addition can be written as an equivalent single-step reaction where the stoichiometric coefficients are a function of the kinetic parameters of the various elementary steps. Note that the stoichiometric coefficients are temperature dependent and reflect the

importance of the reaction path(s) leading to that specific species. In the presented example, these are function of the ratio of the kinetic parameters of both possible hydrogen additions. Hence, if a certain reaction path is favored, this will lead to a higher stoichiometric coefficient for the resulting species.

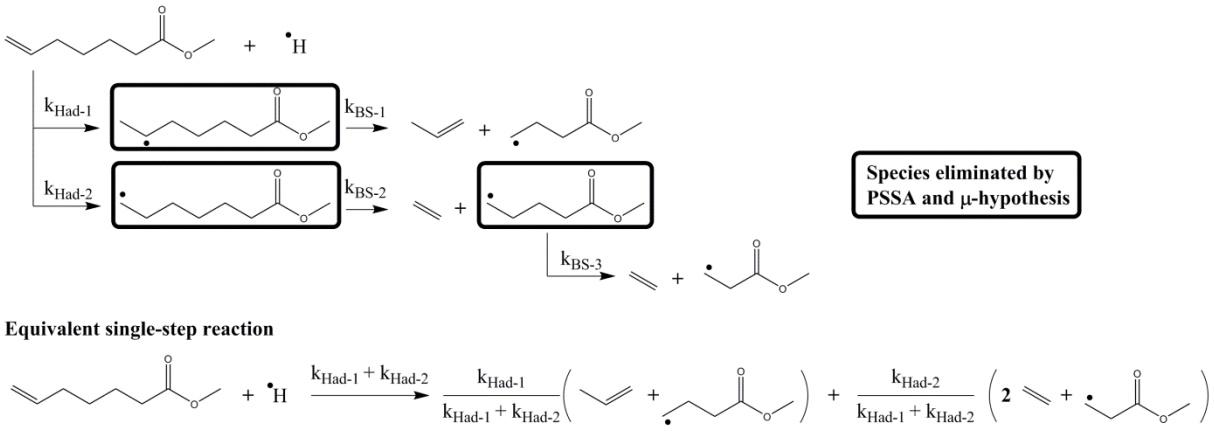

Figure 3.3-1 Hydrogen addition on methyl hept-6-enoate and subsequent decomposition reactions. The equivalent single-step reaction is obtained after elimination of the concentration of the μ-radicals, i.e. methyl heptanoate-6-yl, methyl heptanoate-7-yl and methyl pentanoate-5-yl, considering all the elementary reactions using the pseudo-steady-state approximation.

The validity of the μ-hypothesis and the pseudo-steady-state approximation will be assessed in the next section. Subsequently, the calculation of kinetic and thermodynamic parameters in PRIM-O is discussed.

3.3.4.2.1 Network reduction strategies

Validation of the μ-hypothesis

The μ-hypothesis[26] is a common assumption used to model pyrolysis and steam cracking of hydrocarbons[34]. This assumption allows to drastically reduce the number of differential equations that need to be solved without losing accuracy. The latter is of particular importance if these detailed kinetic models need to be applied in Computational Fluid Dynamics simulations[49, 50]. Bimolecular reactions can be neglected when aliphatic radicals have more than 5 carbon atoms[6, 13, 48]. Given the alkyl chain in esters, the μ-hypothesis may be used for methyl ester derived radicals.

To test this assumption and evaluate the effect of the presence of the ester function, a detailed kinetic model for thermal decomposition of methyl decanoate (MD), a moderately large methyl ester, has been constructed using Genesys[4]. Genesys uses group additivity models to estimate thermodynamic and kinetic data. The C_{6+} part of this mechanism is not a set of

equivalent single-step reactions which would be the case if it would be generated by PRIM-O but, instead, all large radicals and all elementary reactions are explicitly taken into account. Furthermore, the C_{6+} part of the Genesys-generated mechanism contains several reactions which are neglected in the μ-network generated using PRIM-O, e.g. hydrogen abstraction by large radicals, addition of small olefins on methyl decanoate radicals. The Genesys-generated mechanism comprises of 446 species and 2272 reactions and can be used to validate the μ-hypothesis by analyzing the fate of large radicals.

For example, in Figure 3.3-2, the various possible reaction routes of a methyl decanoate radical and the corresponding relative consumption rates, calculated using the Genesys-generated mechanism, are presented. Note that the naming of radicals in this work reflects the name of the corresponding molecule and the position of the unpaired electron. The label of the radical position is consistent with the work by Fisher et al.[51], i.e., "M" if the radical is on the primary carbon atom of the methyl ester group, "2" if the radical is on the carbon α to the ester group, "3" if the radical is on the carbon β to the ester group, etc.

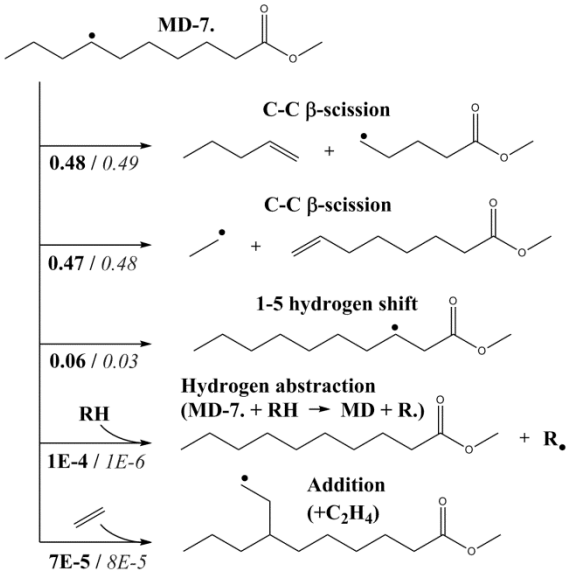

Figure 3.3-2 Possible consumption reactions for the μ-radical MD-7•. Numbers indicate the relative contribution of the corresponding reaction path to the total consumption of MD-7• at 873K (bold) and1073K (italic), which were calculated with CHEMKIN using the plug flow reactor model and the Genesys-generated model, with d_t=6 10^{-3}m, z=2 10^{-2}m, P=0.1 MPa, F_{MD}^{0}=5.4 10^{-4} mol/s.

Reaction paths of the radical can be divided in two groups, i.e. monomolecular and bimolecular reactions. Under the operating conditions investigated in this work[52, 53], monomolecular reactions such as intramolecular hydrogen abstraction and β-scission reactions comprise the vast majority of the MD-7• consumption. Bimolecular reactions, e.g.

addition of small olefins on MD-7• and hydrogen abstraction of MD-7• forming methyl decanoate, are negligible over the entire temperature range. MD-7• can thus be considered a μ-radical and the use of PRIM-O is justified for this species.

The μ-hypothesis has been tested for alkyl and ester radicals in the reaction system. The decomposition of methyl decanoate radicals leads to formation of primary alkyl and methyl ester radicals. Hence, the following discussion will be restricted to these species.

The ratio of monomolecular reaction rate divided by bimolecular reaction rate as a function of carbon atoms for primary alkyl and methyl ester radicals, calculated using the Genesys-generated model, is presented in Figure 3.3-3. Reaction conditions correspond to the most severe conditions for the validity of the μ-hypothesis, i.e. undiluted and low temperature. High radical partial pressures increase the importance of bimolecular reactions. Unimolecular radical reactions, such as C-C β-scission, often have higher activation energies compared to bimolecular radical reactions, such as hydrogen abstraction, see Table 3.3-2.

Hence, the former are more affected by a decrease in temperature[54]. Note that only radicals containing 3 or more carbon atoms are displayed in Figure 3.3-3. Methyl radicals and hydrogen atoms are only involved in bimolecular reactions. The ethyl radical cannot decompose through carbon centered β-scission compared to the other molecules displayed. As such, ethyl follows a different trend regarding μ to β reaction rate ratio. Ethyl has a μ to β reaction ratio of approximately 5 at the operation conditions of Figure 3.3-3.

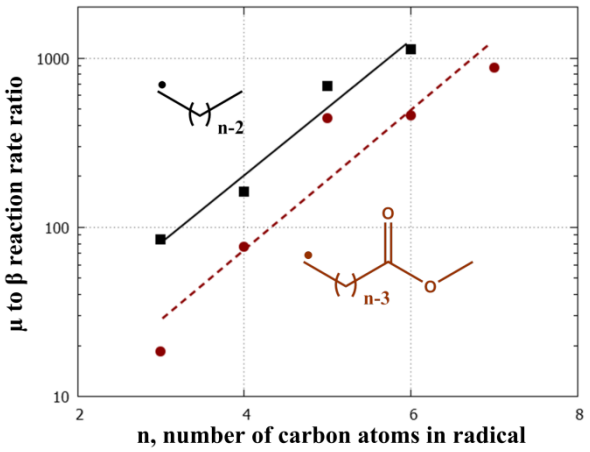

Figure 3.3-3 Calculated μ to β reaction rate ratio as a function of the number of carbon atoms in the radical: ■- primary n-alkyl radicals; ●- primary methyl ester radicals; lines, observed trend. Reaction rates were calculated with CHEMKIN using the plug flow reactor model and the Genesys-generated model, with d_t=6 10^{-3}m, z=2 10^{-2}m, P=0.1 MPa, T=873K, F^0_{MD}=5.4 10^{-4} mol/s.

Overall, small ester radicals appear to have a lower μ to β reaction ratio than alkyl radicals with the same number of carbon atoms. Obviously, their reactivity is influenced by the change in bond dissociation energies due to the ester functionality compared to alkyl radicals [55]. The most important bimolecular reaction for the n-alkyl and ester radicals is hydrogen abstraction from the feed molecule, i.e., methyl decanoate in the case of Figure 3.3-3.

A methyl ethanoate (ME) radical with the radical on the 2 position (ME-2•) is resonantly stabilized causing the rates of possible monomolecular reactions, i.e., decomposition forming ketene plus methoxy and hydrogen shift to ME-M•, to be lower compared to decomposition of 1-propyl to ethene and methyl[56].

A methyl propanoate (MP) radical with a radical on the 3 position (MP-3•) will decompose forming ethene and a methoxy-carbonyl radical. The rate of the latter C-C β-scission reaction is slower than the C-C β-scission of 1-butyl[40, 57].

Decomposition of the methyl butanoate (MB) radical with a radical on the 4 position (MB-4•) will form ethene and ME-2•. As mentioned earlier, the latter species is resonantly stabilized and, thus, the rate of this C-C β-scission is higher than the rate of the C-C β-scission of 1-pentyl[56]. Note that 1-pentyl can isomerize to 2-pentyl through a favorable 5-membered transition state which is not possible in MB-4•. Both MB-4• and 1-pentyl have a comparable and high μ to β reaction rate ratio, $r_\mu/r_\beta \approx 500$. As, 1-pentyl radicals are commonly considered as the largest alkyl radicals with β-properties[6], the largest ester radicals with β-properties are methyl butanoate radicals in this work. The error introduced by neglecting bimolecular reaction for larger ester radicals can assumed to be negligible.

Validation of the pseudo-steady-state approximation

The second assumption is the pseudo-steady-state approximation (PSSA). This has been used in various combustion, pyrolysis and steam cracking models[1, 58-60]. Since the kinetic network generated with PRIM-O makes use of the PSSA for μ-radicals, it is instructive to calculate the error that is introduced.

The pyrolysis of methyl decanoate was simulated with the Genesys-generated network using CHEMKIN at two different temperatures, i.e. 873K and 1073K, and similar reactor conditions as Figure 3.3-2. Subsequently, KINALC[27, 58, 61], a CHEMKIN postprocessor developed to analyze complex reaction mechanisms, is used to evaluate (i) the instantaneous error on the concentration of each species *i* when applying PSSA for this species, denoted as Δc_i^s, and (ii)

the chemical lifetime of each species i, defined as $c_i(z) \Big/ \sum_j v_{ij} r_j(z)$. Details regarding the procedure utilized in KINALC to calculate these properties can be found elsewhere[58, 61].

Table 3.3-1 presents the results for methyl, hydrogen and radicals of methyl decanoate (μ-radicals). Similar values were obtained for the other alkyl and ester radicals. The relative error on the concentration of a radical when applying the PSSA is found to be negligible, below 0.1%. The PSSA is valid for the pyrolysis of methyl esters and it is applied to μ-radicals in the PRIM-O network generation program. The μ-radicals can be eliminated from the model equations. This avoids the need to calculate their concentration during a reactor simulation, which gives rise to considerable speed-up.

Table 3.3-1 Relative error when applying the pseudo-steady-state approximation and the chemical lifetime for a selection of radicals. Reaction simulations were performed with CHEMKIN using the plug flow reactor model and the Genesys-generated model with d_t=6 10^{-3}m, z=2 10^{-2}m, P=0.1 MPa, F_{MD}^0=5.4 10^{-4} mol/s. Subsequently, KINALC, a CHEMKIN postprocessor, was used to calculate $|\Delta c_i^s / c_i|$ and the chemical life of each species i.

	873K		1073K	
	Lifetime (s)	$\|\Delta c_i^s / c_i\|$	**Lifetime (s)**	$\|\Delta c_i^s / c_i\|$
CH_3•	1.94 10^{-6}	1.47 10^{-5}	2.81 10^{-8}	1.53 10^{-4}
H•	6.95 10^{-9}	4.15 10^{-7}	5.71 10^{-10}	1.97 10^{-4}
MD-M•	1.70 10^{-6}	2.54 10^{-6}	7.58 10^{-8}	3.11 10^{-4}
MD-8•	6.04 10^{-8}	2.86 10^{-6}	4.73 10^{-9}	3.63 10^{-4}
MD-3•	5.97 10^{-8}	2.65 10^{-6}	4.68 10^{-9}	3.59 10^{-4}
MD-2•	5.50 10^{-8}	3.87 10^{-7}	8.71 10^{-9}	9.82 10^{-5}
MD-9•	5.06 10^{-8}	1.90 10^{-6}	5.10 10^{-9}	3.25 10^{-4}
MD-7•	5.00 10^{-8}	1.72 10^{-6}	3.71 10^{-9}	2.84 10^{-4}
MD-4•	3.89 10^{-8}	2.09 10^{-6}	2.77 10^{-9}	3.39 10^{-4}
MD-5•	2.49 10^{-8}	8.40 10^{-7}	2.93 10^{-9}	1.97 10^{-4}
MD-6•	7.41 10^{-9}	1.18 10^{-8}	1.94 10^{-9}	1.15 10^{-4}
MD-10•	7.33 10^{-9}	7.74 10^{-7}	1.18 10^{-9}	2.18 10^{-4}

The lifetime of the majority of methyl decanoate radicals is as small as 10^{-9} s. Methyl decanoate with a radical on the methoxy group (MD-M•) has a lifetime which is about two orders of magnitude larger compared to the other methyl decanoate radicals. The direct

decomposition of this type of radical, with formation of formaldehyde and α-carbonyl radicals, is slower than C-C β-scission reactions which are the dominant reaction paths for the other methyl decanoate radicals, explaining their longer lifetime[40].

3.3.4.2.2 Kinetic data

In order to construct decomposition schemes for molecules present in the μ-network, on-the-fly calculation of rate coefficients for decomposition of molecules and (μ-) radicals is needed. In this work, rate coefficients are estimated using a comprehensive group additive data set, mainly derived by Sabbe and coworkers who applied Benson's group additivity concept to transition state theory[62, 63]. Group additive values for radical decomposition reactions that are affected by the ester functionality were derived from the work by Huynh and Violi[40].

In short, the applied group additive concept classifies possible reactions in so called elementary reaction families, see Table 3.3-2. Each reaction is characterized by a rate coefficient which depends on three parameters, i.e., the activation energy E_a, the pre-exponential factor for each single-event $\tilde{A}$ and the number of single events n_e, i.e. the number of energetically equivalent reaction paths from reactant(s) to transition state. The former two are calculated by taking the kinetic parameters of a reference reaction corresponding to the considered reaction family, $E_{a,ref}$ and $\tilde{A}_{ref}$, but adding contributions which take into account the difference in transition state between the considered reaction and the reference reaction, see equations (1) to (3).

$$k(T) = n_e \,.\, \tilde{A} \,.\, \exp\left(-\frac{E_a}{RT}\right) \quad (1)$$

$$E_a = E_{a,ref} + \sum_{i=1}^{n} \Delta GAV_{Ea,i}^{0} \quad (2)$$

$$log(\tilde{A}) = log(\tilde{A}_{ref}) + \sum_{i=1}^{n} \Delta GAV_{\tilde{A},i}^{0} \quad (3)$$

Table 3.3-2 Kinetic data in μ-network

Reaction	Reference Reaction	Log	Ea_{ref}	Ref.
μ-radical formation				
Bond Scission				
C-C	$n\text{-}C_4H_{10} \rightarrow C_2H_5\bullet + C_2H_5\bullet$	16.7	345.5	[64]
C-H	$C_2H_6 \rightarrow C_2H_5\bullet + H\bullet$	16.0	417.8	[65, 66]
C-O	$CH_3\text{-}C(=O)\text{-}O\text{-}CH_3 \rightarrow CH_3\text{-}C(=O)\text{-}O\bullet$ +	15.1	429.9	[52]
Intermolecular hydrogen abstraction				
by C.	$CH_4 + CH_3\bullet \rightarrow CH_3\bullet + CH_4$	6.5	84.4	[67, 68]
by H.	$CH_4 + H\bullet \rightarrow CH_3\bullet + H_2$	8.0	66.4	[69]
Intermolecular radical addition				
by C.	$C_2H_4 + CH_3\bullet \rightarrow C_3H_7\text{-}1\bullet$	6.0	43.1	[62]
by H.	$C_2H_4 + H\bullet \rightarrow C_2H_5\bullet$	7.7	18.5	[56]
μ-radical decomposition				
β-scission				
C-C	$C_3H_7\text{-}1\bullet \rightarrow C_2H_4 + CH_3\bullet$	13.5	128.5	[70]
C-H	$C_2H_5\bullet \rightarrow C_2H_4 + H\bullet$	12.6	162.4	[56]
C-O	$C_3H_7\text{-}C(=O)\text{-}O\text{-}CH_2\bullet \rightarrow C_3H_7\text{-}C(=O)\bullet$ +	13.3	133.5	[40]
α-scission				
CO	$C_3H_7\text{-}C(=O)\bullet \rightarrow C_3H_7\text{-}1\bullet + CO$	13.5	71.8	[40]
Intramolecular hydrogen abstraction				
[1,4]	$n\text{-}C_4H_9\text{-}1\bullet \rightarrow n\text{-}C_4H_9\text{-}1\bullet$	11.0	86.2	[64]
[1,5]	$n\text{-}C_5H_{11}\text{-}1\bullet \rightarrow n\text{-}C_5H_{11}\text{-}1\bullet$	10.2	60.7	[64]
Intramolecular radical addition				
[1,5] endo	pent-1-en-5-yl → cyclopentyl	10.9	62.6	[x]
[1,5] exo	hex-1-en-6-yl → CH_3-cyclopentane	10.8	23.5	[x]
[1,6] endo	hex-1-en-6-yl → cyclohexyl	10.5	32.2	[x]
[1,6] exo	hept-1-en-7-yl → CH_3-cyclohexane	10.2	29.6	[x]
Concerted path reactions				
Retro-ene	$1\text{-}C_5H_{10} \rightarrow C_2H_4 + C_3H_6$	12.8	235.8	[x]
Acetate elimination	$C_3H_7\text{-}C(=O)\text{-}O\text{-}CH_3 \rightarrow CH_3\text{-}C(=O)\text{-}O\text{-}CH_3 + C_2H_4$	12.6	284.5	[71]

[x] Calculated using the methodology described in [56, 62, 67]

3.3.4.2.3 Thermodynamic data

The thermodynamic data for μ-species were determined based on Benson's group additivity method[11]. Various groups have made use of this technique which led to the development of independent, stand-alone programs such as THERGAS[72] and RMG's ThermoDataEstimator[73]. In this work, the thermodynamic data were generated in the NASA polynomial format using Genesys's ThermoGenerator[4] equipped with group additive values derived by Sabbe et al.[74] and Paraskevas et al.[75] from an extensive thermochemical database obtained by ab initio calculations at the CBS-QB3 level of theory.

3.3.4.3 Reactor model

Reactor simulations were performed using CHEMKIN-PRO [76]. Both the perfectly stirred reactor model and the ideal plug flow reactor model were used to model the respective datasets in this work. The plug flow assumption has been verified for the bench scale pyrolysis set up used in this work[30, 53]. Since the constructed kinetic model is comprised of a μ-network, containing equivalent single-step reactions of which the stoichiometric coefficients are temperature dependent, and a β-network, containing reversible elementary reactions, the USRPROD routine was used to couple the kinetic model with the CHEMKIN framework. This option enables the user to define a subroutine that calculates the rate of production of all species for certain reactor conditions. Note that the kinetic model can also be processed using OpenSMOKE++, an open-source software-tool for the simulation of reactors using detailed kinetic models, recently developed by Cuoci et al. [77].

3.3.5 Results and discussion

3.3.5.1 Pyrolysis of methyl decanoate

Methyl decanoate, having a medium-long length alkyl chain, is widely recognized as a good surrogate component for biodiesel. Both its combustion and pyrolysis characteristics have been studied thoroughly[52, 53, 78-80] and several extensive datasets regarding its thermal decomposition are available in literature[52, 53]. In this work, the aforementioned experimental pyrolysis data is used to validate the μ-network generation algorithm and the applied rate rules.

Scission and hydrogen abstraction of methyl decanoate causes μ-radicals to be formed and, thus, these reactions are generated with PRIM-O. The stoichiometric coefficients of the single-step equivalent hydrogen abstraction reaction of methyl decanoate are displayed in Figure 3.3-4 (A) for 873K and 1073K. In this table, methyl esters with a carbon chain of

length X with Y double bonds are denoted as CX:Y. A weak temperature dependence can be observed. The stoichiometric coefficient of the hydrogen atom has the largest relative increase, approximately doubling from 873K to 1073K.

(A)

$MD + R \rightarrow RH + \sum \alpha_i(T)\ species_i$

species	α(873K)	α(1073K)	species	α(873K)	α(1073K)
H.	0,01	0,02	.C(=O)OCH$_3$	0,05	0,05
CH$_3$.	0,03	0,03	ME-2.	0,08	0,08
C$_2$H$_5$.	0,05	0,05	MP-3.	0,19	0,19
1-propyl	0,05	0,05	MB-4.	0,15	0,16
1-butyl	0,17	0,15	CO	0,03	0,08
1-pentyl	0,22	0,23	CH$_2$O	0,03	0,08
C$_2$H$_4$	0,77	0,82	C03:1	0,18	0,13
C$_3$H$_6$	0,10	0,10	C04:1	0,12	0,10
1-butene	0,07	0,06	C05:1	0,02	0,02
1-pentene	0,05	0,05	C06:1	0,05	0,05
1-hexene	0,05	0,05	C07:1	0,05	0,05
1-heptene	0,05	0,05	C08:1	0,05	0,05
1-octene	0,08	0,08	C09:1	0,03	0,03
1-nonene	0,05	0,05	C10:1	0,01	0,01

(B)

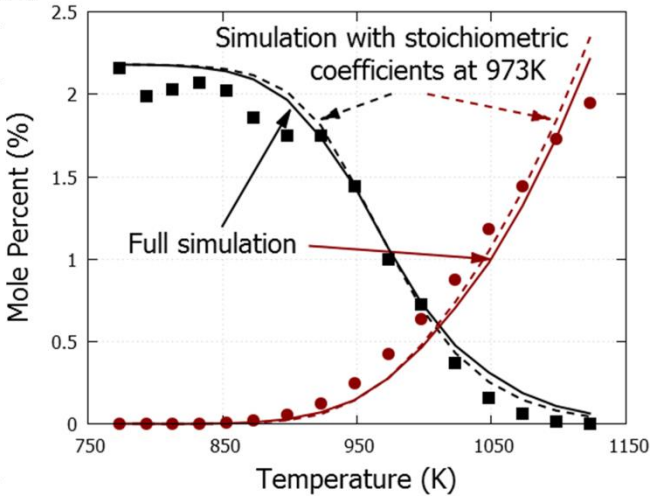

Figure 3.3-4 (A) Hydrogen abstraction reaction of methyl decanoate. The stoichiometric coefficients α are obtained after elimination of the concentration of μ-radicals using the pseudo-steady-state approximation at 873K and 1073K. (B) Mole fractions as a function of temperature for methyl decanoate pyrolysis in a jet stirred reactor[52]: ■- methyl decanoate; ●- H_2; full lines, calculated with CHEMKIN using the perfectly stirred reactor model and the developed kinetic model; dashed lines, calculated with CHEMKIN using the perfectly stirred reactor model and a kinetic model where the stoichiometric coefficients of the equivalent single-step reactions were fixed to their values at 973K.

Hydrogen abstraction from the carbon atom α to the ester group is the favored hydrogen abstracting channel as this leads to a resonantly stabilized radical. Decomposition of this μ-radical leads to formation of methyl propenoate, the unsaturated methyl ester with the highest stoichiometric coefficient and, thus, selectivity, and a 1-heptyl radical, which in turn decomposes to ethene plus 1-pentyl. The selectivity towards C_{5+} 1-olefins and monounsaturated esters is fairly independent of the molecule's chain length. These molecules are formed by the various possible hydrogen abstractions along the alkyl chain of methyl decanoate followed by carbon centered β-scission. As the reaction paths for the production of these unsaturated molecules occur in a similar hydrocarbon moiety, the corresponding reaction rate coefficients, and as such the stoichiometric coefficients, are comparable. Differences are encountered at the oxygenated end, i.e. higher selectivity for octene since the "parent" radical MD-4• prefers this C-C β-scission due to formation of a resonantly stabilized methyl ethanoate radical, and at the alkyl end, i.e. a lower selectivity for methyl nonenoate since the "parent" radical MD-8• disfavors this C-C β-scission due to formation of a methyl radical.

Two extensive data sets for pyrolysis of methyl decanoate are available in literature, one obtained by Herbinet et al. [52] in a jet stirred reactor and one obtained by Pyl et al. [53] in a plug flow reactor. Both were used to test the performance of the kinetic model but only the results using the dataset of Herbinet et al. [52] are reported here. In Figure 3.3-4 (B) experimental methyl decanoate and hydrogen mole fraction profiles are compared to (i) the generated kinetic model and (ii) a kinetic model where the temperature dependence of the stoichiometric coefficients of the reactions in the μ-network has been neglected and fixed to their values at 973K, a selected intermediate temperature.

Fixing the stoichiometric coefficients at an intermediate temperature only has a minor effect on calculated results which is line with earlier observations for hydrocarbons[39]. Even for hydrogen, mainly formed by hydrogen abstraction of hydrogen atoms which experience the largest variation in stoichiometric coefficient, the difference is less than 10% at 1123K. The MAMA program[1, 48], developed by Dente, Ranzi and coworkes, neglects the temperature dependence of the stoichiometric coefficients, which proves to be a reasonable approximation under the conditions studied in this work. Throughout the rest of this work, calculations will be performed using the complete generated kinetic model.

Performance for other detected species is presented in Figure 3.3-5. The ester group decomposes with possible formation of CO and CO_2 [81]. As discussed earlier, the relevant kinetic data for decomposition of the ester functionality was taken from the ab initio study by Huynh and Violi[40]. The model predicts the CO and CO_2 mole fraction profiles accurately and, thus, the rate rules derived from the referred work can assumed to be valid for the considered operating conditions.

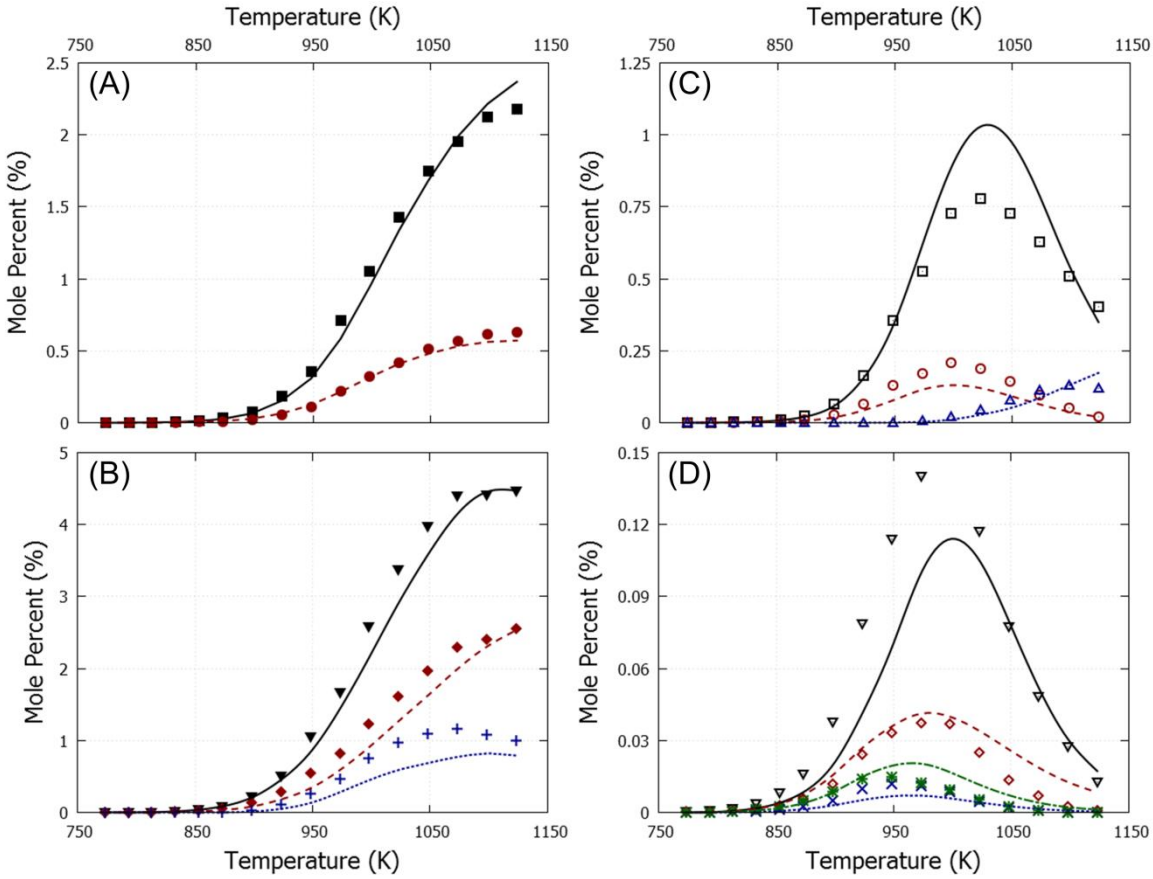

Figure 3.3-5 Mole fractions as a function of temperature for methyl decanoate pyrolysis in a jet stirred reactor[52]: (A) ■- CO, ●- CO_2; (B) ▼- C_2H_4, ◆- CH_4, + - 1,3-butadiene (multiplied by 5); (C) □- C_3H_6, ○ - 1-butene, △ - benzene; (D) ▽- methyl 2-propenoate, ◇- methyl 3-butenoate, ×- methyl 4-pentenoate, ✱ - methyl 5-hexenoate; lines, calculated with CHEMKIN using the perfectly stirred reactor model and the developed kinetic model.

The applied group additivity values describing the decomposition of hydrocarbons has been validated earlier[44]. Ethene, propene and other olefins are formed from the alkyl chain in methyl decanoate. As the model is able to capture the trend of all these species, the accuracy of these values is confirmed here as well. Note that propene has a low stoichiometric coefficient in the hydrogen abstraction reaction of methyl decanoate, see Figure 3.3-4 (A). Retro-ene reactions of the olefins and unsaturated methyl esters, both having a double bond at the end of the carbon chain, are the main source of propene[52].

Both experimental data sets comprise the yield of all esters and olefins with up to 10 carbon atoms. This allows to evaluate the product selectivities generated by the kinetic modeling algorithm. The yield of some unsaturated methyl esters, are displayed in Figure 3.3-5(D). Methyl propenoate is the most abundantly formed ester and the effect of temperature on its mole fraction is captured well by the model. The experimental yield of methyl butenoate, the

largest unsaturated methyl ester of which the decomposition is part of the β-network, matches the model prediction, only at the high temperatures there appears to be a small over prediction. The applied rate rules can be assumed to be valid for methyl decanoate pyrolysis and are extended to the pyrolysis of larger esters such as rapeseed methyl esters.

3.3.5.2 Pyrolysis of rapeseed methyl esters

3.3.5.2.1 Experimental results

An experimental data set regarding rapeseed methyl esters pyrolysis was obtained in the experimental setup discussed above. The inlet molar flow rate of rapeseed methyl esters and N_2 was kept constant at 1.15 10^{-4} mol/s and 2.5 10^{-3} mol/s respectively. The temperature has been varied between 983K and 1063K with 20K increments. A detailed product distribution was obtained at each temperature. Figure 3.3-6 presents the GC×GC-FID chromatogram of the reactor effluent at 983K. There is a clear connection between the position in the GC×GC-chromatogram of the esters, olefins and aromatics based on the number of carbon atoms as observed earlier[32]. At the lowest temperature examined, i.e. 983K, the reactor effluent contains unconverted feed, note however that the conversion already exceeds 95% which is substantially higher than the conversion observed for methyl decanoate pyrolysis at comparable operating conditions. Furthermore, a high fraction of aromatics was found at each temperature which differs from the methyl decanoate pyrolysis effluent discussed earlier.

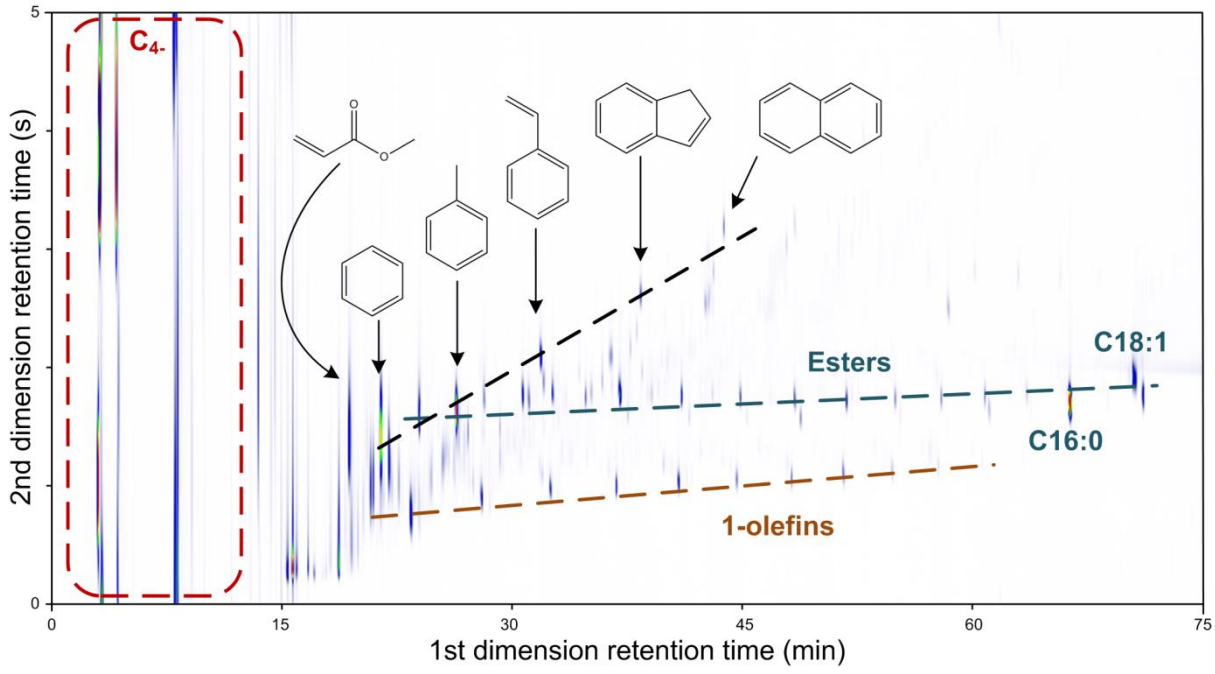

Figure 3.3-6 GC×GC-FID chromatogram of the rapeseed methyl ester pyrolysis effluent at T=983K, P=0.17MPa, F_{RME}=1.15 10^{-4} mol/s and F_{N2}=2.5 10^{-3} mol/s.

3.3.5.2.2 Kinetic Model

Rapeseed methyl esters are typically composed of 5 major components. The major component of the examined RME mixture in this work is methyl oleate (C18:1). The presence of a C=C double bond in the alkyl chain implies that a difference in reactivity compared to methyl decanoate can be expected. The C-C bond dissociation energy between an allylic and a secondary carbon atom is approximately 40 kJ/mol lower than between two secondary carbon atoms[82]. Consequently, C-C scission will be rather fast, leading to a relatively large radical pool explaining the high conversion observed experimentally, even at low temperatures. Besides hydrogen abstraction, small radicals can react with unsaturated methyl esters by addition onto the carbon double bond.

The primary decomposition products following hydrogen abstraction from methyl oleate are presented in Figure 3.3-7. Hydrogen can be abstracted from carbon atoms with label M, 2 to 8 and 11 to 18. Hydrogen abstraction from carbon atoms 9 and 10 is neglected due to the creation of unfavorable vinylic radicals. Decomposition of radicals close to the ester functionality causes formation of small oxygenated species such as •C(=O)OCH3, formaldehyde and CO. Methyl oleate radicals with a radical center along the alkyl chain have similar decomposition routes. For example, methyl oleate radicals with a radical center on carbons atoms with label 11 to 16 can form an alkyl radical and a double unsaturated methyl ester. Analogous reaction routes have been grouped to reduce the size of Figure 3.3-7. Single and double unsaturated esters and olefins are formed by decomposition of radicals along the alkyl chain by C-C β-scission. The presence of a double bond in methyl oleate enables intramolecular addition reactions. In this work, 5-membered and 6-membered intramolecular radical addition reactions, both endo and exo, are considered. For example, a methyl oleate radical with radical center on carbon 5 can form a monounsaturated methyl ester plus an alkenyl radical by C-C β-scission, a diolefin plus a methyl ester radical by C-C β-scission, or a cyclic methyl ester radical. Cyclic methyl ester radicals can react by C-C β-scission, C-H β-scission and intramolecular hydrogen abstraction. A wide variety of unsaturated cyclic molecules can be formed. These molecules consist of a cyclic core with possible alkenyl, alkyl and methyl ester side chains. This complex product spectrum is not presented in Figure 3.3-7, again to reduce the size of the picture, but is part of the developed kinetic model.

The stoichiometric coefficients in the equivalent reaction for hydrogen abstraction from methyl oleate of double unsaturated methyl esters, respectively diolefins, are approximately twice as large as those of monounsaturated methyl esters, respectively 1-olefins. The former

molecules are mainly formed through C-C β-scission of allylic radicals, the most abundantly formed radicals following hydrogen abstraction. Cyclic molecules which are formed following hydrogen abstraction from methyl oleate can be divided in two groups, cyclic molecules with a methyl ester functionality and cyclic molecules without a methyl ester functionality, see Figure 3.3-7. Both types of molecules have similar stoichiometric coefficients in the equivalent reaction for hydrogen abstraction from methyl oleate. These molecules are formed through similar intramolecular radical addition pathways starting from methyl oleate with a radical on carbon 4, 5, 15 or 16. The latter atoms are all secondary carbon atoms and, as such, the corresponding radicals have a similar formation rate.

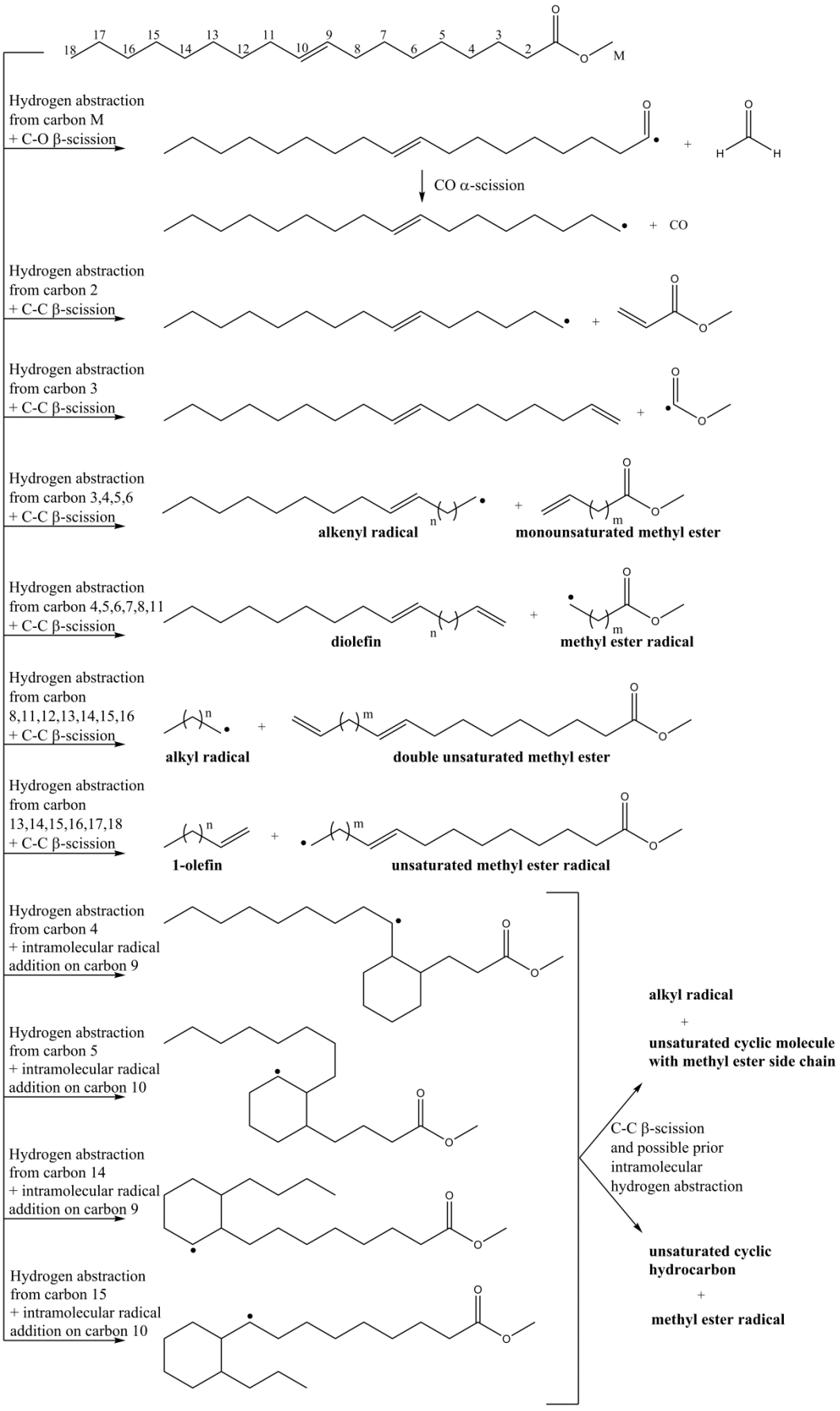

Figure 3.3-7 Reaction routes following hydrogen abstraction from methyl oleate.

3.3.5.2.3 Model performance

Experimental product mole fraction profiles for rapeseed methyl ester pyrolysis were obtained using the tubular reactor, discussed previously, while varying reactor temperature and keeping rapeseed methyl ester and N_2 molar flow rates fixed at 1.15 10^{-4} mol/s and 2.5 10^{-3} mol/s respectively. The obtained experimental results are compared with calculated results using the developed kinetic model in Figure 3.3-8, Figure 3.3-9 and Figure 3.3-10.

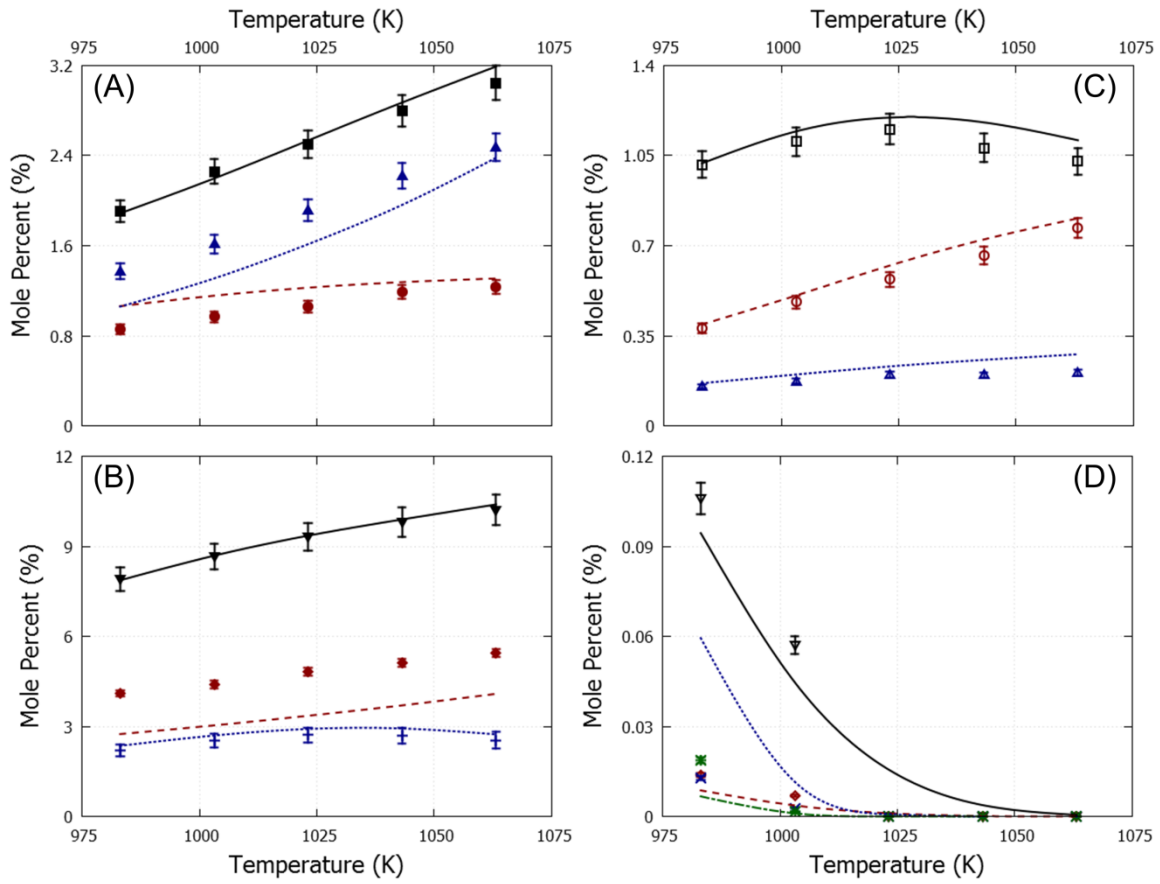

Figure 3.3-8 Mole fractions as a function of temperature for rapeseed methyl ester pyrolysis in a tubular reactor, P=0.17 MPa, F_{RME}=1.15 10^{-4} mol/s, F_{N2}=2.5 10^{-3} mol/s: (A) ■ - CO, ● - CO_2, ▲ - H_2; (B) ▼ - C_2H_4, ◆ - CH_4, + - C_3H_6; (C) □ - 1,3-butadiene, ○ - benzene, △ - toluene; (D) ▽ - methyl palmitate, ◇ - methyl stearate, × - methyl oleate, ✱ - methyl linoleate; lines, mole fraction profiles calculated with CHEMKIN using the plug flow reactor model and the developed kinetic model.

Calculated and experimental results for methyl palmitate (C16:0), methyl stearate (C18:0), methyl oleate (C18:1) and methyl linoleate (C18:2) are displayed in Figure 3.3-8(D). Methyl linolenate (C18:3) was not detected in the reactor effluent. This is in line with model calculations which predict a mole percentage below 0.002 at 983K, i.e., the lowest temperature examined experimentally. Despite the feed being comprised of over 50mol%

methyl oleate, methyl palmitate is the most abundant feed methyl ester remaining in the reactor effluent after pyrolysis at 983K. As discussed earlier, the allylic carbon atoms in methyl oleate enhance its reactivity with respect to hydrogen abstraction and scission reactions. Radical addition reactions on the carbon double bond are responsible for 10% of methyl oleate consumption at 1063K.

Both CO and CO_2 are predicted well by the kinetic model, see Figure 3.3-8(A). Only for CO_2 there is a small overprediction at the lowest investigated temperatures, i.e. 983K. The kinetic data applied for the decomposition of the ester functionality has been validated for methyl decanoate pyrolysis earlier. The double bonds in the feed mixture are separated from the ester group by 7 carbon atoms and, thus, their influence on the formation of carbon oxides can be expected to be negligible.

A high fraction of small olefins was observed which is in line with other works studying long carbon chain feedstocks [83, 84]. The calculated mole fraction profiles of the most abundant olefins, i.e. ethene, propene and 1,3-butadiene match the experimental results, see Figure 3.3-8(B) and (C). The degree of unsaturation of the feedstock has an effect on the relative quantities of these olefins, which is most obvious for 1,3-butadiene. At 1063K, the ratio of 1,3-butadiene to ethene is approximately 1:10 on a molar basis for RME pyrolysis. At comparable conditions for methyl decanoate pyrolysis, i.e. high temperature and conversion, the ratio of 1,3-butadiene to ethene was 1:30. Radicals of saturated molecules, such as methyl decanoate, can decompose by successive C-C β-scissions forming a high number of ethene molecules and a small radical. The presence of a double bond in the alkyl chain can however disrupt this sequence of β-scission reactions leading to resonantly stabilized radicals. These have a lower reactivity compared to their paraffinic counterparts but will eventually isomerize or decompose to 1,3-butadiene[85].

As can be observed from Figure 3.3-8(C), a high yield for aromatics was obtained during rapeseed methyl ester pyrolysis. The kinetic model captures the temperature profile for benzene and toluene quite well. Benzene and toluene exhibit a linear trend compared to the exponential profile observed during methyl decanoate pyrolysis. Especially at the lowest temperatures that were investigated experimentally, other reactions are expected to be dominant towards formation of aromatics compared to methyl decanoate. The kinetic model predicts that the aromatic content for methyl oleate pyrolysis is a factor 10 higher compared to

methyl stearate pyrolysis at 983K and at similar conversion. This effect of a double bond has been observed before[2, 86-90].

As explained earlier, the double bond in unsaturated methyl esters, such as methyl oleate, enables intramolecular radical addition reactions. While it could be hypothesized that the formation of cyclic molecules in highly unsaturated moieties could occur through Diels Alder type reactions[88], recent work showed that this path is of minor importance in thermal cracking of triglycerides compared to intramolecular radical addition[87]. Intramolecular radical addition competes with C-C β-scission for the decomposition of unsaturated methyl ester radicals. Comparison of the kinetic parameters of the reference reactions of both families, see Table 3.3-2, indicate that intramolecular radical addition will be dominant at low temperatures given its relatively low activation energy. At high temperatures the C-C β-scission will become competitive but aromatics will start forming through other reaction paths such as propargyl recombination[91-93] (the C3 pathway), vinyl addition on 1,3-butadiene followed by intramolecular radicals addition[44, 94] (the C4 pathway) and cyclopentadienyl-methyl recombination[46] (the C5 pathway). The linear increase in benzene and toluene yield as a function of temperature for rapeseed methyl esters can thus be considered as a consequence of intramolecular radical addition of unsaturated methyl ester radicals (especially at low temperature) complemented with the C3, C4 and C5 pathway. For esters with a saturated alkyl chain only the latter three pathways contribute to formation of aromatics.

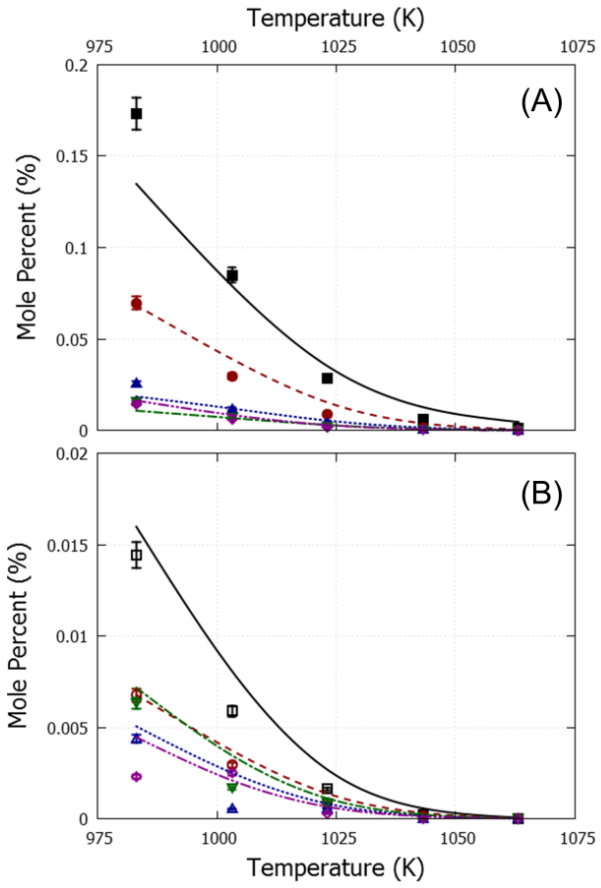

Figure 3.3-9 Mole fractions as a function of temperature for rapeseed methyl ester pyrolysis in a tubular reactor, P=0.17 MPa, F_{RME}=1.15 10^{-4} mol/s, F_{N2}=2.5 10^{-3} mol/s: (A) ■ - 1-hexene, ● - 1-heptene, ▲ - 1-octene, ▼ - 1-nonene, ◆ - 1-decene; (B) □ - 1-undecene, △ - 1-dodecene, ▽ - 1-tridecene, ◇ - 1-tetradecene, ○ - 1-pentadecene; lines, mole fraction profiles calculated with CHEMKIN using the plug flow reactor model and the developed kinetic model.

Figure 3.3-9 and 10 show the experimental and calculated mole fraction profiles of 1-olefins and mono-unsaturated methyl esters respectively, with an alkyl chain varying between 6 and 15 carbon atoms, as a function of temperature. All displayed molecules have a low yield in the investigated operating range and exhibit a monotonic decreasing trend with an approximate zero mole percentage at the highest temperature, i.e., 1063K. Previous works that focused on maximizing the yield of these components[3, 95] were performed in a lower temperature range, i.e., between 600K (high residence time) and 900K (low residence time). The mole fraction profiles are captured accurately by the kinetic model, both quantitatively and qualitatively.

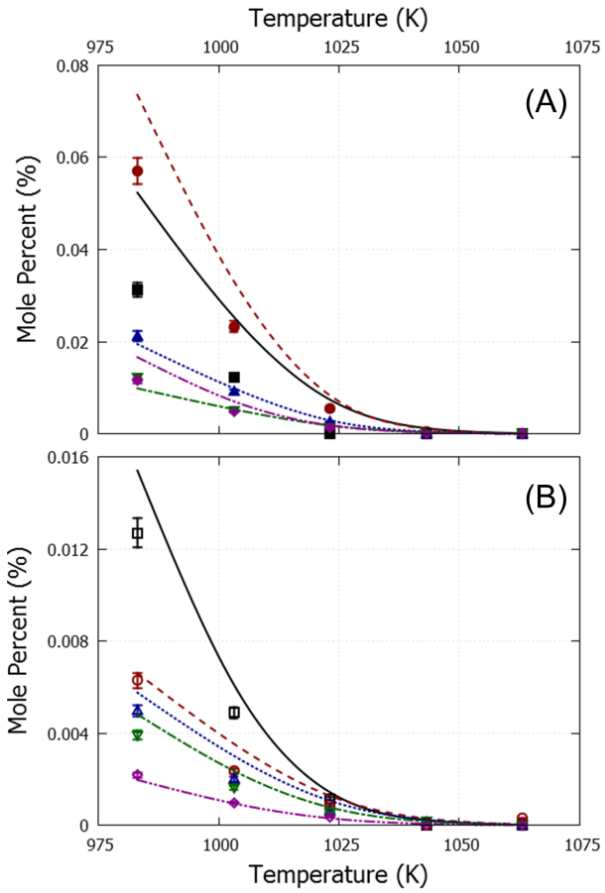

Figure 3.3-10 Mole fractions as a function of temperature for rapeseed methyl ester pyrolysis in a tubular reactor, P=0.17 MPa, F_{RME}=1.15 10^{-4} mol/s, F_{N2}=2.5 10^{-3} mol/s: (A) ■- methyl hex-5-enoate, ●- methyl hept-6-enoate, ▲ - methyl oct-7-enoate, ▼ - methyl non-8-enoate, ◆ - methyl dec-9-enoate; (B) □- methyl undec-10-enoate, △- methyl dodec-11-enoate, ▽- methyl tridec-12-enoate, ◇ - methyl tetradec-13-enoate, ○ - methyl pentadec-14-enoate; lines, mole fraction profiles calculated with CHEMKIN using the plug flow reactor model and the developed kinetic model.

3.3.6 Conclusions

A detailed kinetic model for the pyrolysis of methyl decanoate and rapeseed methyl esters is presented. All reaction rate coefficients are systematically calculated using a comprehensive group additive method. Analysis of the kinetic model shows that the μ-hypothesis and pseudo-steady-state approximation are valid for all radicals with 6 or more carbon atoms, independent of the presence of oxygen. The concentrations of these heavy radicals can be eliminated from the model equations, which allows to come up with equivalent single-step reactions for the decomposition of heavy methyl esters. This also reduces the complexity of the kinetic network substantially, without loss of accuracy. The stoichiometric coefficients of these reactions depend on temperature. In the investigated operating range, neglecting this temperature dependence only has a minor effect on model predictions. Existing and new experimental data for the thermal decomposition of methyl decanoate and rapeseed methyl

esters showed an excellent agreement with model calculations without any adjustment of the reaction rate coefficients. This shows the huge potential of the used approach for modeling the decomposition of other hetero atom containing compound classes.

The ester function has an effect on the reactivity of the neighboring carbon atoms and accurate kinetic data is required to properly predict the formation of small oxygenated species. Most of the dominant elementary reaction families, such as intermolecular/intramolecular hydrogen abstraction and β-scission, occur on the alkyl chain and group additive values originally obtained for pure hydrocarbons are shown to be valid. Intramolecular radical addition onto the C=C double bond present in rapeseed methyl esters are important under the studied conditions. The resulting cyclic intermediates are precursors for aromatics.

3.3.7 References

[1] M. Dente, G. Bozzano, T. Faravelli, A. Marongiu, S. Pierucci, E. Ranzi, Kinetic Modelling of Pyrolysis Processes in Gas and Condensed Phase, Adv. Chem. Eng. 32 (2007) 51-166
[2] F. Billaud, V. Dominguez, P. Broutin, C. Busson, Production of Hydrocarbons by Pyrolysis of Methyl Esters from Rapeseed Oil, J. Am. Oil Chem. Soc. 72 (1995) 1149-1154
[3] D. Archambault, F. Billaud, Experimental and modelling study of methyl oleate pyrolysis between 500 and 650°C, J. Chim. Phys. PCB 96 (1999) 778-796
[4] N. M. Vandewiele, K. M. Van Geem, M.-F. Reyniers, G. B. Marin, Genesys: Kinetic model construction using chemo-informatics, Chem. Eng. J. 207 (2012) 526-538
[5] S. Rangarajan, A. Bhan, P. Daoutidis, Rule-Based Generation of Thermochemical Routes to Biomass Conversion, Ind. Eng. Chem. Res. 49 (2010) 10459-10470
[6] K. M. Van Geem, M.-F. Reyniers, G. B. Marin, J. Song, W. H. Green, D. M. Matheu, Automatic reaction network generation using RMG for steam cracking of n-hexane, AlChE J. 52 (2006) 718-730
[7] F. Buda, R. Bounaceur, V. Warth, P. A. Glaude, R. Fournet, F. Battin-Leclerc, Progress toward a unified detailed kinetic model for the autoignition of alkanes from C4 to C10 between 600 and 1200 K, Combust. Flame 142 (2005) 170-186
[8] L. J. Broadbelt, S. M. Stark, M. T. Klein, Computer-generated Pyrolysis Modeling – on-the-fly Generation of Species, Reactions, and Rates, Ind. Eng. Chem. Res. 33 (1994) 790-799
[9] M. J. De Witt, D. J. Dooling, L. J. Broadbelt, Computer generation of reaction mechanisms using quantitative rate information: Application to long-chain hydrocarbon pyrolysis, Ind. Eng. Chem. Res. 39 (2000) 2228-2237
[10] G. Moreac, E. S. Blurock, F. Mauss, Automatic generation of a detailed mechanism for the oxidation of n-decane, Combust. Sci. Technol. 178 (2006) 2025-2038
[11] S. W. Benson, Thermochemical Kinetics: Methods for the Estimation of Thermochemical Data and Rate Parameters, John Wiley & Sons, New York, 1976
[12] L. J. Broadbelt, J. Pfaendtner, Lexicography of kinetic modeling of complex reaction networks, AlChE J. 51 (2005) 2112-2121
[13] P. J. Clymans, G. F. Froment, Computer generation of the reaction paths and rate equations in the thermal cracking of normal and branched paraffins, Comput. Chem. Eng. 8 (1984) 137-142
[14] M. S. Graboski, R. L. McCormick, Combustion of fat and vegetable oil derived fuels in diesel engines, Prog. Energy Combust. Sci. 24 (1998) 125-164
[15] A. Schönborn, N. Ladommatos, J. Williams, R. Allan, J. Rogerson, The influence of molecular structure of fatty acid monoalkyl esters on diesel combustion, Combust. Flame 156 (2009) 1396-1412
[16] B. Menkiel, A. Donkerbroek, R. Uitz, R. Cracknell, L. Ganippa, Combustion and soot processes of diesel and rapeseed methyl ester in an optical diesel engine, Fuel 118 (2014) 406-415
[17] S. Garner, K. Brezinsky, Biologically derived diesel fuel and NO formation: An experimental and chemical kinetic study, Part 1, Combust. Flame 158 (2011) 2289-2301

[18] J. Sun, J. A. Caton, T. J. Jacobs, Oxides of nitrogen emissions from biodiesel-fuelled diesel engines, Prog. Energy Combust. Sci. 36 (2010) 677-695
[19] S. M. Palash, M. A. Kalam, H. H. Masjuki, B. M. Masum, I. M. Rizwanul Fattah, M. Mofijur, Impacts of biodiesel combustion on NOx emissions and their reduction approaches, Renew. Sust. Energ. Rev. 23 (2013) 473-490
[20] F. Ma, M. A. Hanna, Biodiesel production: a review, Bioresour. Technol. 70 (1999) 1-15
[21] G. Balaji, M. Cheralathan, Potential of Various Sources for Biodiesel Production, Energ. Source Part A 35 (2013) 831-839
[22] P. Zamostny, Z. Belohlav, J. Smidrkal, Production of olefins via steam cracking of vegetable oils, Resour. Conserv. Recycl. 59 (2012) 47-51
[23] J. Šmidrkal, Z. Belohlav, P. Zámostný, V. Filip, Olefin production through pyrolysis of triacylglycerols, Lipid Technol. 21 (2009) 220-223
[24] K. D. Maher, D. C. Bressler, Pyrolysis of triglyceride materials for the production of renewable fuels and chemicals, Bioresour. Technol. 98 (2007) 2351-2368
[25] S. P. Pyl, C. M. Schietekat, M.-F. Reyniers, R. Abhari, G. B. Marin, K. M. Van Geem, Biomass to olefins: Cracking of renewable naphtha, Chem. Eng. J. 176-177 (2011) 178-187
[26] K. J. Laidler, Chemical Kinetics, Harper & Row, New York, 1987
[27] T. Turanyi, A. S. Tomlin, M. J. Pilling, On the error of the quasi-steady-state approximation, J. Phys. Chem.-US 97 (1993) 163-172
[28] G. S. Gusmão, P. Christopher, A general and robust approach for defining and solving microkinetic catalytic systems, AlChE J. 61 (2015) 188-199
[29] G. B. Marin, G. S. Yablonsky, Kinetics of Chemical Reactions, John Wiley & Sons, Inc., New York, 2011
[30] M. R. Harper, K. M. Van Geem, S. P. Pyl, G. B. Marin, W. H. Green, Comprehensive reaction mechanism for n-butanol pyrolysis and combustion, Combust. Flame 158 (2011) 16-41
[31] M. Djokic, H. H. Carstensen, K. M. Van Geem, G. B. Marin, The thermal decomposition of 2,5-dimethylfuran, Proc. Combust. Inst. 34 (2013) 251-258
[32] S. P. Pyl, C. M. Schietekat, K. M. Van Geem, M.-F. Reyniers, J. Vercammen, J. Beens, G. B. Marin, Rapeseed oil methyl ester pyrolysis: On-line product analysis using comprehensive two-dimensional gas chromatography, J. Chromatogr. A 1218 (2011) 3217-3223
[33] Cargill http://www.cargill.be/en/products/grain-oilseeds/biodiesel/
[34] K. M. Van Geem, M.-F. Reyniers, G. B. Marin, Challenges of modeling steam cracking of heavy feedstocks, Oil. Gas. Sci. Technol. 63 (2008) 79-94
[35] D. M. Fake, A. Nigam, M. T. Klein, Mechanism based lumping of pyrolysis reactions: Lumping by reactive intermediates, Appl. Catal. A-Gen. 160 (1997) 191-221
[36] L. P. Hillewaert, J. L. Dierickx, G. F. Froment, Computer-Generation of Reaction Schemes and Rate-Equations for Thermal-Cracking, AlChE J. 34 (1988) 17-24
[37] M. Dente, E. Ranzi, A. G. Goossens, Detailed prediction of olefin yields from hydrocarbon pyrolysis through a fundamental simulation program SPYRO, Comput. Chem. Eng. 3 (1979) 61-75
[38] R. De Bruycker, J. M. Anthonykutty, J. Linnekoski, A. Harlin, J. Lehtonen, K. M. Van Geem, J. Räsänen, G. B. Marin, Assessing the Potential of Crude Tall Oil for the Production of Green-Base Chemicals: An Experimental and Kinetic Modeling Study, Ind. Eng. Chem. Res. 53 (2014) 18430-18442
[39] E. Ranzi, M. Dente, A. Goldaniga, G. Bozzano, T. Faravelli, Lumping procedures in detailed kinetic modeling of gasification, pyrolysis, partial oxidation and combustion of hydrocarbon mixtures, Prog. Energy Combust. Sci. 27 (2001) 99-139
[40] L. K. Huynh, A. Violi, Thermal decomposition of methyl butanoate: Ab initio study of a biodiesel fuel surrogate, J. Org. Chem. 73 (2008) 94-101
[41] L. K. Huynh, K. C. Lin, A. Violi, Kinetic Modeling of Methyl Butanoate in Shock Tube, J. Phys. Chem. A 112 (2008) 13470-13480
[42] A. Farooq, D. F. Davidson, R. K. Hanson, L. K. Huynh, A. Violi, An experimental and computational study of methyl ester decomposition pathways using shock tubes, P. Combust. Inst. 32 (2009) 247-253
[43] A. Farooq, W. Ren, K. Y. Lam, D. F. Davidson, R. K. Hanson, C. K. Westbrook, Shock tube studies of methyl butanoate pyrolysis with relevance to biodiesel, Combust. Flame 159 (2012) 3235-3241
[44] M. K. Sabbe, K. M. Van Geem, M.-F. Reyniers, G. B. Marin, First principle-based simulation of ethane steam cracking, AlChE J. 57 (2011) 482-496
[45] J. Li, Z. W. Zhao, A. Kazakov, M. Chaos, F. L. Dryer, J. J. Scire, A comprehensive kinetic mechanism for CO, CH2O, and CH3OH combustion, Int. J. Chem. Kinet. 39 (2007) 109-136
[46] C. Cavallotti, D. Polino, A. Frassoldati, E. Ranzi, Analysis of Some Reaction Pathways Active during Cyclopentadiene Pyrolysis, J. Phys. Chem. A 116 (2012) 3313-3324

[47] C. Cavallotti, D. Polino, On the kinetics of the C5H5 + C5H5 reaction, P. Combust. Inst. 34 (2013) 557-564
[48] E. Ranzi, M. Dente, S. Plerucci, G. Biardi, Initial product distributions from pyrolysis of normal and branched paraffins, Ind. Eng. Chem. Fund. 22 (1983) 132-139
[49] C. M. Schietekat, M. W. M. van Goethem, K. M. Van Geem, G. B. Marin, Swirl flow tube reactor technology: An experimental and computational fluid dynamics study, Chem. Eng. J. 238 (2014) 56-65
[50] Y. Zhang, F. Qian, C. M. Schietekat, K. M. Van Geem, G. B. Marin, Impact of flue gas radiative properties and burner geometry in furnace simulations, AlChE J. (2015) DOI: 10.1002/aic.14724
[51] E. M. Fisher, W. J. Pitz, H. J. Curran, C. K. Westbrook, Detailed chemical kinetic mechanisms for combustion of oxygenated fuels, P. Combust. Inst. 28 (2000) 1579-1586
[52] O. Herbinet, P.-A. Glaude, V. Warth, F. Battin-Leclerc, Experimental and modeling study of the thermal decomposition of methyl decanoate, Combust. Flame 158 (2011) 1288-1300
[53] S. P. Pyl, K. M. Van Geem, P. Puimège, M. K. Sabbe, M.-F. Reyniers, G. B. Marin, A comprehensive study of methyl decanoate pyrolysis, Energy 43 (2012) 146-160
[54] M. Watanabe, M. Tsukagoshi, H. Hirakoso, T. Adschiri, K. Arai, Kinetics and product distribution of n-hexadecane pyrolysis, AlChE J. 46 (2000) 843-856
[55] A. M. El-Nahas, M. V. Navarro, J. M. Simmie, J. W. Bozzelli, H. J. Curran, S. Dooley, W. Metcalfe, Enthalpies of formation, bond dissociation energies and reaction paths for the decomposition of model biofuels: Ethyl propanoate and methyl butanoate, J. Phys. Chem. A 111 (2007) 3727-3739
[56] M. K. Sabbe, M.-F. Reyniers, M. Waroquier, G. B. Marin, Hydrogen Radical Additions to Unsaturated Hydrocarbons and the Reverse beta-Scission Reactions: Modeling of Activation Energies and Pre-Exponential Factors, ChemPhysChem 11 (2010) 195-210
[57] H. J. Curran, Rate constant estimation for C-1 to C-4 alkyl and alkoxyl radical decomposition, Int. J. Chem. Kinet. 38 (2006) 250-275
[58] T. Turanyi, Applications of sensitivity analysis to combustion chemistry, Reliab. Eng. Syst. Saf. 57 (1997) 41-48
[59] R. Fournet, V. Warth, P. A. Glaude, F. Battin-Leclerc, G. Scacchi, G. M. Côme, Automatic reduction of detailed mechanisms of combustion of alkanes by chemical lumping, Int. J. Chem. Kinet. 32 (2000) 36-51
[60] T. Dijkmans, C. M. Schietekat, K. M. Van Geem, G. B. Marin, GPU based simulation of reactive mixtures with detailed chemistry in combination with tabulation and an analytical Jacobian, Comput. Chem. Eng. 71 (2014) 521-531
[61] T. Kovacs, I. G. Zsely, A. Kramarics, T. Turanyi, Kinetic analysis of mechanisms of complex pyrolytic reactions, J. Anal. Appl. Pyrolysis 79 (2007) 252-258
[62] M. K. Sabbe, M.-F. Reyniers, V. Van Speybroeck, M. Waroquier, G. B. Marin, Carbon-centered radical addition and beta-scission reactions: Modeling of activation energies and pre-exponential factors, ChemPhysChem 9 (2008) 124-140
[63] M. Saeys, M.-F. Reyniers, G. B. Marin, V. Van Speybroeck, M. Waroquier, Ab initio group contribution method for activation energies for radical additions, AlChE J. 50 (2004) 426-444
[64] M. Mehl, G. Vanhove, W. J. Pitz, E. Ranzi, Oxidation and combustion of the n-hexene isomers: A wide range kinetic modeling study, Combust. Flame 155 (2008) 756-772
[65] L. B. Harding, Y. Georgievskii, S. J. Klippenstein, Predictive theory for hydrogen atom - Hydrocarbon radical association kinetics, J. Phys. Chem. A 109 (2005) 4646-4656
[66] L. B. Harding, S. J. Klippenstein, Y. Georgievskii, On the combination reactions of hydrogen atoms with resonance-stabilized hydrocarbon radicals, J. Phys. Chem. A 111 (2007) 3789-3801
[67] M. K. Sabbe, A. Vandeputte, M.-F. Reyniers, M. Waroquier, G. B. Marin, Modeling the influence of resonance stabilization on the kinetics of hydrogen abstractions, Phys. Chem. Chem. Phys. 12 (2010) 1278-1298
[68] P. D. Paraskevas, M. K. Sabbe, M.-F. Reyniers, N. G. Papayannakos, G. B. Marin, Kinetic Modeling of α-Hydrogen Abstractions from Unsaturated and Saturated Oxygenate Compounds by Carbon-Centered Radicals, ChemPhysChem 15 (2014) 1849-1866
[69] P. D. Paraskevas, M. K. Sabbe, M.-F. Reyniers, N. G. Papayannakos, G. B. Marin, Kinetic Modeling of α-Hydrogen Abstractions from Unsaturated and Saturated Oxygenate Compounds by Hydrogen Atoms, J. Phys. Chem. A 118 (2014) 9296-9309
[70] M. K. Sabbe, A. Vandeputte, M.-F. Reyniers, V. Van Speybroeck, M. Waroquier, G. B. Marin, Ab initio thermochemistry and kinetics for carbon-centered radical addition and beta-scission reactions, J. Phys. Chem. A 111 (2007) 8416-8428
[71] W. K. Metcalfe, S. Dooley, H. J. Curran, J. M. Simmie, A. M. El-Nahas, M. V. Navarro, Experimental and Modeling Study of C5H10O2 Ethyl and Methyl Esters, J. Phys. Chem. A 111 (2007) 4001-4014
[72] C. Muller, V. Michel, G. Scacchi, G. M. Come, THERGAS - A computer program for the evaluation of thermochemical data of molecules and free-radicals in the gas-phase, J. Chim. Phys. PCB 92 (1995) 1154-1178

[73] W. H. Green, J. W. Allen, P. Bhoorasingh, B. A. Buesser, R. W. Ashcraft, G. J. Beran, C. A. Class, C. Gao, C. F. Goldsmith, M. R. Harper, A. Jalan, F. S. Khanshan, G. R. Magoon, D. M. Matheu, S. S. Merchant, J. D. Mo, S. Petway, S. Raman, S. Sharma, B. Slakman, J. Song, K. M. Van Geem, J. Wen, R. H. West, A. Wong, H.-W. Wong, P. E. Yelvington, N. Yee, Y. J. Reaction Mechanism Generator. http://rmg.mit.edu/
[74] M. K. Sabbe, F. De Vleeschouwer, M.-F. Reyniers, M. Waroquier, G. B. Marin, First Principles Based Group Additive Values for the Gas Phase Standard Entropy and Heat Capacity of Hydrocarbons and Hydrocarbon Radicals, J. Phys. Chem. A 112 (2008) 12235-12251
[75] P. D. Paraskevas, M. K. Sabbe, M.-F. Reyniers, N. G. Papayannakos, G. B. Marin, Group Additive Values for the Gas-Phase Standard Enthalpy of Formation, Entropy and Heat Capacity of Oxygenates, Chem.-Eur. J. 19 (2013) 16431-16452
[76] R. J. Kee, F. M. Rupley, J. A. Miller, M. E. Coltrin, J. F. Grcar, E. Meeks, H. K. Moffat, A. E. Lutz, G. Dixon-Lewis, M. D. Smooke, J. Warnatz, G. H. Evans, L. R. S., R. E. Mitchell, L. R. Petzold, W. C. Reynolds, M. Caracotsios, W. E. Stewart, P. Glarborg, C. Wang, O. Adigun, in: 15101 ed.; Reaction Design, Inc.: San Diego (CA), 2010.
[77] A. Cuoci, A. Frassoldati, T. Faravelli, E. Ranzi, OpenSMOKE++: An object-oriented framework for the numerical modeling of reactive systems with detailed kinetic mechanisms, Comput. Phys. Commun. (2015) DOI: 10.1016/j.cpc.2015.02.014
[78] R. Grana, A. Frassoldati, C. Saggese, T. Faravelli, E. Ranzi, A wide range kinetic modeling study of pyrolysis and oxidation of methyl butanoate and methyl decanoate – Note II: Lumped kinetic model of decomposition and combustion of methyl esters up to methyl decanoate, Combust. Flame 159 (2012) 2280-2294
[79] P. Dievart, S. H. Won, S. Dooley, F. L. Dryer, Y. G. Ju, A kinetic model for methyl decanoate combustion, Combust. Flame 159 (2012) 1793-1805
[80] S. M. Sarathy, M. J. Thomson, W. J. Pitz, T. Lu, An experimental and kinetic modeling study of methyl decanoate combustion, P. Combust. Inst. 33 (2011) 399-405
[81] A. Farooq, D. F. Davidson, R. K. Hanson, C. K. Westbrook, A comparative study of the chemical kinetics of methyl and ethyl propanoate, Fuel 134 (2014) 26-38
[82] Y. Luo, Handbook of Bond Dissociation Energies in Organic Compounds, CRC Press, Boca Raton, Florida, 2002
[83] S. P. Pyl, T. Dijkmans, J. M. Antonykutty, M.-F. Reyniers, A. Harlin, K. M. Van Geem, G. B. Marin, Wood-derived olefins by steam cracking of hydrodeoxygenated tall oils, Bioresour. Technol. 126 (2012) 48-55
[84] O. Herbinet, P. M. Marquaire, F. Battin-Leclerc, R. Fournet, Thermal decomposition of n-dodecane: Experiments and kinetic modeling, J. Anal. Appl. Pyrolysis 78 (2007) 419-429
[85] K. Zhang, C. Togbé, G. Dayma, P. Dagaut, Experimental and kinetic modeling study of trans-methyl-3-hexenoate oxidation in JSR and the role of CC double bond, Combust. Flame 161 (2014) 818-825
[86] C. Saggese, A. Frassoldati, A. Cuoci, T. Faravelli, E. Ranzi, A lumped approach to the kinetic modeling of pyrolysis and combustion of biodiesel fuels, P. Combust. Inst. 34 (2013) 427-434
[87] A. Kubatova, J. St'avova, W. S. Seames, Y. Luo, S. M. Sadrameli, M. J. Linnen, G. V. Baglayeva, I. P. Smoliakova, E. I. Kozliak, Triacylglyceride Thermal Cracking: Pathways to Cyclic Hydrocarbons, Energ. Fuel. 26 (2012) 672-685
[88] K. D. Maher, D. C. Bressler, Pyrolysis of triglyceride materials for the production of renewable fuels and chemicals, Bioresour. Technol. 98 (2007) 2351-2368
[89] A. Fridlyand, S. S. Goldsborough, K. Brezinsky, S. S. Merchant, W. H. Green, Influence of the double bond position on the oxidation of decene isomers at high pressures and temperatures, P. Combust. Inst. 35 (2015) 333-340
[90] S. M. Sarathy, S. Gail, S. A. Syed, M. J. Thomson, P. Dagaut, A comparison of saturated and unsaturated C-4 fatty acid methyl esters in an opposed flow diffusion flame and a jet stirred reactor, P. Combust. Inst. 31 (2007) 1015-1022
[91] D. M. Matheu, J. M. Grenda, A systematically generated, pressure-dependent mechanism for high-conversion ethane pyrolysis. 1. Pathways to the minor products, J. Phys. Chem. A 109 (2005) 5332-5342
[92] N. Hansen, J. A. Miller, P. R. Westmoreland, T. Kasper, K. Kohse-Höinghaus, J. Wang, T. A. Cool, Isomer-specific combustion chemistry in allene and propyne flames, Combust. Flame 156 (2009) 2153-2164
[93] C. Marchal, J.-L. Delfau, C. Vovelle, G. Moréac, C. Mounaïm-Rousselle, F. Mauss, Modelling of aromatics and soot formation from large fuel molecules, P. Combust. Inst. 32 (2009) 753-759
[94] C. Cavallotti, R. Rota, S. Carrà, Quantum Chemistry Computation of Rate Constants for Reactions Involved in the First Aromatic Ring Formation, J. Phys. Chem. A 106 (2002) 7769-7778
[95] W. Seames, Y. Luo, I. Ahmed, T. Aulich, A. Kubatova, J. Stavova, E. Kozliak, The thermal cracking of canola and soybean methyl esters: Improvement of cold flow properties, Biomass Bioenerg. 34 (2010) 939-946

Chapter 4

Kinetic modeling of thermochemical conversion of cyclic biomass model components

This chapter discusses the pyrolysis of three cyclic oxygenated species, i.e. γ-valerolactone, 2-methyl-tetrahydrofuran and tetrahydropyran. These molecules are considered to be model components for lignocellulosic biomass. Pyrolysis experiments were performed in a dedicated bench pyrolysis setup. Kinetic models were developed to better understand the underlying chemistry. Primary reactions in these kinetic models, describing the decomposition of the cyclic oxygenates species, were taken from quantum chemical calculations.

4.1 Experimental and computational study of the initial decomposition of γ-valerolactone

This section is based on the following paper:

Ruben De Bruycker, Hans-Heinrich Carstensen, John M. Simmie, Kevin M. Van Geem, Guy B. Marin, "Experimental and computational study of the initial decomposition of γ-valerolactone" *Proceedings of the Combustion Institute* 2015, 35 (1), 515-523

4.1.1 Abstract

The thermal decomposition of γ-valerolactone (GVL) diluted 1:10 mol/mol in nitrogen was studied experimentally in a tubular flow reactor. Variation of the temperature from 873 K to 1073 K for a residence time of approximately 400 ms at 0.17 MPa covered the complete GVL conversion range from 1% to 98 %. Comprehensive 2D MS analysis of the effluent revealed that the main products observed at temperatures below 1000 K are CO, CO_2, C4- olefins and 4-pentenoic acid. Initially, GVL is consumed predominantly through isomerization to 4-pentenoic acid, although minor contributions of bimolecular decomposition channels cannot be ruled out. CBS-QB3 level characterization of the $C_5H_8O_2$ potential energy surface reveals the existence of a low energy barrier for ring-opening to 4-pentenoic acid. The weak C-C bond between C_2 and C_3 in 4-pentenoic acid allows formation of radicals that further convert γ-valerolactone or 4-pentenoic acid. The 4-pentenoic acid yield increases steadily with rising temperature before a sharp decrease around 1010 K. The latter can be explained by radical chemistry taking over at high temperatures.

Keywords: γ-valerolactone, pyrolysis, comprehensive 2D GC, 4-pentenoic acid, molecular decomposition

4.1.2 Introduction

The use of biofuels, that is fuels derived from biomass, has been a major focus of scientific research of the last decades. Recently, the potential of γ-valerolactone (GVL), a cyclic ester see Figure 4.1-1, as a platform chemical and biofuel has been highlighted [1, 2]. Proposed production routes include (i) the acid catalyzed transformation of sugars into levulinic acid followed by reduction to GVL on noble-metal catalysts using H_2 [3], and (ii) sequential hydrogenation and hydrolysis of furfural from hemicellulose [4] catalyzed by zeolites with Brønsted and Lewis acid sites [5]. In contrast to some other biofuels such as ethanol, GVL does not form an azeotrope with water. Purification of GVL streams formed by the aforementioned production routes can thus proceed through simple distillation, which is less energy demanding and cheaper.

While some fuel properties of GVL (chemical formula $C_5H_8O_2$) such as its high oxygen content, which is known to decrease soot emissions [6], as well as its high density and high boiling point, are well established, its pyrolysis chemistry is not yet documented and no experimental data regarding its thermal decomposition is currently available to the best of our knowledge. Such data could provide insight in the stability of the molecule, help to identify important intermediate species and evaluate its soot or deposit formation tendency [7, 8]. Therefore, the aim of this work is to provide a first set of GVL pyrolysis data using a continuous flow tubular reactor setup with dedicated online analysis section for product identification and quantification. A qualitative interpretation of the observations is presented, supported by CBS-QB3 calculations of bond dissociation energies of GVL and important intermediates as well as selected aspects of the $C_5H_8O_2$ potential energy surface.

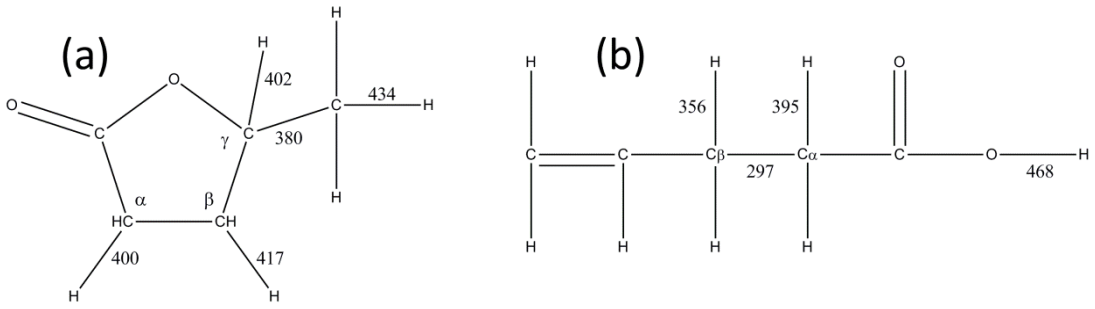

Figure 4.1-1 Structures of and bond dissociation energies (BDE) at 298 K in kJ/mol, calculated at CBS-QB3 level, in (a) γ-valerolactone(GVL) and (b) 4-pentenoic acid (4PA).

4.1.3 Experimental methods

The experimental apparatus has been described extensively by Djokic and Harper [7, 9]. The main features of the experimental and analytical methods used are summarized below.

γ-valerolactone (Sigma Aldrich, stated purity +99%) is fed to an evaporator kept at 573K using a peristaltic pump. Nitrogen (Air Liquide, purity +99,999%) is used as a diluent and its flow rate is controlled using a Coriolis mass flow controller. N_2 is heated to the same temperature as the gaseous GVL feed. Both gasses are mixed prior to entering the reactor.

The reactor is 1.475 m long and has an internal diameter of 6 mm. Eight equally spaced thermocouples allow for continuous temperature measurements. Furthermore, two manometers are present, positioned at the inlet and the outlet of the reactor, respectively. The measured pressure drop across the reactor was found to be negligible.

Products and unconverted feed are identified and quantified online, downstream of the reactor, using several dedicated gas chromatographs. A refinery gas analyzer (RGA) permits detection of all permanent gasses, using a thermal conductivity detector (TCD), as well as the C4- hydrocarbon fraction of the effluent, using a flame ionization detector (FID). Furthermore, a light oxygenates analyzer (LOA), equipped with a TCD, allows quantification of water. Finally, a two dimensional chromatograph (GCxGC) permits identification of the complete reactor effluent ranging from methane to pyrene[10, 11] with a TOF-MS, as well as quantification of these products using a FID. The calibration factors for H_2, CO, CO_2 and C_{4-} hydrocarbons were determined using a gaseous calibration mixture (Air Liquide, Belgium). The response factors of all other species were calculated using the effective carbon number method [12]. N_2 is used as internal standard. The obtained results had good repeatability and the error for the major species is estimated to be 5%, mainly caused by uncertainties in flow rate and calibration factors. Elemental balances typically closed within 3%.

4.1.4 Computational methods

To support the interpretation of the experimental data, electronic structure calculations were performed at the CBS-QB3 level of theory [13] as implemented in the Gaussian 09 suite of programs [14]. Since this method is well-known and established, only deviations will be discussed here. The most important one is that those low frequency vibrations that resemble torsions around single bonds are approximated as 1-dimensional hindered internal rotations. All single bonds, including those in the reactive moiety of the transition state, have been treated in this way. For the reactions considered, rather little coupling between internal rotors

was observed. Rotors with hindrance potentials exceeding 50 kJ/mol were excluded and treated as harmonic oscillators. Hindrance potentials of these rotations are calculated at the B3LYP/6-31G(d) level of theory via relaxed surface scans obtained with a step size of 10 degrees, in which all coordinates except for the dihedral angle of the rotation were re-optimized at each scan angle. The data are then fitted to truncated Fourier series expansions. Reduced moments of inertia for asymmetric internal rotors are calculated at the $I^{(2,3)}$ level as defined by East and Radom [15] based on the equilibrium geometry of the most stable conformer of the species. For each internal rotor, the 1-D Schrödinger equation is solved using the eigenfunctions of the 1-D free rotor basis functions and the energy eigenvalues are used to calculate its contributions to the thermodynamic functions. Inspections of the hindered rotor potentials also help ensure that the optimized geometry of a molecule corresponds to the lowest energy minimum. Transition states are identified by having one imaginary frequency, which is animated to verify that it corresponds to the desired reaction coordinate. In ambiguous cases, intrinsic reaction coordinate analyses ensured that specified transition states were connected to specific reactants and products.

4.1.5 Results and discussion

4.1.5.1 Thermal decomposition of γ-valerolactone: reactivity & product distribution

The thermal decomposition of GVL was studied at a constant inlet GVL mole fraction of 0.09 diluted in N_2 and a constant pressure of 0.17 MPa. A first set of experiments was conducted at constant flow rate but varying the temperature from 873 to 1073 K. Two additional data sets were obtained at constant temperature, 913 K and 993 K respectively, but the residence time was changed from 0.3 to 1s. The observed products may be subdivided in four main groups:

i. Permanent gases H_2/CH_4/CO/CO_2, Figure 4.1-2a
ii. Oxygenated species, Figure 4.1-2b
iii. Unsaturated hydrocarbon species, Figure 4.1-2c
iv. Aromatics, Figure 4.1-2d

The aforementioned temperature interval spans the complete conversion range of GVL, that is 1% at 873 K and 98% at 1073 K. The mole fractions of all permanent gases increase monotonically as a function of the average reactor temperature. CH_4, H_2, CO and CO_2 are already detected at the lowest conversion. As CH_4 and H_2 are generally formed through hydrogen abstraction by methyl and hydrogen atoms, respectively, this indicates that radical chemistry is observed within the entire temperature range. At the highest temperature, 1073

K, more than 93% of the oxygen present in GVL is converted to CO and CO_2. This high yield of CO and CO_2 is comparable to the thermal decomposition of non-cyclic esters such as methyl decanoate [16]. At 1073 K, acetic acid and water are the main other oxygen containing molecules, containing 2% and 5% of the original oxygen content, respectively.

Other identified oxygenated molecules are 4-pentenoic acid (4PA), 5-methyl-2(5H)furanone and methyl vinyl ketone; however their concentration profiles exhibit maxima at intermediate temperatures and they are detected in negligible quantities at the highest temperature studied. The yields of ethene and propene increase monotonically, while the butenes and 1,3-butadiene yields go through a maximum at 1053K. The mole fraction profiles of benzene, toluene and styrene, the main aromatic species, exhibit the typical exponential increase as a function of temperature.

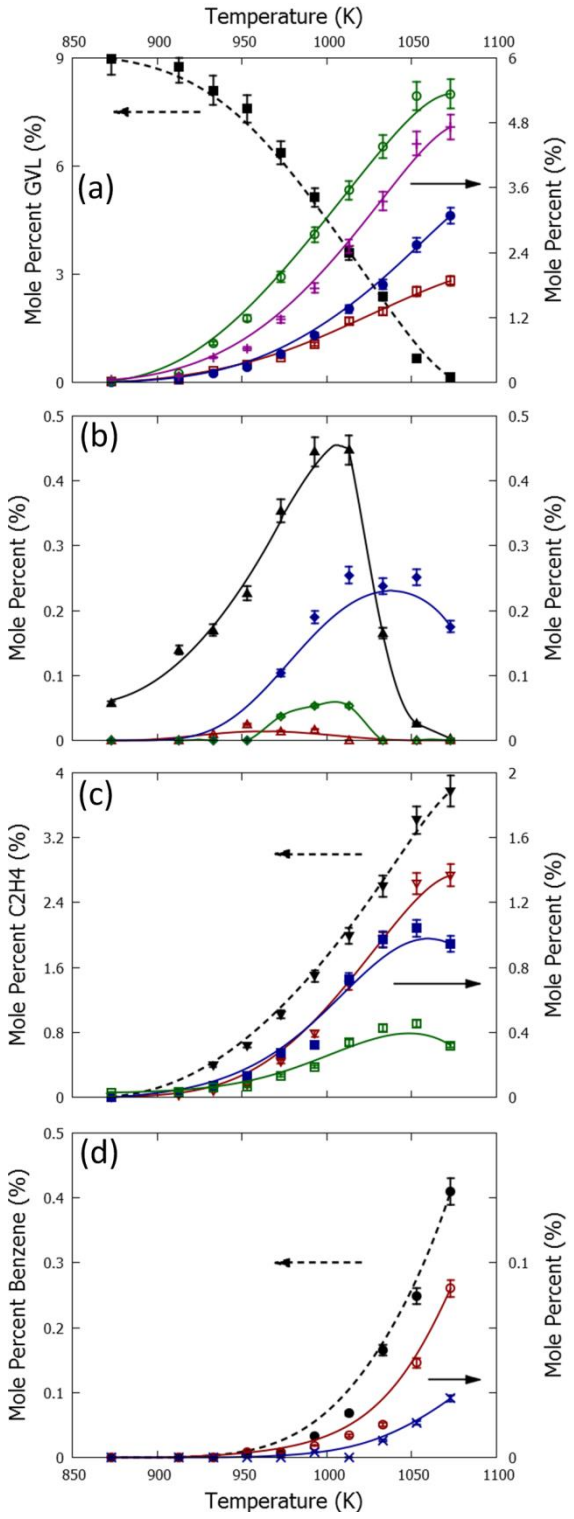

Figure 4.1-2 Mole percentage profiles as a function of reactor temperature for GVL pyrolysis: ■ - GVL (a), □ - H_2 (a), ○ - CH_4 (a), ○ - CO (a), + - CO_2 (a), ▲ - 4PA (b), △ - 5-methyl-2(5H)furanone (b), ◆ - acetic acid (b), ◇ - methyl vinyl ketone (b), ▼ - C_2H_4 (c), ▽ - C_3H_6 (c), ■ - 1,3-butadiene (c), □ - 1-butene (c), ● - benzene (d), ○ - toluene (d), × - styrene (d); lines indicate the observed trend; error bars represent an estimated 5% error on the experimental data.

The mole fractions of GVL and 4PA as a function of residence time at 913 K and 993 K are shown in Figure 4.1-3a. At 913 K increasing the residence time from 0.3 s to 1 s changes GVL conversion from 1 to 6%, while at 993 K the GVL conversion increases from 20 to 60%.

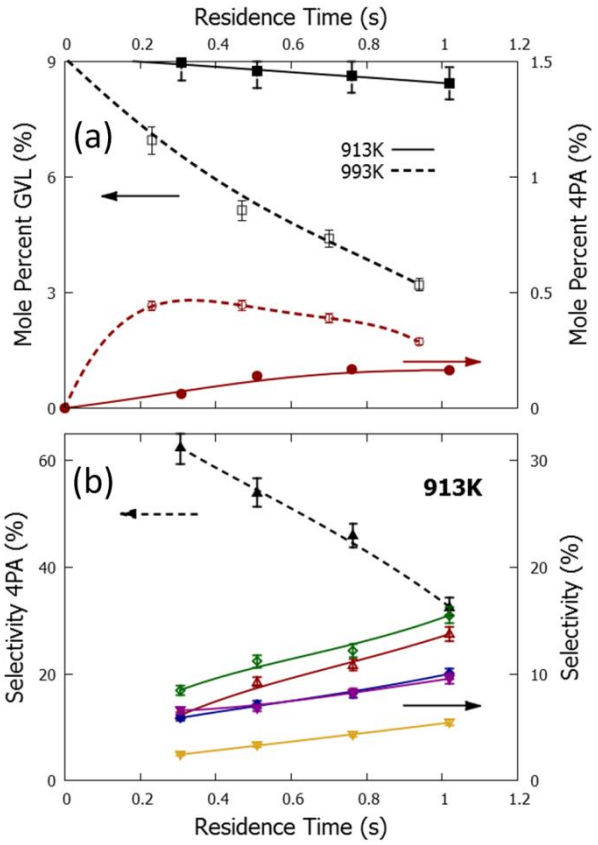

Figure 4.1-3 (a) Mole fractions profiles as a function of residence time for GVL pyrolysis at 913K: ■ - GVL, ● - 4PA; Mole fractions profiles as a function of residence time for GVL pyrolysis at 993K: □ - GVL, ○ - 4PA; (b) Selectivities as a function of residence time for GVL pyrolysis at 913K: ▲ - 4PA, △ - CO, ◆ - CO2, ◇ - C_2H_4, ▼ - 1-butene, ▽ - CH4; lines indicate the observed trend; error bars represent an estimated 5% error on the experimental data.

The 4PA mole fraction increases steadily at 913 K within the investigated residence time range. This clearly proves that 4PA is not an impurity but an initial product, which is already being formed at the low temperature end. The plot of selectivities, Figure 4.1-3b, defined based on the carbon molar balance, of the most abundant products at 913K lends further support to this conclusion because 4PA exhibits an extrapolated selectivity of > 60 % at 0 s residence time, indicating it is a primary product. Its selectivity drops from 60% to about 30% in the investigated residence time range, mostly in favor of CO and ethene.

In contrast to the 913K results, at 993K the 4PA mole fraction exhibits within the investigated residence time range a maximum, which indicates the potential importance of 4PA decomposition reactions at this temperature.

As Figure 4.1-2a demonstrates, the amount of unreacted GVL decreases with increasing temperature in a characteristic fashion which can be described by the assumption of a first order reaction in GVL with an activation energy of ca. 247 kJ/mol, that is, much higher than typical values for surface reactions, hence, ruling out the latter.

4.1.5.2 Mechanistic interpretation

4.1.5.2.1 Unimolecular reactions of GVL

The pyrolysis of GVL obviously begins with unimolecular reactions. Therefore, the relevant part of the $C_5H_8O_2$ potential energy surface was characterized at the CBS-QB3 level of theory (Figure 4.1-4).

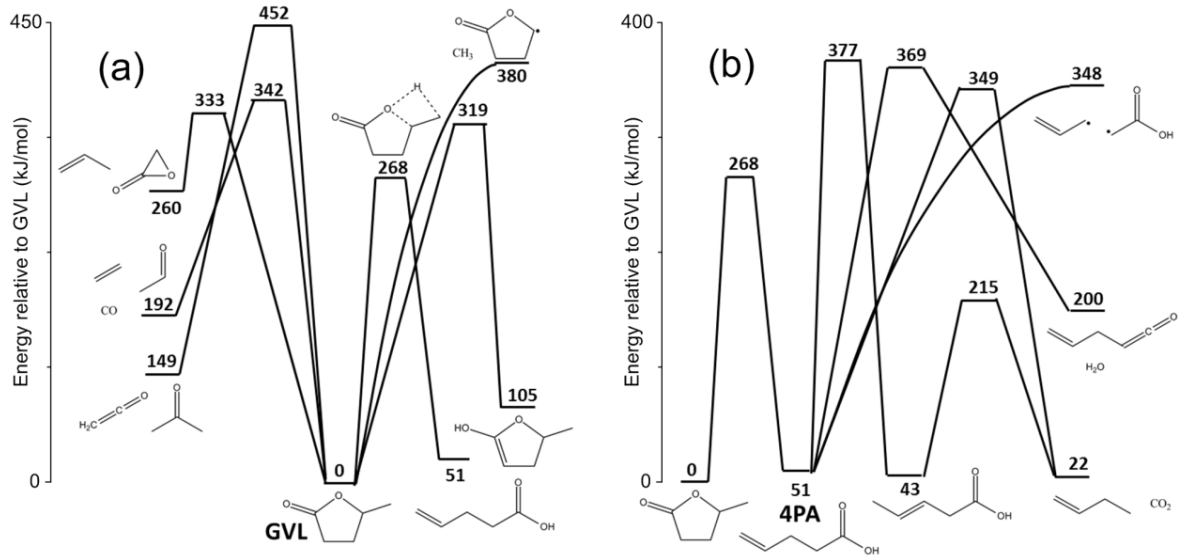

Figure 4.1-4 Selected pathways on the $C_5H_8O_2$ potential energy surface, for (a) GVL and (b) 4PA. The numbers are CBS-QB3 calculated relative enthalpies (kJ/mol) at 298 K

Figure 4.1-4a shows major pathways of GVL. Several molecular decomposition routes exist with barriers below the lowest bond scission channel, which is the 380 kJ/mol endothermic and barrier-less formation of methyl and the γ-radical of γ-butyrolactone. Those decomposition routes are (i) decomposition to propene plus 2-oxiranone, (ii) formation of ethene plus CO plus acetaldehyde, (iii) keto-enol tautomerization, and (iv) ring-opening to 4PA. The energy barrier for the latter ring-opening reaction, which proceeds via a four-membered transition state, is particularly low (268 kJ/mol). This value compares well with similar 1,3-H shift reactions in acyclic ethers such as ethanol and ethene formation from di-ethyl ether and ethyl tert-butyl ether decomposition to tert-butanol and ethene, for which barriers of 273 kJ/mol and 265 kJ/mol , respectively, have been reported [17]. Especially at

low temperature, GVL decomposition is expected to proceed through isomerization to 4PA, in accordance with the experimental results (Figure 4.1-3); the crucial role played by the otherwise unremarkable methyl group is noteworthy. Note that although the heats of formation of both the enol-form of GVL as well as 4PA are 105 and 51 kJ/mol, respectively, *higher* than that of GVL, 4PA possesses substantially more entropy than its cyclic isomer, 388 vs 342 J/mol/K at 298 K. Consequently, the calculations predict it to be the most stable isomer at the highest experimental temperatures.

Figure 4.1-4b shows some selected unimolecular pathways of 4PA. The barrier for isomerization to GVL is clearly the lowest, indicating the possibility for both isomers to (partially) equilibrate. Other investigated pathways are isomerization to 3-pentenoic acid, molecular decomposition to allylketene plus water and 1-butene plus CO_2, as well as C-C-scission yielding an allyl radical and the carboxymethyl radical, $\bullet CH_2COOH$. Given that scission reactions have high pre-exponential factors, this pathway will likely dominate. This is in accordance with the experimental data as allylketene and 3-pentenoic acid were not observed in the reactor effluent. The bond dissociation energy is calculated to be 297 kJ/mol, see Figure 4.1-1, which is 40 kJ/mol higher than the allyl-allyl bond in 1,5-hexadiene[18]. The features of the $C_5H_8O_2$ potential energy surface suggest that the isomerization of GVL to 4PA followed by bond scission could be an important route in the formation of the initial radical pool.

4.1.5.2.2 Plausible products from γ-valerolactone and 4-pentenoic acid through radical chemistry

While molecular chemistry appears to be important in the pyrolysis of GVL, radical chemistry cannot be ruled out. For both GVL and 4PA the C-H bond dissociation energies (BDE) have been calculated at the CBS-QB3 level and are presented in Figure 4.1-1.

In GVL the BDE's increase as follows: C(α-H), resonantly stabilized by the keto-group < C(γ-H), tertiary C-H, stabilized by ring oxygen < C(β-H), secondary C-H < C(methyl-H), primary C-H. The γ-GVL radical and the α-GVL radical will thus be the most stable radicals formed following hydrogen abstraction from GVL. The former will most likely decompose to form CO, ethene and methyl, while the latter can form 5-methyl-2(5H)-furanone or acetaldehyde, CO and vinyl (Figure 4.1-5). As acetaldehyde was not observed among the reaction products and 5-methyl-2(5H)-furanone was, C-H β-scission can be assumed to be the dominating decomposition route. The β-scission of the α-GVL radical forming a species with

a ketene group is assumed to be disfavored in our temperature region since these kinds of reactions often have high energy barriers compared to other reaction routes [16]. Ketenes were not observed in the experimental study. The methyl-GVL radical and the β-GVL radical will most likely react forming CO_2 plus but-1-en-4-yl and but-1-en-3-yl, respectively.

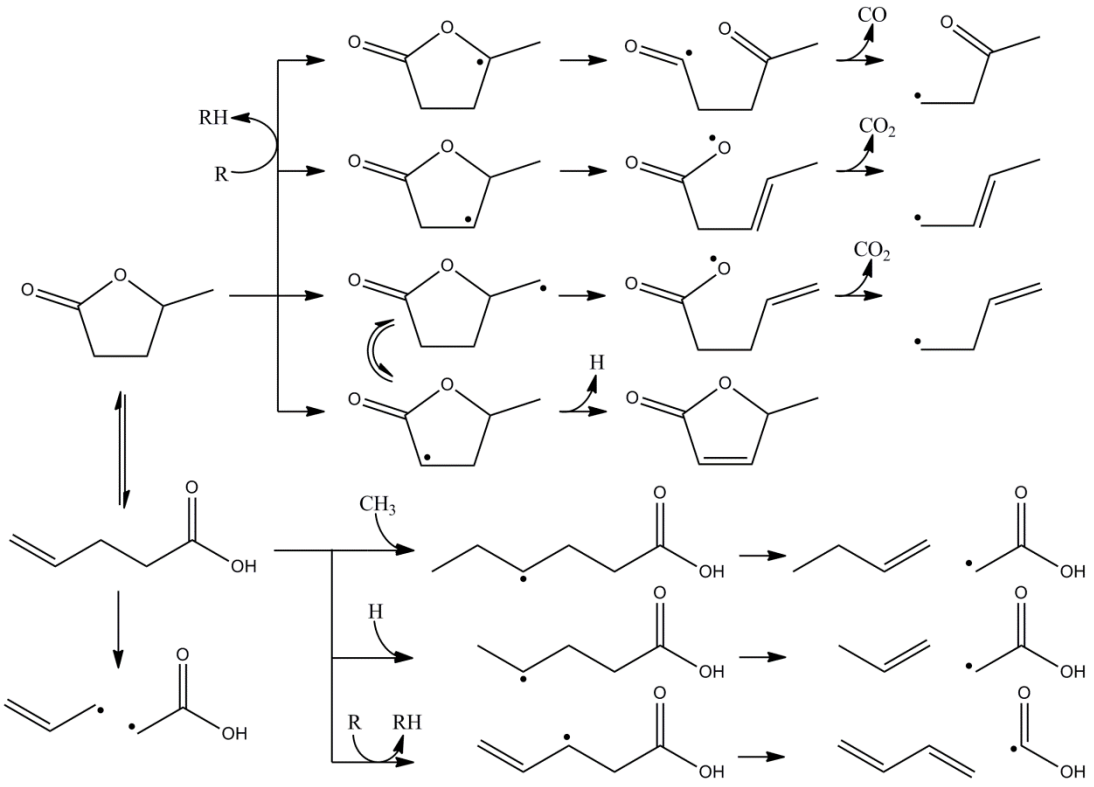

Figure 4.1-5 Some suggested decomposition routes for GVL and 4PA

Besides hydrogen abstraction reactions, hydrogen and carbon radical addition reactions to the carbonyl bond of GVL could be competitive in this temperature range [19]. The radical formed following hydrogen addition on the carbon atom of the carbonyl bond of GVL, which is considered to be the dominant addition route compared to addition at the oxygen atom below 1000 K [19, 20], may decompose to CO, a hydrogen radical, ethene and acetaldehyde. Note that propene, despite being abundantly present in the reactor effluent, cannot be formed through the reaction routes discussed up to now.

As mentioned earlier, unimolecular decomposition of 4-pentenoic acid through C-C scission forming the resonantly stabilized allyl and $\bullet CH_2COOH$ radical will most likely be an important consumption reaction of 4PA over the whole investigated temperature range. However, radical addition and hydrogen abstraction will only be competitive as soon as the radical pool is sufficiently large.

The bond dissociation energy of the hydrogen atom of the acid group is found to be significantly higher than the BDE of the C-H bonds displayed in Figure 4.1-1. The BDE of the C-H bond neighboring the acid group is 395 kJ/mol which is comparable to (i) the energy of the C-H bond neighboring the ester group in methyl butanoate and ethyl propanoate that was calculated to be 394 kJ/mol using the same level of theory [21], and (ii) the C_α-H bond energy in GVL which amounts to 400 kJ/mol. The BDE of the allylic C-H bond in 4PA is 356 kJ/mol. Decomposition of the allylic 4PA radical can occur through C-C β-scission forming 1,3-butadiene and a HOCO radical, as presented in Figure 4.1-5. The latter radical will decompose to CO_2 plus H, or CO plus OH [22]. Abstractions by OH can explain the detection of water.

The reactivity of resonantly stabilized radicals is significantly lower than that of primary radicals [23]. C-C β-scission forming highly energetic radicals such as vinyl are even less favored. This is the case for both radicals formed through hydrogen abstraction of 4PA. Hence, addition reactions can be expected to compete, if not dominate, with 4PA consumption via abstraction reactions. Radical addition to the terminal carbon atom is favored due to the creation of a secondary carbon radical [24, 25]. Hydrogen addition on 4PA followed by C-C β-scission will form propene and $\bullet CH_2COOH$, methyl addition will form 1-butene and $\bullet CH_2COOH$.

The consumption paths of 4PA highlight the importance of the resonantly stabilized $\bullet CH_2COOH$ radical. The β-scission reaction of this radical to ketene plus a hydroxyl radical (Figure 4.1-6) has a rather high barrier and may only contribute at high temperatures. The reaction route of $\bullet CH_2COOH$ involving isomerization to an acetoxyl radical, $CH_3C(O)O\bullet$, through a 4-membered transition state, followed by decomposition to CO_2 plus a relatively more reactive methyl radical, is expected to be dominant in the investigated range of conditions.

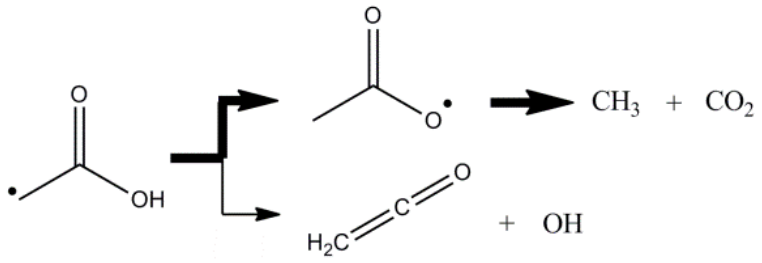

Figure 4.1-6 Decomposition pathways of the carboxymethyl radical

The strong decrease in 4PA yield observed at 1033 K (Figure 4.1-2) can be explained by the reaction paths presented in Figure 4.1-5. The decomposition of •CH_2COOH to a reactive radical and the rate of C-C scission of 4PA will be rather fast at this, relatively high, temperature. Furthermore, hydrogen abstraction followed by C-C β-scission of 4PA to 1,3-butadiene and HOCO will gain importance. The resulting large reactive radical pool can be the cause of the observed experimental result. However a more extensive theoretical and kinetic modeling study is needed to confirm this.

The above considerations are also in accordance with the product spectrum experimentally observed at 913 K. As discussed earlier, at low temperatures, GVL will decompose selectively to 4PA. C-C scission of 4PA will cause radical chemistry to gain in importance resulting in a decline of 4PA selectivity, which is formed through molecular chemistry. Addition of methyl on the carbon-carbon double bond of 4PA, followed by decomposition, can form 1-butene, CO_2 and methyl (eventually formed from •CH_2COOH) which can explain the high selectivity for the former two molecules observed at 913 K. Hydrogen abstraction from GVL will be competitive with radical addition on 4PA. CO and ethene, for which a high selectivity was observed, are decomposition products of the γ-GVL radical, indicative for the importance of this radical at low temperatures.

4.1.5.2.3 Side products

Acetic acid is the most abundantly formed oxygenated intermediate after 4PA (Figure 4.1-2b), with a maximum mole percentage of 0.25% at 1050K. Hydrogen abstraction by the abundantly formed •CH_2COOH radical is expected to be the dominant formation route. Other formation routes such as hydrogen addition on the oxygen atom of the C=O of 4PA followed by C-C β-scission and a keto-enol tautomerization can most likely be neglected in this temperature region [19].

As shown in Figure 4.1-2d, benzene and toluene exhibit a typical exponential profile as function of temperature with a measured mole fraction of 0.41 and 0.09, respectively, at 1073K. Benzene is already observed at 953K. One possible route is through recombination of the resonantly stabilized allyl radicals, formed by C-C scission of 4PA or hydrogen abstraction from propene. 1,5-hexadiene has been detected in the reactor effluent with a maximum mole percentage of approximately 0.03 at intermediate temperatures. Hydrogen abstraction from this molecule followed by cyclization and dehydrogenation can contribute to benzene formation, as for example observed in iso-butanol pyrolysis [26].

4.1.6 Conclusions

The thermal decomposition of γ-valerolactone (GVL) has been investigated at temperatures between 873 K and 1073 K, at a constant pressure of 0.17 MPa in a tubular reactor with quantitative GC analysis. 4-Pentenoic acid (4PA) has been identified as an important oxygenated intermediate although the reactor effluent consists mostly of carbon oxides and olefins with up to 4 carbon atoms. At temperatures greater than 1050 K the yield of 4PA becomes negligible and > 93% of the fuel oxygen is found in CO and CO_2, while acetic acid and water contain most of the remaining oxygen. Several aromatic species are detected at non-negligible concentrations but their yields are, even at 1073 K, below 0.5 mol%.

Important features of the $C_5H_8O_2$ potential energy surface have been calculated at the CBS-QB3 level of theory. These calculations suggest that the isomerization of GVL to 4PA followed by scission of the allyl-carboxymethyl bond could be an important route in the formation of the initial radical pool. As the pre-exponential factors for isomerization and the bond scission are typically quite high, this reaction sequence is crucial in understanding GVL pyrolysis.

Except for 4PA, the reaction paths for all observed products can be hypothesized based on radical chemistry. Radical addition to the carbon-carbon double bond of 4PA is suggested to be an important reaction route. Hydrogen abstraction by allyl radicals is also expected to contribute to the large amounts of propene formed under the studied conditions.

4.1.7 References

[1] I. T. Horvath, H. Mehdi, V. Fabos, L. Boda, L. T. Mika, γ-Valerolactone - a sustainable liquid for energy and carbon-based chemicals, Green Chem. 10 (2008) 238-242
[2] D. M. Alonso, S. G. Wettstein, J. A. Dumesic, Gamma-valerolactone, a sustainable platform molecule derived from lignocellulosic biomass, Green Chem. 15 (2013) 584-595
[3] J. J. Bozell, Connecting Biomass and Petroleum Processing with a Chemical Bridge, Science 329 (2010) 522-523
[4] R. Xing, W. Qi, G. W. Huber, Production of furfural and carboxylic acids from waste aqueous hemicellulose solutions from the pulp and paper and cellulosic ethanol industries, Energ. Environ. Sci. 4 (2011) 2193-2205
[5] L. Bui, H. Luo, W. R. Gunther, Y. Román-Leshkov, Domino Reaction Catalyzed by Zeolites with Brønsted and Lewis Acid Sites for the Production of γ-Valerolactone from Furfural, Angew. Chem. Int. Ed. 52 (2013) 8022-8025
[6] C. K. Westbrook, W. J. Pitz, H. J. Curran, Chemical Kinetic Modeling Study of the Effects of Oxygenated Hydrocarbons on Soot Emissions from Diesel Engines, J. Phys. Chem. A 110 (2006) 6912-6922
[7] M. Djokic, H.-H. Carstensen, K. M. Van Geem, G. B. Marin, The thermal decomposition of 2,5-dimethylfuran, P. Combust. Inst. 34 (2013) 251-258
[8] C. Esarte, M. Abián, Á. Millera, R. Bilbao, M. U. Alzueta, Gas and soot products formed in the pyrolysis of acetylene mixed with methanol, ethanol, isopropanol or n-butanol, Energy 43 (2012) 37-46
[9] M. R. Harper, K. M. Van Geem, S. P. Pyl, G. B. Marin, W. H. Green, Comprehensive reaction mechanism for n-butanol pyrolysis and combustion, Combust. Flame 158 (2011) 16-41

[10] S. P. Pyl, C. M. Schietekat, K. M. Van Geem, M.-F. Reyniers, J. Vercammen, J. Beens, G. B. Marin, Rapeseed oil methyl ester pyrolysis: On-line product analysis using comprehensive two-dimensional gas chromatography, J. Chromatogr. A 1218 (2011) 3217-3223
[11] K. M. Van Geem, S. P. Pyl, M.-F. Reyniers, J. Vercammen, J. Beens, G. B. Marin, On-line analysis of complex hydrocarbon mixtures using comprehensive two-dimensional gas chromatography, J. Chromatogr. A 1217 (2010) 6623-6633
[12] J. Beens, H. Boelens, R. Tijssen, J. Blomberg, Quantitative aspects of comprehensive two-dimensional gas chromatography (GC x GC), J. High. Resolut. Chromatogr. 21 (1998) 47-54
[13] J. A. Montgomery Jr, M. J. Frisch, A complete basis set model chemistry. VI. Use of density functional geometries and frequencies, J. Chem. Phys. 110 (1999) 2822
[14] M. J. Frisch, G. W. Trucks, H. B. Schlegel, e. al., in: Gaussian 09, Revision B.01, Gaussian Inc., Wallingford CT: 2009.
[15] A. L. L. East, L. Radom, An initio statistical thermodynamical models for the computation of third-law entropies, J. Chem. Phys. 106 (1997) 6655
[16] O. Herbinet, P.-A. Glaude, V. Warth, F. Battin-Leclerc, Experimental and modeling study of the thermal decomposition of methyl decanoate, Combust. Flame 158 (2011) 1288-1300
[17] K. Yasunaga, J. M. Simmie, H. J. Curran, T. Koike, O. Takahashi, Y. Kuraguchi, Y. Hidaka, Detailed chemical kinetic mechanisms of ethyl methyl, methyl tert-butyl and ethyl tert-butyl ethers: The importance of uni-molecular elimination reactions, Combust. Flame 158 (2011) 1032-1036
[18] Y. Luo, Handbook of Bond Dissociation Energies in Organic Compounds, CRC Press, Boca Raton, Florida, 2002
[19] H. Hippler, B. Viskolcz, Competition between alkyl radical addition to carbonyl bonds and H-atom abstraction reactions, Phys. Chem. Chem. Phys. 4 (2002) 4663-4668
[20] H. J. Curran, Rate constant estimation for C1 to C4 alkyl and alkoxyl radical decomposition, Int. J. Chem. Kinet. 38 (2006) 250-275
[21] A. M. El-Nahas, M. V. Navarro, J. M. Simmie, J. W. Bozzelli, H. J. Curran, S. Dooley, W. Metcalfe, Enthalpies of formation, bond dissociation energies and reaction paths for the decomposition of model biofuels: Ethyl propanoate and methyl butanoate, J. Phys. Chem. A 111 (2007) 3727-3739
[22] J. S. Francisco, J. T. Muckerman, H.-G. Yu, HOCO Radical Chemistry, Acc. Chem. Res. 43 (2010) 1519-1526
[23] M. Mehl, G. Vanhove, W. J. Pitz, E. Ranzi, Oxidation and combustion of the n-hexene isomers: A wide range kinetic modeling study, Combust. Flame 155 (2008) 756-772
[24] M. K. Sabbe, M.-F. Reyniers, V. Van Speybroeck, M. Waroquier, G. B. Marin, Carbon-centered radical addition and beta-scission reactions: Modeling of activation energies and pre-exponential factors, ChemPhysChem 9 (2008) 124-140
[25] M. K. Sabbe, M.-F. Reyniers, M. Waroquier, G. B. Marin, Hydrogen Radical Additions to Unsaturated Hydrocarbons and the Reverse beta-Scission Reactions: Modeling of Activation Energies and Pre-Exponential Factors, ChemPhysChem 11 (2010) 195-210
[26] S. S. Merchant, E. F. Zanoelo, R. L. Speth, M. R. Harper, K. M. Van Geem, W. H. Green, Combustion and pyrolysis of iso-butanol: Experimental and chemical kinetic modeling study, Combust. Flame 160 (2013) 1907-1929

4.2 An experimental and kinetic modeling study of γ-valerolactone pyrolysis

This section is based on the following paper:

Ruben De Bruycker, Hans-Heinrich Carstensen, Marie-Françoise Reyniers, Guy B. Marin, John M. Simmie, Kevin M. Van Geem, "An experimental and kinetic modeling study of γ-valerolactone pyrolysis" *Combustion and Flame* 2016, 164, 183-200

4.2.1 Abstract

The pyrolysis of γ-valerolactone, a cyclic ester readily obtainable from cellulosic biomass and which has potential as a fuel, was investigated from 873 to 1113 K at 0.17MPa in a tubular continuous flow reactor. Unimolecular decomposition of γ-valerolactone forms 4-pentenoic acid and its selectivity increases upon addition of toluene, a radical scavenger. A kinetic model, consisting of 520 species and 3589 reactions, was developed. Kinetic and thermodynamic data relevant for γ-valerolactone consumption, including hydrogen abstraction, hydrogen addition and fuel radical decomposition, were calculated at the CBS-QB3 level of theory. Experimental and calculated mole fraction profiles are in good agreement. Reaction path analysis shows that γ-valerolactone is mainly consumed by isomerization to 4-pentenoic acid and hydrogen abstraction from the carbon atom α to the carbonyl group and the carbon atom α to the ring oxygen. C-C scission of 4-pentenoic acid forming allyl and carboxy methyl is an important source of radicals.

Keywords: γ-valerolactone, 4-pentenoic acid, pyrolysis, isodesmic reaction, kinetic model

4.2.2 Introduction

There is a growing need for renewable sustainable liquid fuels. Ethanol, the market leader in gasoline alternatives, has several drawbacks such as a low energy density and a high vapor pressure [1]. Current production methods are often competing with the food industry for feedstock. To overcome these issues, new routes for the production of liquid fuels starting from cellulosic biomass are currently being developed. Recently, the potential of γ-valerolactone (GVL), see Figure 4.2-1, has been highlighted [2, 3]. Interesting properties include its high boiling point, high density and high oxygen content which is known to decrease soot formation [4, 5]. Several production routes have been proposed starting from hemicellulose via furfural as intermediate [6, 7] or from cellulose via levulinic acid as intermediate [2, 3, 8-10]. Berecezky et al. studied the combustion performance of diesel/GVL blends in a four-cylinder, turbocharged direct injection diesel engine [11]. The engine performance of the blend was reported to be comparable to 100% fossil diesel while CO and hydrocarbon emissions decreased and smoke concentrations in the exhaust diminished by approximately 50%. Furthermore, GVL has potential as a green solvent [10, 12]. Extensive usage may lead to spills and release of GVL in the atmosphere. Finally, lactones, such as GVL, are products in the oxidation of ketones [13-15].

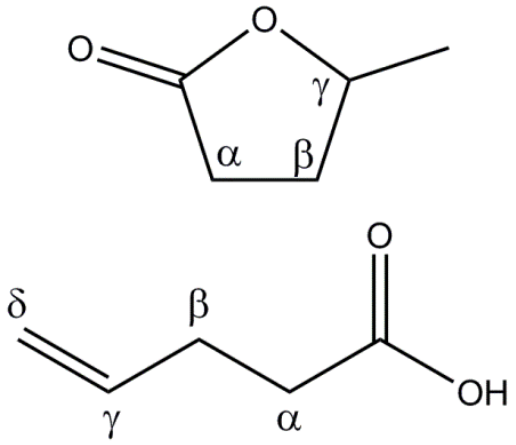

Figure 4.2-1 Molecular representation of γ-valerolactone (top) and 4-pentenoic acid (bottom). Greek letters are atoms labels which will be used throughout this work

The practical implementation of bio-derived fuels requires careful evaluation of the stability of the molecule, assessment of its combustion characteristics and tendency of soot formation [16] and identification of toxic intermediates formed during oxidation/pyrolysis. Previous fundamental work aimed at understanding the decomposition of γ-valerolactone is relatively scarce. In section 4.1, a first experimental dataset regarding pyrolysis of γ-valerolactone along with a qualitative interpretation of the results was presented. Both experiments and CBS-QB3

calculations of the $C_5H_8O_2$ PES highlighted the isomerization of γ-valerolactone to the acyclic 4-pentenoic acid, see Figure 4.2-2(A), as an important reaction path. Recently, Barnes et al. provided a combined experimental and theoretical study regarding hydrogen abstraction by hydroxyl radicals from GVL at room temperature[17]. Hydrogen abstraction by OH is preferred at the C_α and C_γ positions (see Figure 4.2-1), in line with bond dissociation energies [17].

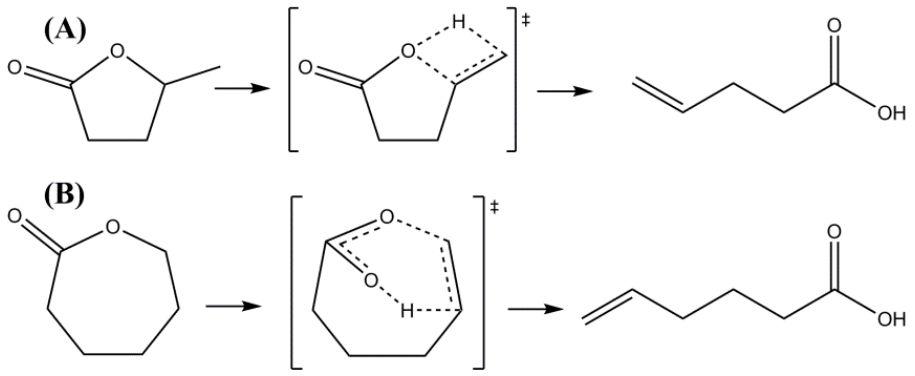

Figure 4.2-2 Formation of unsaturated acids from (A) γ-valerolactone and (B) ε-caprolactone through unimolecular reactions

Thermal decompositions of several GVL related molecules are worth mentioning. Bailey and Bird investigated the pyrolysis of 5- to 12-membered ring lactones at 793K and 863K [18]. At their experimental conditions, pyrolysis of lactones forms unsaturated acids if the lactone contains seven or more ring atoms. The reaction is reported to proceed through a six-membered transition state, in which a hydrogen atom in β-position relative to the ether oxygen bridges to the oxygen atom of the carbonyl group, see Figure 4.2-2(B) for ε-caprolactone, a 7-membered ring lactone. This transition state introduces considerable ring strain for small lactones and is infeasible for γ-butyrolactone (GBL), a 5-membered ring lactone [18]. This reaction is similar to the unimolecular decomposition of acyclic esters that have a hydrogen atom in β-position to the ester functionality, forming an olefin and an acid [19], e.g. ethyl propanoate forming ethene and propanoic acid [20].

The relative stability of 5-membered ring lactones, compared to lactones with a larger ring, motivated some pyrolysis studies of GBL [21, 22]. Rai-Chaudhuri et al. examined its pyrolysis in a continuous flow reactor at low pressure, i.e. 70 Pa [21]. The onset of decomposition was at 1253K. Decarboxylation of GBL forming propene was found to be the major reaction channel. Unimolecular decomposition pathways of GBL were explored at the UMP4/6-31G and UHF/6-31-G levels of theory by Li et al.[22]. Their computations showed that concerted decarbonylation is the energetically preferred reaction path, in contrast to the

experimentally observed decarboxylation. Several studies aimed at understanding the pyrolysis/combustion of 2-methyl-tetrahydrofuran, i.e., a 5-ring ether, have been published recently [23, 24]. A kinetic model was developed by Moshammer et al. and was validated by comparing predicted and experimental mole fraction profiles measured in a fuel-rich pre-mixed laminar low-pressure flames [24]. 2-methyl-tetrahydrofuran is mainly consumed by hydrogen abstraction at the investigated operating conditions [24, 25]. Verdicchio et al. recently investigated the unimolecular decomposition of tetrahydrofuran and showed that diradical, carbenic and pericyclic reactions are important in its pyrolysis [26]. In a follow-up study by Tran et al. a kinetic model was developed for the combustion of tetrahydrofuran, which was validated against laminar low-pressure premixed flame data, atmospheric adiabatic laminar burning velocities and high-pressure ignition delay times [27].

This work aims at providing a first detailed kinetic model describing the pyrolysis of γ-valerolactone. Kinetic and thermodynamic data related to GVL decomposition have been calculated using the CBS-QB3 level of theory. Model simulations are compared with experimental data discussed in 4.1 and new data obtained at higher dilution and shorter residence time. GVL is assumed to be consumed by both isomerization and hydrogen abstraction. The latter is a radical pathway and the relative importance of isomerization should increase by addition of a radical scavenger to the inlet flow. Therefore, to provide experimental evidence of the unimolecular isomerization pathway to 4-pentenoic acid, a dataset of γ-valerolactone and toluene co-pyrolysis has been obtained. The proposed kinetic model can be used as building block for future kinetic models describing the oxidation/combustion of γ-valerolactone.

4.2.3 Experimental methods

The experimental setup, which has been described extensively by Djokic and Harper [28, 29], is the same that was used to obtain the first set of γ-valerolactone pyrolysis data discussed in section 4.1. The main features are summarized below. The interested reader is referred to the aforementioned literature for additional information.

GVL and toluene were purchased from Sigma Aldrich with a stated purity of 99% and 99.8% respectively. The liquid feedstock was fed to an evaporator kept at 573K using a peristaltic pump. Nitrogen (Air Liquide, purity +99.999%) was used as diluent and fed to a heater using a Coriolis mass flow controller. The evaporated liquid feed and heated diluent were mixed before entering the reactor.

The reactor is an Incoloy 800HT tube with an internal diameter of 6 mm and a length of 1.475m. It is positioned in a vertical furnace consisting of four separate heating sections controlled by four thermocouples measuring the process gas temperature. There are four additional thermocouples measuring the gas temperature at fixed positions in the reactor. The pressure was monitored by two manometers positioned at the inlet and outlet of the reactor. The reactor was operated at a fixed pressure of 0.17 MPa. The pressure drop along the reactor was found to be negligible.

The reactor effluent enters a sampling valve kept at 573K. After removal of the condensable products, a part of the effluent is injected on-line on a gas chromatograph dedicated to the quantification of hydrocarbon species with four or less carbon atoms using a flame ionization detector (FID) and all permanent gases using two thermal conductivity detectors (TCD). Species concentrations were calculated based on the known fixed flow rate of N_2. The response factors were determined using a calibration mixture provided by Air Liquide, Belgium. A second fraction of the effluent is injected on a chromatograph dedicated to the identification of small oxygenated molecules, without prior condensation. This GC is able to quantify formaldehyde, methanol and water using propene, quantified on the first GC, as secondary internal standard. Finally, a part of the effluent, again without prior condensation, is injected on-line on a GC×GC, which is used for both species identification, using a time of flight mass spectrometer (TOF-MS), and quantification, using a FID. Flow rates of the detected molecules were calculated using ethene, quantified on the first GC, as secondary internal standard. Response factors were determined using the effective carbon number approach [30]. Transfer lines between sampling oven and GC×GC are heated to prevent condensation. The described experimental procedure allows on-line analysis of the complete product spectrum and avoids separate gas-phase and condensate analysis. Additional details regarding the effluent analysis can be found elsewhere [31]. Elemental balances close within 5%. The estimated uncertainty on experimental mole fractions is approximately 5%, in line with earlier work.

4.2.4 Computational methods

Electronic structure calculations were performed with the Gaussian 09 revision B suite of programs [32].

4.2.4.1 Heats of formation

The heats of formation, $\Delta_f H°$ in Table 4.2-1, of GVL and 4PA were calculated (i) with isodesmic reactions and (ii) with the atomization method combined with bond additive corrections (BAC).

Table 4.2-1 Experimental heats of formation and ab initio calculated enthalpies (298 K) [kJ mol^{-1}]. Abbreviated species names given in parenthesis are used in Table 4.2-2 to specify the isodesmic reaction.

Species	formula	$\Delta_f H^0_{298}$ (experimental)	H(298) CBS-QB3	H(298) G3	H(298) G4
furan	C_4H_4O	-34.7 ±0.8[a] [33]	-34.1	-32.8	-34.4
γ-butyrolactone (GBL)	$C_4H_4O_2$	-365.6 ±0.4 [34]	-374.3	-372.5	-369.0
2-methyl furan (2-MF)	C_5H_6O	-80.3 ±1.0[a] [35]	-77.2	-77.6	-78.0
tetrahydrofuran (THF)	C_4H_8O	-184.2 ±0.7 [36]	-184.2	-183.5	-180.9
2-methyl tetrahydrofuran (2-MTHF)	$C_5H_{10}O$	-225.9 ±1.0[a] [23]	-224.2	-225.4	-222.6
methylcyclopentane (CcyC5)	C_6H_{12}	-106.7 ±0.8 [37]	-97.9	-105.6	103.8
δ-valerolactone (DVL)	$C_5H_8O_2$	-379.6 ±0.9 [38]	-386.6	-386.4	-382.4
cyclohexane (cyC6)	C_6H_{12}	-123.1 ±0.8 [37]	-115.1	-123.1	-121.0
oxetane	C_3H_6O	-80.5 ±0.6 [36]	-81.7	-80.3	-80.3
β-propiolactone (BPL)	$C_3H_4O_2$	-282.9 ±0.8 [39]	-288.9	-286.0	-284.1
tetrahydropyran (THP)	$C_5H_{10}O$	-223.8 ±1.0 [36]	-223.8	-224.7	-222.0
propane (CCC)	C_3H_8	-104.7 ±0.5 [40]	-101.7	-105.7	-103.6
propanoic acid (CCC(=O)OH)	$C_3H_6O_2$	-455.8 ± 2.0 [41][c]	-455.9	-453.5	-450.6
1-pentene (CCCC=C)	C_5H_{10}	-20.9 ± 8.4 [42][b]	-12.6	-20.5	-19.7
ethane (C2H6)	C_2H_6	-83.8 ± 0.3 [40]	-82.4	-85.1	-83.3
acetic acid (CC(=O)OH)	$C_2H_4O_2$	-433.0 ± 3.0 [42][b]	-436.7	-432.9	-431.1
1-butene (CCC=C)	C_4H_8	-0.6 ± 0.8 [43]	6.8	0.4	1.4
Methane (CH4)	CH_4	-74.5 ± 0.4 [40]	-74.5	-75.9	-74.8
formic acid (HC(=O)OH)	CH_2O_2	-379.2 ±0.6 [41][c]	-384.5	-379.1	-379.0
Propene (CC=C)	C_3H_6	20.4 ±2.1 [44][a]	24.7	19.9	20.3
crotonic acid (t-CC=CC(=O)OH)	$C_4H_6O_2$	-368.5 ± 1.4 [45][c]	-361.4	-361.0	-358.9
methacrylic acid (C=C(C)C(=O)OH)	$C_4H_6O_2$	-367.3 ±2.4 [45][c]	-361.7	-361.0	-358.8
acrylic acid (C=CC(=O)OH)	$C_3H_4O_2$	-330.7 ±4.2 [45][c]	-325.2	-323.8	-322.0
butane (CCCC)	C_4H_{10}	-125.6 ±4.2 [40]	-120.5	-125.9	-123.8
butadiene (C=CC=C)	C_4H_6	108.8 ± 0.8 [43]	118.3	111.2	111.0
1,5-hexadiene (C=CCCC=C)	C_6H_{10}	85.0 ±2.0 [46][c]	96.2	86.1	84.6
γ-valerolactone (GVL)	$C_5H_8O_2$	-406.5 ± 1.1 [38]	-416.2	-416.3	-411.7
4-pentenoic acid (4PA)	$C_5H_8O_2$	-366.9 ± 1.1 [47]	-365.2	-366.7	-365.0

[a] uncertainty estimated; [b] averaged value; [c] as cited by NIST Webbook [42]

The enthalpies of the isodesmic reactions were determined with three composite methods: CBS-QB3 [48], G3 [49] and G4 [50]. A set of reactions was constructed in such a way that the number and types of bonds found in the reactants are conserved in the products. Furthermore, the heats of formation of all reactants and products except that of the target molecule must be known experimentally with good accuracy. By combining the calculated reaction enthalpies, $\Delta_R H°$ in Table 4.2-2, with the thermodynamic data of the known species, the heat of formation of the target molecule can be determined with high accuracy because systematic calculation errors cancel out. In this work, atomization enthalpies with internal

rotor corrections were used without any further corrections. The internal rotor treatment is described below.

The use of atomization energies [51] presents an alternative method to calculate heats of formation. Petersson et al. [52] showed that systematic errors of ab initio calculated energies can be largely reduced by applying method-specific BAC to atomization energies. Those BAC parameters are obtained by minimizing the deviations between calculated heats of formation and experimental values reported in the NIST webbook for a large set of molecules via a sum of least-squares procedure. Atomization enthalpies were calculated in this work by applying hindered rotor treatments to all single bonds as long as the barrier of rotation is below 50 kJ mol^{-1}. The frequencies of modes that represent internal rotations were identified via visual inspection of the animated harmonic oscillator vibrations and removed prior to calculating the thermal energy.

Entropies and heat capacities were calculated with established statistical mechanics formulae based on partition functions. The geometry and frequency data were taken from the CBS-QB3 calculations and were therefore based on B3LYP/6-311G(d,p) method. All frequencies were scaled by a factor of 0.99 prior to their use. As mentioned above, internal modes that resemble internal rotations rather than harmonic oscillations were treated separately by replacing the contributions of the corresponding oscillators to the partition function with numerically calculated partition functions of hindered rotors. The required hindrance potentials were obtained from relaxed scans, in which the dihedral angle defining the rotation was varied from 0 to 360 degrees in steps of 10 degrees. In a few cases, step sizes of 5 degrees were used to help the scans to converge. The obtained hindrance potential was fitted to a Fourier series. Together with the reduced moment of inertia calculated at the $I^{(2,3)}$ level as defined by East and Radom [53], the hindrance potential was used to construct the Schrödinger equation for 1-D rotation. The eigenvalues of the solution to this Schrödinger equation represent the energy levels of this mode. They were used to determine the partial partition function as a function of temperature. After correction for symmetry and optical isomers, the total partition function was used to calculate the thermal contribution to the enthalpy, standard entropy and temperature-dependent heat capacity data. All data were stored as NASA polynomials.

4.2.4.2 High-pressure rate coefficients

The rate coefficients of important reactions were calculated at the CBS-QB3 level of theory. First, the thermodynamic properties of reactants, products and the transition state were

calculated with the atomization energy method as described above, however without applying BAC, because (i) those are not available for transition states and (ii) for kinetics, only relative energies are needed. Those uncorrected CBS-QB3 data are used in all following figures that describe potential energy surfaces.

Transition state theory expressed in terms of Free Gibbs energies was used to calculate the rate coefficients:

$$(1) \quad k_{TST}(T) = \chi(T) \cdot \frac{k_B T}{h} \cdot \left(\frac{RT}{p}\right)^{\Delta n - 1} \cdot e^{-\frac{\Delta G^{\ddagger}}{RT}}$$

$\Delta G^{\ddagger}$ is the Gibbs free energy difference between transition state, identified by a single imaginary frequency, and reactant(s), Δn is the molecularity of the reaction (2 for bimolecular, 1 for unimolecular reactions), and $\chi(T)$ accounts for quantum mechanical tunneling. All other symbols have their usual meaning. The asymmetric Eckart potential was used to calculate $\chi(T)$. The Gibbs free energies were obtained from the NASA polynomials discussed above. Rate coefficients were calculated for the temperature range 300 K to 2500 K in 50 K steps and regressed to a modified Arrhenius expression.

4.2.5 Kinetic model development

The kinetic model consists of three parts:

(i) It includes the recent mechanism by Burke et al. for propene oxidation [54]. The mechanism, also known as AramcoMech, was developed hierarchically and has been extensively validated for hydrogen, methane, ethane, ethene, propene, methanol, ethanol and acetaldehyde oxidation [54-56]. It contains all relevant chemistry to describe the thermal decomposition of C_{3-} hydrocarbons and oxygenated molecules.

(ii) Furthermore, the GVL model includes the mechanism by Sabbe et al. for steam cracking of ethane [57]. The latter mechanism contains elementary reactions for the formation and decomposition of C_{6-} hydrocarbons, including benzene.

(iii) Finally, it includes a mechanism with reactions describing GVL consumption and related radical decomposition pathways. Kinetic and thermodynamic data were mostly taken from quantum chemical calculations. Chemistry which involves the formation of unsaturated lactones, furanones, and their consumption by hydrogen abstraction were taken from a recent study by Wurmel and Simmie [58].

The latter submechanism of the kinetic model is the subject of the following paragraphs. The thermodynamic data for GVL and 4PA is extensively discussed in paragraph 4.2.5.1. Reaction rate coefficients related to unimolecular decomposition of GVL and 4PA, hydrogen abstraction from GVL, β-scission of GVL radicals and hydrogen addition to GVL and 4PA will be discussed in paragraph 4.2.5.2.

4.2.5.1 Thermodynamic properties of γ-valerolactone and 4-pentenoic acid

As will be discussed in more detail in the kinetic modeling section, γ-valerolactone (GVL) isomerizes to 4-pentenoic acid (4PA) at the conditions at which the experiments were performed. This implies that the thermodynamic properties of both molecules are important to understand and describe GVL or 4PA pyrolysis. Thus as a first step, the heats of formation of both species were calculated with isodesmic reactions and the atomization method.

4.2.5.1.1 Calculated heats of formation

Table 4.2-1 lists the experimental values as well as the ab initio electronic enthalpies for all species used in the isodesmic reaction method. The resulting heats of formation for GVL and 4PA are reported in Table 4.2-2.

Focusing first on GVL, several observations can be made. (i) The three calculation methods, i.e. CBS-QB3, G3 and G4, are in good agreement, yielding reaction enthalpies that are generally within 1 kJ mol^{-1}. (ii) Of the five considered isodesmic reactions only the first two are close to thermoneutral. This is obviously related to ring strains, which are not conserved in reactions 3-5. (iii) The five heats of formation for GVL are in very good agreement despite the fact that the heats of reaction vary by some 60 kJ mol^{-1}. This suggests that all calculation methods capture ring strain effects well. (iv) Experimental data of sufficient accuracy are available to ensure that the final data has an uncertainty in the order of 3 kJ mol^{-1}. All five obtained heats of formation overlap within their uncertainty limits. (vi) The averaged isodesmic enthalpy of formation for GVL agrees very well with the averaged result of the BAC improved atomization method.

Table 4.2-2 Calculated heats of reactions for a series of isodesmic reactions, and the derived heat of formation for either GVL or 4PA. All data are in kJ mol^{-1}. The reported uncertainties of the averaged values are obtained via error propagation taking the uncertainties of the experimental data into account as well as the standard deviation of the three calculated data. Also provided are the heats of formation obtained with the BAC improved atomization method. See Table 4.2-1 for detailed information on the molecules.

γ-valerolactone

Isodesmic reactions		*CBS-QB3*		*G3*		*G4*		*Average (uncertainty)*
		$\Delta_R H^0_{298}$	$\Delta_f H^0_{298}$	$\Delta_R H^0_{298}$	$\Delta_f H^0_{298}$	$\Delta_R H^0_{298}$	$\Delta_f H^0_{298}$	$\Delta_f H^0_{298}$
1	GVL + Furan ⇌ GBL + 2-MF	-1.1	-410.5	-1.1	-410.5	-0.8	-410.8	-410.6 ± 2.5
2	GVL + THF ⇌ GBL + 2-MTHF	1.9	-409.7	1.8	-409.6	1.0	-408.9	-409.4 ± 2.5
3	GVL + cyC6 ⇌ DVL + CcyC5	46.9	-409.9	47.4	-410.4	46.6	-409.7	-410.0 ± 2.8
4	GVL + oxetane ⇌ BPL + 2-MTHF	-15.2	-413.1	-14.8	-413.5	-14.7	-413.5	-413.4 ± 2.6
5	GVL + THP ⇌ DVL + 2-MTHF	29.2	-410.8	29.2	-410.8	28.7	-410.3	-410.6 ± 3.1

average isodesmic reaction method +/- standard deviation = -410.8 +/- 1.4 kJ mol^{-1}

BAC improved atomization method	*CBS-QB3*	*G3*	*G4*	**Average atomization method +/- standard deviation**
	-409.8	-411.9	-410.4	**-410.7 +/- 0.9 kJ mol^{-1}**

4-pentenoic acid

Isodesmic reactions		*CBS-QB3*		*G3*		*G4*		*Average (uncertainty)*
		$\Delta_R H^0_{298}$	$\Delta_f H^0_{298}$	$\Delta_R H^0_{298}$	$\Delta_f H^0_{298}$	$\Delta_R H^0_{298}$	$\Delta_f H^0_{298}$	$\Delta_f H^0_{298}$
6	4PA + CCC ⇌ CCC(=O)OH + CCCC=C	-1.7	-370.2	-1.5	-370.4	-1.8	-370.1	-370.2 ± 11.0
7	4PA + C2H6 ⇌ CC(=O)OH +CCCC=C	-1.8	-368.3	-1.5	-368.6	-2.6	-367.5	-368.2 ± 11.6
8	4PA + C2H6 ⇌ CCC(=O)OH + CCC=C	-1.5	-370.9	-1.2	-371.2	-0.9	-371.5	-371.2 ± 3.4
9	4PA + CH4 ⇌ CC(=O)OH + CCC=C	9.8	-369.0	10.2	-369.4	10.0	-369.2	-369.2 ± 3.9
10	4PA + 2CH4 ⇌ CCC + HC(=O)OH + CC=C	52.7	-367.1	53.7	-368.1	52.3	-366.7	-367.3 ± 4.4
11	4PA + CH4 ⇌ t-CC=CC(=O)OH + C2H6	-4.1	-373.9	-3.5	-374.5	-2.4	-375.6	-374.7 ± 2.7
12	4PA + C2H6 ⇌ C=C(C)C(=O)OH + CCC	-15.9	-372.3	-14.8	-373.4	-14.1	-374.0	-373.3 ± 4.0
13	4PA + C2H6 ⇌ C=CC(=O)OH + CCCC	1.8	-374.2	2.2	-374.6	2.5	-374.8	-374.5 ± 5.4
14	4PA + C=CC=C ⇌ C=CC(=O)OH + C=CCCC=C	17.9	-371.8	17.9	-371.8	16.5	-370.5	-371.4 ± 7.3

average isodesmic reaction method +/- standard deviation = -371.1 +/- 2.5 kJ mol^{-1}

average isodesmic reaction method without reactions 11-13 +/- standard deviation = -369.6 +/- 1.5 kJ mol^{-1}

BAC improved atomization method	*CBS-QB3*	*G3*	*G4*	**Average atomization method +/- standard deviation**
	-364.3	-365.5	-365.7	**-365.2 +/- 0.6 kJ mol^{-1}**

The results for 4PA, which is more conformationally diverse than GVL, show more variation than for GVL, but most of the observations made above hold for 4PA as well. For example, all three calculation methods seem reliable as they yield similar enthalpies of formation. Also, the results from all nine isodesmic reactions agree with each other within the given uncertainty limits. Another similarity is that some reactions deviate from being thermoneutral, which can be explained with structural differences in reactant and product molecules. For example, including methane as reactant leads to endothermic reactions because of its particularly strong C-H bond. There is one important difference, though, between the data for GVL and those for 4PA: the averaged isodesmic enthalpy of formation for 4PA is found to be 6 kJ mol^{-1} higher than its value obtained with the atomization method. The calculated standard

deviations of the three ab initio results are small and do not provide overlap with the isodesmic value.

A proposed explanation of these deviations is as follows. The BAC values used to improve the atomization method (typically these corrections amount to ~ 2 kJ mol^{-1}) were obtained with a small set of enthalpies of formation of hydrocarbons and oxygenates. This set contains just a single carboxylic acid, namely propionic acid. To test whether this causes systematic errors in predicted enthalpies of formation for carboxylic acids, the thermodynamic data for formic acid, acetic acid, propionic acid, crotonic acid, methacrylic acid and acrylic acid have been calculated. The difference between the experimental and the computed enthalpies of formation of the first three, saturated, carboxylic acids varies between +1.3 and -3.2 kJ mol^{-1}; an agreement that meets expectations. On the other hand, the calculated enthalpies of formation of the last three, unsaturated, carboxylic acids are systematically lower than the corresponding experimental data, leading to deviations of -8.3, -7.1, and -7.2 kJ mol^{-1}, respectively. Note that all experimental data are from the same study. These molecules enter in the isodesmic reactions 11-14, of which the first three lead to substantially lower heats of formation compared to reactions 6-10. Reaction 14 is special as it preserves the conjugation of the double bonds, which could explain why it yields a heat of reaction in-line with reactions 6-10.

In contrast to the BAC values, which are largely obtained from enthalpies of oxygenates other than carboxylic acids, isodesmic reactions heavily depend on accurate experimental enthalpies of formation of carboxylic acids. If latter were on average a few kJ/mol too low, which seems plausible given the high errors reported for some of these molecules, the discrepancy is explained.

The recommended heat of formation for 4PA in the kinetic model is the average value of the heats of formation from both methods after excluding isodesmic reactions 11-13: $\Delta_f H^0_{298}$ (4PA) = -367.4 +/- 2.2 kJ mol^{-1}.

4.2.5.1.2 Comparison to literature

The heat of formation for GVL has been reported by Leitao et al. [38], using bomb calorimetry experiments and corrections for vaporization, as -406.5 +/- 1.1 kJ mol^{-1}. This value is lower but still within the uncertainty range of the heat of formation derived from the isodesmic reactions studied in this work, i.e. -410.7 +/- 3.2 kJ mol^{-1}. Note that the reported

standard deviation of the atomization energy does not reflect the true uncertainty as no error propagation of the BAC data was performed.

Emelyanenko et al. [47] measured the heat of formation of 4PA with combustion calorimetry and supported their data with electronic structure calculations at the G3MP2 level of theory considering several isodesmic reactions. The reported experimental value of -366.9 +/- 1.1 kJ mol^{-1} is in good agreement with the result of this study using the BAC improved atomization method, i.e. -365.2 kJ mol^{-1}. It also agrees very well with the recommended value of -367.4 +/- 2.2 kJ mol^{-1} in this study. The computed heats of formation reported by Emelyanenko et al. range from 364.2 to 369.0 kJ mol^{-1} and confirm the above data.

4.2.5.1.3 Application to GVL pyrolysis

The obtained heats of formation for GVL and 4PA are used together with ab initio entropy and heat capacity data to calculate the equilibrium composition at temperatures relevant for this work. Figure 4.2-3 presents the calculated 4PA/GVL equilibrium ratio as a function of temperature, solely considering the reaction GVL ⇄ 4PA. Thermodynamic equilibrium predicts the 4PA concentration to be very similar to the GVL concentration if only 4PA monomers are considered. Experimentally observed 4PA concentrations are substantially lower than corresponding GVL concentrations, demonstrating that 4PA and GVL do not equilibrate at the conditions of the previous and new experiments (also see paragraph 4.2.6.1).

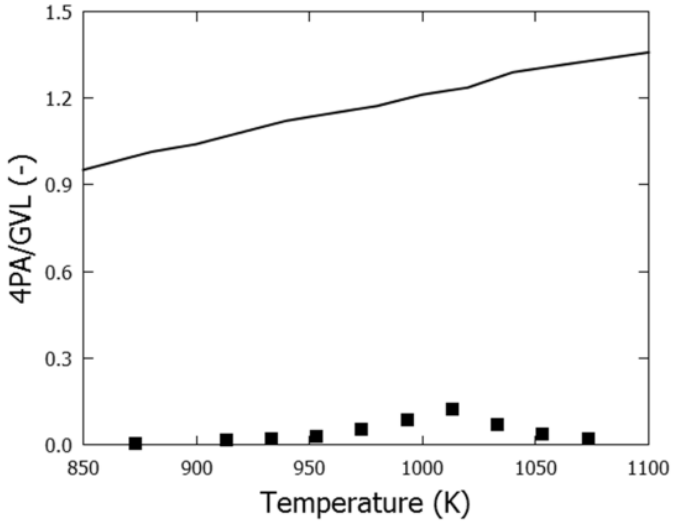

Figure 4.2-3 Ratio of 4PA mole fraction over GVL mole fraction: ■ - experimental ratio during GVL pyrolysis reported in section 4.1; ▬ - calculated using 4PA - GVL equilibrium coefficient

4PA can form dimers. The stabilization energy due to hydrogen bonds is 68.3 kJ mol^{-1} at the CBS-QB3 level of theory. The carboxy groups are quite stiff and the loss in entropy upon

dimerization is moderate. Equilibrium calculations have been performed where solely the reactions GVL ⇄ 4PA and 2 4PA ⇄ $(4PA)_2$ have been considered. At the experimental conditions reported in section 4.1, that is, a total pressure of 0.17 MPa and a mole ratio of 10:1 nitrogen to GVL, the ratio of 4PA in dimer form to the total 4PA concentration, i.e. 4PA dimers plus 4PA monomers, is below 1.5%. Without dilution, this ratio increases to approximately 12%.

4.2.5.2 Kinetic data

The experimental study regarding GVL pyrolysis highlighted the importance of isomerization of GVL to 4PA and radical chemistry, i.e. hydrogen abstraction, radical addition and radical decomposition, see section 4.1. Therefore, these reactions were evaluated using the methodology described in paragraph 4.2.4 and will be discussed in this paragraph. Several of these reactions and their corresponding rate coefficients are listed in Table 4.2-3.

Table 4.2-3 Rate coefficients for selected reactions in the GVL pyrolysis network, calculated at the CBS-QB3 level of theory unless stated differently. Units: A T^n [s^{-1} monomolecular or m^3 mol^{-1} s^{-1} bimolecular], Ea [kJ mol^{-1}], k = A T^n exp(-Ea/RT) [s^{-1} monomolecular or m^3 mol^{-1} s^{-1} bimolecular].

No.	Reaction	A	n	Ea	k(1000K)
Unimolecular decomposition reactions					
1	O=cy(COC(C)CC)→C=CCCC(=O)OH	1.10E+07	1.97	255.64	3.96E-01
2	O=cy(COC(C)CC)→C3H6+O=cy(CCO)	2.90E+13	0.68	335.14	9.91E-03
3[a]	O=cy(COC(C)CC) →CH3+O=cy(COC•CC)	1.40E+22	-1.50	384.51	3.64E-03
4	C=CCCC(=O)OH→C=CC•+C•C(=O)OH	1.70E+20	-1.40	300.41	2.18E+00
Hydrogen abstraction from GVL					
5	H+O=cy(COC(C)CC)→H2+O=cy(COC•(C)CC)	2.70E+01	1.90	16.74	1.81E+06
6	H+O=cy(COC(C)CC)→H2+O=cy(COC(C•)CC)	3.80E+01	2.02	41.00	3.15E+05
7	H+O=cy(COC(C)CC)→H2+O=cy(COC(C)C•C)	1.50E+01	2.07	30.96	5.87E+05
8	H+O=cy(COC(C)CC)→H2+O=cy(COC(C)CC•)	1.10E+01	2.07	25.52	8.28E+05
9	CH3+O=cy(COC(C)CC)→CH4+O=cy(COC•(C)CC)	8.20E-04	2.88	26.36	1.50E+04
10	CH3+O=cy(COC(C)CC)→CH4+O=cy(COC(C•)CC)	6.50E-04	2.99	45.61	2.52E+03
11	CH3+O=cy(COC(C)CC)→CH4+O=cy(COC(C)C•C)	1.90E-04	3.02	37.66	2.35E+03
12	CH3+O=cy(COC(C)CC)→CH4+O=cy(COC(C)CC•)	2.60E-04	2.99	31.80	5.30E+03
13	C=CC•+O=cy(COC(C)CC)→C3H6+O=cy(COC•(C)CC)	4.80E-04	3.12	64.43	4.74E+02
14	C=CC•+O=cy(COC(C)CC)→C3H6+O=cy(COC(C•)CC)	7.10E-04	3.15	92.88	2.81E+01
15	C=CC•+O=cy(COC(C)CC)→C3H6+O=cy(COC(C)C•C)	3.90E-04	3.17	81.17	7.26E+01
16	C=CC•+O=cy(COC(C)CC)→C3H6+O=cy(COC(C)CC•)	3.80E-04	3.26	68.20	6.27E+02
17	C•C(=O)OH+O=cy(COC(C)CC)→O=cy(COC•(C)CC)+ CC(=O)OH	1.50E-04	2.95	21.34	8.16E+03
18	C•C(=O)OH+O=cy(COC(C)CC)→O=cy(COC(C•)CC)+ CC(=O)OH	7.50E-08	3.96	38.91	5.28E+02
19	C•C(=O)OH+O=cy(COC(C)CC)→O=cy(COC(C)C•C)+ CC(=O)OH	2.00E-04	3.08	38.91	3.22E+03
20	C•C(=O)OH+O=cy(COC(C)CC)→O=cy(COC(C)CC•)+ CC(=O)OH	3.10E-05	3.29	31.38	5.27E+03
21	OH+O=cy(COC(C)CC)→H2O+O=cy(COC•(C)CC)	4.08E+00	1.81	-4.84	1.95E+06
22	OH+O=cy(COC(C)CC)→H2O+O=cy(COC(C•)CC)	5.46E+01	1.47	5.85	6.71E+05
23	OH+O=cy(COC(C)CC)→H2O+O=cy(COC(C)C•C)	8.61E+05	0.40	22.42	9.46E+05
24	OH+O=cy(COC(C)CC)→H2O+O=cy(COC(C)CC•)	4.65E+03	1.03	10.89	1.57E+06
Hydrogen abstraction from 4PA					
25	H+C=CCCC(=O)OH→H2+C=CCCC(=O)O•	4.80E+01	1.87	61.92	1.14E+04
26	H+C=CCCC(=O)OH→H2+C=CCC•C(=O)OH	1.40E+00	2.32	20.50	1.08E+06
27	H+C=CCCC(=O)OH→H2+C=CC•CC(=O)OH	9.60E+00	2.16	16.74	3.87E+06
28	CH3+C=CCCC(=O)OH→CH4+C=CCCC(=O)O•	1.00E-03	2.73	38.91	1.44E+03
29	CH3+C=CCCC(=O)OH→CH4+C=CCC•C(=O)OH	3.40E-05	3.29	24.27	1.36E+04
30	CH3+C=CCCC(=O)OH→CH4+C=CC•CC(=O)OH	4.40E-05	3.29	20.50	2.77E+04
Ring opening of GVL radicals					
	α-GVL radical				
31	O=cy(COC(C)CC•)→O=cy(COC(C•)CC)	4.40E+07	1.27	129.29	5.01E+04
32	O=cy(COC(C)CC•)→O=cy(COC(C)C•C)	1.10E+09	1.28	159.83	3.41E+04

33	O=cy(COC(C)CC•)→C=CC(=O)OC•C	2.40E+12	0.42	162.34	1.45E+05
34	C=CC(=O)OC•C→ C=CC• (=O)+CC=O	3.50E+10	0.69	89.54	8.65E+07
35	C=CC(=O)OC•C→O=y(COC(C)C(C•))	1.50E+12	0.00	51.46	3.07E+09
36	O=y(COC(C)C(C•))→C=CC(C)OC•(=O)	2.00E+11	0.57	56.48	1.15E+10
37	C=CC(C)OC•(=O)→C=CC•C+CO2	2.20E+12	0.18	30.54	1.94E+11
	β-GVL radical				
38	O=cy(COC(C)C•C)→O=cy(COC(C•)CC)	7.90E+06	1.64	159.83	2.94E+03
39	O=cy(COC(C)C•C)→O=cy(COC•(C)CC)	4.80E+08	1.25	160.25	1.15E+04
40	O=cy(COC(C)C•C)→ C=CC•C +CO2	1.80E+13	-0.06	107.95	2.73E+07
41	O=cy(COC(C)C•C)→C=CC(C)OC•(=O)	4.70E+12	0.27	141.42	1.24E+06
	γ-GVL radical				
42	O=cy(COC•(C)CC)→O=cy(COC(C•)CC)	4.90E+06	1.97	180.75	1.44E+03
43	O=cy(COC•(C)CC)→CC(=O)CCC•(=O)	3.30E+12	0.37	123.01	1.60E+07
44	CC(=O)CCC•(=O)→CO+C•CC(=O)C	4.80E+13	0.14	67.36	3.82E+10
45	O=cy(COC•(C)CC)→C=C(C)OC(=O)C•	5.50E+11	0.67	144.35	1.62E+06
46	C=C(C)OC(=O)C•→CC(=O)C•+C=C=O	3.10E+10	0.81	115.06	8.15E+06
	methyl-GVL radical				
47	O=cy(COC(C•)CC)→C=CCCC(=O)O•	2.30E+11	0.54	89.12	2.12E+08
48	O=cy(COC(C•)CC)→C=COC(=O)CC•	4.40E+10	0.91	114.64	2.43E+07
49	C=CCCC(=O)O•→C=CCC•+CO2	5.30E+11	0.50	6.28	7.88E+12
50	C=CCCC(=O)O•→C=CC•CC(=O)OH	1.90E+06	1.74	29.30	9.31E+09
51	C=CC•CC(=O)OH→C=CC=C+HOCO	9.40E+08	1.53	149.37	5.76E+05
Radical addition on GVL and 4PA					
	Hydrogen addition GVL				
52	H+O=cy(COC(C)CC) →O•cy(COC(C)CC)	1.40E+02	1.54	41.0032	4.21E+04
53	H+O=cy(COC(C)CC) →HOcy(C•OC(C)CC)	1.80E+02	1.68	46.4424	7.40E+04
	Hydrogen addition 4PA				
54	H+C=CCCC(=O)OH→CC•CCC(=O)OH	6.50E+03	1.17	0.42	2.00E+07
55	CC•CCC(=O)OH→C3H6+C•C(=O)OH	5.10E+09	1.11	93.30	1.46E+08
56	H+C=CCCC(=O)OH→C•CCCC(=O)OH	3.70E+02	1.54	8.79	5.36E+06
57	C•CCCC(=O)OH→C2H4+C•CC(=O)OH	2.00E+11	0.74	117.15	2.52E+07
	Methyl addition 4PA				
58	CH3+C=CCCC(=O)OH→CCC•CCC(=O)OH	9.60E-01	2.06	20.08	1.30E+05
59	CCC•CCC(=O)OH→C4H8-1+C•C(=O)OH	1.60E+09	1.21	94.14	8.25E+07
60	CH3+C=CCCC(=O)OH→C•C(C)CCC(=O)OH	5.10E-04	2.84	23.43	1.01E+04
61	C•C(C)CCC(=O)OH→C3H6+C•CC(=O)OH	2.00E+12	0.41	115.06	3.32E+07
Acid radical decomposition					
62	C•CC(=O)OH→C2H4+HOCO	2.70E+09	1.18	116.73	7.47E+06
63	C•C(=O)OH→CC(=O)O•	9.10E+08	1.15	161.08	9.88E+03
64	CC(=O)O•→CH3+CO2	5.00E+12	0.19	21.76	1.36E+12
65	C•C(=O)OH→OH+C=C=O	9.80E+13	0.25	225.52	9.14E+02
66[b]	HOCO→CO+OH	4.54E+26	-5.12	115.36	1.87E+05
67[b]	HOCO→CO2+H	1.07E+36	-8.11	121.60	2.27E+05
Furanone formation and decomposition					
68[c]	H+O=cy(COC(C)C=C)→O=cy(COC(C)C•C)	1.35E+02	1.34	14.47	2.55E+05
69[c]	H+O=cy(COC(C)C=C)→O=cy(COC(C)CC•)	1.20E+02	1.60	14.16	1.33E+06
70[c]	H+O=cy(COC(C)=CC)→O=cy(COC•(C)CC)	5.01E+02	1.47	8.53	4.49E+06
71[c]	H+O=cy(COC(C)=CC)→O=cy(COC(C)C•C)	5.39E+01	1.65	18.92	5.04E+05
72[c]	CH3+O=cy(COC=CC)→O=cy(COC(C)C•C)	2.46E-02	2.23	37.51	1.29E+03
73	O=cy(COC(C)C=C)→C=CC=CC(=O)OH	2.30E+06	2.19	269.03	7.56E-02
74	O=cy(COC(C)C=C)→CC(=O)CC=C=O	7.00E+10	0.82	202.51	5.33E+02
75	O=cy(COC(C)=CC)→CC(=O)CC=C=O	3.90E+10	0.95	233.89	1.67E+01
76	O=cy(COC(C)=CC)→CO+C=CC(=O)C	5.90E+13	0.39	224.68	1.60E+03

[a] calculated from the equilibrium coefficient and assuming that the rate coefficient for CH3+ O=cy(COC•CC)→ O=cy(COC(C)CC) is 1E+7 $m^3 mol^{-1} s^{-1}$, [b] from [54], [c] from [58]

This paragraph refers to a reaction in Table 4.2-3 by using the name convention "RX", where X is the number of the referred reaction in Table 4.2-3.

4.2.5.2.1 Unimolecular decomposition reactions

The importance of unimolecular decomposition reactions in GVL pyrolysis has been highlighted in section 4.1. Ring opening of GVL to 4-pentenoic acid (R1) proceeds through a 4-membered transition state, in which a hydrogen atom from the methyl group is transferred to the ring oxygen, see Figure 4.2-2(A). This is believed to be the most important unimolecular reaction channel. The calculated rate coefficient is comparable to that of the

unimolecular reaction of diethyl ether to ethene and ethanol which proceeds through a similar transition state [59], for example at 1000K:

$$\begin{array}{ll} GVL \rightarrow 4PA & k(1000K) = 0.40\ s^{-1} \\ C_2H_5OC_2H_5 \rightarrow C_2H_5OH + CH_2{=}CH_2 & k(1000K) = 0.55\ s^{-1} \end{array}$$

It dominates over other competing unimolecular reactions. The second most important channel is formation of propene plus 2-oxiranone (R2) which is approximately a factor 40 slower in the investigated operating range. C-C scission of the methyl group is a factor of 100 slower (R3). Note that despite the importance of ring opening of GVL to 4PA, its rate is slow relative to the time scale of the experiments, explaining the deviation of the experimental 4PA to GVL ratio from equilibrium as observed in Figure 4.2-3.

4-Pentenoic acid has a weak allyl-carboxymethyl bond with a bond dissociation energy of approximately 297 kJ mol^{-1}, see 4.1. Even at low temperatures, scission of this bond (R4) is relatively fast and can be an important source of radicals.

4.2.5.2.2 Hydrogen abstraction from GVL

The kinetics for hydrogen abstraction by hydrogen atoms (R5-R8), methyl (R9-R12), ethyl, vinyl, allyl (R13-R16), carboxy methyl (R17-R20), and hydroxyl radicals (R21-R24) have been calculated at the CBS-QB3 level of theory. The calculated reaction rate coefficients for hydrogen abstraction by hydrogen atoms and methyl radicals are displayed in Figure 4.2-4. Hydrogen abstraction can occur from four positions in GVL. In the investigated temperature range, the hydrogen abstraction rate coefficients increases in the order $C_{methyl} < C_\beta < C_\alpha < C_\gamma$. Hydrogen abstraction from GVL by hydrogen atoms at the γ-position is a factor of two faster than hydrogen abstraction by hydrogen atoms at the α-position at 1000K. In the case of methyl radicals, the C_γ hydrogen abstraction rate coefficient is only 10% larger than the C_α hydrogen abstraction rate coefficient.

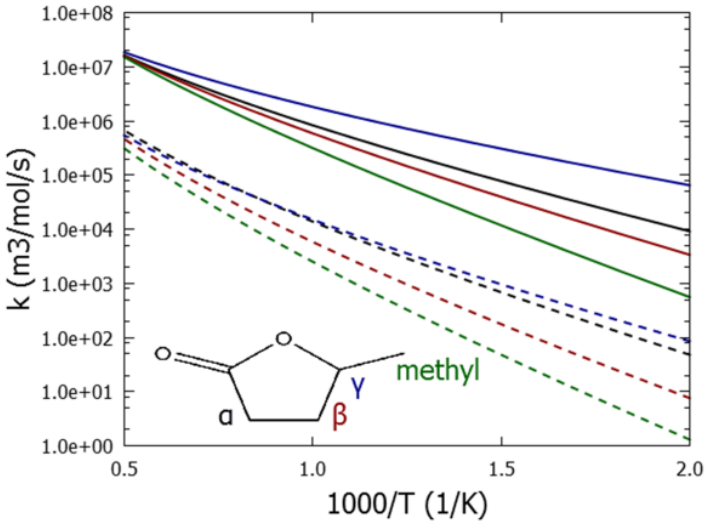

Figure 4.2-4 Reaction rate coefficients for GVL hydrogen abstraction by hydrogen atoms: ——— - from C_{α}, ——— - from C_{β}, ——— - from C_{γ}, ——— - from C_{methyl}; and by methyl radicals: - - - - from C_{α}, - - - - from C_{β}, - - - - from C_{γ}, - - - - from C_{methyl}

Hydrogen abstraction by other carbon centered radicals were estimated by taking the rate coefficients for hydrogen abstraction by methyl and adding a group additive contribution to the pre-exponential factor and activation energy, which takes into account the stabilization of the considered radical compared to methyl [60, 61].

4.2.5.2.3 Ring opening of GVL radicals

Computed barrier heights and rate coefficients for important reaction channels of GVL-radicals are presented in Table 4.2-3 and Figure 4.2-5. The α-GVL radical is resonantly stabilized by the carbonyl group. The fate of this radical is depicted in Figure 4.2-5(A). Ring opening by C-O β-scission forms a ketene. This reaction has a high energy barrier, similar to acyclic esters[62, 63], and is not shown. Ring opening by C-C β-scission has an energy barrier of 160 kJ mol^{-1}, forming an ethyl propenoate radical (R33). The latter radical can decompose to acetaldehyde plus propenoyl by C-O β-scission (R34). Intramolecular radical addition of the ethyl propenoate radical to a methyl crotonolactone radical (R35) is an alternative low energy pathway. The latter radical can ring-open to a but-1-en-3-yloxy formyl radical (R35) and subsequently fragment to CO_2 and but-1-en-3-yl (R36), similar to n-butoxy formyl forming CO_2 and n-butyl [64].

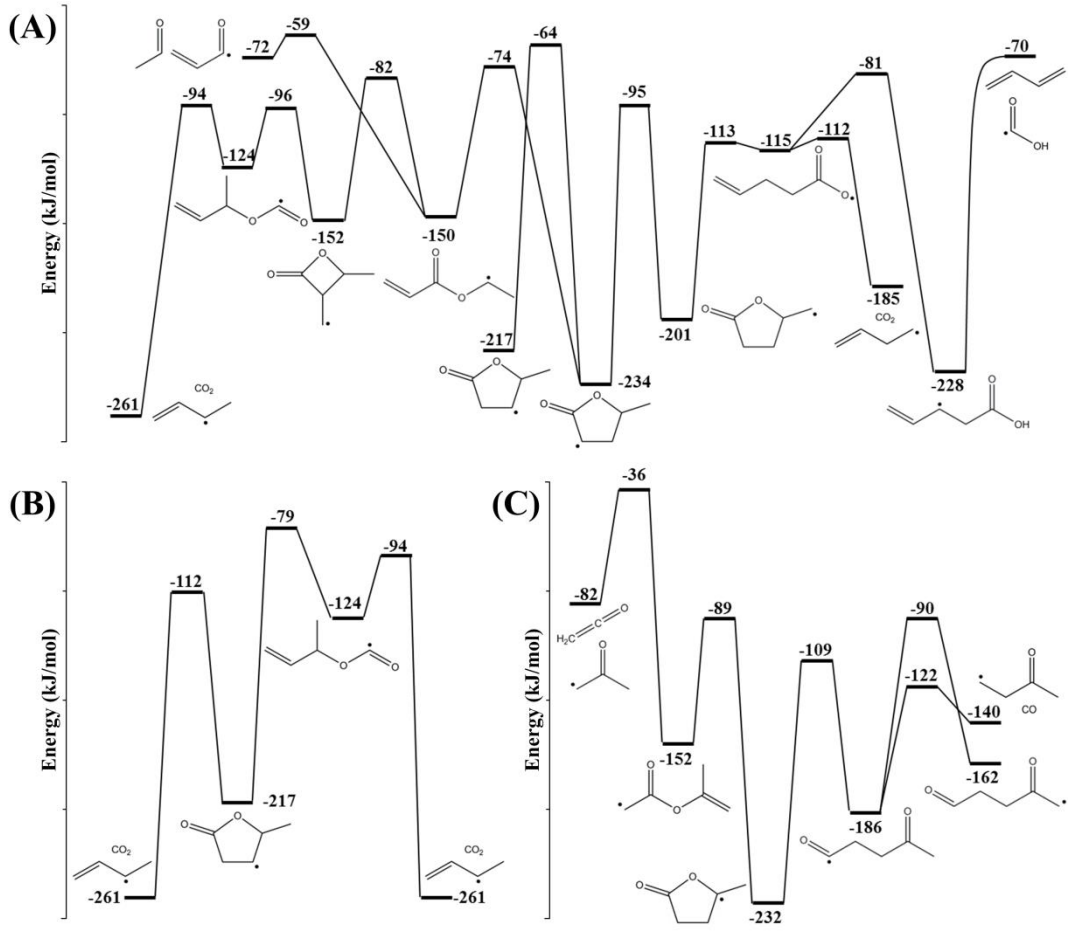

Figure 4.2-5 Selected pathways on the $C_5H_7O_2$ potential energy surface for (A) α-GVL radical and methyl-GVL radical, (B) β-GVL radical and (C) γ-GVL radical. The numbers are CBS-QB3 calculated enthalpies (kJ mol^{-1}) at 298 K.

Note that acetaldehyde, the product of the high energy decomposition channel, was not observed during the performed experiments in section 4.1. The α-GVL radical can also form the methyl-GVL radical (R31) and β-GVL (R32) radical by intramolecular hydrogen abstractions, which have barriers of 139 and 170 kJ mol^{-1}, respectively. Reaction of the α-GVL radical to the methyl-GVL radical has the lowest energy barrier but also the lowest pre-exponential factor, as the methyl rotor is tightened up in the transition state. At the investigated operating conditions, intramolecular hydrogen abstractions are competitive with C-C β-scission. Intramolecular hydrogen abstraction to the methyl-GVL radical dominates α-GVL radical decomposition below 800K. At higher temperatures, ring opening by C-C β-scission has the highest rate coefficient.

The methyl-GVL radical, formed by intramolecular hydrogen abstraction of the α-GVL radical or directly from GVL by hydrogen abstraction, preferentially decomposes by C-O β-scission (R47). The reaction rate coefficient of the competing C-C β-scission (R48) is

approximately a factor 10 lower at 1000K. Decarboxylation of the O-4PA radical has a very low energy barrier, yielding CO_2 and but-1-en-4-yl (R49). Alternatively, it can form a β-4PA radical by intramolecular hydrogen abstraction (R50) which may decompose to 1,3-butadiene and the carboxy radical (R51). Note that both O-4PA and β-4PA radicals are products of hydrogen abstraction from 4PA, the main unimolecular decomposition product of GVL.

The β-GVL radical may ring-open via C-O β-scission (R40) and by C-C β-scission (R41). C-O β-scission is found to be the dominating channel. The formed product, pent-3-enoyloxy, readily decomposes to CO_2 and but-1-en-3-yl. The latter reaction has a very low energy barrier and is not shown in Figure 4.2-5(B). Intramolecular hydrogen abstraction to form isomeric GVL-radicals have substantially higher energy barriers compared to C-O β-scission.

The γ-GVL radical can also decompose by C-O β-scission (R43) and by C-C β-scission (R45). Ring opening by C-O β-scission has again the lowest energy barrier, i.e. 123 kJ mol^{-1}, and is favored within the experimentally investigated temperature range. The ring opened radical, 4-oxopentanoyl, mainly forms 3-oxobutyl by CO α-scission (R44). Ring opening of the γ-GVL radical by C-C β-scission has an energy barrier of 143 kJ mol^{-1} and forms a resonantly-stabilized propen-2-yl acetate radical. The high-energy C-O β-scission channel of the latter radical forms ketene and 2-oxopropyl (R46).

4.2.5.2.4 Radical addition on GVL and 4PA

A selected number of computed barrier heights and rate coefficients for hydrogen addition to GVL and 4PA are listed in Table 4.2-3 and presented in Figure 4.2-6. Hydrogen abstraction by hydrogen atoms from GVL is approximately a factor 30 faster than hydrogen addition on GVL (R52 & R53) at 1000K, hence hydrogen addition to GVL will have a minor effect in the investigated operating range.

In contrast, addition of hydrogen atoms to the C=C double bond of 4PA (R54 & R56) is kinetically favored compared to hydrogen abstraction from 4PA by hydrogen atoms. This part of the $C_5H_9O_2$ potential energy surface is depicted in Figure 4.2-6. Formation of the secondary radical is favored over the primary radical formation. The secondary radical, 5-carboxypent-2-yl, can decompose by C-C β-scission to propene plus the resonantly stabilized carboxy methyl radical (R55). The corresponding rate coefficient at 1000K is a factor 30 larger than that of the competing isomerization to pentanoloxy, despite the lower energy barrier for the latter reaction. The other product following hydrogen addition on 4PA, 5-

carboxypentyl, is expected to decompose by C-C β-scission forming ethene and 2-carboxyethyl (R57).

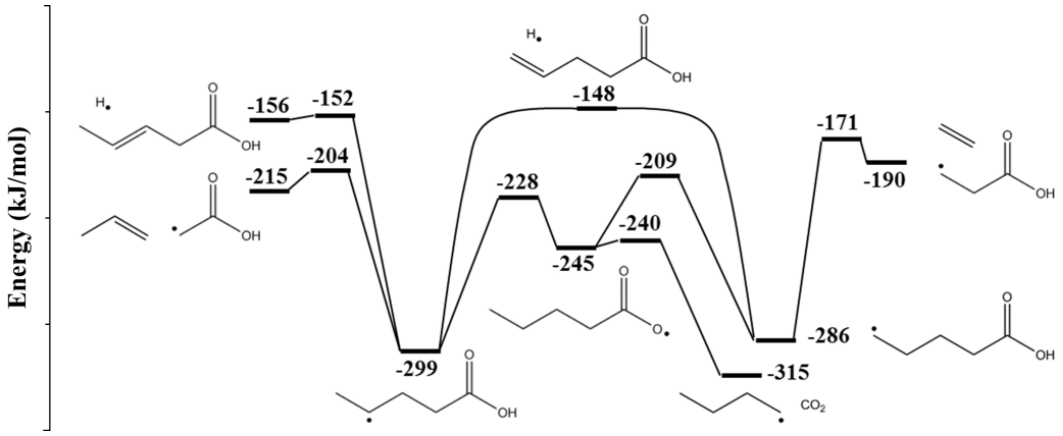

Figure 4.2-6 Selected pathways on the $C_5H_9O_2$ potential energy surface for 4PA+H. The numbers are CBS-QB3 calculated enthalpies (kJ mol^{-1}) at 298K

4.2.5.2.5 Acid radical decomposition

The importance of the carboxy methyl radical during pyrolysis of GVL has been mentioned earlier. It can be formed through C-C scission of 4-pentenoic acid (R4) or through a 4PA radical addition – decomposition sequence (R54-R55 & R58-R59 in Table 4.2-3). The relevant aspects of the $C_2H_3O_2$ PES are presented in Figure 4.2-7. Isomerization of carboxy methyl to acetyloxy (R61), which decomposes rapidly to carbon dioxide and methyl (R62) [65], has an energy barrier of 173 kJ mol^{-1}. Direct decomposition to hydroxyl and ketene (R63) requires an approximately 50 kJ mol^{-1} higher activation energy than the isomerization reaction and this pathway will thus only contribute at the highest temperatures investigated.

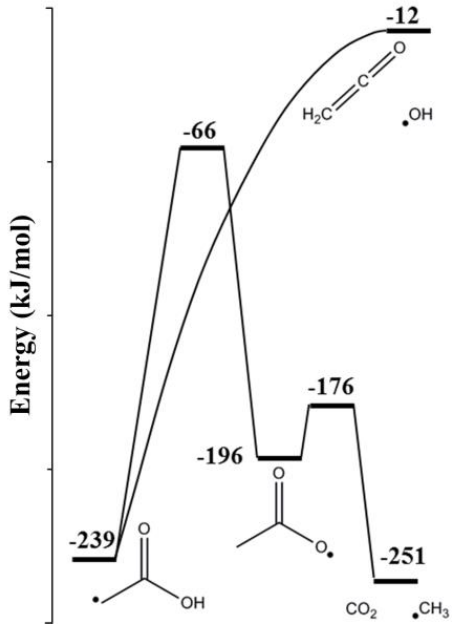

Figure 4.2-7 Selected pathways on the $C_2H_3O_2$ potential energy surface. The numbers are CBS-QB3 level calculated enthalpies (kJ mol^{-1}) at 298K

4.2.5.2.6 Furanone formation and decomposition

In earlier experimental GVL pyrolysis studies, 5-methyl-2(5H)-furanone was the only detected furanone and had a carbon selectivity, defined as the fraction of carbon atoms transferred to a product at certain conversion, below 2%. It can be formed by C-H β-scission of the α- and β-GVL radical. Other furanones which can be formed in GVL pyrolysis include 5-methyl-2(3H)-furanone by C-H β-scission of the β- and γ-GVL radical, and 2(3H)-furanone by C-C β-scission of the methyl group in the β-GVL radical. Recently, Simmie et al. and Wurmel and Simmie provided thermochemistry for furanones [58, 66] and rate coefficients for hydrogen abstraction by hydrogen and methyl radicals and addition of hydrogen and methyl radicals [58]. Their rate coefficients (R68-R72) were adopted in this study.

Unimolecular reactions have been shown to be important in the pyrolysis of furanones. 2(3H)-Furanone and their methyl-substituted analogs can undergo decarbonylation by scission of two sigma bonds at the carbonyl group [67]. In the case of 5-methyl -2(3H)-furanone, this leads to formation of CO and but-3-en-2-one. Pyrolysis of 2(5H)-furanone was found to have a similar product spectrum as pyrolysis of 2(3H)-furanone [67]. 2(5H)-furanone is proposed to isomerize to 2(3H)-furanone before decarbonylation. Isomerization by a 1,3-H shift is insufficient to explain the interconversion [58, 67]. Wurmel et al. hypothesized that trace impurities of an H atom source could interconvert both furanones via 2(5H)-furanone + H• ⇄ β-GBL radical ⇄ 2(3H)-furanone + H• [58].

Several unimolecular reactions for 5-methyl-2(3H)-furanone and 5-methyl-2(5H)-furanone were investigated at the CBS-QB3 level of theory, considering the known isomerization of the unsaturated, heterocyclic 2,3-dihydrofuran[24, 68] and GVL, see Figure 4.2-8. Isomerization of 5-methyl-2(5H)-furanone to 2,4-pentadienoic acid (R73), formed through a 4-membered transition state, has an energy barrier which is approximately 80 kJ mol^{-1} higher than isomerization to 1-pentene-1,4-dione (R74), formed through a hydrogen shift from C_γ to C_β and carbonyl – ring oxygen scission. The latter product can also be formed by isomerization of 5-methyl-2(3H)-furanone (R75), through a hydrogen shift from C_α to C_β and carbonyl – ring oxygen scission. Thus, interconversion between both furanones is possible with 1-pentene-1,4-dione as intermediate. Decarbonylation of 5-methyl-2(3H)-furanone has an energy barrier of approximately 222 kJ mol^{-1} and forms but-3-en-2-one along with CO (R76).

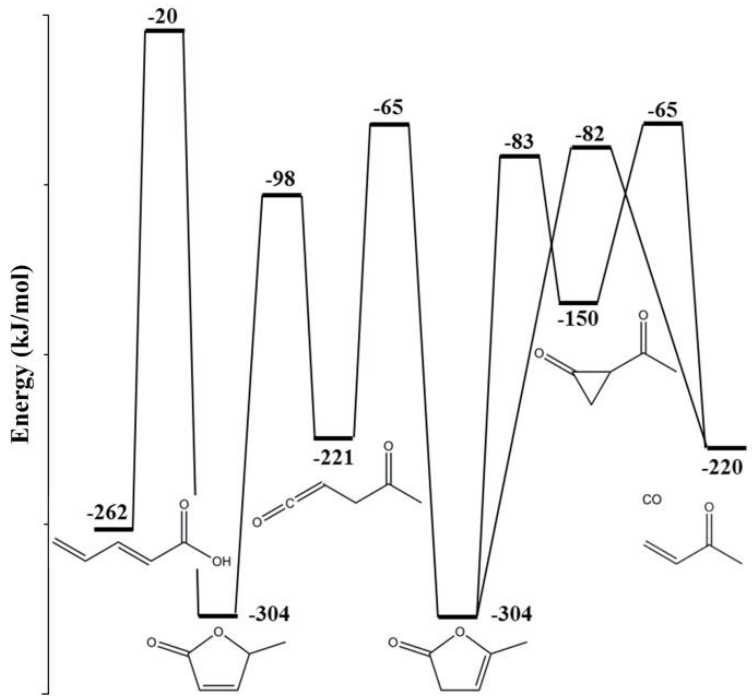

Figure 4.2-8 Selected pathways for 5-methyl-2(3H)-furanone and 5-methyl-2(5H)-furanone isomerization. The numbers are CBS-QB3 calculated enthalpies (kJ mol^{-1}) at 298K

4.2.6 Results and discussion

4.2.6.1 Experimental results

In section 4.1, an experimental dataset for GVL pyrolysis was obtained at constant pressure, P = 0.17 MPa, constant GVL and N_2 inlet molar flow rates of 1.67 10^{-4} mol/s and1.67 10^{-3} mol/s respectively, while varying the temperature. The experimental results are shown in Figure 4.2-9. Two new experimental datasets were obtained for GVL pyrolysis in this work. The first dataset was obtained at a similar pressure but higher dilution, 50:1 mole ratio of

nitrogen to GVL, compared to the dataset obtained in section 4.1, i.e. 10:1. Both product spectra are similar. Higher dilution shifts the conversion and species mole fraction profiles towards higher temperatures — which is a consequence of the decrease in GVL inlet partial pressure. Pyrolysis of GVL has a high selectivity to 4PA at low temperature and low conversion. This is consistent with the quantum chemical calculations discussed in 4.2.5.2.1. At higher conversion, hydrogen abstraction becomes an increasingly important GVL consumption channel. A large number of hydrocarbons are formed in the pyrolysis of GVL. As illustrated in Figure 4.2-5 and discussed in 4.2.5.2.3, GVL radicals have low-energy pathways to hydrocarbons and the oxygen atoms mainly end up in CO and CO_2. Minor fractions of 5-methyl-2(5H)-furanone were detected experimentally. Note that besides 4-pentenoic acid, also acetic acid was observed in the reactor effluent. The combustion of GVL in an engine likely leads to an elevated fraction of acids in the exhaust compared to combustion of traditional fossil feedstock's. Acids impact air quality and further studies regarding the combustion of GVL are required[69].

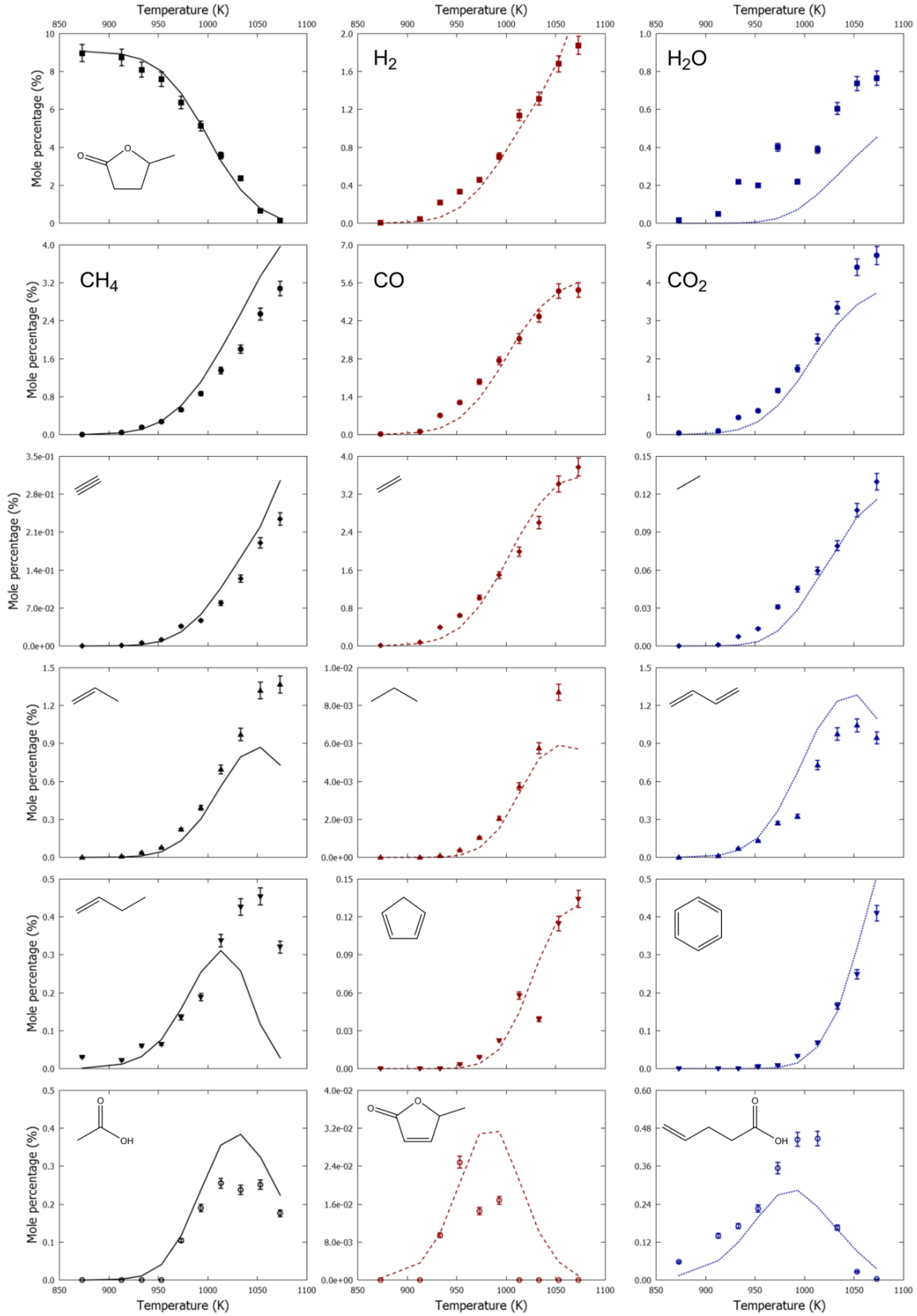

Figure 4.2-9 Mole fractions as a function of temperature for GVL pyrolysis in a tubular reactor, P=0.17 MPa, F_{GVL}=1.67 10^{-4} mol/s, F_{N2}=1.67 10^{-3} mol/s: symbols, experimental mole fraction profile of molecule represented in graph; lines, mole fraction profiles calculated with CHEMKIN using the plug flow reactor model and the developed kinetic model, discussed in paragraph 4.2.5

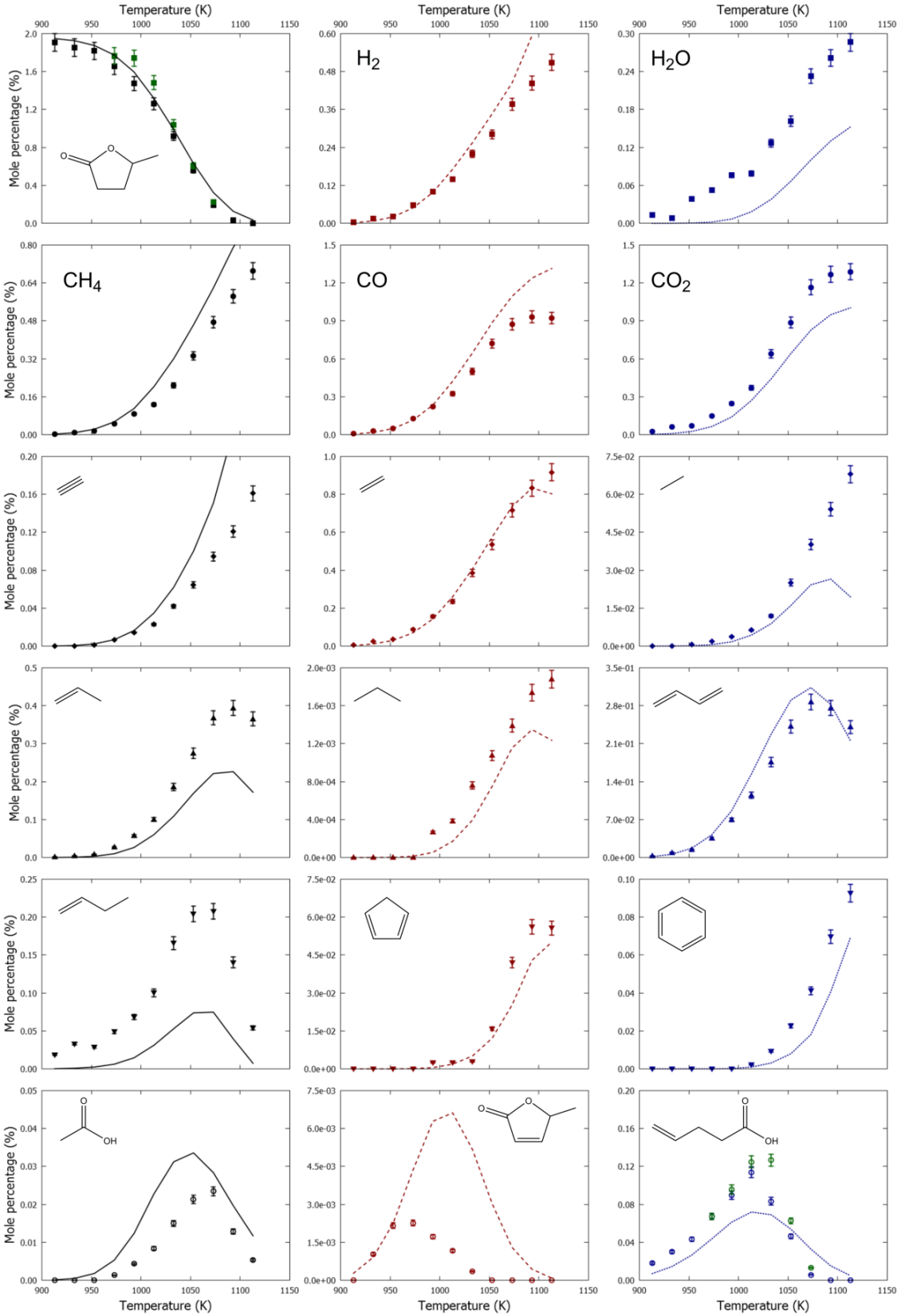

Figure 4.2-10 Mole fractions as a function of temperature for GVL pyrolysis in a tubular reactor, P=0.17 MPa, F_{GVL}=8.33 10^{-5} mol/s, F_{N2}=4.17 10^{-3} mol/s: symbols, experimental mole fraction profile of molecule represented in graph; P=0.17 MPa, F_{GVL}=8.33 10^{-5} mol/s, $F_{toluene}$=4.17 10^{-4} mol/s, F_{N2}=3.75 10^{-3} mol/s: green symbols, experimental mole fraction profile of molecule represented in graph; lines, mole fraction profiles calculated with CHEMKIN using the plug flow reactor model and the developed kinetic model, discussed in paragraph 4.2.5

The second dataset was obtained for a GVL/toluene mixture, in which the GVL inlet partial pressure was kept at the same value as in the high dilution case and the toluene to GVL inlet molar ratio was set to 5:1. This experiment is aimed at investigating the effect of a radical scavenger (toluene) [70, 71] on the product yields. Besides the typical product spectrum in GVL pyrolysis, non-negligible fractions of benzylacetic acid, but-3-enyl-benzene, bibenzyl, stilbene, anthracene and phenanthrene were detected.

The new high dilution experimental dataset is shown in Figure 4.2-10. The GVL mole fraction profile follows a first order reaction profile with an activation energy of 247 kJ mol^{-1}. This value would be significantly lower if surface reactions would play a role.

Experimental GVL and 4PA mole fraction profiles of the toluene dataset are added to Figure 4.2-10 for comparison. The addition of toluene reduces conversion and increases selectivity to 4PA. This can be understood as follows. Radicals formed by decomposition of GVL can react with both GVL and toluene. Hydrogen abstraction from toluene forms benzyl. Decomposition of benzyl is slow at the investigated operating conditions [72-75]. Furthermore, reaction rate coefficients for hydrogen abstraction by benzyl radicals are substantially lower than hydrogen abstraction by methyl as they are resonantly stabilized[60]. Recombination reactions are important for resonantly stabilized radicals as they have a prolonged lifetime[74, 76]. This is confirmed experimentally by the presence of ethylbenzene, a recombination product of benzyl plus methyl, benzylacetic acid, a recombination product of benzyl plus carboxy methyl, and but-3-enyl-benzene, a recombination production of benzyl plus allyl.

Compared to methyl radicals and hydrogen atoms, a higher fraction of benzyl will recombine, resulting in a net decrease of reactive radicals . This will reduce conversion and, furthermore, decrease the relative contribution of hydrogen abstraction from GVL (radical pathway) compared to ring opening to 4PA (unimolecular pathway).

4.2.6.2 Model performance

Reactor simulations, using the kinetic model discussed in paragraph 4.2.5, were conducted with the CHEMKIN PRO package[77] using the plug flow reactor module. The validity of the plug flow assumption has been shown earlier[29]. Figure 4.2-9 and Figure 4.2-10 show the model calculated mole fraction profiles for the low, 10:1, and high dilution, 50:1 nitrogen to GVL mole ratios, data sets, respectively, as function of the set temperature of the reactor heating elements. There is a good agreement between experimental and model calculated conversion profiles for both dilutions / inlet GVL partial pressures, especially considering the

novel chemistries being explored. Generally, there is a good qualitative and even quantitative agreement between experiment and model calculated mole fraction profiles for most species.

More detailed comparisons show that the maximum 4PA yield is underpredicted in both, the low and high dilution data sets. Furthermore, the model predicts a more gradual decline compared to the steep drop in experimental 4PA yields. Both propene and 1-butene are underpredicted by the kinetic model, and the deviations are more pronounced at high dilution. Water is underpredicted in both datasets. Experimental mole fraction profiles of other hydrocarbons and oxygenated molecules are in good agreement with the predictions.

At higher temperature, and higher conversion, secondary reactions become increasingly important. These reactions are part of the mechanism of Burke et al.[54] and Sabbe et al.[57], see paragraph 4. These mechanisms have been validated at other operating conditions than what has been investigated here. This might explain some of the model discrepancies at high temperatures.

Figure 4.2-11 shows the experimental and model calculated values for GVL mole fraction as a function of residence time. Figure 4.2-11 also shows the experimental and model calculated values for 4PA carbon selectivity, defined as the fraction of carbon atoms transferred to a product at certain conversion, as a function of residence time. Experimental values are in good agreement with model calculations in both cases.

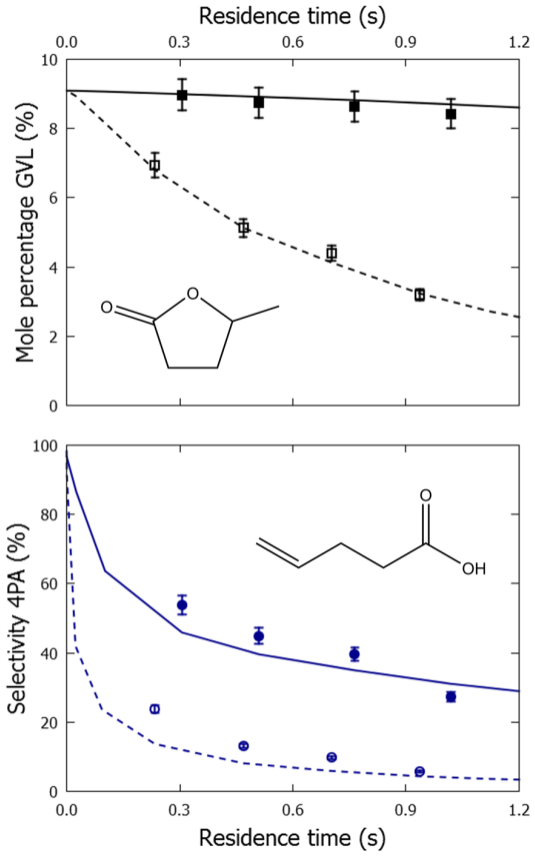

Figure 4.2-11 GVL mole fraction and 4PA carbon selectivity as a function of residence time for GVL pyrolysis in a tubular reactor, P=0.17 MPa, F_{N2}/F_{GVL} =10:1 mol_{N2}/mol_{GVL}: symbols, experimental mole fraction profile of molecule represented in graph, filled symbols correspond to T=913K, open symbols correspond to T=993K; lines, mole fraction profiles calculated with CHEMKIN using the plug flow reactor model and the developed kinetic model, discussed in paragraph 4.2.5, full lines correspond to T=913K, dashed lines correspond to T=993K

4.2.6.3 Consumption of γ-valerolactone

4.2.6.3.1 Sensitivity analysis

The model calculated carbon selectivity is close to 100% for 4PA in GVL pyrolysis at residence time 0s as can be observed from Figure 4.2-11. The selectivity for 4PA decreases gradually at 913K while its profile is steeper at 993K. As mentioned earlier, 4PA formation and decomposition is an important aspect in GVL pyrolysis. A sensitivity analysis was performed at 913K to quantitatively assess the importance of each reaction on GVL conversion. Sensitivity coefficients of reactions with respect to GVL were calculated using CHEMKIN-PRO. The sensitivity coefficient of a reaction is a measure for the relative change in GVL mole fraction upon varying the pre-exponential factor of that reaction. The sensitivity coefficients of the eight most sensitive reactions are presented in Figure 4.2-12 as a function of position axial position.

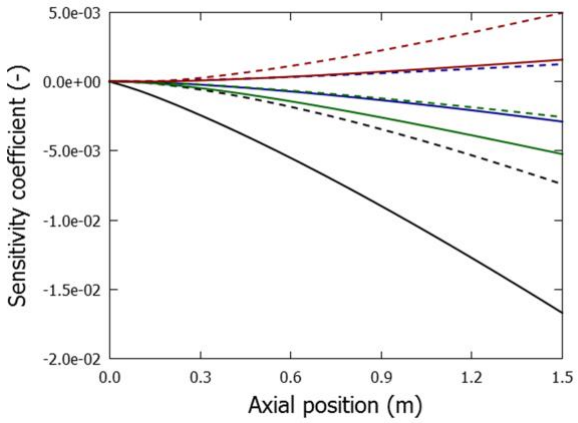

Figure 4.2-12 Sensitivity coefficients for GVL calculated using CHEMKIN-PRO as a function of axial position. Operating conditions: P=0.17 MPa, F_{GVL}=1.67 10^{-4} mol/s, F_{N2}=1.67 10^{-3} mol/s, T = 913K. ▬ - GVL→4PA, ▪▪▪ - 4PA→allyl+carboxy methyl, ▬ - GVL+CH_3→γ-GVL+CH_4, ▪▪▪ - GVL+CH_3→β-GVL+CH_4, ▬ - 1,3-butadiene+H→but-1en-3-yl, ▪▪▪ - GVL+ but-1en-3-yl →γ-GVL+1-butene, ▬ - but-1-en-3-yl+but-1-en-3-yl→1,3-butadiene+1-butene, ▪▪▪ - but-1-en-3-yl +CH_3→pent-2-ene

Ring opening of GVL to 4PA has the highest sensitivity on the GVL mole fraction. This is the only reaction which has a significant impact on conversion initially in the reactor, in agreement with Figure 4.2-11. C-C scission of 4PA is the reaction with the second highest sensitivity. It is the sole reaction displayed in Figure 4.2-12 that results in a net increase of radicals. Hydrogen abstraction by methyl radical from the β-carbon atom has a positive coefficient while hydrogen abstraction from the γ-carbon atom has a negative coefficient. This indicates that increasing the pre-exponential factor of the former reaction increases GVL mole fraction while increasing the pre-exponential factor of the latter reaction decreases GVL mole fraction. As mentioned earlier, decomposition of the β-GVL radical forms CO_2 and but-1-en-3-yl while decomposition of the α-GVL radicals forms CO and 3-oxobutyl. The latter radical will form ethene, CO and methyl radical by successive C-C β-scission and CO α-scission. The methyl radical can, again, consume GVL by hydrogen abstraction. But-1-en-3-yl has multiple reaction possibilities and the appearance of four of those reactions in Figure 4.2-12 demonstrates the importance of this radical. The four reactions are: C-H β-scission, forming 1,3-butadiene plus hydrogen atom, and hydrogen abstraction from GVL have negative sensitivity coefficients while recombination with methyl, forming pentene, and disproportionation have positive sensitivity coefficients. But-1-en-3-yl is resonantly stabilized and has a relatively long lifetime[78]. Reactions with other radicals, including recombination and disproportionation, are important. These reactions decrease the radical pool. Hence, GVL conversion depends on the hydrogen abstraction branching ratio as decomposition of the β-GVL radical forms less-reactive but-1-en-3-yl radials which are prone to radical chain termination.

4.2.6.3.2 Reaction path analysis

The main decomposition pathways of GVL are shown in Figure 4.2-13 for 0.17 MPa, dilution 10:1 nitrogen to GVL, 10% conversion of GVL and at 913 and 1073K. The rates of the important reactions are shown as a percentage relative to the total decomposition rate of GVL and are calculated using CHEMKIN[77]. Hydrogen addition to GVL only accounts for 1% of total GVL consumption and is not presented in Figure 4.2-13. Temperature has a minor effect on the relative importance of the various GVL decomposition channels. Ring opening to 4PA accounts for 29% of the total GVL consumption at 913K under the studied conditions and decreases to 26% at 1073K. Hydrogen abstraction from GVL accounts for approximately 70% of the total GVL consumption.

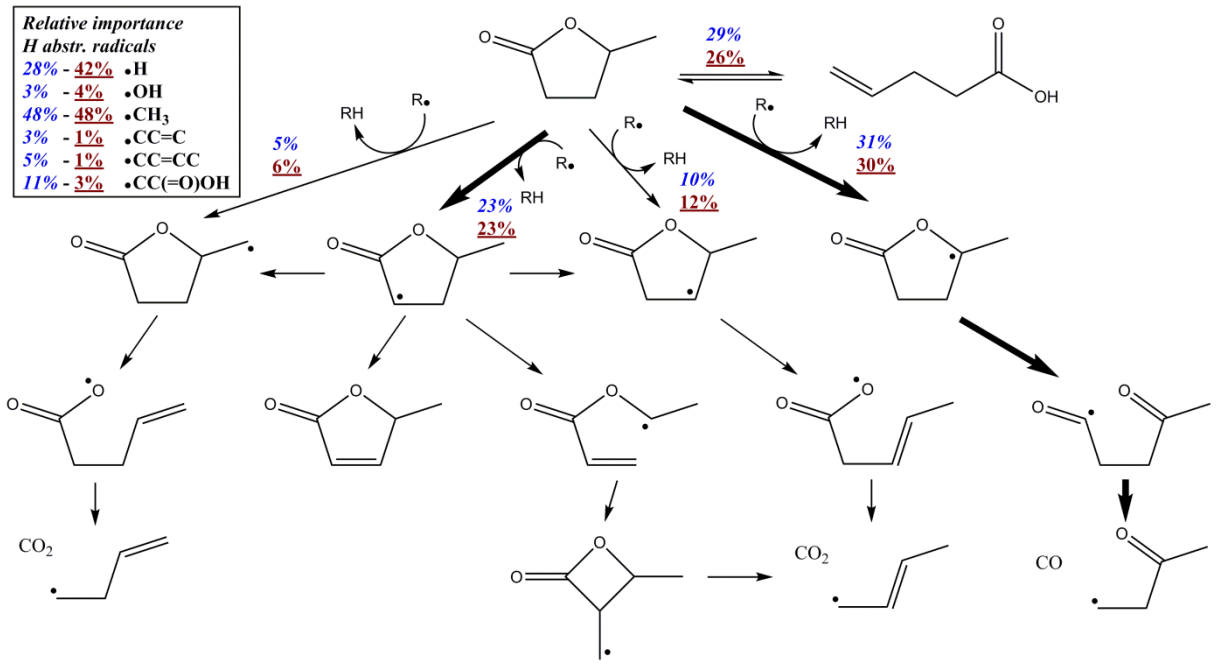

Figure 4.2-13 Reaction path analysis for the decomposition of GVL. Operating conditions: P=0.17 MPa, F_{GVL}/F_{N2} = 1:10 mol_{GVL}/mol_{N2}, $conversion_{GVL}$ = 10%, T = 913K (blue & italic) and 1073K (red & underlined). Percentages on a reaction path represent the reaction rate relative to the total GVL decomposition rate. The relative importance of a radical for hydrogen abstraction from GVL is the hydrogen abstraction reaction rate by this radical divided by the total GVL hydrogen abstraction rate

Several radicals contribute to hydrogen abstraction of GVL in non-negligible amounts. Hydrogen abstraction by methyl radicals are responsible for approximately 50% of the total GVL hydrogen abstraction rate. Hydrogen atoms contribute for 28% at 913K but their importance increases to 42% at 1073K. Abstraction by OH contributes to just 3% or 4 %. Other important hydrogen abstracting radicals include allyl, but-1-en-3-yl and carboxy methyl. These radicals are resonantly stabilized. Note that allyl and carboxy methyl are formed by C-C scission of 4PA and that but-1-en-3-yl is a decomposition product of GVL

radicals, see paragraph 4.2.5.2.3. The importance of hydrogen abstraction by these radicals diminishes at higher temperatures. Unimolecular reactions of resonantly stabilized radicals typically have rather high energy barriers [79]. Hence, at higher temperatures, the decomposition of such radicals will become, relatively, faster than hydrogen abstraction. For example, C-H β-scission of but-1-en-3-yl becomes more important compared to competing reaction channels such as hydrogen abstraction. This reaction partially explains the relative increase in hydrogen abstraction reaction rate by hydrogen atoms at 1073K.

Hydrogen abstraction from the γ carbon atom is favored. As mentioned earlier, the γ-GVL radical readily decomposes to CO plus but-4-yl-2-one of which the latter, in turn, decomposes to ethene, CO plus methyl. This GVL decomposition channel is the main formation path for ethene, CO and methyl.

The second most important hydrogen abstraction channel is that from the α carbon site. At the studied conditions, 50% of the α-GVL radical decomposes by C-C β-scission, 20% by C-H β-scission, 15% by intramolecular hydrogen abstraction to the methyl-GVL radical and 5% by intramolecular hydrogen abstraction to the β-GVL radical. The product of C-H β-scission, 5-methyl-2(5H)-furanone, is only measured in small quantities in the reactor effluent. It is mainly consumed by a sequence of unimolecular reactions: isomerization to 1-pentene-1,4-dione, isomerization to 5-methyl-2(3H)-furanone and decarbonylation to but-3-ene-2-one.

Over 99% of the methyl-GVL radical decomposes by ring opening and formation of but-1-en-4-yl and CO_2. At the selected operating conditions, but-1-en-4-yl preferrably undergoes C-C β-scission channel to ethene plus vinyl.

Hydrogen abstraction from the β-carbon accounts for approximately 10% of GVL consumption. The dominant decomposition channel of the β-GVL radical is formation of CO_2 and but-1-en-3-yl, which has a selectivity of approximately 97%. C-C β-scission of the methyl side group, forming 2(3H)-furanone, and contribute for approximately 2%. Note that in the case of the isoelectronic 2-methyl-cyclopent-1-yl radical, β-scission of the C-C bond forming cyclopentene and methyl is favored over ring opening forming hexenyl [80] and that in the case of the isoelectronic 2-methyl-cyclohex-1-yl radical, β-scission of the C-C bond forming cyclohexene and methyl is favored over ring opening forming heptenyl [81]. Clearly, the oxygen functionality enhances ring opening as observed earlier for 2-methyl-tetrahydrofuran[23]. The model predicts negligible concentrations of 2(3H)-furanone given

the very fast decarbonylation reaction, see paragraph 4.2.5.2.6, which is in line with experimental observations.

4.2.6.4 Consumption of 4-pentenoic acid

Besides being a primary product in GVL pyrolysis, subsequent decomposition of 4PA can easily introduce radicals by C-C scission, see paragraph 4.2.5.2.1. This reaction channel accounts for approximately 20% of the total 4PA consumption and its contribution increases with temperature. C-C scission and other consumption paths are presented in Figure 4.2-14. Reaction path analysis was performed at the same conditions as paragraph 4.2.6.3. Hydrogen abstraction of 4PA contributes for 10% of the total 4PA consumption. Hydrogen abstraction from the β-carbon atom is favored over hydrogen abstraction from the α-carbon atom. Hydrogen abstraction of the acidic hydrogen atom is negligible. C-C β-scission of the β-4PA radical yields 1,3-butadiene and the carboxy radical. Radical addition to 4PA is the main consumption route, approximately 70% of the total consumption. Addition to the C_δ site of 4PA is favored over addition to C_γ. The latter reaction channel leads to primary radicals. In the case of methyl addition, radical decomposition forms propene plus 2-carboxyethyl. In the case of hydrogen addition, radical decomposition forms ethene plus 2-carboxyethyl. 2-carboxyethyl readily forms ethylene plus a carboxy radical. Addition of radicals to the γ-carbon atom of 4PA and subsequent decomposition is the main source of carboxy radicals in the GVL pyrolysis system. Hydrogen and methyl addition to the δ-carbon atom are responsible for approximately 30% and 20% of the total 4PA consumption. C-C β-scission of the resulting radicals is the main source of carboxy methyl.

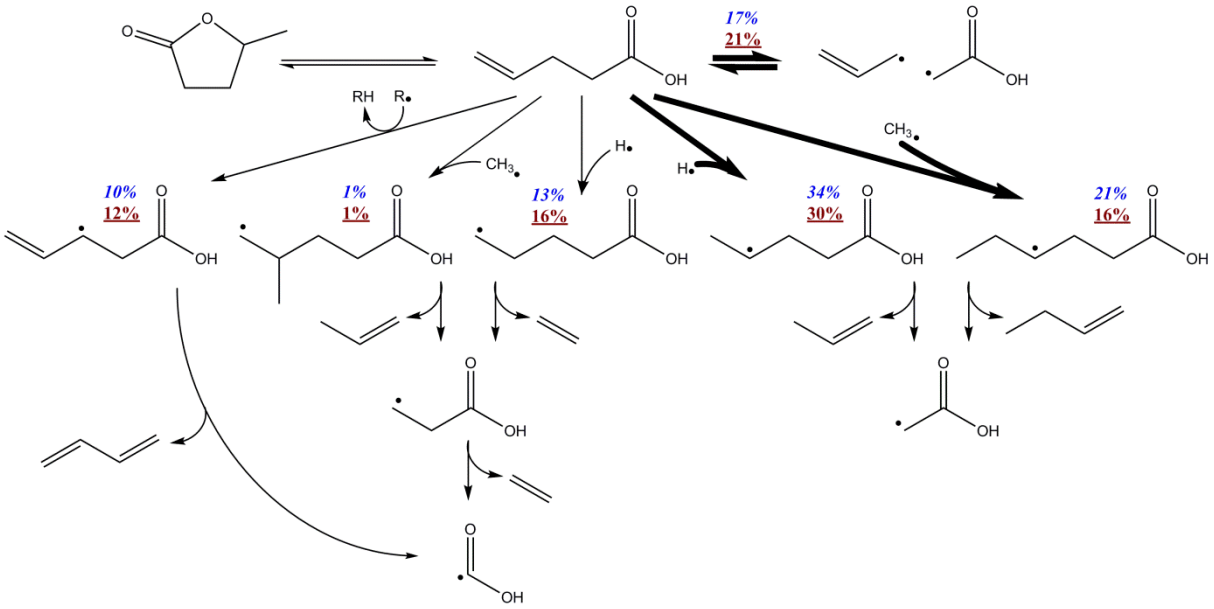

Figure 4.2-14 Reaction path analysis for the decomposition of 4PA. Operating conditions: P=0.17 MPa, F_{GVL}/F_{N2} = 1:10 mol_{GVL}/mol_{N2}, $conversion_{GVL}$ = 10%, T = 913K (blue & italic) and 1073K (red & underlined). Percentages on a reaction path represent the reaction rate relative to the total 4PA decomposition rate.

4.2.6.5 Product formation channels

4.2.6.5.1 CO and CO_2

CO is mainly formed by decomposition of the γ-GVL radical, as mentioned earlier. It is, thus, sensitive to (i) the ratio of unimolecular decomposition of GVL versus hydrogen abstraction from GVL and (ii) the branching ratio of hydrogen abstraction from GVL. Minor paths include decomposition of the carboxy radical, see Figure 4.2-15, and decarbonylation of 5-methyl-2(3H)-furanone.

Formation of CO_2 is not dominated by a single reaction. Instead, five important reaction channels are revealed by reaction path analysis: decomposition of the β-GVL radical by C-O β-scission, decomposition of the methyl-GVL radical by C-O β-scission, decomposition of the α-GVL radical by C-C β-scission, decarboxylation of acetyloxy, decomposition of carboxy radical (see Figure 4.2-15) accounting for respectively 35%, 25%, 20%, 10% and 5% of the total CO_2 formation rate at 1073K.

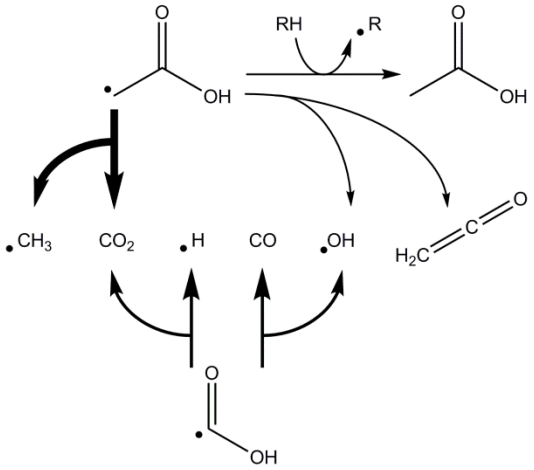

Figure 4.2-15 Decomposition of carboxy and carboxy methyl radical

4.2.6.5.2 Water

Water is formed from hydrogen abstraction by hydroxyl radicals. Hydroxyl radicals are mainly formed by decomposition of the carboxy radical, see Figure 4.2-15. Formation of hydroxyl by C-O β-scission of carboxy methyl is negligible over the investigated temperature range. Carboxy to hydroxyl plus CO (R66) is in competition with carboxy to CO_2 plus H (R67).

These reactions are part of the AramcoMech submechanism [54] and the kinetics are taken from the extensive work by Barker and coworkers who performed master equation calculations on the carboxy system [82-84]. The ratio of the reaction rate coefficients of both competing carboxy decomposition channels is approximately 1 at 1073K. Obviously, changing this ratio in favor of the hydroxyl plus CO channel would improve the agreement between model calculated and experimental mole fraction profiles of water. The effect on CO, CO_2 and H_2 mole fraction profiles would be minor as carboxy decomposition contributes less than 10% to their total formation rate. Note that recent work regarding ethyl propanoate pyrolysis proposed to reduce this ratio to improve model agreement [85]. Their experiments were performed at higher dilution, 1 mol ethyl propanoate / 100 mol argon, and higher temperatures (T=1250K-1750K).

The carboxy radical is produced by consumption of 4PA as stated earlier. The model performance for water can be improved by changing the reaction rate coefficients of the various 4PA consumption pathways, favoring formation of carboxy. Note that the maximum mole fraction of 4PA is underpredicted by the kinetic model. Increasing the isomerization of GVL to 4PA would be beneficial for the model performance of both 4PA and water.

4.2.6.5.3 Acetic acid

Acetic acid is formed by hydrogen abstraction of carboxy methyl and accounts for approximately 20% of the total carboxy methyl consumption at 913K and decreases with temperature. At the highest investigated temperatures acetic acid is mainly consumed by unimolecular dehydration, $CC(=O)OH \rightarrow C=C=O+H_2O$, and unimolecular decarboxylation, $CC(=O)OH \rightarrow CO_2+CH_4$ [86]. Rate coefficients in the kinetic model were taken from a recent experimental study by Elwardany et al. [87].

4.2.6.5.4 C_{4-} hydrocarbons

Formation paths of most small hydrocarbons are directly related to GVL and 4PA decomposition. Ethene is mainly produced by decomposition of the γ-GVL radical and by subsequent decomposition of the product formed by hydrogen addition to C_δ of 4PA. Hydrogen addition to C_γ of 4PA is the major source of propene. C-H β-scission of but-1-en-3-yl, formed by decomposition of the α-GVL radical and β-GVL radical, contributes for 70% of the total 1,3-butadiene formation while C-H β-scission of but-1-en-3-yl, formed by decomposition of the methyl-GVL radical, and C-C β-scission of the β-4PA radical contribute for 15% and 5% respectively. Formation paths of 1-butene include hydrogen abstraction from but-1-en-3-yl from GVL (25%), methyl addition to C_δ of 4PA (35%) and recombination of allyl plus methyl (30%). Consumption of 1-butene by hydrogen abstraction becomes significant at high conversion.

4.2.6.5.5 Aromatics

Several reaction pathways to benzene are included in the kinetic model. Figure 4.2-16 represents the rate of each such reaction divided by the total benzene formation rate as a function of temperature. In the investigated temperature range, C-H β-scission of cyclohexadienyl is the dominant formation channel. From 1153K onwards, reactions involving propargyl radicals start to compete and eventually dominate. Reaction path analysis shows that cyclohexadienyl is mainly formed by cyclization of hexadienyl and subsequent C-H β-scission and hydrogen abstraction[57]. There are two pathways forming hexadienyl, i.e. vinyl addition to 1,3-butadiene and allyl recombination followed by hydrogen abstraction. These reactions have been highlighted earlier as important source for aromatic precursors [57, 88, 89]. The former pathway is responsible for 80% of the total hexadienyl formation. Note that vinyl, allyl and 1,3-butadiene are primary decomposition products of GVL and 4PA and are present in relatively high quantities.

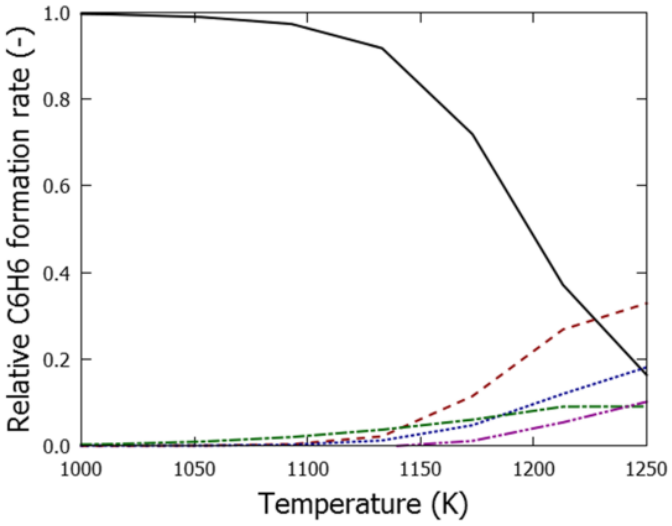

Figure 4.2-16 Benzene formation rate of several reactions divided by the total benzene formation rate as a function of temperature, calculated with CHEMKIN using the plug flow reactor model and the developed kinetic model, discussed in paragraph 4.2.5, ——— - cyclohexadienyl→benzene+H, - - - - $C_3H_3+C_3H_3$→benzene, ····· - $C_3H_4+C_3H_3$→benzene+H, -·-·- $C_4H_5+C_2H_2$→benzene+H, -··-··- toluene+H→benzene+CH_3

As can be observed from Figure 4.2-9 and Figure 4.2-10, the benzene mole fraction profile is accurately predicted at low dilution while it is slightly underpredicted at high dilution. Typically, benzene is formed by bimolecular reactions which are, thus, affected by a change in GVL inlet partial pressure. While benzene formation at high temperature through reactions involving propargyl is relatively well understood [90], this is less so for benzene formation at low/intermediate temperatures [89]. Often there are several reactions contributing, all involving resonantly stabilized radicals such as allyl, cyclopentadienyl and hexadienyl [88, 91-93]. Recently, Fridlyand et al. investigated allyl recombination in a shock tube with temperatures of 650 to 1300K and observed low temperature benzene formation pathways[94]. Further combined experimental and modeling work is required in this respect.

4.2.7 Conclusions

The pyrolysis of γ-valerolactone has been investigated experimentally in a continuous flow reactor from 873 to 1113 K and at 0.17MPa, and computationally, through detailed kinetic modeling. Relevant GVL decomposition chemistry has been calculated at the CBS-QB3 level of theory. A kinetic model has been assembled based on AramcoMech, an ethane pyrolysis network, and novel ab initio calculated rate expressions for GVL/4PA and related PES. Predicted mole fractions are in good agreement with the experimental data. Sensitivity analysis showed that GVL conversion is mainly affected by isomerization to 4PA, C-C scission of 4PA, hydrogen abstraction and the reactivity of resonantly stabilized radicals. Experimental data and the ab initio calculations show that consumption of GVL by

unimolecular ring opening is in competition with consumption by hydrogen abstraction. Hydrogen abstraction from the γ-carbon atom is favored and is a major source of ethene and CO in the reactor effluent. Hydrogen abstraction from other carbon atoms have a high selectivity to CO_2 and butenyl. 4PA is mainly consumed by addition of methyl radicals and hydrogen atoms to the C=C double bond. Subsequent decomposition forms small radicals derived from carboxylic acids, i.e. 2-carboxyethyl, carboxy methyl and carboxy. These radicals, and their relative reaction paths, are important to accurately describe the product spectrum.

The propensity of GVL to form carboxylic acids can be troublesome for environmental reasons. The potential increase of carboxylic acids in the exhaust of an engine upon combustion of GVL compared to combustion of fossil fuels warrants further investigation.

4.2.8 References

[1] J. R. Regalbuto, Cellulosic Biofuels—Got Gasoline?, Science 325 (2009) 822-824
[2] J. J. Bozell, Connecting Biomass and Petroleum Processing with a Chemical Bridge, Science 329 (2010) 522-523
[3] D. M. Alonso, S. G. Wettstein, J. A. Dumesic, Gamma-valerolactone, a sustainable platform molecule derived from lignocellulosic biomass, Green Chem. 15 (2013) 584-595
[4] C. K. Westbrook, W. J. Pitz, H. J. Curran, Chemical Kinetic Modeling Study of the Effects of Oxygenated Hydrocarbons on Soot Emissions from Diesel Engines, J. Phys. Chem. A 110 (2006) 6912-6922
[5] C. Esarte, Á. Millera, R. Bilbao, M. U. Alzueta, Gas and soot products formed in the pyrolysis of acetylene–ethanol blends under flow reactor conditions, Fuel Process. Technol. 90 (2009) 496-503
[6] R. Xing, W. Qi, G. W. Huber, Production of furfural and carboxylic acids from waste aqueous hemicellulose solutions from the pulp and paper and cellulosic ethanol industries, Energ. Environ. Sci. 4 (2011) 2193-2205
[7] L. Bui, H. Luo, W. R. Gunther, Y. Román-Leshkov, Domino Reaction Catalyzed by Zeolites with Brønsted and Lewis Acid Sites for the Production of γ-Valerolactone from Furfural, Angew. Chem. Int. Ed. 52 (2013) 8022-8025
[8] I. T. Horvath, H. Mehdi, V. Fabos, L. Boda, L. T. Mika, γ-Valerolactone - a sustainable liquid for energy and carbon-based chemicals, Green Chem. 10 (2008) 238-242
[9] F. M. A. Geilen, B. Engendahl, A. Harwardt, W. Marquardt, J. Klankermayer, W. Leitner, Selective and Flexible Transformation of Biomass-Derived Platform Chemicals by a Multifunctional Catalytic System, Angew. Chem. 122 (2010) 5642-5646
[10] X. Tang, X. Zeng, Z. Li, L. Hu, Y. Sun, S. Liu, T. Lei, L. Lin, Production of γ-valerolactone from lignocellulosic biomass for sustainable fuels and chemicals supply, Renew. Sust. Energ. Rev. 40 (2014) 608-620
[11] Á. Bereczky, K. Lukács, M. Farkas, S. Dóbé, Effect of γ-Valerolactone Blending on Engine Performance, Combustion Characteristics and Exhaust Emissions in a Diesel Engine, Natural Resources 5 (2014) 177-179
[12] G. Strappaveccia, E. Ismalaj, C. Petrucci, D. Lanari, A. Marrocchi, M. Drees, A. Facchetti, L. Vaccaro, A biomass-derived safe medium to replace toxic dipolar solvents and access cleaner Heck coupling reactions, Green Chem. 17 (2015) 365-372
[13] A. M. Scheer, O. Welz, J. Zádor, D. L. Osborn, C. A. Taatjes, Low-temperature combustion chemistry of novel biofuels: resonance-stabilized QOOH in the oxidation of diethyl ketone, Phys. Chem. Chem. Phys. 16 (2014) 13027-13040
[14] J. Zádor, C. A. Taatjes, R. X. Fernandes, Kinetics of elementary reactions in low-temperature autoignition chemistry, Prog. Energy Combust. Sci. 37 (2011) 371-421
[15] J. W. Allen, A. M. Scheer, C. W. Gao, S. S. Merchant, S. S. Vasu, O. Welz, J. D. Savee, D. L. Osborn, C. Lee, S. Vranckx, Z. Wang, F. Qi, R. X. Fernandes, W. H. Green, M. Z. Hadi, C. A. Taatjes, A coordinated investigation of the combustion chemistry of diisopropyl ketone, a prototype for biofuels produced by endophytic fungi, Combust. Flame 161 (2014) 711-724

[16] K. Alexandrino, Á. Millera, R. Bilbao, M. U. Alzueta, Novel aspects in the pyrolysis and oxidation of 2,5-dimethylfuran, P. Combust. Inst. 35 (2015) 1717-1725
[17] I. Barnes, S. Kirschbaum, J. M. Simmie, Combined Experimental and Theoretical Study of the Reactivity of γ-Butyro- and Related Lactones, with the OH Radical at Room Temperature, J. Phys. Chem. A 118 (2014) 5013-5019
[18] W. J. Bailey, C. N. Bird, Pyrolysis of esters. 27. Pyrolysis of lactones, J. Org. Chem. 42 (1977) 3895-3899
[19] C. D. Hurd, F. H. Blunck, The Pyrolysis of Esters, J. Am. Chem. Soc. 60 (1938) 2419-2425
[20] W. K. Metcalfe, C. Togbé, P. Dagaut, H. J. Curran, J. M. Simmie, A jet-stirred reactor and kinetic modeling study of ethyl propanoate oxidation, Combust. Flame 156 (2009) 250-260
[21] A. Rai-Chaudhuri, W. S. Chin, D. Kaur, C. Y. Mok, H. H. Huang, Gas phase pyrolysis of γ-butyrolactone and γ-thiobutyrolactone, J. Chem. Soc., Perkin Trans. 2 (1993) 1249-1250
[22] Z.-H. Li, W.-N. Wang, K.-N. Fan, M. W. Wong, H.-H. Huang, W. Huang, Ab initio study on thermal decomposition of γ-butyrolactone, Chem. Phys. Lett. 305 (1999) 474-482
[23] J. M. Simmie, Kinetics and Thermochemistry of 2,5-Dimethyltetrahydrofuran and Related Oxolanes: Next Next-Generation Biofuels, J. Phys. Chem. A 116 (2012) 4528-4538
[24] K. Moshammer, S. Vranckx, H. K. Chakravarty, P. Parab, R. X. Fernandes, K. Kohse-Höinghaus, An experimental and kinetic modeling study of 2-methyltetrahydrofuran flames, Combust. Flame 160 (2013) 2729-2743
[25] A. Sudholt, L. Cai, J. Heyne, F. M. Haas, H. Pitsch, F. L. Dryer, Ignition characteristics of a bio-derived class of saturated and unsaturated furans for engine applications, P. Combust. Inst. 35 (2015) 2957-2965
[26] M. Verdicchio, B. Sirjean, L. S. Tran, P.-A. Glaude, F. Battin-Leclerc, Unimolecular decomposition of tetrahydrofuran: Carbene vs. diradical pathways, P. Combust. Inst. 35 (2015) 533-541
[27] L.-S. Tran, M. Verdicchio, F. Monge, R. C. Martin, R. Bounaceeur, B. Sirjean, P.-A. Glaude, M. U. Alzueta, F. Battin-Leclerc, An experimental and modeling study of the combustion of tetrahydrofuran, Combust. Flame 162 (2015) 1899-1918
[28] M. Djokic, H.-H. Carstensen, K. M. Van Geem, G. B. Marin, The thermal decomposition of 2,5-dimethylfuran, P. Combust. Inst. 34 (2013) 251-258
[29] M. R. Harper, K. M. Van Geem, S. P. Pyl, G. B. Marin, W. H. Green, Comprehensive reaction mechanism for n-butanol pyrolysis and combustion, Combust. Flame 158 (2011) 16-41
[30] J. Beens, H. Boelens, R. Tijssen, J. Blomberg, Quantitative aspects of comprehensive two-dimensional gas chromatography (GC x GC), J. High. Resolut. Chromatogr. 21 (1998) 47-54
[31] S. P. Pyl, C. M. Schietekat, K. M. Van Geem, M.-F. Reyniers, J. Vercammen, J. Beens, G. B. Marin, Rapeseed oil methyl ester pyrolysis: On-line product analysis using comprehensive two-dimensional gas chromatography, J. Chromatogr. A 1218 (2011) 3217-3223
[32] M. J. Frisch, G. W. Trucks, H. B. Schlegel, G. E. Scuseria, M. A. Robb, J. R. Cheeseman, G. Scalmani, V. Barone, B. Mennucci, G. A. Petersson, H. Nakatsuji, M. Caricato, X. Li, H. P. Hratchian, A. F. Izmaylov, J. Bloino, G. Zheng, J. L. Sonnenberg, M. Hada, M. Ehara, K. Toyota, R. Fukuda, J. Hasegawa, M. Ishida, T. Nakajima, Y. Honda, O. Kitao, H. Nakai, T. Vreven, J. Montgomery, J. A., J. E. Peralta, F. Ogliaro, M. Bearpark, J. J. Heyd, E. Brothers, K. N. Kudin, V. N. Staroverov, T. Keith, R. Kobayashi, J. Normand, K. Raghavachari, A. Rendell, J. C. Burant, S. S. Iyengar, J. Tomasi, M. Cossi, N. Rega, J. M. Millam, M. Klene, J. E. Knox, J. B. Cross, V. Bakken, C. Adamo, J. Jaramillo, R. Gomperts, R. E. Stratmann, O. Yazyev, A. J. Austin, R. Cammi, C. Pomelli, J. W. Ochterski, R. L. Martin, K. Morokuma, V. G. Zakrzewski, G. A. Voth, P. Salvador, J. J. Dannenberg, S. Dapprich, A. D. Daniels, O. Farkas, J. B. Foresman, J. V. Ortiz, J. Cioslowski, D. J. Fox, in: Revision B.01 ed.; Gaussian, Inc.: Wallingford CT, 2010.
[33] G. B. Guthrie, D. W. Scott, W. N. Hubbard, C. Katz, J. P. McCullough, M. E. Gross, K. D. Williamson, G. Waddington, Thermodynamic Properties of Furan, J. Am. Chem. Soc. 74 (1952) 4662-4669
[34] W. V. Steele, R. D. Chirico, A. Nguyen, I. A. Hossenlopp, N. K. Smith, Determination of some pure compound ideal-gas enthalpies of formation, AIChE Symp. Ser. 85 (1989) 140-162
[35] D. Feller, J. M. Simmie, High-Level ab Initio Enthalpies of Formation of 2,5-Dimethylfuran, 2-Methylfuran, and Furan, J. Phys. Chem. A 116 (2012) 11768-11775
[36] A. S. Pell, G. Pilcher, Measurements of heats of combustion by flame calorimetry. Part 3.-Ethylene oxide, trimethylene oxide, tetrahydrofuran and tetrahydropy, Trans. Faraday. Soc. 61 (1965) 71-77
[37] E. J. Prosen, W. H. Johnson, F. D. Rossini, Heats of formation and combustion of the normal alkylcyclopentanes and cyclohexanes and the increment per CH2 group for several homologous series of hydrocarbons, J. Res. NBS 37 (1946) 51-56
[38] M. L. P. Leitão, G. Pilcher, Y. Meng-Yan, J. M. Brown, A. D. Conn, Enthalpies of combustion of γ-butyrolactone, γ-valerolactone, and δ-valerolactone, J. Chem. Thermodyn. 22 (1990) 885-891
[39] B. Borjesson, Y. Nakase, S. Sunner, The heat of combustion and polymerization of β-propiolactone, Acta Chem. Scand. 20 (1966) 803-810

[40] D. A. Pittam, G. Pilcher, Measurements of heats of combustion by flame calorimetry. Part 8.-Methane, ethane, propane, n-butane and 2-methylpropane, J. Chem. Soc. Faraday Trans. 68 (1972) 2224-2229
[41] N. D. Lebedeva, Heats of combustion of monocarboxylic acids, Russ. J. Phys. Chem. 38 (1964) 1435-1437
[42] NIST Chemistry WebBook. http://webbook.nist.gov/chemistry/
[43] E. J. Prosen, F. W. Maron, F. D. Rossini, Heats of combustion, formation, and insomerization of ten C4 hydrocarbons, J. Res. NBS 46 (1951) 106-112
[44] J. R. Lacher, C. H. Walden, K. R. Lea, J. D. Park, Vapor Phase Heats of Hydrobromination of Cyclopropane and Propylene, J. Am. Chem. Soc. 72 (1950) 331-333
[45] Y. Y. Van-chin-syan, V. V. Kochubei, V. V. Sergeev, Y. A. Raevskii, S. I. Gerasimchuk, K. Z. Kotovich, Thermodynamic properties of some acids and aldehydes of the acrylic series, Sov. J. Chem. Phys. 70 (1996) 1789-1794
[46] W. Fang, D. W. Rogers, Enthalpy of hydrogenation of the hexadienes and cis- and trans-1,3,5-hexatriene, J. Org. Chem. 57 (1992) 2294-2297
[47] V. N. Emel'yanenko, S. P. Verevkin, E. N. Burakova, G. N. Roganov, M. K. Georgieva, The thermodynamic properties of 4-pentenoic acid, Russ. J. Phys. Chem. A 82 (2008) 1521-1526
[48] J. A. Montgomery Jr, M. J. Frisch, A complete basis set model chemistry. VI. Use of density functional geometries and frequencies, J. Chem. Phys. 110 (1999) 2822
[49] L. A. Curtiss, K. Raghavachari, P. C. Redfern, V. Rassolov, J. A. Pople, Gaussian-3 (G3) theory for molecules containing first and second-row atoms, J. Chem. Phys. 109 (1998) 7764-7776
[50] L. A. Curtiss, P. C. Redfern, K. Raghavachari, Gaussian-4 theory using reduced order perturbation theory, J. Chem. Phys. 127 (2007) 124105
[51] L. A. Curtiss, K. Raghavachari, P. C. Redfern, J. A. Pople, Assessment of Gaussian-2 and density functional theories for the computation of enthalpies of formation, J. Chem. Phys. 106 (1997) 1063-1079
[52] G. A. Petersson, D. K. Malick, W. G. Wilson, J. W. Ochterski, J. A. Montgomery, M. J. Frisch, Calibration and comparison of the Gaussian-2, complete basis set, and density functional methods for computational thermochemistry, J. Chem. Phys. 109 (1998) 10570-10579
[53] A. L. L. East, L. Radom, An initio statistical thermodynamical models for the computation of third-law entropies, J. Chem. Phys. 106 (1997) 6655
[54] S. M. Burke, W. Metcalfe, O. Herbinet, F. Battin-Leclerc, F. M. Haas, J. Santner, F. L. Dryer, H. J. Curran, An experimental and modeling study of propene oxidation. Part 1: Speciation measurements in jet-stirred and flow reactors, Combust. Flame 161 (2014) 2765-2784
[55] W. K. Metcalfe, S. M. Burke, S. S. Ahmed, H. J. Curran, A Hierarchical and Comparative Kinetic Modeling Study of C1 − C2 Hydrocarbon and Oxygenated Fuels, Int. J. Chem. Kinet. 45 (2013) 638-675
[56] M. M. Kopp, N. S. Donato, E. L. Petersen, W. K. Metcalfe, S. M. Burke, H. J. Curran, Oxidation of Ethylene–Air Mixtures at Elevated Pressures, Part 1: Experimental Results, J. Propul. Power 30 (2014) 790-798
[57] M. K. Sabbe, K. M. Van Geem, M.-F. Reyniers, G. B. Marin, First principle-based simulation of ethane steam cracking, AlChE J. 57 (2011) 482-496
[58] J. Wurmel, J. M. Simmie, Thermochemistry and Kinetics of Angelica and Cognate Lactones, J. Phys. Chem. A 118 (2014) 4172-4183
[59] K. Yasunaga, J. M. Simmie, H. J. Curran, T. Koike, O. Takahashi, Y. Kuraguchi, Y. Hidaka, Detailed chemical kinetic mechanisms of ethyl methyl, methyl tert-butyl and ethyl tert-butyl ethers: The importance of uni-molecular elimination reactions, Combust. Flame 158 (2011) 1032-1036
[60] M. K. Sabbe, A. Vandeputte, M.-F. Reyniers, M. Waroquier, G. B. Marin, Modeling the influence of resonance stabilization on the kinetics of hydrogen abstractions, Phys. Chem. Chem. Phys. 12 (2010) 1278-1298
[61] P. D. Paraskevas, M. K. Sabbe, M.-F. Reyniers, N. G. Papayannakos, G. B. Marin, Kinetic Modeling of α-Hydrogen Abstractions from Unsaturated and Saturated Oxygenate Compounds by Carbon-Centered Radicals, ChemPhysChem 15 (2014) 1849-1866
[62] O. Herbinet, P.-A. Glaude, V. Warth, F. Battin-Leclerc, Experimental and modeling study of the thermal decomposition of methyl decanoate, Combust. Flame 158 (2011) 1288-1300
[63] L. K. Huynh, A. Violi, Thermal decomposition of methyl butanoate: Ab initio study of a biodiesel fuel surrogate, J. Org. Chem. 73 (2008) 94-101
[64] S. Vranckx, J. Beeckmann, W. A. Kopp, C. Lee, L. Cai, H. K. Chakravarty, H. Olivier, K. Leonhard, H. Pitsch, R. X. Fernandes, An experimental and kinetic modelling study of n-butyl formate combustion, Combust. Flame 160 (2013) 2680-2692
[65] Y. L. Wang, D. J. Lee, C. K. Westbrook, F. N. Egolfopoulos, T. T. Tsotsis, Oxidation of small alkyl esters in flames, Combust. Flame 161 (2014) 810-817
[66] J. M. Simmie, K. P. Somers, W. K. Metcalfe, H. J. Curran, Substituent effects in the thermochemistry of furans: A theoretical (CBS-QB3, CBS-APNO and G3) study, J. Chem. Thermodyn. 58 (2013) 117-128

[67] Z. Ping Xu, C. Yew Mok, W. Shong Chin, H. Hua Huang, S. Li, W. Huang, Interconversion and decomposition of furanones, J. Chem. Soc., Perkin Trans. 2 (1999) 725-730
[68] F. Dubnikova, A. Lifshitz, Isomerization of 2,3-Dihydrofuran and 5-Methyl-2,3-dihydrofuran: Quantum Chemical and Kinetics Calculations, J. Phys. Chem. A 106 (2002) 1026-1034
[69] F. Battin-Leclerc, E. Blurock, R. Bounaceur, R. Fournet, P.-A. Glaude, O. Herbinet, B. Sirjean, V. Warth, Towards cleaner combustion engines through groundbreaking detailed chemical kinetic models, Chem. Soc. Rev. (2011)
[70] R. Bounaceur, G. Scacchi, P.-M. Marquaire, F. Dominé, O. Brévart, D. Dessort, B. Pradier, Inhibiting Effect of Tetralin on the Pyrolytic Decomposition of Hexadecane. Comparison with Toluene, Ind. Eng. Chem. Res. 41 (2002) 4689-4701
[71] F. Lannuzel, R. Bounaceur, R. Michels, G. r. Scacchi, P.-M. Marquaire, Reassessment of the Kinetic Influence of Toluene on n-Alkane Pyrolysis, Energ. Fuel. 24 (2010) 3817-3830
[72] L. Zhang, J. Cai, T. Zhang, F. Qi, Kinetic modeling study of toluene pyrolysis at low pressure, Combust. Flame 157 (2010) 1686-1697
[73] C. Cavallotti, M. Derudi, R. Rota, On the mechanism of decomposition of the benzyl radical, P. Combust. Inst. 32 (2009) 115-121
[74] W. Yuan, Y. Li, P. Dagaut, J. Yang, F. Qi, Investigation on the pyrolysis and oxidation of toluene over a wide range conditions. I. Flow reactor pyrolysis and jet stirred reactor oxidation, Combust. Flame 162 (2015) 3-21
[75] W. Yuan, Y. Li, P. Dagaut, J. Yang, F. Qi, Investigation on the pyrolysis and oxidation of toluene over a wide range conditions. II. A comprehensive kinetic modeling study, Combust. Flame 162 (2015) 22-40
[76] L. B. Harding, S. J. Klippenstein, Y. Georgievskii, On the combination reactions of hydrogen atoms with resonance-stabilized hydrocarbon radicals, J. Phys. Chem. A 111 (2007) 3789-3801
[77] R. J. Kee, F. M. Rupley, J. A. Miller, M. E. Coltrin, J. F. Grcar, E. Meeks, H. K. Moffat, A. E. Lutz, G. Dixon-Lewis, M. D. Smooke, J. Warnatz, G. H. Evans, L. R. S., R. E. Mitchell, L. R. Petzold, W. C. Reynolds, M. Caracotsios, W. E. Stewart, P. Glarborg, C. Wang, O. Adigun, in: 15101 ed.; Reaction Design, Inc.: San Diego (CA), 2010.
[78] Y. Fenard, G. Dayma, F. Halter, F. Foucher, Z. Serinyel, P. Dagaut, Experimental and Modeling Study of the Oxidation of 1-Butene and cis-2-Butene in a Jet-Stirred Reactor and a Combustion Vessel, Energ. Fuel. 29 (2015) 1107-1118
[79] M. K. Sabbe, M.-F. Reyniers, V. Van Speybroeck, M. Waroquier, G. B. Marin, Carbon-centered radical addition and beta-scission reactions: Modeling of activation energies and pre-exponential factors, ChemPhysChem 9 (2008) 124-140
[80] B. Sirjean, P. A. Glaude, M. F. Ruiz-Lopèz, R. Fournet, Theoretical Kinetic Study of Thermal Unimolecular Decomposition of Cyclic Alkyl Radicals, J. Phys. Chem. A 112 (2008) 11598-11610
[81] K. Narayanaswamy, H. Pitsch, P. Pepiot, A chemical mechanism for low to high temperature oxidation of methylcyclohexane as a component of transportation fuel surrogates, Combust. Flame 162 (2015) 1193-1213
[82] J. R. Barker, Energy transfer in master equation simulations: A new approach, Int. J. Chem. Kinet. 41 (2009) 748-763
[83] T. L. Nguyen, B. C. Xue, R. E. Weston, J. R. Barker, J. F. Stanton, Reaction of HO with CO: Tunneling Is Indeed Important, J. Phys. Chem. Lett. 3 (2012) 1549-1553
[84] R. E. Weston, T. L. Nguyen, J. F. Stanton, J. R. Barker, HO + CO Reaction Rates and H/D Kinetic Isotope Effects: Master Equation Models with ab Initio SCTST Rate Constants, J. Phys. Chem. A 117 (2013) 821-835
[85] A. Farooq, D. F. Davidson, R. K. Hanson, C. K. Westbrook, A comparative study of the chemical kinetics of methyl and ethyl propanoate, Fuel 134 (2014) 26-38
[86] K. R. Doolan, J. C. Mackie, C. R. Reid, High temperature kinetics of the thermal decomposition of the lower alkanoic acids, Int. J. Chem. Kinet. 18 (1986) 575-596
[87] A. Elwardany, E. F. Nasir, E. Es-sebbar, A. Farooq, Unimolecular decomposition of formic and acetic acids: A shock tube/laser absorption study, P. Combust. Inst. 35 (2015) 429-436
[88] S. S. Merchant, E. F. Zanoelo, R. L. Speth, M. R. Harper, K. M. Van Geem, W. H. Green, Combustion and pyrolysis of iso-butanol: Experimental and chemical kinetic modeling study, Combust. Flame 160 (2013) 1907-1929
[89] C. Cavallotti, R. Rota, S. Carrà, Quantum Chemistry Computation of Rate Constants for Reactions Involved in the First Aromatic Ring Formation, J. Phys. Chem. A 106 (2002) 7769-7778
[90] N. Hansen, J. A. Miller, P. R. Westmoreland, T. Kasper, K. Kohse-Höinghaus, J. Wang, T. A. Cool, Isomer-specific combustion chemistry in allene and propyne flames, Combust. Flame 156 (2009) 2153-2164
[91] M. R. Djokic, K. M. Van Geem, C. Cavallotti, A. Frassoldati, E. Ranzi, G. B. Marin, An experimental and kinetic modeling study of cyclopentadiene pyrolysis: First growth of polycyclic aromatic hydrocarbons, Combust. Flame 161 (2014) 2739-2751

[92] C. Cavallotti, D. Polino, A. Frassoldati, E. Ranzi, Analysis of Some Reaction Pathways Active during Cyclopentadiene Pyrolysis, J. Phys. Chem. A 116 (2012) 3313-3324
[93] A. Goldaniga, T. Faravelli, E. Ranzi, The kinetic modeling of soot precursors in a butadiene flame, Combust. Flame 122 (2000) 350-358
[94] A. Fridlyand, P. T. Lynch, R. S. Tranter, K. Brezinsky, Single Pulse Shock Tube Study of Allyl Radical Recombination, J. Phys. Chem. A 117 (2013) 4762-4776

4.3 An experimental and kinetic modeling study of 2-methyl-tetrahydrofuran pyrolysis and combustion

4.3.1 Abstract

Saturated cyclic ethers are being proposed as next-generation bio-derived fuels. However, their pyrolysis and combustion chemistry has not been well established. In this work, the pyrolysis and combustion chemistry of 2-methyl-tetrahydrofuran (MTHF) was investigated through experiments and detailed kinetic modeling. Pyrolysis experiments were performed in a dedicated plug flow reactor at 170 kPa, temperatures between 900 and 1100K and a N_2 (diluent) to MTHF molar ratio of 10. The combustion chemistry of MTHF was investigated by measuring mole fraction profiles of stable species in premixed flat flames at 6.7 kPa and equivalence ratios 0.7, 1.0 and 1.3 and by determining laminar burning velocities of MTHF/air flat flames with unburned gas temperatures of 298, 358 and 398K and equivalence ratios between 0.6 and 1.6. Furthermore, a kinetic model for pyrolysis and combustion of MTHF was developed, which contains a detailed description of the reactions of MTHF and its derived radicals with the aid of new high-level theoretical calculations. Model calculated mole fraction profiles and laminar burning velocities are in relatively good agreement with the obtained experimental data. At the applied pyrolysis conditions, unimolecular decomposition of MTHF by scission of the methyl group and concerted ring opening to 4-penten-1-ol dominates over scission of the ring bonds; the latter reactions were significant in tetrahydrofuran pyrolysis. MTHF is mainly consumed by hydrogen abstraction reactions. Subsequent decomposition of the resulting radicals by β-scission results in the observed product spectrum including small alkenes, formaldehyde, acetaldehyde and ketene. In the studied flames, unimolecular ring opening of MTHF is insignificant and consumption of MTHF through radical chemistry dominates. Recombination of 2-oxo-ethyl and 2-oxo-propyl, primary radicals in MTHF decomposition, with hydrogen atoms and carbon-centered radicals results in a wide range of oxygenated molecules.

Keywords: 2-methyl-tetrahydrofuran, pyrolysis, premixed flames, detailed kinetic model

4.3.2 Introduction

There is an increased demand for a sustainable production of chemicals and fuels. Currently, a lot of effort is dedicated to the conversion of lignocellulosic biomass through catalytic, fermentative and pyrolytic processes. These conversion routes result in a wide variety of molecules that may be processed further into other high-value chemicals, so-called platform molecules, or that can be used directly, for example as bio-fuel.

Recently, several production routes to saturated cyclic ethers, such as 2-methyl-tetrahydrofuran (MTHF) and 2,5-dimethyl-tetrahydrofuran (DMTHF), have been proposed [1-3]. This class of molecules has lower heating values that range between ~28.5 MJ l^{-1} and 29.5 MJ l^{-1}, which are close to those of furans (~27.7-30.0 MJ l^{-1}) and of gasoline (~31.6 MJ l^{-1}), but clearly higher than that of ethanol (~21.3 MJ l^{-1}). MTHF has good antiknock characteristics (RON=86, MON=73), and satisfactory performance when mixed with gasoline in a conventional internal combustion engine [4-7].

The potential of cyclic ethers to serve as next-generation bio-derived fuels has triggered several fundamental studies that aim at understanding their combustion chemistry. Tetrahydrofuran (THF), the simplest five-membered cyclic ether, has received most attention. Verdicchio et al. investigated the unimolecular decomposition of THF using quantum chemical methods [8]. The calculations show that biradical and carbene intermediates play an important role in the initial ring-opening steps, but that a concerted molecular channel is also active. Model simulations with a kinetic model based on the mentioned ab initio study are in good agreement with shock tube experiments [9]. Tran et al. expanded the model to describe the combustion chemistry of THF. The model was validated with data obtained from premixed flames and shock tube measurements [10]. Kasper et al. investigated the structure of laminar premixed low-pressure THF flames using photoionization (PI) and electron-ionization (EI) molecular-beam mass spectrometry (MBMS) [11]. THF oxidation and ignition has been studied in jet-stirred reactors and a rapid compression machine [12, 13]. The available experimental data and developed kinetic models of the aforementioned studies indicate that THF decomposition is dominated by radical chemistry as soon a radical pool is established.

The pyrolysis and combustion chemistry of alkylated cyclic ethers is less well established. A theoretical study by Simmie provides thermochemistry for THF, MTHF, DMTHF and the derived radicals, and kinetic data for a selection of hydrogen abstraction and radical decomposition reactions [14]. Other quantum chemical studies have focused on hydrogen

abstraction from MTHF and DMTHF by hydroperoxy radicals [15] and intramolecular hydrogen abstraction of the various peroxy radicals formed from 3-methyl-tetrahydrofuran [16]. Fuel rich (φ=1.7), low pressure, premixed laminar MTHF flames were investigated by Moshammer et al. [17]. Reaction products were identified and quantified using molecular beam mass spectrometry with electron ionization and synchrotron-based tunable VUV photoionization. A kinetic model was developed using the theoretical study by Simmie [14] and analogy with other molecules.

This work aims to improve the understanding the pyrolysis and combustion chemistry of MTHF, see Figure 4.3-1. Firstly, the experimental database for MTHF reactions is expanded in several ways. The pyrolysis chemistry is investigated in a tubular plug flow reactor. Furthermore, temperature and mole fraction profiles are measured in three low-pressure premixed flames while laminar burning velocities are obtained at atmospheric pressure using the heat flux method. Secondly, a new detailed kinetic model for MTHF pyrolysis and combustion has been developed. Kinetic data related to the decomposition of MTHF has been calculated using the CBS-QB3 level of theory. Thirdly, predictions of the new kinetic model are compared to the obtained experimental data. Reaction path and sensitivity analyses are performed to better understand the MTHF chemistry. The proposed kinetic model is meant to serve as a building block for biomass pyrolysis and gasification processes as the cyclic ether structure is present in some biomass model compounds.

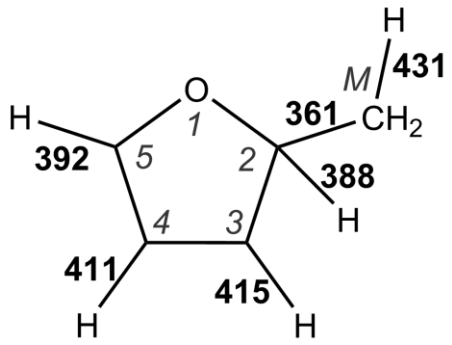

Figure 4.3-1 Structure of MTHF with atom labels (italic) and bond bond energy in kJ mol^{-1} [14] (bold)

4.3.3 Experimental methods

The pyrolysis chemistry of MTHF was studied in a plug flow reactor. The combustion chemistry was studied using premixed, laminar flames. A detailed description of the experimental setups used in this study has been given elsewhere [18-23]. Only the main

features of the experimental and analytical methods used are summarized below. Operating conditions are listed in Table 4.3-1.

Table 4.3-1 Operating conditions for MTHF flames and pyrolysis

	φ	F^0_{MTHF} (mol s^{-1})	F^0_{O2} (mol s^{-1})	F^0_{Ar} (mol s^{-1})	P (kPa)	C/O	$x_{0,diluent}$	Flow velocity at T=333K (cm s^{-1})
Low-pressure premixed flame	0.7	1.15E-04	1.15E-03	3.29E-03	6.7	0.24	0.72	67
	1	1.39E-04	9.74E-04	3.45E-03	6.7	0.33	0.76	67
	1.3	2.02E-04	1.09E-03	3.27E-03	6.7	0.42	0.72	67

Atmospheric premixed laminar flame	φ	P (kPa)	$T_{unburned\ gas}$ (K)
	0.60 – 1.55	101.3	298 - 398

	φ	F^0_{MTHF} (mol s^{-1})	F^0_{O2} (mol s^{-1})	F^0_{N2} (mol s^{-1})	P (kPa)	C/O	$x_{0,diluent}$	T-range (K)
Flow reactor	∞	1.68E-04	0.00E+00	1.67E-03	170	5.00	0.91	913 - 1073

4.3.3.1 Tubular flow reactor for pyrolysis

MTHF (Sigma Aldrich, state purity +99 %) is fed to an evaporator kept at 573K using a Coriolis flow meter controlled pump. Nitrogen (Air Liquide, purity +99.999 %) is used as diluent and its flow rate is controlled using a Coriolis mass flow controller. It is heated to the same temperature as MTHF and both gasses are mixed before entering the reactor.

The tubular reactor has an internal diameter of 6 mm and is 1.475 m long. The reactor is placed in an electrically heated furnace. In total, eight thermocouples are positioned along the reactor length, measuring the gas temperature. The reactor consists of 4 separate sections and the temperature in each section is controlled by a thermocouple. Furthermore, two manometers, positioned at the inlet and outlet of the reactor, measure the pressure. The pressure was kept fixed at 0.17 MPa using a valve positioned downstream of the reactor. The pressure drop across the reactor was found to be negligible (<0.001 MPa).

Products and unconverted feed are identified and quantified online, downstream of the reactor, using several dedicated gas chromatographs. The reactor effluent is first sent to a heated sampling system kept at 573 K to avoid condensation. A part of the mixture is injected on a refinery gas analyzer (RGA) after removal of the condensable fraction. This chromatograph is able to calculate the flow rate of all permanent gases using two thermal conductivity detectors (TCD) and C_{4-} hydrocarbons using a flame ionization detector (FID) based on the fixed flow rate of N_2, i.e. primary internal standard. The response factors were

determined using a calibration mixture provided by Air Liquide, Belgium. A different fraction of the effluent is injected on a two dimensional gas chromatograph (GCxGC) and a light oxygenates analyzer (LOA) through heated transfer lines, without prior condensation. The flow rate of water, formaldehyde and methanol are calculated using the LOA, equipped with a TCD, with propene, identified and quantified on the RGA, as secondary internal standard. The GCxGC allows identification, using a time-of-flight mass spectrometer (TOF-MS), and quantification, using a FID, of all hydrocarbons and oxygenated molecules that have two or more carbon atoms. Methane, identified and quantified on the RGA, acts as secondary internal standard. Response factors were calculated using the effective carbon number approach[24]. This methodology allows online analysis of the complete product spectrum and avoids separate gas-phase and condensate analysis. A more detailed description of data quantification can be found elsewhere[25].

The procedure described above allowed closing C, H and O molar balances within 5%. Several repeat experiments were performed and the average uncertainty on the mole fraction for most products is 5%, in line with previous experiments.

4.3.3.2 Low-pressure premixed flat flame structure

The flow rates of oxygen (Messer, purity +99.995 %) and argon (Messer, purity +99.999 %), the diluent, are controlled by two mass flow controllers (Bronkhorst). The flow rate of liquid MTHF (Sigma Aldrich, purity +99%) is regulated using a mass flow controller connected to a evaporator/mixer (Bronkhorst). There, MTHF is evaporated and mixed with argon. Subsequently, the gaseous stream is mixed with oxygen and fed to a McKenna burner (60 mm diameter) housed in a vacuum chamber. The temperature of the burner is kept at 333K using water cooling.

Three premixed flames, i.e. φ=0.7, 1.0 and 1.3,were stabilized on the burner. The volumetric flow rate of the unburned gas was constant for all equivalence ratios, see Table 4.3-1. The pressure was fixed at 6.7 kPa (50 Torr). The flame was connected with three gas chromatographs (GC) through a quartz probe, with a 0.18 mm diameter orifice at the tip and an angle to vertical of 22°, and heated transfer lines kept at 423 K. The first GC was equipped with a carbosphere column and was used to quantify oxygen and hydrogen using a TCD detector. The second GC was equipped with a HP-PLOT Q column and was used to quantify CO, CO_2, oxygenates, hydrocarbons using a FID detector preceded by a methanizer and water using a TCD detector. This GC was also equipped with a HP-Molsieve column and was used

to quantify CO and CH_4 using a FID detector and argon using a TCD detector. The third GC was equipped with a HP-PLOT Q column and a mass spectrometer and was used for species identification. The burner can be moved in vertical direction while the position of the sampling probe was fixed during experiment which allowed to obtain species mole fraction profiles as function of height above the burner.

Flame temperature profiles were measured with a PtRh(6 %)–PtRh(30 %) type B thermocouple (diameter 0.10 mm). The thermocouple junction was located at the center of the burner. The thermocouple was coated with a ceramic layer of BeO-Y_2O_3 to reduce catalytic effects. The electrical compensation method was used to correct for radiative heat losses. The estimated uncertainty of the measured temperature values is approximately 5%.

A sighting telescope (cathetometer) was used to evaluate the position of the probe and the thermocouple with respect to the burner, accuracy +/- 0.05mm.

The described procedure allowed closing the C molar balance within 5% and the O and H molar balances within 10%.

4.3.3.3 Laminar burning velocities measurements in atmospheric flat flame

Laminar burning velocities were measured using the heat flux method applied to a flat flame adiabatic burner [26]. The apparatus consists of a plenum chamber attached to a brass burner plate. The temperature of the plenum chamber was set to the desired unburned gas temperature using a thermostatic oil jacket. The brass burner plate is 2 mm thick and has a diameter of 30 mm. The plate is perforated with holes of diameter 0.5 mm, with the pitch between them being 0.7 mm. Eight thermocouples are embedded into the plate surface at different distances and angles from the center to the periphery of the burner to measure the radial temperature profile. Heating around the burner plate was provided by thermostatic oil, at 50 K higher than the unburned gas temperature. The heat flux from the heated burner to the unburned gas can compensate for heat losses from the flame toward the heated burner, which results in adiabatic conditions. The radial burner temperature profile becomes flat and the gas speed equals the adiabatic burning velocity.

In the present study, the measurements of laminar burning velocity were performed at atmospheric pressure (101.3 kPa), for unburned flame temperatures ranging from 298 to 398 K, and equivalence ratios from 0.60 to 1.55.

The estimated error of the laminar burning velocity is ~4 %. In addition, the error in the equivalence ratio is about 1%, resulting mainly from the error in the mass flow measurements for oxygen and liquid fuel.

4.3.4 Computational methods

4.3.4.1 Theoretical rate coefficients

The rate coefficients for the concerted MTHF decomposition, several hydrogen abstraction reactions and unimolecular decomposition channels of the resulting radicals were calculated in two steps. First, electronic structure calculations at the CBS-QB3 level of theory [27] were performed using the Gaussian 09 revision D suite of programs [28]. Using methods from statistical mechanics, the output of the ab initio calculations was used to determine the thermodynamic properties of reactants, products and transition states. Heats of formation are obtained from the electronic energies by converting those with the atomization method. B3LYP/6-311G(d,p) level rotational constants and scaled (factor 0.99) harmonic frequencies, except those that represent internal rotations, were used to calculate the thermal contributions to the enthalpies as well as entropies and heat capacities. Hindrance potentials of internal rotors, which are not well described as harmonic oscillators, were determined *via* relaxed scans by increasing the corresponding dihedral angle in 10 degrees steps until complete rotation was achieved. These potentials were regressed to Fourier series prior to their use. The reduced moments of inertia were calculated at the $I^{(2,3)}$ level as defined by East and Radom [29]. With this information, the Schroedinger equation for one-dimensional axis-fixed rotation could be solved and the resulting energy eigenvalues were employed to calculate the contributions of these modes to the thermodynamic functions. Finally, the thermodynamic data was stored in form of NASA polynomials.

In the second step, transition state theory expressed in terms of Gibbs free energies was used to calculate the rate coefficients:

$$k_{TST}(T) = \chi(T) \cdot \frac{k_B T}{h} \cdot \left(\frac{RT}{p}\right)^{\Delta n - 1} \cdot e^{-\frac{\Delta G^{\ddagger}}{RT}} \quad (1)$$

Here $\Delta G^{\ddagger}$ is the Gibbs free energy difference between transition state without the transitional mode and reactant(s), Δn is the molecularity of the reaction (2 for bimolecular, 1 for unimolecular reactions), and $\chi(T)$ is a correction factor that accounts for quantum mechanical tunneling. All other symbols have their usual meaning. The asymmetric Eckart potential was

used in this work to calculate $\chi(T)$. The Gibbs free energies were obtained from the NASA polynomials calculated in the first step. Rate coefficients were calculated for temperatures ranging between 300 K and 2500 K in 50 K steps. The individual rate coefficients were finally regressed to modified Arrhenius expressions.

4.3.4.2 Simulations

Simulations were performed using the CHEMKIN package [30].

The plug flow reactor module was used to simulate the pyrolysis experiments. The plug flow assumption has been validated earlier for the used reactor setup [31].

The simulations for the low-pressure premixed flames were conducted using the premixed laminar burning-stabilized flame module. Composition and flow rate of the inlet stream, pressure and temperature profile were provided as input. In this work, the input temperature profile is the average of the measured temperature profile with and without the sampling probe, in line with earlier studies [10]. The use of the average temperature profile tries to account for the distortion of the flame structure induced by sampling probe and thermocouple: (i) The measured temperature profile without the sampling probe overestimates the temperature as the sampling probe acts as a heat sink; (ii) The measured temperature profile with the sampling probe underestimates the temperature as the probe mainly affects the temperature of the gas near the probe, and not necessarily the temperature of the gas near the burner. The measured temperature profile with the sampling probe, the measured temperature profile without the sampling probe and the temperature profile used for simulation at φ = 1.0 are presented in Figure 4.3-2 as example.

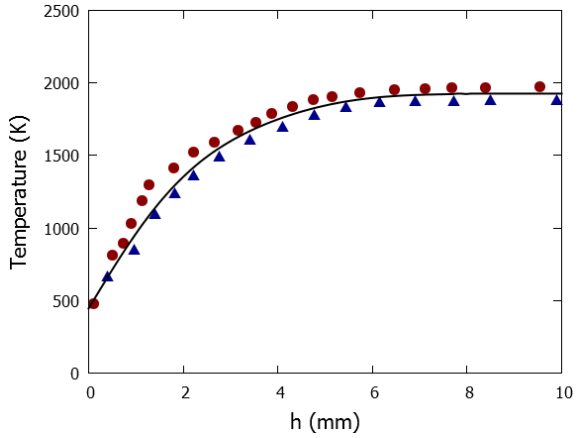

Figure 4.3-2 MTHF flame temperature profiles as a function of height above burner h at φ = 1.0: ●- measured profile without the sampling probe, ▲- measured profile and with the sampling probe, ——- temperature profile used for simulation

Simulations of adiabatic laminar burning velocities were carried out using the premixed laminar flame-speed module with GRAD and CURV parameters of 0.05. Thermal diffusion effects were included in the simulations.

4.3.5 Kinetic model development

A detailed kinetic model has been developed to describe the pyrolysis and combustion of MTHF. The model consist of three main parts: (1) a primary mechanism, describing the combustion and pyrolysis of MTHF and derived radicals, (2) a base mechanism, describing the combustion and pyrolysis of small hydrocarbons and oxygenates, (3) a secondary mechanism, describing the combustion and pyrolysis of products originating from MTHF decomposition and not described by the base mechanism. A selection of key reactions of the primary mechanism and their corresponding rate coefficients are presented in Table 4.3-2. The three parts of the model are described in the following sections.

Table 4.3-2 Primary mechanism of the high-temperature pyrolysis and oxidation of MTHF. The rate coefficients are given ($k = AT^n exp(-E_a/RT)$) in m^3, mol, s, kJ units

Nr.	Reaction	A	n	Ea	k (1000K)	Comment
	C-H and methyl scission					
1	C•cy(COCCC)+H→Ccy(COCCC)	1.0E+08	0.0	0.0	1.0E+08	a
2	Ccy(C•OCCC)+H→Ccy(COCCC)	1.0E+08	0.0	0.0	1.0E+08	a
3	Ccy(COC•CC)+H→Ccy(COCCC)	1.0E+08	0.0	0.0	1.0E+08	a
4	Ccy(COCC•C)+H→Ccy(COCCC)	1.0E+08	0.0	0.0	1.0E+08	a
5	Ccy(COCCC•)+H→Ccy(COCCC)	1.0E+08	0.0	0.0	1.0E+08	a
6	cy(OC•CCC)+CH_3→Ccy(COCCC)	1.0E+07	0.0	0.0	1.0E+07	a
	Carbene and biradical pathways					
7	Ccy(COCCC)→C=CCOCC	4.8E+49	-10.1	467.3	1.3E-05	b, 1.0atm
8	Ccy(COCCC)→C=CC(C)OC	4.8E+49	-10.1	467.3	1.3E-05	b, 1.0atm
9	Ccy(COCCC)→C=COC(C)C	1.8E+51	-10.4	474.9	1.3E-05	b, 1.0atm
10	Ccy(COCCC)→C=C(C)OCC	1.8E+51	-10.4	474.9	1.3E-05	b, 1.0atm
11	Ccy(COCCC)→CCCCCHO	6.6E+46	-9.4	430.6	1.1E-04	b, 1.0atm
12	Ccy(COCCC)→CCCC(=O)C	6.6E+46	-9.4	430.6	1.1E-04	b, 1.0atm
13	Ccy(COCCC)→CC=CCCOH	1.7E+41	-7.7	416.1	2.2E-04	b, 1.0atm
14	Ccy(COCCC)→C=CCC(C)OH	1.7E+41	-7.7	416.1	2.2E-04	b, 1.0atm
15	Ccy(COCCC)→CH_2O+C=CCC	2.7E+35	-5.8	409.1	4.2E-04	b, 1.0atm
16	Ccy(COCCC)→CH_3CHO+C=CC	2.7E+35	-5.8	409.1	4.2E-04	b, 1.0atm
17	Ccy(COCCC)→Ccy(COC)+C_2H_4	9.3E+64	-14.1	549.4	1.2E-06	b, 1.0atm
18	Ccy(COCCC)→cy(COC)+C=CC	9.3E+64	-14.1	549.4	1.2E-06	b, 1.0atm
	Concerted ring opening					
19	Ccy(COCCC)→C=CCCCOH	1.1E+05	2.3	248.5	8.5E-02	c
20	Ccy(COCCC)→CC=CCCOH	1.0E+12	0.6	342.6	6.7E-05	b
21	Ccy(COCCC)→C=CCC(C)OH	1.0E+12	0.6	342.6	6.7E-05	b
	Hydrogen abstraction					
	by H					
22	Ccy(COCCC)+H→Ccy(COC•CC)+H_2	3.3E+01	1.9	13.8	2.6E+06	c
23	Ccy(COCCC)+H→Ccy(COCC•C)+H_2	1.1E+01	2.0	23.9	7.2E+05	c

24	Ccy(COCCC)+H→Ccy(COCCC•)+H_2	1.0E+01	2.0	25.1	5.6E+05	c
25	Ccy(COCCC)+H→Ccy(C•OCCC)+H_2	1.7E+02	1.7	9.2	6.6E+06	c
26	Ccy(COCCC)+H→C•cy(COCCC)+H_2	4.2E+01	2.0	39.3	2.8E+05	c
	by CH3					
27	Ccy(COCCC)+CH_3→Ccy(COC•CC)+CH_4	4.7E-04	3.0	27.6	1.2E+04	c
28	Ccy(COCCC)+CH_3→Ccy(COCC•C)+CH_4	3.2E-04	3.0	34.3	5.5E+03	c
29	Ccy(COCCC)+CH_3→Ccy(COCCC•)+CH_4	2.6E-04	3.0	35.6	3.9E+03	c
30	Ccy(COCCC)+CH_3→Ccy(C•OCCC)+CH_4	3.9E-04	2.9	22.2	1.5E+04	c
31	Ccy(COCCC)+CH_3→C•cy(COCCC)+CH_4	5.0E-04	3.0	45.6	2.4E+03	c
	by OH					
32	Ccy(COCCC)+OH→Ccy(COC•CC)+H_2O	2.4E+00	2.0	-12.3	1.1E+07	d
33	Ccy(COCCC)+OH→Ccy(COCC•C)+H_2O	2.4E+00	2.0	-2.7	3.3E+06	d
34	Ccy(COCCC)+OH→Ccy(COCCC•)+H_2O	2.4E+00	2.0	-0.4	2.5E+06	d
35	Ccy(COCCC)+OH→Ccy(C•OCCC)+H_2O	1.2E+00	2.0	-13.9	6.4E+06	d
36	Ccy(COCCC)+OH→C•cy(COCCC)+H_2O	3.6E+00	2.0	7.2	1.5E+06	d
	by O					
37	Ccy(COCCC)+O→Ccy(COC•CC)+OH	3.4E+02	1.5	-0.3	1.1E+07	d
38	Ccy(COCCC)+O→Ccy(COCC•C)+OH	3.4E+02	1.5	14.0	2.0E+06	d
39	Ccy(COCCC)+O→Ccy(COCCC•)+OH	3.4E+02	1.5	17.5	1.3E+06	d
40	Ccy(COCCC)+O→Ccy(C•OCCC)+OH	1.7E+02	1.5	-2.8	7.5E+06	d
41	Ccy(COCCC)+O→C•cy(COCCC)+OH	5.1E+02	1.5	28.9	5.0E+05	d
	by HO2					
42	Ccy(COCCC)+HO_2→Ccy(COC•CC)+H_2O_2	7.8E-06	3.5	33.0	5.7E+03	e
43	Ccy(COCCC)+HO_2→Ccy(COCC•C)+H_2O_2	7.2E-08	4.1	48.0	5.5E+02	e
44	Ccy(COCCC)+HO_2→Ccy(COCCC•)+H_2O_2	1.2E-06	3.7	50.9	3.8E+02	e
45	Ccy(COCCC)+HO_2→Ccy(C•OCCC)+H_2O_2	6.5E-05	3.3	26.8	1.7E+04	e
46	Ccy(COCCC)+HO_2→C•cy(COCCC)+H_2O_2	1.7E-04	3.5	71.5	7.9E+02	e
	MTHF radical decomposition					
	Ccy(COC•CC)					
47	Ccy(COC•CC)→C=COCC2•	4.6E+11	0.7	140.3	2.7E+06	c
48	C=COCC2•→C=CO•+CC=C	3.2E+11	0.5	68.6	2.2E+09	c
49	C=COCC2•→CH_3+C=COC=C	1.6E+12	0.5	128.6	6.9E+06	c
50	C=COCC2•→a-C•cy(COC(C)C)	1.0E+09	0.6	59.0	5.2E+07	anti , c
51	C=COCC2•→s-C•cy(COC(C)C)	1.1E+09	0.6	55.6	7.0E+07	syn, c
52	Ccy(COC•CC)→CC•CCCHO	3.3E+12	0.3	94.4	3.2E+08	c
53	CC•CCCHO→C=CO•+CC=C	3.6E+09	1.0	85.5	9.9E+07	c
54	CC•CCCHO→CCCCC•(=O)	7.3E+04	1.9	62.1	1.9E+07	c
55	CCCCC•(=O)→CCCC•+CO	1.0E+11	0.0	40.2	8.0E+08	c
56	Ccy(COC•CC)→H+Ccy(COC=CC)	2.8E+04	2.7	191.1	3.6E+02	b
	Ccy(COCC•C)					
57	Ccy(COCC•C)→C=CCOC•C	4.4E+12	0.2	136.1	1.7E+06	c
58	C=CCOC•C→CH_3CHO+C=CC•	4.4E+09	1.1	58.1	7.4E+09	c
59	C=CCOC•C→a-C•cy(CCOC(C))	6.1E+07	0.9	54.6	3.8E+07	anti, c
60	C=CCOC•C→s-C•cy(CCOC(C))	1.2E+08	0.9	57.7	4.4E+07	syn, c
61	Ccy(COCC•C)→C=CCC(C)O•	2.0E+12	0.3	130.4	2.2E+06	c
62	C=CCC(C)O•→CH_3CHO+C=CC•	1.8E+12	0.4	19.9	2.1E+12	c
63	C=CCC(C)O•→CH_3+C=CCCHO	4.7E+13	0.2	60.1	1.2E+11	c
64	C=CCC(C)O•→C=CC•C(C)OH	2.3E+08	1.3	74.0	2.5E+08	anti , c
65	C=CCC(C)O•→a-C•cy(COC(C)C)	4.7E+10	0.4	49.7	1.8E+09	syn, c
66	C=CCC(C)O•→s-C•cy(COC(C)C)	2.2E+10	0.4	46.0	1.3E+09	c
67	Ccy(COCC•C)→H+Ccy(COC=CC)	9.2E+09	1.1	137.6	1.5E+06	b
68	Ccy(COCC•C)→H+Ccy(COCC=C)	1.7E+10	1.1	149.4	5.1E+05	b
	Ccy(COCCC•)					
69	Ccy(COCCC•)→C=CC(C)OC•	1.4E+12	0.5	136.6	2.8E+06	c

70	C=CC(C)OC•→CH_2O+c-CC=CC•	8.0E+11	0.5	67.5	6.9E+09	c
71	C=CC(C)OC•→CH_2O+t-CC=CC•	1.4E+11	0.8	63.3	1.3E+10	c
72	C=CC(C)OC•→a-C•cy(CCOC(C))	2.9E+09	0.5	60.1	8.2E+07	anti , c
73	C=CC(C)OC•→s-C•cy(CCOC(C))	1.2E+09	0.6	66.9	2.7E+07	syn, c
74	Ccy(COCCC•)→t-CC=CCCO•	2.8E+13	-0.1	127.0	4.8E+06	trans, c
75	Ccy(COCCC•)→c-CC=CCCO•	6.3E+12	0.1	136.7	7.8E+05	cis, c
76	t-CC=CCCO•→t-C=CC•CCOH	3.1E+04	1.9	132.5	2.5E+03	trans, c
77	t-CC=CCCO•→t-CC=CC•COH	8.1E+07	1.4	80.8	9.5E+07	trans, c
78	c-CC=CCCO•→c-C=CC•CCOH	2.1E+06	1.4	18.8	3.5E+09	cis, c
79	c-CC=CCCO•→c-CC=CC•COH	3.1E+07	1.5	79.5	7.6E+07	cis, c
80	t-CC=CCCO•→CH_2O+t-CC=CC•	5.7E+11	0.5	25.7	6.8E+11	trans, c
81	c-CC=CCCO•→ CH_2O +c-CC=CC•	1.1E+12	0.4	24.7	9.2E+11	cis, c
82	Ccy(COCCC•)→H+Ccy(C=CCCO)	9.2E+09	1.1	137.6	1.5E+06	b
83	Ccy(COCCC•)→H+Ccy(COCC=C)	1.7E+10	1.1	149.4	5.1E+05	b
84	Ccy(COCCC•)→CH_3+cy(OC=CCC)	1.5E+13	0.3	129.2	2.7E+07	c
	Ccy(C•OCCC)					
85	Ccy(C•OCCC)→C•CCC(=O)C	1.4E+12	0.5	90.7	9.2E+08	c
86	C•CCC(=O)C→C2•C=O+C_2H_4	1.2E+11	0.7	92.4	2.2E+08	c
87	C•CCC(=O)C→CCCC(=O)C•	2.5E+04	1.9	56.1	1.4E+07	c
88	Ccy(C•OCCC)→C=C(C)OCC•	7.2E+11	0.7	136.9	4.6E+06	c
89	C=C(C)OCC•→C2•C=O+C_2H_4	2.8E+13	0.1	75.9	4.8E+09	c
90	Ccy(C•OCCC)→H+Ccy(C=CCCO)	2.8E+04	2.7	191.1	3.6E+02	b
	C•cy(COCCC)					
91	C•cy(COCCC)→C=CCCCO•	4.8E+10	0.6	75.8	2.4E+08	c
92	C=CCCCO•→CH_2O+C=CCC•	1.3E+14	0.0	57.4	1.7E+11	c
93	C=CCCCO•→cy(OCC•CCC)	1.1E+09	0.3	12.3	2.2E+09	c
94	C=CCCCO•→C=CC•CCOH	3.6E+07	1.2	51.1	3.0E+08	c
95	C•cy(COCCC)→C•CCOC=C	1.1E+10	0.8	90.0	7.2E+07	c
96	C•CCOC=C→C=COC•+C_2H_4	1.2E+12	0.4	116.4	1.9E+07	c
97	C•CCOC=C→cy(OC•CCCC)	2.0E+08	0.6	48.4	3.0E+07	c
	Substitution					
98	Ccy(COCCC)+H→CC•CCCOH	3.9E+00	2.0	99.6	2.0E+01	c

a estimated
b reaction rate coefficient taken from its THF analogue [10]
c CBS-QB3 calculated value, see Section 4.3.4
d estimated from Evans-Polanyi relationship [32]
e taken from [15]

4.3.5.1 Primary mechanism

The primary mechanism consists of reactions describing the consumption of MTHF by unimolecular reactions and bimolecular reactions, e.g. hydrogen abstraction, and decomposition of MTHF-derived radicals, e.g. β-scission reactions.

4.3.5.1.1 Unimolecular fuel decomposition

Scission of the methyl – ring bond and scission of the C-H bonds produce radical species. Reaction rate coefficients were estimated in the reverse direction, i.e. recombination (reactions 1-6).

Unimolecular ring opening by scission of one of the ring bonds produces diradical or carbenic species. These reactions were found to be important in THF pyrolysis [8]. Similar reactions for MTHF have been considered in this work, see reactions 7-20 in Table 4.3-2. Corresponding reaction rate coefficients were taken from their THF-analogues [10]. Diradical and carbenic species are unstable and react to molecular products. These unstable species are not included explicitly in the kinetic model. Instead, they are replaced by their molecular product(s) following stabilization by intramolecular hydrogen abstraction or β-scission.

For example, C-O scission in THF may form 3-hydroxypropyl carbene [8], see Figure 4.3-3. Isomerization of the carbene to but-3-en-1-ol is favored over decomposition to ethenol and ethene [8]. The analogous reactions for MTHF are added to Figure 4.3-3. C-O scission in MTHF can form methyl,3-hydroxypropyl carbene which can react to pent-3-en-1-ol. The equivalent single-step reaction is reaction number 13 in Table 4.3-2. C-O scission in MTHF can also form 3-methyl-3-hydroxypropyl carbene which can react to pent-4-en-2-ol. The equivalent single-step reaction is reaction number 14 in Table 4.3-2. Rate coefficients for the latter two reactions are taken from their THF analogue [10].

Note that the use of the reaction rate coefficients of THF for MTHF introduces some error to the kinetic model. In the case of the analogous reactions in Figure 4.3-3, C-O scission in THF forms 3-hydroxypropyl carbene where a primary carbon atom has valence two while C-O scission in MTHF can form methyl-3-hydroxypropyl carbene where a secondary carbon atom has valence two. The effect of this error on the performance of the kinetic model is expected to be minor as scission of one of the ring bonds is typically of lower importance compared to C-C scission of the alkyl side group, as in methyl-cyclohexane [33].

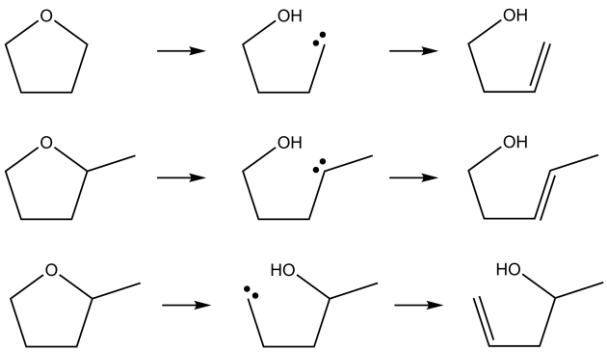

Figure 4.3-3 C-O scission in THF and MTHF forming carbene intermediates and subsequent decomposition.

Ethers can react through a 4-membered transition state where a hydrogen atom of a carbon atom in β-position bridges to the oxygen atom forming an alkene and an alcohol [34]. Three

such reactions are considered for MTHF. Hydrogen atoms from ring carbon atoms in the β-position can bridge to the oxygen atom forming pent-3-en-1-ol and pent-4-en-2-ol respectively, reactions 20 and 21 in Table 4.3-2. Rate coefficients were taken from the analogous THF reaction [8]. Furthermore, a hydrogen atom of the methyl groups can bridge to the ring oxygen forming 4-penten-1-ol, reaction 19 in Table 4.3-2. Rate coefficients were obtained from CBS-QB3 calculations.

4.3.5.1.2 Hydrogen abstraction from MTHF

Reaction rate coefficients for hydrogen abstraction reactions from MTHF by hydrogen atoms and methyl radicals (reactions 22-31) were derived from quantum calculations in the present study. Reaction rate coefficients for hydrogen abstraction by oxygen atoms, hydroxyl radicals (reactions 32-41) were deduced from Evans-Polanyi correlations proposed by Dean and Bozelli [32], analogous to recently developed tetrahydrofuran and tetrahydropyran kinetic models [10, 35]. Kinetics for hydrogen abstraction from MTHF by hydroperoxy radicals (reactions 42-46) were taken from the theoretical calculations by Chakravarty et al. [15]. Hydrogen abstraction reactions by carbon centered radicals, such as ethyl and allyl, were estimated from hydrogen abstraction by methyl but taking into consideration the effect of resonance stabilization [36, 37].

4.3.5.1.3 MTHF radical decomposition

Decomposition reactions of all MTHF radicals and ring-opened MTHF radicals have been calculated at the CBS-QB3 level of theory, see Table 4.3-2 (reactions 47-55, 57-66, 69-81, 85-89, 91-97). MTHF radicals can undergo ring opening reactions by C-C β-scission and C-O β-scission. Previous studies regarding THF and MTHF indicated that ring opening by C-O β-scission is favored over C-C β-scission [10, 14]. The same trend is observed in this work. Unsaturated cyclic ethers can be formed by C-H β-scission of MTHF radicals (reactions 56, 67, 68, 82, 83, 90) and C-C β-scission of the methyl side group (reaction 74) in the case of tetrahydro-2-methyl-3-furanyl. Note that the decomposition of MTHF radicals is more detailed in this new kinetic model compared to the model proposed by Moshammer et al.[17].

The ring-opened MTHF radicals can fragment by β-scission or react by intramolecular hydrogen abstraction and intramolecular radical addition. Ring opening of tetrahydro-2-methyl-4-furanyl and subsequent decomposition is presented as example in Figure 4.3-4. The dominant consumption path of 1-allyloxy-ethyl radical, formed by C-C β-scission of

tetrahydro-2-methyl-4-furanyl, is C-O β-scission to acetaldehyde plus allyl. A minor path is exo-intramolecular radical addition to 3-methylene-2-methyl-oxetane. The latter radical is also formed by exo-intramolecular radical addition of the 3-buten-2-yloxy-methyl radical, formed by C-C β-scission of tetrahydro-2-methyl-3-furanyl. Hence, tetrahydro-2-methyl-3-furanyl and tetrahydro-2-methyl-4-furanyl can interconvert with 3-methylene-2-methyl-oxetane as intermediate. Decomposition of 4-penten-2-oxy, formed by C-O β-scission of tetrahydro-2-methyl-4-furanyl, by C-C β-scission to acetaldehyde and allyl is favored over C-C β-scission to 3-butenal plus methyl, intramolecular hydrogen abstraction to 2-hydroxy-4-penten-3-yl and exo-intramolecular radical addition to 2-methylene-4-methyl-oxetane. The latter radical is also formed by exo-intramolecular radical addition of the 2-vinyloxy-propyl radical, formed by C-C β-scission of tetrahydro-2-methyl-5-furanyl. Hence, tetrahydro-2-methyl-5-furanyl and tetrahydro-2-methyl-4-furanyl can interconvert with 2-methylene-4-methyl-oxetane as intermediate.

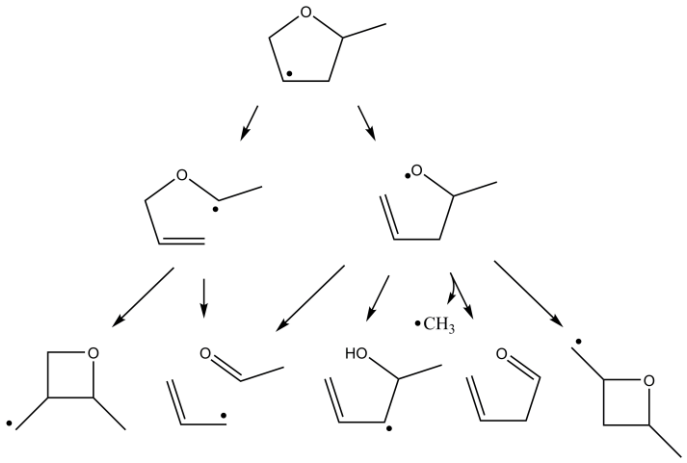

Figure 4.3-4 Unimolecular consumption reactions of tetrahydro-2-methyl-4-furanyl and derived radicals

At the investigated operating conditions, β-scission reactions of the radicals formed following ring opening of tetrahydro-2-methyl-2-furanyl, tetrahydro-2-methyl-3-furanyl, tetrahydro-2-methyl-4-furanyl and tetrahydro-2-methyl-5-furanyl are kinetically favored over intramolecular hydrogen abstraction and radical addition reactions. Only in the case of 3-vinyloxy-propyl, which is formed by C-C β-scission of the 2-methylene-tetrahydrofuran radical, endo-intramolecular radical addition to tetrahydro-2-pyranyl is favored over C-C β-scission to vinyloxy-methyl plus ethene below 1050 K.

4.3.5.1.4 Substitution of hydrogen atom on MTHF

As will be discussed in 4.3.6.1, water yields are underpredicted in pyrolysis conditions. Hydrogen atom addition on the ring oxygen atom of MTHF forms 2-pentyl-5-ol, reaction 98. The latter radical can react by subsequent C-C β-scissions forming two ethene molecules plus hydroxyl radical. The calculated reaction rate coefficient for reaction 98 is five orders lowers than the competing hydrogen abstraction reactions. Therefore, this reaction path does not contribute significantly to hydroxyl radical and water formation.

4.3.5.2 Base mechanism

The mechanism developed for propene oxidation and combustion by Burke et al. served as reaction base [38, 39]. This model was developed hierarchically and has been validated for hydrogen, methane, ethane, ethene, propene, methanol, ethanol and acetaldehyde combustion.

4.3.5.3 Secondary mechanism

The third part of the developed kinetic model is a secondary mechanism which contains the reactions of species formed in the primary mechanism and for which no consumption routes are included in the base mechanism.

Submechanisms for tetrahydrofuran and tetrahydropyran pyrolysis and combustion were taken from recently developed kinetic models by Tran et al.[10, 35]. Isomerization of alkylated dihydrofurans were implemented as suggested by Dubnikova and Lifshitz [40]. Rate coefficients for reactions describing the decomposition of aldehydes and ketones, products detected in the premixed laminar low-pressure flames, were estimated using the EXGAS database [41].

Pathways to benzene were included in the developed kinetic model. Self-recombination of allyl radicals followed by hydrogen abstraction and addition of vinyl on 1,3-butadiene lead to 2,5-hexadien-1-yl which can react to cyclohexen-3-yl by intramolecular radical addition. Subsequent dehydrogenation steps of cyclohexen-3-yl lead to benzene. Reaction rate coefficients were taken from Wang et al. [42, 43]. Recombination of cyclopentadienyl with methyl, followed by hydrogen abstraction and ring enlargement is another possible formation pathway for benzene. Reaction rate coefficients were taken from Green and coworkers [44, 45]. Reactions involving propargyl are known to be important for benzene formation in

flames. Kinetics regarding self-recombination of propargyl radicals and recombination of propargyl with allyl were taken from Georgievskii et al.[46] and Miller et al. [47].

4.3.5.4 Thermochemistry and transport data

Thermochemical data for species and radicals were taken from extensive databases whenever possible[48, 49]. Otherwise, this data was calculated using the software THERGAS [50] which is based on the group additivity method proposed by Benson [51].

Thermochemistry for MTHF was taken from the Third Millennium Thermochemical Database [48]. The enthalpy of formation at 298K is -225.1 kJ mol^{-1}, which agrees well with the recommended value of -225.4 kJ mol^{-1} by Simmie [14] and -228.4 kJ mol^{-1} by Wijaya et al. [52].

Transport properties of species, for which no data is available from literature, were estimated using the RMG TransportDataEstimator [53].

4.3.6 Results and discussion

The pyrolysis results obtained in a flow reactor and combustion results obtained in low-pressure and atmospheric premixed flames are presented in this section.

4.3.6.1 Thermal decomposition of MTHF in a tubular flow reactor

4.3.6.1.1 Experimental and simulated results

An experimental dataset was obtained for the pyrolysis of MTHF in a tubular flow reactor, described in section 4.3.3.1. The pressure was kept constant at 0.17 MPa. MTHF and N_2 inlet molar flow rates correspond to 1.67 10^{-4} and 1.67 10^{-3}mol s^{-1} respectively. The temperature was varied between 900 and 1100 K. Besides hydrocarbons, several oxygenated products were detected in the reactor effluent, including CO, H_2O, formaldehyde, acetaldehyde, ketene and 4-penten-1-ol.

Figure 4.3-5 shows the experimental and model calculated mole fraction profiles of MTHF and a selected number of product species as a function of temperature. The calculated conversion profile agrees well with the experimental data. Furthermore, the model is in qualitative agreement with the experimental product profiles, i.e. it is able to capture the effect of temperature on mole fractions. The model is also in qualitative agreement with most product mole fraction profiles, the main exception being H_2O, see Figure 4.3-5 (C), which is

underpredicted by a factor 4 and ketene, see Figure 4.3-5 (I), which is overpredicted by a factor 2. Note that calibration factor for ketene was determined using the effective carbon number approach, as mentioned 4.3.3.1. This is a rough approximation and, therefore, the uncertainty on the experimental ketene yield is substantial.

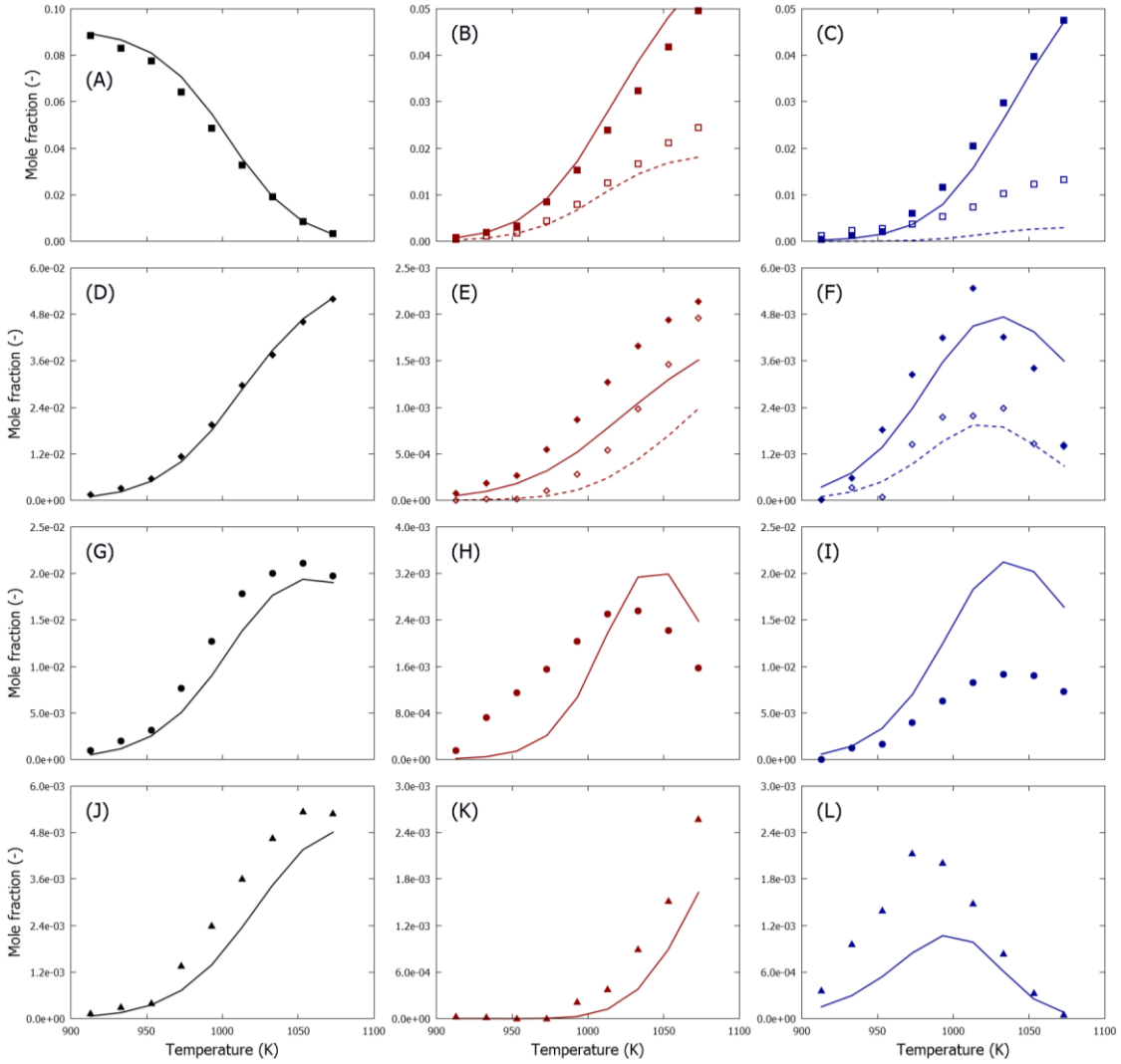

Figure 4.3-5 Mole fractions as a function of temperature for MTHF pyrolysis in a tubular reactor, P=0.17 MPa, F_{MTHF}=1.67 10^{-4} mol s^{-1}, F_{N2}=1.67 10^{-3} mol^{-1}: ■ - MTHF (A), ■ - CH_4 (B),□ - H_2 (B),■ - CO (C),□ - H_2O (C), ◆ - C_2H_4 (D), ◆ - C_2H_6 (E), ◇ - C_2H_2(E),◆ - acetaldehyde (F),◇ - formaldehyde (F),● - C_3H_6 (G), ● - 1-butene (H), ● - ketene (I), ▲ - 1,3-butadiene (J), ▲ - benzene (K), ▲ - 4-penten-1-ol (L); lines, mole fraction profiles calculated with CHEMKIN-PRO using the plug flow reactor model and the developed kinetic model, discussed in section 4.3.5

4.3.6.1.2 Reaction path analysis

A first reaction path analysis was performed with CHEMKIN-PRO using the plug flow reactor model and operating conditions corresponding to P = 0.17 MPa, T = 1000K, F_{MTHF} = 1.67 10^{-4} mol s^{-1}, F_{N2}= 1.67 10^{-3} mol s^{-1} at the inlet of the reactor, see Figure 4.3-6.

The unimolecular decomposition of MTHF is dominated by the pericyclic ring opening reaction forming 4-penten-1-ol, where a hydrogen atom of the methyl group bridges to the ring oxygen, and C-C scission forming tetrahydro-2-furanyl plus methyl. At 1000K, these paths account for respectively 61 % and 38 % of the total unimolecular decomposition rate. Scission of the ring bonds forming carbene and biradical intermediates and pericyclic ring opening reactions involving hydrogen atoms of ring carbon atoms contribute less than 1% of the total unimolecular decomposition rate. Note that latter reactions are significant in the pyrolysis of THF [8]. Hence, the presence of a methyl-group in MTHF completely changes the unimolecular decomposition paths compared to THF.

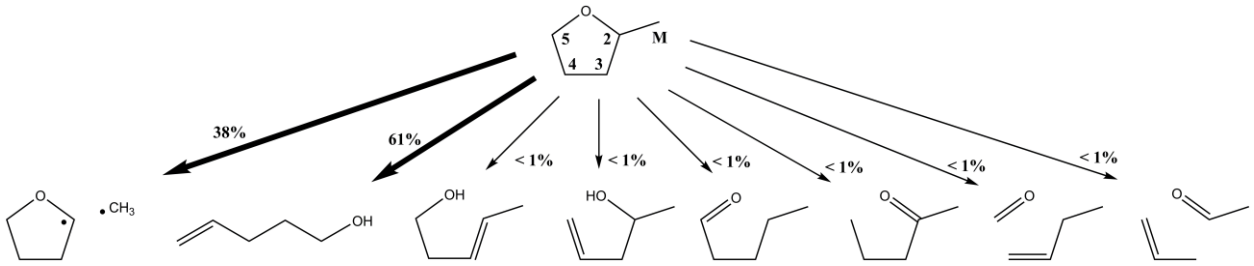

Figure 4.3-6 Main reaction paths in MTHF pyrolysis, identified using CHEMKIN-PRO. Operating conditions correspond to P = 0.17 MPa, T = 1000K, F_{MTHF} = 1.67 10^{-4} mol s^{-1}, F_{N2}= 1.67 10^{-3} mol s^{-1}, $conversion_{MTHF}$= 0%. A percentage next to a reaction pathway represents the rate of that reaction relative to the total MTHF consumption rate.

A second reaction path analysis was performed with CHEMKIN-PRO using the plug flow reactor model and operating conditions corresponding to P = 0.17 MPa, T = 1000 K, F_{MTHF} = 1.67 10^{-4} mol s^{-1}, F_{N2}= 1.67 10^{-3} mol s^{-1}, $conversion_{MTHF}$= 10% .The main reaction pathways from MTHF are presented in Figure 4.3-7.

In these conditions, a radical pool is established and 91 % of MTHF is consumed by hydrogen abstraction reactions. Ring opening to 4-penten-1-ol and C-C scission of the methyl side-group correspond to 6 and 3 % of the total MTHF consumption respectively.

The main hydrogen abstracting species are methyl radicals and hydrogen atoms. Hydrogen abstraction from carbon atom 2 is favored, followed by carbon atoms 5, 4, 3 and the methyl carbon atom.

Tetrahydro-2-methyl-2-furanyl mainly reacts by C-O β-scission, forming 2-oxo-pent-5-yl. At 1000K, the rate coefficient is 200 times larger than the rate coefficient of the competing C-C β-scission and 2E+6 times larger than the rate coefficient of the competing C-H β-scission to 5-methyl-2,3-dihydrofuran, see Table 4.3-2. The 2-oxo-pent-5-yl radical can form ethene plus

2-oxo-propyl by C-C β-scission. This path contributes for approximately 70% of the total ethene formation rate.

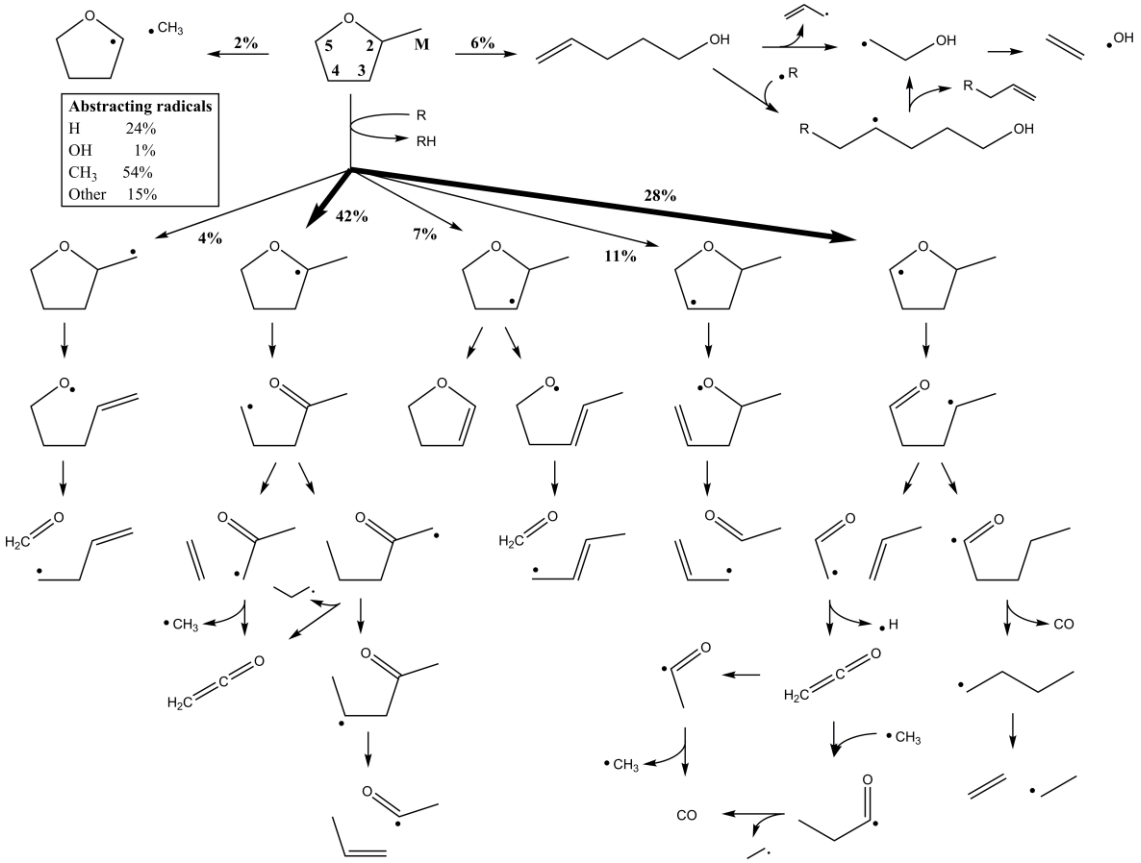

Figure 4.3-7 Main reaction paths in MTHF pyrolysis, identified using CHEMKIN-PRO. Operating conditions correspond to P = 0.17 MPa, T = 1000K, F_{MTHF} = 1.67 10^{-4} mol s^{-1}, F_{N2}= 1.67 10^{-3} mol s^{-1}, $conversion_{MTHF}$= 10%. A percentage next to a reaction pathway represents the rate of that reaction relative to the total MTHF consumption rate.

Tetrahydro-2-methyl-5-furanyl mainly reacts by C-O β-scission, forming 1-oxo-pent-4-yl. Consumption of 1-oxo-pent-4-yl is dominated by C-C β-scission to propene plus vinoxy and intramolecular hydrogen abstraction to 1-oxo-pent-1-yl. The former path contributes for approximately 50% of the total propene formation rate. 1-oxo-pent-1-yl rapidly forms 1-butyl plus CO following CO α-scission. C-C β-scission of 1-butyl to ethene plus ethyl radical and C-H β-scission of ethyl to ethene plus hydrogen atom contribute for approximately 25% of the total ethene formation rate.

The other three MTHF-radicals, tetrahydro-2-methyl-3-furanyl, tetrahydro-2-methyl-4-furanyl and 2-methylene-tetrahydrofuran, are formed in lower amounts. Decomposition of tetrahydro-2-methyl-4-furanyl and 2-methylene-tetrahydrofuran by C-O β-scission forms formaldehyde plus but-1-en-3-yl and formaldehyde plus but-1-en-4-yl respectively. Formaldehyde is almost exclusively formed by the latter two pathways, which is accurately predicted by the kinetic

model. Decomposition of tetrahydro-2-methyl-4-furanyl by C-O β-scission is the main source of acetaldehyde, next to hydrogen abstraction by 2-oxo-ethyl from MTHF.

Water is formed by hydrogen abstraction of hydroxyl radicals. Hydroxyl is formed by several consumption pathways of 4-penten-1-ol. C-C scission of 4-penten-1-ol, forming allyl plus 2-hydroxy-ethyl, and radical addition on the terminal carbon atom of the C=C double bond followed by C-C β-scission contribute for approximately 90% of the total 4-penten-1-ol consumption. Both pathways form 2-hydroxy-ethyl which is the main source of hydroxyl radicals, through C-O β-scission forming ethene as second product. Water yields are, thus, highly sensitive to the formation of 4-penten-1-ol. The experimental yield of the latter molecule is underpredicted by the kinetic model, especially at the lowest investigated temperatures. As mentioned in 4.3.5.1, 4-penten-1-ol is formed by a concerted ring opening reaction of MTHF. Obviously, increasing the corresponding reaction rate coefficient would have a beneficial effect on the model performance regarding 4-penten-1-ol and water.

Ketene is formed by C-H β-scission of 2-oxo-ethyl and C-C β-scission of 2-oxo-propyl. The overprediction of oxygen selectivity towards ketene matches the underprediction of oxygen selectivity towards water. Note that both 2-oxo-ethyl and 2-oxo-propyl are formed by hydrogen abstraction from MTHF and subsequent β-scission reactions. Hence, increasing the fraction of MTHF that reacts by unimolecular decomposition would reduce the fraction of MTHF that reacts by hydrogen abstraction and, thus, reduce ketene yields.

4.3.6.2 Combustion of MTHF in low-pressure premixed flat flame

4.3.6.2.1 Experimental and simulated results

The chemical structure of MTHF flames were investigated at three equivalences ratios, which are φ=0.7, 1.0 and 1.3. Some 50 species were identified and quantified. Compared to the experimental pyrolysis results, a considerably higher number of oxygenated molecules were detected and quantified. Figure 4.3-8, Figure 4.3-9, Figure 4.3-10 and Figure 4.3-11 present mole fraction profiles of feed molecules and products as a function of distance above the burner. The selected products in these figures have high yields and/or are important intermediates according to reaction path analysis.

MTHF, see Figure 4.3-8 (A), is completely consumed at a height of 2.0 mm above the burner which corresponds with temperatures higher than 1200K in the flame. Model calculated mole

fraction profiles of complete-combustion products CO_2 and H_2O, see Figure 4.3-8 (B), and CO and H_2, see Figure 4.3-8 (C), agree well with experimental mole fraction profiles.

Experimental yields of most hydrocarbon products and oxygenated molecules have maxima at a height of approximately 2.0 mm above the burner.

The kinetic model is in qualitative agreement with the experimental data of all hydrocarbon products, see Figure 4.3-8 and Figure 4.3-9. As mentioned earlier, the volumetric flow rate of the unburned gas was constant for all equivalence ratios. At fuel-rich conditions (φ=1.3), the operating conditions caused the flame to be relatively close to the burner; therefore, flame temperature and species profiles were significantly disturbed by the sampling probe resulting in a higher experimental error. For propene, 1-butene and 1,3-butadiene, model agreement deteriorates at higher equivalence ratios, underpredicting the experimental mole fraction profile. Interestingly, at the fuel-rich conditions (φ = 1.7) by Moshammer at al. [17], model calculated mole fraction profile for propene is in good agreement with the experimental data while 1-butene and 1,3-butadiene yields are overpredicted, see Figure 4.3-12.

Aldehydes, having between one and five carbon atoms, were detected in the reactor effluent. Experimental and model calculated mole fraction profiles are presented in Figure 4.3-10. The model calculated peak in 2-butenal is approximately a factor 5 larger than experimental observations. A similar overprediction is observed for 2,3-dihydrofuran, see Figure 4.3-11 (E). Tran et al. proposed that 2,3-dihydrofuran rapidly isomerizes to cyclopropanecarboxaldehyde and 2-butenal [10]. In their modeling of low-pressure premixed tetrahydrofuran flames, the same disagreement for 2-butenal and 2,3-dihydrofuran was observed. Note that in this work, reactions and associated rate coefficients for consumption of 2,3-dihydrofuran, 2-butenal and cyclopropanecarboxaldehyde were adopted from Tran et al. [10].

A second class of oxygenated molecules in the reactor effluent is ketones. Note that acetone was the only ketone measured in tetrahydrofuran premixed laminar flames and its maximum mole fraction is approximately a factor 10 lower than what is measured here, under comparable conditions. Model calculated mole fraction profiles are in relatively good agreement with experimental mole fraction profiles, see Figure 4.3-11.

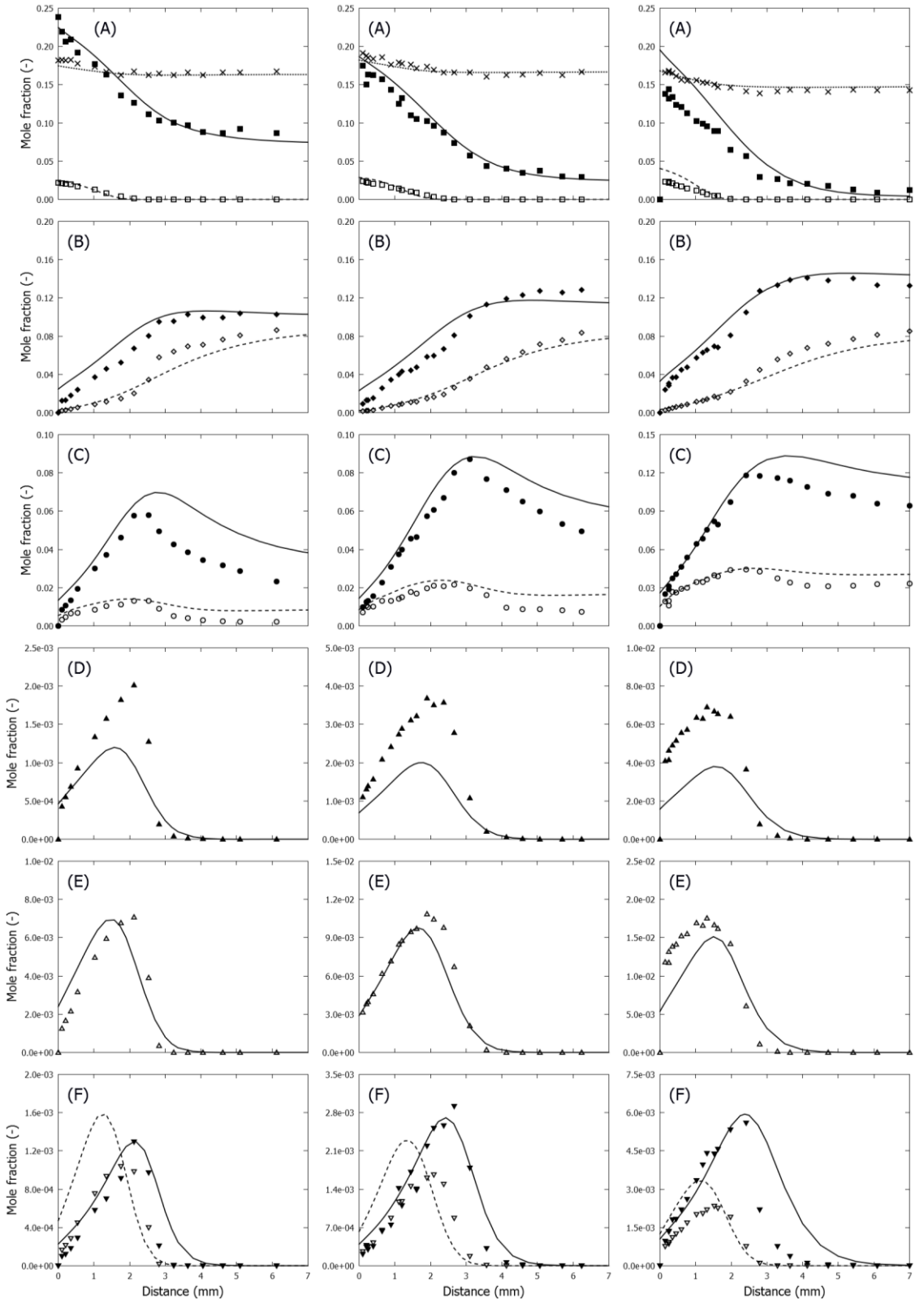

Figure 4.3-8 Mole fraction profiles as a function of height above burner for φ = 0.7 (left), φ = 1.0 (middle) and φ = 1.3 (right): ■ - O_2 (A), □- MTHF (A), ✕- Argon/4 (A), ◆- H_2O (B), ◇ - CO_2 (B), ● - CO (C), ○ - H_2 (C), ▲ - CH_4 (D), △ - C_2H_4 (E), ▼ - C_2H_2 (F), ▽ - C_2H_6 (F); lines, mole fraction profiles calculated with CHEMKIN using the premixed laminar flame model and the developed kinetic model, discussed in section 4.3.5

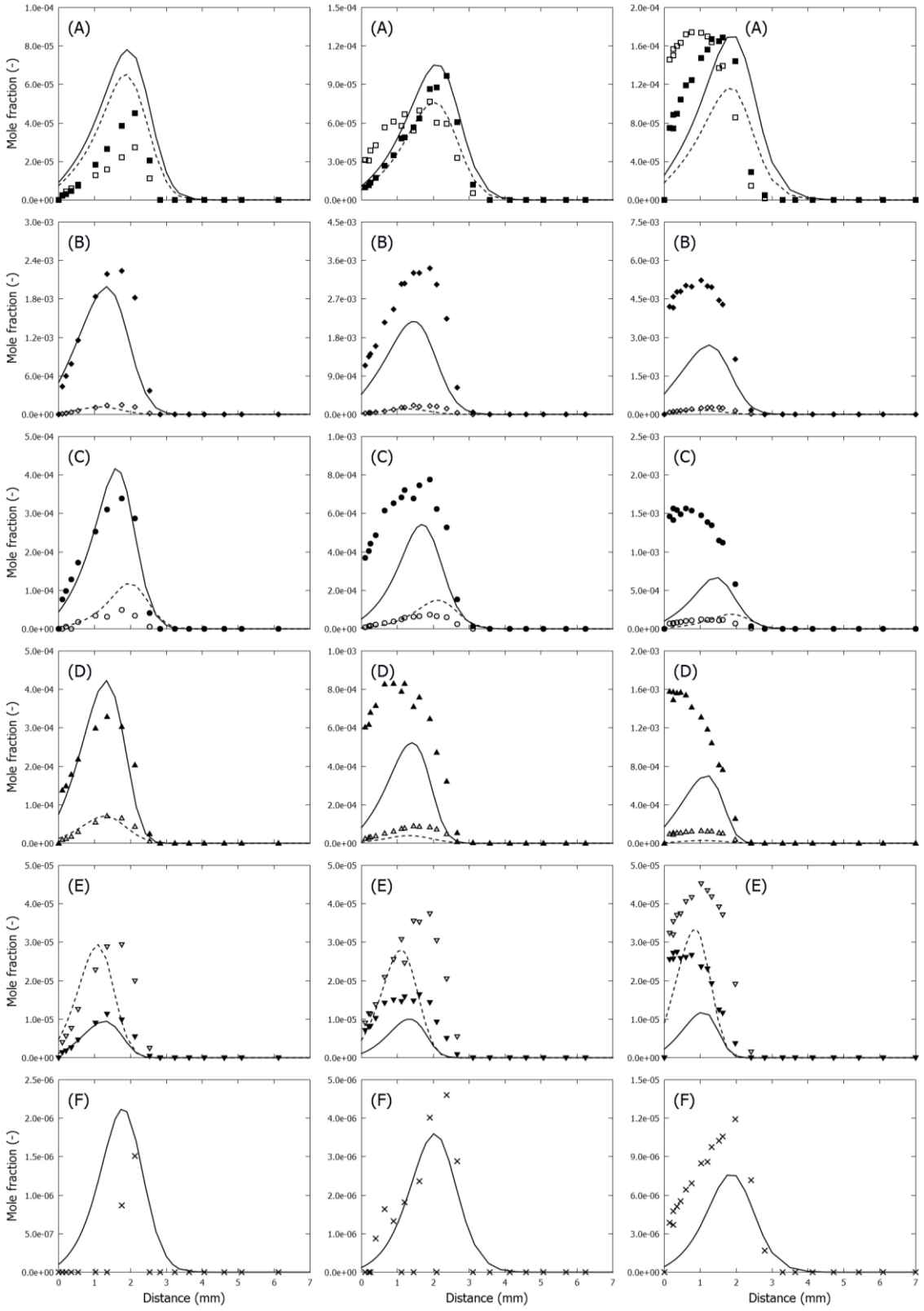

Figure 4.3-9 Mole fraction profiles as a function of height above burner for φ = 0.7 (left), φ = 1.0 (middle) and φ = 1.3 (right): ■ - allene (A), □- propyne (A), ◆ - C_3H_6 (B), ◇ - C_3H_8 (B), ● - 1,3-butadiene (C), ○ - 1,2-butadiene x 10 (C), ▲ - 1-butene (D), △ - 2-butene (D), ▼ - 1-pentene (E), ▽- 2-pentene (E), ✕- benzene (F); lines, mole fraction profiles calculated with CHEMKIN using the premixed laminar flame model and the developed kinetic model, discussed in section 4.3.5

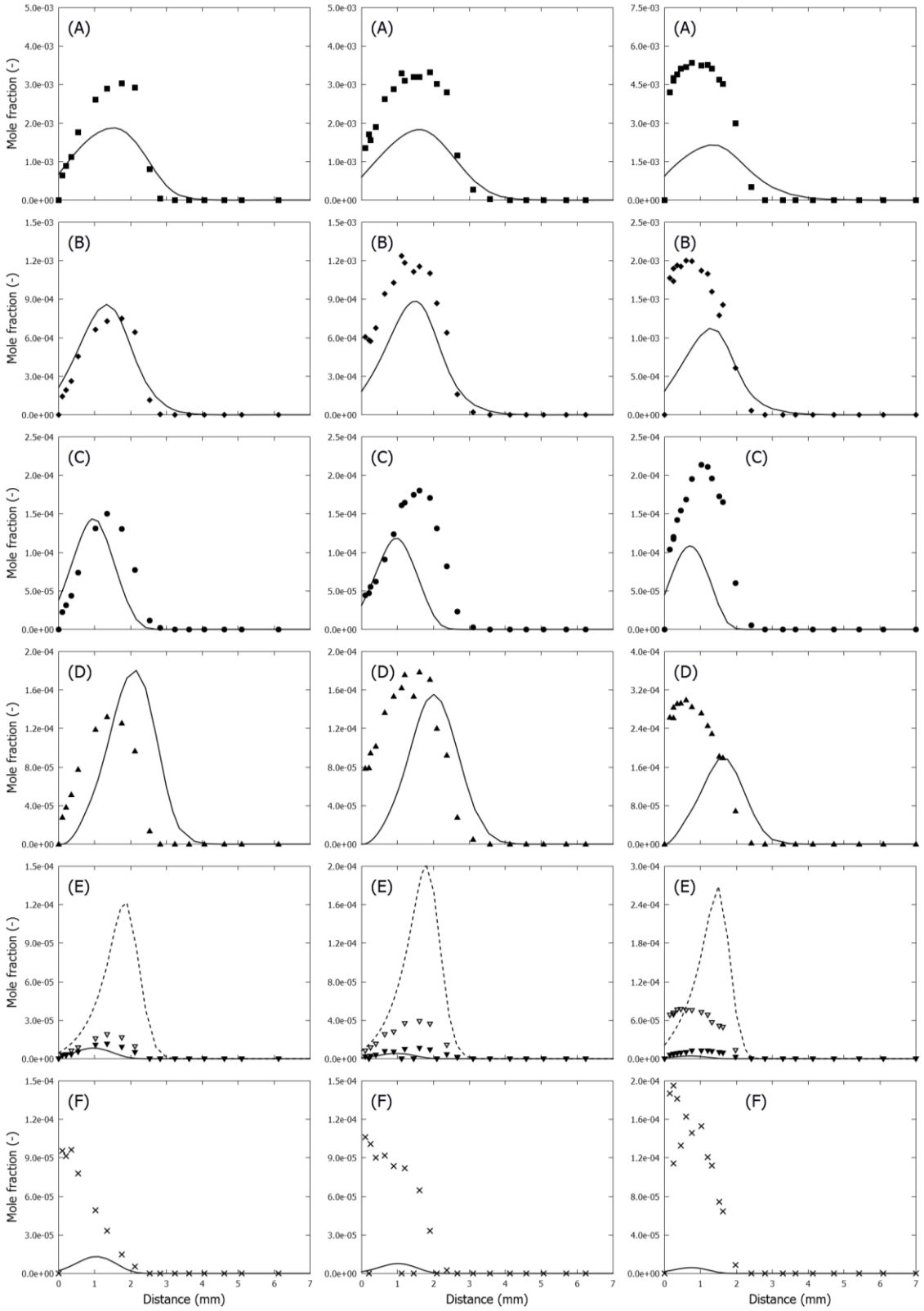

Figure 4.3-10 Mole fraction profiles as a function of height above burner for φ = 0.7 (left), φ = 1.0 (middle) and φ = 1.3 (right): ■ - formaldehyde (A), ◆ - acetaldehyde (B), ● - propanal (C), ▲ - acrolein (D), ▼ - butanal (E), ▽ - 2-butenal (E), ✕ - pentenal (F); lines, mole fraction profiles calculated with CHEMKIN using the premixed laminar flame model and the developed kinetic model, discussed in section 4.3.5

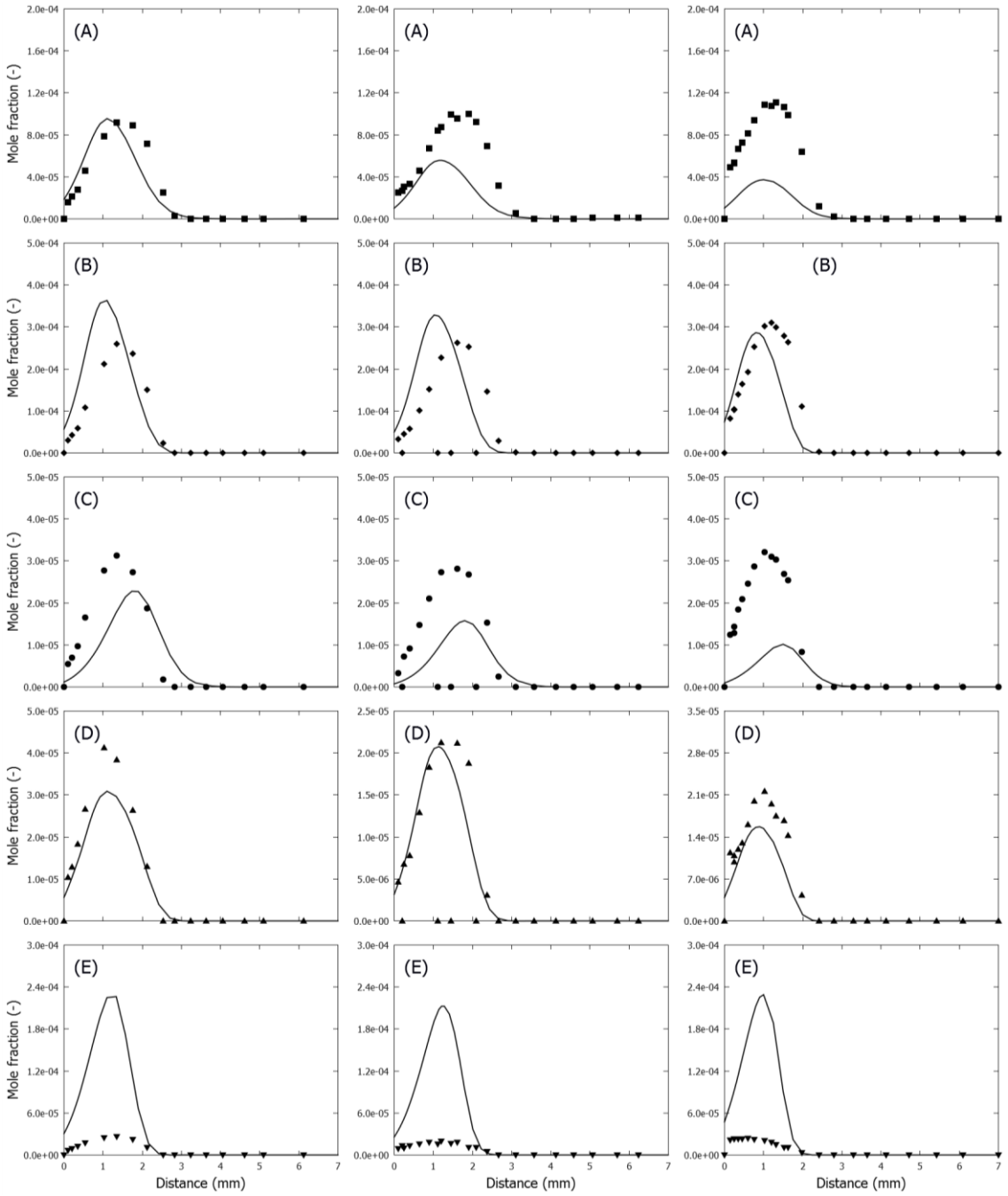

Figure 4.3-11 Mole fraction profiles as a function of height above burner for φ = 0.7 (left), φ = 1.0 (middle) and φ = 1.3 (right): ■ - acetone (A), ◆ - butanone (B), ● - butenone (C), ▲ - 2-pentanone (D), ▼ - 2,3-dihydrofuran (E) ; lines, mole fraction profiles calculated with CHEMKIN using the premixed laminar flame model and the developed kinetic model, discussed in section 4.3.5

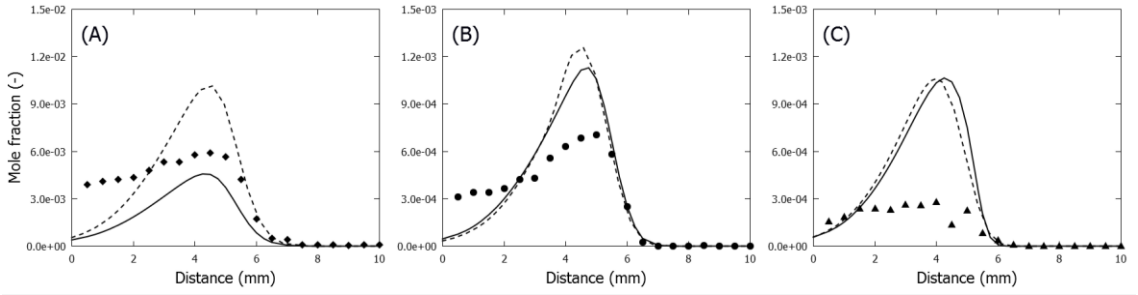

Figure 4.3-12 Mole fraction profiles as a function of height above burner for φ = 1.7 using synchrotron-based tunable VUV PI-MBMS obtained by Moshammer et al.[17]: ◆-propene (A), ● - 1,3-butadiene (B), ▲ - 1-butene (C); lines, mole fraction profiles calculated with CHEMKIN using the premixed laminar flame model: ——- the developed kinetic model, discussed in section 4.3.5, - - - - the kinetic model developed by Moshammer et al. [17]

4.3.6.2.2 Reaction path analysis

A reaction path analysis was performed with CHEMKIN-PRO using the premixed laminar flame model and operating conditions: φ=1 and $conversion_{MTHF}$=90 % . This corresponds to a height of 1.8 mm above the burner and a temperature of approximately 1300K. Most products have a maximum in their mole fraction profile at these conditions. The reaction path analysis helps to identify the dominant product formation paths. This is presented in Figure 4.3-13.

The MTHF consumption reactions resemble those in pyrolysis.

Compared to pyrolysis, a higher fraction of MTHF is consumed by C-C scission of the methyl side-group. The latter reaction has a high activation energy and therefor has a higher flux in the high temperature flames compared to the relatively low-temperature pyrolysis experiments. Ring opening to 4-penten-1-ol accounts for less than 1% of the total MTHF consumption at the conditions investigated in Figure 4.3-13. 4-penten-1-ol is rapidly consumed, e.g. by scission of the weak allyl – 2-hydroxy-ethyl bond in 4-penten-1-ol. The peak in model calculated mole fraction profile is below 10 ppm, explaining why it was not possible to identify and quantify this species experimentally.

The majority of MTHF is consumed by hydrogen abstraction. Hydrogen atoms are the main hydrogen abstracting radicals, followed by hydroxyl. Hydrogen abstraction from MTHF by methyl, the main hydrogen abstracting radical in the pyrolysis conditions investigated in Figure 4.3-7, is now insignificant. Methyl is mainly consumed by reaction with oxygen and recombination with other radicals. Methyl plus atomic oxygen to formaldehyde plus atomic hydrogen is the main source of formaldehyde at the reactor conditions of Figure 4.3-13, rather than formation by decomposition of MTHF radicals.

Hydrogen abstraction from MTHF forming tetrahydro-2-methyl-2-furanyl is favored, but less pronounced compared to the pyrolysis conditions investigated in Figure 4.3-7. The higher temperature in the MTHF flame and the high contribution of hydroxyl radicals to the total hydrogen abstraction rate decrease selectivity to tetrahydro-2-methyl-2-furanyl.

Obviously, the same radicals and molecules are formed following ring opening and C-O/C-C β-scission of MTHF radicals in the MTHF flame and pyrolysis. Their formation paths will not be repeated here. The presence of molecular oxygen and the augmented radical concentration in the MTHF flames, given the higher temperature and lower pressure, changes the consumption of primary radicals and molecules. This is especially the case for the resonantly stabilized radicals allyl, 2-oxo-ethyl and 2-oxo-propyl. Consumption pathways of the latter 3 radicals are emphasized in Figure 4.3-13.

The majority of allyl radicals reacts by recombination. Recombination with hydrogen atoms and methyl radicals are important allyl consumption routes. These paths accounts for 25% of the total propene formation and 90% of the total 1-butene formation, respectively, at the given conditions. Hydrogen abstraction from 1-butene and subsequent C-H β-scission is an important source of 1,3-butadiene. Hence, formation paths of propene, 1-butene and 1,3-butadiene, for which model disagreement increased with increasing equivalence ratio, are all linked to these allyl recombination reactions. Other allyl consumptions to products presented in Figure 4.3-8, Figure 4.3-9, Figure 4.3-10 and Figure 4.3-11 are allyl plus ethyl to 1-pentene, allyl plus atomic oxygen to acrolein plus atomic hydrogen, recombination of allyl plus hydroperoxy which eventually forms acrolein, a hydrogen atom and a hydroxyl radical following decomposition of the hydroperoxide [54].

The 2-oxo-ethyl radical is mainly formed by decomposition of the 2-methyl-5-furanyl radical. The 2-oxo-ethyl radical is resonantly stabilized and, thus, has a relatively long lifetime. It mainly forms methyl plus CO and ketene plus hydrogen atom [55], Recombination reactions with hydrogen atom, methyl, ethyl and allyl form acetaldehyde, propanal, butanal and 4-pentenal respectively, see Figure 4.3-10.

The 2-oxo-propyl radical is formed by decomposition of the tetrahydro-2-methyl-2-furanyl radical. It mainly reacts by C-C β-scission forming ketene and methyl, similar as in pyrolysis. Recombination with hydrogen, methyl and ethyl forms acetone, butanone and 2-pentanone respectively, see Figure 4.3-11.

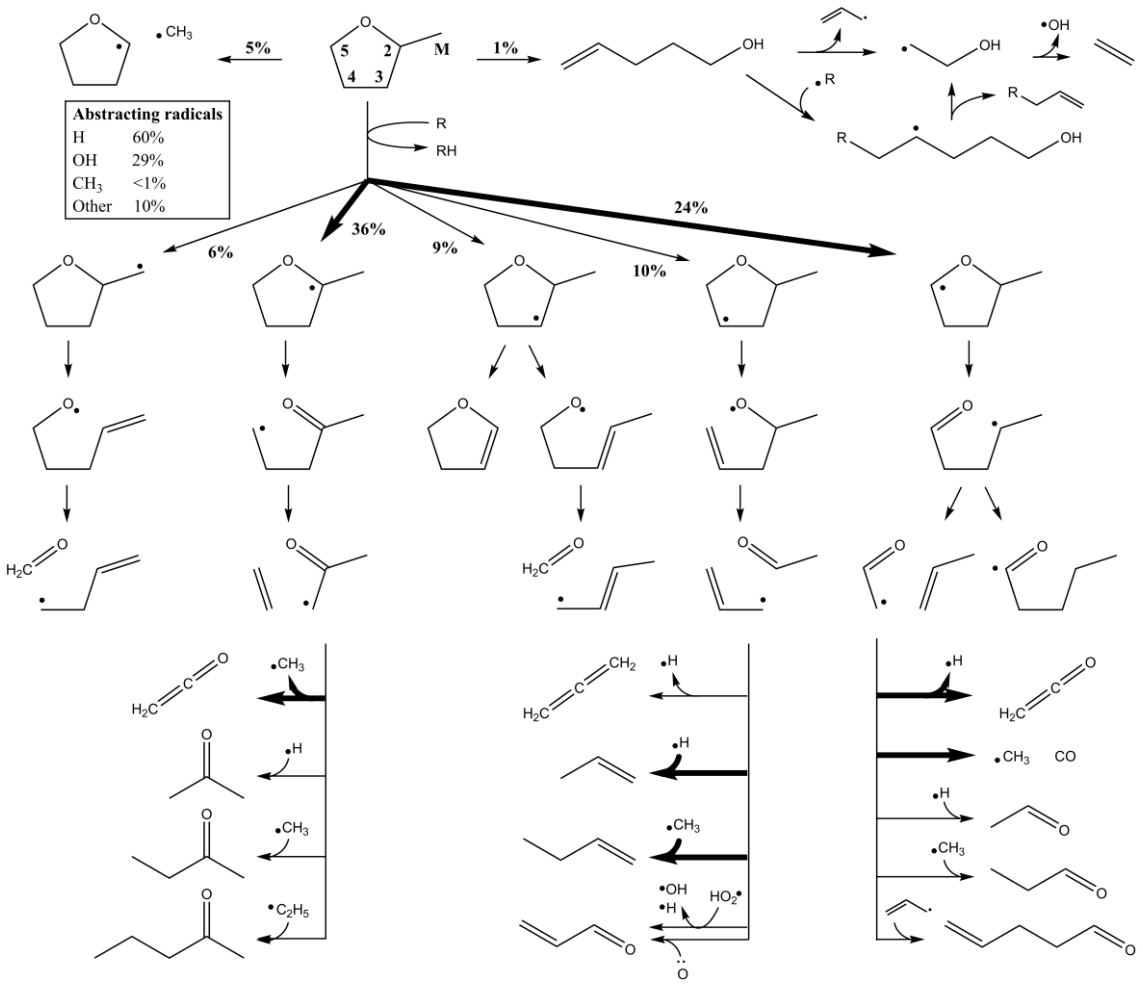

Figure 4.3-13 Main reaction paths in MTHF premixed low-pressure laming flames, identified using CHEMKIN-PRO. Operating conditions correspond to P = 6.66 kPa, T = 1300K, h = 1.8mm, conversion$_{MTHF}$= 90%. A percentage next to a reaction pathway represents the rate of that reaction relative to the total MTHF consumption rate.

4.3.6.3 Laminar burning velocities of MTHF at atmospheric pressure

4.3.6.3.1 Experimental and simulated results

To our knowledge, no investigation on the adiabatic laminar burning velocities of MTHF in air has been published prior to the present study. Experimental data for the adiabatic laminar burning velocities of MTHF-air mixtures were measured on a flat flame burner at atmospheric pressure, with unburned gas temperatures ranging between 298 and 398 K and equivalence ratios ranging between 0.6 and 1.55.The obtained results are displayed in Figure 4.3-14. These profiles exhibit maxima at φ = 1.1, similar to most hydrocarbons and oxygenated molecules [56].

Model calculated laminar burning velocities are added to Figure 4.3-14. Satisfactory agreement is observed for all unburned gas temperatures and equivalence ratios.

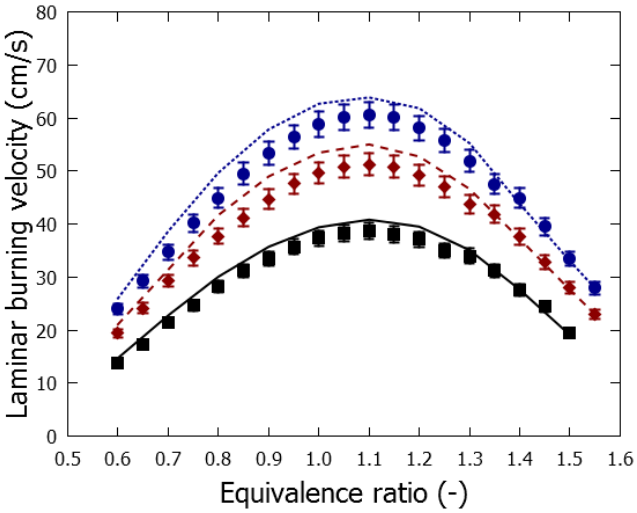

Figure 4.3-14 Laminar burning velocities for MTHF–air flames at 0.101 MPa: ■ - unburned gas temperature of 298K, ◆- unburned gas temperature of 358K, ● - unburned gas temperature of 398K; lines, profiles calculated with CHEMKIN using the premixed laminar flame model and the developed kinetic model, discussed in section 4.3.5

4.3.6.3.2 Sensitivity analysis

A sensitivity analysis with respect to laminar burning velocity was performed at an unburned gas temperature of 298K and equivalence ratio of 1.1. Such an analysis is able to identify reactions that influence laminar burning velocity most significantly. Selected results are presented in Figure 4.3-15. A reaction with a positive sensitivity coefficient indicates that raising the associated pre-exponential factor increases the laminar burning velocity, a reaction with a negative sensitivity coefficient indicates that reducing the associated pre-exponential factor increases the laminar burning velocity.

Laminar burning velocities are mainly controlled by reactions of small species [56]. Also in this work, the chain branching reaction of molecular oxygen with a hydrogen atom forming atomic oxygen and a hydroxyl radical is the most sensitive reaction for laminar burning velocities. Other sensitive reactions involve the consumption and production of hydrogen atoms, as these can react with molecular oxygen through the aforementioned chain branching reaction. For example, decomposition of the formyl radical has a positive sensitivity coefficient as this produces a hydrogen atom while reaction of the formyl radical with a hydrogen atom to carbon monoxide and molecular hydrogen has a negative sensitivity coefficient as this consumes a hydrogen atom and a formyl radical, which could otherwise decompose forming a hydrogen atom.

Some reactions that are related to MTHF consumption are displayed in Figure 4.3-15. As discussed previously, MTHF produces high yields of ketene via C-C β-scission of 2-oxo-propyl and C-H β-scission of 2-oxo-ethyl. Ketene can be consumed by hydrogen abstraction by hydrogen atoms and by hydrogen addition forming 1-oxo-ethyl. The former reaction has a positive sensitivity coefficient as the resulting ketenyl react can react with molecular oxygen forming carbon monoxide, carbon dioxide plus a hydrogen atom [57] while the latter reaction has a negative sensitivity coefficient as 1-oxo-ethyl forms a relatively unreactive methyl radical by CO α-scission, which can recombine with a hydrogen atom forming methane.

The recombination of allyl radical, which is formed by decomposition of the tetrahydro-2-methyl-4-furanyl radical and by hydrogen abstraction from propene, with a hydrogen atom has negative sensitivity coefficient as it results in a decrease of radicals in the reactive system. Scission of MTHF to methyl plus tetrahydro-2-furanyl radicals has a positive sensitivity coefficient as it results in an increase of radicals in the reactive system.

Hydrogen abstraction from MTHF by hydrogen atoms forming tetrahydro-2-methyl-2-furanyl and tetrahydro-2-methyl-5-furanyl are displayed in Figure 4.3-15. The former radical mainly decomposes to ethene while the latter radical mainly decomposes to propene. Hydrogen abstraction from ethene yields vinyl radicals, which may form hydrogen atoms upon C-H β-scission or lead to chain branching by reaction with molecular oxygen [58]. Consumption of propene by hydrogen abstraction creates unreactive allyl radicals.

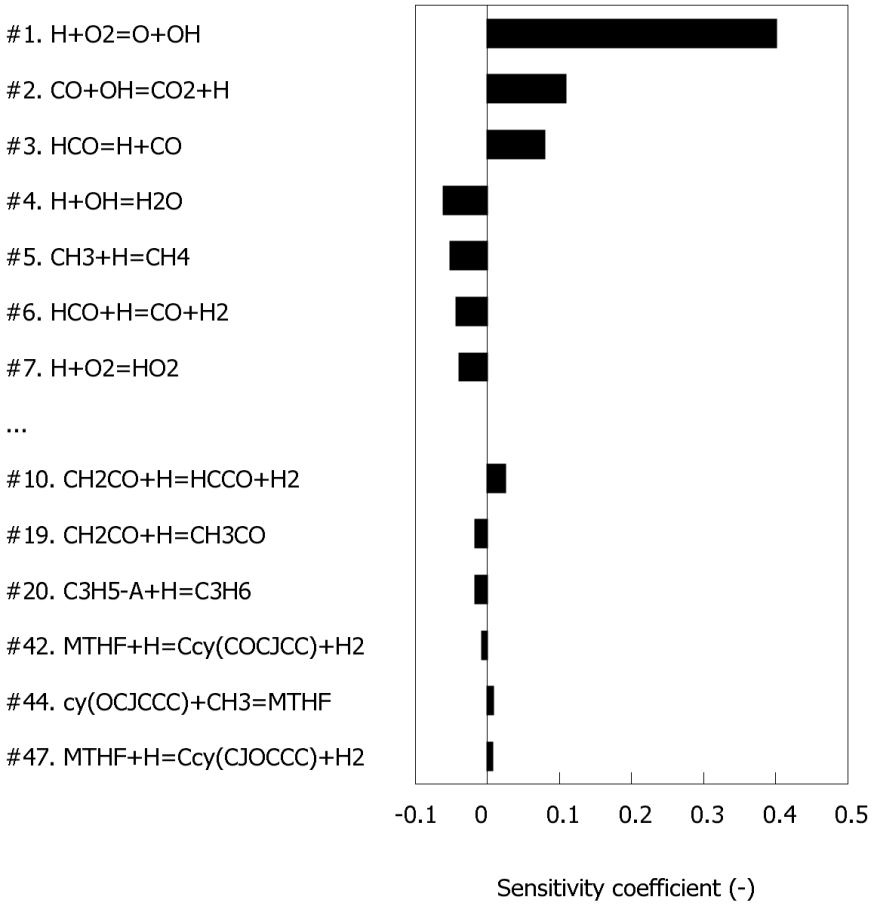

Figure 4.3-15 Sensitivity coefficients for MTHF laminar burning velocities. Operating conditions correspond to φ = 1.1, P = 0.101 MPa and unburned gas temperature of 298K. Coefficients for the seven most sensitive reactions and coefficients for six other reactions, related to consumption of MTHF and related decomposition products, are displayed.

4.3.6.3.3 Comparison of adiabatic laminar burning velocity with other cyclic biofuels

The adiabatic laminar burning velocities of several other cyclic oxygenated biofuels have been investigated using the same experimental setup and similar operating conditions. These biofuels include tetrahydrofuran [10], tetrahydropyran [35], 2-methyl-furan [59], and 2,5-dimethylfuran [60]. These biofuels exhibit a maximum in laminar burning velocity at φ = 1.1, similar to MTHF. Figure 4.3-16 compares the laminar burning velocity's at φ = 1.1 and $T_{initial}$=298 K.

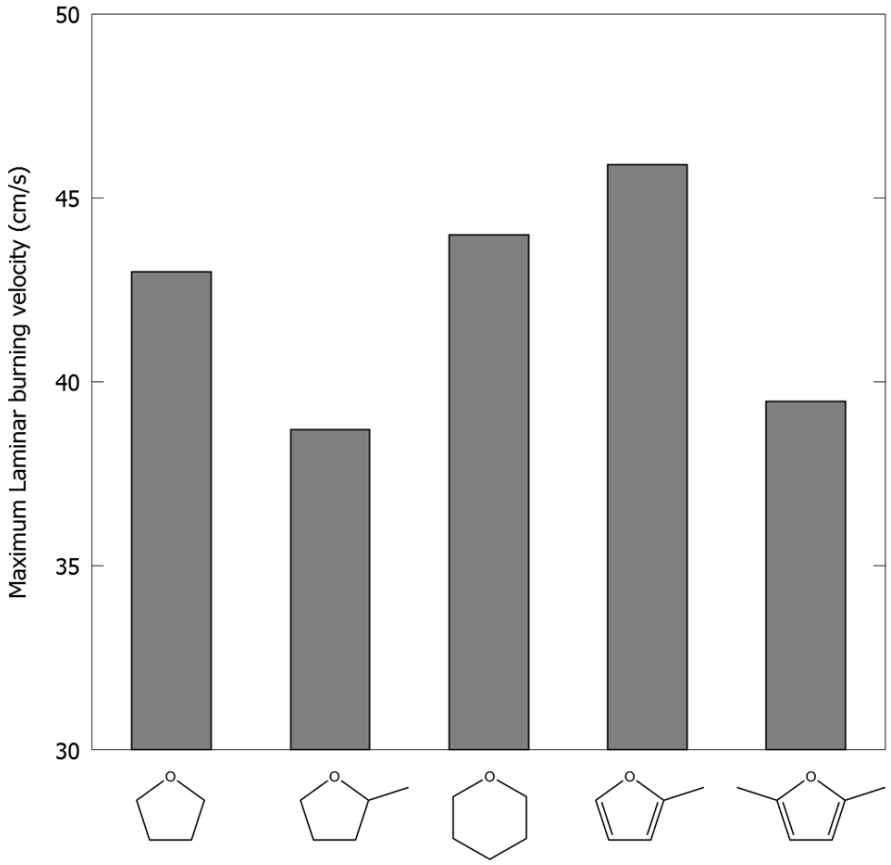

Figure 4.3-16 Experimental laminar burning velocity at 0.101 MPa, unburned gas temperature of 298K, φ = 1.1 for tetrahydrofuran [10], 2-methyl-tetrahydrofuran (this work), tetrahydropyran [35], 2-methyl-furan [59] and 2,5-dimethylfuran [60]

Laminar burning velocities for MTHF are lower compared to THF. Methyl substitution is known to reduce flame speeds in alkanes and cycloalkanes [56, 61]. In these hydrocarbons, this is considered to be mainly a kinetic effect due to an increase in methyl and propene formation. The latter two species affect hydrogen atom concentration, i.e. methyl radicals reduce flame speed by removing hydrogen atoms from the system through recombination while propene is consumed by hydrogen abstraction forming allyl which can recombine with hydrogen atoms. Note the concentration of propene is approximately two times higher in MTHF flames compared to THF flames under comparable conditions [10].

MTHF has a lower burning velocity than 2-methyl-furan. Earlier studies have shown that 2-methyl-furan is mainly consumed by hydrogen abstraction and hydrogen addition reactions [59, 62]. These reaction channels produce high yields of vinylic radicals in 2-methyl-furan flames. For example, the 2-furanyl-methyl radical, formed by hydrogen abstraction from the methyl group in 2-methyl-furan, mainly forms CO and 1,3-butandien-1-yl [59, 62]. Vinylic radicals, which are produced in significantly lower quantities in MTHF flames, have a beneficial effect on laminar burning velocities[56].

4.3.7 Conclusions

This works presents new experimental data for the pyrolysis and combustion of MTHF obtained in a plug flow reactor and premixed laminar flames (flame structure and burning velocity measurements). The pyrolysis experimental data provides insight in the main MTHF consumption pathways and associated product spectrum. The number of detected oxygenated species in flames is substantially higher due to the presence of molecular oxygen. At similar conditions, a lower burning velocity is observed for MTHF than for previously studied saturated and unsaturated cyclic ethers.

The experimental data was interpreted using a newly developed kinetic model. The basis for the model is an existing, validated, propene oxidation model. Chemistry related to the decomposition of MTHF was either based on quantum chemical calculations or estimated by analogy with previous work regarding the pyrolysis and combustion of tetrahydrofuran and tetrahydropyran.

Model calculated and experimental data profiles are in reasonable agreement. The most important unimolecular decomposition reactions for MTHF are scission of the methyl group and concerted ring opening to 4-penten-1-ol. Scission of the ring bonds forming diradical and carbene species, important in the pyrolysis of THF, is negligible. As soon a radical pool is established, MTHF is mainly consumed by hydrogen abstraction reactions. Hydrogen abstraction from the carbon atoms α to the ring oxygen is favored, comparable to tetrahydrofuran and tetrahydropyran. At pyrolysis conditions, the decomposition pathways of the resulting MTHF radicals are able to explain the majority of the product spectrum. At combustion conditions, the same reaction paths are important. However, an increased importance for recombination reactions, given the higher radical concentration due to the higher temperature in flames compared to pyrolysis conditions, is observed. This is particularly the case for recombination reaction involving 2-oxo-ethyl and 2-oxo-propyl, which results in a variety of aldehydes and ketones.

4.3.8 References

[1] W. Yang, A. Sen, One-Step Catalytic Transformation of Carbohydrates and Cellulosic Biomass to 2,5-Dimethyltetrahydrofuran for Liquid Fuels, ChemSusChem 3 (2010) 597-603
[2] M. R. Grochowski, W. Yang, A. Sen, Mechanistic Study of a One-Step Catalytic Conversion of Fructose to 2,5-Dimethyltetrahydrofuran, Chem.-Eur. J. 18 (2012) 12363-12371
[3] J.-P. Lange, E. van der Heide, J. van Buijtenen, R. Price, Furfural—A Promising Platform for Lignocellulosic Biofuels, ChemSusChem 5 (2012) 150-166
[4] T. W. Rudolph, J. J. Thomas, NOx, NMHC and CO emissions from biomass derived gasoline extenders, Biomass 16 (1988) 33-49
[5] A. J. Janssen, F. W. Kremer, J. H. Baron, M. Muether, S. Pischinger, J. Klankermayer, Tailor-Made Fuels from Biomass for Homogeneous Low-Temperature Diesel Combustion, Energ. Fuel. 25 (2011) 4734-4744
[6] Y. Kar, H. Deveci, Importance of P-Series Fuels for Flexible-Fuel Vehicles (FFVs) and Alternative Fuels, Energy Sources, Part A: Recovery, Utilization, and Environmental Effects 28 (2006) 909-921
[7] W. R. Leppard, The Autoignition Chemistries of Octane-Enhancing Ethers and Cyclic Ethers: A Motored Engine Study, SAE Int. 100 (1991) 589-604
[8] M. Verdicchio, B. Sirjean, L. S. Tran, P.-A. Glaude, F. Battin-Leclerc, Unimolecular decomposition of tetrahydrofuran: Carbene vs. diradical pathways, P. Combust. Inst. 35 (2015) 533-541
[9] A. Lifshitz, M. Bidani, S. Bidani, Thermal reactions of cyclic ethers at high temperatures. Part 3. Pyrolysis of tetrahydrofuran behind reflected shocks, The Journal of Physical Chemistry 90 (1986) 3422-3429
[10] L.-S. Tran, M. Verdicchio, F. Monge, R. C. Martin, R. Bounaceeur, B. Sirjean, P.-A. Glaude, M. U. Alzueta, F. Battin-Leclerc, An experimental and modeling study of the combustion of tetrahydrofuran, Combust. Flame 162 (2015) 1899-1918
[11] T. Kasper, A. Lucassen, W. Jasper Ahren, W. Li, R. Westmoreland Philip, K. Kohse-Höinghaus, B. Yang, J. Wang, A. Cool Terrill, N. Hansen, in: *Zeitschrift für Physikalische Chemie International journal of research in physical chemistry and chemical physics*, 2011; Vol. 225, p 1237.
[12] P. Dagaut, M. McGuinness, J. M. Simmie, M. Cathonnet, The Ignition and Oxidation of Tetrahydrofuran: Experiments and Kinetic Modeling, Combust. Sci. Technol. 135 (1998) 3-29
[13] G. Vanhove, Y. Yu, M. A. Boumehdi, O. Frottier, O. Herbinet, P.-A. Glaude, F. Battin-Leclerc, Experimental Study of Tetrahydrofuran Oxidation and Ignition in Low-Temperature Conditions, Energ. Fuel. 29 (2015) 6118-6125
[14] J. M. Simmie, Kinetics and Thermochemistry of 2,5-Dimethyltetrahydrofuran and Related Oxolanes: Next Next-Generation Biofuels, J. Phys. Chem. A 116 (2012) 4528-4538
[15] H. K. Chakravarty, R. X. Fernandes, Reaction Kinetics of Hydrogen Abstraction Reactions by Hydroperoxyl Radical from 2-Methyltetrahydrofuran and 2,5-Dimethyltetrahydrofuran, The Journal of Physical Chemistry A 117 (2013) 5028-5041
[16] P. R. Parab, N. Sakade, Y. Sakai, R. Fernandes, K. A. Heufer, Theoretical Investigation of Intramolecular Hydrogen Shift Reactions in 3-Methyltetrahydrofuran (3-MTHF) Oxidation, The Journal of Physical Chemistry A 119 (2015) 10917-10928
[17] K. Moshammer, S. Vranckx, H. K. Chakravarty, P. Parab, R. X. Fernandes, K. Kohse-Höinghaus, An experimental and kinetic modeling study of 2-methyltetrahydrofuran flames, Combust. Flame 160 (2013) 2729-2743
[18] M. R. Harper, K. M. Van Geem, S. P. Pyl, G. B. Marin, W. H. Green, Comprehensive reaction mechanism for n-butanol pyrolysis and combustion, Combust. Flame 158 (2011) 16-41
[19] M. Djokic, H.-H. Carstensen, K. M. Van Geem, G. B. Marin, The thermal decomposition of 2,5-dimethylfuran, P. Combust. Inst. 34 (2013) 251-258
[20] E. Pousse, P. A. Glaude, R. Fournet, F. Battin-Leclerc, A lean methane premixed laminar flame doped with components of diesel fuel: I. n-Butylbenzene, Combust. Flame 156 (2009) 954-974
[21] P. Dirrenberger, H. Le Gall, R. Bounaceur, O. Herbinet, P.-A. Glaude, A. Konnov, F. Battin-Leclerc, Measurements of Laminar Flame Velocity for Components of Natural Gas, Energ. Fuel. 25 (2011) 3875-3884
[22] L.-S. Tran, B. Sirjean, P.-A. Glaude, K. Kohse-Höinghaus, F. Battin-Leclerc, Influence of substituted furans on the formation of Polycyclic Aromatic Hydrocarbons in flames, P. Combust. Inst. 35 (2015) 1735-1743
[23] P. Dirrenberger, P. A. Glaude, R. Bounaceur, H. Le Gall, A. P. da Cruz, A. A. Konnov, F. Battin-Leclerc, Laminar burning velocity of gasolines with addition of ethanol, Fuel 115 (2014) 162-169
[24] J. Beens, R. Tijssen, J. Blomberg, Prediction of comprehensive two-dimensional gas chromatographic separations - A theoretical and practical exercise, J. Chromatogr. A 822 (1998) 233-251
[25] S. P. Pyl, C. M. Schietekat, K. M. Van Geem, M.-F. Reyniers, J. Vercammen, J. Beens, G. B. Marin, Rapeseed oil methyl ester pyrolysis: On-line product analysis using comprehensive two-dimensional gas chromatography, J. Chromatogr. A 1218 (2011) 3217-3223

[26] L. P. H. de Goey, A. van Maaren, R. M. Quax, Stabilization of Adiabatic Premixed Laminar Flames on a Flat Flame Burner, Combust. Sci. Technol. 92 (1993) 201-207
[27] J. A. Montgomery, M. J. Frisch, J. W. Ochterski, G. A. Petersson, A complete basis set model chemistry. VI. Use of density functional geometries and frequencies, The Journal of Chemical Physics 110 (1999) 2822-2827
[28] M. J. Frisch, G. W. Trucks, H. B. Schlegel, G. E. Scuseria, M. A. Robb, J. R. Cheeseman, G. Scalmani, V. Barone, B. Mennucci, G. A. Petersson, H. Nakatsuji, M. Caricato, X. Li, H. P. Hratchian, A. F. Izmaylov, J. Bloino, G. Zheng, J. L. Sonnenberg, M. Hada, M. Ehara, K. Toyota, R. Fukuda, J. Hasegawa, M. Ishida, T. Nakajima, Y. Honda, O. Kitao, H. Nakai, T. Vreven, J. A. Montgomery, J. E. Peralta, F. Ogliaro, M. Bearpark, J. J. Heyd, E. Brothers, K. N. Kudin, V. N. Staroverov, R. Kobayashi, J. Normand, K. Raghavachari, A. Rendell, J. C. Burant, S. S. Iyengar, J. Tomasi, M. Cossi, N. Rega, J. M. Millam, M. Klene, J. E. Knox, J. B. Cross, V. Bakken, C. Adamo, J. Jaramillo, R. Gomperts, R. E. Stratmann, O. Yazyev, A. J. Austin, R. Cammi, C. Pomelli, J. W. Ochterski, R. L. Martin, K. Morokuma, V. G. Zakrzewski, G. A. Voth, P. Salvador, J. J. Dannenberg, S. Dapprich, A. D. Daniels, Farkas, J. B. Foresman, J. V. Ortiz, J. Cioslowski, D. J. Fox, in: Wallingford CT, 2009.
[29] A. L. L. East, L. Radom, An initio statistical thermodynamical models for the computation of third-law entropies, J. Chem. Phys. 106 (1997) 6655
[30] R. J. Kee, F. M. Rupley, J. A. Miller, M. E. Coltrin, J. F. Grcar, E. Meeks, H. K. Moffat, A. E. Lutz, G. Dixon-Lewis, M. D. Smooke, J. Warnatz, G. H. Evans, L. R. S., R. E. Mitchell, L. R. Petzold, W. C. Reynolds, M. Caracotsios, W. E. Stewart, P. Glarborg, C. Wang, O. Adigun, in: 15101 ed.; Reaction Design, Inc.: San Diego (CA), 2010.
[31] S. S. Merchant, E. F. Zanoelo, R. L. Speth, M. R. Harper, K. M. Van Geem, W. H. Green, Combustion and pyrolysis of iso-butanol: Experimental and chemical kinetic modeling study, Combust. Flame 160 (2013) 1907-1929
[32] A. Dean, J. Bozzelli, in: Gas-Phase Combustion Chemistry, W. C. Gardiner, Jr., (Ed.) Springer New York: 2000; pp 125-341.
[33] Z. Wang, L. Ye, W. Yuan, L. Zhang, Y. Wang, Z. Cheng, F. Zhang, F. Qi, Experimental and kinetic modeling study on methylcyclohexane pyrolysis and combustion, Combust. Flame 161 (2014) 84-100
[34] K. Yasunaga, J. M. Simmie, H. J. Curran, T. Koike, O. Takahashi, Y. Kuraguchi, Y. Hidaka, Detailed chemical kinetic mechanisms of ethyl methyl, methyl tert-butyl and ethyl tert-butyl ethers: The importance of uni-molecular elimination reactions, Combust. Flame 158 (2011) 1032-1036
[35] L.-S. Tran, R. De Bruycker, H.-H. Carstensen, P.-A. Glaude, F. Monge, M. U. Alzueta, R. C. Martin, F. Battin-Leclerc, K. M. Van Geem, G. B. Marin, Pyrolysis and combustion chemistry of tetrahydropyran: Experimental and modeling study, Combust. Flame 162 (2015) 4283-4303
[36] M. K. Sabbe, A. Vandeputte, M.-F. Reyniers, M. Waroquier, G. B. Marin, Modeling the influence of resonance stabilization on the kinetics of hydrogen abstractions, Phys. Chem. Chem. Phys. 12 (2010) 1278-1298
[37] P. D. Paraskevas, M. K. Sabbe, M.-F. Reyniers, N. G. Papayannakos, G. B. Marin, Kinetic Modeling of α-Hydrogen Abstractions from Unsaturated and Saturated Oxygenate Compounds by Carbon-Centered Radicals, ChemPhysChem 15 (2014) 1849-1866
[38] S. M. Burke, U. Burke, R. Mc Donagh, O. Mathieu, I. Osorio, C. Keesee, A. Morones, E. L. Petersen, W. Wang, T. A. DeVerter, M. A. Oehlschlaeger, B. Rhodes, R. K. Hanson, D. F. Davidson, B. W. Weber, C.-J. Sung, J. Santner, Y. Ju, F. M. Haas, F. L. Dryer, E. N. Volkov, E. J. K. Nilsson, A. A. Konnov, M. Alrefae, F. Khaled, A. Farooq, P. Dirrenberger, P.-A. Glaude, F. Battin-Leclerc, H. J. Curran, An experimental and modeling study of propene oxidation. Part 2: Ignition delay time and flame speed measurements, Combust. Flame 162 (2015) 296-314
[39] S. M. Burke, W. Metcalfe, O. Herbinet, F. Battin-Leclerc, F. M. Haas, J. Santner, F. L. Dryer, H. J. Curran, An experimental and modeling study of propene oxidation. Part 1: Speciation measurements in jet-stirred and flow reactors, Combust. Flame 161 (2014) 2765-2784
[40] F. Dubnikova, A. Lifshitz, Isomerization of 2,3-Dihydrofuran and 5-Methyl-2,3-dihydrofuran: Quantum Chemical and Kinetics Calculations, J. Phys. Chem. A 106 (2002) 1026-1034
[41] V. Warth, N. Stef, P. A. Glaude, F. Battin-Leclerc, G. Scacchi, G. M. Côme, Computer-Aided Derivation of Gas-Phase Oxidation Mechanisms: Application to the Modeling of the Oxidation of n-Butane, Combust. Flame 114 (1998) 81-102
[42] K. Wang, S. M. Villano, A. M. Dean, Reactions of allylic radicals that impact molecular weight growth kinetics, Phys. Chem. Chem. Phys. 17 (2015) 6255-6273
[43] K. Wang, S. M. Villano, A. M. Dean, Fundamentally-based kinetic model for propene pyrolysis, Combust. Flame 162 (2015) 4456-4470
[44] S. Sharma, M. R. Harper, W. H. Green, Modeling of 1,3-hexadiene, 2,4-hexadiene and 1,4-hexadiene-doped methane flames: Flame modeling, benzene and styrene formation, Combust. Flame 157 (2010) 1331-1345
[45] S. Sharma, W. H. Green, Computed Rate Coefficients and Product Yields for c-C(5)H(5) + CH(3) -> Products, J. Phys. Chem. A 113 (2009) 8871-8882

[46] Y. Georgievskii, J. A. Miller, S. J. Klippenstein, Association rate constants for reactions between resonance-stabilized radicals: C3H3 + C3H3, C3H3 + C3H5, and C3H5 + C3H5, Phys. Chem. Chem. Phys. 9 (2007) 4259-4268
[47] J. A. Miller, S. J. Klippenstein, Y. Georgievskii, L. B. Harding, W. D. Allen, A. C. Simmonett, Reactions between Resonance-Stabilized Radicals: Propargyl + Allyl, J. Phys. Chem. A 114 (2010) 4881-4890
[48] E. Goos, A. Burcat, B. Ruscic, Extended Third Millennium Thermodynamic Database for Combustion and Air-Pollution Use with Updates from Active Thermochemical Tables, 2014
[49] P. D. Paraskevas, M. K. Sabbe, M.-F. Reyniers, N. G. Papayannakos, G. B. Marin, Group Additive Values for the Gas-Phase Standard Enthalpy of Formation, Entropy and Heat Capacity of Oxygenates, Chem.-Eur. J. 19 (2013) 16431-16452
[50] C. Muller, V. Michel, G. Scacchi, G. M. Come, THERGAS - A computer program for the evaluation of thermochemical data of molecules and free-radicals in the gas-phase, J. Chim. Phys. PCB 92 (1995) 1154-1178
[51] S. W. Benson, Thermochemical Kinetics: Methods for the Estimation of Thermochemical Data and Rate Parameters, John Wiley & Sons, New York, 1976
[52] C. D. Wijaya, R. Sumathi, W. H. Green, Thermodynamic Properties and Kinetic Parameters for Cyclic Ether Formation from Hydroperoxyalkyl Radicals, The Journal of Physical Chemistry A 107 (2003) 4908-4920
[53] C. W. Gao, J. W. Allen, W. H. Green, R. H. West, Reaction Mechanism Generator: Automatic construction of chemical kinetic mechanisms, Comput. Phys. Commun.)
[54] C. F. Goldsmith, S. J. Klippenstein, W. H. Green, Theoretical rate coefficients for allyl + HO2 and allyloxy decomposition, P. Combust. Inst. 33 (2011) 273-282
[55] J. P. Senosiain, S. J. Klippenstein, J. A. Miller, Pathways and Rate Coefficients for the Decomposition of Vinoxy and Acetyl Radicals, The Journal of Physical Chemistry A 110 (2006) 5772-5781
[56] E. Ranzi, A. Frassoldati, R. Grana, A. Cuoci, T. Faravelli, A. P. Kelley, C. K. Law, Hierarchical and comparative kinetic modeling of laminar flame speeds of hydrocarbon and oxygenated fuels, Prog. Energy Combust. Sci. 38 (2012) 468-501
[57] P. Zou, D. L. Osborn, On the mechanism of the HCCO + O2 reaction: Probing multiple pathways to a single product channel, Phys. Chem. Chem. Phys. 6 (2004) 1697-1705
[58] C. F. Goldsmith, L. B. Harding, Y. Georgievskii, J. A. Miller, S. J. Klippenstein, Temperature and Pressure-Dependent Rate Coefficients for the Reaction of Vinyl Radical with Molecular Oxygen, J. Phys. Chem. A 119 (2015) 7766-7779
[59] K. P. Somers, J. M. Simmie, F. Gillespie, U. Burke, J. Connolly, W. K. Metcalfe, F. Battin-Leclerc, P. Dirrenberger, O. Herbinet, P. A. Glaude, H. J. Curran, A high temperature and atmospheric pressure experimental and detailed chemical kinetic modelling study of 2-methyl furan oxidation, P. Combust. Inst. 34 (2013) 225-232
[60] K. P. Somers, J. M. Simmie, F. Gillespie, C. Conroy, G. Black, W. K. Metcalfe, F. Battin-Leclerc, P. Dirrenberger, O. Herbinet, P.-A. Glaude, P. Dagaut, C. Togbé, K. Yasunaga, R. X. Fernandes, C. Lee, R. Tripathi, H. J. Curran, A comprehensive experimental and detailed chemical kinetic modelling study of 2,5-dimethylfuran pyrolysis and oxidation, Combust. Flame 160 (2013) 2291-2318
[61] F. Wu, A. P. Kelley, C. K. Law, Laminar flame speeds of cyclohexane and mono-alkylated cyclohexanes at elevated pressures, Combust. Flame 159 (2012) 1417-1425
[62] L.-S. Tran, C. Togbé, D. Liu, D. Felsmann, P. Oßwald, P.-A. Glaude, R. Fournet, B. Sirjean, F. Battin-Leclerc, K. Kohse-Höinghaus, Combustion chemistry and flame structure of furan group biofuels using molecular-beam mass spectrometry and gas chromatography – Part II: 2-Methylfuran, Combust. Flame 161 (2014) 766-779

4.4 An experimental and kinetic modeling study of tetrahydropyran pyrolysis

This section is based on the following paper:

Luc-Sy Tran, Ruben De Bruycker, Hans-Heinrich Carstensen, Pierre-Alexandre Glaude, Fabiola Monge, Maria U. Alzueta, Roberto Colino Martin, Frédérique Battin-Leclerc, Kevin M. Van Geem, Guy B. Marin, "Pyrolysis and Combustion Chemistry of Tetrahydropyran: Experimental and Modeling Study" *Combustion and Flame* 2015, 162, 4283-4303

4.4.1 Abstract

This section reports new experimental and numerical data for the pyrolysis of tetrahydropyran (THP) - a model component for carbohydrates and next-generation heterocyclic oxygenated fuels. Pyrolysis experiments were performed using a plug flow reactor at 170 kPa, over the temperature range 913-1133 K at residence times of approximately 0.5 and 0.2 s, with 90% and 96% N_2 dilution, respectively. Ethene, 1,3-butadiene, formaldehyde, and acrolein were the most important intermediates. A new detailed kinetic model for THP pyrolysis was developed by EXGAS, complemented with theoretical calculations for the most sensitive reactions. Good agreement between experimental and model calculated data was obtained. Reaction path analysis shows that THP is mainly consumed by hydrogen abstractions at pyrolysis conditions. The pyrolysis simulations are sensitive to the unimolecular initiations involving C−C and C−O bond scission.

Keywords: tetrahydropyran, pyrolysis, carbohydrates, model component, detailed kinetic model.

4.4.2 Introduction

Strategies are being developed to transform biomass into transportation fuels and chemicals. Among the main biomass conversion technologies, oxidation and fast pyrolysis of lignocellulose is a promising route for the production of renewable fuels and chemicals. Tetrahydropyran (THP) is a liquid cyclic ether at standard conditions and has a structure, see Figure 4.4-1, that resembles the core structure of many polysaccharides, such as cellulose, and sugars, such as glucose which is a common raw material for production of bio-chemicals and bio-fuels [1-3].

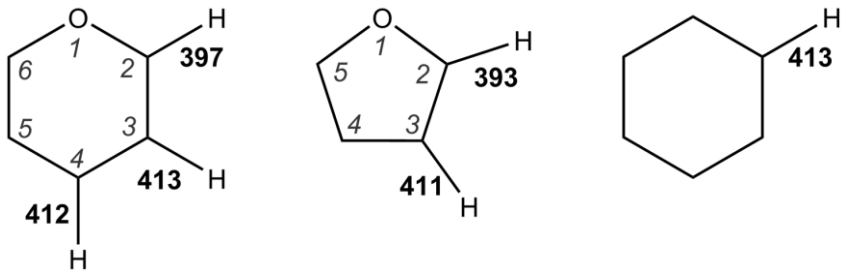

Figure 4.4-1 Structure of tetrahydropyran (THP), tetrahydrofuran (THF) and cyclohexane with atom labels (italic) and bond bond energy in kJ mol^{-1} [4, 5]

Cyclic ethers, such as tetrahydropyran, are also considered as next-generation bio-derived fuels [4]. A motored engine study of auto-ignition chemistry of ethers [6] has shown that cyclic ethers have different antiknock characteristics than acyclic ethers, with octane numbers slightly below those of cyclic alkanes with a same ring size. The combustion properties of tetrahydropyran have not yet been fully investigated, but it is expected to have a heating value close to that of gasoline. Due to the presence of an oxygen atom in the molecule, the combustion of tetrahydropyran is expected to form more oxygenated pollutants but less soot than hydrocarbon containing fuels. This trend is well reported in previous studies on combustion of oxygenated fuels [7, 8].

Furthermore, THP and its derivatives are important intermediates during the low-temperature oxidation of alkanes. The subsequent reactions of these cyclic ethers are believed to have an effect on the overall kinetics of alkane oxidation [9, 10].

In order to better understand the aforementioned processes, several oxidation and combustion studies related to THP have been carried out.

The first THP combustion study dates from 1991 by Leppard who studied the auto-ignition chemistry of six acyclic and cyclic ethers, including THP, using a piston engine [6]. The auto-

ignition of THP was studied at an equivalence ratio (φ) of 0.95 to 1.0, a temperature of 358 K, and a pressure of 60 kPa in the intake manifold. Products formed during the auto-ignition were mainly measured by gas chromatography (GC). The chemical reactions, which are responsible for the auto-ignition of acyclic and cyclic ethers, are used to explain the differences in antiknock characteristics of these ethers. Later, in 1997, ignition delay times and the oxidation of THP were studied by Dagaut et al. [11] behind reflected shock waves (T = 1000-1700 K, P = 200-500 kPa, φ = 0.5-2) and in a jet-stirred reactor (T = 800-1100 K, P = 1000 kPa, φ = 0.5-2), respectively. The chemical species formed during the oxidation of THP were measured by GC. On the basis of these results a detailed kinetic mechanism for the oxidation of THP was proposed. These authors found aldehydes (formaldehyde, acetaldehyde, propanal) to be important intermediates. Most recently, in 2013, Labbe et al. [12] investigated the chemical structure of a fuel-rich premixed low-pressure flame (P = 2.66 kPa, φ = 1.75) using vacuum-ultraviolet (VUV)-photoionization molecular-beam mass spectrometry (PI-MBMS). A detailed kinetic model for the oxidation of THP was developed to interpret the results. Associated reaction rate coefficients were estimated using an analogy with cyclohexane reactions and theoretical calculations. Pyrolysis studies regarding THP are unavailable to the best of the author's knowledge.

This work aims at improving the current understanding of the thermal decomposition of THP, a core building block in polysaccharides. Firstly, THP pyrolysis experiments were performed in a dedicated bench scale setup. Secondly, a detailed kinetic model has been developed through a combination of automatic network generation and quantum chemical calculations. Finally, model calculations are performed using the kinetic model and are compared with the experimental data. Dominant thermal decomposition paths are identified.

4.4.3 Experimental methods

The pyrolysis experiments were performed in a tubular flow reactor. A detailed description of the setup can be found elsewhere [13, 14]. The apparatus consists of a feed, reactor and analysis section.

Liquid THP (Sigma Aldrich, stated purity +99%) is fed to an evaporator kept at 573K using a pump coupled to a Bronkhorst mini-CORI-FLOW mass flow to monitor the liquid fuel flow rate. Nitrogen (Air Liquide, purity +99,999%) is used as a diluent and its flow rate is controlled using a Coriolis mass flow controller. Both gasses are mixed prior to entering the reactor.

The reactor has an internal diameter of 6 mm and a length of 1475 mm. It is placed inside an electrically heated oven which consist of four sections, controlled by four thermocouples. In total, eight thermocouples are positioned along the reactor length, continuously measuring the gas temperature. In the first part of the reactor, the gaseous inlet stream is heated to the set reactor temperature. After approximately 200 mm, the gas temperature reaches the set reactor temperature and remains constant for about 1000 mm. This is followed by a temperature decrease in the final 300 mm of the reactor. The inlet and outlet pressures are measured by two manometers. The measured pressure drop across the reactor was found to be negligible in all experiments (below 1 kPa).

The reactor effluent was analyzed on-line using two regular gas chromatographs (GC) and one two-dimensional chromatograph (GC×GC). The first gas chromatograph is equipped with two thermal conductivity detectors and one flame ionization detector and is used to quantify all permanent gasses and small hydrocarbons (C_{4-}). The second gas chromatograph, equipped with a single thermal conductivity detector, is dedicated to the quantification of formaldehyde and water. The GC×GC is connected to a time-of-flight mass spectrometer and a flame ionization detector. It permits the identification and quantification of the complete reactor effluent ranging from methane to large polycyclic aromatic hydrocarbons (PAH) such as pyrene [15, 16]. The calibration factors for H_2, N_2, CO, CO_2 and C_{4-} hydrocarbons were determined using a calibration mixture (Air Liquide, Belgium). The response factors of all other species were estimated using the effective carbon number method [17]. N_2 was used as diluent and as internal standard.

Experiments were performed at a constant pressure of 170 kPa and a constant THP molar flow rate of 1.67×10^{-4} mol s^{-1} over the temperature range of 913-1133 K. Two N_2 dilutions were investigated, i.e. 90 and 96%, corresponding to residence times of approximately 0.5 and 0.2 s (at 1000 K). Triplicate pyrolysis experiments were carried out for all conditions. The obtained results for these triplicates were generally found to be in good agreement. The mole fractions of all species were averaged at each experimental condition. Elemental balances typically closed within 5%. The error was estimated to be 5%, in line with previous work.

4.4.4 Computational methods

4.4.4.1 Theoretical rate coeffcients

The rate coefficients of several important THP-related reactions were calculated in two steps. First, the CBS-QB3 method [18] as implemented in the Gaussian 09 revision B suite of programs [19] was used to calculate thermodynamic properties of reactants, products and transition states. The electronic energies were converted with the atomization method to the corresponding heats of formation. B3LYP/6-311G(d,p) level rotational constants and scaled (factor 0.99) harmonic frequencies, except those that represent internal rotations, were used to calculate the entropies, heat capacities and thermal contributions to the enthalpies. Hindrance potentials of internal rotors were determined *via* relaxed scans by increasing the corresponding dihedral angle in 10 degrees steps until complete rotation was achieved. These potentials were fitted to Fourier series prior to their use. The reduced moments of inertia were calculated at the $I^{(2,3)}$ level as defined by East and Radom [20]. With this information, the Schroedinger equation for one-dimensional axis-fixed rotation could be solved and the resulting energy eigenvalues were employed to calculate the contributions of these modes to the thermodynamic functions. Finally, the thermodynamic data was stored in form of NASA polynomials. In the second step, transition state theory expressed in terms of Gibbs free energies was used to calculate the rate coefficients:

$$k_{TST}(T) = \chi(T) \cdot \frac{k_B T}{h} \cdot \left(\frac{RT}{p}\right)^{\Delta n - 1} \cdot e^{-\frac{\Delta G^{\ddagger}}{RT}} \quad (1)$$

$\Delta G^{\ddagger}$ is the Gibbs free energy difference between transition state without the transitional mode and reactant(s), Δn is the molecularity of the reaction (2 for bimolecular, 1 for unimolecular reactions), and $\chi(T)$ accounts for quantum mechanical tunneling. All other symbols have their usual meaning. The asymmetric Eckart potential was used in this work to calculate $\chi(T)$. The Gibbs free energies were obtained from the NASA polynomials calculated in the first step. Rate coefficients were calculated for the temperature range 300 K to 2500 K in 50 K steps and fitted to a modified Arrhenius expression.

4.4.4.2 Simulations

Reactor simulations were performed using CHEMKIN [21]. The plug flow reactor (PLUG) module was employed for modeling the tubular reactor, supplied with the inlet flow compositions, measured temperature profiles (including temperature increase at the inlet and

temperature decrease at the outlet), measured pressure and reactor dimensions. The plug flow assumption for the experimental reactor setup has been verified earlier [14].

4.4.5 Kinetic model development

A new detailed chemical kinetic model for the pyrolysis of THP has been developed. The model was developed in two steps:

In the first step, a kinetic mechanism, including thermochemical and transport data, for THP pyrolysis was generated by EXGAS [22-25] starting from a C_0-C_6 reactions base.

In the second step, some key kinetic parameters in the automatically generated mechanism were updated. The kinetic parameters provided by EXGAS are mainly derived and validated for alkanes and alkenes and, hence, they do not take into account the specificity of cyclic ether reactivity. Updated kinetic parameters were taken from quantum calculations, Evans-Polanyi correlations or analogy with structurally similar species.

Both steps will be discussed in the following paragraphs.

Table 4.4-1 Primary mechanism of the high-temperature pyrolysis and oxidation of THP. The rate coefficients are given ($k = AT^n exp(-E_a/RT)$) in m^3, mol, s, kJ units

Nr.	Reaction	A	n	Ea	k (1000K)	Comment
	C-H scission					
1	cy(OCCCCC)→H+cy(OC•CCCC)	4.8E+14	0.0	397.8	8.0E-07	a
2	cy(OCCCCC)→H+cy(OCC•CCC)	4.9E+14	0.0	413.4	1.3E-07	a
3	cy(OCCCCC)→H+cy(OCCC•CC)	4.9E+14	0.0	413.0	1.3E-07	a
	Carbene and biradical pathways					
4	cy(OCCCCC)→C=CCCCOH	4.2E+05	2.6	306.7	2.5E-03	b
5	cy(OCCCCC)→CCCCCHO	6.5E+19	-0.6	377.1	2.1E-02	c
6	cy(OCCCCC)→CCCOC=C	6.5E+19	-0.6	393.4	2.9E-03	c
7	cy(OCCCCC)→C=CCCOC	6.5E+19	-0.6	382.5	1.1E-02	c
8	cy(OCCCCC)→C=CCC+CH2O	1.1E+26	-3.0	397.9	1.8E-04	d
	Hydrogen abstraction					
9	cy(OCCCCC)+H→cy(OC•CCCC)+H_2	2.5E+00	2.4	16.7	5.3E+06	b
10	cy(OCCCCC)+H→cy(OCC•CCC)+H_2	3.7E+01	2.0	28.5	1.2E+06	b
11	cy(OCCCCC)+H→cy(OCCC•CC)+H_2	2.1E+01	2.0	25.1	1.0E+06	b
12	cy(OCCCCC)+OH→cy(OC•CCCC)+H_2O	4.8E+00	2.0	-8.8	1.4E+07	e
13	cy(OCCCCC)+OH→cy(OCC•CCC)+H_2O	4.8E+00	2.0	-1.1	5.5E+06	e
14	cy(OCCCCC)+OH→cy(OCCC•CC)+H_2O	2.4E+00	2.0	-1.3	2.8E+06	e
15	cy(OCCCCC)+CH_3→cy(OC•CCCC)+CH_4	2.0E-04	3.2	31.8	1.7E+04	b
16	cy(OCCCCC)+CH_3→cy(OCC•CCC)+CH_4	9.0E-04	3.0	37.7	9.7E+03	b
17	cy(OCCCCC)+CH_3→cy(OCCC•CC)+CH_4	5.6E-04	3.0	36.4	7.0E+03	b

18	cy(OCCCCC)+C_2H_3→cy(OC•CCCC) +C_2H_4	4.0E+05	0.0	46.0	1.6E+03	a
19	cy(OCCCCC)+C_2H_3→cy(OCC•CCC)+C_2H_4	4.0E+05	0.0	46.0	1.6E+03	a
20	cy(OCCCCC)+C_2H_3→cy(OCCC•CC)+C_2H_4	2.0E+05	0.0	46.0	7.9E+02	a
21	cy(OCCCCC)+C_2H_5→cy(OC•CCCC)+C_2H_6	4.0E+05	0.0	46.0	1.6E+03	a
22	cy(OCCCCC)+C_2H_5→cy(OCC•CCC)+C_2H_6	4.0E+05	0.0	46.0	1.6E+03	a
23	cy(OCCCCC)+C_2H_5→cy(OCCC•CC)+C_2H_6	2.0E+05	0.0	46.0	7.9E+02	a
24	cy(OCCCCC)+C=CC•→cy(OC•CCCC)+C_3H_6	3.7E-05	3.6	73.2	3.5E+02	b
25	cy(OCCCCC)+C=CC•→cy(OCC•CCC)+C_3H_6	1.2E-03	3.2	83.3	2.1E+02	b
26	cy(OCCCCC)+C=CC•→cy(OCCC•CC)+C_3H_6	1.2E-03	3.1	80.8	1.4E+02	b
27	cy(OCCCCC)+CHO→cy(OC•CCCC)+CH_2O	2.2E+01	1.9	71.1	2.1E+03	a
28	cy(OCCCCC)+CHO→cy(OCC•CCC)+CH_2O	2.2E+01	1.9	71.1	2.1E+03	a
29	cy(OCCCCC)+CHO→cy(OCCC•CC)+CH_2O	1.0E+01	1.9	71.1	9.6E+02	a
30	cy(OCCCCC)+CH_2OH→cy(OC•CCCC)+CH_3OH	1.2E-04	3.0	50.2	2.9E+02	a
31	cy(OCCCCC)+CH_2OH→cy(OCC•CCC)+CH_3OH	1.2E-04	3.0	50.2	2.9E+02	a
32	cy(OCCCCC)+CH_2OH→cy(OCCC•CC)+CH_3OH	6.0E-05	3.0	50.2	1.4E+02	a
33	cy(OCCCCC)+CH_3O→cy(OC•CCCC)+CH_3OH	2.9E+05	0.0	18.8	3.0E+04	a
34	cy(OCCCCC)+CH_3O→cy(OCC•CCC)+CH_3OH	2.9E+05	0.0	18.8	3.0E+04	a
35	cy(OCCCCC)+CH_3O→cy(OCCC•CC)+CH_3OH	1.5E+05	0.0	18.8	1.6E+04	a
	THP radical decomposition					
	cy(OC•CCCC)					
36	cy(OC•CCCC)→C•CCCCHO	5.8E+11	0.6	96.7	3.3E+08	b
37	C•CCCCHO→C•CCHO+C_2H_4	2.0E+11	0.7	119.7	1.4E+07	b
38	C•CCCCHO→CCC•CCHO	3.3E+09	1.0	154.8	2.7E+04	a
39	CCC•CCHO→CHO+C=CCC	2.0E+13	0.0	115.9	1.8E+07	a
40	CCC•CCHO→CH_3+C=CCCHO	2.0E+13	0.0	129.7	3.4E+06	a
41	CCC•CCHO→CCCCC•(=O)	1.7E+09	1.0	138.1	1.0E+05	a
42	C•CCCCHO→CCCC•CHO	5.7E+08	1.0	72.4	9.4E+07	a
43	CCCC•CHO→C_2H_5+C_2H_3CHO	2.0E+13	0.0	120.1	1.1E+07	a
44	CCCC•CHO→CC•CCCHO	3.3E+09	1.0	154.8	2.7E+04	a
45	CC•CCCHO→CH_2CHO+C_3H_6	2.0E+13	0.0	120.1	1.1E+07	a
46	C•CCCCHO→CCCCC•(=O)	4.9E+07	1.0	33.5	8.7E+08	a
47	CCCCC•(=O)→CCCC•+CO	2.8E+13	0.0	71.8	5.0E+09	a
48	cy(OC•CCCC)→C•CCOC=C	1.0E+12	0.8	140.6	1.1E+07	b
49	C•CCOC=C→C•OC=C+C_2H_4	2.4E+12	0.4	116.3	3.2E+07	b
50	C•CCOC=C→CCC•OC=C	3.3E+09	1.0	153.3	3.2E+04	a
51	CCC•OC=C→C_2H_3+C_2H_5CHO	2.0E+13	0.0	100.4	1.1E+08	a
52	CCC•OC=C→CH_3+C=COC=C	2.0E+13	0.0	129.7	3.4E+06	a
53	cy(OC•CCCC)→cy(OC=CCCC)+H	2.8E+04	2.7	191.1	3.7E+02	d
	cy(OCC•CCC)					
54	cy(OCC•CCC)→C=CCCCO•	4.8E+12	0.3	91.6	6.2E+08	b
55	C=CCCCO•→C=CCC•+CH2O	1.3E+14	0.0	57.3	1.3E+11	b
56	cy(OCC•CCC)→C•COCC=C	1.5E+12	0.6	127.6	2.0E+07	b
57	C•COCC=C→C=CCO•+C_2H_4	2.6E+10	0.9	96.2	1.2E+08	b
58	C•COCC=C→CCOC•C=C	5.7E+08	1.0	70.9	1.1E+08	a
59	CCOC•C=C→C_2H_5+C_2H_3CHO	4.3E+12	0.0	138.9	2.4E+05	a
60	CCOC•C=C→CC•OCC=C	3.3E+09	1.0	194.6	2.3E+02	a

61	CC•OCC=C→C=CC•+CH_3CHO	2.0E+13	0.0	100.4	1.1E+08	a
62	cy(OCC•CCC)→cy(OC=CCCC)+H	1.2E+11	0.9	128.4	1.2E+07	b
63	cy(OCC•CCC)→cy(OCC=CCC)+H	1.4E+11	0.9	142.7	2.5E+06	b
	cy(OCCC•CC)					
64	cy(OCCC•CC)→C•OCCC=C	2.0E+12	0.5	117.6	4.6E+07	b
65	C•OCCC=C→C=CCC•+CH_2O	6.4E+12	0.4	102.1	4.7E+08	b
66	C•OCCC=C→COC•CC=C	3.3E+09	1.0	178.4	1.6E+03	a
67	COC•CC=C→CH_3+C=CCCHO	2.0E+13	0.0	100.4	1.1E+08	a
68	COC•CC=C→C_2H_3+COC=C	2.0E+13	0.0	148.5	3.5E+05	a
69	C•OCCC=C→COCC•C=C	5.7E+08	1.0	104.3	2.0E+06	a
70	COCC•C=C→CH_3O+C=CC=C	4.3E+12	0.0	138.9	2.4E+05	a
71	cy(OCCC•CC)→cy(OCC=CCC)+H	1.4E+11	0.9	150.2	1.0E+06	b
	Retro-Diels-Alder dihydropyran					
72	cy(OC=CCCC) →C_2H_4+C_2H_3CHO	1.1E+12	0.9	213.4	3.0E+03	b
73	cy(OCC=CCC) →C=CC=C+CH_2O	1.8E+12	0.8	202.5	9.7E+03	b

[a]: Directly provided by EXGAS software [23]
[b]: Calculated using CBS-QB3 methods.
[c]: Analogy with cyclohexane [26]. Difference in BDE between C−C and C−O in THP molecule, and difference between ring strain of THP and that of cyclohexane have been taken into account.
[d]: Analogy with THF [27].
[e]: Estimated using the Evans-Polanyi correlation proposed by Dean and Bozelli [28].

4.4.5.1 Mechanism generated with EXGAS

The kinetic model generated with the EXGAS software consists of three parts:

(i) The first part is a C_0-C_6 reactions base mechanism [25], which consists of a C_0-C_2 sub-mechanism [23] with associated kinetic data mainly taken from [29, 30], reactions of C_3-C_6 species [31-33], and reactions of small aromatic compounds up to ethylbenzene [25]. Reaction pathways involving fulvene and leading to benzene formation have been added as proposed by Li et al. [34]

(ii) The second part is a comprehensive *primary mechanism* of the THP high-temperature oxidation containing fuel consumption reactions, i.e. unimolecular initiation by C−H bond scission (reactions 1-3), hydrogen abstractions (reactions 9-35) and THP radical decomposition reactions (reactions 36-71). Note that, the unimolecular initiations of THP by C−O and C−C bond scissions (reactions 4-8) cannot be generated by EXGAS. This part of the *primary mechanism* will be discussed separately below.

(iii) The third part is a global *secondary mechanism* that contains the reactions of the molecular products formed by the *primary mechanism*. Reactions of some of these products are already included in the C_0-C_6 reactions base.

4.4.5.2 Kinetic parameters in the primary mechanism of THP

Some key kinetic parameters in the *primary mechanism* of THP were updated with quantum calculations, Evans-Polanyi correlations, and analogy with similar structured species.

4.4.5.2.1 Unimolecular decomposition

Recently, Verdicchio et al. [27] performed a detailed study of the unimolecular decomposition of tetrahydrofuran (THF) by means of high-level quantum chemical calculations. Five types of unimolecular initiation pathways were examined for the THF decomposition: (i) initial C−H bond scission involving CH_2 moieties of the THF-ring, (ii) ring-opening by C−O and C−C bond scissions yielding C_4 unsaturated ethers and n-butanal via diradical species, (iii) a pericyclic rearrangement to yield an unsaturated alcohol (1-buten-4-ol), (iv) ring-opening by C−O and C−C bond scission with internal hydrogen atom transfer leading to the formation of carbenic intermediates that isomerize and decompose into molecular products, and (v) a pericyclic hydrogen elimination involving the formation of cyclic diradical.

Both THF and THP are saturated cyclic ethers and, thus, their unimolecular decomposition can assumed to be similar as a first approximation. However, the difference in ring size (5 atoms in THF, 6 atoms in THP; see Figure 4.4-1) will obviously result in different ring strains. This will have an effect on rate coefficients and branching ratios of their respective decomposition pathways. Therefore, one cannot directly use the rate coefficients from the THF calculations by Verdicchio et al. [27] for THP. Considering the ring corrections to the group additivity method of Benson for thermodynamic properties, it can be noted that the contributions of the THP ring strain to $\Delta_f H°$ (298K) and $S°$ (298K) are around 2.1 kJ mol^{-1} and around 78.7 J mol^{-1} K^{-1}, respectively, and are very different to those of the THF ring strain, i.e., 24.7 kJ mol^{-1} to $\Delta_f H°$ (298K) and 105.9 J mol^{-1} K^{-1} to $S°$ (298K) [35]. However, the contributions of THP ring strain are very close to those of the cyclohexane ring, i.e. 0 kJ mol^{-1} to $\Delta_f H°$ (298K) and 78.7 J mol^{-1} K^{-1} to $S°$ (298K) [35]. These values are summarized in Table 4.4-2. Like THP, cyclohexane is a saturated ring molecule with 6 heavy atoms in the ring.

Table 4.4-2 Ring corrections to the group additivity method of Benson for thermodynamic properties [35]

Group	$\Delta_f H°$ (298K) (kJ mol^{-1})	$S°$ (298K) (J mol^{-1} K^{-1})
Tetrahydropyran (THP) ring	2.1	78.7
Tetrahydrofuran (THF) ring	24.7	105.9
Cyclohexane ring	0.0	78.7

Since a complete set of kinetic data for the unimolecular reactions of THP (C−H bond breaking, pericyclic, diradical, and carbenic mechanisms) is unavailable, most of the required rate coefficients were estimated by analogy between cyclohexane and THP.

The rate coefficients for ring-opening by C–O and C–C bond scission yielding either n-pentanal (CCCCCHO) (reaction 5), or one of the two possible unsaturated ethers (CCCOC=C and C=CCCOC; reactions 6 and 7) *via* diradicals, were estimated by analogy with cyclohexane [26]. Unlike cyclohexane, there are three different distinct carbon sites on THP (Figure 4.4-1): C2 and C6 (carbons directly adjacent to the ether oxygen); C3 and C5 (the next neighboring two carbons); and C4 (carbon opposite the oxygen). Therefore, the activation energies were modified considering (i) the difference in BDE between C−C and C−O bonds in THP molecule and (ii) the difference between ring strain between THP and cyclohexane.

As the α-carbene (produced from ring-opening by C1–C2 bond scission) is a relatively stable intermediate in the cyclic ether chemistry [27], its formation pathway from THP has been considered in the present model. This α-carbene (structure in Table S4) can decompose to 1-butene and formaldehyde (reaction 8). The kinetic parameters of this reaction were taken from the THF calculations [4, 27] without any further modifications, even though this creates a rather large uncertainty. Given that THF contains more ring strain than THP, the used activation energy should be a lower limit for THP and consequently the used rate coefficient can be considered an upper limit.

The rate coefficients for C−H bond scission (reactions 1-3) were automatically generated by EXGAS and were kept unchanged.

The rate coefficient for the isomerization (pericyclic rearrangement) of THP to 4-penten-1-ol (C=CCCCOH) (reaction 4) has been calculated at the CBS-QB3 level of theory.

4.4.5.2.2 Hydrogen abstraction

Given the symmetry of THP (Figure 4.4-1) three types of hydrogen atoms can be abstracted by radicals: at C2 (or C6) producing the tetrahydro-2-pyranyl radical, at C3 (or C5) producing the tetrahydro-3-pyranyl radical, and at C4 producing the tetrahydro-4-pyranyl radical. The rate coefficients for hydrogen abstractions by hydrogen atoms, methyl radicals and allyl radicals (reactions 9-11, 15-17, 24-26) were obtained from quantum calculations, whereas rate coefficients for hydrogen abstractions by hydroxyl radicals (reactions 12-14) were deduced

from the Evans-Polanyi correlation proposed by Dean and Bozelli [28]. The rate coefficients for hydrogen abstractions by other radicals were provided by the EXGAS software.

4.4.5.2.3 Decomposition of cyclic C_5H_9O radicals

The decomposition of the tetrahydro-2-pyranyl, tetrahydro-3-pyranyl, and tetrahydro-4-pyranyl radicals is an essential part of the high-temperature chemistry of THP. This set of reactions includes ring-opening by C-C and C-O β-scission and C–H bond β-scissions forming dihydropyrans. Rate coefficients were obtained from theoretical calculations, apart from reaction 53 which is based on an analogy with THF [27] because the CBS-QB3 calculation failed to locate the transition state for this barrier-less reaction.

The ring in the tetrahydro-2-pyranyl radical can open by β-scission of C–O and C–C bond to form C•CCCCHO (reaction 36) and C•CCOC=C (reaction 48), respectively. In the case of the tetrahydro-3-pyranyl radical, ring-opening by β-scission leads to the formation of a carbon-centered radical, i.e. C•COCC=C (reaction 60), or an oxygen-centered radical, i.e. C=CCCCO• (reaction 54). The rate coefficient for C−O β-scission is found to be significantly larger than for C−C fissions β-scission, hence ring-opening via C−O β-scission is favored. In the case of the tetrahydro-4-pyranyl radical, ring-opening by C-C β-scission leads to the formation of a single product, the C•OCCC=C radical (reaction 64).

The C−H β-scission of tetrahydro-2-pyranyl, tetrahydro-3-pyranyl, and tetrahydro-4-pyranyl radicals forms dihydropyrans, i.e. 3,4-dihydropyran (reactions 53, 62) and 3,6-dihydropyran (reactions 63, 71).

4.4.5.2.4 Decomposition of acyclic C_5H_9O radicals

The C•CCCCHO, C•CCOC=C, C•COCC=C, C=CCCCO•, and C•OCCC=C radicals, produced by ring-opening reactions of tetrahydropyran radicals as described above, can decompose by β-scission of C−C an C-O bonds to give smaller (unsaturated) species, including ethene and formaldehyde, two key products in THP combustion as observed by Labbe et al. [12] and Dagaut et al. [11]. This set of reactions, i.e. β-scissions, has been calculated using the CBS-QB3 method. Rate coefficients for intramolecular hydrogen abstraction and subsequent decomposition by β-scission were taken from EXGAS.

4.4.5.3 Kinetic parameters in the secondary mechanism of THP

The reactions involved in the *primary mechanism* described above lead to formation of a large number of products such as ethene, propene, 1,3-butadiene, 1-butene, formaldehyde, acetaldehyde, propanal, acrolein, butenal, methoxy-ethene, ethenyloxy-ethene, methoxy-butene, ethenyloxy-propane, 4-penten-1-ol, 3,4-dihydropyran and 3,6-dihydropyran. The *secondary mechanism* includes the reactions of these primary products. The reactions of some of these products are included in the reaction database, see 4.4.5.1. The reactions of other secondary products have been generated automatically using EXGAS. Some rate coefficients were subsequently updated with results from theoretical calculations or by using analogy with structurally similar species. Retro-Diels-Alder reactions for 3,4-dihydropyran and 3,6-dihydropyran (reactions 72 and 73, respectively) were calculated using the CBS-QB3 method and added in the mechanism.

4.4.5.4 Thermodynamic and transport data

Thermochemical data is provided and stored as 14 polynomial coefficients by EXGAS (coupled with THERGAS [36] based on the group additivity method proposed by Benson [37]). This thermochemical data was used also to determinate rate coefficients by Evans-Polanyi correlations described earlier. The enthalpy of formation for THP used in the present model agrees with those found in the literature [11, 12, 38-40] to within 4 kJ mol^{-1}, see Table 4.4-3.

Table 4.4-3 Thermochemical parameters for tetrahydropyran at 298.15K

	This work	Labbe et al. [12]	Dagaut et al. [11]	Burcat database [38]	Pell and Pilcher [39]; Dorofeeva [40]
$\Delta_f H°$ (kJ mol^{-1})	-227.3	-223.8	-227.3	-224.3	-223.8±1.0
S° (J mol^{-1} K^{-1})	312.3	308.7	312.3	301.9	308.2
Cp° (J mol^{-1} K^{-1})	98.8	98.4	128.2	96.4	99.1±3.5

4.4.6 Results and discussion

4.4.6.1 Experiment and simulated results

The mole fraction profiles of THP and selected products, measured as a function of the temperature, are presented in Figure 4.4-2 for N_2 dilution 90% and residence time 0.5s, and in Figure 4.4-3 for N_2 dilution 96% and residence time 0.2s.

In the low dilution dataset, THP starts to decompose from 920 K, fuel conversion reaches 50% at around 1030 K, and is almost complete at 1120 K. The conversion profile is shifted to higher temperatures in the high dilution dataset.

The thermal decomposition of THP leads to the formation of more than twenty products. Light products such as methane, carbon monoxide, ethene, ethane, acetylene, and hydrogen were detected in large amounts with mole fractions increasing with temperature. Ethene is the most abundant product in the THP pyrolysis.

The mole fraction profiles of several C_3-C_4 products including allene, propyne, propene, propane, 1,3-butadiene and 1-butene are also presented in Figure 4.4-2 and Figure 4.4-3. Among these species, 1,3-butadiene and propene have the highest yields. The mole fraction profiles of most of C_3-C_4 species (except for C_3H_4 isomers) go through maxima at an intermediate temperature.

Several important soot precursors have been identified in the reactor effluent, including 1,3-cyclopentadiene, benzene, toluene, styrene, indene and naphthalene. Their profiles exhibit a typical exponential increase as a function of temperature. Among these cyclic products, 1,3-cyclopentadiene and benzene have the highest yields.

Two oxygenated intermediates have been identified in the reactor effluent, i.e. acrolein and formaldehyde. The associated mole fraction profiles have maxima at intermediate temperature. Furthermore, THP pyrolysis has high selectivity to these molecules at low THP conversion, indicating that they are primary products, in agreement with the studies by Labbe et al. [12] and by Dagaut et al. [11].

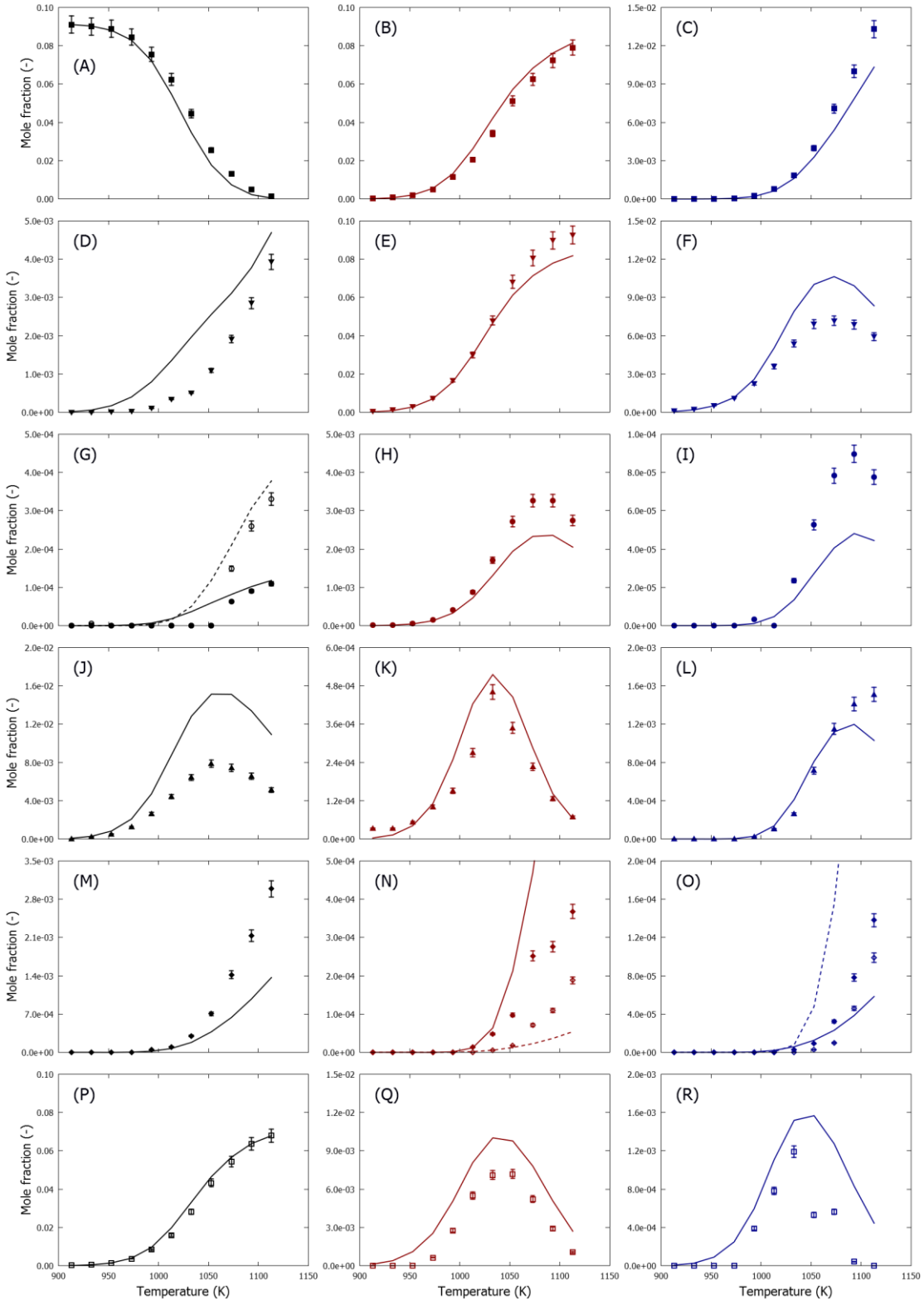

Figure 4.4-2 Mole fractions as a function of temperature for THP pyrolysis in a tubular reactor, P=0.17 MPa, F_{THP}=1.67 10^{-4} mol s^{-1}, F_{N2}=1.67 10^{-3} mol $^{-1}$: ■ - THP (A), ■ - H_2 (B), ■ - CH_4 (C), ▼ - C_2H_2 (D), ▼ - C_2H_4 (E), ▼ - C_2H_6 (F), ● - allene (G), ○ - propyne (G), ● - propene (H), ● - propane (I), ▲ - 1,3-butadiene (J), ▲ - 1-butene (K), ▲ - 1,3-cyclopentadiene (L), ◆ - benzene (M), ◆ - toluene (N), ◇ - styrene (N), ◆ - indene (F),◇ - naphthalene (F), □ - CO (P), □ - formaldehyde (Q), □ - acrolein (R); lines, mole fraction profiles calculated with CHEMKIN-PRO using the plug flow reactor model and the developed kinetic model, discussed in section 4.4.5

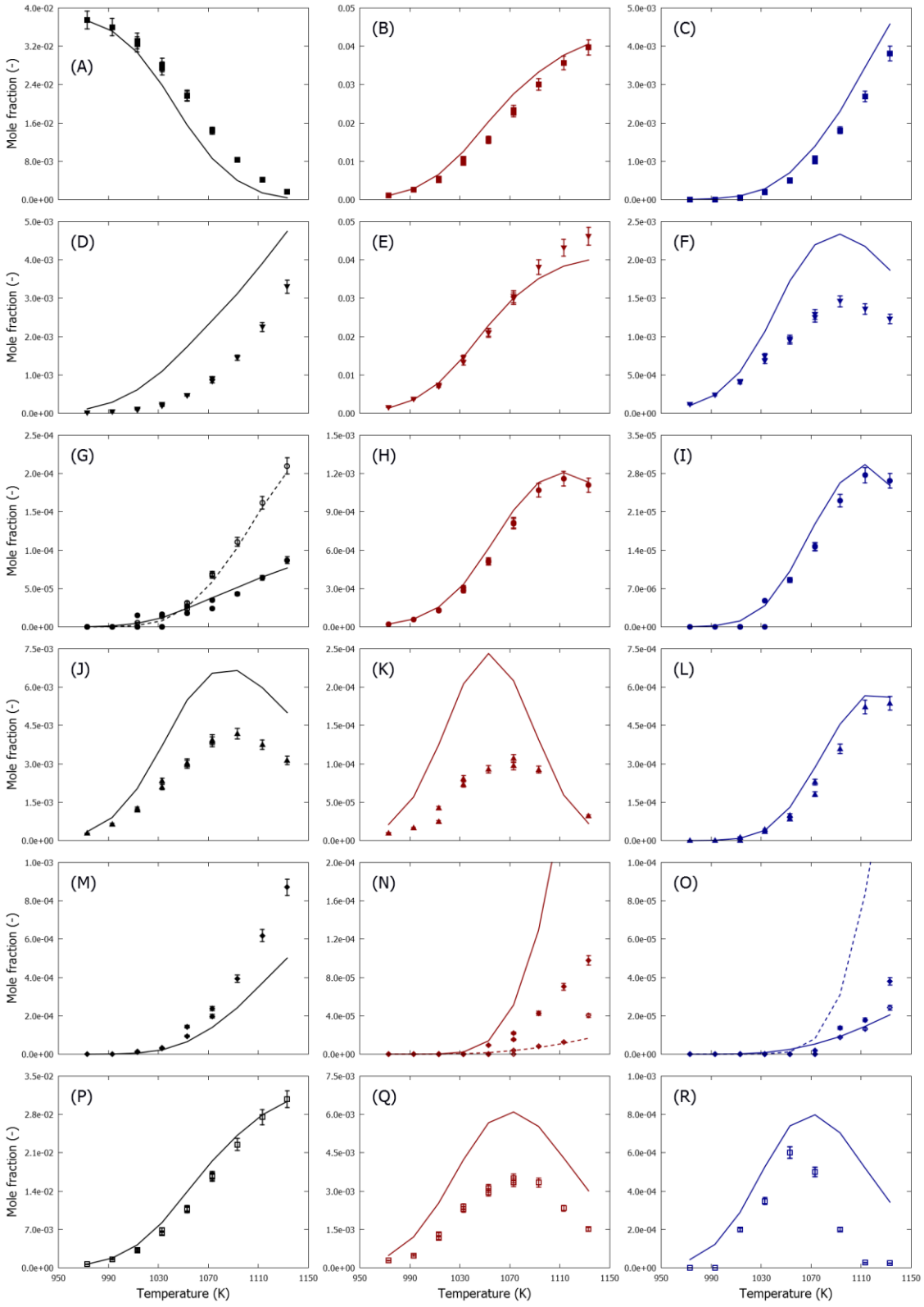

Figure 4.4-3 Mole fractions as a function of temperature for THP pyrolysis in a tubular reactor, P=0.17 MPa, F_{THP}=1.67 10^{-4} mol s^{-1}, F_{N2}=4.15 10^{-3} mol l^{-1}: ■ - THP (A), ■ - H_2 (B), ■ - CH_4 (C), ▼ - C_2H_2 (D), ▼ - C_2H_4 (E), ▼ - C_2H_6 (F), ● - allene (G), ○ - propyne (G), ● - propene (H), ● - propane (I), ▲ - 1,3-butadiene (J), ▲ - 1-butene (K), ▲ - 1,3-cyclopentadiene (L), ◆ - benzene (M), ◆ - toluene (N), ◇ - styrene (N), ◆ - indene (F), ◇ - naphthalene (F), □ - CO (P), □ - formaldehyde (Q), □ - acrolein (R); lines, mole fraction profiles calculated with CHEMKIN-PRO using the plug flow reactor model and the developed kinetic model, discussed in section 4.4.5

Model calculated mole fraction profiles are added to Figure 4.4-2 and Figure 4.4-3. The presented model is in qualitative agreement with all species displayed, i.e. it accurately predicts the temperatures at which the mole fraction profiles increase, decrease or peak. Conversion is slightly overpredicted. For most products, the calculated mole fraction profiles agree within the stated uncertainty with the experimental results. Dihydropyrans, formed by C-H β-scission of tetrahydropyran radicals, were not detected in the reactor effluent. This is in agreement with model calculations which predict yields below 0.1 ppm.

Note that at higher temperatures, the role of secondary, molecular growth, chemistry becomes increasingly important, evidenced by the increase in experimental aromatic yield. The corresponding reactions are part of the base mechanism and not the focus of this work. These reactions can however have an impact on the model performance at the highest investigated temperatures. In this respect, the role of cyclopentadienyl in the formation of (poly-)aromatics has been investigated by several authors [41, 42]. Currently, there is no consensus regarding rate coefficients of the involved reactions. For example, the rate coefficient for recombination of two cyclopentadienyl radicals to naphthalene plus hydrogen atoms varies over two orders of magnitude, depending on the literature source [13, 43][44].

4.4.6.2 Reaction path analysis

To gain more insight in the pyrolysis chemistry of THP, a rate of production analysis has been performed for THP pyrolysis at 1053 K and 500 mm from the reactor inlet which corresponds to a THP conversion of 50%. The results are displayed in Figure 4.4-4.

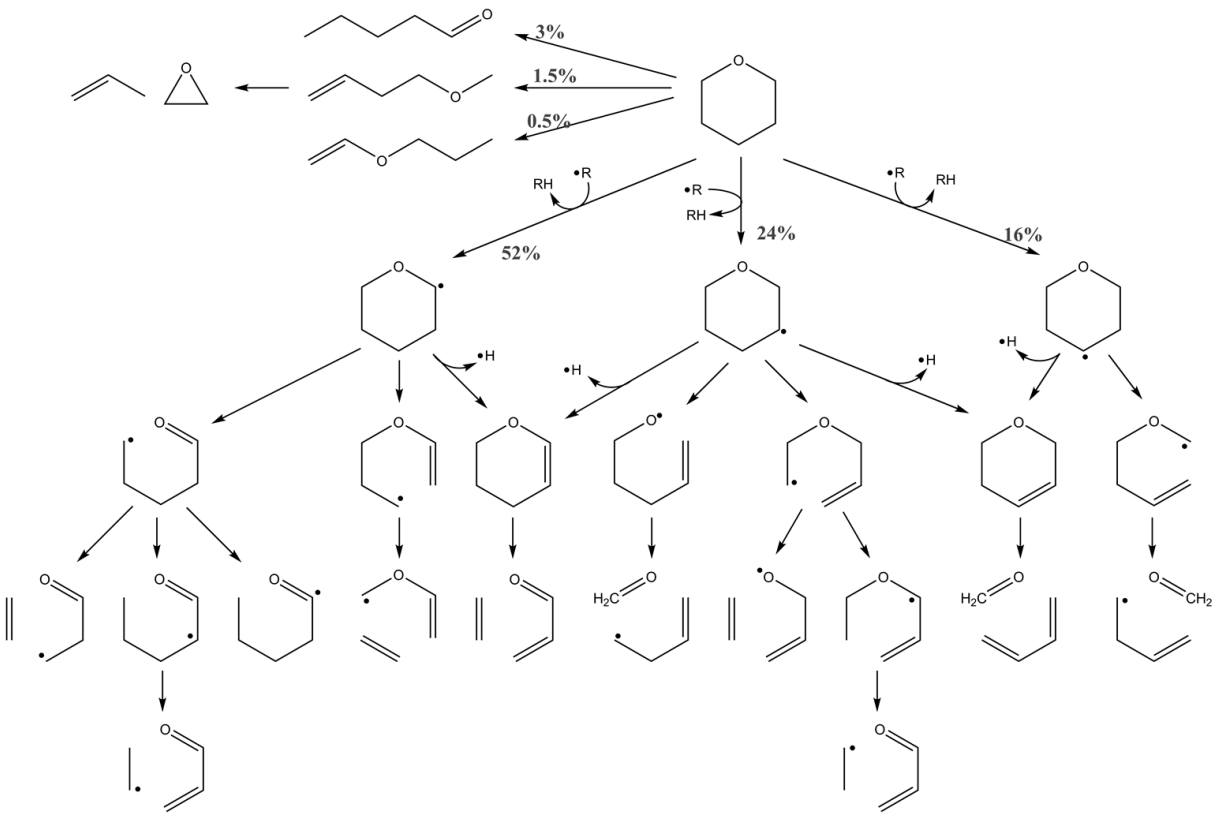

Figure 4.4-4 Main reaction paths in THP pyrolysis, identified using CHEMKIN-PRO. Operating conditions correspond to P = 0.17 MPa, T = 1053K, F_{THP} = 1.67 10^{-4} mol s^{-1}, F_{N2}= 1.67 10^{-3} mol s^{-1}, $conversion_{MTHF}$= 50%. A percentage next to a reaction pathway represents the rate of that reaction relative to the total MTHF consumption rate.

Unimolecular decomposition via diradical pathways contribute for approximately 5% of the total THP consumption. The main stable species formed following C-C and C-O scission of the ring bonds are pentanal, 1-methoxy-3-butene and 1-ethenyloxy-propane. These species further decompose by hydrogen abstraction and unimolecular reactions.

At the investigated conditions, most of THP is consumed by hydrogen abstractions. Hydrogen abstraction from the C2 (or C6) position of THP (the carbon atoms bound to the oxygen atom), which produces the tetrahydro-2-pyranyl radical, is the most important hydrogen-abstracting channel, followed by hydrogen abstractions from the C3 (or C5) position and those from the C4 position, yielding the tetrahydro-3-pyranyl and tetrahydro-4-pyranyl radicals respectively. The contributions of these three hydrogen abstraction channels with respect to fuel consumption are consistent with the difference in the dissociation energies of C–H bonds and number of H-atoms between the different positions in the THP molecule. As shown in Figure 4.4-1, the bond dissociation energy (BDE) of a C2–H bond (397 kJ mol^{-1}) is much lower than those for a C3-H bond (413 kJ mol^{-1}) and a C4–H bond (412 kJ mol^{-1}).

Hydrogen atoms are the main hydrogen abstracting radicals, followed by methyl radicals, ethyl radicals and allyl radicals.

Tetrahydro-2-pyranyl mainly reacts by the C–O bond β-scission leading to the formation of the C•CCCCHO radical. Less important consumption channels of the tetrahydro-2-pyranyl radical are C–C bond β-scission yielding the C•CCOC=C radical and C–H bond β-scission producing 3,4-dihydropyran. C•CCCCHO and C•CCOC=C radicals, acyclic C_5H_9O isomers, decompose by β-scission of the C–C bonds to produce ethene and C_3H_5O radicals. The C•CCCCHO radical can also react by intramolecular hydrogen abstraction to CCCC•CHO and CCCCC(=O)•, which decompose to produce ethyl plus acrolein and CO plus n-butyl, respectively. Decomposition of tetrahydro-2-pyranyl is a major source of ethene, CO, 1-butene and acrolein. The presented model reproduces the mole fraction profiles of these abundant species quite well, as shown in Figure 4.4-2 and Figure 4.4-3

The tetrahydro-3-pyranyl radical reacts by β-scission of C–O, C–C, or C–H bonds to produce C=CCCCO•, C•COCC=C radicals, and dihydropyrans (3,4-dihydropyran and 3,6-dihydropyran), respectively. The C=CCCCO• radical decomposes into formaldehyde and the but-3-en-1-yl radical. This is an important formaldehyde formation path. As shown in Figure 4.4-2 and Figure 4.4-3, the formaldehyde profiles are quite well reproduced by the model. The C•COCC=C radical reacts *via* C–O bond β-scission or *via* intramolecular hydrogen abstraction to produce ethene plus •OCC=C and CCOC•C=C radical, respectively. β-scission reactions of the latter two radicals are minor acrolein formation paths.

The tetrahydro-4-pyranyl radical is mainly consumed by C–C bond β-scissions to form C=CCCOC•, which subsequently decomposes to formaldehyde and the but-3-en-1-yl radical. The but-3-en-1-yl radical decomposes into ethene plus vinyl or hydrogen atom plus 1,3-butadiene. The latter pathway is a significant 1,3-butadiene pathway, the most abundant C4 intermediate.

4.4.6.3 Sensitivity analysis

A sensitivity analysis has been performed to identify the reactions that have the most impact on THP mole fraction. The sensitivity coefficients for the most critical reactions at 1053K are displayed in Figure 4.4-5 as a function of axial position. A reaction with a positive sensitivity coefficient indicates that raising the associated pre-exponential factor increases the mole

fraction of THP, a reaction with a negative sensitivity coefficient indicates that reducing the associated pre-exponential factor increases the mole fraction of THP.

In the first section of the reactor, radical concentration is low and unimolecular decomposition of THP is important, for example to C=CCCOC and CCCCCHO. Such reactions have negative sensitivity coefficients. The acyclic $C_5H_{10}O$ isomers decompose further, possibly with formation of radicals. As indicated in Figure 4.4-4, C=CCCOC mainly reacts to oxirane and propene. In turn, oxirane can decompose to formyl plus methyl or to acetaldehyde. The former reaction has a negative sensitivity coefficients as this leads to a net increase of radicals in the system and, thus, increases reactivity. Hydrogen abstraction reactions from THP have negative sensitivity coefficients. As the radical pool gets established throughout the reactor, their sensitivity coefficients decrease.

Several reactions involving ethyl radicals are also found to be important. Ethyl is formed by several THP decomposition reactions. Ethyl can decompose by C-H β-scission forming ethene plus a reactive hydrogen atom, which has a negative sensitivity coefficient. Ethyl can also recombine, for example with ethyl forming n-butane, which has a positive sensitivity coefficient as this results in a net decrease of radicals in the system.

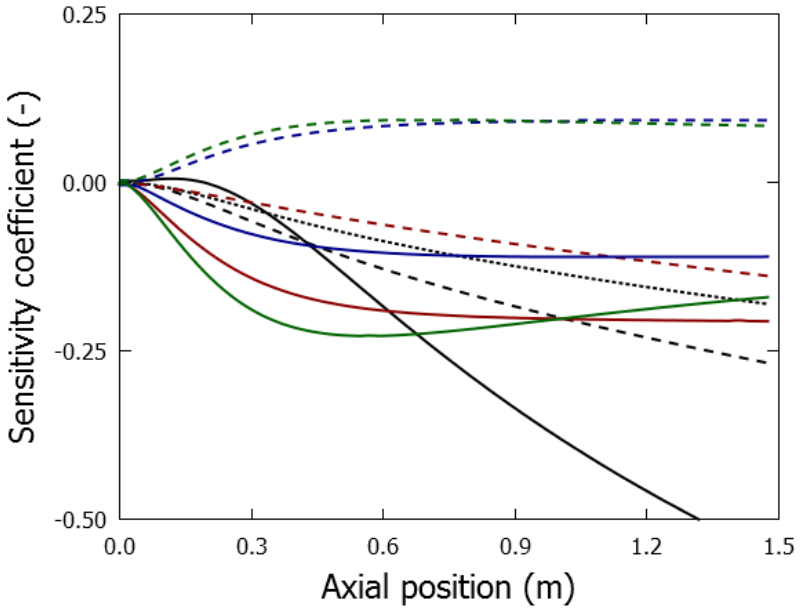

Figure 4.4-5 Sensitivity coefficients for THP calculated using CHEMKIN-PRO as a function of axial position. Operating conditions: P=0.17 MPa, F_{THP}=1.67 10^{-4} mol/s, F_{N2}=1.67 10^{-3} mol/s, T = 1053K: - cy(OCCCCC)+H →cy(OC•CCCC)+H_2, - cy(OCCCCC)+H →cy(OCC•CCC)+H_2, - cy(OCCCCC)+H →cy(OCCC•CC)+H_2, - cy(OCCCCC) →C=CCCOC, - cy(OCCCCC) →CCCCCHO, - cy(OCC) →CHO+CH_3, - cy(OCC) →CH_3CHO, - C_2H_5 →C_2H_4+H, - C_2H_5 +C_2H_5 →C_4H_{10}

4.4.7 Summary and conclusion

The pyrolysis of tetrahydropyran (THP) has been investigated experimentally in a tubular flow reactor. Over 20 species have been identified and quantified in these experiments. Ethene has the highest yield during the pyrolysis of THP. 1,3-Butadiene, formaldehyde, and acrolein are important intermediates.

To gain further insight in the pyrolysis chemistry of THP, a new kinetic model was constructed through automatic model generation and quantum chemical calculations. Model calculated mole fraction profiles are in relatively good agreement with the experimental data. Reaction path analysis shows that THP is largely consumed by hydrogen abstractions in pyrolysis conditions. The majority of the reactor effluent composition is formed by subsequent β-scission reactions. Nevertheless, model agreement would benefit from additional quantum chemical calculations regarding unimolecular THP reactions, evidenced by sensitivity analysis.

4.4.8 References

[1] G. W. Huber, S. Iborra, A. Corma, Synthesis of transportation fuels from biomass: Chemistry, catalysts, and engineering, Chem. Rev. 106 (2006) 4044-4098
[2] R.-J. van Putten, J. C. van der Waal, E. de Jong, C. B. Rasrendra, H. J. Heeres, J. G. de Vries, Hydroxymethylfurfural, A Versatile Platform Chemical Made from Renewable Resources, Chem. Rev. 113 (2013) 1499-1597
[3] A. Osmont, L. Catoire, P. Escot Bocanegra, I. Gökalp, B. Thollas, J. A. Kozinski, Second generation biofuels: Thermochemistry of glucose and fructose, Combust. Flame 157 (2010) 1230-1234
[4] L.-S. Tran, M. Verdicchio, F. Monge, R. C. Martin, R. Bounaceeur, B. Sirjean, P.-A. Glaude, M. U. Alzueta, F. Battin-Leclerc, An experimental and modeling study of the combustion of tetrahydrofuran, Combust. Flame 162 (2015) 1899-1918
[5] Z. Serinyel, O. Herbinet, O. Frottier, P. Dirrenberger, V. Warth, P. A. Glaude, F. Battin-Leclerc, An experimental and modeling study of the low- and high-temperature oxidation of cyclohexane, Combust. Flame 160 (2013) 2319-2332
[6] W. R. Leppard, The Autoignition Chemistries of Octane-Enhancing Ethers and Cyclic Ethers: A Motored Engine Study, SAE Int. 100 (1991) 589-604
[7] J. Bünger, J. Krahl, K. Baum, O. Schröder, M. Müller, G. Westphal, P. Ruhnau, G. T. Schulz, E. Hallier, Cytotoxic and mutagenic effects, particle size and concentration analysis of diesel engine emissions using biodiesel and petrol diesel as fuel, Arch. Toxicol. 74 (2000) 490-498
[8] K. Kohse-Hoinghaus, P. Osswald, T. A. Cool, T. Kasper, N. Hansen, F. Qi, C. K. Westbrook, P. R. Westmoreland, Biofuel Combustion Chemistry: From Ethanol to Biodiesel, Angew. Chem. Int. Ed. 49 (2010) 3572-3597
[9] P. Dagaut, M. Reuillon, M. Cathonnet, High Pressure Oxidation of Liquid Fuels from Low to High Temperature. 2. Mixtures of n-Heptane and iso-Octane, Combust. Sci. Technol. 103 (1994) 315-336
[10] O. Herbinet, S. Bax, P.-A. Glaude, V. Carré, F. Battin-Leclerc, Mass spectra of cyclic ethers formed in the low-temperature oxidation of a series of n-alkanes, Fuel 90 (2011) 528-535
[11] P. Dagaut, M. McGuinness, J. M. Simmie, M. Cathonnet, The Ignition and Oxidation of Tetrahydropyran: Experiments and Kinetic Modeling, Combust. Sci. Technol. 129 (1997) 1-16
[12] N. J. Labbe, V. Seshadri, T. Kasper, N. Hansen, P. Oßwald, P. R. Westmoreland, Flame chemistry of tetrahydropyran as a model heteroatomic biofuel, P. Combust. Inst. 34 (2013) 259-267

[13] M. R. Djokic, K. M. Van Geem, C. Cavallotti, A. Frassoldati, E. Ranzi, G. B. Marin, An experimental and kinetic modeling study of cyclopentadiene pyrolysis: First growth of polycyclic aromatic hydrocarbons, Combust. Flame 161 (2014) 2739-2751
[14] M. R. Harper, K. M. Van Geem, S. P. Pyl, G. B. Marin, W. H. Green, Comprehensive reaction mechanism for n-butanol pyrolysis and combustion, Combust. Flame 158 (2011) 16-41
[15] S. P. Pyl, C. M. Schietekat, K. M. Van Geem, M.-F. Reyniers, J. Vercammen, J. Beens, G. B. Marin, Rapeseed oil methyl ester pyrolysis: On-line product analysis using comprehensive two-dimensional gas chromatography, J. Chromatogr. A 1218 (2011) 3217-3223
[16] K. M. Van Geem, S. P. Pyl, M.-F. Reyniers, J. Vercammen, J. Beens, G. B. Marin, On-line analysis of complex hydrocarbon mixtures using comprehensive two-dimensional gas chromatography, J. Chromatogr. A 1217 (2010) 6623-6633
[17] J. Beens, H. Boelens, R. Tijssen, J. Blomberg, Quantitative aspects of comprehensive two-dimensional gas chromatography (GC x GC), J. High. Resolut. Chromatogr. 21 (1998) 47-54
[18] J. A. Montgomery, M. J. Frisch, J. W. Ochterski, G. A. Petersson, A complete basis set model chemistry. VI. Use of density functional geometries and frequencies, The Journal of Chemical Physics 110 (1999) 2822-2827
[19] M. J. Frisch, G. W. Trucks, H. B. Schlegel, G. E. Scuseria, M. A. Robb, J. R. Cheeseman, G. Scalmani, V. Barone, B. Mennucci, G. A. Petersson, H. Nakatsuji, M. Caricato, X. Li, H. P. Hratchian, A. F. Izmaylov, J. Bloino, G. Zheng, J. L. Sonnenberg, M. Hada, M. Ehara, K. Toyota, R. Fukuda, J. Hasegawa, M. Ishida, T. Nakajima, Y. Honda, O. Kitao, H. Nakai, T. Vreven, J. A. Montgomery, J. E. Peralta, F. Ogliaro, M. Bearpark, J. J. Heyd, E. Brothers, K. N. Kudin, V. N. Staroverov, R. Kobayashi, J. Normand, K. Raghavachari, A. Rendell, J. C. Burant, S. S. Iyengar, J. Tomasi, M. Cossi, N. Rega, J. M. Millam, M. Klene, J. E. Knox, J. B. Cross, V. Bakken, C. Adamo, J. Jaramillo, R. Gomperts, R. E. Stratmann, O. Yazyev, A. J. Austin, R. Cammi, C. Pomelli, J. W. Ochterski, R. L. Martin, K. Morokuma, V. G. Zakrzewski, G. A. Voth, P. Salvador, J. J. Dannenberg, S. Dapprich, A. D. Daniels, Farkas, J. B. Foresman, J. V. Ortiz, J. Cioslowski, D. J. Fox, in: Wallingford CT, 2009.
[20] A. L. L. East, L. Radom, An initio statistical thermodynamical models for the computation of third-law entropies, J. Chem. Phys. 106 (1997) 6655
[21] R. J. Kee, F. M. Rupley, J. A. Miller, M. E. Coltrin, J. F. Grcar, E. Meeks, H. K. Moffat, A. E. Lutz, G. Dixon-Lewis, M. D. Smooke, J. Warnatz, G. H. Evans, L. R. S., R. E. Mitchell, L. R. Petzold, W. C. Reynolds, M. Caracotsios, W. E. Stewart, P. Glarborg, C. Wang, O. Adigun, in: 15101 ed.; Reaction Design, Inc.: San Diego (CA), 2010.
[22] V. Warth, N. Stef, P. A. Glaude, F. Battin-Leclerc, G. Scacchi, G. M. Côme, Computer-Aided Derivation of Gas-Phase Oxidation Mechanisms: Application to the Modeling of the Oxidation of n-Butane, Combust. Flame 114 (1998) 81-102
[23] F. Buda, R. Bounaceur, V. Warth, P. A. Glaude, R. Fournet, F. Battin-Leclerc, Progress toward a unified detailed kinetic model for the autoignition of alkanes from C4 to C10 between 600 and 1200 K, Combust. Flame 142 (2005) 170-186
[24] B. Heyberger, N. Belmekki, V. Conraud, P.-A. Glaude, R. Fournet, F. Battin-Leclerc, Oxidation of small alkenes at high temperature, Int. J. Chem. Kinet. 34 (2002) 666-677
[25] B. Husson, M. Ferrari, O. Herbinet, S. S. Ahmed, P.-A. Glaude, F. Battin-Leclerc, New experimental evidence and modeling study of the ethylbenzene oxidation, P. Combust. Inst. 34 (2013) 325-333
[26] B. Sirjean, P. A. Glaude, M. F. Ruiz-Lopez, R. Fournet, Detailed Kinetic Study of the Ring Opening of Cycloalkanes by CBS-QB3 Calculations, The Journal of Physical Chemistry A 110 (2006) 12693-12704
[27] M. Verdicchio, B. Sirjean, L. S. Tran, P.-A. Glaude, F. Battin-Leclerc, Unimolecular decomposition of tetrahydrofuran: Carbene vs. diradical pathways, P. Combust. Inst. 35 (2015) 533-541
[28] A. Dean, J. Bozzelli, in: Gas-Phase Combustion Chemistry, W. C. Gardiner, Jr., (Ed.) Springer New York: 2000; pp 125-341.
[29] W. Tsang, R. F. Hampson, Chemical Kinetic Data Base for Combustion Chemistry. Part I. Methane and Related Compounds, J. Phys. Chem. Ref. Data 15 (1986) 1087-1279
[30] D. L. Baulch, C. T. Bowman, C. J. Cobos, R. A. Cox, T. Just, J. A. Kerr, M. J. Pilling, D. Stocker, J. Troe, W. Tsang, R. W. Walker, J. Warnatz, Evaluated Kinetic Data for Combustion Modeling: Supplement II, J. Phys. Chem. Ref. Data 34 (2005) 757-1397
[31] R. Fournet, J. C. Bauge, F. Battin-Leclerc, Experimental and modeling of oxidation of acetylene, propyne, allene and 1,3-butadiene, Int. J. Chem. Kinet. 31 (1999) 361-379
[32] N. Belmekki, P. A. Glaude, I. Da Costa, R. Fournet, F. Battin-Leclerc, Experimental and modeling study of the oxidation of 1-butyne and 2-butyne, Int. J. Chem. Kinet. 34 (2002) 172-183
[33] H. A. Gueniche, J. Biet, P. A. Glaude, R. Fournet, F. Battin-Lederc, A comparative study of the formation of aromatics in rich methane flames doped by unsaturated compounds, Fuel 88 (2009) 1388-1393
[34] W. Li, M. E. Law, P. R. Westmoreland, T. Kasper, N. Hansen, K. Kohse-Höinghaus, Multiple benzene-formation paths in a fuel-rich cyclohexane flame, Combust. Flame 158 (2011) 2077-2089

[35] B. E. Poling, J. M. Prausnitz, J. P. O'Connell, in: 5 ed.; McGraw-Hill Companies: 2001.
[36] C. Muller, V. Michel, G. Scacchi, G. M. Come, THERGAS - A computer program for the evaluation of thermochemical data of molecules and free-radicals in the gas-phase, J. Chim. Phys. PCB 92 (1995) 1154-1178
[37] S. W. Benson, Thermochemical Kinetics: Methods for the Estimation of Thermochemical Data and Rate Parameters, John Wiley & Sons, New York, 1976
[38] E. Goos, A. Burcat, B. Ruscic, Extended Third Millennium Thermodynamic Database for Combustion and Air-Pollution Use with Updates from Active Thermochemical Tables, 2014
[39] A. S. Pell, G. Pilcher, Measurements of heats of combustion by flame calorimetry. Part 3.-Ethylene oxide, trimethylene oxide, tetrahydrofuran and tetrahydropy, Trans. Faraday. Soc. 61 (1965) 71-77
[40] O. V. Dorofeeva, Ideal gas thermodynamic properties of oxygen heterocyclic compounds, Thermochim. Acta 200 (1992) 121-150
[41] H. Richter, J. B. Howard, Formation of polycyclic aromatic hydrocarbons and their growth to soot - a review of chemical reaction pathways, Prog. Energy Combust. Sci. 26 (2000) 565-608
[42] J. A. Miller, M. J. Pilling, J. Troe, Unravelling combustion mechanisms through a quantitative understanding of elementary reactions, P. Combust. Inst. 30 (2005) 43-88
[43] N. A. Slavinskaya, P. Frank, A modelling study of aromatic soot precursors formation in laminar methane and ethene flames, Combust. Flame 156 (2009) 1705-1722
[44] V. Chernov, M. J. Thomson, S. B. Dworkin, N. A. Slavinskaya, U. Riedel, Soot formation with C1 and C2 fuels using an improved chemical mechanism for PAH growth, Combust. Flame 161 (2014) 592-601

Chapter 5

Oxidation of unsaturated intermediates in biomass conversion

This chapter discusses the pyrolysis and oxidation of three unsaturated species, i.e. 3-methyl-2-butenol, 3-methyl-3-butenol and 1,5-hexadiene. These molecules are considered to be intermediates in the thermochemical conversion of biomass. The first paper investigates the effect of the position of the hydroxyl group with respect to the C=C double bond on the reactivity of unsaturated alcohols. The second paper investigates the pyrolysis of 1,5-hexadiene, a molecule which has a high selectivity towards 1,3-cyclopentadiene and aromatics, see section 3.1 and section 4.2. Experiments were performed in a jet-stirred reactor. Kinetic models were developed using Genesys, an automatic network generation tool.

5.1 Experimental and kinetic modeling study of the pyrolysis and oxidation of 3-methyl-2-butenol and 3-methyl-3-butenol: Understanding the reactivity of unsaturated alcohols

5.1.1 Abstract

The reactivity of unsaturated alcohols with a C=C double bond in the β- and γ-positions to the hydroxyl group is not well established. The pyrolysis and oxidation of two such unsaturated alcohols have been studied, i.e. 3-methyl-2-butenol (prenol) and 3-methyl-3-butenol (isoprenol). Experiments at three equivalence ratios, i.e. $\varphi = 0.5$, $\varphi = 1.0$ and $\varphi = \infty$ (pyrolysis), were performed using an isothermal jet-stirred quartz reactor at temperatures ranging from 500 to 1100K and a pressure of 0.107 MPa. The reactant and product concentrations were quantified using gas chromatography. A kinetic model has been developed using the automatic network generation tool "Genesys". Several important rate coefficients are obtained from new quantum chemical calculations. Overall, there is a good agreement between model calculated mole fraction profiles and experimental data. Reaction path analysis reveals that isoprenol consumption is dominated by a unimolecular reaction to formaldehyde and isobutene. At the applied operating conditions, the equivalence ratio has no effect on the isoprenol conversion profile. Pyrolysis and oxidation of prenol is dominated by radical chemistry, with hydrogen abstractions from prenol forming resonantly stabilized radicals as dominating conversion path. Oxidation and decomposition of the resulting radicals are predicted to form 3-methyl-2-butenal and 2-methyl-1,3-butadiene, which have been detected as important products in the reactor effluent.

Keywords: unsaturated alcohols, pyrolysis, oxidation, kinetic model, unimolecular decomposition

5.1.2 Introduction

Alcohols are attractive alternative fuels as they can be produced from renewable feedstocks and as their combustion leads to reduced levels of NOx and soot in the exhaust compared to traditional fossil fuels[1]. Ethanol is a first generation bio-derived fuel and the current biofuel market leader. Disadvantages of ethanol, including high hygroscopicity and low energy density, and novel alcohol-production routes from cellulosic biomass have triggered fundamental research towards understanding the combustion chemistry of larger alcohols, i.e. alcohols having 4 or more carbon atoms. Longer chain alcohols have improved physical properties compared to ethanol but their combustion chemistry is less well documented, except that alcohol combustion results in a wide range of products, including ketones, aldehydes and unsaturated alcohols[2-7]. Unsaturated alcohols are important intermediates[1] and understanding their reactivity is of interest to improve kinetic models for alcohol combustion[8]. Besides being intermediates unsaturated alcohols themselves can be considered next-generation bio-derived fuels for spark-ignition combustion engines. Recently, several groups proposed metabolic engineering of Escherichia coli for the highly selective production of prenol and isoprenol from glucose[9, 10].

Unsaturated alcohols have both a hydroxyl group and a C=C double bond incorporated in their molecular structure. The individual effect of either type of functional group has been investigated previously. The presence and position of a hydroxyl group has an impact on the reactivity of the molecule. Ignition delay times are typically higher for alcohols compared to the analogous alkanes at low temperatures (< 750K) while they are lower at high temperatures (< 1000K)[11]. The difference in ignition delay times diminishes as the length of the alkyl chain increases[5, 11]. The hydroxyl group in alcohols changes the bond dissociation energies (BDE) of nearby C-C and C-H bonds compared to the analogous alkanes[12, 13]. Those BDE changes have an impact on, e.g. the rate coefficients of hydrogen abstraction reactions, the main consumption channels of fuels in combustion and pyrolysis. In alcohols, hydrogen abstraction reactions from the α-carbon are favored and the resulting radicals react at oxidizing conditions mainly with molecular oxygen forming an aldehyde and a hydroperoxy radical[14-16], which is rather unreactive at low temperature.

The presence and position of a C=C double bond in hydrocarbons and its effect on combustion characteristics has been investigated previously[17-19]. The C-H bond of the carbon atom in the α-position to the C=C bond and the C-C bond between the carbon atoms in α and β-positions are weak as scission leads to resonantly stabilized radicals[17]. The

resonance stabilization in these radicals is lost upon addition of molecular oxygen, important for autoignition and chain branching at low temperatures, and redissociation of the adduct to the initial reactants is therefore a major reaction channel[20]. The low-temperature reactivity of alkenes is reduced compared to alkanes[19].

Studies regarding the combined effect of both a hydroxyl group and a C=C double bond on the reactivity of a molecule have focused on enols[21]. Enols are unsaturated alcohols of the general structure RC=C(R)OH, where a hydroxyl group is attached to a vinylic carbon atom. In the pyrolysis and oxidation of saturated alcohols, they are produced by hydrogen abstraction from the carbon atom in alpha position of the hydroxyl group followed by subsequent β-scission[1]. They are also formed in the oxidation of hydrocarbons[21, 22], e.g. hydroxyl plus ethene[23] and hydroxyl plus propene[24, 25]. Enols may isomerize to their corresponding aldehydes by keto-enol tautomerization, which is catalyzed by hydrogen atoms, hydroperoxy radicals[26] and carboxylic acids[27] in the gas phase.

In the past, the reactivity of unsaturated alcohols, in which the hydroxyl group is separated from the C=C double bond by one or more carbon atoms, has not received much attention accept for studies that focused at atmospheric or low-pressure conditions[28]. Recently, Welz et al. investigated the oxidation of 3-methyl-2-buten-1-ol (prenol) and 3-methyl-3-buten-1-ol (isoprenol), see Figure 5.1-1, at 550K and low pressure (8 torr)[29]. In their experiments, chlorine atoms, which were generated from Cl_2 by pulsed laser photolysis, abstract hydrogen from prenol and isoprenol. The radicals reacted with oxygen and the product spectrum was analyzed using multiplexed synchrotron photoionization mass spectrometry. The main products during prenol and isoprenol oxidation were the corresponding aldehydes, 3-methyl-2-butenal and 3-methyl-3-butenal respectively. The formation of these aldehydes were supported mechanistically with quantum chemical calculations. As reaction to aldehyde and HO_2 was the only energetically accessible reaction path starting from the prenol and isoprenol radicals with O_2, Welz et al. concluded that unsaturated alcohols have reduced low-temperature reactivity compared to saturated alcohols, similar to saturated and unsaturated methyl esters[30].

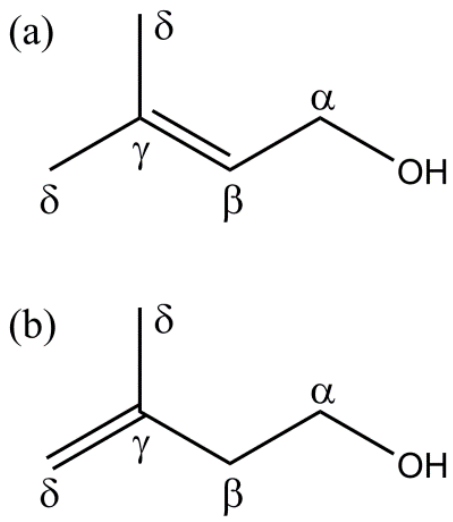

Figure 5.1-1 Molecular representation of prenol (a) and isoprenol (b). Greek letters are atom labels which will be used throughout this work

This work aims at providing a better understanding of the reactivity of unsaturated alcohols in which the double bond is separated from the hydroxyl group by one and two carbon atoms. An extensive experimental dataset was obtained for the oxidation and pyrolysis of prenol and isoprenol in a dedicated jet-stirred reactor. Furthermore, a kinetic model was developed with the automated network generation code Genesys[31, 32]. Several high level theoretical calculations were conducted to describe special reactions that could not be treated automatically. The model calculated mole fraction profiles were compared with the newly obtained experimental data and important reactions were identified. The developed kinetic model should be helpful to improve existing kinetic models for the oxidation and pyrolysis of saturated alcohols.

5.1.3 Experimental methods

The applied experimental setup has been extensively described by Herbinet and coworkers[33-35] and only the main features are summarized below. The interested reader is referred to the aforementioned literature for additional information. The setup consists of three parts: feed section, reactor section and analysis section.

The feed section ensures a stable, continuous stream of helium, oxygen and prenol or isoprenol to the reactor. Helium and oxygen were provided by Messer (purities of 99.99% and 99.999% respectively). Their flow rates to the reactor was controlled using two gas-mass-flow controllers. Prenol and isoprenol were provided by Sigma Aldrich (purity of 98%). The flow rate to the reactor was controlled using a liquid-Coriolis-flow-controller. The liquid flow was

mixed with helium and passed through an evaporator. The fuel/helium blend was subsequently mixed with oxygen. Prior to entering the reactor, the gaseous mixture is heated to the reactor temperature in an annular pre-heating zone. Heating is provided by Thermocoax resistance wires. The residence time in this zone is short compared to the residence time in the reactor.

The reactor is a spherical jet-stirred reactor made out of quartz. The reactive mixture enters the reactor through four nozzles, positioned in the center of the reactor. The nozzles were designed to ensure thermal homogeneity and avoid concentration gradients inside the reactor. Heating of the reactor is again provided by Thermocoax resistance wires. The reaction temperature is measured by a type K thermocouple positioned in the center of the reactor. The pressure in the reactor is controlled using a needle valve positioned downstream of the reactor.

The reactor effluent was analyzed using three dedicated gas chromatographs. The first gas chromatograph is equipped with a thermal conductivity detector and a Carbosphere packed column. It was used to quantify O_2, CO and CO_2. The second gas chromatograph is equipped with a flame-ionization detector and a PlotQ capillary column. The flame-ionization detector was preceded by a methanizer to detect CO, CO_2 and formaldehyde with improved sensitivity. This gas chromatograph was used to quantify molecules containing up to five carbon atoms. The third gas chromatograph is equipped with a flame-ionization detector and a HP-5MS capillary column for quantifying molecules containing at least five carbon atoms. Response factors were determined by injecting calibration mixtures or using the effective carbon number method.

The exit of the reactor is connected with the aforementioned gas chromatographs through heated transfer lines kept at 473K to avoid condensation. Online sampling allowed to obtain reproducible results for the majority of molecules detected in this work. In the case of prenol oxidation and pyrolysis, offline sampling was used to accurately quantify the reactant. During offline sampling, a glass trap, cooled by liquid nitrogen, is connected to the reactor exit. Products exiting the reactor accumulate in the trap. After a known period of time, typically 10 min, the glass trap is disconnected and heated to ambient temperature. Subsequently, a solvent (acetone) and internal standard (n-octane) are added. The resulting mixture is injected into the third gas chromatograph and analyzed. This method proved to be efficient to avoid

repeatability problems due to the condensation and/or adsorption of prenol on the walls of the transfer line.

In this work, the prenol and isoprenol inlet mole fraction was kept constant at 0.008. The inlet volumetric flow rate was fixed at 4.06 10^{-5} m^3 s^{-1} which corresponds to a residence time of 2s. The relative uncertainty in gas flow rate is approximately 5% which results in an uncertainty in residence time of 0.1s. For both unsaturated alcohols, three equivalence ratios were investigated, i.e. φ = 0.5, 1.0 and ∞. Experiments were performed at temperatures ranging from 500 to 1100K and at a constant pressure of 0.107 MPa. The uncertainty on experimental mole fractions is approximately 6% in isoprenol oxidation and pyrolysis and 7% in prenol oxidation and pyrolysis based on repeat experiments. The preceding procedure allowed to close the carbon molar balance within 5%. Note that H_2O was not quantified in this work, therefore, hydrogen and oxygen molar balances could not be verified.

5.1.4 Computational methods

All electronic structure calculations reported in this study were performed with the Gaussian 09 revision D suite of programs[36] as implemented on the high-performance supercomputing facility at Ghent University. The CBS-QB3 level of theory[37] was used exclusively to obtain thermodynamic data for prenol, isoprenol, their radicals and related peroxy species, and to provide input data for transition state theory, which was used to calculate rate expressions. The primary information obtainable from CBS-QB3 calculations are geometries, external moments of inertia, harmonic oscillator frequencies and the electronic energy at 0 K. The first three properties are utilized in statistical mechanics calculations to calculate entropies, heat capacities and thermal contributions to the enthalpy. Except for internal rotations, which were treated separately, all internal modes were assumed to behave as harmonic oscillators. A scaling factor of 0.99 was applied as usual. Internal modes that resemble rotations around a single bond were treated separately by replacing the contributions of the corresponding oscillators to the partition function by numerically calculated partition functions of hindered rotors. The required hindrance potentials were obtained from scans, in which the dihedral angle defining the rotation was varied from 0 to 360 degrees in steps of 10 degrees while all other molecule parameters were allowed to optimize. The obtained hindrance potential was then expressed as a Fourier series. Together with the reduced moment of inertia calculated at the $I^{(2,3)}$ level as defined by East and Radom[38], the hindrance potential was used to construct the Schrödinger equation for 1-D rotation. The eigenvalues of the solution to this Schrödinger equation represent the energy levels of this mode. They were used to determine

the partial partition function as a function of temperature. After corrections for symmetry and optical isomers, the total partition function was used to calculate the thermal contribution to the enthalpy, standard entropy and temperature-dependent heat capacity data.

Enthalpies of formation were calculated with the atomization method[39]. Two additional corrections accounting for spin-orbit interactions[40, 41] and systematic bond corrections (BAC)[40] significantly improve these values as has been shown in previous work[42]. However, such corrections are only needed to calculate the thermodynamic properties. All transition state calculations used uncorrected enthalpy data because BACs are not known for transition states. All data were stored as NASA polynomials.

Transition state theory expressed in terms of Free Gibbs energies was used to calculate the rate coefficients:

$$k_{TST}(T) = \chi(T) \cdot \frac{k_B T}{h} \cdot \left(\frac{RT}{p}\right)^{\Delta n - 1} \cdot e^{-\frac{\Delta G^{\ddagger}}{RT}}$$

$\Delta G^{\ddagger}$ is the Gibbs free energy difference between transition state without the transitional mode and reactant(s), Δn is the molecularity of the reaction (2 for bimolecular, 1 for unimolecular reactions), and $\chi(T)$ accounts for quantum mechanical tunneling. All other symbols have their usual meaning. We used the asymmetric Eckart potential to estimate tunneling contributions $\chi(T)$. The Gibbs free energies were obtained from the NASA polynomials. Rate coefficients were calculated for the temperature range 300 K to 2500 K in steps of 50 K and the results were regressed to a modified Arrhenius expression.

5.1.5 Kinetic model development

5.1.5.1 Mechanism construction

A kinetic model has been developed for the oxidation and pyrolysis of prenol and isoprenol. The prenol and isoprenol submechanism has been generated automatically using Genesys[31, 32, 43]. The latter program produces a CHEMKIN readable input file based on a set of initial molecules, thermochemical databases, and a set of reaction families. The main features of the algorithm for network generation are summarized below, details can be found elsewhere[31, 32].

Each reaction family in Genesys contains a description of how atoms and bonds in a reactive moiety are rearranged through the course of a reaction. The user can provide constraints to a

reaction family to prevent the generation of kinetically insignificant reactions. Each reaction family has to be accompanied with a methodology to assign reaction rate coefficients to reactions belonging to the reaction family. Possible methods include Evans-Polanyi relationship, group additivity for pre-exponential factors and activation energies, and reactivity-structure-based rate rules. The initial set of molecules is iteratively tested whether it is eligible to undergo a reaction family. If a molecule contains the required reactive moiety and passes the molecular constraints, the reaction family is executed and products are generated. The reaction network systematically grows until all initial molecules and generated products are tested against the set of reaction families.

Thermochemical data for molecules and radicals are taken from databases when possible[44-47], otherwise the thermodynamic functions are estimated using Benson's group additivity concept for thermochemistry[42, 45, 46, 48].

The developed kinetic model also includes an isobutene oxidation mechanism by Zhou et al., developed at the Combustion Chemistry Centre at National University of Ireland (Galway)[49]. The isobutene mechanism has been constructed hierarchically. It contains submechanisms for the oxidation of hydrogen, methane, ethane, ethene, propene, methanol, ethanol and acetaldehyde[50-52]. Kinetic and thermochemical data were assembled from high-level theoretical calculations and experimental measurements. The isobutene mechanism has been validated over a wide range of experimental data, including flame speed, ignition delays and speciation measurements in a jet-stirred reactor[53].

The first generated kinetic model, which consisted of the Genesys-generated prenol/isoprenol submechanim and the isobutene oxidation mechanism by Zhou et al. as seed, highlighted the importance of several reactions for model performance. These reactions include hydrogen abstraction from prenol, β-scission of primary radicals and unimolecular decomposition of isoprenol to isobutene plus formaldehyde. The corresponding reaction rate coefficients have been calculated at the CBS-QB3 level of theory and were implemented in the kinetic model. These reactions are listed in Table 5.1-1. This preliminary version of the kinetic model severely underpredicted observed acetaldehyde profiles. Reaction path analysis revealed that this was linked to hydrogen abstraction from ethenol by hydroxyl radicals forming vinoxy plus water. Reaction rate coefficients in the isobutene oxidation mechanism by Zhou et al. were replaced with those proposed by Paraskevas et al.[54] which resulted in satisfactory model performance, as will be shown later.

Table 5.1-1 Rate coefficients for selected reactions in the prenol and isoprenol kinetic model. Units: A T^n [s^{-1} monomolecular or m^3 mol^{-1} s^{-1} bimolecular], Ea [kJ mol^{-1}], k = A T^n exp(-Ea/RT) [s^{-1} monomolecular or m^3 mol^{-1} s^{-1} bimolecular].

No.	Reaction	A	n	Ea	Reference/Note
	Unimolecular decomposition reactions				
1	Isoprenol ⇄ C2C=C + CH_2O	7.31E+05	1.68	145.4	CBS-QB3
2	C2•C=C + •CH_2OH ⇄ Isoprenol	1.00E+07	0.00	0.00	Estimated
3	C2C=CC• + •OH ⇄ Prenol	2.50E+07	0.00	0.00	Estimated
	Hydrogen abstraction from unsaturated alcohols				
	by hydroxyl radicals				
4	•OH + Isoprenol ⇄ H_2O + C=C(C)CC•OH	5.10E-02	2.60	-133.0	[a,] [54]
5	•OH + Isoprenol ⇄ H_2O + C=C(C)C•COH	1.50E-01	2.40	-3.9	[b,] [54]
6	•OH + Isoprenol ⇄ H_2O + C=C(C•)CCOH	7.80E-01	2.30	-5.7	[c,] [54]
7	•OH + Prenol ⇄ H_2O + CC(C)=CC•OH	2.30E-02	2.60	-8.7	[d,] [54]
8	•OH + Prenol ⇄ H_2O + C=C(C)C•COH	1.56E+00	2.30	-5.7	[a,] [54]
	by H atoms				
9	H• + Isoprenol ⇄ H_2 + C=C(C)CC•OH	8.52E-01	2.42	17.5	CBS-QB3
10	H• + Isoprenol ⇄ H_2 + C=C(C)C•COH	7.90E-01	2.45	14.6	CBS-QB3
11	H• + Isoprenol ⇄ H_2 + C=C(C•)CCOH	2.23E+00	2.30	17.7	CBS-QB3
12	H• + Prenol ⇄ H_2 + CC(C)=CC•OH	1.19E+03	1.58	9.2	CBS-QB3
13	H• + Prenol ⇄ H_2 + C=C(C)C•COH	3.50E+00	2.31	18.0	CBS-QB3
	by methyl radicals				
14	•CH_3 + Isoprenol ⇄ CH_4 + C=C(C)CC•OH	1.63E-05	3.44	31.1	CBS-QB3
15	•CH_3 + Isoprenol ⇄ CH_4 + C=C(C)C•COH	4.80E-06	3.62	23.4	CBS-QB3
16	•CH_3 + Isoprenol ⇄ CH_4 + C=C(C•)CCOH	3.60E-05	3.33	29.0	CBS-QB3
17	•CH_3 + Prenol ⇄ CH_4 + C=C(C)C•COH	3.50E-05	3.37	27.2	CBS-QB3
18	•CH_3 + Prenol ⇄ CH_4 + CC(C)=CC•OH	5.56E-04	3.01	20.7	CBS-QB3
	by hydroperoxy radicals				
19	HO_2• + Isoprenol ⇄ H_2O_2 + C=C(C)CC•OH	2.46E-11	5.26	31.3	[a,] [55]
20	HO_2• + Isoprenol ⇄ H_2O_2 + C=C(C)C•COH	5.12E-08	4.40	56.7	[c,] [56]
21	HO_2• + Isoprenol ⇄ H_2O_2 + C=C(C•)CCOH	7.68E-08	4.40	56.7	[c,] [56]
22	HO_2• + Prenol ⇄ H_2O_2 + CC(C)=CC•OH	2.70E-07	3.79	24.3	CBS-QB3
23	HO_2• + Prenol ⇄ H_2O_2 + C=C(C)C•COH	1.54E-07	4.40	56.7	[c,] [56]
	by molecular oxygen				
24	O_2 + Isoprenol ⇄ HO_2• + C=C(C)CC•OH	2.00E+07	0.00	198.6	[e,] [57]
25	O_2 + Isoprenol ⇄ HO_2• + C=C(C)C•COH	2.00E+07	0.00	144.5	[e,] [57]
26	O_2 + Isoprenol ⇄ HO_2• + C=C(C•)CCOH	3.00E+07	0.00	164.4	[e,] [57]
27	O_2 + Prenol ⇄ HO_2• + CC(C)=CC•OH	2.00E+07	0.00	131.3	[e,] [57]
28	O_2 + Prenol ⇄ HO_2• + C=C(C)C•COH	3.00E+07	0.00	162.4	[e,] [57]
	Radical decomposition				
29	C=C(C)CC•OH ⇄ C=C•C + C=COH	3.07E+14	0.00	147.7	[f,] [58]
30	C=C(C)CC•OH ⇄ C=C(C•)CCOH	9.00E+11	0.00	109.7	[f,] [59, 60]
31	C=C(C)C=C + •OH ⇄ C=C(C)C•COH	1.30E-02	2.55	-24.3	CBS-QB3
32	C=C(C•)CCOH ⇄ C=C=C + C•COH	3.11E+15	0.00	236.8	[f,] [58]
33	CC(C)=CC•OH ⇄ CC(C)=CC=O + H•	6.40E+10	1.03	179.0	CBS-QB3
34	CC(C)=CC•OH ⇄ C=C(C)C•COH	2.30E+06	1.95	149.0	CBS-QB3
	Hydroxyl addition and subsequent reaction channels				
34	Prenol + •OH ⇄ C2C(OH)C•COH	7.80E+01	1.29	-11.1	[c,] [24]
35	C2C(OH)C•COH ⇄ C2C(OH)C=C+ •OH	3.00E+13	0.00	112.1	[a]
36	C2C(OH)C•COH ⇄ •CH3 + CC(OH)=CCOH	9.39E+13	0.00	124.4	[f,] [58]
37	O2 + C2C(OH)C•COH ⇄ C2C(OH)C(OO•)COH	1.51E+09	-0.92	-0.5	[g,] [61]
38	C2C(OH)C(OO•)COH ⇄ C2C(O•)C(OOH)COH	2.91E+12	-0.23	93.3	[h,] [62]
39	C2C(O•)C(OOH)COH ⇄ CC(=O)C + C(=O)COH + •OH	6.00E+13	0.22	59.0	[i]
40	C2C(OH)C(OO•)COH ⇄ C2C(OH)C(OOH)CO•	2.91E+12	-0.23	93.3	[h,] [62]
41	C2C(OH)C(OOH)CO• ⇄ C2C(OH)C=O + CH_2O + •OH	6.00E+13	0.22	59.0	[i]
42	Prenol + •OH ⇄ C2C•C(OH)COH	7.80E+01	1.29	-11.1	[c,] [24]
43	C2C•C(OH)COH ⇄ C2C=COH + •CH_2OH	7.68E+13	0.00	127.6	CBS-QB3
44	O2 + C2C•C(OH)COH ⇄ C2C(OO•)C(OH)COH	4.95E+05	0.40	-3.4	[g,] [61]
45	C2C(OO•)C(OH)COH ⇄ C2C(OOH)C(O•)COH	2.91E+12	-0.23	93.3	[h,] [62]
46	C2C(OOH)C(O•)COH ⇄ CC(=O)C + C(=O)COH + •OH	6.00E+13	0.22	59.0	[i]
	Reactions of prenol radicals with molecular oxygen				
47	O_2 + CC(C)=CC•OH ⇄ CC(C)=CC(OO•)OH	2.90E+01	1.59	4.5	[c,] [63]
48	CC(C)=CC(OO•)OH ⇄ CC(C)=CC=O + HO_2•	1.20E+12	0.20	41.0	CBS-QB3
49	O_2 + C=C(C)C•COH ⇄ •OOCC(C)=CCOH	2.90E+01	1.59	4.5	[c,] [63]
50	•OOCC(C)=CCOH ⇄ HOOCC(C)=CC•OH	4.48E+06	1.29	59.6	[j,] [64]
51	O_2 + HOOCC(C)=CC•OH ⇄ HOOCC(C)=CC(OO•)OH	2.90E+01	1.59	4.5	[c,] [63]
52	HOOCC(C)=CC(OO•)OH ⇄ HOOCC(C)=CC=O + HO_2•	1.20E+12	0.20	41.0	[k]

[a] generated using Genesys, reaction rate coefficient is estimated from the analogous ethanol/2-hydroxy-ethyl reaction
[b] generated using Genesys, reaction rate coefficient is estimated from the analogous 1-butene reaction
[c] generated using Genesys, reaction rate coefficient is estimated from the analogous propene/allyl reaction
[d] generated using Genesys, reaction rate coefficient is estimated from the analogous 2-propen-1-ol reaction

[e] generated using Genesys, reaction rate coefficient is estimated using Evans-Polanyi relationship
[f] generated using Genesys, reaction rate coefficient is estimated using group additivity method
[g] generated using Genesys, reaction rate coefficient is estimated from the analogous alkyl reaction
[h] generated using Genesys, reaction rate coefficient is estimated from the analogous isobutene/isobutenyl reaction
[i] generated using Genesys, reaction rate coefficient is estimated from the analogous acetone/2-oxy-propane reaction
[j] generated using Genesys, reaction rate coefficient is estimated from the analogous 2-pentene reaction
[k] generated using Genesys, reaction rate coefficient is estimated from the analogous prenol reaction

The following paragraphs focuses on three essential aspects of the kinetic model, i.e. the utilized reaction families in Genesys, the unimolecular decomposition of isoprenol to isobutene plus formaldehyde and thermochemistry of prenol peroxy radicals.

5.1.5.2 Reaction families

Genesys requires the user to define all reaction families that shall be considered in the network generation process. The reaction families utilized in this work are listed in Table 5.1-2. Reaction rate coefficients for these families were taken from various sources including estimation techniques, such as group additivity, Evans-Polanyi, reactivity-structure-based rate rules, or analogy of known reactions.

Table 5.1-2 Reaction families

Reaction family	
Hydrogen abstraction	
Intermolecular	by C• by H• by •OH by HO_2• by O_2
Intramolecular	C-$(C)_n$-C• ⇄ •C-$(C)_n$-C C-$(C)_n$-O-O• ⇄ •C-$(C)_n$-O-OH C(O-O•)-C-OH ⇄ C(O-OH)-C-O•
β-scission / radical addition	
Carbon centered radicals	•C-C-C ⇄ C=C + •C •C-C-H ⇄ C=C + •H •C-C-OH ⇄ C=C+ •OH •C-O-H ⇄ C=O+ •H •C-C-O-OH ⇄ C=C+ HO_2•
Oxygen centered radicals	•O-C-C ⇄ C=O+ •C •O-C-H ⇄ C=O+ •H
α-scission	
CO α-scission	C-C(=O)• ⇄ C• + CO
Concerted reaction paths	
Peroxy-alkyl to alkene and HO_2	C-C-O-O• ⇄ C=C + HO_2•
Hydroperoxy-alkene to cyclic ether and OH	•C-$(C)_n$-O-OH ⇄ cy(C-$(C)_n$-O) + •OH
Oxidation of α-hydroxyalkyl	C(-O-O•)-OH + O_2 ⇄ C=O + HO_2•
Radical + O_2	
Oxygen addition to carbon-centered radicals	C• + O_2 ⇄ C-O-O•
Scission / radical recombination	
Recombination allylic radicals with HO_2	•C-C=C + HO_2• ⇄ C-C=C-O-OH
Scission of O-O bond	C-O-OH ⇄ C-O• + •OH

For several reaction families, only a limited number of kinetics studies are available in literature. Reaction rate coefficients of a reaction belonging to such a reaction family are assigned based on analogy to similar hydrocarbon/alcohol reactions. For example, reaction

rate coefficients for hydrogen abstraction by hydroperoxy radicals from the δ-carbon atom in prenol were taken from a theoretical study by Zador et al. regarding propene plus hydroperoxy[56] (cf. reaction no. 23 in Table 5.1-1 and Figure 5.1-2). The pre-exponential factor of hydrogen abstraction by a hydroperoxy radical from the δ-carbon atom in prenol is a factor two higher than hydrogen abstraction by a hydroperoxy radical from the allylic carbon atom in propene, given the increase in number of energetically equivalent reaction paths (when neglecting the effect of the hydroxyl-methyl group).

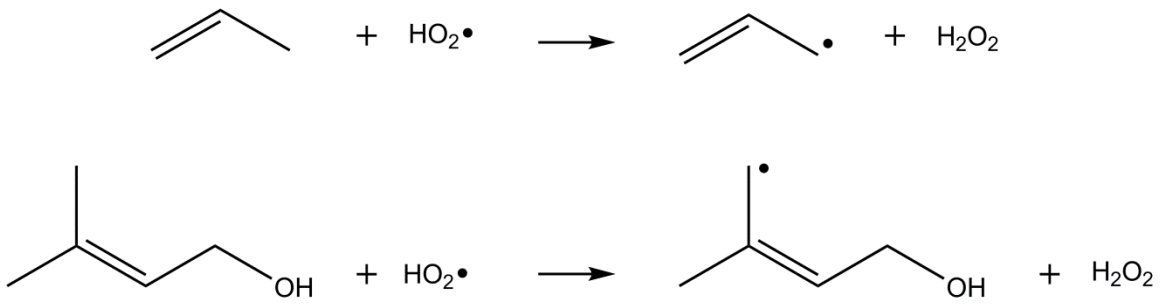

Figure 5.1-2 Hydrogen abstraction by hydroperoxy forming resonantly stabilized radicals

The sources of rate expressions for a selected number of reaction families are discussed in the following paragraphs. All reaction families, along with details regarding reaction rate coefficients, are listed in Appendix B.

5.1.5.2.1 Hydrogen abstraction and radical decomposition reactions

Reaction rate coefficients of reactions belonging to the reaction families (i) hydrogen abstraction by carbon-centered radicals, (ii) hydrogen abstraction by hydrogen atoms, (iii) carbon-centered β-scission / carbon-centered radical addition and (iv) hydrogen-centered β-scission / hydrogen atom addition were calculated using the group additive databases developed by Marin and co-workers [58, 65-67]. These authors applied Benson's group additivity concept to transition state theory and derived group additive values from CBS-QB3 calculations at the high-pressure limit. If group values were not available, e.g. for hydrogen abstraction from the carbonyl group in aldehydes, reaction rate coefficients were taken from literature, e.g. Mendes et al.[68].

Reaction rate coefficients for hydrogen abstraction by hydroxyl radicals from primary/secondary/tertiary C-H moieties forming alkyl radicals are provided by an experimental study by Sivaramakrishnan et al.[69] and Badra et al.[70]. If hydrogen abstraction by a hydroxyl radical forms a resonantly stabilized radical, reaction rate coefficients are taken from the analogous alkene reactions[54]. Reaction rate coefficients for

hydrogen abstraction by a hydroxyl radical from a carbon atom connected to a C=C double bond and a hydroxyl group are assumed to be analogous to hydrogen abstraction by hydroxyl from allyl alcohol[54].

Reaction rate coefficients for hydrogen abstraction by hydroperoxy radicals from primary/secondary/tertiary carbon atoms forming alkyl radicals are provided by a theoretical study by Aguilera-Iparraguirre et al.[71]. If hydrogen abstraction by hydroperoxy forms an α-hydroxy-alkyl radical or a resonantly stabilized radical, reaction rate coefficients are taken from the analogous ethanol (HO_2• + CH_3CH_2OH ⇄ H_2O_2 + CH_3CH(•)OH)[55] or propene (HO_2• + $CH_3CH=CH_2$ ⇄ H_2O_2 + •$CH_2CH=CH_2$)[56] reactions.

Intramolecular hydrogen abstractions proceed through a cyclic transition state. The activation energy of such reactions can be considered to consist of two components, the ring strain induced by the transition state and the activation energy of the analogous bimolecular hydrogen abstraction reaction[60]. The pre-exponential factor is correlated with the loss of hindered rotors in the transition state[60]. In this work, rate coefficients for intramolecular hydrogen abstraction reactions of carbon-centered radicals are estimated using the reactivity-structure-based rate rules proposed by Wang et al.[60].

5.1.5.2.2 Low temperature oxidation pathways

Bugler et al. recently recommended rate rules for oxygen addition to alkyl radicals (R + O_2 ⇄ ROO), concerted decomposition of peroxy radicals to alkenes and hydroperoxy (ROO ⇄ alkene + HO_2), intramolecular hydrogen abstraction of peroxy radicals (ROO ⇄ QOOH), β-scission of β-hydroperoxy-alkyl radicals to alkenes and hydroperoxy (β-QOOH ⇄ alkene + HO_2) and decomposition of hydroperoxy-alkyl radicals to cyclic ethers plus hydroxyl (QOOH ⇄ cyclic ether + OH)[61]. These reaction pathways were implemented in this work. For all reaction families mentioned above, reaction rate coefficients were taken from Bugler et al. in the case of alkyl radicals[61] or from the analogous alkene system in the case of resonantly stabilized radicals[63, 64]. For example, reaction rate coefficients for oxygen addition on resonantly stabilized radicals were taken from oxygen addition on allyl[63].

5.1.5.2.3 Reaction pathways characteristic for alkene and alcohol oxidation

Alkenes and alcohols have several characteristic oxidation pathways. Resonantly stabilized radicals, such as allyl radicals, have a relatively long life time compared to alkyl radicals. Recombination with hydroperoxy radicals therefore is an important consumption channel, as shown for allyl in propene oxidation[50] and 2-methyl-butenyl in 2-methyl-2-butene

oxidation[72]. The resulting hydroperoxide has a weak O-O bond and scission results in a hydroxyl radical and an oxy radical. Rate coefficients for recombination reactions of resonantly stabilized radicals with hydroperoxy and associated reactions were taken from the theoretical study by Goldsmith et al. on allyl plus hydroperoxy[73].

One of the most important reaction pathways of hydroxyl radicals, the main chain carrying radical at low-temperatures, is addition to the C=C double bond of alkenes, forming a β-hydroxy-alkyl radical. Oxygen addition to this radical yields a hydroxyl-alkyl-peroxy radical. Intramolecular hydrogen abstraction of the latter radical, in which the hydrogen of the hydroxyl group migrates to the peroxy group, has a relatively low energy barrier[62]. The formed hydroperoxy-alkoxy radical dissociates by C-O β-scission forming a α-hydroperoxy-keto-alkyl radical. It is unstable and decomposes rapidly by O-O β-scission. The described reaction sequence, known as the Waddington reaction, plays an important role in the oxidation of alkenes[18]. Reaction rate coefficients were estimated from a theoretical study by Sun et al.[62].

Oxidation of alcohols have a high selectivity to aldehydes. The reaction of molecular oxygen with an α-hydroxyalkyl radical to hydroperoxy and the corresponding aldehyde has a low energy barrier[14, 74]. Therefore, this reaction family was included in the current work. Reaction rate coefficients were taken from a theoretical study by da Silva et al. for α-hydroxyethyl plus molecular oxygen[14].

5.1.5.3 Isoprenol molecular decomposition

As will be discussed in the results, isoprenol oxidation and pyrolysis have a high selectivity to isobutene and formaldehyde. The molecular decomposition of isoprenol to isobutene plus formaldehyde has been investigated at the CBS-QB3 level of theory, using the methodology described above. This reaction is analogous to the retro-ene reaction of alkenes[18] and proceeds through a six-membered transition state, in which the hydrogen atom of the hydroxyl group bridges to the C=C double bond, as illustrated in Figure 5.1-3. The retro-ene reaction family is known to be an important unimolecular consumption channel of olefins and unsaturated methyl esters[35, 75, 76]. The rate coefficient for the reaction of isoprenol to isobutene plus formaldehyde is displayed in Figure 5.1-3 as a function of temperature, and the retro-ene reaction of 1-pentene to propene plus ethene has been added for comparison. At 500K and 1000K, the lowest and highest temperatures at which isoprenol oxidation and pyrolysis experiments were performed, the reaction rate coefficients for isoprenol to isobutene

plus formaldehyde are, respectively, 1E+7 and 3E+2 times faster than the retro-ene reaction of 1-pentene to propene plus ethene. The large reactivity differences are caused by substantially different activation energies as shown in Figure 5.1-3. The activation energy for isoprenol to isobutene plus formaldehyde is 159 kJ mol^{-1}, the activation energy for 1-pentene to propene plus ethene is 236 kJ mol^{-1}. This can be related to differences in the endothermicity of the reactions: at 298K, the reaction enthalpy of isoprenol to isobutene plus formaldehyde is 64.2 kJ mol^{-1} and the reaction enthalpy of 1-pentene to propene plus ethene is 86.3 kJ mol^{-1}.

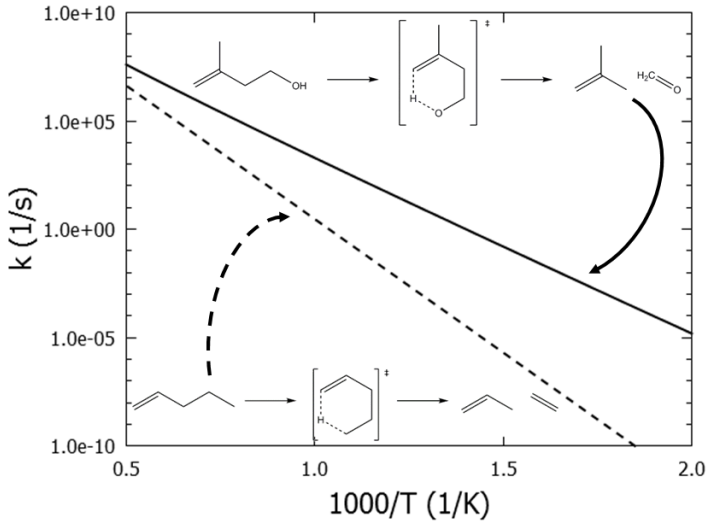

Figure 5.1-3 Comparison of the retroene-like decomposition reaction of isoprenol with the prototypical retro-ene reaction of 1-pentene, ——- isoprenol ⇄ isobutene + formaldehyde, - - - - - 1-pentene ⇄ propene + ethene

5.1.5.4 Thermochemistry of peroxy radicals

Peroxy radicals are formed by reaction of molecular oxygen with carbon-centered radicals. In this work, the thermochemistry of peroxy prenol radicals has been calculated at the CBS-QB3 level of theory. The stability of peroxy radicals can be evaluated by calculating the bond dissociation energy (BDE) of the C-O_2 bond. The C-O_2 BDE of several radicals are compared in Table 5.1-3.

Table 5.1-3 C-O_2 bond dissociation energies at 298K for several peroxy radicals, calculated at the CBS-QB3 level of theory

Structure	BDE C-O_2 (kJ mol^{-1})	Structure	BDE C-O_2 (kJ mol^{-1})
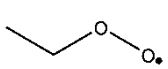	148	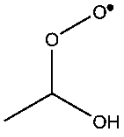	166

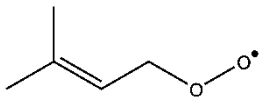	77	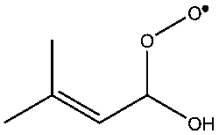	100
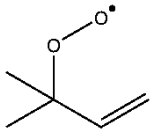	90	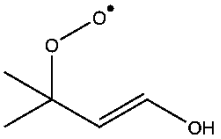	95
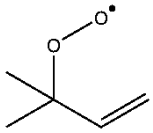	90	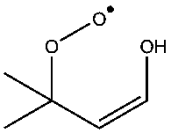	105

Hydroxy-alkyl peroxy radicals have higher C-O_2 BDE than alkyl peroxy radicals. The hydroxyl group has a stabilizing effect on the C-O_2 bond through formation of a hydrogen bond. For example, ethyl-peroxy radicals have a C-O_2 BDE of 148 kJ mol^{-1} while 2-hydroxy-ethyl peroxy radicals have a C-O_2 BDE of 166 kJ mol^{-1}, see Table 5.1-3.

Allylic peroxy radicals, such as prenol peroxy radicals, have weaker C-O_2 bonds due to loss of resonance stabilization. The C-O_2 BDE of several prenol peroxy radicals are compared with their isopentene analogs in Table 5.1-3. Similar to saturated alcohols, the presence of a hydroxyl group has a stabilizing effect on the C-O_2 bond in unsaturated alcohols. For example, the C-O_2 BDE of the 3-methyl-but-2-en-1-ol-1-peroxy radical is 100 kJ mol-1, 23 kJ mol^{-1} higher than the C-O_2 BDE of the 3-methyl-but-2-en-1-peroxy radical. The effect of the hydroxyl group diminishes when the distance between the hydroxyl and peroxy group increases. The C-O_2 BDE of trans- and cis-3-methyl-but-1-en-1-ol-3-peroxy radicals are 5 and 15 kJ mol^{-1} higher than the C-O_2 BDE of the 3-methyl-but-1-en-3-peroxy radical.

5.1.6 Results and discussion

5.1.6.1 Isoprenol

5.1.6.1.1 Experimental data

Forty-three molecules were detected and quantified in the reactor effluent during isoprenol oxidation and pyrolysis. These include carbon oxides, hydrocarbons ranging from methane to phenanthrene and oxygenates containing a single oxygen atom. The experimental isoprenol mole fraction profiles and the mole fraction profiles of the most representative products are presented in Figure 5.1-4 as a function of temperature, for φ = 0.5, 1.0 and ∞ (pyrolysis).

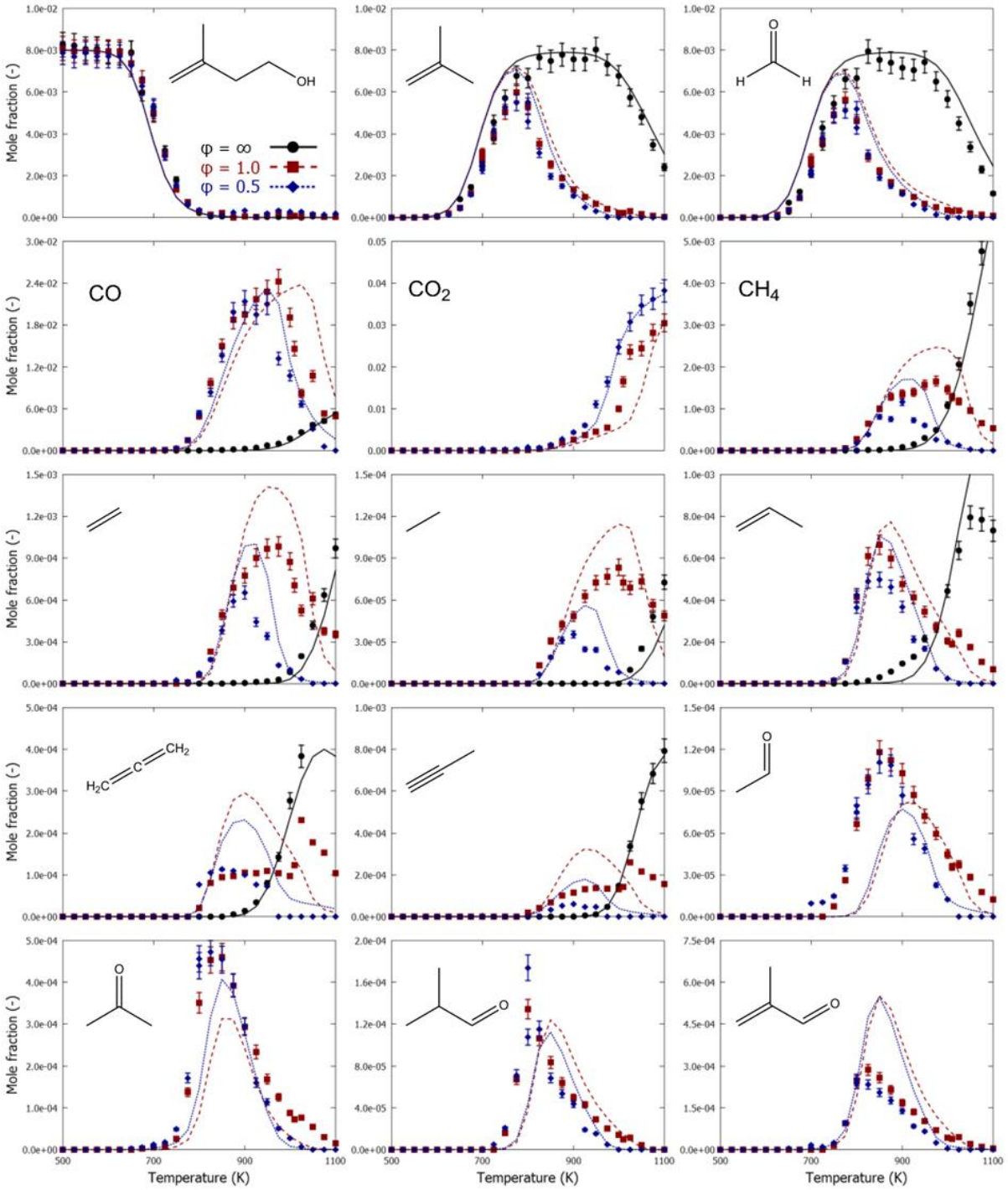

Figure 5.1-4 Mole fractions as a function of temperature for isoprenol oxidation and pyrolysis in a jet-stirred reactor, P=0.107 MPa, F_V =4.06 10^{-5} m^3 s^{-1}, $x_{isoprenol,0}$=0.008, φ=0.5 (blue), φ=1.0 (red) and φ=∞ (black): symbols, experimental mole fraction profile of molecule represented in graph; lines, mole fraction profiles calculated with CHEMKIN using the perfectly stirred reactor model and the developed kinetic model

The isoprenol mole fraction profiles for all equivalence ratios are very similar. At the applied operating conditions, isoprenol starts to decompose at 625K and conversion is approximately complete at 800K. The reactivity of isoprenol cannot be attributed to low-temperature oxidation chemistry as the conversion profile is independent of the presence of oxygen and as

isoprenol pyrolysis and oxidation has a very high selectivity to isobutene and formaldehyde, the two products formed by molecular decomposition of isoprenol. Unlike alkanes[34, 77, 78], no "negative temperature coefficient" (NTC) zone, in which reactivity decreases with increasing temperature, is observed.

In the case of isoprenol pyrolysis, the isobutene and formaldehyde mole fraction increases to approximately 0.008, which corresponds to the initial isoprenol mole fraction in the feed, at 800K. The mole fractions of isobutene and formaldehyde in the reactor effluent remain relatively constant at 0.008 between 800K and 950K. At higher temperatures, isobutene and formaldehyde mole fractions decrease, while mole fractions of other products, such as CO, CH_4, ethene, propene, propyne and allene increase.

In the case of isoprenol oxidation, the isobutene and formaldehyde mole fractions reach their maxima around 775K. At higher temperatures both mole fractions decrease and a wide variety of hydrocarbons and oxygenated molecules are formed, including 2-methyl-2-propenal, 2-methyl-propanal and acetone. The latter molecules are known products of isobutene oxidation[53, 79] and motivates the inclusion of the low-temperature oxidation chemistry of this molecule into the current kinetic model.

5.1.6.1.2 Kinetic model performance

Reactor simulations, using the developed kinetic model, were conducted with the CHEMKIN PRO package using the perfectly stirred reactor module[80]. Calculated mole fraction profiles for isoprenol and products as a function of temperature have been added to Figure 5.1-4 for φ = 0.5, 1.0 and ∞. The predicted mole fraction profiles for isoprenol are independent of the equivalence ratio, which is in agreement with the experimental observation. Model calculated mole fraction profiles for isobutene and formaldehyde are in good agreement with the experimental data, i.e. a constant isobutene and formaldehyde mole fraction of approximately 0.008 between 800 and 950K at $\varphi = \infty$, while both molecules reach their maxima in mole fraction around 775K at φ = 0.5 and 1.0.

The kinetic model accurately reproduces the effect of temperature and equivalence ratio on the mole fraction of the other products displayed in Figure 5.1-4. The main deviations of the kinetic model can be observed for propyne and allene, for which model calculated mole fraction profiles deviate from experimental mole fraction fractions at φ = 1.0.

5.1.6.1.3 Reaction path analysis

A reaction path analysis was performed and the results are displayed in Figure 5.1-5. Operating conditions correspond to φ = 1.0, $x_{isoprenol}$ = 0.008, P = 0.107 MPa,T = 800K and 1000K..

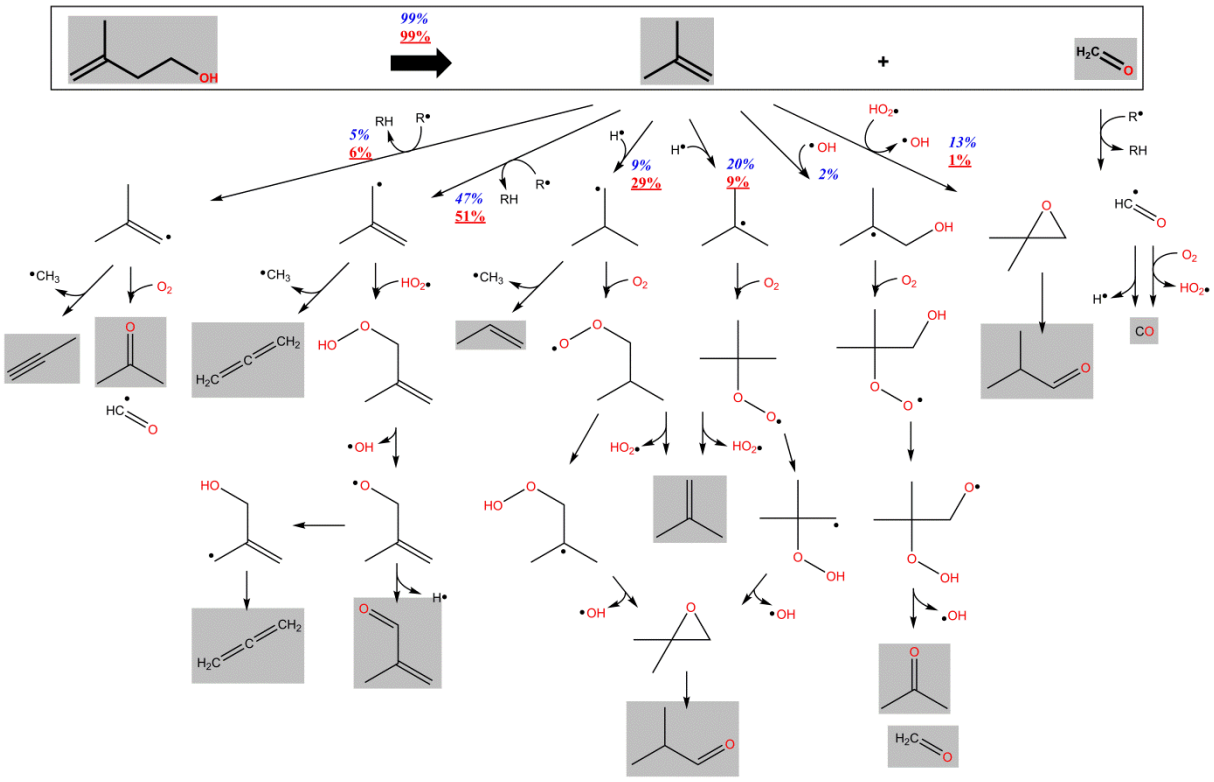

Figure 5.1-5 Reaction path analysis for the decomposition of isoprenol. Operating conditions: F_V =4.06 10^{-5} m^3 s^{-1}, $x_{isoprenol,0}$=0.008, φ=1.0, T = 800K (blue & italic) and 1000K (red & underlined). Percentages on a reaction path represent the reaction rate relative to the total isoprenol decomposition rate. Species with a shaded background have been detected experimentally.

Isoprenol is almost exclusively consumed via unimolecular decomposition to isobutene and formaldehyde. This channel accounts for more than 99% of the total isoprenol consumption. Oxidation of isobutene leads to the majority of products detected in the reactor effluent. Hence, the performance of the kinetic model regarding the obtained experimental dataset depends on two key elements, i.e. correct prediction of unimolecular decomposition of isoprenol to isobutene and formaldehyde and the accuracy of the isobutene oxidation submechanism. The remainder of this paragraph focusses on the reaction paths leading to the major oxygenated intermediates displayed in Figure 5.1-4.

The major consumption path of isobutene is hydrogen abstraction from the allylic C-H site forming the resonantly stabilized isobutenyl radical. Isobutenyl radicals preferentially

recombine with hydroperoxy forming isobutenyl hydroperoxide. The O-O bond in the latter molecule is weak and scission leads to isobutenyloxy plus hydroxyl radicals. C-H β-scission of isobutenyloxy radical forms 2-methyl-2-propenal, one of the major intermediate oxygenated molecules detected experimentally. Isobutenyloxy radical can also isomerize forming a resonantly stabilized radical and subsequent decomposition is an important formation path of allene. At higher temperature and pyrolysis conditions, C-C β-scission of isobutenyl radical to allene plus methyl is a non-negligible consumption channel of isobutenyl radicals.

Hydrogen abstraction from the vinylic carbon atom in isobutene is relatively slow compared to hydrogen abstraction from the allylic carbon atom. The product, 2-methyl-prop-1-en-1-yl radical, either reacts with molecular oxygen forming acetone plus formyl radical, or, it produces propyne plus methyl through C-C β-scission. Note that the calculated mole fraction profiles of propyne and allene deviate from experimental observations at oxidizing conditions. At low temperatures, both C_3H_4 species are over-predicted, and the observed sudden increase for Phi=1.0 is not captured. Rate coefficients of several reactions related to propyne and allene formation were estimated from analogous reactive systems in the isobutene submechanism, e.g. reaction rate coefficients for 2-methyl-prop-1-en-1-yl radical plus molecular oxygen were estimated from vinyl plus molecular oxygen[81]. The observed model performance suggests that additional theoretical calculations regarding radicals derived from isobutene and their interaction with oxygen would be beneficial.

Besides their involvement in hydrogen abstraction reactions, radicals can also add to the C=C double bond of isobutene. Addition of hydroperoxy radical to isobutene leads to 2,2-dimethyloxirane plus hydroxyl[53, 79]. The major consumption path of 2,2-dimethyloxirane is unimolecular decomposition to 2-methyl-propanal. According to the developed model, addition of hydroperoxy radical to isobutene becomes insignificant at higher temperatures. Hydroxyl addition to the C=C double bond is a minor consumption channel of isobutene. Molecular oxygen can add to the formed adduct. Intramolecular hydrogen abstraction of the hydroxyl-peroxy radical forming a hydroperoxy-alkoxy radical and subsequent β-scission leads to acetone, formaldehyde plus hydroxyl. Addition of hydrogen atoms to isobutene can form tert-butyl and isobutyl radicals. β-scission reactions of butyl radicals are in competition with addition of molecular oxygen to butyl radicals forming peroxy radicals. At low temperatures, addition of hydrogen atoms on isobutene forming tert-butyl and subsequent addition of molecular oxygen dominates. At high temperatures, C-H β-scission of tert-butyl

radical, back to isobutene, becomes more important. In contrast to tert-butyl radicals, isobutyl radicals can decompose by C-C β-scission. The latter reaction path dominates over C-H β-scission of isobutyl, back to isobutene, and addition of molecular oxygen on isobutyl. Consumption of isobutene by addition of hydrogen atoms forming isobutyl radical is therefore larger than addition of hydrogen atoms forming tert-butyl radical at high temperatures.

5.1.6.2 Prenol

5.1.6.2.1 Experimental data

Forty-two molecules were detected and quantified in the reactor effluent during prenol oxidation and pyrolysis. The experimental prenol mole fraction profiles and the mole fraction profiles of the most representative products are presented in Figure 5.1-6 as a function of temperature, for $\varphi = 0.5$, 1.0 and ∞.

In contrast to isoprenol, the presence of oxygen in the reactor inlet has a significant influence on the prenol conversion. At $\varphi = 0.5$ and 1.0, prenol conversion starts at approximately 650K and is almost complete at 900K. At $\varphi = \infty$, prenol conversion starts at approximately 850K and is almost complete at 1050K. No clear NTC-zone is observed, but several product mole fraction evolutions (e.g. 3-methyl-2-butenal, acetone, 2-methyl-propanal) display two maxima, one below and one above 750K.

Prenol oxidation and pyrolysis have high selectivities to 3-methy-2-butenal and 2-methyl-1,3-butadiene at the conditions investigated. 3-methyl-2-butenal has a higher yield at $\varphi = 0.5$ and 1.0 than at $\varphi = \infty$. This is consistent with other comparable study's regarding alcohols[1, 82]. The reaction of the α-hydroxyalkyl radical with molecular oxygen is a known important reaction path to aldehydes in the oxidation of alcohols[1, 83]. Obviously, this reaction path is of no significance in the pyrolysis of alcohols.

Besides hydrocarbons and small oxygenated molecules, the reactor effluent includes acetone, 2-methyl-2-propenal and 3-buten-2-one. A recent kinetic modeling study regarding the oxidation of 2-methyl-2-butene, which is the hydrocarbon backbone of prenol, highlighted the importance of hydroperoxy recombination with allylic radicals[72]. Reaction path analysis showed that the latter reactions, and subsequent decomposition, can lead to 2-methyl-2-propenal and 3-buten-2-one. Hydroxyl radical addition on 2-methyl-2-butene and reaction with molecular oxygen, the Waddington mechanism, leads to acetaldehyde, acetone and hydroxyl radical[72].

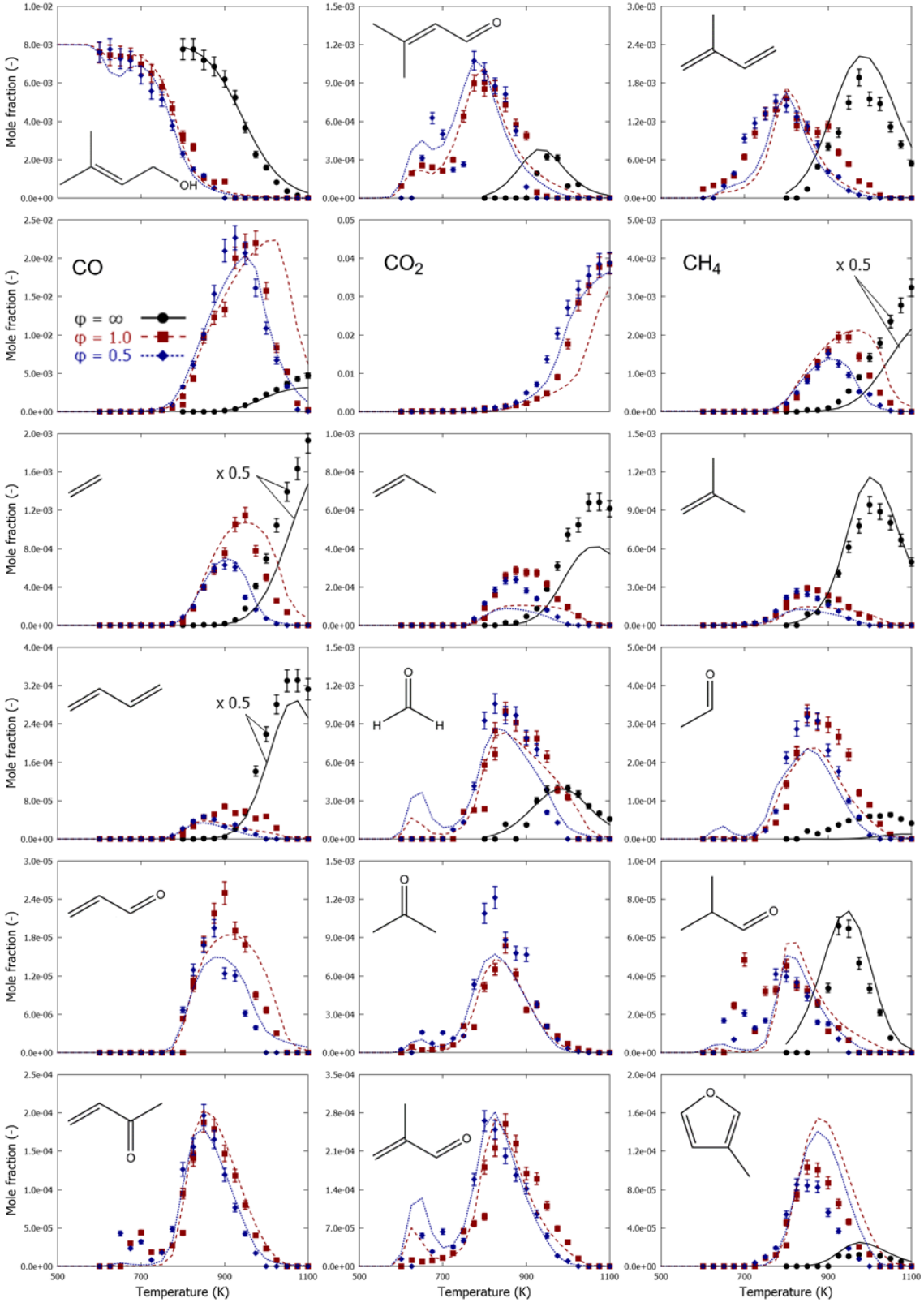

Figure 5.1-6 Mole fractions as a function of temperature for prenol oxidation and pyrolysis in a jet-stirred reactor, P=0.107 MPa, F_V =4.06 10^{-5} m^3 s^{-1}, $x_{prenol,0}$=0.008, φ=0.5 (blue), φ=1.0 (red) and φ=∞ (black): symbols, experimental mole fraction profile of molecule represented in graph; lines, mole fraction profiles calculated with CHEMKIN using the perfectly stirred reactor model and the developed kinetic model

5.1.6.2.2 Kinetic model performance

Reactor simulations, using the developed kinetic model, were conducted with the CHEMKIN PRO package using the perfectly stirred reactor module[80]. Model calculated mole fraction profiles for prenol and products as a function of temperature have been added to Figure 5.1-6 for $\varphi = 0.5$, 1.0 and ∞.

The calculated prenol mole fraction profiles are generally in good agreement with the experimental data, i.e. the effect of temperature and equivalence ratio is accurately reproduced by the kinetic model. Prenol conversion is slightly overestimated below 700K (NTC behavior) for $\varphi = 0.5$.

The 3-methyl-2-butenal profiles, including the local maxima below 700K, are also well reproduced by the kinetic model. The predicted 2-methyl-1,3-butadiene mole fraction profiles matches the experimental mole fraction profile at pyrolysis conditions, while in the presence of oxygen, the kinetic model underestimates 2-methyl-1,3-butadiene yields below 750K. The calculated mole fraction profiles of other products are in reasonable agreement with the experimental data.

5.1.6.2.3 Reaction path analysis

A reaction path analysis was performed to highlight important prenol consumption routes and to identify critical product formation channels. Operating conditions correspond to $\varphi = 1.0$, $x_{prenol} = 0.008$, P = 0.107 MPa, T = 700K and 900K. Prenol conversion is 6% at 700K and 96% at 900K respectively. The results are displayed in Figure 5.1-7.

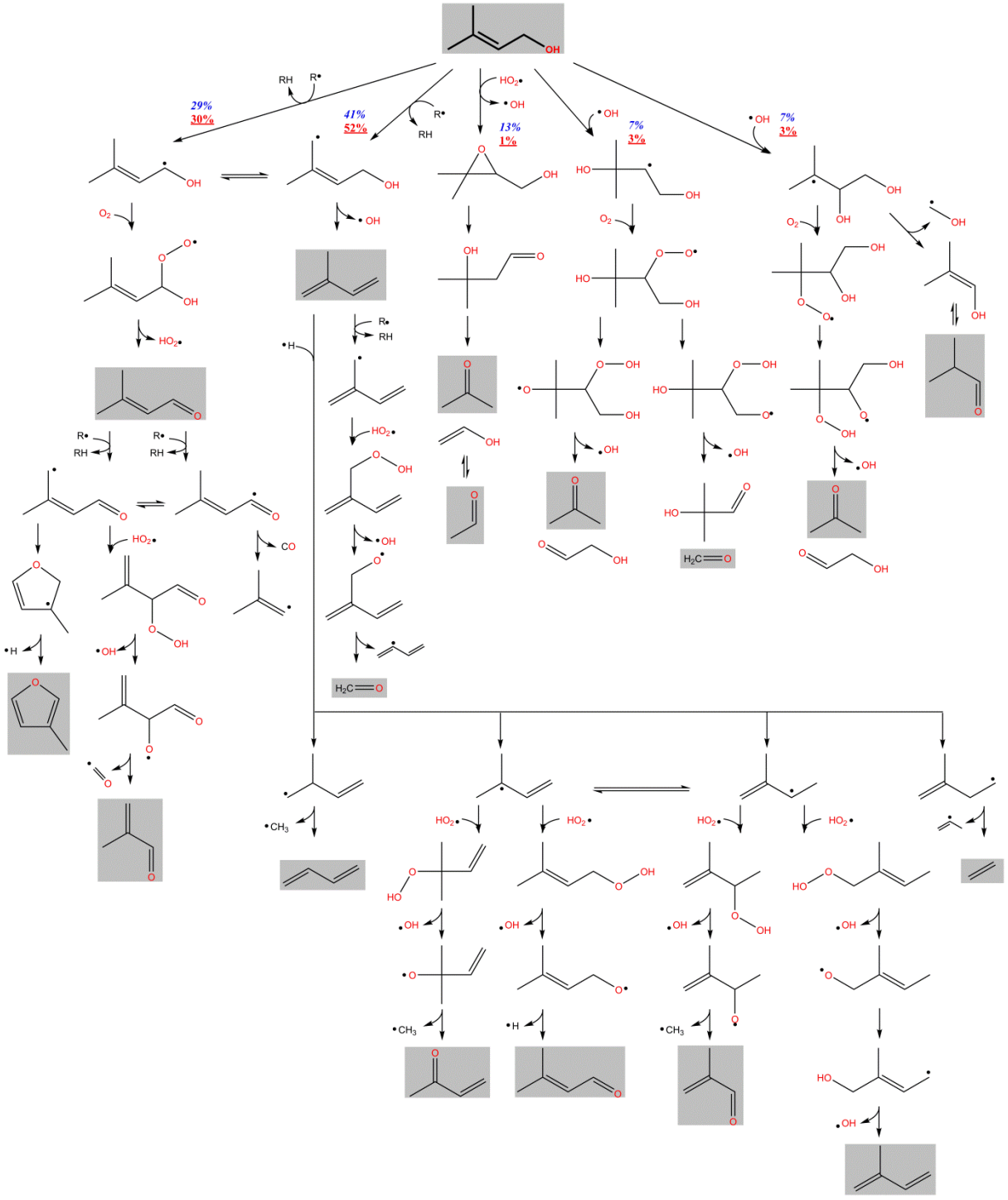

Figure 5.1-7 Reaction path analysis for the decomposition of prenol. Operating conditions: F_V =4.06 10^{-5} m^3 s^{-1}, $x_{prenol,0}$=0.008, φ=1.0, T = 700K (blue & italic) and 900K (red & underlined). Percentages on a reaction path represent the reaction rate relative to the total prenol decomposition rate. Species with a shaded background have been detected experimentally.

5.1.6.2.3.1 Prenol decomposition paths

Prenol consumption is dominated by hydrogen abstraction. Hydrogen abstraction from the α- and δ-carbon atoms leads to resonantly stabilized radicals. The α-prenol radicals can react

with molecular oxygen forming 3-methyl-2-butenal plus hydroperoxy radical (reactions 49 and 50 in Table 5.1-1). In their study regarding the chlorine atom-initiated low-temperature oxidation of prenol, Welz et al. highlighted that this is a low-energy reaction path[29]. At pyrolysis conditions, 3-methyl-2-butenal is formed by direct O-H β-scission of α-prenol radicals (reaction 31 in Table 5.1-1).

Hydrogen abstraction from the δ-carbon atom is the main prenol consumption channel. Intramolecular hydrogen abstraction of the δ-prenol radical forms the α-prenol radical, and vice versa, which proceeds through a 5-membered transition state (reaction 34 in Table 5.1-1). β-scission of the C-O bond is the dominant δ-prenol radical decomposition channel and the main formation route of 2-methyl-1,3-butadiene (reaction 33 in Table 5.1-1).

The hydroperoxy radical can add to the C=C double bond forming 3,3-dimethyl-2-methanol-oxiran plus hydroxyl radical. This type of reaction is known to be important in the oxidation of alkenes as it consumes a relatively unreactive hydroperoxy radical and produces a reactive hydroxyl radical[19]. 3,3-dimethyl-2-methanol-oxiran isomerizes to 3-methyl-3-hydroxy-butanal following hydrogen migration from the hydroxyl group to the ring oxygen atom. 3-methyl-3-hydroxy-butanal can react by a retro-ene reaction to acetone and ethenol. Addition of hydroperoxy radicals is a minor prenol consumption path at higher temperatures. Note that oxygenated molecules with both a hydroxyl and an oxo-functionality, such as 3-methyl-3-hydroxy-butanal and 2-hydroxy-acetaldehyde, were not detected in the reactor effluent.

Hydroxyl radical addition to the C=C double bond (reactions 34 and 42 in Table 5.1-1), followed by addition of molecular oxygen leads to hydroxylated peroxy radicals (reactions 37 and 44 in Table 5.1-1), which can isomerize to hydroperoxy-alkoxy radicals by intermolecular hydrogen abstraction (reactions 38, 40 and 45 in Table 5.1-1). These radicals likely decompose by β-scission of the C-C bond, forming a hydroxyl radical and two carbonyl-containing molecules, the Waddington mechanism.

5.1.6.2.3.2 Decomposition of primary products

The reaction path analysis reveals that a large fraction of the product spectrum formed during the oxidation and pyrolysis of prenol originates from the consumption of 3-methyl-2-butenal and 2-methyl-1,3-butadiene.

Similar to prenol, 3-methyl-2-butenal mainly reacts by hydrogen abstraction forming resonantly stabilized radicals, 3-methyl-but-2-en-1-oxo-1-yl and 3-methyl-but-3-en-1-oxo-2-

yl, see Figure 5.1-7. Both radicals can interconvert by intramolecular hydrogen abstraction. CO α-scission of 3-methyl-but-2-en-1-oxo-1-yl radical forms 2-methyl-prop-1-en-1-yl radical. The latter radical can react with molecular oxygen or by C-C β-scission forming propyne and methyl. 3-methyl-but-3-en-1-oxo-2-yl can recombine with a hydroperoxy radical. Scission of the O-O bond and subsequent decomposition may form 2-methyl-2-propenal and a formyl radical. Alternatively, 3-methyl-but-3-en-1-oxo-2-yl radical can react by intramolecular radical addition forming a 5-membered ring. C-H β-scission of the cyclic radical forms 3-methyl-furan, which was experimentally observed in this work and in the oxidation study by Welz et al.[29].

Besides 3-methyl-2-butenal, 2-methyl-1,3-butadiene is an important product in the oxidation and pyrolysis of prenol. One possible reaction route is hydrogen abstraction from the allylic carbon atom. C-C β-scission of the resulting radical is slow at the investigated operating conditions. Instead, the radical will mainly abstract hydrogen from other species, reforming 2-methyl-1,3-butadiene, or recombine with a hydroperoxy radical. The main consumption path of 2-methyl-1,3-butadiene is addition of hydrogen atoms to one of its double bonds. Hydrogen addition forming resonantly stabilized radicals, 3-methyl-but-2-en-1-yl and 2-methyl-but-2-en-1-yl, is favored. Both radicals can interconvert by intramolecular hydrogen abstraction. Similar to some of the other resonantly stabilized radicals encountered in this work, recombination with hydroperoxy radicals is the major reaction channel. This is in agreement with the conclusions by Welz et al. for 2-methyl-2-butene oxidation[72]. Hydrogen addition to 2-methyl-1,3-butadiene can also form non-resonantly stabilized radicals, i.e. 2-methyl-but-3-en-1-yl and 3-methyl-but-3-en-1-yl. These radicals mainly react by C-C β scission forming 1,3-butadiene plus methyl and ethene plus propen-2-yl radical, respectively.

5.1.6.2.3.3 Low-temperature reactivity

Characteristic for the oxidation of prenol is the occurrence of aldehyde peaks below 700K. Such early formation of oxygenated products has not been observed during the oxidation of 2-methyl-2-butene[72], the hydrocarbon backbone of prenol.

According to the model, this difference can be explained by stabilization effects of the hydroxyl group on peroxy radicals, as has been discussed earlier. The higher stability enables intramolecular hydrogen abstractions which can be followed by fragmentation to aldehydes and/or chain branching reactions.

Reaction path analysis reveals that addition of molecular oxygen to the δ-position is responsible for the chain branching, necessary to trigger low-temperature chemistry. Intramolecular hydrogen abstraction of the peroxy radical through a 7-membered cyclic transition state and subsequent reaction with molecular oxygen will form 4-hydroperoxy-3-methyl-2-butenal (reactions 50, 51 and 52 in Table 5.1-1), see Figure 5.1-8. The latter hydroperoxide reacts by O-O scission.

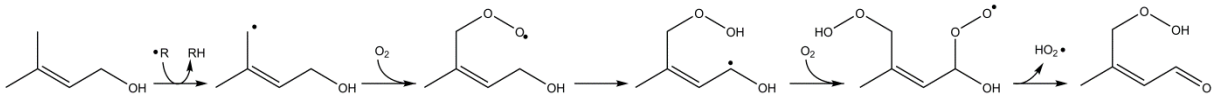

Figure 5.1-8 Chain branching reaction path in the oxidation of prenol

Addition of molecular oxygen to δ-prenol radicals is in competition with addition of molecular oxygen to α-prenol radicals. The latter reaction path leads to 3-methyl-2-butenal plus a hydroperoxy radical and reduces reactivity.

Due to the strong non-nearest neighbor stabilization effects observed in hydroxylated peroxy radicals, group-additivity is not an accurate means to provide the thermochemistry. Similarly, rate coefficients deduced from reactions of reactants that do not contain the hydroxyl functionality have high uncertainties. Improved predictions of the developed kinetic model thus require a systematic quantum-mechanical study of all important reactions. This is beyond the scope of the current study and subject to future work.

5.1.7 Conclusions

The oxidation and pyrolysis of two unsaturated alcohols, prenol and isoprenol, have been studied in the temperature range of 500 to 1100K. It is shown that they react entirely different and that a newly constructed kinetic model reproduces these reactivity differences well.

Isoprenol oxidation and pyrolysis is dominated by a single unimolecular reaction giving formaldehyde and isobutene. The reaction proceeds through a 6-membered transition state and is likely to be important for all unsaturated alcohols which contain the C=C double bond in γ-position relative to the hydroxyl group. Other molecules in the reactor effluent are formed by oxidation and pyrolysis of isobutene and formaldehyde.

The prenol results show that the different position of the double bond completely changes the reactivity, i.e. from molecular channels to radical chemistry. Though prenol reacts through typical pathways, such as hydrogen abstraction and radical addition on the C=C double bond,

the presence of a hydroxyl functional group has a clear impact on the thermochemistry. This enables minor low-temperature chemistry in prenol oxidation, resulting in the formation of aldehydes and ketones. Low-temperature chemistry is not observed during the oxidation of 2-methyl-2-butene, which has the same hydrocarbon structure as prenol.

5.1.8 References

[1] S. M. Sarathy, P. Oßwald, N. Hansen, K. Kohse-Höinghaus, Alcohol combustion chemistry, Prog. Energy Combust. Sci. 44 (2014) 40-102
[2] K. Kohse-Hoinghaus, P. Osswald, T. A. Cool, T. Kasper, N. Hansen, F. Qi, C. K. Westbrook, P. R. Westmoreland, Biofuel Combustion Chemistry: From Ethanol to Biodiesel, Angew. Chem. Int. Ed. 49 (2010) 3572-3597
[3] G. Wang, W. Yuan, Y. Li, L. Zhao, F. Qi, Experimental and kinetic modeling study of n-pentanol pyrolysis and combustion, Combust. Flame 162 (2015) 3277-3287
[4] X. Y. Zhang, B. Yang, W. H. Yuan, Z. J. Cheng, L. D. Zhang, Y. Y. Li, F. Qi, Pyrolysis of 2-methyl-1-butanol at low and atmospheric pressures: Mass spectrometry and modeling studies, P. Combust. Inst. 35 (2015) 409-417
[5] L. Cai, Y. Uygun, C. Togbé, H. Pitsch, H. Olivier, P. Dagaut, S. M. Sarathy, An experimental and modeling study of n-octanol combustion, P. Combust. Inst. 35 (2015) 419-427
[6] Q. Li, C. Tang, Y. Cheng, L. Guan, Z. Huang, Laminar Flame Speeds and Kinetic Modeling of n-Pentanol and Its Isomers, Energ. Fuel. 29 (2015) 5334-5348
[7] M. V. Johnson, S. S. Goldsborough, Z. Serinyel, P. O'Toole, E. Larkin, G. O'Malley, H. J. Curran, A Shock Tube Study of n- and iso-Propanol Ignition, Energ. Fuel. 23 (2009) 5886-5898
[8] R. Van de Vijver, N. M. Vandewiele, P. L. Bhoorasingh, B. L. Slakman, F. Seyedzadeh Khanshan, H.-H. Carstensen, M.-F. Reyniers, G. B. Marin, R. H. West, K. M. Van Geem, Automatic Mechanism and Kinetic Model Generation for Gas- and Solution-Phase Processes: A Perspective on Best Practices, Recent Advances, and Future Challenges, Int. J. Chem. Kinet. 47 (2015) 199-231
[9] Y. Zheng, Q. Liu, L. Li, W. Qin, J. Yang, H. Zhang, X. Jiang, T. Cheng, W. Liu, X. Xu, M. Xian, Metabolic engineering of Escherichia coli for high-specificity production of isoprenol and prenol as next generation of biofuels, Biotechnol. Biofuels 6 (2013) 57
[10] K. W. George, M. G. Thompson, A. Kang, E. Baidoo, G. Wang, L. J. G. Chan, P. D. Adams, C. J. Petzold, J. D. Keasling, T. S. Lee, Metabolic engineering for the high-yield production of isoprenoid-based C-5 alcohols in E-coli, Sci. Rep. 5 (2015)
[11] K. A. Heufer, J. Bugler, H. J. Curran, A comparison of longer alkane and alcohol ignition including new experimental results for n-pentanol and n-hexanol, P. Combust. Inst. 34 (2013) 511-518
[12] K. A. Heufer, S. M. Sarathy, H. J. Curran, A. C. Davis, C. K. Westbrook, W. J. Pitz, Detailed Kinetic Modeling Study of n-Pentanol Oxidation, Energ. Fuel. 26 (2012) 6678-6685
[13] S. Mani Sarathy, S. Park, B. W. Weber, W. Wang, P. S. Veloo, A. C. Davis, C. Togbe, C. K. Westbrook, O. Park, G. Dayma, Z. Luo, M. A. Oehlschlaeger, F. N. Egolfopoulos, T. Lu, W. J. Pitz, C.-J. Sung, P. Dagaut, A comprehensive experimental and modeling study of iso-pentanol combustion, Combust. Flame 160 (2013) 2712-2728
[14] G. da Silva, J. W. Bozzelli, L. Liang, J. T. Farrell, Ethanol Oxidation: Kinetics of the α-Hydroxyethyl Radical + O2 Reaction, J. Phys. Chem. A 113 (2009) 8923-8933
[15] O. Welz, J. Zádor, J. D. Savee, L. Sheps, D. L. Osborn, C. A. Taatjes, Low-Temperature Combustion Chemistry of n-Butanol: Principal Oxidation Pathways of Hydroxybutyl Radicals, J. Phys. Chem. A 117 (2013) 11983-12001
[16] O. Welz, J. Zador, J. D. Savee, M. Y. Ng, G. Meloni, R. X. Fernandes, L. Sheps, B. A. Simmons, T. S. Lee, D. L. Osborn, C. A. Taatjes, Low-temperature combustion chemistry of biofuels: pathways in the initial low-temperature (550 K-750 K) oxidation chemistry of isopentanol, Phys. Chem. Chem. Phys. 14 (2012) 3112-3127
[17] A. Fridlyand, S. S. Goldsborough, K. Brezinsky, S. S. Merchant, W. H. Green, Influence of the double bond position on the oxidation of decene isomers at high pressures and temperatures, P. Combust. Inst. 35 (2015) 333-340
[18] M. Mehl, G. Vanhove, W. J. Pitz, E. Ranzi, Oxidation and combustion of the n-hexene isomers: A wide range kinetic modeling study, Combust. Flame 155 (2008) 756-772
[19] F. Battin-Leclerc, A. Rodriguez, B. Husson, O. Herbinet, P.-A. Glaude, Z. Wang, Z. Cheng, F. Qi, Products from the Oxidation of Linear Isomers of Hexene, J. Phys. Chem. A 118 (2014) 673-683

[20] R. Bounaceur, V. Warth, B. Sirjean, P. A. Glaude, R. Fournet, F. Battin-Leclerc, Influence of the position of the double bond on the autoignition of linear alkenes at low temperature, P. Combust. Inst. 32 (2009) 387-394
[21] C. A. Taatjes, N. Hansen, J. A. Miller, T. A. Cool, J. Wang, P. R. Westmoreland, M. E. Law, T. Kasper, K. Kohse-Höinghaus, Combustion Chemistry of Enols: Possible Ethenol Precursors in Flames, J. Phys. Chem. A 110 (2006) 3254-3260
[22] C. A. Taatjes, N. Hansen, A. McIlroy, J. A. Miller, J. P. Senosiain, S. J. Klippenstein, F. Qi, L. Sheng, Y. Zhang, T. A. Cool, J. Wang, P. R. Westmoreland, M. E. Law, T. Kasper, K. Kohse-Höinghaus, Enols Are Common Intermediates in Hydrocarbon Oxidation, Science 308 (2005) 1887-1889
[23] J. P. Senosiain, S. J. Klippenstein, J. A. Miller, Reaction of Ethylene with Hydroxyl Radicals: A Theoretical Study, J. Phys. Chem. A 110 (2006) 6960-6970
[24] J. Zador, A. W. Jasper, J. A. Miller, The reaction between propene and hydroxyl, Phys. Chem. Chem. Phys. 11 (2009) 11040-11053
[25] L. K. Huynh, H. R. Zhang, S. Zhang, E. Eddings, A. Sarofim, M. E. Law, P. R. Westmoreland, T. N. Truong, Kinetics of Enol Formation from Reaction of OH with Propene, J. Phys. Chem. A 113 (2009) 3177-3185
[26] G. da Silva, J. W. Bozzelli, Role of the α-hydroxyethylperoxy radical in the reactions of acetaldehyde and vinyl alcohol with HO2, Chem. Phys. Lett. 483 (2009) 25-29
[27] G. da Silva, Carboxylic Acid Catalyzed Keto-Enol Tautomerizations in the Gas Phase, Angew. Chem. Int. Ed. 49 (2010) 7523-7525
[28] A. Rodríguez, D. Rodríguez, A. Soto, I. Bravo, Y. Diaz-de-Mera, A. Notario, A. Aranda, Products and mechanism of the reaction of Cl atoms with unsaturated alcohols, Atmos. Environ. 50 (2012) 214-224
[29] O. Welz, J. D. Savee, D. L. Osborn, C. A. Taatjes, Chlorine atom-initiated low-temperature oxidation of prenol and isoprenol: The effect of CC double bonds on the peroxy radical chemistry in alcohol oxidation, P. Combust. Inst. 35 (2015) 401-408
[30] C. K. Westbrook, W. J. Pitz, S. M. Sarathy, M. Mehl, Detailed chemical kinetic modeling of the effects of CC double bonds on the ignition of biodiesel fuels, P. Combust. Inst. 34 (2013) 3049-3056
[31] R. Van de Vijver, N. M. Vandewiele, A. G. Vandeputte, K. M. Van Geem, M.-F. Reyniers, W. H. Green, G. B. Marin, Rule-based ab initio kinetic model for alkyl sulfide pyrolysis, Chem. Eng. J. 278 (2015) 385-393
[32] N. M. Vandewiele, K. M. Van Geem, M.-F. Reyniers, G. B. Marin, Genesys: Kinetic model construction using chemo-informatics, Chem. Eng. J. 207 (2012) 526-538
[33] O. Herbinet, F. Battin-Leclerc, Progress in Understanding Low-Temperature Organic Compound Oxidation Using a Jet-Stirred Reactor, Int. J. Chem. Kinet. 46 (2014) 619-639
[34] O. Herbinet, B. Husson, Z. Serinyel, M. Cord, V. Warth, R. Fournet, P.-A. Glaude, B. Sirjean, F. Battin-Leclerc, Z. Wang, M. Xie, Z. Cheng, F. Qi, Experimental and modeling investigation of the low-temperature oxidation of n-heptane, Combust. Flame 159 (2012) 3455-3471
[35] O. Herbinet, P. M. Marquaire, F. Battin-Leclerc, R. Fournet, Thermal decomposition of n-dodecane: Experiments and kinetic modeling, J. Anal. Appl. Pyrolysis 78 (2007) 419-429
[36] M. J. Frisch, G. W. Trucks, H. B. Schlegel, G. E. Scuseria, M. A. Robb, J. R. Cheeseman, G. Scalmani, V. Barone, B. Mennucci, G. A. Petersson, H. Nakatsuji, M. Caricato, X. Li, H. P. Hratchian, A. F. Izmaylov, J. Bloino, G. Zheng, J. L. Sonnenberg, M. Hada, M. Ehara, K. Toyota, R. Fukuda, J. Hasegawa, M. Ishida, T. Nakajima, Y. Honda, O. Kitao, H. Nakai, T. Vreven, J. A. Montgomery, J. E. Peralta, F. Ogliaro, M. Bearpark, J. J. Heyd, E. Brothers, K. N. Kudin, V. N. Staroverov, R. Kobayashi, J. Normand, K. Raghavachari, A. Rendell, J. C. Burant, S. S. Iyengar, J. Tomasi, M. Cossi, N. Rega, J. M. Millam, M. Klene, J. E. Knox, J. B. Cross, V. Bakken, C. Adamo, J. Jaramillo, R. Gomperts, R. E. Stratmann, O. Yazyev, A. J. Austin, R. Cammi, C. Pomelli, J. W. Ochterski, R. L. Martin, K. Morokuma, V. G. Zakrzewski, G. A. Voth, P. Salvador, J. J. Dannenberg, S. Dapprich, A. D. Daniels, Farkas, J. B. Foresman, J. V. Ortiz, J. Cioslowski, D. J. Fox, in: Wallingford CT, 2009.
[37] J. A. Montgomery Jr, M. J. Frisch, A complete basis set model chemistry. VI. Use of density functional geometries and frequencies, J. Chem. Phys. 110 (1999) 2822
[38] A. L. L. East, L. Radom, An initio statistical thermodynamical models for the computation of third-law entropies, J. Chem. Phys. 106 (1997) 6655
[39] L. A. Curtiss, K. Raghavachari, P. C. Redfern, J. A. Pople, Assessment of Gaussian-2 and density functional theories for the computation of enthalpies of formation, J. Chem. Phys. 106 (1997) 1063-1079
[40] G. A. Petersson, D. K. Malick, W. G. Wilson, J. W. Ochterski, J. A. Montgomery, M. J. Frisch, Calibration and comparison of the Gaussian-2, complete basis set, and density functional methods for computational thermochemistry, J. Chem. Phys. 109 (1998) 10570-10579
[41] L. A. Curtiss, K. Raghavachari, P. C. Redfern, V. Rassolov, J. A. Pople, Gaussian-3 (G3) theory for molecules containing first and second-row atoms, J. Chem. Phys. 109 (1998) 7764-7776

[42] M. K. Sabbe, M. Saeys, M.-F. Reyniers, G. B. Marin, V. Van Speybroeck, M. Waroquier, Group additive values for the gas phase standard enthalpy of formation of hydrocarbons and hydrocarbon radicals, J. Phys. Chem. A 109 (2005) 7466-7480
[43] N. M. Vandewiele, R. Van de Vijver, K. M. Van Geem, M.-F. Reyniers, G. B. Marin, Symmetry calculation for molecules and transition states, J. Comput. Chem. 36 (2015) 181-192
[44] C. F. Goldsmith, G. R. Magoon, W. H. Green, Database of Small Molecule Thermochemistry for Combustion, J. Phys. Chem. A 116 (2012) 9033-9057
[45] M. K. Sabbe, F. De Vleeschouwer, M.-F. Reyniers, M. Waroquier, G. B. Marin, First Principles Based Group Additive Values for the Gas Phase Standard Entropy and Heat Capacity of Hydrocarbons and Hydrocarbon Radicals, J. Phys. Chem. A 112 (2008) 12235-12251
[46] P. D. Paraskevas, M. K. Sabbe, M.-F. Reyniers, N. G. Papayannakos, G. B. Marin, Group Additive Values for the Gas-Phase Standard Enthalpy of Formation, Entropy and Heat Capacity of Oxygenates, Chem.-Eur. J. 19 (2013) 16431-16452
[47] E. Goos, A. Burcat, B. Ruscic, Extended Third Millennium Thermodynamic Database for Combustion and Air-Pollution Use with Updates from Active Thermochemical Tables, 2014
[48] S. W. Benson, Thermochemical Kinetics: Methods for the Estimation of Thermochemical Data and Rate Parameters, John Wiley & Sons, New York, 1976
[49] C.-W. Zhou, Y. Li, E. O'Connor, K. P. Somers, S. Thion, C. Keesee, O. Mathieu, E. L. Petersen, T. A. DeVerter, M. A. Oehlschlaeger, G. Kukkadapu, C.-J. Sung, M. Alrefae, F. Khaled, A. Farooq, P. Dirrenberger, P.-A. Glaude, F. Battin-Leclerc, J. Santner, Y. Ju, T. Held, F. M. Haas, F. L. Dryer, H. J. Curran, A comprehensive experimental and modeling study of isobutene oxidation, Combust. Flame (Accepted)
[50] S. M. Burke, W. Metcalfe, O. Herbinet, F. Battin-Leclerc, F. M. Haas, J. Santner, F. L. Dryer, H. J. Curran, An experimental and modeling study of propene oxidation. Part 1: Speciation measurements in jet-stirred and flow reactors, Combust. Flame 161 (2014) 2765-2784
[51] M. M. Kopp, N. S. Donato, E. L. Petersen, W. K. Metcalfe, S. M. Burke, H. J. Curran, Oxidation of Ethylene–Air Mixtures at Elevated Pressures, Part 1: Experimental Results, J. Propul. Power 30 (2014) 790-798
[52] W. K. Metcalfe, S. M. Burke, S. S. Ahmed, H. J. Curran, A Hierarchical and Comparative Kinetic Modeling Study of C1 − C2 Hydrocarbon and Oxygenated Fuels, Int. J. Chem. Kinet. 45 (2013) 638-675
[53] P. Dagaut, M. Cathonnet, Isobutene Oxidation and Ignition: Experimental and Detailed Kinetic Modeling Study, Combust. Sci. Technol. 137 (1998) 237-275
[54] P. D. Paraskevas, M. K. Sabbe, M.-F. Reyniers, N. G. Papayannakos, G. B. Marin, Group Additive Kinetics for Hydrogen Transfer Between Oxygenates, J. Phys. Chem. A (2015)
[55] G. Mittal, S. M. Burke, V. A. Davies, B. Parajuli, W. K. Metcalfe, H. J. Curran, Autoignition of ethanol in a rapid compression machine, Combust. Flame 161 (2014) 1164-1171
[56] J. Zádor, S. J. Klippenstein, J. A. Miller, Pressure-Dependent OH Yields in Alkene + HO2 Reactions: A Theoretical Study, J. Phys. Chem. A 115 (2011) 10218-10225
[57] H. J. Curran, P. Gaffuri, W. J. Pitz, C. K. Westbrook, A comprehensive modeling study of n-heptane oxidation, Combust. Flame 114 (1998) 149-177
[58] M. K. Sabbe, M.-F. Reyniers, V. Van Speybroeck, M. Waroquier, G. B. Marin, Carbon-centered radical addition and beta-scission reactions: Modeling of activation energies and pre-exponential factors, ChemPhysChem 9 (2008) 124-140
[59] P. D. Paraskevas, M. K. Sabbe, M.-F. Reyniers, N. G. Papayannakos, G. B. Marin, Kinetic Modeling of α-Hydrogen Abstractions from Unsaturated and Saturated Oxygenate Compounds by Carbon-Centered Radicals, ChemPhysChem 15 (2014) 1849-1866
[60] K. Wang, S. M. Villano, A. M. Dean, Reactivity–Structure-Based Rate Estimation Rules for Alkyl Radical H Atom Shift and Alkenyl Radical Cycloaddition Reactions, J. Phys. Chem. A 119 (2015) 7205-7221
[61] J. Bugler, K. P. Somers, E. J. Silke, H. J. Curran, Revisiting the Kinetics and Thermodynamics of the Low-Temperature Oxidation Pathways of Alkanes: A Case Study of the Three Pentane Isomers, J. Phys. Chem. A 119 (2015) 7510-7527
[62] H. Sun, J. W. Bozzelli, C. K. Law, Thermochemical and Kinetic Analysis on the Reactions of O2 with Products from OH Addition to Isobutene, 2-Hydroxy-1,1-dimethylethyl, and 2-Hydroxy-2-methylpropyl Radicals: HO2 Formation from Oxidation of Neopentane, Part II, J. Phys. Chem. A 111 (2007) 4974-4986
[63] J. Lee, J. W. Bozzelli, Thermochemical and kinetic analysis of the allyl radical with O2 reaction system, P. Combust. Inst. 30 (2005) 1015-1022
[64] F. Zhang, T. S. Dibble, Effects of Olefin Group and Its Position on the Kinetics for Intramolecular H-Shift and HO2 Elimination of Alkenyl Peroxy Radicals, J. Phys. Chem. A 115 (2011) 655-663
[65] P. D. Paraskevas, M. K. Sabbe, M.-F. Reyniers, N. G. Papayannakos, G. B. Marin, Kinetic Modeling of α-Hydrogen Abstractions from Unsaturated and Saturated Oxygenate Compounds by Hydrogen Atoms, J. Phys. Chem. A 118 (2014) 9296-9309

[66] M. K. Sabbe, A. Vandeputte, M.-F. Reyniers, M. Waroquier, G. B. Marin, Modeling the influence of resonance stabilization on the kinetics of hydrogen abstractions, Phys. Chem. Chem. Phys. 12 (2010) 1278-1298
[67] M. K. Sabbe, M.-F. Reyniers, M. Waroquier, G. B. Marin, Hydrogen Radical Additions to Unsaturated Hydrocarbons and the Reverse beta-Scission Reactions: Modeling of Activation Energies and Pre-Exponential Factors, ChemPhysChem 11 (2010) 195-210
[68] J. Mendes, C.-W. Zhou, H. J. Curran, Theoretical Chemical Kinetic Study of the H-Atom Abstraction Reactions from Aldehydes and Acids by Ḣ Atoms and ȮH, HȮ2, and ĊH3 Radicals, J. Phys. Chem. A 118 (2014) 12089-12104
[69] R. Sivaramakrishnan, J. V. Michael, Rate Constants for OH with Selected Large Alkanes: Shock-Tube Measurements and an Improved Group Scheme, J. Phys. Chem. A 113 (2009) 5047-5060
[70] J. Badra, A. Elwardany, A. Farooq, Shock tube measurements of the rate constants for seven large alkanes + OH, P. Combust. Inst. 35 (2015) 189-196
[71] J. Aguilera-Iparraguirre, H. J. Curran, W. Klopper, J. M. Simmie, Accurate Benchmark Calculation of the Reaction Barrier Height for Hydrogen Abstraction by the Hydroperoxyl Radical from Methane. Implications for CnH2n+2 where n = 2 → 4, J. Phys. Chem. A 112 (2008) 7047-7054
[72] C. K. Westbrook, W. J. Pitz, M. Mehl, P.-A. Glaude, O. Herbinet, S. Bax, F. Battin-Leclerc, O. Mathieu, E. L. Petersen, J. Bugler, H. J. Curran, Experimental and Kinetic Modeling Study of 2-Methyl-2-Butene: Allylic Hydrocarbon Kinetics, J. Phys. Chem. A 119 (2015) 7462-7480
[73] C. F. Goldsmith, S. J. Klippenstein, W. H. Green, Theoretical rate coefficients for allyl + HO2 and allyloxy decomposition, P. Combust. Inst. 33 (2011) 273-282
[74] J. Zádor, R. X. Fernandes, Y. Georgievskii, G. Meloni, C. A. Taatjes, J. A. Miller, The reaction of hydroxyethyl radicals with O2: A theoretical analysis and experimental product study, P. Combust. Inst. 32 (2009) 271-277
[75] S. P. Pyl, K. M. Van Geem, P. Puimège, M. K. Sabbe, M.-F. Reyniers, G. B. Marin, A comprehensive study of methyl decanoate pyrolysis, Energy 43 (2012) 146-160
[76] R. De Bruycker, J. M. Anthonykutty, J. Linnekoski, A. Harlin, J. Lehtonen, K. M. Van Geem, J. Räsänen, G. B. Marin, Assessing the Potential of Crude Tall Oil for the Production of Green-Base Chemicals: An Experimental and Kinetic Modeling Study, Ind. Eng. Chem. Res. 53 (2014) 18430-18442
[77] J. Zádor, C. A. Taatjes, R. X. Fernandes, Kinetics of elementary reactions in low-temperature autoignition chemistry, Prog. Energy Combust. Sci. 37 (2011) 371-421
[78] J. Biet, M. H. Hakka, V. Warth, P. A. Glaude, F. Battin-Leclerc, Experimental and modeling study of the low-temperature oxidation of large alkanes, Energ. Fuel. 22 (2008) 2258-2269
[79] J. C. Bauge, F. Battin-Leclerc, F. Baronnet, Experimental and modeling study of the oxidation of isobutene, Int. J. Chem. Kinet. 30 (1998) 629-640
[80] R. J. Kee, F. M. Rupley, J. A. Miller, M. E. Coltrin, J. F. Grcar, E. Meeks, H. K. Moffat, A. E. Lutz, G. Dixon-Lewis, M. D. Smooke, J. Warnatz, G. H. Evans, L. R. S., R. E. Mitchell, L. R. Petzold, W. C. Reynolds, M. Caracotsios, W. E. Stewart, P. Glarborg, C. Wang, O. Adigun, in: 15101 ed.; Reaction Design, Inc.: San Diego (CA), 2010.
[81] C. F. Goldsmith, L. B. Harding, Y. Georgievskii, J. A. Miller, S. J. Klippenstein, Temperature and Pressure-Dependent Rate Coefficients for the Reaction of Vinyl Radical with Molecular Oxygen, J. Phys. Chem. A 119 (2015) 7766-7779
[82] J. Cai, L. Zhang, F. Zhang, Z. Wang, Z. Cheng, W. Yuan, F. Qi, Experimental and Kinetic Modeling Study of n-Butanol Pyrolysis and Combustion, Energ. Fuel. 26 (2012) 5550-5568
[83] S. M. Sarathy, S. Vranckx, K. Yasunaga, M. Mehl, P. Oßwald, W. K. Metcalfe, C. K. Westbrook, W. J. Pitz, K. Kohse-Höinghaus, R. X. Fernandes, H. J. Curran, A comprehensive chemical kinetic combustion model for the four butanol isomers, Combust. Flame 159 (2012) 2028-2055

5.2 Experimental and kinetic modeling study of the pyrolysis and oxidation of 1,5-hexadiene: The reactivity of allylic radicals and their role in the formation of aromatics

5.2.1 Abstract

Resonantly stabilized radicals play an important role in the formation of aromatics. In this section, the pyrolysis and oxidation (φ=1 and 2) of 1,5-hexadiene, diluted in He, has been studied experimentally in a jet-stirred reactor at atmospheric pressure. The temperature was varied between 500 and 1100K and the residence time was fixed at 2s. Gas chromatography was used to determine the reactor effluent composition. The pyrolysis of 1,5-hexadiene results in the formation of small alkenes and cyclic hydrocarbons, with a particularly high selectivity towards 1,3-cyclopentadiene and benzene. In the presence of molecular oxygen, various oxygenated intermediates, including acrolein, prop-2-en-1-ol and but-3-enyl-oxiran, were detected in the outlet gases, besides the pyrolysis products. A detailed kinetic model was developed, mainly using an automatic network generation tool, and used to simulate and interpret the performed experiments. Model calculated and experimental mole fraction profiles are in relatively good agreement. In low-temperature pyrolysis conditions, 1,5-hexadiene is in quasi-equilibrium with allyl radicals. Hydrogen abstraction from 1,5-hexadiene by allyl is the most sensitive reaction for conversion. The resulting hexa-2,5-dien-1-yl radical can react by intramolecular radical addition and eventually form 1,3-cyclopentadiene and benzene. Recombination of cyclopentadienyl with alkyl radicals followed by hydrogen abstraction and ring enlargement is an important aromatic formation path. In oxidation, the pyrolysis reaction pathways are in competition with reactions involving hydroxyl and hydroperoxy radicals, as well as oxygen. Above 900K, 1,5-hexadiene is mainly consumed by C-C scission. The reactivity and product spectrum in 1,5-hexadiene oxidation is sensitive towards the reactions of allyl with hydroperoxy radicals. Recombination and O-O scission of the resulting hydroperoxide forms hydroxyl and allyloxy radicals. Allyl plus hydroperoxy radical can also form propene plus molecular oxygen which decreases the number of radicals in the system.

Keywords 1,5-hexadiene, allyl, jet-stirred reactor, recombination reactions, formation of aromatics

5.2.2 Introduction

The pyrolysis and oxidation of hydrocarbon and oxygenated molecules often leads to the formation of polycyclic aromatic hydrocarbons (PAH) which are considered the main precursors for deposits or soot particles [1]. Resonantly stabilized radicals, such as propargyl, allyl and cyclopentadienyl, have been identified as important intermediates for PAH formation [2-5]. They have prolonged lifetimes compared to non-resonantly stabilized radicals and can therefore accumulate at fuel-rich oxidation or pyrolysis conditions. Recombination with other radicals in the reactive system is an important consumption route leading to molecular weight growth [6]. In this respect, the self-recombination of propargyl radicals to benzene has been investigated thoroughly [5, 7, 8]. Other important recombination channels routes that eventually lead to benzene include allyl plus propargyl and allyl plus allyl [2, 6]. Self-recombination of allyl results in 1,5-hexadiene, which upon hydrogen abstraction from the allylic carbon atoms forms hexa-2,5-dien-1-yl. Cyclization of hexa-2,5-dien-1-yl produces C5 and C6 ring species [9, 10]. Note that hexa-2,5-dien-1-yl is also formed by addition of vinyl on 1,3-butadiene [11]. The latter reaction channel has been recognized as a potential benzene formation channel [11], especially at relatively low temperatures.

This study provides an experimental dataset regarding the oxidation and pyrolysis of 1,5-hexadiene, the self-recombination product of allyl, in a jet-stirred reactor. This is motivated by the interest to comprehend the role that 1,5-hexadiene and allylic radicals play in the formation of aromatics. In order to interpret the data, a kinetic model has been developed using an automatic network generation tool. This model was augmented with kinetic data from several recent literature-reported theoretical calculations. The model was used to simulate the obtained experimental data and to identify the main reaction pathways.

5.2.3 Experimental methods

The applied experimental setup is an isothermal quartz jet-stirred reactor with a dedicated feed section and analysis section for outlet gases. The main features of the apparatus are discussed below, details can be found elsewhere[12, 13].

Helium and oxygen were provided by Messer (purities of 99.99% and 99.999% respectively) while 1,5-hexadiene was provided by Sigma-Aldrich (purity of 98%). The helium and oxygen flow rates to the reactor are controlled with two gas-mass-flow controllers (Bronkhorst). The 1,5-hexadiene flow rate is regulated using a liquid-Coriolis-flow controller (Bronkhorst). The

liquid is mixed with helium and passes through an evaporator (kept at 450K). Afterwards, oxygen is added to the gaseous flow.

The gaseous mixture flows through an annular preheating zone, where it is heated to the reactor temperature, and enters the jet-stirred reactor through four nozzles. The nozzles and reactor are designed to avoid thermal and concentration gradients. Thermocoax resistance wires provide heating for the annular preheating zone and the reactor. A type K thermocouple measures the temperature in the center of the reactor (measured temperature gradients < 5K). The pressure is set with a needle valve downstream of the reactor.

The exit of the reactor is connected to several gas chromatographs through heated transfer lines, kept at 473K, to avoid condensation. The reactor effluent composition is quantified using three gas chromatographs. Response factors were determined by injecting known amounts of pure substances or using the effective carbon number method. The first gas chromatograph is equipped with a thermal conductivity detector and uses a Carbosphere packed column for separation. The second gas chromatograph has a flame-ionization detector, preceded by a methanizer, and is equipped with a PlotQ capillary column. The third gas chromatograph is equipped with a flame-ionization detector and a HP-5MS capillary column. A forth gas chromatograph, which is used for product identification only, uses a PlotQ or HP-5MS capillary column for separation and a quadrupole mass spectrometer as detector.

In this work, the 1,5-hexadiene inlet mole fraction was kept constant at 0.008 and the inlet volumetric flow rate was fixed at $4.06\ 10^{-5}$ $m^3\ s^{-1}$, which corresponds to a residence time of 2s. Three equivalence ratios were investigated, i.e. φ=1.0, 2.0 and ∞, for which the effluent compositions were quantitatively analyzed. The pressure was fixed at 0.107 MPa for all experiments and the reactor temperature was varied between 500 and 1100K. The experimental procedure allowed to close the carbon molar balance within 5%. The hydrogen molar balance closed within 5% in pyrolysis conditions. Since water was not quantified in this work, hydrogen and oxygen molar balances could not be verified at φ=1.0 and 2.0. The uncertainty on experimental mole fractions is approximately 6% in 1,5-hexadiene oxidation and pyrolysis based on repeat experiments.

5.2.4 Kinetic model development

A kinetic model has been developed for the oxidation and pyrolysis of 1,5-hexadiene, consisting of two parts. The first part is a submechanism containing reactions describing the consumption of 1,5-hexadiene and derived radicals. The second part of the developed kinetic

model describes the pyrolysis and oxidation of propene, 1,3-cyclopentadiene and aromatics. The complete kinetic model is in CHEMKIN [14] format.

5.2.4.1 Submechanism for the pyrolysis and oxidation of 1,5-hexadiene

The majority of the 1,5-hexadiene submechanism has been generated automatically using Genesys
[15]. After model generation, several key reactions and associated thermochemical data were replaced with literature-reported quantum chemical calculations and experimental observations.

5.2.4.1.1 Kinetic model construction

Genesys requires a set of initial molecules, i.e. reactants, and a set of reaction families as input. Each reaction family describes how reactants are transformed into products through the course of that specific reaction. For each reaction of a specific reaction family, Genesys assigns reaction rate coefficients using a methodology provided by the user, e.g. Evans-Polanyi relationships, group additivity for pre-exponential factors and activation energies, reactivity-structure-based rate rules or simple analogy with similar reactions. Thermochemical data for generated molecules and radicals are taken from extensive databases whenever possible [16, 17]. Otherwise, Benson's group additivity concept for thermochemistry is used [18]. The algorithm in Genesys starts by reacting the initial molecules using the considered reaction families. The generated reactions and species are added to the reaction network. The algorithm continues until all generated species have reacted according to the provided reaction families. The user can add constraints to reaction families to prevent the generation of kinetically insignificant reactions.

5.2.4.1.2 Reaction families

The reaction families considered in the automated mechanism development step are listed below and more details are given in Appendix B.

The rate coefficients for hydrogen abstraction by hydrogen atoms and carbon-centered radicals, and C-C and C-H β-scission reactions were estimated using a group additive framework for pre-exponential factors and activation energies [19-21].

Reaction rate coefficients for hydrogen abstraction by hydroxyl and hydroperoxy radicals from carbon atoms were estimated from analogous hydrogen abstraction reactions from alkanes and alkenes [22-25].

Kinetic parameters for intramolecular radical addition and hydrogen abstraction were estimated using reactivity-structure-based estimation rules [26]. These reactions proceed through a cyclic transition state. The pre-exponential factor is correlated with the number of hindered rotors in the transition state and the activation energy is the sum of analogous bimolecular reaction and the ring strain in the transition state.

The reaction rate coefficients for addition reactions of molecular oxygen to carbon-centered radicals and subsequent reactions were estimated from analogous alkane and alkene reactions [27, 28]. The reaction rate coefficient for the allyl plus hydroperoxy reaction system [29] was used to estimate the recombination of hydroperoxy radicals with resonantly stabilized radicals and the subsequent decomposition of the hydroperoxide. These reactions were shown to be important in the oxidation of propene and 2-methyl-2-butene [30, 31].

5.2.4.1.3 Updated C_6H_{10}, C_6H_9, C_6H_8, C_6H_6 and C_7H_{11} chemistry

After model generation, several reaction rate coefficients of key reactions and the associated thermochemical data of several species were replaced with literature-reported quantum chemical calculations and experimental observations. For example, the unimolecular decomposition of 1,5-hexadiene to allyl plus allyl has recently been investigated in a shock tube [32]. The recommended kinetic and thermodynamic data were incorporated in the developed kinetic model. Wang et al. [9] investigated the reactivity of allylic radicals and calculated the C_6H_9 potential energy surface, which includes decomposition routes of hexa-2,5-dien-1-yl, and the C_7H_{11} potential energy surface, which includes addition of allyl on 1,3-butadiene, at the CBS-QB3 level of theory [9]. The proposed reaction rate coefficients were implemented in the kinetic model. Reaction rate coefficient for the self-reaction of propargyl and reaction of propargyl with allyl were taken from Miller and coworkers[7, 33, 34].

5.2.4.2 Pyrolysis and oxidation of propene, 1,3-cyclopentadiene and aromatics

Propene, 1,3-cyclopentadiene and aromatics are important products in the oxidation and pyrolysis of 1,5-hexadiene and consumption pathways for these species need to be included for an adequate performance of the kinetic model. Therefore, the thoroughly validated propene oxidation model by Burke et al. [30, 35] was added to the 1,5-hexadiene submechanism to describe the propene chemistry. The subsequent chemistry of 1,3-cyclopentadiene was taken from Green and coworkers [10, 36]. Finally, submechanisms for the oxidation of aromatics, including benzene/toluene/styrene, were taken from Herbinet et al.[12].

5.2.5 Results and discussion

5.2.5.1 Experimental and modeling results

Experiments were performed at pyrolysis (φ=∞), stoichiometric (φ=1.0) and fuel rich (φ=2.0) oxidation conditions. No "negative temperature coefficient" zone, in which the reactivity decreases with increasing temperature, was observed in the oxidation experiments. Alkenes are known to have reduced low-temperature reactivity compared to alkanes [37]. Hexa-2,5-dien-1-yl, the radical formed following hydrogen abstraction from the allylic carbon atom in 1,5-hexadiene, is resonantly stabilized. The resonance stabilization is lost upon addition of molecular oxygen. Redissociation of the adduct to the reactants is likely to be the major reaction path, rather than intramolecular hydrogen abstraction, which can trigger chain branching and low-temperature reactivity [37].

Sixty products were detected and quantified in the reactor outlet gases. A selection of mole fraction profiles are displayed in Figure 5.2-1 (φ=∞), Figure 5.2-2 (φ=1.0) and Figure 5.2-3 (φ=2.0). These species were chosen because they (a) have high yields in 1,5-hexadiene pyrolysis and oxidation, (b) are important intermediates of 1,5-hexadiene decomposition and/or (c) are PAH precursors.

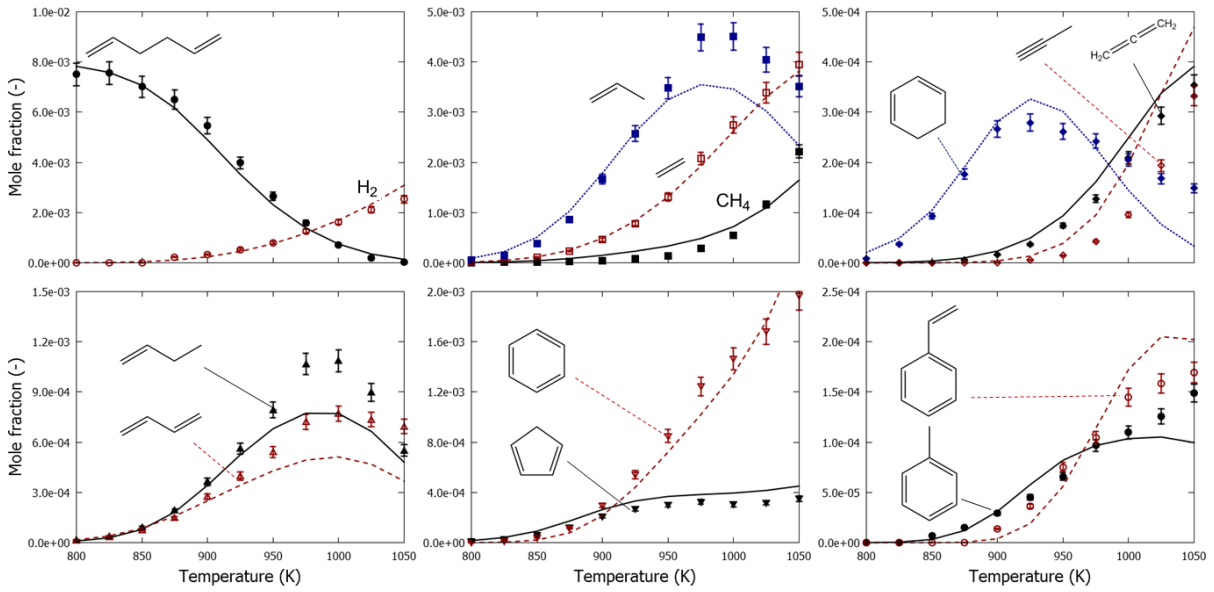

Figure 5.2-1 Mole fractions as function of temperature for 1,5-hexadiene pyrolysis in a jet-stirred reactor, P=0.107 MPa, F_V=4.06 10^{-5} m^3 s^{-1}, $x_{1,5\text{-hexadiene},0}$=0.008: symbols, experimental mole fraction profile of molecule represented in graph; lines, mole fraction profiles calculated with CHEMKIN using the perfectly stirred reactor model and the developed kinetic model

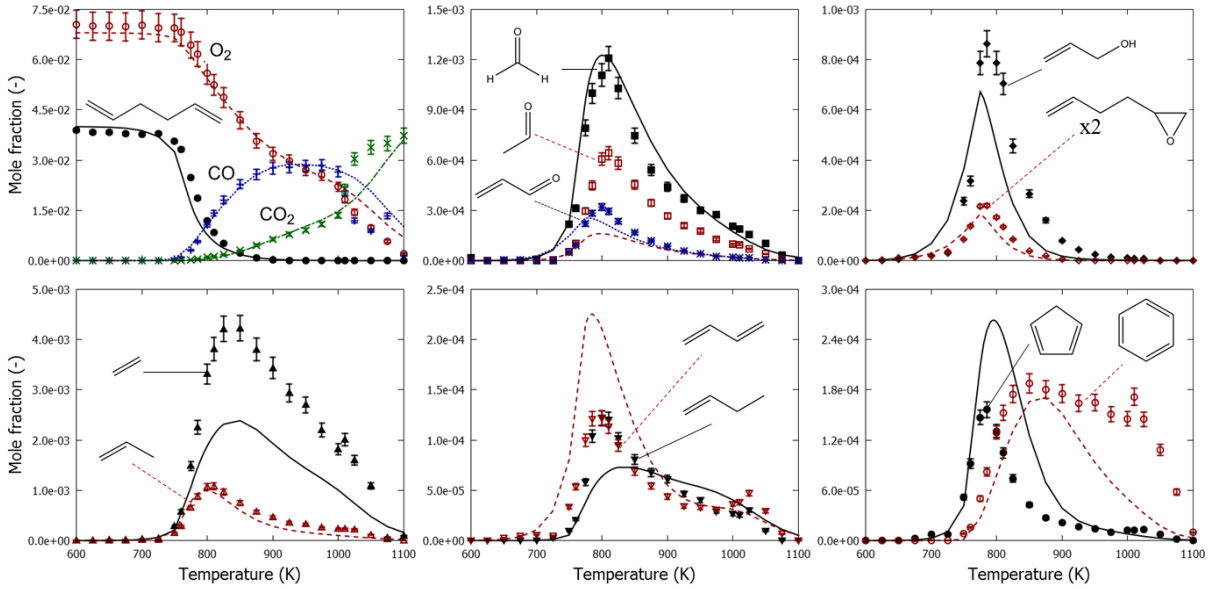

Figure 5.2-2 Mole fractions as function of temperature for 1,5-hexadiene oxidation in a jet-stirred reactor, P=0.107 MPa, φ=1.0, F_V=4.06 10^{-5} m^3 s^{-1}, $x_{1,5\text{-hexadiene},0}$=0.008: symbols, experimental mole fraction profile of molecule represented in graph; lines, mole fraction profiles calculated with CHEMKIN using the perfectly stirred reactor model and the developed kinetic model

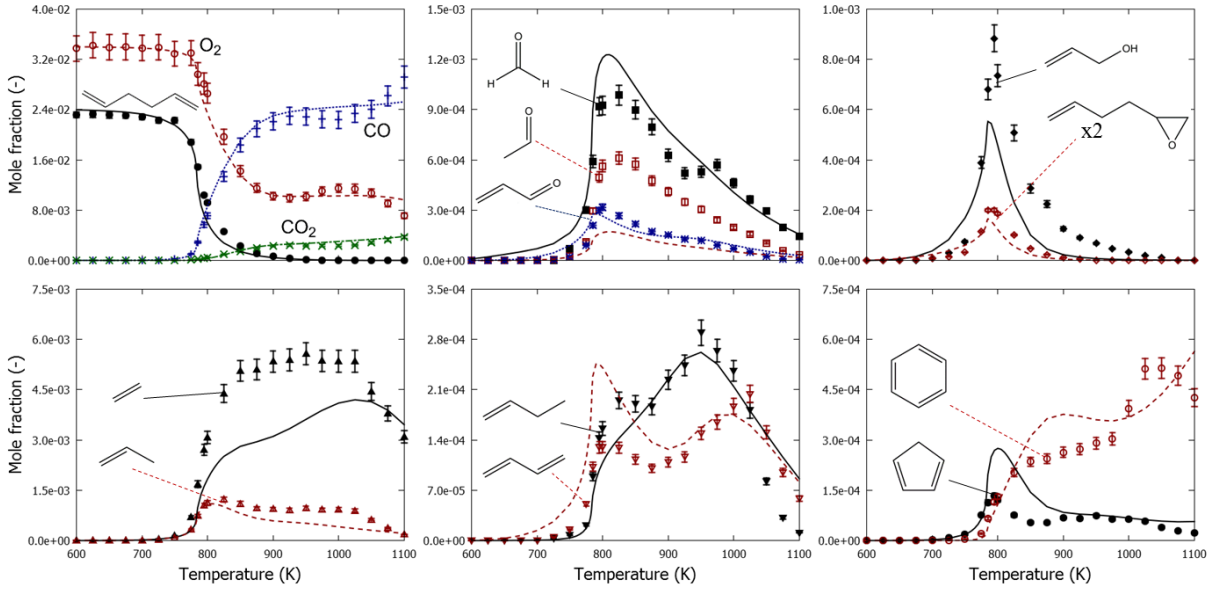

Figure 5.2-3 Mole fractions as function of temperature for 1,5-hexadiene oxidation in a jet-stirred reactor, P=0.107 MPa, φ=2.0, F_V=4.06 10^{-5} m^3 s^{-1}, $x_{1,5\text{-hexadiene},0}$=0.008: symbols, experimental mole fraction profile of molecule represented in graph; lines, mole fraction profiles calculated with CHEMKIN using the perfectly stirred reactor model and the developed kinetic model

The pyrolysis of 1,5-hexadiene results in the formation of small alkenes and a wide variety of cyclic hydrocarbons, such as cyclohexene, cyclohexadiene, 1,3-cyclopentadiene, methyl-cyclopentadiene, benzene and larger aromatics.

The same products are also detected in the oxidation of 1,5-hexadiene, though their yields are generally lower and decrease with increasing oxygen content. Furthermore, several oxygenated species were identified. Acrolein, prop-2-en-1-ol and but-3-enyl-oxiran were detected in relatively high quantities which can be attributed to several fuel decomposition channels as will be discussed in section 5.2.5.2.

Reactor simulations were performed using the perfectly-stirred reactor module in CHEMKIN-PRO[14] and the developed kinetic model. Model calculated mole fraction profiles are added to Figure 5.2-1, Figure 5.2-2 and Figure 5.2-3. The developed kinetic model is in qualitative agreement with most experimental data, i.e. the effect of temperature and equivalence ratio on mole fraction is accurately reproduced. For pyrolysis, the major products are also in quantitative agreement, as can be observed in Figure 5.2-1. The deviations between experimental and model calculated mole fractions are overall larger in oxidation conditions. The main discrepancies can be observed for ethene, which is underpredicted by a factor 2, and acetaldehyde, which is underpredicted by a factor 3. These differences are further discussed in section 5.2.5.2 and 5.2.5.3.

5.2.5.2 Primary decomposition paths of 1,5-hexadiene

1,5-hexadiene is consumed by hydrogen abstraction, radical addition to the C=C double bonds and C-C scission. The importance of each consumption path depends on temperature and equivalence ratio. A reaction path analysis was performed at 800K and 1000K at φ=2.0 and is presented in Figure 5.2-4.

Unimolecular decomposition of 1,5-hexadiene by C-C scission is fast and forms two allyl radicals. At low temperature and conversion, allyl is relatively unreactive and recombination back to 1,5-hexadiene is an important reaction route. At higher temperatures, 1,5-hexadiene and allyl concentrations deviate from equilibrium, mainly due to consumption of 1,5-hexadiene by hydrogen abstraction and radical addition reactions and consumption of allyl radicals. In fuel-rich oxidation, C-C scission accounts for only 10% of the total 1,5-hexadiene consumption at 800K, while it accounts for 92% of the total 1,5-hexadiene consumption at 1000K.

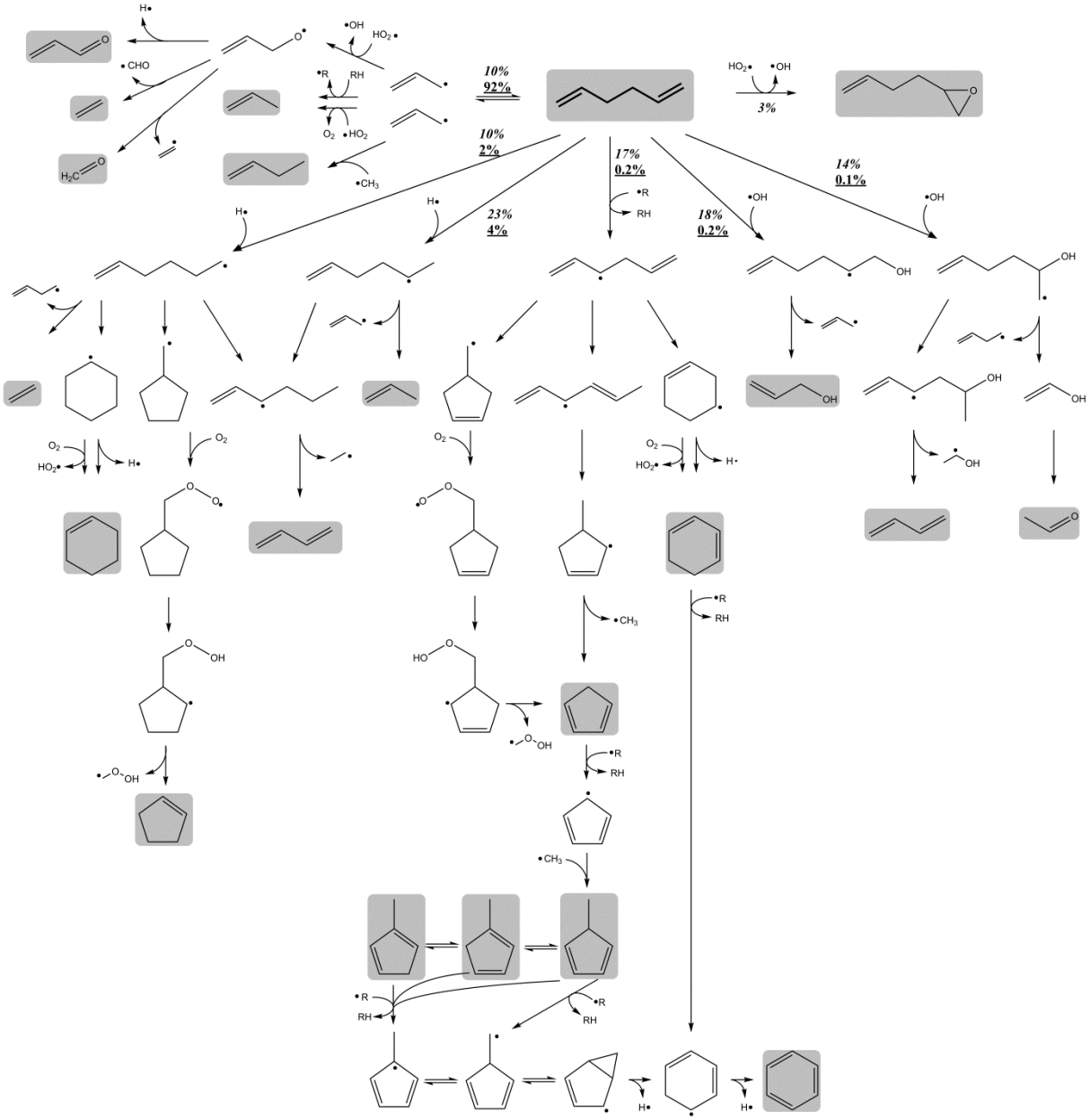

Figure 5.2-4 Reaction path analysis for the decomposition of 1,5-hexadiene. Operating conditions: F_V=4.06 10^{-5} m^3 s^{-1}, $x_{1,5\text{-hexadiene},0}$=0.008, φ=2.0, T=800K (italic) and 1000K (underlined). Percentages on a reaction path represent the reaction rate relative to the total 1,5-hexadiene decomposition rate. Species with a shaded background have been detected experimentally.

Radicals can add to the terminal and the non-terminal carbon-atom of the C=C double bonds. Hydrogen atoms, hydroxyl radicals and methyl radicals are the main adding radicals at the investigated operating conditions. Addition to the terminal carbon-atom of the C=C double bond forms a secondary radical which can decompose by C-C β-scission forming allyl and an unsaturated species, e.g. propene, prop-2-en-1-ol, 1-butene in the case of hydrogen atom, hydroxyl radical, methyl radical addition, respectively. Addition to the non-terminal carbon-atom of the C=C double bond forms a primary radical. C-C β-scission of the primary radical

is in competition with intramolecular hydrogen abstraction through a five-membered transition state forming a resonantly stabilized radical, exo-intramolecular radical addition forming a five-membered ring and endo-intramolecular radical addition forming a six-membered ring. In the case of hydrogen atom addition, these pathways may lead to ethene plus but-1-en-4-yl radical, 1,3-butadiene plus ethyl radical, cyclopentane-carbinyl radical and cyclohexyl radical as indicated in Figure 5.2-4. In the case of hydroxyl radical addition, C-C β-scission of the primary radical forms ethenol plus but-1-en-4-yl and intramolecular hydrogen abstraction followed by C-C β-scission forms 1-hydoxy-ethyl plus 1,3-butadiene, see Figure 5.2-4. Keto-enol tautomerization of ethenol and oxidation of 1-hydoxy-ethyl are the main formation paths of acetaldehyde at 800K. Re-evaluation of thermodynamic and kinetic parameters following addition of hydroxyl radical on 1,5-hexadiene can have a positive effect on acetaldehyde model performance. Addition of hydroperoxy to the C=C double bond and decomposition to cyclic ether leads to but-3-enyl-oxiran plus hydroxyl radical and is a minor pathway at low temperatures.

Hydrogen abstraction from the allylic carbon atom in 1,5-hexadiene forms the hexa-2,5-dien-1-yl radical. This radical mainly reacts by intramolecular radical addition and intramolecular hydrogen abstraction at the investigated operating conditions. Recombination of hexa-2,5-dien-1-yl with hydroperoxy radical and reaction of hexa-2,5-dien-1-yl with molecular oxygen forming 1,3,5-hexatriene and hydroperoxy radical were found to be unimportant. Intramolecular hydrogen abstraction of hexa-2,5-dien-1-yl forms hexa-2,4-dien-1-yl radical. Exo-intramolecular radical addition to a five-membered ring and subsequent β-scission of the methyl group leads to 1,3-cyclopentadiene. Intramolecular radical addition of hexa-2,5-dien-1-yl through a five-membered transition state forms cyclopentene-4-carbinyl radical. Consumption pathways of the latter radical to 4-methyl-cyclopentene-3-yl radical or to methylene-cyclopentene plus a hydrogen atom have relatively high energy barriers. Cyclopentene-4-carbinyl and hexa-2,5-dien-1-yl radicals are in quasi-equilibrium at low temperature pyrolysis conditions. In oxidation conditions, molecular oxygen can add on cyclopentene-4-carbinyl. The dominant reaction path of the adduct is intramolecular hydrogen abstraction from the allylic carbon atom and subsequent β-scission of the side group, which leads to 1,3-cyclopentadiene plus hydroperoxy-methyl radical, see Figure 5.2-4. Endo-intramolecular radical addition of hexa-2,5-dien-1-yl to a six-membered ring forms cyclohexene-4-yl. C-H β-scission of cyclohexene-4-yl forms 1,3-cyclohexadiene and 1,4-

cyclohexadiene. The latter two molecules can also be formed through reaction of cyclohexene-4-yl with molecular oxygen.

Sensitivity analyses were performed to better understand the effect of the aforementioned reactions on the 1,5-hexadiene mole fraction profile. In the presented sensitivity analyses, a positive sensitivity coefficient for a certain reaction indicates that increasing the associated pre-exponential factor increases the mole fraction of the target molecule. Analogously, a negative sensitivity coefficient for a certain reaction indicates that increasing the associated pre-exponential factor decreases the mole fraction of the target molecule.

Sensitivity analysis with respect to 1,5-hexadiene mole fraction profile for pyrolysis conditions is displayed in Figure 5.2-5. The conversion profile of 1,5-hexadiene in pyrolysis is very sensitive towards hydrogen abstraction by allyl from 1,5-hexadiene. This reaction consumes 1,5-hexadiene and an unreactive allyl radical is converted to hexa-2,5-dien-1-yl which may decompose and result in the formation of methyl radical or hydrogen atom, see Figure 5.2-4. Hydrogen abstraction by hydrogen atoms and methyl radicals from 1,5-hexadiene also have negative sensitivity coefficients. Hydrogen addition on the C=C double bond forming hex-5-en-2-yl has a positive sensitivity coefficient as hex-5-en-2-yl mainly decomposes to an unreactive allyl radical while hydrogen addition on the C=C double bond forming hex-5-en-1-yl has a negative sensitivity coefficient as decomposition of hex-5-en-2-yl mainly results in reactive hydrogen atoms.

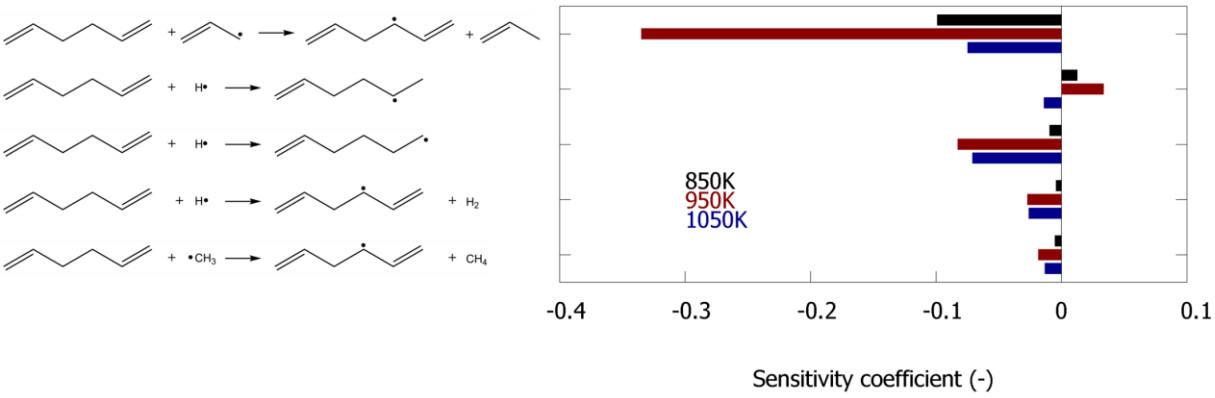

Figure 5.2-5 Sensitivity coefficients for 1,5-hexadiene mole fraction in 1,5-hexadiene pyrolysis. Operating conditions correspond to P=0.107 MPa, F_V=4.06 10^{-5} m^3 s^{-1}, $x_{1,5\text{-hexadiene},0}$=0.008, T = 850K (black), 950K (red), and 1050K (blue).

Sensitivity analysis with respect to 1,5-hexadiene mole fraction profile for fuel-rich oxidations conditions at T = 700K, 800K, 900K, 1000K and 1100K is displayed in Figure 5.2-6.

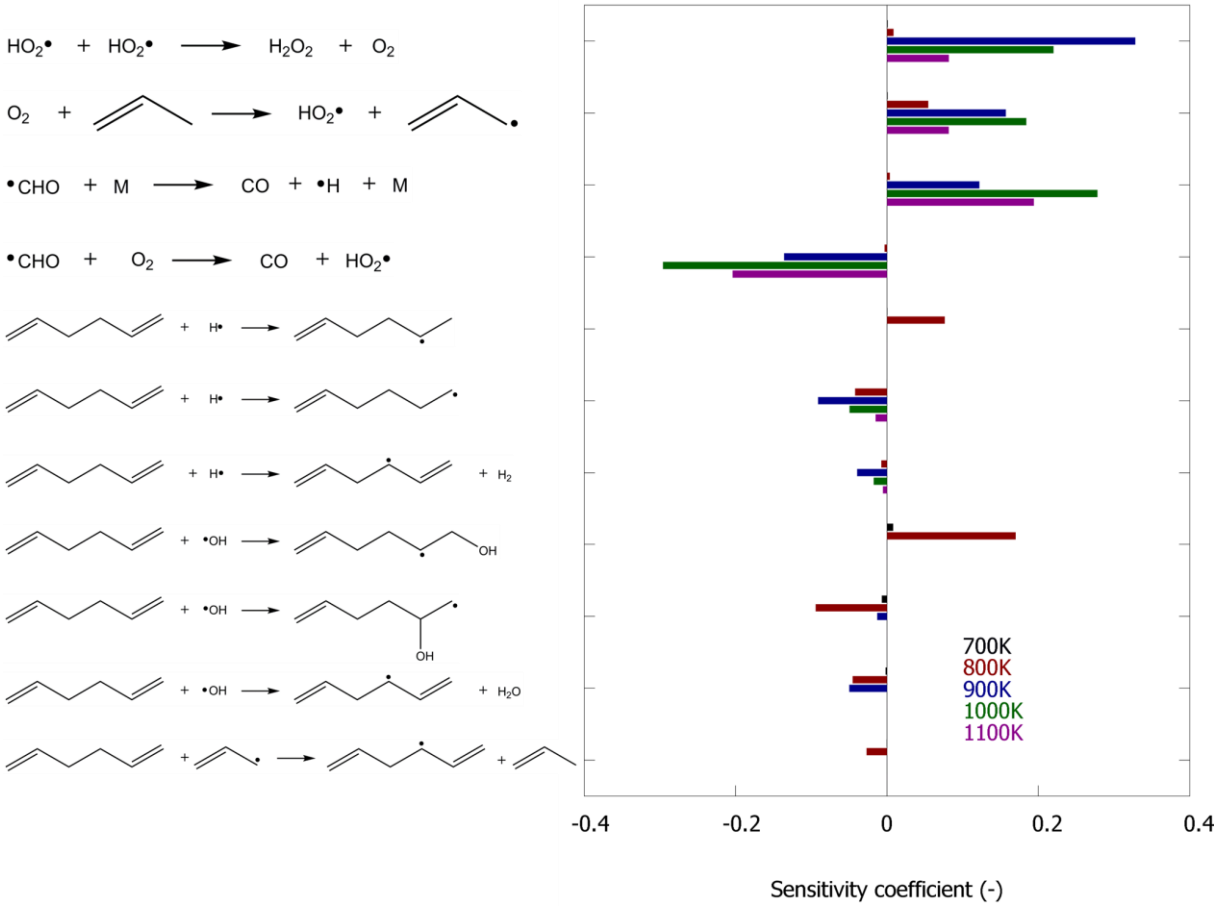

Figure 5.2-6 Sensitivity coefficients for 1,5-hexadiene mole fraction in 1,5-hexadiene oxidation. Operating conditions correspond to P=0.107 MPa, φ=2.0, F_V=4.06 10^{-5} m^3 s^{-1}, $x_{1,5\text{-hexadiene},0}$=0.008, T = 700K (black), 800K (red), 900K (blue), 1000K (green) and 1100K (purple).

1,5-hexadiene mole fraction is sensitive to reactions of small oxygenated radicals. Self-reaction of hydroperoxy radicals to hydrogen peroxide plus molecular oxygen has a positive sensitivity coefficient as this results in a net decrease of radicals in the system. Reaction of formyl radical with molecular oxygen to carbon monoxide plus hydroperoxy radical has a positive sensitivity coefficient as hydroperoxy can self-react through the aforementioned reaction. Decomposition of formyl radical to carbon monoxide and a reactive hydrogen atom has a negative sensitivity coefficient. Hydrogen atom abstraction from hydroperoxy by allyl has a positive sensitivity coefficient as this reduces the number of radicals and thus the reactivity.

Reactions related to 1,5-hexadiene decomposition are important below 900K, where 1,5-hexadiene conversion in incomplete. The most sensitive reactions in pyrolysis conditions are also important in 1,5-hexadiene oxidation. Addition of hydroxyl radicals on the C=C double bonds and hydrogen abstraction by hydroxyl radicals appear in the sensitivity analysis for 1,5-hexadiene oxidation. Hydroxyl addition on the C=C double bond forming hex-5-en-1-ol-2-yl has a positive sensitivity coefficient as hex-5-en-1-ol-2-yl mainly decomposes to an unreactive allyl radicals, similar to addition of hydrogen atom forming hex-5-en-2-yl.

5.2.5.3 Allyl reaction pathways

The allyl radical, which is formed in large quantities, has several consumption pathways including abstraction reactions forming propene and recombination reactions with hydrogen atoms or radicals. C-H β-scission to allene plus hydrogen atom is a minor allyl consumption pathway, analogous to the oxidation of propene under comparable operating conditions[30].

The recombination of allyl with methyl radical is a significant pathway in fuel-rich oxidation and pyrolysis conditions. At 1000K and φ=2.0, this is the dominant 1-butene formation pathway. Note that this recombination reaction is part of the base mechanism and reaction rate coefficients are taken from Kynazev and Slagle [38]. Subsequent consumption of 1-butene by hydrogen abstraction and C-H β-scission leads to 1,3-butadiene and is the cause of the second maximum in 1,3-butadiene yield at 1000K.

At oxidizing conditions, an important pathway for allyl radicals is recombination with a hydroperoxy radical. The resulting hydroperoxide reacts by O-O scission forming allyloxy and a hydroxyl radical. Allyloxy can decompose by C-C β-scission, forming vinyl plus formaldehyde, by C-H β-scission, forming acrolein plus a hydrogen atom, and by a 1,2-H-shift forming 3-oxo-propyl. These reaction pathways are important for accurate predictions of the observed product spectrum. C-H β-scission of allyloxy is the dominant acrolein formation path at the investigated conditions. C-C β-scission of 3-oxo-propyl to formyl plus ethene contributes for approximately 50% of the total ethene production at 800K and φ=2.0. The ethene mole fraction profile is sensitive to the allyloxy decomposition routes. Re-evaluation of the branching ratio of the competing reactions can help to improve the agreement between model and experiment. The recombination of allyl with hydroperoxy radicals competes with hydrogen atom abstraction from hydroperoxy by allyl.

5.2.5.4 Formation of aromatics

Benzene is the most abundant aromatic in the oxidation and pyrolysis of 1,5-hexadiene. Cyclohexadiene and 1,3-cyclopentadiene are important benzene precursors. Cyclohexadiene yields benzene after hydrogen abstraction and subsequent C-H β-scission. Cyclopentadienyl can recombine with a methyl radical. Hydrogen abstraction from methyl-cyclopentadiene and ring enlargement may result in benzene, as indicated in Figure 5.2-4. This pathway has been described extensively in the past [6, 10]. Above 1000K, the reaction of allyl with propargyl radical to benzene is non-negligible.

As mentioned earlier, the benzene precursors cyclohexadiene and 1,3-cyclopentadiene are products of hexa-2,5-dien-1-yl. This radical can be formed by hydrogen abstraction from the feed structure and by addition of vinyl on 1,3-butadiene. The former pathway to hexa-2,5-dien-1-yl is important below 900K at φ =2.0 while the latter pathway is important in the fuel rich oxidation of 1,5-hexadiene above 900K at φ =2.0. A different route to 1,3-cyclopentadiene at high temperature is addition of allyl on ethene, followed by intramolecular radical addition and dehydrogenation reactions.

Under oxidation conditions, the pathways to benzene and 1,3-cyclopentadiene that are related to decomposition of the feed molecular structure give rise to the first peak in yield while the pathways that are related to reactions of small molecules, such as vinyl, allyl, ethene, 1,3-butadiene give rise to the second peak in yield. This is evidenced by the sensitivity analyses with respect to benzene and 1,3-cyclopentadiene mole fraction profiles in fuel rich oxidation, displayed in Figure 5.2-7 and Figure 5.2-8 respectively. At 700K, 800K and 900K, 1,3-cyclopentadiene and benzene mole fraction profiles are sensitive to (i) reactions that have an effect on 1,5-hexadiene conversion and (ii) reactions that are important for the formation benzene and 1,3-cyclopentadiene directly from the fuel structure, e.g. intramolecular radical addition of hexa-2,5-dien-1-yl to cyclohexene-4-yl, which may form benzene following dehydrogenation reactions, and intramolecular hydrogen abstraction of hexa-2,5-dien-1-yl to hexa-2,5-dien-1-yl to hexa-2,4-dien-1-yl, which may form 1,3-cyclopentadiene following intramolecular radical addition and C-C β-scission of the methyl side group. At 1000K and 1100K, other reactions have an increased importance in the sensitivity analysis. Benzene mole fraction profiles are sensitive to addition of vinyl on 1,3-butadiene to hexa-2,5-dien-1-yl and C-C β-scission of but-1-en-4-yl to vinyl plus ethene, which is in competition with C-H β-scission of but-1-en-4-yl to 1,3-butadiene plus hydrogen atom. 1,3-cyclopentadiene mole

fraction profiles are sensitive to addition of allyl radical on ethene and intramolecular radical addition to cyclopentyl.

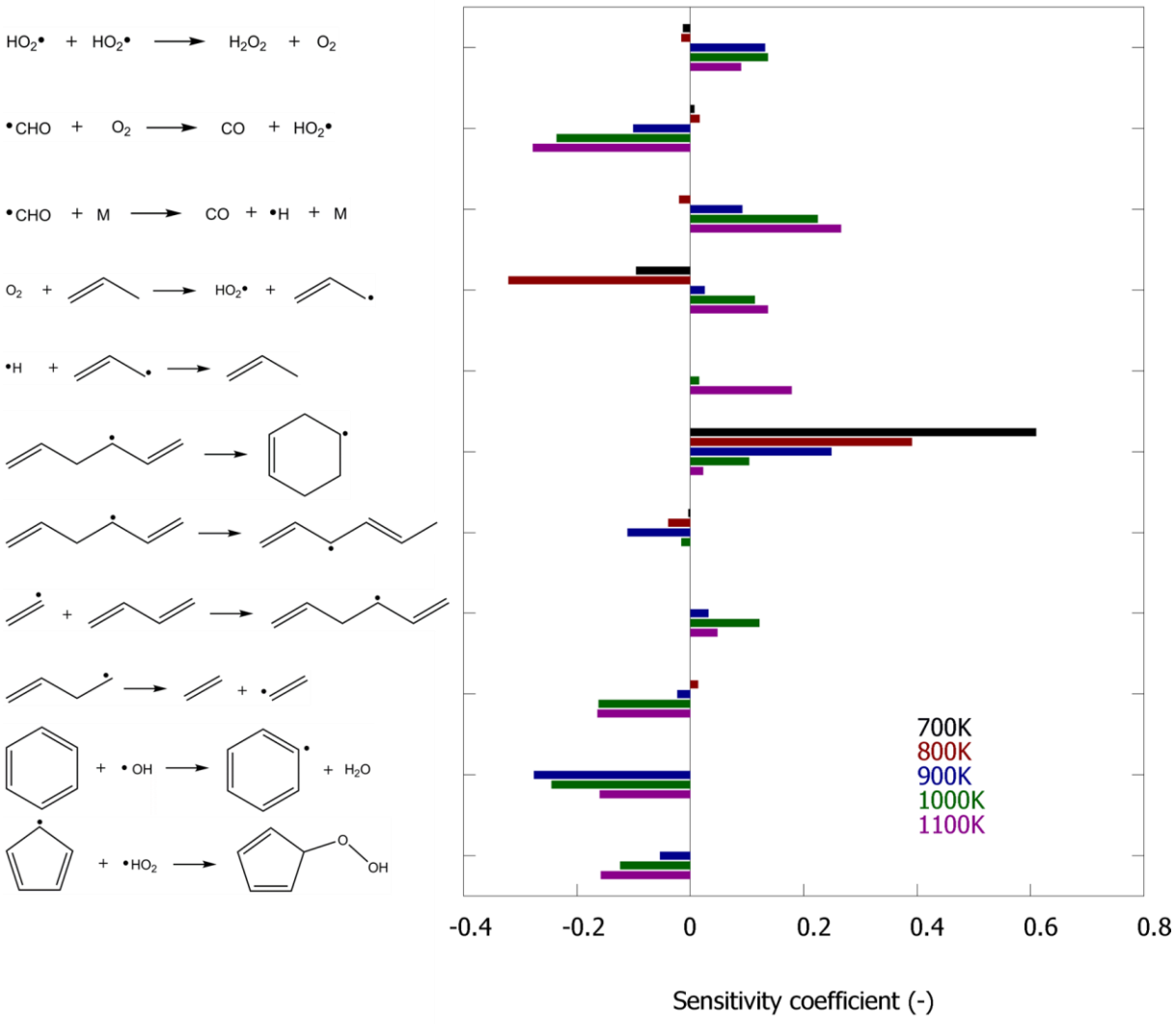

Figure 5.2-7 Sensitivity coefficients for benzene mole fraction in 1,5-hexadiene oxidation. Operating conditions correspond to P=0.107 MPa, φ=2.0, F_V=4.06 10^{-5} m^3 s^{-1}, $x_{1,5\text{-hexadiene},0}$=0.008, T = 700K (black), 800K (red), 900K (blue), 1000K (green) and 1100K (purple).

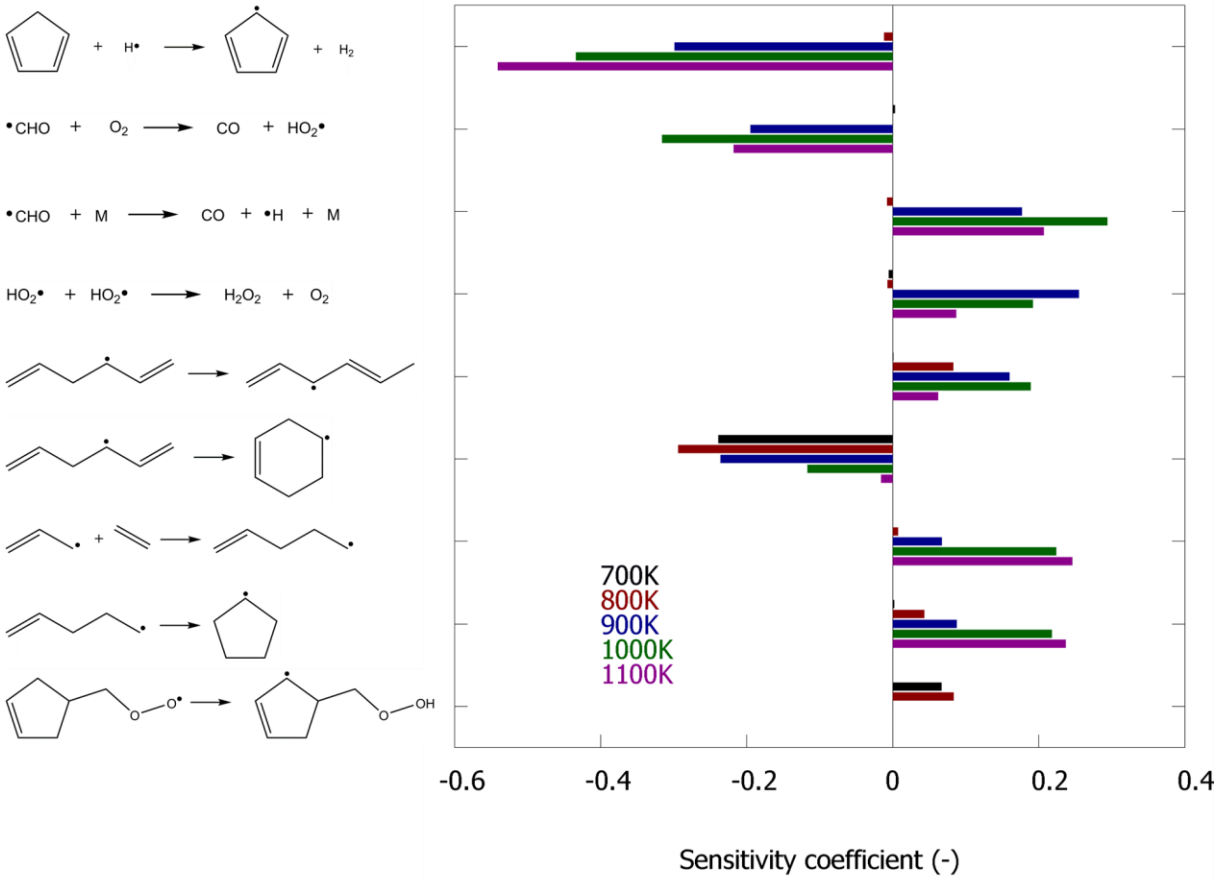

Figure 5.2-8 Sensitivity coefficients for 1,3-cyclopentadiene mole fraction in 1,5-hexadiene oxidation. Operating conditions correspond to P=0.107 MPa, φ=2.0, F_V=4.06 10^{-5} m^3 s^{-1}, $x_{1,5\text{-hexadiene},0}$=0.008, T = 700K (black), 800K (red), 900K (blue), 1000K (green) and 1100K (purple).

Several other aromatics were detected in the reactor outlet gases, e.g. toluene, styrene, indene and naphthalene. Especially in pyrolysis, they have relatively high yields. The pathways to substituted aromatics, such as toluene and styrene, are similar to the discussed benzene pathways see Figure 5.2-9. Toluene is mainly formed by recombination of allyl with but-1-en-3-yl followed by hydrogen abstraction and intramolecular radical addition reaction, analogous to the formation of benzene starting from 1,5-hexadiene. A second route to toluene is the recombination of ethyl with 1,3-cyclopentadienyl, followed by hydrogen abstraction and ring enlargement, analogous to the formation of benzene starting from the recombination of methyl with 1,3-cyclopentadienyl radical. Recombination of allyl with 1,3-cyclopentadienyl is the dominant path to styrene. The subsequent reaction sequence is, again, analogous to methyl plus 1,3-cyclopentadienyl giving benzene.

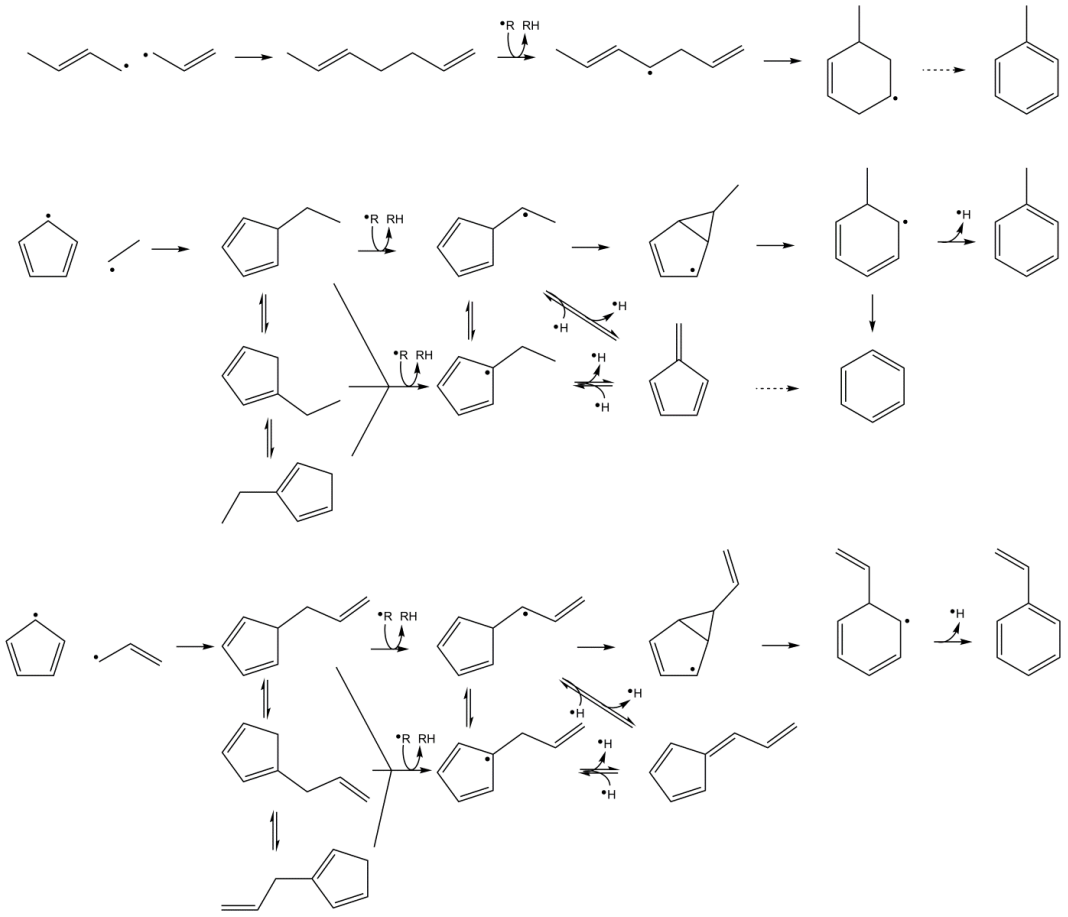

Figure 5.2-9 Formation of aromatics in the pyrolysis of 1,5-hexadiene

5.2.6 Conclusions

1,5-hexadiene is an excellent molecule to study the role of allylic radicals in the formation of aromatic molecules. Therefore, oxidation and pyrolysis experiments were performed in a jet-stirred reactor, below 1100K. The experimental data is supported by a new detailed kinetic model, which was developed using a combination of automatic network generation and literature-reported quantum chemical calculations. Without any adjustments, the model describes all experimental data qualitatively well, but for some compounds, such as ethene and acetaldehyde, quantitative differences exist, especially in the presence of oxygen. At the investigated operating conditions, the reactor effluent composition is sensitive towards reactions involving allyl radicals, e.g. hydrogen abstraction from 1,5-hexadiene by allyl and its reaction with hydroperoxy radicals. The pyrolysis and oxidation of 1,5-hexadiene has a high selectivity to benzene. It can be formed directly from 1,5-hexadiene as precursor or alternatively, by a reaction sequence that starts with the recombination of cyclopentadienyl and methyl radicals. The pathways responsible for benzene formation can be extrapolated to substituted aromatics such as toluene and styrene.

5.2.7 References

[1] H. Richter, J. B. Howard, Formation of polycyclic aromatic hydrocarbons and their growth to soot - a review of chemical reaction pathways, Prog. Energy Combust. Sci. 26 (2000) 565-608
[2] N. Hansen, W. Li, M. E. Law, T. Kasper, P. R. Westmoreland, B. Yang, T. A. Cool, A. Lucassen, The importance of fuel dissociation and propargyl + allyl association for the formation of benzene in a fuel-rich 1-hexene flame, Phys. Chem. Chem. Phys. 12 (2010) 12112-12122
[3] M. R. Djokic, K. M. Van Geem, C. Cavallotti, A. Frassoldati, E. Ranzi, G. B. Marin, An experimental and kinetic modeling study of cyclopentadiene pyrolysis: First growth of polycyclic aromatic hydrocarbons, Combust. Flame 161 (2014) 2739-2751
[4] J. A. Miller, M. J. Pilling, J. Troe, Unravelling combustion mechanisms through a quantitative understanding of elementary reactions, P. Combust. Inst. 30 (2005) 43-88
[5] J. A. Miller, C. F. Melius, Kinetic and thermodynamic issues in the formation of aromatic compounds in flames of aliphatic fuels, Combust. Flame 91 (1992) 21-39
[6] K. Wang, S. M. Villano, A. M. Dean, Fundamentally-based kinetic model for propene pyrolysis, Combust. Flame 162 (2015) 4456-4470
[7] Y. Georgievskii, J. A. Miller, S. J. Klippenstein, Association rate constants for reactions between resonance-stabilized radicals: C3H3 + C3H3, C3H3 + C3H5, and C3H5 + C3H5, Phys. Chem. Chem. Phys. 9 (2007) 4259-4268
[8] N. Hansen, J. A. Miller, P. R. Westmoreland, T. Kasper, K. Kohse-Höinghaus, J. Wang, T. A. Cool, Isomer-specific combustion chemistry in allene and propyne flames, Combust. Flame 156 (2009) 2153-2164
[9] K. Wang, S. M. Villano, A. M. Dean, Reactions of allylic radicals that impact molecular weight growth kinetics, Phys. Chem. Chem. Phys. 17 (2015) 6255-6273
[10] S. Sharma, M. R. Harper, W. H. Green, Modeling of 1,3-hexadiene, 2,4-hexadiene and 1,4-hexadiene-doped methane flames: Flame modeling, benzene and styrene formation, Combust. Flame 157 (2010) 1331-1345
[11] Z. J. Buras, E. E. Dames, S. S. Merchant, G. Liu, R. M. I. Elsamra, W. H. Green, Kinetics and Products of Vinyl + 1,3-Butadiene, a Potential Route to Benzene, J. Phys. Chem. A 119 (2015) 7325-7338
[12] O. Herbinet, B. Husson, M. Ferrari, P.-A. Glaude, F. Battin-Leclerc, Low temperature oxidation of benzene and toluene in mixture with n-decane, P. Combust. Inst. 34 (2013) 297-305
[13] O. Herbinet, F. Battin-Leclerc, Progress in Understanding Low-Temperature Organic Compound Oxidation Using a Jet-Stirred Reactor, Int. J. Chem. Kinet. 46 (2014) 619-639
[14] R. J. Kee, F. M. Rupley, J. A. Miller, M. E. Coltrin, J. F. Grcar, E. Meeks, H. K. Moffat, A. E. Lutz, G. Dixon-Lewis, M. D. Smooke, J. Warnatz, G. H. Evans, L. R. S., R. E. Mitchell, L. R. Petzold, W. C. Reynolds, M. Caracotsios, W. E. Stewart, P. Glarborg, C. Wang, O. Adigun, in: 15101 ed.; Reaction Design, Inc.: San Diego (CA), 2010.
[15] N. M. Vandewiele, K. M. Van Geem, M.-F. Reyniers, G. B. Marin, Genesys: Kinetic model construction using chemo-informatics, Chem. Eng. J. 207 (2012) 526-538
[16] C. F. Goldsmith, G. R. Magoon, W. H. Green, Database of Small Molecule Thermochemistry for Combustion, J. Phys. Chem. A 116 (2012) 9033-9057
[17] E. Goos, A. Burcat, B. Ruscic, Extended Third Millennium Thermodynamic Database for Combustion and Air-Pollution Use with Updates from Active Thermochemical Tables, 2014
[18] S. W. Benson, Thermochemical Kinetics: Methods for the Estimation of Thermochemical Data and Rate Parameters, John Wiley & Sons, New York, 1976
[19] M. K. Sabbe, A. Vandeputte, M.-F. Reyniers, M. Waroquier, G. B. Marin, Modeling the influence of resonance stabilization on the kinetics of hydrogen abstractions, Phys. Chem. Chem. Phys. 12 (2010) 1278-1298
[20] M. K. Sabbe, M.-F. Reyniers, M. Waroquier, G. B. Marin, Hydrogen Radical Additions to Unsaturated Hydrocarbons and the Reverse beta-Scission Reactions: Modeling of Activation Energies and Pre-Exponential Factors, ChemPhysChem 11 (2010) 195-210
[21] M. K. Sabbe, M.-F. Reyniers, V. Van Speybroeck, M. Waroquier, G. B. Marin, Carbon-centered radical addition and beta-scission reactions: Modeling of activation energies and pre-exponential factors, ChemPhysChem 9 (2008) 124-140
[22] R. Sivaramakrishnan, J. V. Michael, Rate Constants for OH with Selected Large Alkanes: Shock-Tube Measurements and an Improved Group Scheme, J. Phys. Chem. A 113 (2009) 5047-5060
[23] P. D. Paraskevas, M. K. Sabbe, M.-F. Reyniers, N. G. Papayannakos, G. B. Marin, Group Additive Kinetics for Hydrogen Transfer Between Oxygenates, J. Phys. Chem. A (2015)
[24] J. Aguilera-Iparraguirre, H. J. Curran, W. Klopper, J. M. Simmie, Accurate Benchmark Calculation of the Reaction Barrier Height for Hydrogen Abstraction by the Hydroperoxyl Radical from Methane. Implications for CnH2n+2 where n = 2 → 4, J. Phys. Chem. A 112 (2008) 7047-7054
[25] J. Zádor, S. J. Klippenstein, J. A. Miller, Pressure-Dependent OH Yields in Alkene + HO2 Reactions: A Theoretical Study, J. Phys. Chem. A 115 (2011) 10218-10225

[26] K. Wang, S. M. Villano, A. M. Dean, Reactivity–Structure-Based Rate Estimation Rules for Alkyl Radical H Atom Shift and Alkenyl Radical Cycloaddition Reactions, J. Phys. Chem. A 119 (2015) 7205-7221
[27] J. Bugler, K. P. Somers, E. J. Silke, H. J. Curran, Revisiting the Kinetics and Thermodynamics of the Low-Temperature Oxidation Pathways of Alkanes: A Case Study of the Three Pentane Isomers, J. Phys. Chem. A 119 (2015) 7510-7527
[28] F. Zhang, T. S. Dibble, Effects of Olefin Group and Its Position on the Kinetics for Intramolecular H-Shift and HO2 Elimination of Alkenyl Peroxy Radicals, J. Phys. Chem. A 115 (2011) 655-663
[29] C. F. Goldsmith, S. J. Klippenstein, W. H. Green, Theoretical rate coefficients for allyl + HO2 and allyloxy decomposition, P. Combust. Inst. 33 (2011) 273-282
[30] S. M. Burke, W. Metcalfe, O. Herbinet, F. Battin-Leclerc, F. M. Haas, J. Santner, F. L. Dryer, H. J. Curran, An experimental and modeling study of propene oxidation. Part 1: Speciation measurements in jet-stirred and flow reactors, Combust. Flame 161 (2014) 2765-2784
[31] C. K. Westbrook, W. J. Pitz, M. Mehl, P.-A. Glaude, O. Herbinet, S. Bax, F. Battin-Leclerc, O. Mathieu, E. L. Petersen, J. Bugler, H. J. Curran, Experimental and Kinetic Modeling Study of 2-Methyl-2-Butene: Allylic Hydrocarbon Kinetics, J. Phys. Chem. A 119 (2015) 7462-7480
[32] P. T. Lynch, C. J. Annesley, C. J. Aul, X. Yang, R. S. Tranter, Recombination of Allyl Radicals in the High Temperature Fall-Off Regime, J. Phys. Chem. A 117 (2013) 4750-4761
[33] J. A. Miller, S. J. Klippenstein, Y. Georgievskii, L. B. Harding, W. D. Allen, A. C. Simmonett, Reactions between Resonance-Stabilized Radicals: Propargyl + Allyl, J. Phys. Chem. A 114 (2010) 4881-4890
[34] J. A. Miller, S. J. Klippenstein, The recombination of propargyl radicals and other reactions on a C6H6 potential, J. Phys. Chem. A 107 (2003) 7783-7799
[35] S. M. Burke, U. Burke, R. Mc Donagh, O. Mathieu, I. Osorio, C. Keesee, A. Morones, E. L. Petersen, W. Wang, T. A. DeVerter, M. A. Oehlschlaeger, B. Rhodes, R. K. Hanson, D. F. Davidson, B. W. Weber, C.-J. Sung, J. Santner, Y. Ju, F. M. Haas, F. L. Dryer, E. N. Volkov, E. J. K. Nilsson, A. A. Konnov, M. Alrefae, F. Khaled, A. Farooq, P. Dirrenberger, P.-A. Glaude, F. Battin-Leclerc, H. J. Curran, An experimental and modeling study of propene oxidation. Part 2: Ignition delay time and flame speed measurements, Combust. Flame 162 (2015) 296-314
[36] S. S. Merchant. Molecules to Engines: Combustion Chemistry of Alcohols and their Application to Advanced Engines. Massachusetts Institute of Technology, Massachusetts, United States, 2015.
[37] J. Zádor, C. A. Taatjes, R. X. Fernandes, Kinetics of elementary reactions in low-temperature autoignition chemistry, Prog. Energy Combust. Sci. 37 (2011) 371-421
[38] V. D. Knyazev, I. R. Slagle, Kinetics of the Reactions of Allyl and Propargyl Radicals with CH3, J. Phys. Chem. A 105 (2001) 3196-3204

Chapter 6

Conclusions and perspectives

6.1 Conclusions

Ecological, social and political incentives push for an increased production of chemicals from bio-derived, renewable feedstocks. The production of green chemicals has currently difficulties to compete with well-established technologies that use fossil resources. In order to be environmentally and economically viable, the development of every new process requires careful evaluation and optimization. Yields of valuable products need to be maximized in particular. In this thesis, the focus is on two novel thermochemical processes, i.e. steam cracking of triglyceride-based biomass and fast pyrolysis of lignocellulose. Improved understanding about these processes is obtained by a combination of novel experimental data and first principles based detailed kinetic modeling.

Kinetic models for thermochemical processes are characterized by a large number of reactions, radicals and intermediates. Manual construction of such kinetic models requires an expert kineticist and is inherently error-prone. In this work, a network generation tool PRIM-O is presented which (i) automatically generates thermal decomposition schemes and (ii) applies the pseudo steady state approximation to μ-radicals. Compared to the previous version, i.e. PRIM, the framework has been extended to generate decomposition schemes for oxygenates and the considered number of reaction families has been extended. As case study, a kinetic model for the pyrolysis of rapeseed methyl esters has been generated and a good agreement was obtained between model-calculated and experimental mole fraction profiles. The PRIM-O framework allows extension to other oxygenates, relevant for biomass pyrolysis.

The first thermochemical process for production of green chemicals that has been investigated in this thesis is steam cracking of triglyceride-based biomass. Triglycerides and fatty acids differentiate themselves from other types of biomass by their low oxygen content and low molecular weight. Therefore, the two-step process that involves (i) catalytically upgrading by deoxygenation of triglycerides to hydrocarbons and (ii) steam cracking of the resulting hydrocarbon mixture, is a viable route for the production of bio-derived alkenes and aromatics. These chemicals can be processed in existing petrochemical facilities. Steam cracking experiments of two such deoxygenated feedstocks were performed in a dedicated

bench scale set-up. The first hydrocarbon mixture is hydrodeoxygenated crude tall oil, i.e. a mixture of long chain alkanes and cycloalkanes. The second hydrocarbon mixture is hydrodexoygenated and isomerized vegetable oil, i.e. a mixture of normal and branched alkanes. High ethene and propene yields were obtained following steam cracking, relative to petroleum-derived naphtha cracking. The steam cracking experiments were accurately reproduced by means of a detailed kinetic model. This kinetic model can on one hand be used to identify operating conditions that maximize alkene/aromatic yield. On the other hand, it can provide information to the foregoing deoxygenation step to "optimize" hydrocarbon composition. For example, a large fraction of crude tall oil consists of resin acids. Hydrodeoxygenation of resin acids at high temperatures favors formation of naphtheno-aromatics while hydrodeoxygenation of resin acids at low temperature favors formations of poly-naphthenes. As pyrolysis of poly-naphthenes has a higher selectivity towards valuable alkenes and mono-aromatics compared to pyrolysis of naphtheno-aromatics, hydrodeoxygenation of resin acids should be performed at temperatures that maximize formation of poly-naphthenes and that allow complete deoxygenation.

The second thermochemical process for production of green chemicals that has been investigated in this thesis is fast pyrolysis of lignocellulose. Lignocellulose is a complex bio-polymer and understanding its pyrolysis requires prior knowledge regarding the pyrolysis of its core-constituents and reactive intermediates. In this respect, the pyrolysis for 2-methyl-tetrahydrofuran, tetrahydropyran, γ-valerolactone, unsaturated alcohols and 1,5-hexadiene has been investigated. Note that the former three molecules can also be produced through biochemical and catalytic routes from lignocellulose. They have been suggested as potential next generation bio-derived fuels, although their application is unlikely in the coming decade. For 2-methyl-tetrahydrofuran, experiments have been performed using premixed laminar flames. Detailed kinetic models have been developed for the decomposition of all investigated species. The presence of oxygen atoms increases the importance of unimolecular decomposition reactions compared to hydrocarbons. For 2-methyl-tetrahydrofuran and γ-valerolactone, a concerted ring-opening reaction was identified producing 4-penten-1-ol and 4-pentenoic acid respectively. For 3-methyl-3-buten-1-ol, a retro-ene reaction producing isobutene and formaldehyde dominates decomposition. Finally, 1,5-hexadiene has been identified as an important precursor of aromatics in the pyrolysis of hydrocarbon and oxygenated molecules, either fossil or renewable based. The new experimental dataset and

kinetic model for 1,5-hexadiene improves the current understanding of polycyclic aromatic hydrocarbon formation.

6.2 Perspectives

The processing of bio-derived feedstocks in existing steam cracking facilities is the simplest method to produce green chemicals. Several companies are actually considering this and commercial tests are being carried out. However, diversification of renewable feedstocks, other than triglyceride-based biomass, is necessary for production of chemicals on a larger scale. One interesting option is depolymerization and complete defunctionalization of lignocellulose, producing a renewable naphtha for steam crackers. Further development of this process is still needed and requires fundamental understanding of both the catalytic and the pyrolysis step. Furthermore, oxygenated impurities in the steam cracker feedstock, inherent to the catalytic step, have to be identified and the effect on steam cracker effluent evaluated.

The mechanistic understanding of fast pyrolysis of lignocellulose is still far from complete. The model components investigated in this work can mainly be linked with fast pyrolysis of carbohydrates. The pyrolysis of lignin model components, e.g. phenols and phenyl ethers, have received little attention thus far. It is known that the methyl – phenoxy bonds in lignin and lignin model components are weak and, therefore, scission is an important unimolecular reaction route. This is drastically different from cyclic ethers. Improving the understanding of their thermochemical decomposition chemistry requires new experimental data and detailed kinetic models.

Pyrolysis of biomass model components provides valuable qualitative insight in the dominant product formation paths in biomass fast pyrolysis. Bridging the gap to predictive mechanistic model for biomass fast pyrolysis requires: (i) detailed description of biomass feedstock composition, (ii) automated network generation algorithm to develop kinetic models for the pyrolysis of polymers, (iii) intrinsic kinetic data for biomass pyrolysis. It is clear that this task is inherently multi-disciplinary and requires collaboration between biologists, chemists and engineers.

The network generation tool PRIM-O should be used to develop kinetic models for the pyrolysis of a wide range of oxygenated molecules. Thus far, only a kinetic model for the pyrolysis of methyl esters has been developed. Depending on the type of oxygenated molecule, minor to extensive adjustments to PRIM-O are required. The extension of PRIM-O

towards other types of biomass with low oxygen content, such as fatty acids, fatty alcohols, resin acids, sterols solely requires extension of the kinetic library and list of pre-defined molecules. Generation of decomposition schemes for oxygenated molecules with multiple functional groups requires extension of the list of available reaction families, e.g. unimolecular decomposition reactions for unsaturated alcohols. The use of PRIM-O for the pyrolysis of lignin model components requires assessment of the reactivity of phenoxy and benzylic radicals. These radicals are resonantly stabilized and the μ-hypothesis may not be valid, especially at low temperature.

Finally, PRIM-O can be extended to generate decomposition schemes for molecules with hetero-atoms other than oxygen. The extension of PRIM to PRIM-O can serve as example. The presence of oxygen atoms in molecules is tracked through an oxygen atom vector in PRIM-O. A similar approach can be used for the tracking of nitrogen and sulphur atoms. Generation of decomposition schemes for nitrogen- and sulphur-containing molecules requires extension of the list of reaction families and the kinetic library.

Appendix A

Defined molecules in PRIM-O

Table A-1 Overview of molecules defined in PRIM-O

Defined PRIM-O structures	Class
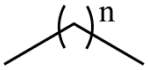	Normal alkanes
	1-alkenes
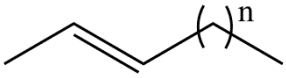	Other straight chain alkenes
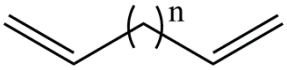	Dienes, non-conjugated C=C double bond
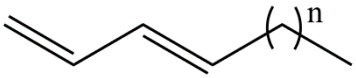	Dienes, conjugated C=C double bond
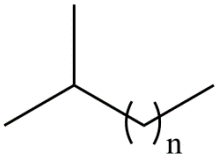	Branched alkanes
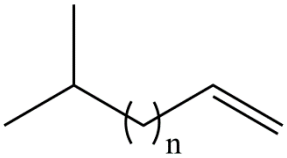	Branched alkenes
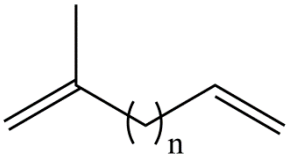	Branched dienes
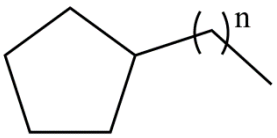	Alkyl-cyclopentanes
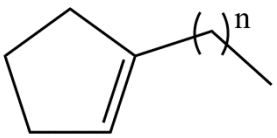	Alkyl-cyclopentenes
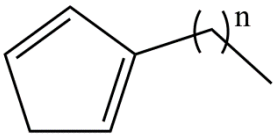	Alkyl-cyclopentadienes

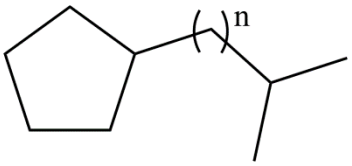

Branched alkyl-cyclopentanes

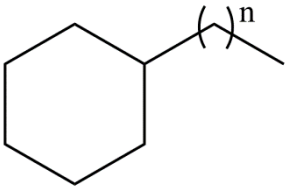

Alkyl-cyclohexanes

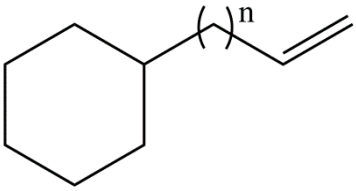

Alkenyl-cyclohexanes

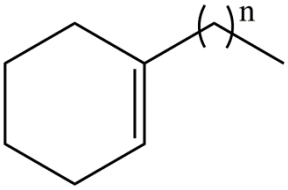

Alkyl-cyclohexenes

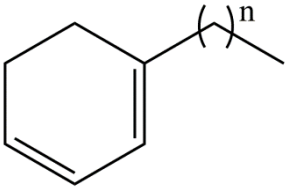

Alkyl-cyclohexadienes

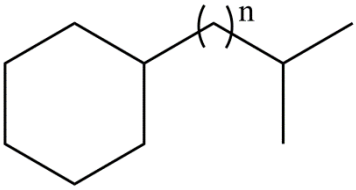

Branched alkyl-cyclohexanes

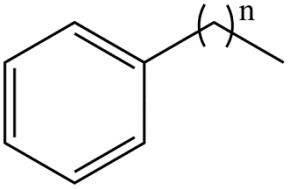

Alkyl-aromatics

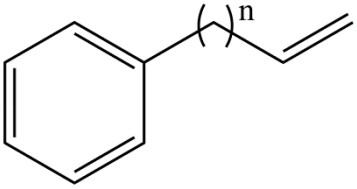

Alkenyl-aromatics

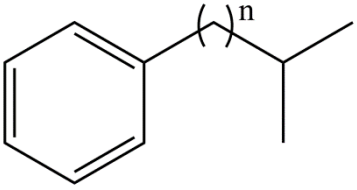

Branched alkyl-aromatics

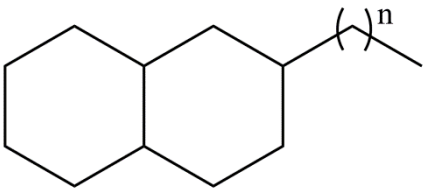

Alkyl-decahydronaphthalenes

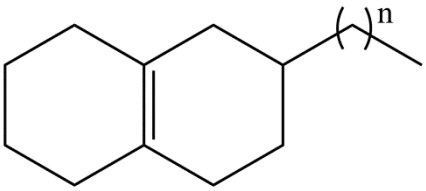

Alkyl-octahydronaphthalenes

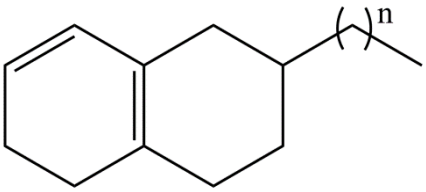

Alkyl-hexahydronaphthalenes

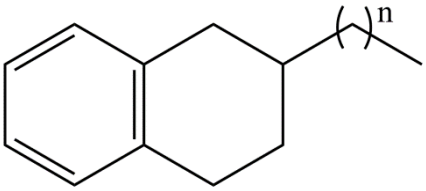

Alkyl-tetrahydronaphthalenes

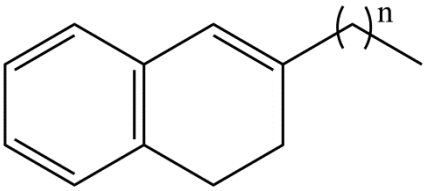

Alkyl-dihydronaphthalenes

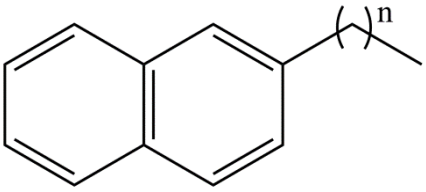

Alkyl-naphthalenes

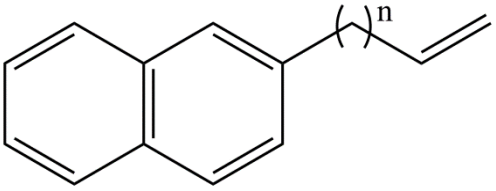

Alkenyl-naphthalenes

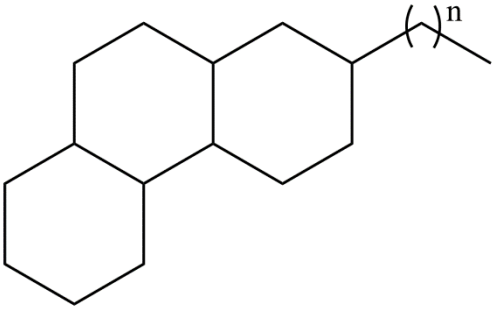

Alkyl-tetradecahydrophenanthrenes

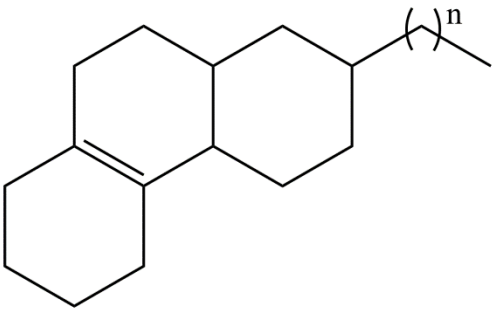

Alkyl-dodecahydrophenanthrenes

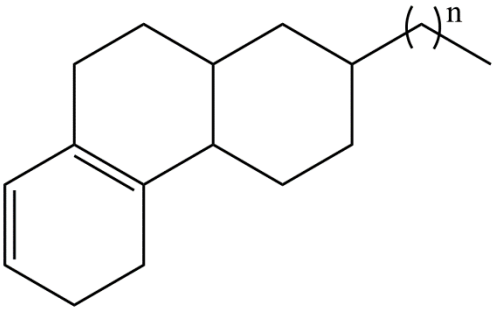

Alkyl-decahydrophenanthrenes

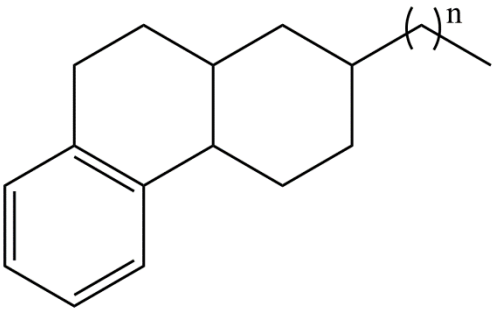

Alkyl-octahydrophenanthrenes

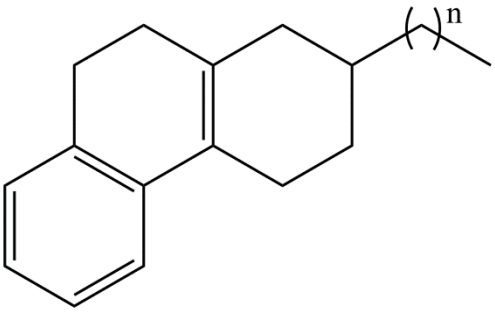

Alkyl-hexahydrophenanthrenes

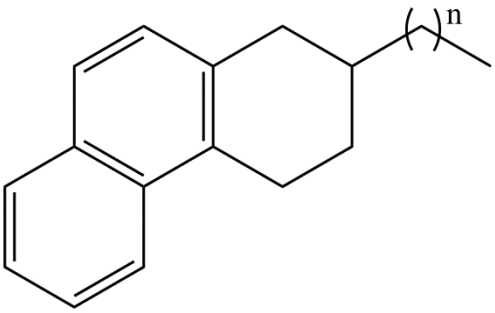

Alkyl-tetrahydrophenanthrenes

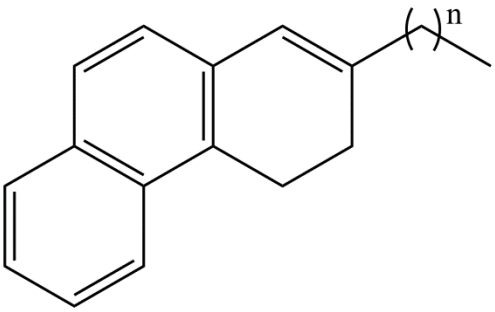

Alkyl-dihydrophenanthrenes

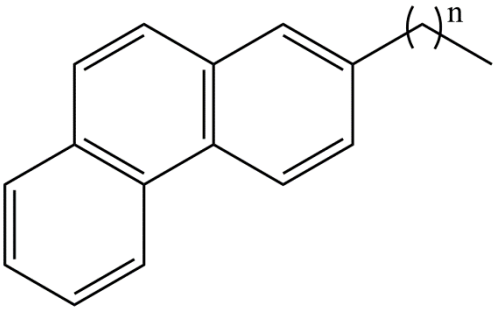

Alkyl-phenanthrenes

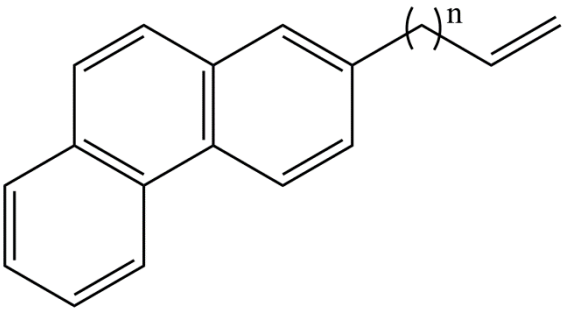

Alkenyl-phenanthrenes

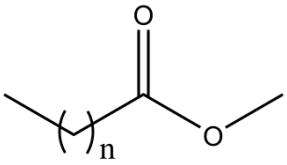

Esters

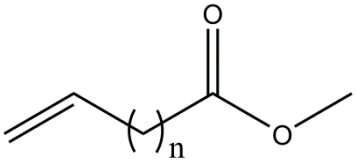

Mono-unsaturated esters

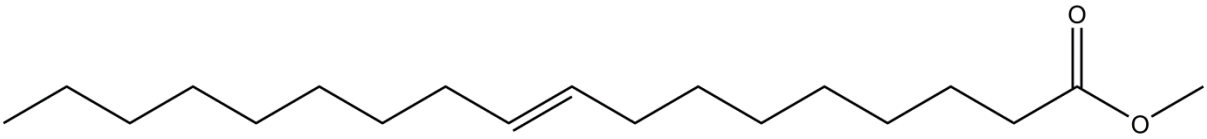

Methyl oleate

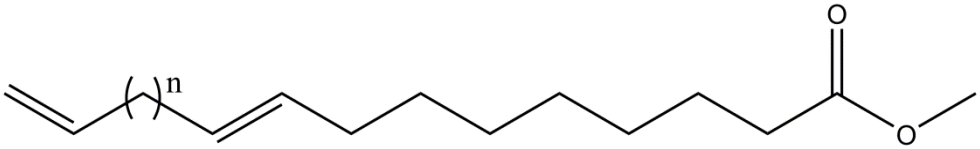

Double-unsaturated methyl esters

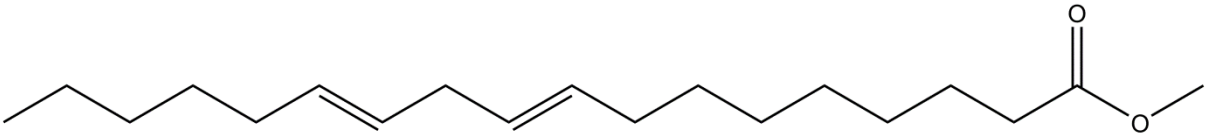

Methyl linoeate

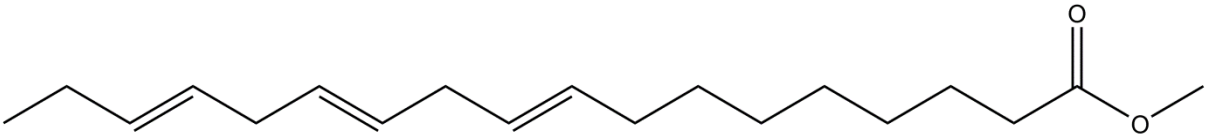

Methyl linolenate

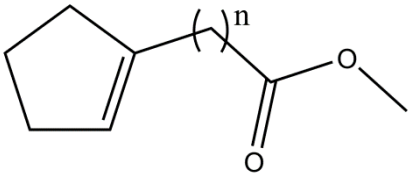

Cyclopentene with methyl ester side chain

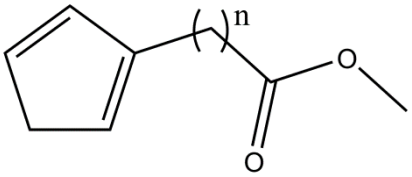

Cyclopentadiene with methyl ester side chain

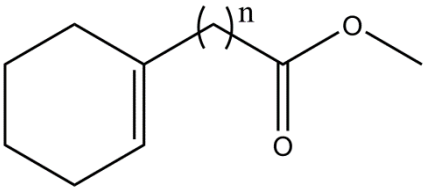

Cyclohexene with methyl ester side chain

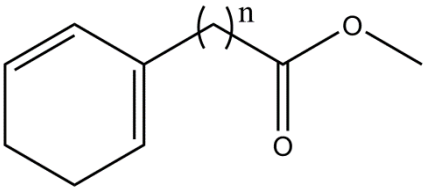

Cyclohexadiene with methyl ester side chain

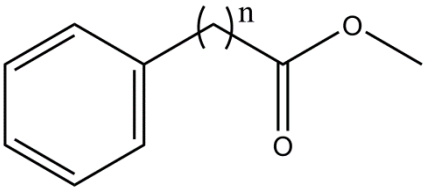

Benzene with methyl ester side chain

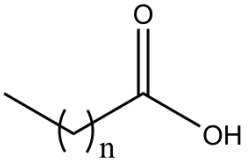

Acids

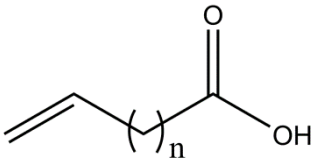

Mono-unsaturated acids

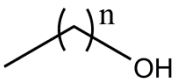

Alcohols

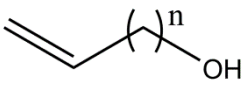

Mono-unsaturated alcohols

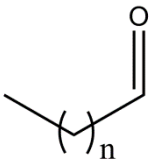

Aldehydes

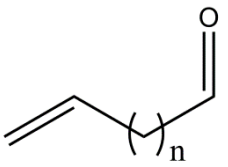

Mono-unsaturated aldehydes

Appendix B

Defined reaction families in Genesys

Table B-1 k [bimolecular - $m^3\ mol^{-1}\ s^{-1}$; unimolecular - s^{-1}] = A T^n exp(-Ea/RT) where R = 8.314 10^{-3} kJ K^{-1} mol^{-1}

Reaction family	Comment	Kinetic parameters			Ref
		A	*n*	*Ea*	
Hydrogen abstraction					
Intermolecular					
by C• from C-H		Group additivity			[1, 2]
	H abstr from C(=O)-**H** by CH_3	2.5e-6	3.6	18.1	[3]
by H• from C-H		Group additivity			[4]
	H abstr from C(=O)-**H**	7.15e-1	2.4	6.6	[3]
by •OH from C-H	R_1, R_2, R_3 alkyl chains or H atoms	Rate rules for alkanes			[5, 6]
	R_1, R_2 H atoms R_3 C=C	7.80e-1	2.3	-5.7	[7]
	R_1 H atom R_2 alkyl chain R_3 C=C	7.50e-2	2.4	-3.9	[7]
	R_1 H atom R_2 OH R_3 alkyl chain	1.15e-2	2.6	-8.7	[7]
	R_1 H atom R_2 OH R_3 C=C	2.55e-2	2.6	-13.3	[7]
	H abstr from C(=O)-**H**	6.13e-2	2.7	-19.2	[3]

by HO_2• from C-H	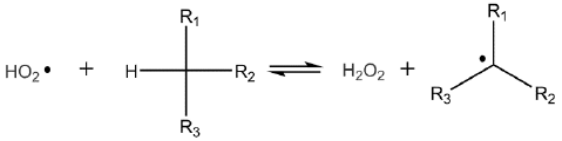	R_1, R_2, R_3 alkyl chains or H atoms	Rate rules for alkanes			[8]
		R_1, R_2 or R_3 OH	1.23e-11	5.26	31.3	[9]
		R_1, R_2 or R_3 C=C	7.68e-2	4.4	56.7	[10]
		H abstr from C(=O)-**H**	1.18e-10	4.9	15.4	[3]
by O_2 from C-H	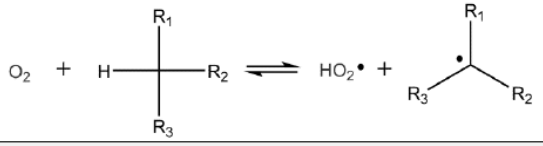		1.00e7	0.0	ΔH_r	[11, 12]
Intramolecular						

by C• from C-H	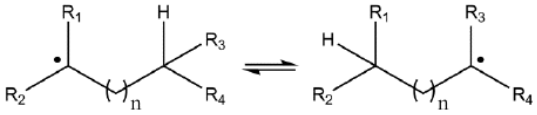		Group additivity + rate rule
			A = function of # hindered rotors in TS
			Ea = ring strain in TS + activation energy analogous bimolecular reaction
						[1, 2, 13, 14]

by R-O-O• from C-H	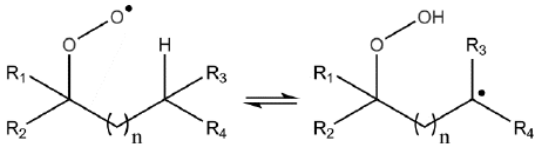	Formation of an alkyl radical	Rate rules for alkanes			[15]
		Formation of an allylic radical	2.24e6	1.29	59.6	[16]
by R-O-O• from O-H	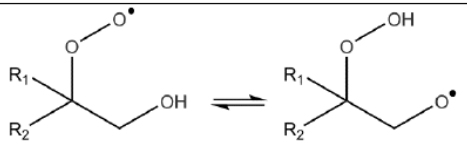	Analogy with 2-peroxy-2-methyl-propan-1-ol	2.91e12	-0.23	93.3	[17]
by cyclopentadienyl from C-H through 3-membered transition state	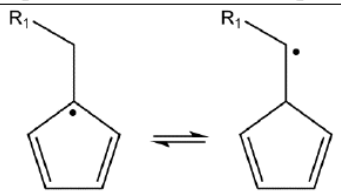	Analogy with methyl-cyclopentadienyl	2.20e-3	4.91	169.0	[18]

β-scission / radical addition						
Intermolecular						
•C-C-C ⇄ C=C + •C	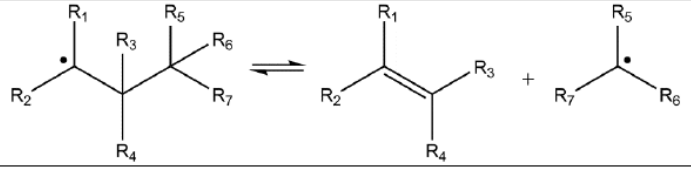		Group additivity			[19]
•C-C-H ⇄ C=C + •H	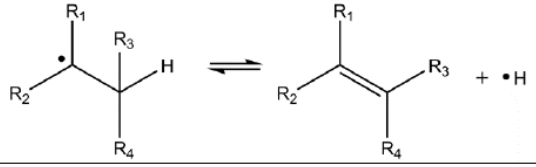		Group additivity			[20]
•C-C-OH ⇄ C=C+ •OH	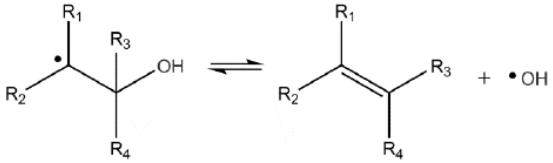	Analogy with 2-hydroxy-ethyl to ethene plus OH	3.00e13	0.0	112.1	[a]
•C-O-H ⇄ C=O+ •H	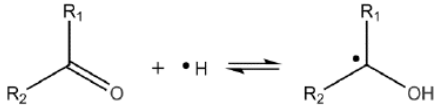	Analogy with acetaldehyde plus H to 1-hydroxy-ethyl	1.10e8	0.0	44.7	[a]
•C-O-OH ⇄ C=O+ •OH	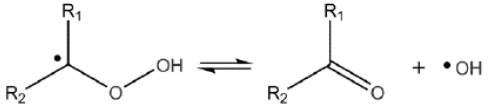		9.00e14	0.0	6.28	
•C-C-O-O-H ⇄ C=C+ HO_2•	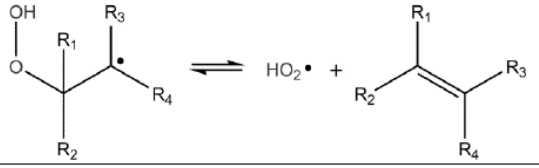		Rate rules for alkanes			[15]

•O-C-C ⇄ C=O+ •C	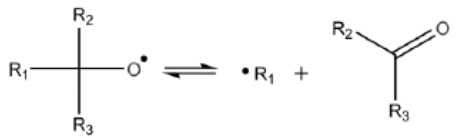	R_1 alkyl Analogy with 2-oxy-propane	6.00e13	0.22	59.0	[a]
		R_1 C=C Analogy with allyloxy	2.70e14	0.00	100.0	[21]
•O-C-H ⇄ C=O+ •H	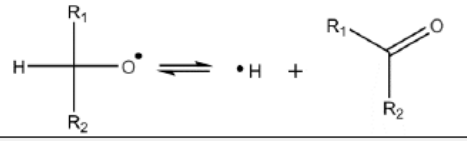	R_1 or R_2 C=C. Analogy with allyloxy	1.17e10	1.00	77.6	[21]
Intramolecular						

exo-addition	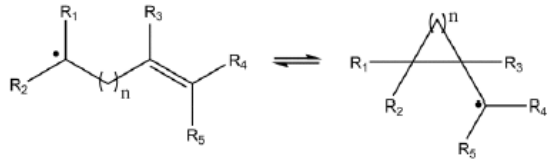		Group additivity + rate rule
			A = function of # hindered rotors in TS
			Ea = ring strain in TS + activation energy analogous bimolecular reaction
						[13, 19]

endo-addition	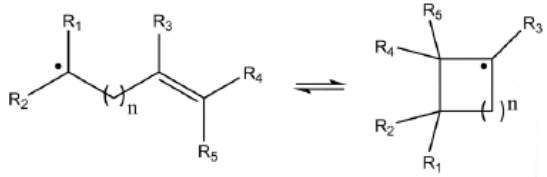		Group additivity + rate rule
			A = function of # hindered rotors in TS
			Ea = ring strain in TS + activation energy analogous bimolecular reaction
						[13, 19]

endo-addition forming bicyclic species	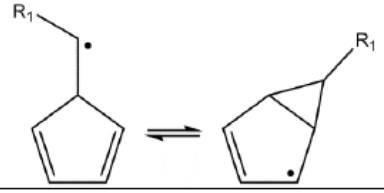	Analogy with methyl-cyclopentadienyl	3.20e11	0.17	18.4	[18]
ring-enlargement	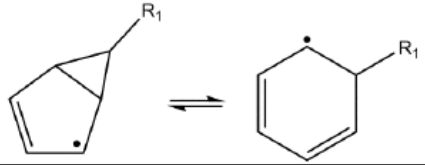	Analogy with hexadienyl	8.50e11	0.41	69.9	[18]

α-scission					
C-C(=O)• ⇄ C• + CO		Analogy with acetyl radical	3.30e12	0.62	72.4 [a]
Concerted reactions					
•O-O-C-C-H ⇄ HO_2• + C=C			Rate rules for alkanes		[15]
Formation of cyclic ethers from hydoperoxyl-alkyl radicals			Rate rules for alkanes		[15]
•O-O-C-OH ⇄ HO_2• + C=O		Analogy with alpha-hydroxy-ethylperoxy	2.60e8	1.128	44.5 [22]
Sigmatropic hydrogen shift of 5-alkyl-1,3-cyclopentadiene to 1-alkyl-1,3-cyclopentadiene		Analogy with methyl-cyclopentadiene	7.03e8	1.20	103.8 [23]
Sigmatropic hydrogen shift of 1-alkyl-1,3-cyclopentadiene to 2-alkyl-1,3-cyclopentadiene		Analogy with methyl-cyclopentadiene	1.65e7	2.10	105.0 [23]

Oxygen addition on carbon-centered radicals						
C• + O_2 ⇄ C-O-O•		R_1, R_2, R_3 alkyl chains or H atoms	Rate rules for alkanes			[15]
		R_1 C=C	5.78e1	1.59	4.5	[24]
		R_1 OH	4.05e7	-0.31	-1.4	[9]
Recombination / scission						
C-O-O-H ⇄ CO• + •OH		Analogy with allylhydroperoxide	3.35e10	0.60	-8.8	[21]
C• + HO_2• ⇄ C-O-O-H		Analogy with allylhydroperoxide	1.59e20	-1.50	179.3	[21]
Recombination of cyclopentadienyl with carbon-centered radicals		Analogy with cyclopentadienyl plus methyl	8.34e9	-0.70	-2.1	[23]

[a] CBS-QB3 calculations

References

[1] M. K. Sabbe, A. Vandeputte, M.-F. Reyniers, M. Waroquier, G. B. Marin, Modeling the influence of resonance stabilization on the kinetics of hydrogen abstractions, Phys. Chem. Chem. Phys. 12 (2010) 1278-1298

[2] P. D. Paraskevas, M. K. Sabbe, M.-F. Reyniers, N. G. Papayannakos, G. B. Marin, Kinetic Modeling of α-Hydrogen Abstractions from Unsaturated and Saturated Oxygenate Compounds by Carbon-Centered Radicals, ChemPhysChem 15 (2014) 1849-1866

[3] J. Mendes, C.-W. Zhou, H. J. Curran, Theoretical Chemical Kinetic Study of the H-Atom Abstraction Reactions from Aldehydes and Acids by Ḣ Atoms and ȮH, HȮ2, and ĊH3 Radicals, J. Phys. Chem. A 118 (2014) 12089-12104

[4] P. D. Paraskevas, M. K. Sabbe, M.-F. Reyniers, N. G. Papayannakos, G. B. Marin, Kinetic Modeling of α-Hydrogen Abstractions from Unsaturated and Saturated Oxygenate Compounds by Hydrogen Atoms, J. Phys. Chem. A 118 (2014) 9296-9309

[5] R. Sivaramakrishnan, J. V. Michael, Rate Constants for OH with Selected Large Alkanes: Shock-Tube Measurements and an Improved Group Scheme, J. Phys. Chem. A 113 (2009) 5047-5060

[6] J. Badra, A. Elwardany, A. Farooq, Shock tube measurements of the rate constants for seven large alkanes + OH, P. Combust. Inst. 35 (2015) 189-196

[7] P. D. Paraskevas, M. K. Sabbe, M.-F. Reyniers, N. G. Papayannakos, G. B. Marin, Group Additive Kinetics for Hydrogen Transfer Between Oxygenates, J. Phys. Chem. A (2015)

[8] J. Aguilera-Iparraguirre, H. J. Curran, W. Klopper, J. M. Simmie, Accurate Benchmark Calculation of the Reaction Barrier Height for Hydrogen Abstraction by the Hydroperoxyl Radical from Methane. Implications for CnH2n+2 where n = 2 → 4, J. Phys. Chem. A 112 (2008) 7047-7054

[9] G. Mittal, S. M. Burke, V. A. Davies, B. Parajuli, W. K. Metcalfe, H. J. Curran, Autoignition of ethanol in a rapid compression machine, Combust. Flame 161 (2014) 1164-1171

[10] J. Zádor, S. J. Klippenstein, J. A. Miller, Pressure-Dependent OH Yields in Alkene + HO2 Reactions: A Theoretical Study, J. Phys. Chem. A 115 (2011) 10218-10225

[11] H. J. Curran, P. Gaffuri, W. J. Pitz, C. K. Westbrook, A comprehensive modeling study of n-heptane oxidation, Combust. Flame 114 (1998) 149-177

[12] H. J. Curran, P. Gaffuri, W. J. Pitz, C. K. Westbrook, A comprehensive modeling study of iso-octane oxidation, Combust. Flame 129 (2002) 253-280

[13] K. Wang, S. M. Villano, A. M. Dean, Reactivity–Structure-Based Rate Estimation Rules for Alkyl Radical H Atom Shift and Alkenyl Radical Cycloaddition Reactions, J. Phys. Chem. A 119 (2015) 7205-7221

[14] K. Wang, S. M. Villano, A. M. Dean, The Impact of Resonance Stabilization on the Intramolecular Hydrogen-Atom Shift Reactions of Hydrocarbon Radicals, Chemphyschem 16 (2015) 2635-2645

[15] J. Bugler, K. P. Somers, E. J. Silke, H. J. Curran, Revisiting the Kinetics and Thermodynamics of the Low-Temperature Oxidation Pathways of Alkanes: A Case Study of the Three Pentane Isomers, J. Phys. Chem. A 119 (2015) 7510-7527

[16] F. Zhang, T. S. Dibble, Effects of Olefin Group and Its Position on the Kinetics for Intramolecular H-Shift and HO2 Elimination of Alkenyl Peroxy Radicals, J. Phys. Chem. A 115 (2011) 655-663

[17] H. Sun, J. W. Bozzelli, C. K. Law, Thermochemical and Kinetic Analysis on the Reactions of O2 with Products from OH Addition to Isobutene, 2-Hydroxy-1,1-dimethylethyl, and 2-Hydroxy-2-methylpropyl Radicals: HO2 Formation from Oxidation of Neopentane, Part II, J. Phys. Chem. A 111 (2007) 4974-4986

[18] S. Sharma, M. R. Harper, W. H. Green, Modeling of 1,3-hexadiene, 2,4-hexadiene and 1,4-hexadiene-doped methane flames: Flame modeling, benzene and styrene formation, Combust. Flame 157 (2010) 1331-1345

[19] M. K. Sabbe, M.-F. Reyniers, V. Van Speybroeck, M. Waroquier, G. B. Marin, Carbon-centered radical addition and beta-scission reactions: Modeling of activation energies and pre-exponential factors, ChemPhysChem 9 (2008) 124-140

[20] M. K. Sabbe, M.-F. Reyniers, M. Waroquier, G. B. Marin, Hydrogen Radical Additions to Unsaturated Hydrocarbons and the Reverse beta-Scission Reactions: Modeling of Activation Energies and Pre-Exponential Factors, ChemPhysChem 11 (2010) 195-210

[21] C. F. Goldsmith, S. J. Klippenstein, W. H. Green, Theoretical rate coefficients for allyl + HO2 and allyloxy decomposition, P. Combust. Inst. 33 (2011) 273-282

[22] G. da Silva, J. W. Bozzelli, L. Liang, J. T. Farrell, Ethanol Oxidation: Kinetics of the α-Hydroxyethyl Radical + O2 Reaction, J. Phys. Chem. A 113 (2009) 8923-8933

[23] S. Sharma, W. H. Green, Computed Rate Coefficients and Product Yields for c-C(5)H(5) + CH(3) -> Products, J. Phys. Chem. A 113 (2009) 8871-8882

[24] J. Lee, J. W. Bozzelli, Thermochemical and kinetic analysis of the allyl radical with O2 reaction system, P. Combust. Inst. 30 (2005) 1015-1022